

De Gruyter. All rights reserved. May not be reproduced in any form without permission from the publisher.
Copyright 2017. All rights reserved. May not be reproduced in any form without permission from the publisher.
except fair use as permitted under U.S. or applicable copyright law.

DE GRUYTER

REFERENCE

Alfred Golloch (Ed.)

HANDBOOK OF RARE EARTH ELEMENTS

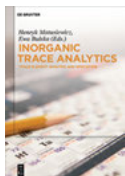
ANALYTICS



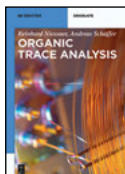
EE 0 Pub
AM 130
AC 111

Golloch (Ed.)
Rare Earth Elements
De Gruyter Reference

Also of interest



Inorganic Trace Analytical Chemistry.
Trace Element Analysis and Speciation
Matusiewicz, Bulska (Eds.), 2017
ISBN 978-3-11-037194-9, e-ISBN 978-3-11-036673-0



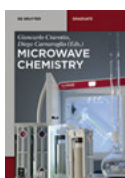
Organic Trace Analysis.
Niessner, Schaeffer; 2016
ISBN 978-3-11-044114-7, e-ISBN 978-3-11-044115-4



Series: Metal Ions in Life Sciences Volume 17
Lead – Its Effects on Environment and Health
Sigel, Sigel, Sigel (Eds.), 2017
ISBN 978-3-11-044107-9, e-ISBN 978-3-11-043433-0
ISSN 1559-0836



Research Laboratory Safety.
Kuespert, 2016
ISBN 978-3-11-044439-1, e-ISBN 978-3-11-044443-8



Microwave Chemistry.
Cravotto, Carnaroglio (Eds.), 2017
ISBN 978-3-11-047992-8, e-ISBN 978-3-11-047993-5



Physical Sciences Reviews
e-ISSN 2365-659X

Alfred Golloch

Rare Earth Elements

Analytics

Edited by
Alfred Golloch

DE GRUYTER

Editor

Prof. Dr. Alfred Golloch
Schönauer Bach 21
52072 Aachen
Germany

ISBN 978-3-11-036523-8
e-ISBN (PDF) 978-3-11-036508-5
e-ISBN (EPUB) 978-3-11-039125-1
Set-ISBN 978-3-11-036509-2

Library of Congress Cataloging-in-Publication Data

A CIP catalog record for this book has been applied for at the Library of Congress.

Bibliographic information published by the Deutsche Nationalbibliothek

The Deutsche Nationalbibliothek lists this publication in the Deutsche Nationalbibliografie; detailed bibliographic data are available on the Internet at <http://dnb.dnb.de>.

© 2017 Walter de Gruyter GmbH, Berlin/Boston
Typesetting: Integra Software Services Pvt. Ltd.
Printing and binding: CPI books GmbH, Leck
Cover image: Science Photo Library C013/2672
♻️ Printed on acid-free paper
Printed in Germany

www.degruyter.com

Preface

The use of rare earth elements for the production of high-tech devices is continuously increasing which in turn increases attention on quality of starting materials and products. Application of powerful analytical instruments and validated analysis methods ensure the quality of the materials.

This handbook contains a summary of the most important tools of instrumental analysis on rare earth elements and is supplemented with the special applications report. The combination of analytical tool and its application could offer analytical chemists a chance to find solutions for certain problems.

The methods for the determination of rare earth elements can often only be efficiently applied if a separation of mixtures of rare earth elements is previously carried out. Therefore, two contributions such as separation and enrichment come first in the determination methods.

It is obvious that all the specified important determinations are based on atomic effect methods since especially instrumental techniques based on atomic effects are powerful enough for the determination of low concentrations of rare earth elements.

Neutron activation (atomic nucleus), x-ray fluorescence (electron shells near the atomic nucleus) or optical atomic emission (outer electron shells) is used for the method development of rare earth elements determination.

These applications are selected under the aspect of usage of the presented tools, where they demonstrate how complex problems in rare earth elements analysis can be solved. Nevertheless, the selection is a subjective one. The sequence of the contributions describing instrumental analytical tools and their applications is therefore mixed. But a mixture has been chosen to point out interactions and to make the book less monotonous.

The state of the art presented in this handbook could only be realized by the dedication and competent commitment of the authors. There was a good opportunity for the authors to compare and share their knowledge by presentation of their contributions on the “Analysis of Rare Earth Elements, Methods and Application” colloquium, which was held on 5–6 October 2015, organized at the Rhine-Waal University of Applied Sciences (Kleve, Germany). I thank Dr Myint Myint Sein for perfectly organizing the colloquium. I am also thankful to the authors!

The team at De Gruyter, especially Dr Ria Fritz, has patiently endured my phone calls and emails. I thank them for their support and for their professionalism in preparing the chapters for the publication of this handbook.

I thank Dipl.-Ing. Gerd Fischer for his friendly advices and competent support in preparing the chapters; he was patient enough to help find missing data and references.

I would like to thank my wife Dorothee for her patience and understanding, as well as for allowing me to spend time at my desk.

Alfred Golloch

Contents

Preface — V

List of Contributing Authors — XV

Alfred Golloch

1 Introduction — 1
References — 3

Alfred Golloch

2 Analytics of Rare Earth Elements – Basics and Methods — 4

2.1 Electronic configurations of RE elements and analytical properties — 4

2.1.1 Chemistry of Ln^{3+} ions — 5

2.1.2 Chemistry of Ln^{2+} and Ln^{4+} ions — 5

2.2 The development of rare earth analytics from 1940 to present — 6

2.2.1 Determination methods applied during the period from 1940 to 1960 — 7

2.2.2 Separation methods applied during the period 1940–1960 — 8

2.2.3 RE analysis during the period 1960–1980 — 9

2.2.4 Literature review 1978 — 12

2.2.5 Situation of RE analytics from 1980 to present — 12

References — 12

Bin Hu, Man He, Beibei Chen and Zucheng Jiang

3 Separation/Preconcentration Techniques for Rare Earth Elements Analysis — 14

3.1 Introduction — 14

3.2 Chemical separation techniques for REEs — 15

3.2.1 Precipitation/coprecipitation — 15

3.3 Liquid–liquid extraction — 16

3.3.1 Affecting factors for LLE of REEs — 16

3.3.2 Extractants for REEs — 18

3.3.3 Extractant concentration and extraction equilibrium constant — 26

3.3.4 Medium pH — 26

3.3.5 Salting-out agent — 28

3.3.6 Extraction systems for REEs and their application — 29

3.4 Liquid phase microextraction — 33

3.4.1 Operation modes and mechanism — 34

3.4.2 Single-drop microextraction — 35

3.4.3 Hollow fiber liquid phase microextraction — 37

3.4.4	Two-phase HF-LPME —	38
3.4.5	Three-phase HF-LPME —	38
3.4.6	Dispersive liquid–liquid microextraction —	40
3.4.7	Solidified floating organic drop microextraction —	42
3.4.8	Affecting factors in LPME —	44
3.4.9	Cloud point extraction —	47
3.5	Solid phase extraction —	50
3.5.1	Carbon nanotubes and graphene oxide —	51
3.5.2	Silica-based materials —	56
3.5.3	Chelating resin and ionic-exchange resin —	57
3.5.4	Metal oxide nanostructured materials —	58
3.5.5	Ion-imprinted materials —	60
3.5.6	Metal-organic frameworks (MOFs) —	60
3.5.7	Restricted access materials —	61
3.5.8	Capillary microextraction —	61
	References —	65

Beibei Chen, Man He, Huashan Zhang, Zucheng Jiang and Bin Hu

4 Chromatographic Techniques for Rare Earth Elements Analysis — 74

4.1	Introduction —	74
4.2	Liquid chromatography —	75
4.2.1	Ion-exchange chromatography —	75
4.2.2	Ion chromatography —	86
4.2.3	Reverse-phase ion pair chromatography (RPIPC) —	90
4.2.4	Extraction chromatography —	97
4.2.5	Thin layer chromatography (TLC) and Paper chromatography (PC) —	102
4.3	Gas chromatography —	107
4.4	Capillary Electrophoresis (CE) —	108
4.4.1	Basic knowledge and principle —	108
4.4.2	Influencing factors on CE separation —	110
4.4.3	Applications in REEs analysis —	111
4.5	Supercritical fluid chromatography —	115
	References —	116

Lena Telgmann, Uwe Lindner, Jana Lingott and Norbert Jakubowski

5 Analysis and Speciation of Lanthanoides by ICP-MS — 124

5.1	Introduction —	124
5.2	Fundamentals of ICP-MS —	125
5.2.1	Sample preparation —	126
5.2.2	Sample introduction —	126
5.2.3	The ion source —	127

- 5.2.4 Interface — **128**
- 5.2.5 Lens system — **129**
- 5.2.6 Mass analyzers — **129**
- 5.2.7 Detector and computer — **134**
- 5.3 Analytical figures of merit — **134**
- 5.4 Speciation of Gd-based contrast agents — **135**
- 5.5 Analysis of Gd-based contrast agents in medical samples — **139**
- 5.6 Analysis of Gd-based contrast agents in environmental samples — **140**
- 5.7 Summary and outlook — **142**
- References — **142**

Man He, Bin Hu, Beibei Chen and Zucheng Jiang

6 Inductively Coupled Plasma Optical Emission Spectrometry for Rare Earth Elements Analysis — 145

- 6.1 Introduction — **145**
 - 6.1.1 Spectral interference — **148**
 - 6.1.2 Matrix effect — **155**
 - 6.1.3 Acid effect — **158**
 - 6.1.4 Sensitivity-enhancing effect of organic solvent — **159**
- 6.2 Sample introduction for ICP — **166**
 - 6.2.1 Pneumatic nebulization and ultrasonic nebulization — **166**
 - 6.2.2 Flow injection — **166**
 - 6.2.3 Laser ablation — **170**
 - 6.2.4 Electrothermal vaporization — **173**
- 6.3 ETV-ICP-OES for REE analysis — **177**
 - 6.3.1 Fluorination-assisted (F)ETV-ICP-OES for REEs analysis — **177**
 - 6.3.2 Low-temperature ETV-ICP-OES for REEs analysis — **184**
- 6.4 Application of ICP-OES in the analysis of high-purity REE, alloys and ores — **187**
 - 6.4.1 High-purity REE analysis by ICP-OES — **187**
 - 6.4.2 REE ores analysis by ICP-OES — **191**
 - 6.4.3 Trace REE analysis by ICP-OES in alloys — **192**
- References — **193**

Jörg Niederstraßer

7 Application of Spark Atomic Emission Spectrometry for the Determination of Rare Earth Elements in Metals and Alloys — 197

- 7.1 Introduction — **197**
- 7.2 Spark emission spectrometry basics — **197**
- 7.3 Setup of a spark emission spectrometer — **200**

7.3.1	Argon supply —	201
7.3.2	Spark stand —	201
7.3.3	Spectrometer optical system —	202
7.3.4	Spark generator —	203
7.3.5	Power supply —	203
7.3.6	Operation and evaluation PC —	204
7.4	The analysis process —	204
7.5	Quantitative analysis —	206
7.5.1	Calibration and recalibration —	206
7.5.2	Evaluation of calibration and analysis results —	208
7.6	Using spark emission spectrometry —	209
7.7	Analysing rare earths using spark emission spectrometry —	210
7.7.1	Industrial use of rare earths —	211
7.7.2	Spectrometric prerequisites —	212
7.7.3	Calibration samples —	212
7.8	Analysis of aluminium alloys —	215
7.8.1	Calibration (analysis function) and accuracy —	215
7.8.2	Detection limits —	217
7.8.3	Repeatability —	217
7.9	Analysis of magnesium alloys —	218
7.9.1	Calibration (analysis function) and accuracy —	218
7.9.2	Detection limits —	220
7.9.3	Repeatability —	220
7.10	Analysis of iron alloys —	222
7.10.1	Calibration (analysis function) and accuracy —	222
7.10.2	Detection limits —	223
7.10.3	Repeatability —	224
7.10.4	Long-term stability —	224
7.11	Analysis of zinc alloys —	226
7.11.1	Calibration (analysis function) and accuracy —	226
7.11.2	Detection limits —	226
7.11.3	Repeatability —	228
7.12	Conclusion —	228
	References —	229

Rainer Schramm

8	Use of X-ray Fluorescence Analysis for the Determination of Rare Earth Elements —	231
8.1	Introduction —	231
8.2	Principle of X-ray fluorescence analysis —	231
8.3	XRF methods —	233
8.3.1	Energy-dispersive X-ray fluorescence analysis —	233

- 8.3.2 Wavelength-dispersive X-ray analysis — 235
- 8.3.3 Comparison of EDXRF–WDXRF — 236
- 8.3.4 Other XRF techniques — 236
- 8.4 Sample preparation — 236
- 8.4.1 Pressed pellets techniques — 236
- 8.4.2 Fusion technology — 238
- 8.4.3 Additional sample preparation techniques — 240
- 8.5 Practical application of REEs determination — 240
- 8.5.1 Reference materials — 240
- 8.5.2 Measuring parameters — 241
- 8.5.3 Analyte lines — 245
- 8.5.4 Lower limit of detection (LLD) — 249
- 8.6 Calibration — 249
- 8.6.1 Other calibration strategies mentioned in literature — 251
- 8.7 Summary — 251
- References — 251

Heinz-Günter Stosch

- 9 Neutron Activation Analysis of the Rare Earth Elements (REE) – With Emphasis on Geological Materials — 253**
- 9.1 Introduction — 253
- 9.2 Principles of neutron activation: activation equation, cross sections — 253
- 9.3 Equipment — 258
- 9.3.1 Neutron sources — 258
- 9.3.2 The counting system — 261
- 9.4 Practical considerations — 266
- 9.4.1 Instrumental versus radiochemical NAA — 266
- 9.4.2 Samples and standards — 267
- 9.4.3 Counting strategies — 273
- 9.4.4 Radiochemical neutron activation analysis (RNAA) – a fast separation scheme — 275
- 9.4.5 Data reduction and sources of error — 279
- 9.5 Conclusion — 283
- Acknowledgements — 283
- References — 284

Sven Sindern and F. Michael Meyer

- 10 Automated Quantitative Rare Earth Elements Mineralogy by Scanning Electron Microscopy — 286**
- 10.1 Introduction — 286
- 10.2 Quantitative mineralogy — 288
- 10.3 Scanning electron microscopy — 289

- 10.4 SEM-based automated quantitative mineralogy — **290**
- 10.4.1 Quantitative Evaluation of Minerals by Scanning Electron Microscopy — **291**
- 10.4.2 Mineral Liberation Analyser — **294**
- 10.4.3 Tescan-Integrated Mineral Analyser — **294**
- 10.4.4 ZEISS Mineralogic Mining — **294**
- 10.5 Quantitative REE mineralogy — **295**
- 10.6 Concluding remarks — **298**
Acknowledgements — **298**
References — **299**

Larissa Müller, Heike Traub and Norbert Jakubowski

11 Novel Applications of Lanthanoides as Analytical or Diagnostic Tools in the Life Sciences by ICP-MS-based Techniques — 301

- 11.1 Introduction — **301**
- 11.2 Bio-conjugation of biomolecules — **302**
- 11.2.1 Fundamentals — **302**
- 11.2.2 Bio-conjugation of antibodies — **303**
- 11.3 Applications — **304**
- 11.3.1 Development of identification and quantification strategies for DNA, peptides and proteins in mass spectrometry — **304**
- 11.3.2 Analytical and diagnostic applications of lanthanoides — **305**
- 11.4 Outlook — **316**
References — **317**

Jürgen Meinhardt, Martin Kilo, Ferdinand Somorowsky and Werner Hopp

12 Lanthanoides in Glass and Glass Ceramics — 321

- 12.1 Introduction — **321**
- 12.2 Literature survey of rare earth chemical analysis in glass — **322**
- 12.2.1 Laser-ablation inductively coupled plasma mass spectrometry (LA-ICP-MS) — **322**
- 12.2.2 Laser-ablation inductively coupled plasma atomic emission spectrometry (LA-ICP-AES) — **323**
- 12.2.3 ICP-MS analysis of solutions — **323**
- 12.2.4 X-ray fluorescence analysis (XRF) — **323**
- 12.3 Analytical methods for the determination of main components of glass (except lanthanoides) — **323**
- 12.4 Preparation of sample solutions for glass analysis by ICP-OES — **324**
- 12.4.1 Hydrofluoric acid digestion — **324**
- 12.4.2 Melt digestion — **325**

- 12.5 ICP-OES analysis of rare earth elements — 325
- 12.6 Analysis of special optical glass — 325
- 12.7 Analysis of glass by topochemical analysis — 327
- References — 331

Sven Sindern

- 13 Analysis of Rare Earth Elements in Rock and Mineral Samples by ICP-MS and LA-ICP-MS — 334**
 - 13.1 Introduction — 334
 - 13.2 Technical development — 338
 - 13.3 Physical and chemical effects on concentration and isotope ratio determination — 340
 - 13.4 Determination of REE concentrations — 343
 - 13.4.1 Sample preparation — 343
 - 13.4.2 Quantification — 343
 - 13.5 Determination of isotope ratios by multi-collector (MC)-ICP-MS — 345
 - 13.5.1 Solution-MC-ICP-MS — 346
 - 13.5.2 LA-MC-ICP-MS — 347
 - 13.6 Concluding remarks — 349
 - Acknowledgements — 349
 - References — 349

Tom Lorenz and Martin Bertau

- 14 Recycling of Rare Earth Elements — 357**
 - 14.1 Recycling of rare earth elements — 357
 - 14.2 Recycling from fluorescent lamp scraps — 358
 - 14.2.1 Starting material — 359
 - 14.2.2 Solid-state chlorination — 361
 - 14.2.3 Optimization of the solid-state chlorination — 365
 - 14.2.4 Recycling process — 375
 - 14.2.5 Summary — 376
 - 14.3 RE metal recycling from Fe₁₄Nd₂B magnets — 378
 - 14.3.1 Starting material — 379
 - 14.3.2 Preliminary tests — 380
 - 14.3.3 Optimization of the solid-state chlorination — 382
 - 14.3.4 Recycling process — 389
 - 14.3.5 Summary — 391
 - References — 391

Index — 395

List of Contributing Authors

Chapter 1, 2

Alfred Golloch

Schönauer Bach 21, 52072 Aachen
A.u.D.Golloch@t-online.de

Chapter 3 + 4

Bin Hu*

Key Laboratory of Analytical Chemistry
for Biology and Medicine
(Ministry of Education)
College of Chemistry and Molecular Sciences
Wuhan University
Wuhan, Hubei, 400372, China
Phone: 86-27-68752162
Fax: 86-27-68754067
E-mail: binhu@whu.edu.cn

Man He

Key Laboratory of Analytical Chemistry
for Biology and Medicine
(Ministry of Education)
College of Chemistry and Molecular
Sciences
Wuhan University
Wuhan, Hubei, 400372, China

Beibei Chen

Key Laboratory of Analytical Chemistry
for Biology and Medicine
(Ministry of Education)
College of Chemistry and Molecular
Sciences
Wuhan University
Wuhan, Hubei, 400372, China

Zucheng Jiang

Key Laboratory of Analytical Chemistry
for Biology and Medicine
(Ministry of Education)
College of Chemistry and Molecular
Sciences
Wuhan University
Wuhan, Hubei, 400372
China

Chapter 5

Lena Telgmann

Federal Institute for Materials Research
and Testing – BAM
Richard-Willstaetter-Str. 11
12489 Berlin

Uwe Lindner

Federal Institute for Materials Research
and Testing – BAM
Richard-Willstaetter-Str. 11
12489 Berlin

Jana Lingott

Federal Institute for Materials Research
and Testing – BAM
Richard-Willstaetter-Str. 11
12489 Berlin

Norbert Jakubowski

Federal Institute for Materials Research
and Testing – BAM
Richard-Willstaetter-Str. 11
12489 Berlin

Chapter 6

Man He*

Key Laboratory of Analytical Chemistry
for Biology and Medicine
(Ministry of Education)
College of Chemistry and Molecular
Sciences
Wuhan University
Wuhan, Hubei, 400372, China
Phone: 86-27-68752162
Fax: 86-27-68754067
E-mail: heman@whu.edu.cn

Bin Hu

Key Laboratory of Analytical Chemistry for
Biology and Medicine (Ministry of Education)
College of Chemistry and Molecular Sciences
Wuhan University
Wuhan, Hubei, 400372, China

Beibei Chen

Key Laboratory of Analytical Chemistry for
Biology and Medicine (Ministry of Education)
College of Chemistry and Molecular Sciences
Wuhan University
Wuhan, Hubei, 400372, China

Zucheng Jiang

Key Laboratory of Analytical Chemistry for
Biology and Medicine (Ministry of Education)
College of Chemistry and Molecular Sciences
Wuhan University
Wuhan, Hubei, 400372, China

Chapter 7

Jörg Niederstraßer

OBLF Gesellschaft für Elektronik
und Feinwerktechnik GmbH
Salinger Feld 44
58454 Witten, Germany

Chapter 8

Dr. Rainer Schramm

Bonhoefferweg 1
47551 Bedburg-Hau
rschramm@fluxana.de

Chapter 9

Heinz-Günter Stosch

Karlsruher Institut für Technologie (KIT)
Institut für Angewandte
Geowissenschaften
Adenauerring 20b
76131 Karlsruhe, Germany

Chapter 10

Sindern, S.

Institute of Applied Mineralogy
and Mineral Deposits
RWTH Aachen University
Wüllnerstrasse 2
52056 Aachen
Germany

Meyer, F.M.

German-Mongolian Institute of Resource
Technology
GMIT Campus, 2nd khoro
Nalaikh district, Ulaanbaatar, Mongolia
And
Institute of Applied Mineralogy
and Mineral Deposits
RWTH Aachen University
Wüllnerstrasse 2
52056 Aachen, Germany

Chapter 11

Larissa Müller

Federal Institute for Materials Research
and Testing (BAM)
Richard-Willstaetter-Str. 11
12489 Berlin, Germany

Heike Traub

Federal Institute for Materials Research
and Testing (BAM)
Richard-Willstaetter-Str. 11
12489 Berlin, Germany

Norbert Jakobowski

Federal Institute for Materials Research
and Testing (BAM)
Richard-Willstaetter-Str. 11
12489 Berlin, Germany

Chapter 12

Jürgen Meinhardt

Fraunhofer Institut für
Silicatforschung ISC
Neunerplatz 2
97080 Würzburg

Martin Kilo

Fraunhofer Institut für
Silicatforschung ISC
Neunerplatz 2
97080 Würzburg

Ferdinand Somorowsky

Fraunhofer Institut für
Silicatforschung ISC
Neunerplatz 2, 97080 Würzburg

Werner Hopp

Fraunhofer Institut für
Silicatforschung ISC
Neunerplatz 2, 97080 Würzburg

Chapter 13

Sindern, S.

Institute of Applied Mineralogy
and Mineral Deposits
RWTH Aachen University
Wüllnerstrasse 2
52056 Aachen, Germany

Chapter 14

Tom Lorenz

Institut für Technische Chemie
TU Bergakademie Freiberg
Leipziger Straße 29
09599 Freiberg, Germany

Martin Bertau*

Institut für Technische Chemie
TU Bergakademie Freiberg
Leipziger Straße 29
09599 Freiberg
Germany
Tel.: +49 3731 39-2384,
Fax: +49 3731 39-2324
martin.bertau@chemie.tu-freiberg.de

Alfred Golloch

1 Introduction

Rare earth elements (REEs) are a group of chemical elements in the periodic table, including the 15 elements from lanthanum (La, 57) to lutetium (Lu, 71), scandium (Sc, 21) and yttrium (Y, 39). This grouping was agreed by the IUPAC [1]. The elements scandium and yttrium differ in their atomic structure from the lanthanides but their chemical and physical properties are very similar (Figure 1.1).

The abundance of the REEs in the earth's crust follows a pattern in the periodic table. Lanthanides with even atomic numbers are more common in nature than lanthanides with odd atomic numbers.

Figure 1.2 shows the pattern of REE abundance in the earth's crust and it can also be noted that the abundance of REEs with lower atomic numbers is higher than the abundance of REEs with higher atomic numbers. Regarding this scope the first group is called "light REEs (LREEs)" and the second one "heavy REEs (HREEs)" (see Table 1.1). Other attempts have been made to subdivide REEs into groups.

Main groups		Transition groups										Main groups						
1	2	3	4	5	6	7	8	9	10	11	12	13	14	15	16	17	18	
Ia	IIa	IIIb	IVb	Vb	VIb	VIIb	VIIIb			Ib	IIb	IIIa	IVa	Va	VIa	VIIa	VIIIa	
s ¹	s ²	d ¹	d ²	d ³	d ⁴	d ⁵	d ⁶	d ⁷	d ⁸	d ⁹	d ¹⁰	p ¹	p ²	p ³	p ⁴	p ⁵	p ⁶	
1 1s	1 H																2 He	
2 2s 2p	3 Li	4 Be											5 B	6 C	7 N	8 O	9 F	10 Ne
3 3s 3p	11 Na	12 Mg											13 Al	14 Si	15 P	16 S	17 Cl	18 Ar
4 4s 3d 4p	19 K	20 Ca	21 Sc	22 Ti	23 V	24 *Cr	25 Mn	26 Fe	27 Co	28 Ni	29 *Cu	30 Zn	31 Ga	32 Ge	33 As	34 Se	35 Br	36 Kr
5 5s 4d 5p	37 Rb	38 Sr	39 Y	40 Zr	41 *Nb	42 *Mo	43 Tc	44 *Ru	45 *Rh	46 *Pd	47 *Ag	48 Cd	49 In	50 Sn	51 Sb	52 Te	53 I	54 Xe
6 6s 4f 5d 6p	55 Cs	56 Ba	57 *La	72 Hf	73 Ta	74 W	75 Re	76 Os	77 Ir	78 *Pt	79 *Au	80 Hg	81 Tl	82 Pb	83 Bi	84 Po	85 At	86 Rn
7 7s 5f 6d	87 Fr	88 Ra	89 *Ac	104 Rf	105 Db	106 Sg	107 Bh	108 Hs	109 Mt	110 Ds	111 Rg	112 Cn	113 Nh	114 Fl	115 Mc	116 Lv	117 Ts	118 Og
Lanthanoids (4f-elements)		58 Ce	59 Pr	60 Nd	61 Pm	62 Sm	63 Eu	64 *Gd	65 Tb	66 Dy	67 Ho	68 Er	69 Tm	70 Yb	71 Lu			
Actinoids (5f-elements)		90 *Th	91 *Pa	92 *U	93 *Np	94 Pu	95 Am	96 *Cm	97 Bk	98 Cf	99 Es	100 Fm	101 Md	102 No	103 Lr			

Figure 1.1: Periodic table of elements.

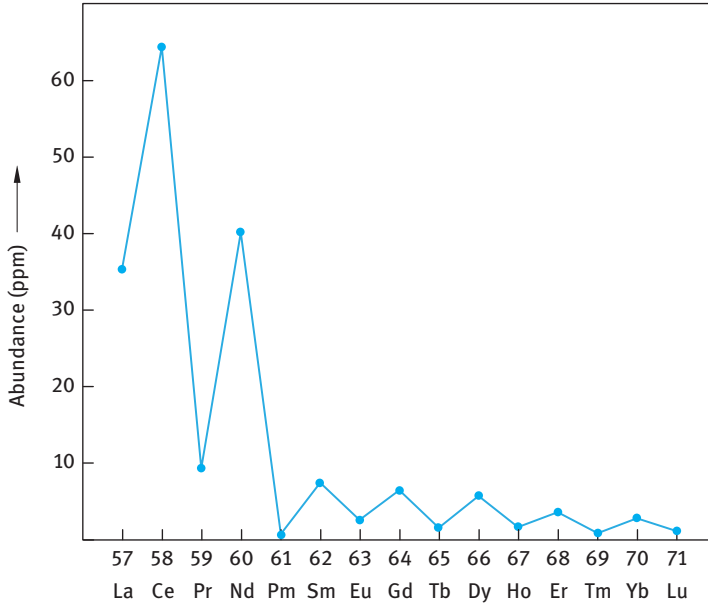


Figure 1.2: Abundance of the rare earth elements in the earth's crust (Harkins rule) [2].

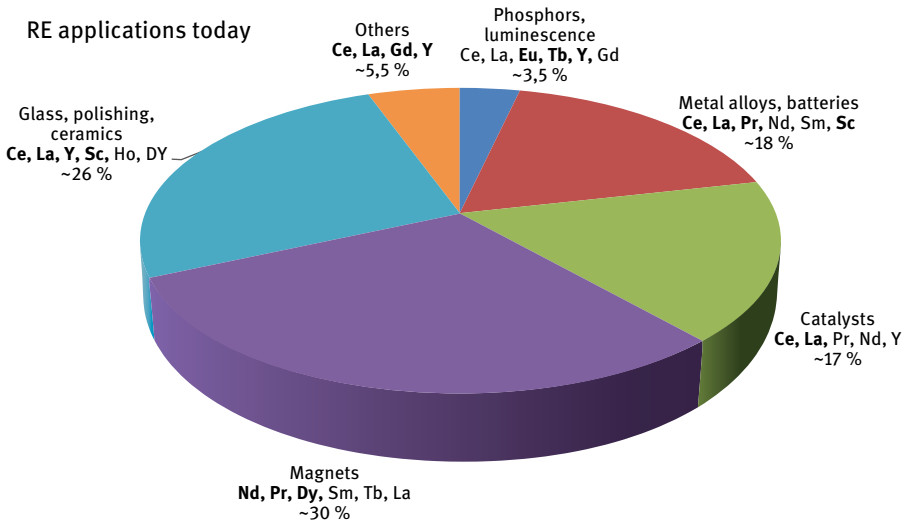


Figure 1.3: Main applications of rare earth elements (Source: Öko-Institut e.V.).

Table 1.1: List of light and heavy REEs.

LREE	Atomic number	HREE	Atomic number
Sc	21	Y	30
La	57	Gd	64
Ce	58	Tb	65
Pr	59	Dy	66
Nd	60	Ho	67
Pm	61	Er	68
Sm	62	Tm	69
Eu	63	Yb	70
		Lu	71

In most deposits of REEs, the share in LREEs is higher than 90 % and the percentage of HREEs is 2–3 %. For “High-Tech” applications mainly HREEs are used and the demand for these elements is obvious.

Figure 1.3 presents the most important applications of REEs [3].

References

- [1] International Union of Pure and Applied Chemistry (IUPAC): Nomenclature of Inorganic Chemistry, Definition Rules 1970. London, Butterworths, 1971.
- [2] Riedel E, Janiak C. Anorganische Chemie. Berlin and New York, DeGruyter, 2011.
- [3] Öko-Institut e.v. Hintergrundpapier Seltene Erden, Stand: Januar 2011, Seltene Erden-Daten und Fakten, S. 5

Alfred Golloch

2 Analytics of Rare Earth Elements – Basics and Methods

Abstract: A short summary of the electronic configuration of the RE elements gives proof for the analytical properties of the lanthanoides ions. The chemical reactions of the Ln^{3+} ions and of RE elements with “unusual” oxidation states are compared. The introduction to the scientific contributions of the handbook is realized by the presentation of the historical development of REE analytics from 1940 to present.

2.1 Electronic configurations of RE elements and analytical properties

The electronic configuration of the rare earth elements (REEs) is the key for understanding the analytical properties of the elements [1, 2]. Table 2.1 shows the electronic configurations of the ground state of REE atoms and of the ions.

The ground state configurations for the majority of lanthanoides can be summarized as $4f^{n+1} 6s^2$, except the following elements:

Lanthanum	$5d^1 6s^2$
Gadolinium	$4f^7 5d^1 6s^2$
Lutetium	$4f^{14} 5d^1 6s^2$
Scandium	$3d^1 4s^2$
Yttrium	$4d^1 5s^2$

In general, the f-levels of the lanthanoid atoms are filled with electrons and the N shell is filled up to the maximum of 32 electrons. The energy of 6s, 5d and 4f levels are very similar and as a result there is an irregular fill of the energy levels. It can be noted that the half-filled ($4f^7$) and the completely filled 4f subshell are preferred. The fill of the inlying 4f subshell with electrons slightly affects the chemical properties of the elements. The ground state configurations are not important for the analytical behaviour, but the trivalent ionic configurations are more important. The trivalent ions are formally generated when the valence electrons are removed. The radii of the Ln^{3+} ions are very similar to the radii of Sc^{3+} and Y^{3+} ions. This electronic similarity causes the chemical similarity and that is the reason for including elements of group 3 of the periodic table in considerations of the chemistry of lanthanoides.

Table 2.1: Electronic configuration of the rare earth elements [1].

Atomic number	Name	Symbol	Electronic configuration	
			Atom	Ion Ln^{3+}
57	Lanthanum	La	$5d^1 6s^2$	[Xe]
58	Cerium	Ce	$4f^2 6s^2$	$4f^1$
59	Praseodymium	Pr	$4f^3 6s^2$	$4f^2$
60	Neodymium	Nd	$4f^4 6s^2$	$4f^3$
61	Promethium	Pm	$4f^5 6s^2$	$4f^4$
62	Samarium	Sm	$4f^6 6s^2$	$4f^5$
63	Europium	Eu	$4f^7 6s^2$	$4f^6$
64	Gadolinium	Gd	$4f^7 5d^1 6s^2$	$4f^7$
65	Terbium	Tb	$4f^9 6s^2$	$4f^8$
66	Dysprosium	Dy	$4f^{10} 6s^2$	$4f^9$
67	Holmium	Ho	$4f^{11} 6s^2$	$4f^{10}$
68	Erbium	Er	$4f^{12} 6s^2$	$4f^{11}$
69	Thulium	Tm	$4f^{13} 6s^2$	$4f^{12}$
70	Ytterbium	Yb	$4f^{14} 6s^2$	$4f^{13}$
71	Lutetium	Lu	$4f^{14} 5d^1 6s^2$	$4f^{14}$
21	Scandium	Sc	$3d^1 4s^2$	[Ar]
39	Yttrium	Y	$3d^1 5s^2$	[Kr]

2.1.1 Chemistry of Ln^{3+} ions

The radii of the Ln^{3+} ions continuously decrease with the increasing atomic number of the elements (lanthanoid contraction) (Figure 2.1).

The lanthanoid contraction is the reason for the resemblance of 4d and 5d elements of the subgroups of the periodic table. The lanthanoid contraction is responsible for the regular amendment of some lanthanoid properties. The chemistry of the Ln^{3+} ions is similar to the chemistry of Sc^{3+} and Y^{3+} ions. The solubility of the trifluorides LnF_3 is poor, whereas the chlorides, bromides and iodides are slightly soluble. The oxalates can be used for the precipitation of the Ln^{3+} ions. All the Ln^{3+} ions react with EDTA (ethylenediaminetetraacetic acid) to form chelates in a ratio of (1:1).

2.1.2 Chemistry of Ln^{2+} and Ln^{4+} ions

Additional to the oxidation state (+3), the oxidation states (+2) and (+4) can be formed from the atoms of some lanthanoides. Table 2.2 presents the elements with “unusual” oxidation states.

The stability of compounds with the oxidation state (+2) decreases as follows: $\text{Eu}^{2+} > \text{Yb}^{2+} > \text{Sm}^{2+} > \text{Tm}^{2+}$. In aqueous solution only Eu^{2+} ions are stable, and the other Ln^{2+} ions decompose water. Compounds containing Ln^{2+} ions are similar to compounds of alkaline earth elements.

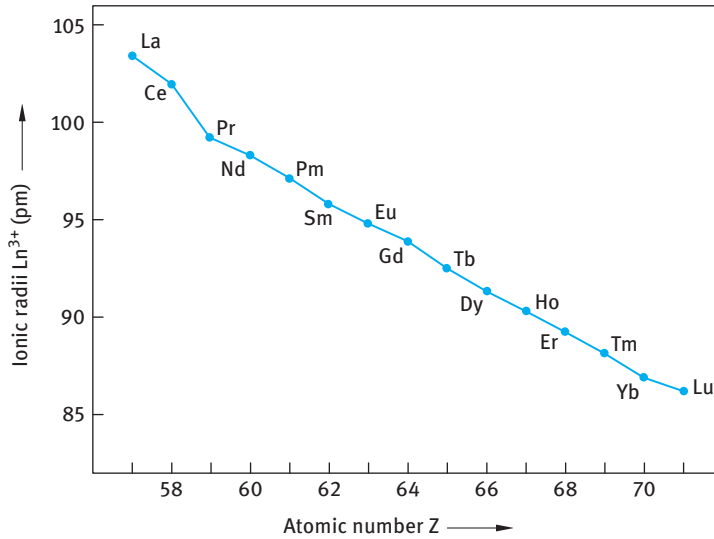
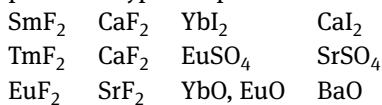


Figure 2.1: Lanthanoid contraction.

Table 2.2: Some lanthanoids with “unusual” oxidation states.

Ce	Pr	Nd	Pm	Sm	Eu	Gd	Tb	Dy	Ho	Er	Tm	Yb	Lu
				+2	+2						+2	+2	
+3	+3	+3	+3	+3	+3	+3	+3	+3	+3	+3	+3	+3	+3
+4	+4	+4					+4	+4					

Examples of isotype compounds are:



Comparing the compounds with Ln⁴⁺ ions it can be noted that compounds with Ce⁴⁺ are the most stable ones. In aqueous solution only Ce⁴⁺ ions can exist but all other Ln⁴⁺ ions oxidize water. Only few solid compounds with Ln⁴⁺ ions exist, for example, oxides like CeO₂, PrO₂ and TbO₂ or fluorides like Cs₃NdF₇ and Cs₃DyF₇.

2.2 The development of rare earth analytics from 1940 to present

Before World War II, the rare earth were frequently determined as a group with a nonselective precipitant such as oxalic acid, hydrofluoric acid or ammonium hydroxide. Indeed as recently as 1943, well-known textbooks on quantitative analysis contained such statements as “Beyond simply isolating the rare earth in this manner, there is little the analyst can do”. During and since World War II, however, knowledge of rare earths and the literature on their analytical chemistry have grown tremendously. [3]

An approach to review the development of REE analytics from 1940 to present results in the realization of subdividing the time period. The study of corresponding publications showed that it would be useful to analyse and describe three time periods:

1940–1960

1960–1980

1980–present

2.2.1 Determination methods applied during the period from 1940 to 1960

Two publications appeared in 1961 as chapter of a book [3] or in book form [4], dealing with the analytical chemistry of the REEs. Both of the publications have been prepared in order to describe the development of the analytical chemistry during the 20 years from the beginning of World War II.

In addition to these two books a collection of papers was published, which was presented at the conference on REEs held in June 1956 at the Institute of Geochemistry and Analytical Chemistry im V.I. Vernadskii of the Academy of Sciences of USSR [5]. It was the aim of the conference to summarize the experience on REEs gained in Russia during the past 20 years.

The publications stated earlier resumed for the first time the knowledge and experience on analytical chemistry of the REEs after 20 years.

Only few methods for the determination of REEs were available:

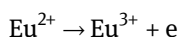
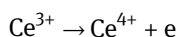
- Gravimetric methods
- Titrimetric methods
- Spectrophotometry
- Spectrography (Emission spectrometry)
- X-ray absorption and emission spectrometry
- Radiochemical methods (NAA, tracer)

Gravimetric methods

Various methods have been proposed. The precipitation of the rare earths (RE) as oxalates is the most frequently used method. The oxalates are thermally decomposed.

Titrimetric methods

Volumetric determination of individual RE in mixtures is restricted to cerium and possibly europium. Valence state variations are basis for the methods:



Spectrophotometry

The analytical methods of spectrophotometry are based upon the following:

Absorption spectra of the RE ions (350–750 nm region); Sc, Y, and La have no absorption spectra in this region.

Absorption spectra of coloured dye complexes.

Instrumentation

Filter photometers (Standard)

Increasing application of monochromatic spectrophotometers.

Spectrography (emission spectrometry)

Instrumentation

Grating spectrograph

Excitation source dc-arc discharge

Graphite electrodes for non-conducting samples

Photoplate detection.

Calibration

Techniques of internal standard

Observation of selected lines of intensity ratio.

Problems

Many spectra of REEs are very complex. Finding excitation conditions in order to produce spectra of sufficient precision.

X-ray absorption and emission spectrometry

Radiochemical methods (NAA, tracer)

These methods have been of no great importance for routine analysis of REEs.

2.2.2 Separation methods applied during the period 1940–1960

The number of methods for separation of REEs was limited

- Fractional precipitation
- Organic solvent extraction of complex compounds
- Ion exchange
- Paper or cellulose chromatography
- Electrolytic methods (reduction at a lithium-amalgam cathode)

All these separation methods were not efficient and unsuitable for the separation of complex mixtures of REE, except ion exchange. This technique was continuously developed during this time period, and the quality of separations was improved.

Conclusion: REE analysis 1940–1960

Spectrography was the only available method for the trace analysis of REEs.

2.2.3 RE analysis during the period 1960–1980

A distinct progress in RE analysis made during the period 1960–1972 was presented on a conference in Norway in 1972 [6]. The results presented on the conference are substantially in accord with the progress reviewed in an additional publication [7]. New determination techniques were developed and implemented ones were significantly improved:

- Determination of REs by complexometry
- Emission spectrometry (arc/spark)
- Flame and plasma atomic absorption, emission, and fluorescence spectrometry
- X-ray excited optical fluorescence spectrometry (XEOF)
- X-ray fluorescence (XRF) spectrometry
- Mass spectrometry and isotope dilution
- Neutron activation analysis

Determination of REs by complexometry [8]

The development of complexometric determination of the REs is a useful supplement of the gravimetric and titrimetric methods. The application of the method is limited by the determination of mixtures or pure REEs isolated from the others.

The volumetric determination of the REs was practically unknown before EDTA and related compounds (polyaminopolycarboxylic acids) were introduced in analytical chemistry.

Atomic emission spectrometry (arc/spark)

Readers are referred to De Kalb EL in Ref. [6].

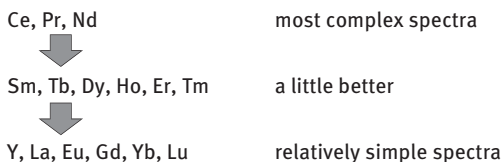
Atomic emission spectrometry is the most powerful tool for the analysis of RE materials. The efficiency of the method depends on the character of the spectrum. The spectra of many of the RE elements are very complex, and the choice of a suitable spectrometer is restricted to those which can provide adequate resolution. A rough classification of spectra of the REEs is listed in Figure 2.2.

Atomic emission spectrometry can be used for the following applications:

- Determination of REs in a “pure” RE.
- Determination of other impurities in a RE.
- Determination of REs in a mixture of various REs.
- Determination of RE impurities in other materials.

The methods for the determination of RE impurities in an RE metal or oxide were developed by Fassel and coworkers [9–13]. Later the methods were modified by several analysts. The use of an ac-arc instead of a dc-arc improved the detection limits and the precision. Detection limits of 10–0.01 ppm RE impurity in RE matrix could be achieved.

Complexity of the REE Emission Spectra



In general, the lowest detection limits are obtained for elements with a simple spectrum

Figure 2.2: Structure of REE emission spectra.

Flame and plasma atomic absorption, emission, and fluorescence spectrometry

Readers are referred to Fassel et al. in Ref. [6].

As mentioned earlier, the atomic emission spectrometry (arc/spark) is available for the analysis of solid REE samples. A method for the determination of REEs in aqueous solutions is missing. During this time period several studies were prepared to ascertain if emission spectra of REEs can be generated using combustion flames. The result of the studies showed that with oxygen/hydrogen flames, REE spectra could be generated. The character of the spectra did not correspond to atomic lines but to molecule emission bands. The analytical application was limited.

Flame emission spectrometry (FES) was improved by the studies of Fassel et al. [14]. They detected that flame chemistry was an important consideration in the production of free atoms of the REs rather than flame temperature. Fuel-rich hydrocarbon flames significantly enhanced the emission intensities. The spectra are relatively simple.

Flame atomic absorption spectrometry (FAAS) and flame atomic fluorescence spectrometry have also been investigated for the application of REE analysis. A comparison of the results illustrated the much better detection limits of FES than those observed in FAAS.

Atomic FES was successfully applied for mixtures of REEs.

The power and the potential of inductively coupled plasma-atomic emission spectrometry (ICP-AES) was presented in the conference [6]. Some characteristics of ICP-AES were discussed, and the arguments for use in analysis of REEs were convincing.

XEOF spectrometry and cathode-ray excited emission spectrometry

These two special analytical methods have been developed and improved during the period 1960–1972. The application was focussed on special challenges, for example, trace analysis of REEs. These methods could not be established for routine analysis.

XRF analysis

The first prototype of XRF (secondary emission) spectrometer was launched 1948. Since then the technique was fast developed. Important contributions on XRF analysis were published in 1955–1961 [15–18]. The method was well established in 1972, and all sample types can be analysed: Liquids, powders, metals or fused beads. XRF is applicable to the concentration range of REEs from 100 % down to absolute 0.01 %. These results were obtained with spectrometers equipped with wavelength-dispersive optics. Spectrometers with energy-dispersive detection technique were not available.

Mass spectrometry and isotope dilution

Mass spectrometry is a method that can be applied for trace REE analysis and is preferred for the analysis of small samples. Different instruments were applied. Some technical details are mentioned:

Two types of ion sources were used: surface ionization filaments (Re wires) and high-frequency spark. The sample preparation depends on the ion source; for Re filaments small amounts of the sample were dissolved. For spark source sample powder was mixed with high-purity graphite, and tiny electrodes were pressed.

Mass spectrometers

Single- or double-focussing instruments

Registration of the spectra using electron multiplier or photoplate

Limits of determination: 0.1 ppm

Neutron activation analysis

Readers are referred to Eiliv Steinnes in Ref. [6].

The method was well established in 1972 and the preferred applications of REE analysis are:

- Geological samples
- Reactor material
- High-purity chemicals
- Metals
- Biological tissues
- Water

Advantages of the method

High sensitivity for a great number of elements

Good specificity

Freedom from reagent contamination

Relative freedom from matrix effects

Multi-element determination

Drawbacks

Nuclear reactors are not easily accessible.

The equipment is relatively expensive.

In some cases, considerable amounts of radioactivity are released.

Sometimes it is time-consuming to wait for the result.

2.2.4 Literature review 1978 [18]

This review compiled by Jones and Dixon confirmed the state of REE analytics presented in the conference in Norway [6]:

- Spectroscopic methods were preferred for the determination of REEs.
- NAA = Neutron activation analysis.
- Application of atomic absorption spectrometry was increased.
- Spark-source mass spectrometry was applied more often.

Important separation methods with improved efficiency are:

- Liquid–liquid extraction
- Cation exchange
- Anion exchange

2.2.5 Situation of RE analytics from 1980 to present

Since about 1980 the very effective method of “inductively coupled plasma-optical emission spectrometry (ICP-OES)” was available. This tool was a breakthrough for RE analytics. Both liquid samples and solid material could be analysed. Efficiency and precision of the method are excellent and the method was widely accepted.

Around 1990, the superior technique of the “inductively coupled plasma- mass spectrometry ICP-MS” was developed and available for RE analytics. This method was an ideal supplement to ICP-OES and both of the methods are the workhorses in RE analytics.

The following review summarizes the experience gained with the application of spectroscopic methods for REE analytics: Zawisza B, Pytlakowska K, Feist B, Polowniak M, Kita A, Sitko R. Determination of rare earth elements by spectroscopic techniques: a review. *J Anal At Spectrom* 2011, 26, 2373–90.

References

- [1] Riedel E, Janiak C, *Anorganische Chemie*. 8.Aufl. Berlin and New York, W.DeGruyter, 2011.
- [2] De Bettencourt-Dias An. The electronic structure of the lanthanides. In: Atwood David A. ed. *The Rare Earth Elements, Fundamentals and Applications*. Chichester, UK, John Wiley & Sons, Ltd 2012, 27–34.
- [3] Banks CV, Klingman DW. Analytical chemistry of the rare earth, in: Spedding FH, Daane AH (ed.) *The Rare Earths*. New York and London, Wiley & Sons, Inc., 1961 (Chapter 23).

- [4] Vickery RC. *Analytical Chemistry of the Rare Earths*. New York, Oxford, London and Paris, Pergamon Press, 1961.
- [5] *Rare Earth Elements (Extraction, Analysis, Applications)*. Papers presented at a conference on REEs held in June 1956 at the Institute of Geochemistry and Analytical Chemistry im V.I. Vernadskii of the Academy of Sciences of USSR. Translated: Israel Program for Scientific translations, Jerusalem, 1960.
- [6] Michelsen Odd B (ed.) *Analysis and Application of Rare Earth Materials*. NATO Advanced Study Institute, Kjeller, Norway, 23–29 August 1972, Universitetsforlaget Oslo, Bergen, Tromsø.
- [7] Brusdeylins A. *Analytische Verfahren zur Bestimmung der Seltenen Erden*. *Chemiker-Zeitung* 1973, 97(10), 543–7.
- [8] Pribil R. Present state of complexometry-IV Determination of rare earths. *Talanta* 1967, 14, 619–27.
- [9] Fassel VA, Wilhelm HA. The quantitative spectrographic analysis of the rare earth elements; determination of samarium in neodymium; determination of europium in samarium. *J Opt Soc Am* 1948, 38, 518.
- [10] Fassel VA, Cook HD, Krotz LC, Kehres PW. Quantitative spectrographic analysis of the rare earth elements. IV. Determination of cerium, praseodymium, and neodymium in lanthanum. V. Determination of lanthanum, praseodymium, and neodymium in cerium. VI. Determination of lanthanum, cerium, and neodymium in praseodymium. VII. Determination of praseodymium in neodymium. *Spectrochim Acta* 1952, 5, 201.
- [11] Fassel VA, Quinney BB, Krotz LC, Lentz CF. Quantitative spectrographic analysis of rare earth elements – determination of holmium, erbium, yttrium, and terbium in dysprosium, and determination of yttrium, dysprosium, and erbium in holmium, and determination of yttrium, dysprosium, holmium, thulium, and ytterbium in erbium. *Anal Chem* 1955, 27, 1010–14.
- [12] Kniseley RN, Fassel VA, Quinney BB, Tremmel C, Gordon WA, Hayles WJ. Quantitative spectrographic analysis of rare earth elements. IX. Determination of rare earth impurities commonly associated with purified samarium, gadolinium, terbium, and yttrium. *Spectrochim Acta* 1958, 12, 332–7.
- [13] Kniseley RN, Fassel VA, Tabeling RW, Hurd BG, Quinney BB. Quantitative spectrographic analysis of the rare earth elements. X. Determination of rare earth impurities commonly associated with purified thulium, ytterbium, lutetium, and scandium. *Spectrochim Acta* 1959, 13, 300–03.
- [14] Fassel VA, Curry RH, Kniseley RN. Flame spectra of the rare earth elements. *Spectrochim Acta* 1962, 18, 1127–53.
- [15] Dunn HW. A study of x-ray fluorescence for the analysis of rare earths and other complex groups. Oak Ridge National Laboratory, 1955, 30.
- [16] Lytle FW, Heady H. X-ray emission spectrographic analysis of high-purity rare earth oxides. *Anal Chem* 1959, 31, 809.
- [17] Heidel RH, Fassel VA. X-ray fluorescent spectrometric determination of yttrium in rare earth mixtures. *Anal Chem* 1958, 30, 176–9.
- [18] Jones EA, Dixon K. A review of the literature on the separation and determination of rare-earth elements. 23 March 1978. Report No. 1943. National Institute for Metallurgy of South Africa.

Bin Hu, Man He, Beibei Chen and Zucheng Jiang

3 Separation/Preconcentration Techniques for Rare Earth Elements Analysis

Abstract: The main aim of this chapter exactly characterizes the contribution. The analytical chemistry of the rare earth elements (REEs) very often is highly complicated and the determination of a specific element is impossible without a sample pre-concentration. Sample preparation can be carried out either by separation of the REEs from the matrix or by concentrating the REEs. The separation of REEs from each other is mainly made by chromatography.

At the beginning of REE analysis, the method of precipitation/coprecipitation was applied for the treatment of REE mixtures. The method is not applicable for the separation of trace amounts of REEs. The majority of the methods used are based on the distribution of REEs in a two-phase system, a liquid–liquid or a liquid–solid system. Various techniques have been developed for the liquid–liquid extraction (LLE), in particular the liquid phase micro-extraction. The extraction is always combined with a pre-concentration of the REEs in a single drop of extractant or in a hollow fiber filled with the extractant. Further modified techniques for special applications and for difficult REE separation have been developed. Compared to the LLE, the solid phase micro-extraction is preferred. The method is robust and easy to handle, in which the solid phase loaded with the REEs can be used directly for subsequent determination methods. At present, very new solid materials, like nanotubes, are developed and tested for solid phase extraction.

3.1 Introduction

Rare earth elements (REEs) have been widely used in functional materials, catalysts, and other products in industry, diagnosis reagents of magnetic resonance imaging (MRI) in medicine and some fertilizers in agriculture (especially in China). As a result of their usage, more and more REEs are getting into the environment, food chain and organisms. The concentration of REEs in biological samples and environmental samples such as atmosphere, soil and natural water is around ppm–ppb level; the concentration of REEs in sea water is around ppt level; the requirements for ultra-high purity rare earth materials demand for a detection limit of ppb–ppt level for the ultra-trace REE impurities. Accordingly, much higher sensitivity is demanded for the quantification of trace/ultra-trace REEs in real-world samples. On the other hand, the separation among REEs has always been a challenging hot topic due to their similar chemical properties.

3.2 Chemical separation techniques for REEs

For the determination of trace REEs in biological and environmental samples, appropriate separation/preconcentration techniques are usually required to separate the complex matrix, preconcentrate interesting REEs and bring REEs in a suitable form for subsequent instrumental analysis. The most widely used techniques for the separation and/or preconcentration of trace REEs include precipitation/coprecipitation, liquid–liquid extraction (LLE), liquid phase microextraction (LPME), solid phase extraction (SPE) and solid phase microextraction.

3.2.1 Precipitation/coprecipitation

3.2.1.1 Oxalate precipitation

Precipitants for REEs include oxalic acid, diphenyl glycolic acid, cinnamic acid, mandelic acid (for the precipitation of Sc), methylene phosphoric acid (for the precipitation of La) and 8-hydroxy quinoline (for the precipitation of Eu, Gd and Sm). Among them, oxalic acid is the mostly employed precipitant for REEs. Oxalate gravimetric method based on the precipitation of RE oxalate had been used as a routine analytical method for the determination of total REEs and is suitable for the samples with content of REEs of above 5 %.

Oxalate gravimetric method is performed by weighing the burned precipitate obtained by oxalate precipitation and separation. Oxalic acid is spiked into the weak acidic solution containing REEs, resulting in colored RE oxalate precipitation as $RE_2(C_2O_4)_3 \cdot nH_2O$, $n = 5, 6, 9$ or 10 . Dimethyl oxalate or oxalic acid acetone is usually used as the precipitant in homogeneous precipitation; ammonium oxalate is preferred for a good separation when the content of iron is 40 times higher than that of REEs. Alkali metal oxalates are unsuitable as the precipitant for REEs for that alkali metal would form insoluble complex salt with REEs which would be introduced into the precipitate, or form soluble oxalic acid complexes with yttrium group REEs which lead to incomplete precipitation of REEs.

There are series of factors influencing oxalate gravimetric method, including solubility of RE oxalate, oxalate activity, temperature, stirring and aging time, ammonium salt and other coexisting ions, and the medium. The details could be found in the book on REEs [1].

3.2.1.2 Coprecipitation

Coprecipitation is a conventional separation/preconcentration technique, which is suitable for the separation of trace REEs from the large number of common elements in complicated samples.

The carrier (also called trapping agent) is very important in coprecipitation. Generally, the carrier should meet the following requirements: (1) featuring with similar chemical composition and structure to RE precipitate; (2) the usage should be as low

as possible; (3) no interference for subsequent analysis and no need for secondary separation. The fluorides, hydroxides, oxalates or metal organic chelates of REEs are generally used as the carrier for their coprecipitation. It should be noted that if inductively coupled plasma-optical emission spectrometry/mass spectrometry (ICP-OES/MS) is employed for the subsequent detection, small amounts of interfering substances that remained in the precipitation will not interfere with the determination of REEs due to the good elemental selectivity of ICP-OES/MS. In other words, the requirement for separation efficiency in coprecipitation is not very stringent when ICP-OES/MS detection is used after coprecipitation.

Flotation technique for separation of REEs is another form of coprecipitation. Zhang et al. [2] employed $\text{Fe}(\text{OH})_3$ as the precipitant, oleic acid as the surfactant and processed the precipitation and flotation of trace REEs effectively under pH 8–9. Some representatives for the trace REEs analysis by using coprecipitation and ICP-OES/MS determination are listed in Table 3.1.

3.3 Liquid–liquid extraction

LLE is generally a two-phase solvent extraction, aiming to separate interesting analyte based on its different distribution coefficients in two immiscible solvents. The greater the difference in the solubility of interesting analyte between the extraction solvent and original aqueous solution is, along with greater distribution coefficient, the better is the extraction performance for separation. The distribution coefficient depends on the extraction temperature, solvent and the characteristics of target analyte. And the factors affecting the extraction performance mainly include the extraction solvent (extractant), the solubility difference between the extractant and original aqueous solution and the contacting of two phases during extraction. Under a certain condition for a specific analyte, the selection of extractant significantly determines the extraction performance.

Since acetone, ether or alcohols were employed for the extraction of REEs in 1937, new extractants and strategies for the extraction of REEs are emerging prominently. Tributyl phosphate was used to extract Ce^{4+} and RE^{3+} first in 1949 and then to separate RE^{3+} from each other successfully. Di(2-ethylhexyl)phosphate (P204), naphthenic acid and methyl trialkylammonium chloride were employed for the separation and purification of REEs in the production process from the 1970s.

3.3.1 Affecting factors for LLE of REEs

LLE is commonly used for the separation of REEs from non-REEs, group separation of REEs and separation of single REE to improve the sensitivity and selectivity for REEs analysis. And the affecting factors for LLE of REEs are mainly the selection of extractants, extractant concentration, medium pH and salting-out agents.

Table 3.1: Application of coprecipitation-ICP-OES/MS for trace REEs analysis.

Sample	Analytes	Carrier	Operation process	Ref.
Soil, plant and environmental water	Ce, La, Y and Yb	Mixture of PAN and 5-Br-PADAP 2-(5-bromo-2-pyridylazo)5-(diethylamino)phenol	Samples are adjusted to pH 8, spiked with co-precipitating agent (carrier), maintained at 60–80°C for 30 min, filtered after 2 h settling; the precipitate is dissolved by HNO ₃ and HClO ₄ prior to ICP-OES detection	[2]
Silicate rocks	REEs and Y	Calcium oxalates	The rock sample was decomposed by HF and HClO ₄ , followed by precipitation of REE and Y as oxalates, with calcium as carrier. The oxalate precipitate is ignited to the oxide and then dissolved in diluted HNO ₃ for ICP-OES detection	[3]
Geological samples	REEs	Calcium oxalates	The sample was decomposed by HF, HNO ₃ and HClO ₄ , and the residue was dissolved in HCl. The solution was adjusted to pH 3.5–4, followed by precipitation of REE as oxalates and cation-exchange column separation in 6 mol/L HNO ₃	[4]
Soils and sediments	REE, Cd, In, Tl, Th, Nb, Ta, Zr and Hf	Ti(OH) ₄ –Fe(OH) ₃	The sample was alkaline fused by NaOH–Na ₂ O ₂ and co-precipitated by Ti(OH) ₄ –Fe(OH) ₃ . The precipitate was dissolved with inverse aqua regia and determined by ICP-MS	[5]
Sea water	REEs and Y, Mn, Co and Cr	Mg(OH) ₂	The sample was adjusted to pH 9.5 by aqueous NH ₃ , which led to precipitation of magnesium hydroxides. The Mg(OH) ₂ precipitate was dissolved in diluted HNO ₃ solution for subsequent ICP-MS detection	[6]

3.3.2 Extractants for REEs

In practical analysis, an appropriate extractant is required to feature with good selectivity, low water solubility, high extraction capacity, good stability and safety; in terms of chemical property, low density, high surface tension, low viscosity and high boiling point and flash point are required. According to the structure and property, along with the extraction mechanism, the extractants for REEs can be divided into neutral phosphorus compounds, acidic phosphorus compounds, organic amines, neutral oxygen-containing compounds, chelates and others (including supramolecule, e.g., crown ethers and calixarene).

3.3.2.1 Neutral phosphorus compounds

The basic structure is $(RO)_3PO$ or R_3PO , without dissociable H, alkyl or alkoxy connected with P. Their structure, property and other constants are listed in Table 3.2.

These extractants have phosphoryl (P=O), and the high electron density on O atom favors the coordination with RE ions. The electronegativity of RO-group is higher than that of R-group (R is electron-donating group), and the electron density on O atom in P=O is decreased, decreasing the complexation ability with REE ions (Table 3.3).

TBP and P350 are specific representatives of neutral phosphorus. REE ions could be well extracted by TBP in nitric acid above 10 mol/L and the partition coefficient is listed in Table 3.4. The extracted complex is $RE(NO_3)_3 \cdot 3TBP$. As can be seen from Table 3.4, the extraction ability of TBP for heavy RE ions is better than that for light RE ions, and the separation factor for neighboring RE ions is relative low, making it

Table 3.2: Neutral phosphorus extractants for REEs extraction.

Name	Structural formula	Trade names and abbreviation	Solubility (H ₂ O, g/L)
Dibutyl phosphate	$(nC_4H_9O)_3PO$	TBP	0.38
Diisoamyl methyl phosphonate	$CH_3P(O)(C_5H_{11}-i)$	P218, DAMP	3.39
Dimethyl methyl phosphate heptyl ester	$CH_3PO(OCHCH_3)(CH_2)_5CH_3$	P350	0.14
Isopropyl bis-(2-ethylhexyl)phosphate	$i-C_3H_7(O)(OC_8H_{17}-i)_2$	P277	0.01
Dibutyl butanephosphonate	$C_4H_9P(O)(OC_4H_9)_2$	P205, DBBP	
Dibutyl butyl phosphate	$(C_4H_9)_2PO(OC_4H_9)$	P203, BDBP	
Trioctylphosphine oxide	$(nC_8H_{17})_3PO$	P201, TOPO	0.09
Dibutyltin oxide	$(nC_4H_9)_3PO$	TBPO	
Oxide di-(2-ethylhexyl) phosphine	$(CH_3(CH_2)_3)CH(C_2H_5)CH_2)_3PO$	TEHPO	

Table 3.3: The effect of substituents on REEs extraction by neutral phosphorus agents [7].

D_{RE}	The structure of extractants			
	$Bu_3PO(TBP)$	$Bu_2(BuO)PO$	$Bu(BuO)_2PO$	$(BuO)_3PO$
Ce	4.25	1.96	0.291	0.026
Pm	6.00	2.95	0.613	0.050
Y	12.3	3.61	0.419	0.044

Note: Extractant: 0.1 mol/L (benzene as solvent); $[HNO_3]$ 3 mol/L, Ce¹⁴⁴, Pm¹⁴⁷, Y⁹⁰.

Table 3.4: Distribution coefficient (D) for REEs extraction by TBP [8].

RE	La	Ce	Pr	Nd	Sm	Eu	Gd	Tb	Dy	Ho	Er	Tm	Yb	Lu	Y
HNO_3 (mol/L)	14	14	14	12.3	12.3	12.3	12.3	12.3	12.3	12.3	12.3	12.3	12.3	12.3	12.0
D	0.09	0.3	1.1					1.0	1.6	2.1	2.9	4.4	5.9	7.2	14

very difficult for the separation of neighboring single RE ions. P350 can extract RE ions well under low-acidity condition; compared with TBP, P350 presents higher extraction efficiency, higher separation factor and lower water solubility. The extracted complex is in the form of $RE(NO_3)_3 \cdot 3P350$, and the distribution ratio is increasing with the increase of the atomic number.

3.3.2.2 Acidic phosphorus compounds

The basic structure is $(RO)_2PO(OH)$ or $(RO)PO(OH)_2$, and $R(RO)PO(OH)$ or $R_2PO(OH)$. Neutral phosphorus is alkyl phosphates and acidic phosphorus is alkyl phosphoric acid, by substitution or esterification of one or two $-OH$ in orthophosphate molecule. H^+ would easily dissociate from the left hydroxyl and make the molecule acidic. These compounds are called acidic phosphorus (Table 3.5).

There are hydroxyl groups in these extractants, and H is easily substituted by RE^{3+} ; $P=O$ would easily coordinate with RE^{3+} ; thus, these acidic phosphorus extractants exhibit good extraction ability for RE ions either under low-acidity or high-acidity condition. In $(RO)_2PO(OH)$, R-substitutes RO-group, increasing the electron density on O atom in $-OH$, making H difficult to dissociate and decreasing the replacement extent for RE^{3+} (Table 3.6).

3.3.2.3 Oxygen-containing organic extractants

Some alcohols, ketones and carboxylic acids can also be used as the extractants for REEs (Table 3.7). RE^{3+} is a hard acid; oxygen-containing organic extractants are hard bases, and they can form complexes according to HSAB theory, while the extraction mechanisms are different. For alcohols, ketones, ether and ester, RE ions are extracted

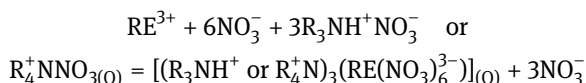
Table 3.5: Acidic phosphorus extractants.

Name	Structural formula and pK_a	Trade names and abbreviation	Solubility (H ₂ O, g/L)
Di(isooctyl)phosphate	(C ₄ H ₉ CH(C ₂ H ₅)CH ₂ O) ₂ PO(OH) 3.32	P204, D2EHPA, HDEHP	0.02
Phosphoric acid ethylhexylester	(C ₄ H ₉ CH(C ₂ H ₅)CH ₂ O)PO (C ₄ H ₉ CH(C ₂ H ₅)CH ₂)(OH) 4.10	P507, HEHEHP, PC88A	0.08
Bis(1-methylheptyl)phosphate	(C ₆ H ₁₃ CH(CH ₃)O) ₂ PO(OH) 3.22	P215	0.02
Di-iso-octyl Phosphonate	(C ₄ H ₉ CH(C ₂ H ₅)CH ₂) ₂ PO(OH) 4.98	P227	
Lauryl alcohol phosphate acid ester	<i>n</i> -C ₁₂ H ₂₅ OPO(OH) ₂	P501, DDPA	0.20
Phosphoric acid diphenyl ethylhexyl ester	(C ₄ H ₉ CH(C ₂ H ₅)CH ₂ O)C ₆ H ₅ PO(OH) 3.12	P406, HEHPHP	
Dibutyl phosphate	(C ₄ H ₉ O) ₂ PO(OH)	DBP	
Monoalkyl phosphate	RCHR-CH ₂ OPO(OH) ₂	P538	0.05

by oxygen-based coordination or hydrogen bonding. For carboxylic acids, RE ions are extracted by ion exchanging between H⁺ and RE ions; the acidity affects the extraction significantly; to decrease the water solubility of the carboxylic acids, carbochain of C₇–C₉ are usually employed, and carbochain longer than C₁₀ is unsuitable for the extraction due to the decreasing *K_a*. Fatty acid with branched-chain exhibits good extraction selectivity, along with steric effect.

3.3.2.4 Nitrogen-containing compounds

Amine-based extractants are one of the most useful nitrogen-containing extractants for RE ions, including primary amines, secondary amines, tertiary and quaternary ammonium salts. Organic amines with molecular weight of around 250–600 are suitable for the extraction of RE ions because they are insoluble in water; they can form stable salts in strong acid and the anion exchange ability in salts follow the order of ClO₄⁻ > NO₃⁻ > HSO₄⁻ > F⁻; they form associated complex with RE anionic complex and can be extracted by organic solvents, thus amine-based extractants are also called as liquid ionic extractants.



Quaternary ammonium salts can extract RE anionic complex in acidic or neutral solution. Table 3.8 lists some nitrogen-containing extractants for RE ions.

Table 3.6: The structure of acidic phosphate extractants and their properties for REE extraction [9].

Number	Structural formula	pKa	Extraction equilibrium constants(K)				Separation factor(α)	
			Nd	Sm	Y	Yb	Sm/Nd	Yb/Y
1	(iso-C ₈ H ₁₇ O) ₂ P(O)OH	2.74	6.8 × 10 ⁻³	4.9 × 10 ⁻²	1.0 × 10 ⁻¹	3.7 × 10 ⁻¹	7.2	3.7
2	(sec-C ₈ H ₁₇ O) ₂ P(O)OH	3.19	5.6 × 10 ⁻⁴	6.4 × 10 ⁻³	4.1 × 10 ⁻¹	3.3	11.4	8.0
3	<i>i</i> -C ₈ H ₁₇ PO (OC ₈ H _{17-<i>i</i>}) ₂	4.09	8.4 × 10 ⁻⁵	8.8 × 10 ⁻⁴	1.4 × 10 ⁻¹	8.9 × 10 ⁻¹	10.5	6.4
4	C ₆ H ₅ PO (OC ₈ H _{17-<i>i</i>})	2.99	2.2	4.2 × 10	1.7 × 10 ³	2.2 × 10 ⁻⁴	19.1	12.9
5	Cyc-C ₆ H ₁₁ PO (OC ₈ H _{17-<i>i</i>})	3.87	1.6 × 10 ⁻³	2.8 × 10 ⁻²	3.4	3.5 × 10	17.5	10.3
6	(iso-C ₈ H ₁₇) ₂ PO(OH)	5.45	4.0 × 10 ⁻⁸	3.2 × 10 ⁻⁹	4.1 × 10 ⁻⁵	6.1 × 10 ⁻⁴	8.0	14.8
7	(<i>n</i> -C ₈ H ₁₇) ₂ PO(OH)	5.71	1.2 × 10 ⁻⁴	1.8 × 10 ⁻³	4.1 × 10	1.8	15	4.4
8	(iso-C ₈ H ₁₇ O) PO(OH) ₂	3.60	6.7 × 10 ⁻⁴	2.2 × 10 ⁵	6.4 × 10 ⁻⁴	2.0 × 10 ⁵	3.3	3.1
9	(iso-C ₁₈ H ₃₇ O) PO(OH) ₂	9.10	3.8 × 10 ⁵	4.1 × 10 ⁵	2.9 × 10 ⁵	9.8 × 10 ⁵	1.1	3.4
10	iso-C ₈ H ₁₇ PO(OH) ₂	4.72 10.40	3.7 × 10 ⁻³	1.2 × 10 ⁻⁴	6.3 × 10 ³	8.1 × 10 ⁻³		
11	iso-C ₁₈ H ₃₇ PO(OH) ₂	3.88 9.37	7.6 × 10 ²	1.3 × 10 ³	9.4 × 10 ²	4.3 × 10 ³	1.6	4.6

Table 3.7: Some oxygen-containing extractants for REEs.

Name	Structural formula	Trade names and abbreviation	Solubility (H ₂ O, g/L)
Naphthenic acid	R ₁ R ₂ R ₃ R ₄ C ₅ H ₁₀ (CH ₂) _{<i>n</i>} COOH	Naphthenic acid, nphthanic	0.09
Versatic acid	R ₁ R ₂ C(CH ₃)COOH	C547, Versatic911	2.50
Methyl isobutyl ketone	CH ₃ CH(CH ₃)CH ₂ COCH ₃	4-Methyl-2-pentanone, MIBK, hexone	19.1
sec-Caprylic alcohol	C ₆ H ₁₃ CH(CH ₃)OH	2-Octanol, octanol 2	1.0
β-Primary alcohol	RCHRCH ₂ OH	A1416	

The separation performance of primary amine is unsatisfying to single RE, and the extraction of La to Sm by primary amine can be easily obtained while the extraction efficiency is decreased after Sm. Li et al. [10] used N1923 to extract REEs from sulfuric acid matrix, and found that the extraction efficiency of REEs decreases as

Table 3.8: Some nitrogen-containing extractants for REEs.

Name	Structural formula	Trade names and abbreviation	Solubility (H ₂ O, g/L)
Se-carbon primary amine	(C _n H _{2n+1}) ₂ CHNH ₂ (<i>n</i> = 9–11)	N1923, AH:9	0.04
Multi-branched hexadecyl tertiary carbon primary amine	CH ₃ C(CH ₃) ₂ [CH ₂ C(CH ₃) ₂] ₃ NH ₂	N116, Primene JM.T	0.05 g (0.5 mol/L H ₂ SO ₄)
<i>N</i> -Dodecyl (trialkyl methyl) amine	CH ₃ [C(CH ₂) ₂ CH ₂] ₂ C(CH ₃) ₂ NHCH ₂ CHCH(CH ₂ C(CH ₂) ₂)-CH ₃	AmberliteL A-1	0.015–20 g (0.5 mol/L H ₂ SO ₄)
<i>N</i> -Lauryl (meth alkyl) amine	C(R ₁)(R ₂)R ₃ NHCH ₂ (CH ₂) ₁₀ CH ₃	AmberliteL A-2	
Dioctylamine	(CH ₃ (CH ₂) ₇) ₃ N	N204, TOA, and TNOA	
Triisooctylamine	(CH ₃ C(CH ₃) ₂ CH ₂ CH(CH ₃)CH ₂) ₃ N	TIOA	
Triheptylamine	(C ₇ H ₁₅) ₃ N	N208	
Tribromoaniline	(C ₆ H ₅ CH ₂) ₃ N	TBA	
Trialkylamine	(C _n H _{2n-1}) ₃ N, <i>n</i> = 8–10	N235, Alamine336	0.01
Chloride methyl trialkyl amine	[(C _n H _{2n-1}) ₃ NCH ₃]Cl, <i>n</i> = 6–10	N263, Aliquat336	0.04

atomic number increases, exhibiting “tetrad effect”; while in perchloric acid medium, the extraction efficiency of REEs increases as atomic number increases, also exhibiting “tetrad effect” [11]. Secondary amine, e.g., N235, is mainly octyl, similar to trioctylamine, and can extract REEs in the presence of salting-out agents. Trioctylamine as a colorless viscous liquid is soluble in organic solvents, and its applications in metal ions extraction is reviewed [12].

N263, trialkyl methyl ammonium chloride, consisting of 8–10 carbon atoms in its alkyl carbon chain, is a quaternary ammonium salt that frequently used in REEs extraction. Its performance and composition are similar to Aliquat336. It is a viscous liquid, with high extraction capacity and excellent selectivity, and is suitable for a variety of inorganic acid system. The distribution ratio of REEs in the N263-LiNO₃ system is decreased with increasing the atomic number of REEs, showing an “inverted order” (Table 3.9); while a “positive sequence” is obtained in the N263-NH₄SCN system (Table 3.10). For amine extractants, the effect of their structure and spatial effects on the extraction efficiency is also very significant.

Table 3.9: Distribution ratio of REEs in N263–nitrate system.

RE ³⁺	La	Pr	Nd	Sm	Gd	Tb	Dy	Ho	Er	Tm	Yb	Lu	Y
Distribution ratio (D)	4.4	4.0	1.59	0.41	0.15	0.13	0.13	0.086	0.058	0.022	0.021	0.013	0.031
Separation factor (α _{RE} /γ)	140	128	50.7	13.2	4.8	4.3	4.2	2.7	1.86	0.70	0.67	0.43	

Note: HNO₃, 0.1 mol/L; N263, 400 g/L; V(o)/V(aq) = 4:1.

Table 3.10: Distribution ratio of REEs in N263–thiocyanic acid system.

RE ³⁺	La	Pr	Nd	Sm	Gd	Tb	Dy	Ho	Er	Tm	Yb	Lu	Y
Distribution ratio (D)	0.52	1.09	1.29	2.06	7.19	3.05	3.30	4.76	7.26	17.87	30.94	59.30	2.14
Separation factor ($\alpha_{RE/\gamma}$)	0.25	0.51	0.60	0.96	3.36	1.43	1.55	2.23	3.40	8.32	14.5	27.8	

Note: NH₄NCS, pH = 1; N263, 0.7 mol/L; V(o)/V(aq) = 4:1.

3.3.2.5 Chelate extractant for REEs

Chelate extractants can form stable electrically neutral complex with RE ions which can be extracted by organic solvents. Besides β -diketones (e.g., acetylacetone, thenoyltrifluoroacetone [TTA], 1-phenyl-3-methyl-4-benzoyl-pyrazolone [PMBP]), homologs of 8-hydroxyquinoline and ketoxime derivatives (Table 3.11) are also commonly used chelating extractants for REEs.

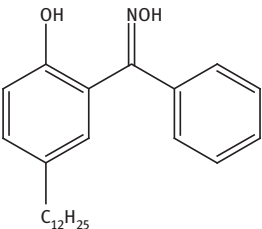
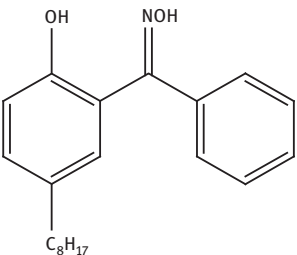
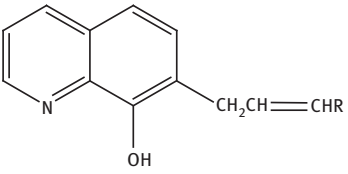
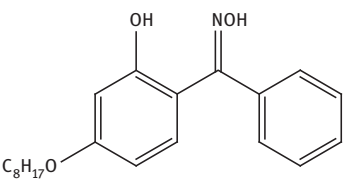
TTA, colorless acicular crystal, is soluble in benzene, methylbenzene and other organic solvents. And RE³⁺ can be extracted by TAA at pH 3–4 (Table 3.12). TTA is usually employed to synergistically extract REEs with other solvents such as ethylenediamine, 2,2,2-terpyridine and neutral phosphorus reagents.

PMBP [5] is also a good β -diketone reagent for REEs extraction, with higher extraction capacity, acidity and faster reaction dynamic compared with TTA, and it has become one of the main extraction agent for the separation and preconcentration of REEs. 1-phenyl-3-methyl-4-acetyl-pyrazolone is a homolog of PMBP, and the extraction efficiency of heavy REEs could reach more than 90 % under pH3. Oxime and hydroxylamine compounds have been investigated for heavy REEs extraction. Haraguchi et al. [14] synthesized several *N*-phenyl hydroxamic acid, among them, 2-hexyl-*N*-phenyl-decyl hydroxyl oxime acid is considered as the most suitable agent for the extraction of heavy REEs; the extraction capacity of *N*-*p*-methoxybenzoyl, -*p*(*n*, *iso*, *t*)-butylbenzoyl, -propoxybenzoyl, -*m*-nitrobenzoyl, -*m*-cyanobenzoyl-*N*-phenylhydroxylamine for REEs was discussed, along with, the effects of substituent in extractant molecules and the acidity of the reagents on the separation factor between REEs; it was found that the smaller the pK value of the extractant is, the greater the extraction constant is [15–18].

3.3.2.6 Supramolecular extractants and others

Crown ethers and calixarenes are supramolecular compounds which can be used for the complexing and extraction of REEs [19, 20]. In the presence of counter anions, 18-crown-6 and benzo15-crown-5 exhibit very high extraction efficiency for REEs; Inoue et al. [21] used dicrown ether to extract REEs-picric acid complexes, and the extraction efficiency was increased. Calixarene has also been studied for the extraction of REEs [22], and some supramolecular compounds as REEs extractants are listed in Table 3.13. Calixarene 1,3-bis(diethylamide)generation of calixarenes [4] exhibits

Table 3.11: Some chelating agent for REEs extraction.

Name	Structural formula	Trade names and abbreviation	Solubility (H ₂ O, g/L)
Lauryl hydroxamic acid	$i\text{-C}_{11}\text{H}_{23}\text{CONHOH}$	H106	0.02
5,8-Diethyl-7-hydroxy-6-dodecanone oxime	$\text{CH}_8(\text{CH}_2)_3\text{CH}(\text{C}_2\text{H}_5)\text{CH}(\text{OH})\text{C}(\text{NOH})\text{CH}(\text{C}_2\text{H}_5)(\text{CH}_2)_3\text{CH}_3$	N509, LIX-63	
2-Hydroxy-5-dodecyl benzophenone oxime		3045, LIX64	
2-Hydroxy-5-octyl benzophenone oxime		N510	0.005
2-Hydroxy-5-sec-octyl oxy benzophenone oxime		N530	0.001
7-Dodecenyloxy-8-hydroxyquinoline		N601, Kelex100	0.003

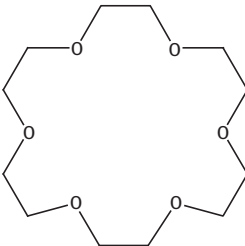
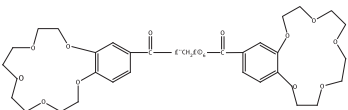
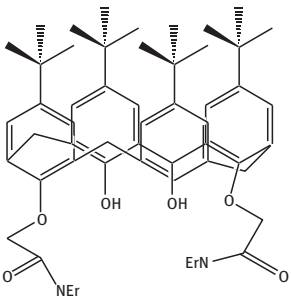
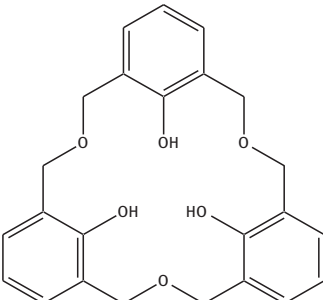
a high extraction efficiency for REEs, which is 20–22 % higher than that obtained by crown ether and dicrown ether.

Sulfoxide with S–O bond is also a good extractant for REEs. Among them, dimethylsulfoxide was one of the most commonly used, which can form ionic

Table 3.12: Extraction constants for REEs extraction by PMBP and TTA [13].

RE ³⁺	La	Ce	Pr	Nd	Pm	Sm	Gd	Tb	Dy	Ho	Er	Tm	Yb	Lu	Y
pK _α (TTA)	10.51	9.45	8.85	8.58	8.06	7.68	7.57	7.51	7.03	7.25	7.2	6.96	6.72	6.77	
pK _α (PMBP)	7.19	6.56	5.81	5.67		5.00	4.77		4.42				3.89		

Table 3.13: Some supramolecular compounds as REEs extractants.

Name	Structural formula	RE ³⁺	Counter anion	Solvent	Ref.
18-Crown-6		La–Lu La–Ga	ClO ₄ ⁻ Picric acid	CH ₂ Cl ₂ CH ₂ Cl ₂	[20] [23]
Octanedione 1,8-bis(4-benzo- 15-crown-5)		La–Gd	Picric acid	CH ₂ Cl ₂	[21]
1,3-bis(ethylenedioxy amide) is substituted calixarene		La–Lu	Picric acid	CH ₂ Cl ₂	[24]
Hexahomotrioxacalix [3]arene		Sc, La, Y and Lu	DMSO		[25]

associates soluble in benzene in the presence of anions, such as ClO_4^- or SCN^- . Besides, pentylsulfoxide, di-*n*-octylsulfoxide and tetramethylenesulfoxide were also effective in REE's extraction. Bis (2-ethylhexyl) sulfoxide can extract REE- SCN^- complex into benzene.

Light REEs can be extracted by employing crown ether 18-crown-6 [26] and benzo-15-crown-5 [27]; with the existence of pentadecafluorinecaprilate, light REEs could be extracted by 18-crown-6 in ionic association form [28].

3.3.3 Extractant concentration and extraction equilibrium constant

Distribution coefficient (D) is proportional to n th power of free extractant concentration; if free extractant concentration is increased by two times, D is increased by 2^n times. When P204 is used for the extraction of RE ions, D is proportional to 3 power of the concentration of P204 dimer; the increase of the concentration of the extractant is beneficial to the extraction of interesting ions.

The higher the stability constant for the complex is formed by REE ions and the extractant, the complex is more stable and more easily to be extracted. Given a specific extractant for the extraction of RE ions, the stability of the complex is related to the charge and radius of RE ions. For RE ions with the same valence, the radius decreases with the increase of the atomic number, and the formed complex stability and extraction equilibrium constant increase with the increase of atomic number (Table 3.14), while the separation factors for the neighboring RE ions are not increasing with the increase of atomic number (Table 3.15). Thus, the extraction efficiency of REE ions and the separation factors for neighboring RE ions should be considered simultaneously, and the latter is sometimes more important.

3.3.4 Medium pH

In acidic complex extraction system for REEs, the effect of pH on D of REE ions in two phases is very obvious. Within a specific acidic complex extraction system, D will

Table 3.14: Extraction equilibrium constants (K) for REE extraction by P204.

RE ³⁺	Pm	Sm	Eu	Tb	Dy	Ho	Er	Yb	Lu	Y
log K	-1.73	-0.95	-0.83	0.4	0.88	1.25	1.75	2.27	2.94	1.63

Table 3.15: Separation factor for REE extraction by P204.

REE pair	Ce/La	Pr/Ce	Nd/Pr	Pm/Nd	Sm/Pm	Eu/Sm	Gd/Eu
Separation factor	2.8	1.5	1.3	2.7	3.2	2.2	1.5
REE pair	Tb/Gd	Dy/Tb	Ho/Dy	Er/Ho	Tm/Er	Yb/Tm	Lu/Yb
Separation factor	5.3	2.8	2.2	3.0	3.5	3.0	2.0

increase by $10n$ times (n is the valence of RE ions) when pH is increased by 1 unit. If the volume of two phases are the same, when $D = 1$, half of RE ions are extracted, and the pH is called half extraction pH value, denoted by $\text{pH}_{1/2}$.

$$\text{pH}_{1/2} = -1/n \log K - \log(\text{HL})_o$$

where K is the extraction equilibrium constant and $(\text{HL})_o$ is the concentration of extractant (HL) in organic phase. As can be seen, the higher K or $[\text{HL}]_o$ is, the lower the $\text{pH}_{1/2}$ is, indicating RE ions can be extracted more easily. So $\text{pH}_{1/2}$ is used to show the extraction ability for metal ions with the same valence. The $\text{pH}_{1/2}$ for Y extraction by naphthenic acid is the highest among other ions (Table 3.16), indicating D of Y is the lowest.

P204 and P507 are specific representatives of acidic phosphorus extractants. The extraction ability of P204 is increasing with the increasing of the atomic number of REE (Table 3.17), and the difference between light and heavy REEs is obvious. P204 form dimeric polymer through hydrogen bonding in nonpolar solvents (e.g., benzene, CCl_4), REE ions coordinates with three dimers by replacing three H in it and form neutral six coordinate complex, which is easily dissolved in organic solvents, with the extraction mechanism of cation exchange. In the nitric acid or hydrochloric acid matrix, the extraction efficiency of P204 for REEs will decrease with the increase of the matrix acidity. The basic structure of P507 is similar to that of P204, the reaction for the extraction of REEs is similar along with the performance variation. Due to the C–P bond in P507, the extraction ability of P507 is lower than that of P204, while P507 is featured with easy back-extraction and uneasy emulsification.

Table 3.16: $\text{pH}_{1/2}$ for RE ions extraction by naphthenic acid.

RE ³⁺	La	Ce	Pr	Nd	Pm	Sm	Eu	Gd	Tb	Dy	Ho	Er	Tm	Yb	Lu	Y
$\text{pH}_{1/2}$	3.95	3.89	3.78	3.74	4.1	3.73	3.62	3.76	–	3.73	3.97	3.84	3.92	4.02	–	4.30

Table 3.17: Distribution ratio and separation factors (α) of REEs (III) by P204*.

RE(III)	La	Ce	Pr	Nd	Pm	Sm	Eu	Gd
D	1.3×10^{-4}	3.6×10^{-4}	5.4×10^{-4}	7.0×10^{-4}	1.9×10^{-4}	5.9×10^{-4}	0.013	0.019
$a_{Z_{n+1}/n}$	2.8	1.5	1.3	2.7	3.2	2.2	1.6	5.3
RE	Tb	Dy	Ho	Er	Tm	Yb	Lu	Y
D	0.100	0.28	0.62	1.4	4.9	14.7	39.4	1.00
$a_{Z_{n+1}/n}$	2.8	2.2	3.0	3.5	3.0	2.0		

*Extraction medium: HClO_4 .

3.3.5 Salting-out agent

In a neutral complex extraction system (e.g., REEs extraction by TBP), the extraction efficiency would be improved by adding salting-out agents (e.g., LiNO_3 , NH_4NO_3), because the concentration of NO_3^- would be increased with the addition of salting-out agents, benefiting the increasing of D . Additionally, the hydration of salting-out agents would decrease the concentration of free water molecules in the extraction system, reducing the concentration of hydrated RE ions and increasing the activity of RE ions.

Dimethyl methyl phosphate heptyl ester (P350) presents much better performance for REEs extraction than TBP, the effect of concentration of salting-out agents LiNO_3 on D and separation factor (α) in the separation of La and Pr is very significant (Table 3.18).

In the ion association complex extraction system, the addition of salting-out agents would also help the extraction of REE ions (Table 3.19). In the extraction of REE ions by N263, salting-out agents can participate the ion association complex formation as reactants, and increase the average activity coefficient of $\text{RE}(\text{NO}_3)_n$. On the other hand, salting-out agents as complexing agents can improve the complexing of REE, and decrease the distribution ratio.

Table 3.18: Effect of LiNO_3 on the extraction of La^{3+} and Pr^{3+} by P350.

LiNO_3 (mol/L)	Distribution ratio		Separation factor (α) $\text{Pr}^{3+}/\text{La}^{3+}$
	$D(\text{Pr}^{3+})$	$D(\text{La}^{3+})$	
1	0.201	0.151	1.33
2	0.426	0.155	2.72
3	0.594	0.186	3.19
4	0.697	0.183	3.81
5	1.28	0.240	5.34
6	1.47	0.254	5.78

Table 3.19: Effect of salting-out agents on the extraction efficiency of Eu^{3+}

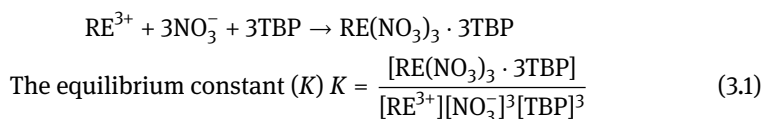
$\text{Al}(\text{NO}_3)_3$		LiNO_3		NH_4NO_3	
C (mol/L)	EE (%)	C (mol/L)	EE (%)	C (mol/L)	EE (%)
0.2	2.2	0.6	3.6	2.0	16.6
0.4	12.2	1.2	18.9	4.1	51.1
0.8	62.1	2.4	74.5	5.1	67.1
1.2	92.7	3.7	95.9	7.1	88.8
1.6	98.8	4.9	99.5	8.2	94.0

C, Concentration; EE, extraction efficiency.

3.3.6 Extraction systems for REEs and their application

3.3.6.1 Neutral complex extraction system

In this extraction system, the extracted RE complexes are neutral salts such as $\text{RE}(\text{SCN})_3$ and $\text{RE}(\text{NO}_3)_3$, and the employed extractants are neutral organics such as TBP and trioctylphosphine oxide (TOPO). >P=O in neutral extractants would complex with RE ions and form insoluble neutral complexes such as $\text{La}(\text{NO}_3)_3 \cdot 3\text{TBP}$ and $\text{Ce}(\text{SCN})_3 \cdot 4\text{TOPO}$ which can be extracted by organic solvents. The neutral extraction system is discussed as follows by using extraction REEs with TBP as the representative:



The distribution coefficient (D) of REE ions between two phases:

$$D = \frac{[\text{RE}(\text{NO}_3)_3 \cdot 3\text{TBP}]}{[\text{RE}^{3+}]} \quad (3.2)$$

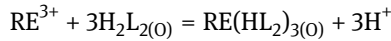
Combining eqs (3.1) and (3.2),

$$D = K[\text{NO}_3^-]^3[\text{TBP}]^3 \quad (3.3)$$

As can be seen, D of REE ions between two phases is proportional to the equilibrium constant, the concentration of NO_3^- in aqueous phase and concentration of TBP in organic phase under equilibrium condition. The size and charge of RE ions also affect the extraction process, and D for RE^{4+} is higher than the corresponding RE^{3+} ; for RE^{3+} , the smaller the radius, much more stable for the formed RE complexes. The order of the D for REEs extraction by TBP is as follows: $\text{Lu} > \text{Yb} > \text{Tm} > \text{Er} > \text{Ho} > \text{Dy} > \text{Y} > \text{Tb} > \text{Gd} > \text{Eu} > \text{Sm} > \text{Pm} > \text{Nd} > \text{Pr} > \text{Ce} > \text{La}$. In other words, D increases with the increase of atomic number, or with the decrease of atomic radius. The effect of NO_3^- concentration in aqueous phase on the extraction of light and heavy REEs is different [29].

3.3.6.2 Acidic complex extraction system

In acidic complex extraction system, organic weak acid (HL or H_2L) acts as the extractants, which can be chelate extractants (e.g., β -diketones), acidic phosphorus extraction agent (e.g., P204) or carboxylic acid (e.g., naphthenic acid). The extraction mechanism is based on the cation ions exchange between RE ions and H^+ in the employed extractants, and the hydrophobic complex formed by RE ions and the extractant is extracted into the organic solvents. P204 is a commonly used extractant for REEs extraction and separation, the reaction is as follows.



The extraction equilibrium constant (K):

$$K = \frac{[\text{RE}(\text{HL}_2)_3]_{(\text{o})}[\text{H}^+]^3}{[\text{RE}^{3+}][\text{H}_2\text{L}_2]_{(\text{o})}^3} \quad (3.4)$$

The distribution ratio (D) of REE ions between two phases:

$$D = \frac{[\text{RE}(\text{HL}_2)_3]_{(\text{o})}}{[\text{RE}^{3+}]} \quad (3.5)$$

Substituting eq. (3.4) into eq. (3.5),

$$D = \frac{K[\text{H}_2\text{L}_2]_{(\text{o})}^3}{[\text{H}^+]^3} \quad (3.6)$$

For REE ions with any valence, eq. (3.6) is changed into

$$D = \frac{K[\text{HL}]_{(\text{o})}^n}{[\text{H}^+]^n} \quad (3.7)$$

Taking the logarithm on both sides of the formula

$$\log D = \log K + n \log[\text{HL}]_{(\text{o})} + n\text{pH} \quad (3.8)$$

Equation (3.8) is the basic formula for acidic extraction system for REEs.

Butyric acid, α -ethylbutyric acid, α -chloro fatty acid can be used to extract and separate REEs from non-REEs. The distribution ratio of REEs during the extraction by α -ethylbutyric acid shows “tetrad effect” with the increasing of their atomic numbers.

PMBP–benzene could extract REEs and Th into organic phase under pH 5.5, and the extracted REEs can be back-extracted by 2–3 mol/L formic acid, while Th left in the organic phase which can be back-extracted by 2.4–6 mol/L HCl. By using Arsenazo III, the determination of Th and REEs could be achieved simultaneously in one sample. In the solution of 15 % ammonium thiocyanate and 60 % sulfosalicylic acid, PMBP–benzene solution also can be used to separate REEs from a large amount of common elements under pH 5–5.7. After back-extracted by 0.01 mol/L HCl, the trace REEs in the steel and alloy could be determined by the arsenazo III spectrophotometry [30].

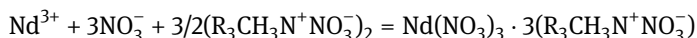
With P204 as the extractant, crude separation of yttrium and heavy REEs from light REEs groups in sulfuric acid system could be achieved by changing pH, extractant concentration and extraction series. Heavy REEs could be separated from light REEs in 0.7–0.9 mol/L HNO_3 by using P204-benzene extractant. In the extraction of REEs from 0.1 mol/L HCl into toluene by using 2-ethylhexyl-(3-pentadecylphenyl)phosphate acid, it could be found that the extraction of heavy REEs was better than medium and light REEs and the obtained extraction efficiency

was higher than that obtained by other organophosphorus extractants [31]. Bis(4-dicyclohexyl)phosphate acid (D4DCHPA)–xylene can also be used for REEs group separation [32].

3.3.6.3 Ion association complex extraction system

The extractants used in this system are organic amines and quaternary ammonium salt or oxygen-containing ketones, alcohols and ether, the extracted compounds are RE complex cations or anions. Organic amines associate with RE complex anions by ammonium, and oxygen-containing organic solvents associate with RE complex anions, forming associated complex which can be extracted into organic solvents. During the extraction process, the exchange between anions and anions occurs, and the extraction system and affecting factors are discussed as follows by using extraction of Nd^{3+} by N263 as the representative.

Before use, N263 is transformed into methyl trialkyl ammonium nitrate by nitric acid or nitrate, and the reaction is



The effect of acidity on the reaction is complicated because there are a variety of existing species of the complex anions and the extractant which affected by the acidity. Increasing the concentration of nitric acid help the formation of $\text{Nd}(\text{NO}_3^-)_{3-6}$ and the extraction; while $\text{R}_3\text{CH}_3\text{N}^+ \cdot \text{NO}_3^- \cdot \text{H}_3\text{O}^+ \cdot \text{NO}_3^-$ forms with the increase of nitric acid concentration, decreasing the concentration of $\text{R}_3\text{CH}_3\text{N}^+ \cdot \text{NO}_3^-$ and deteriorating the extraction. Thus, the effect of acidity in a certain range on the extraction of RE ions is negligible. High concentration of the extractant is beneficial to REE extraction, while polymerization would occur among the extractants, worsening the separation factors between RE ions.

Above all, in the ion association complex extraction system, the extraction by using quaternary ammonium salts can be performed in diluted acidic matrix; the oxygen-containing organic extractants exhibit good extraction performance for REEs under high acidity and the extraction efficiency is affected by the acidity significantly.

N263–xylene was used to separate REEs in the steel from other coexisting elements, while the interference of Zr was masked by adding EDTA before extraction. Benzyl chloride dimethyl myristyl ammonium and 2,3-naphthalenediol–chloroform solution were used to extract REEs from sodium acetate buffer based on ionic association reaction, followed by ICP-OES detection [33].

3.3.6.4 Synergistic extraction system

As early as in 1954, it was found that the distribution ratio for RE ions obtained by using TTA and TBP simultaneously is higher than the sum of the distribution obtained by either of them. With the development of extraction chemistry, the synergistic extraction of REEs has been getting more and more attention. The synergistic

Table 3.20: Classification of the synergistic extraction system.

Classification		Example
Dual heterogeneous synergistic extraction system	Chelating and neutral complexing	$\text{Eu}^{3+}/\text{H}_2\text{O}-\text{HNO}_3/\text{TTA} + \text{TBP}$ (cyclohexane)
	Chelating and ion association	$\text{Th}^{4+}/\text{HCl} + \text{LiCl}/\text{TTA} + \text{TOA}$ (benzene)
Dual homogeneous synergistic extraction system	Neutral complexing and ion association	$\text{PuO}_2^{2+}/\text{H}_2\text{O} - \text{HNO}_3/\text{TBP} + \text{TBAN}$ (kerosene)
	Chelating synergistic extraction	$\text{RE}^{3+}/\text{H}_2\text{O}-\text{HNO}_3//\text{HA} + \text{TTA}$ (benzene)
	Neutral complexing synergistic extraction	$\text{RE}^{3+}/\text{H}_2\text{O}-\text{HNO}_3//\text{TBPO} + \text{TOPO}$ (kerosene)
Other synergistic extraction system	Ion association synergistic extraction	$\text{Pa}^{3+}/\text{H}_2\text{O}-\text{HCl}/\text{RCOR} + \text{ROH}$
	Ternary system involving chelating, neutral complexing and ion association	$\text{UO}_2^{2+}/\text{H}_2\text{O} - \text{H}_2\text{SO}_4/\text{D2EHPA} + \text{TBP} + \text{R3A}$ (kerosene)

extraction system consisting of TTA and neutral phosphorus extractants is the most concerned one, three extraction systems as mentioned above can all be involved in the synergistic extraction system (Table 3.20). The system combining acidic chelating with neutral complexing also exhibits significant synergistic effect.

The mechanism for synergistic extraction is complicated. For the synergistic extraction system involving acidic and neutral extractants, it is based on adducting and substitution mechanism, also affected by the size, charge and coordination geometry of the ion (Table 3.21).

The system of TTA–TBP was applied for the separation of Eu^{3+} from Am [34]. PMBP–TOPO–benzene system can be effectively used to separate REEs, U and Th from niobite [35]. The extraction performance of the 5, 7-dichloro-8-hydroxyquinoline–chloroform solution for REEs (La, Eu and Lu) could be improved in the presence of tetrabutyl ammonium or TOPO [36].

Table 3.21: Synergistic extraction of REEs by β -diketones and TBP.

RE^{3+}	Extractants (cyclohexane as the solvent)					
	HFA–TBP		TAA–TBP		FHD–TBP	
	log	log <i>K</i>	log	log <i>K</i>	log	log <i>K</i>
Eu	10.84	5.05	–	–2.22	10.00	10.06
Nd	10.50	4.35	–	–2.77	9.96	9.95
Tm	10.76	4.63	–	–2.62	10.20	10.47

3.4 Liquid phase microextraction

LPME is developed based on LLE [37, 38]. Compared with traditional LLE, LPME is environmentally friendly with the consumption of very small amount of organic solvent (only a few microliters or tens of microliters); the operation of LPME is much simpler, avoiding time-consuming step in LLE; and LPME can provide a comparable or even better enrichment factor (EF). LPME integrates the sampling, extraction and concentration in one step, and can be easily combined with various modern analytical instruments (e.g., HPLC, CE, GC, GFAAS). It has been employed in the fields of environmental monitoring, food safety and pharmaceutical analysis.

In 1996, Liu and Dasgupta [38] reported a drop-in-drop system (Figure 3.1) to extract sodium dodecyl sulfate, in which a 1.3- μL microdrop of a water-immiscible organic solvent was immersed into a large flowing aqueous drop to accomplish the extraction process. At almost the same time, Jeannot and Cantwell [37] introduced a procedure that they termed solvent microextraction. In this configuration (Figure 3.2), a droplet of 1-octanol was held at the end of a Teflon rod and suspended in a stirred aqueous sample solution. After extraction, the Teflon rod was withdrawn from the aqueous solution; the organic phase was sampled with a microsyringe and injected into a GC system for analysis. One disadvantage of the aforementioned methods is that extraction and injection have to be performed separately with different apparatus. In order to overcome this shortcoming, Jeannot and Cantwell [39] developed a microextraction method in 1997, which was performed simply by suspending a 1- μL drop directly from the tip of a microsyringe needle immersed in a stirred aqueous solution containing target analytes, the post-extraction microdrop was retracted back

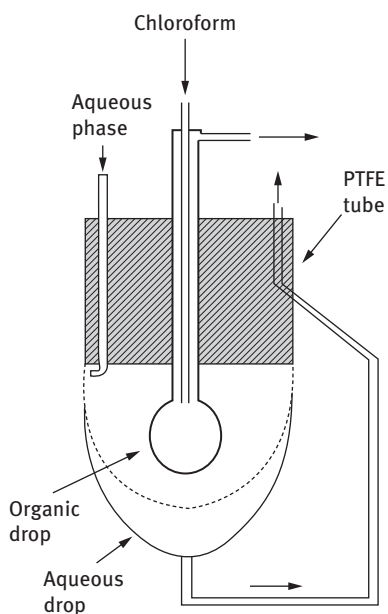


Figure 3.1: Schematic diagram of “drop in drop” system [38].

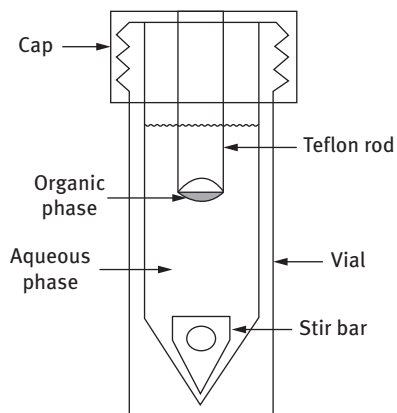


Figure 3.2: Schematic diagram of solvent microextraction based on Teflon rod [37].

into the microsyringe and transferred into GC for further analysis. In this configuration, the microsyringe served as both the solvent holder and the GC sampling injector, which make the extraction and injection integrated in a single device (Figure 3.3). This represents a desirable convenience of the microextraction operation, and led to the appearance of some new LPME configurations, such as single-drop microextraction (SDME) and hollow fiber (HF)-LPME.

3.4.1 Operation modes and mechanism

To extremely decrease the volume of the extractant phase and simplify the experimental apparatus and operation procedure, analysts have spent a lot of energy on the configuration of experimental apparatus and exploration of microextraction mechanisms. So far, the most representative techniques in LPME include SDME,

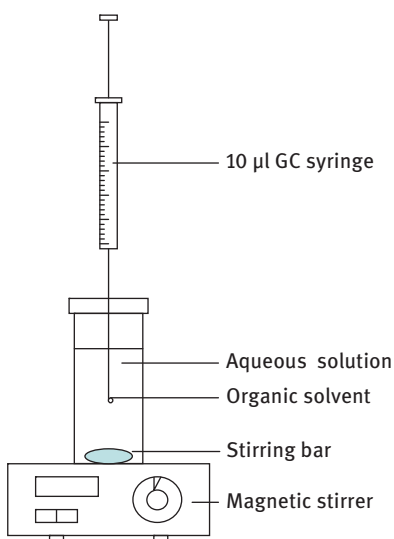


Figure 3.3: Schematic diagram of solvent microextraction based on microsyringe [39].

HF-LPME, dispersive liquid–liquid microextraction (DLLME) and solidified floating organic drop microextraction (SFODME).

3.4.2 Single-drop microextraction

In this extraction mode (Figure 3.6), the extractant is suspended on the needle tip of the microsyringe, and immersed in the sample solution, contacting directly with target analytes and sample matrix. Since the extraction medium is in the form of a single drop, this type of microextraction is called SDME. Direct-SDME or direct immersion (DI)-SDME, in which the extraction medium without any special supporter, is simple and inexpensive.

In direct-SDME, the analyte (A) is distributed between aqueous sample solution and organic solvent [40]:



The distribution coefficient of A between two phases ($K_{\text{org/d}}$) can be defined as

$$K_{\text{org/d}} = \frac{C_{\text{eq,ord}}}{C_{\text{eq,d}}} \quad (3.10)$$

where $C_{\text{eq,org}}$ and $C_{\text{eq,d}}$ are the concentration of A in organic phase (acceptor phase) and sample solution (donor phase), respectively, under equilibrium.

Then $C_{\text{eq,ord}}$ can be calculated by eq. (3.11):

$$C_{\text{eq,ord}} = \frac{K_{\text{org/d}} C_i V_d}{K_{\text{org/d}} V_{\text{org}} + V_d} \quad (3.11)$$

where C_i is the initial concentration of A in sample solution, V_d and V_{org} are the volume of sample solution and organic solvent, respectively.

As can be seen from eq. (3.11), a high $K_{\text{org/d}}$ is beneficial to the extraction.

The two-phase micro-extraction mode is only applicable to a strong or moderate lipophilic analyte ($K_{\text{org/d}} > 500$) instead of strongly hydrophilic analyte [40]; for acidic or alkaline analyte, the analyte should be existing in deprotonated form for extraction by adjusting sample pH to increase the partition coefficient.

To achieve the LPME of REE ions, PMBP–benzene was used as the extraction solvent (10 μL), and a 500-fold EF for La was obtained [41]. In this microextraction procedure as shown in Figure 3.4, perfluoroalkoxy (PFA) tubing was used to connect the extraction chamber, and a constant-flow pump and a 10-L microsyringe were employed to introduce the aqueous solution and extraction solvent, respectively. The sample solution was continuously pumped “around” the drop, allowing the analytes

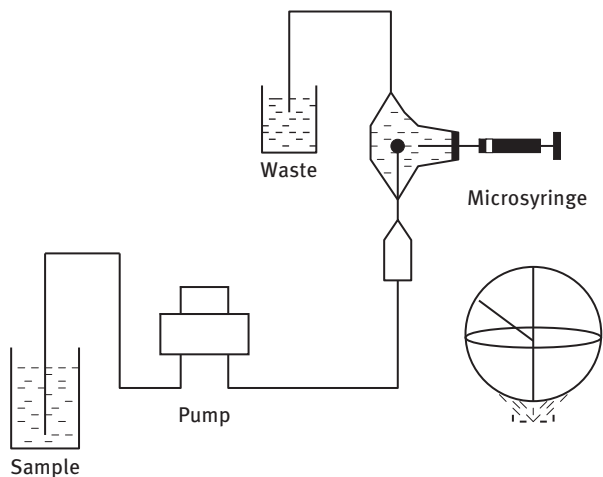


Figure 3.4: The experimental setup for continuous-flow SDME [41, 42].

to be extracted efficiently. It is called continuous-flow microextraction. With some modification to the continuous-flow SDME setup that the waste outlet of tubing was placed into the sample reservoir, cycle-flow SDME was developed and successfully applied in the determination of trace metals in biological samples [42]. It allows further reduction in the sample size and non-attended operation since there is no danger of the sample vial running out.

Besides the two-phase microextraction mode mentioned above, Ma and Cantwell [43] combined solvent microextraction with simultaneous back extraction into a single microdrop, which was called three-phase (liquid–liquid–liquid) microextraction. As shown in Figure 3.5, *n*-octane was employed as an organic liquid membrane, confined inside a Teflon ring over a buffered aqueous sample solution. With the help of a microsyringe, a microdrop was left suspended inside the organic liquid membrane. The target analytes were initially extracted into the organic liquid membrane (neutral at high pH) and back extracted simultaneously into the acidic microdrop (protonated at low pH).

In three-phase SDME, the analytes are extracted from an aqueous donor phase to an aqueous acceptor drop covered with an organic layer. Due to the large volume ratio between the sample donor phase and the acceptor drop as well as the thin organic layer, high EFs can be obtained with three-phase SDME in a short time. The convenience and efficiency of in-line coupling with some analytical instrument, e.g., CE, are additional advantages of three-phase SDME. Most acidic or basic analytes can be enriched by adjusting the pH to promote neutral forms of the analytes in the donor phase and their charged forms in the acceptor phase in three-phase SDME.

Besides the acidic or basic analytes, three-phase microextraction coupled with CE-UV was employed for the analysis of trace REEs by using 40 mmol/L PMBP as

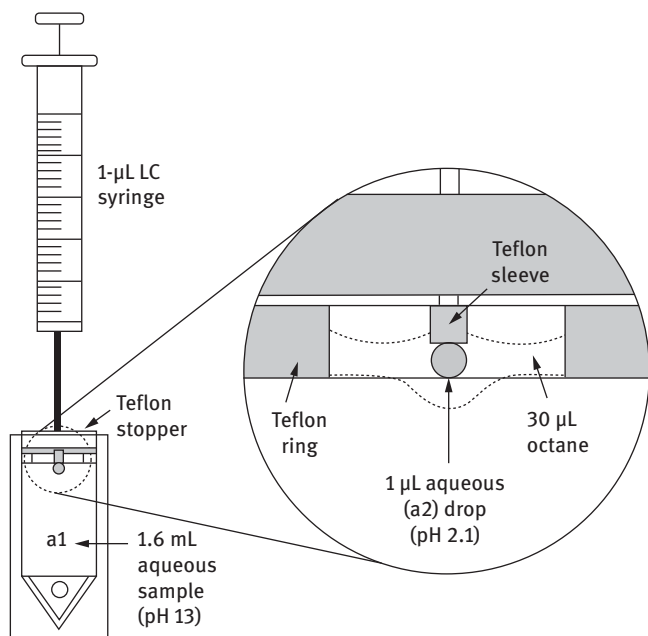


Figure 3.5: Schematic diagram of “Ma and Cantwell” type three-phase SDME [43].

the extractant and 4 % (v/v) formic acid as back-extraction solution [44]. Under the optimized conditions, the LODs of REEs were in the range of 0.19–0.70 ng/mL. The developed method was successfully applied to the determination of trace amounts of REEs in water samples.

3.4.3 Hollow fiber liquid phase microextraction

SDME is simple, inexpensive, rapid and available for headspace extraction, whereas requires careful and elaborate manual operations to overcome the problem of drop dislodgment, which would deteriorate the reproducibility. Prolonged extraction times and faster stirring rates are unfavorable in SDME, since they typically result in drop dissolution and/or dislodgment. In order to solve this problem, in 1999, Pedersen-Bjergaard and coworkers [45] introduced a method named HF-LPME, in which the micro-extract is contained within the lumen of a porous hollow fiber. With the hollow fiber supporting/protecting the micro-extract, HF-LPME is much more robust than SDME with extra sample clean-up ability. Similar to SDME, HF-LPME can also be performed in both two-phase and three-phase microextraction modes. In the two-phase HF-LPME, the analyte is extracted from the aqueous sample into the organic phase immobilized in the pores and lumen of the hollow fiber. In the three-phase mode (hollow fiber liquid–liquid–liquid microextraction [HF-LLLME]), the analyte is extracted from the aqueous sample through the organic solvent immobilized in the pores of the

hollow fiber into another aqueous phase (acceptor phase) presented inside the lumen of the hollow fiber.

3.4.4 Two-phase HF-LPME

Figure 3.6 presents the schematic diagram of two-phase HF-LPME. In this operation mode, the extractants immobilized in the pores and the lumen of the hollow fiber are the same organic solvent, and the analytes are extracted from the aqueous sample (donor phase) directly into the organic acceptor solution. The extraction mechanism is similar to that specified in the section of Direct-SDME. HF-LPME is the most used LPME mode and it can be applied for the analytes with solubility in an organic solvent immiscible with water substantially higher than that in an aqueous medium.

Compared with direct-SDME, two-phase HF-LPME is much stable and simple in terms of operation due to the accommodation and protection of the organic solvents in the hollow fiber.

3.4.5 Three-phase HF-LPME

Figure 3.7 presents the schematic diagram of three-phase HF-LPME, also called HF-LLME. The analyte is extracted from aqueous sample solution through a thin phase

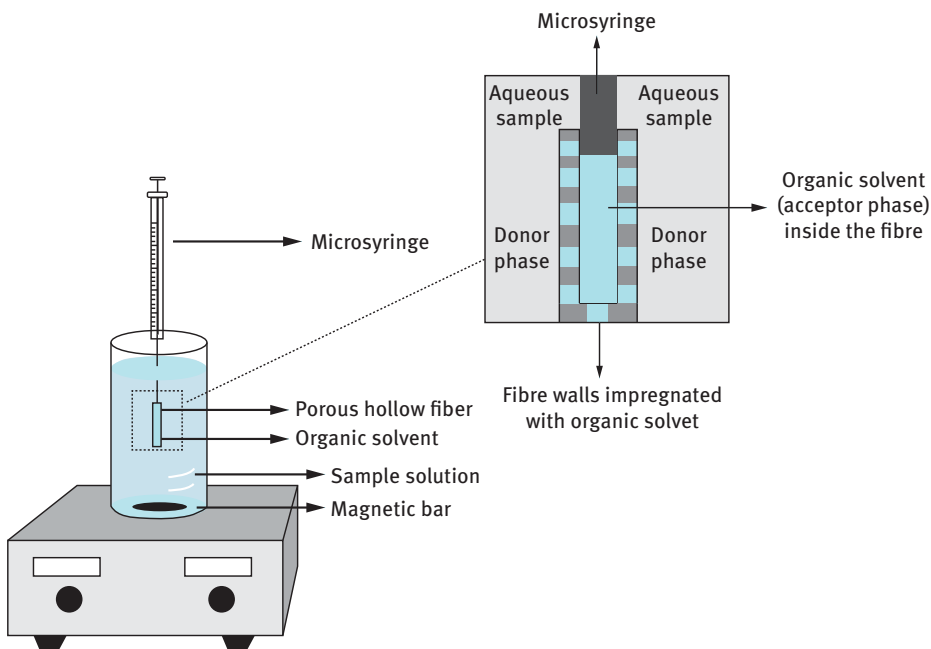


Figure 3.6: Schematic diagram of two-phase HF-LPME.

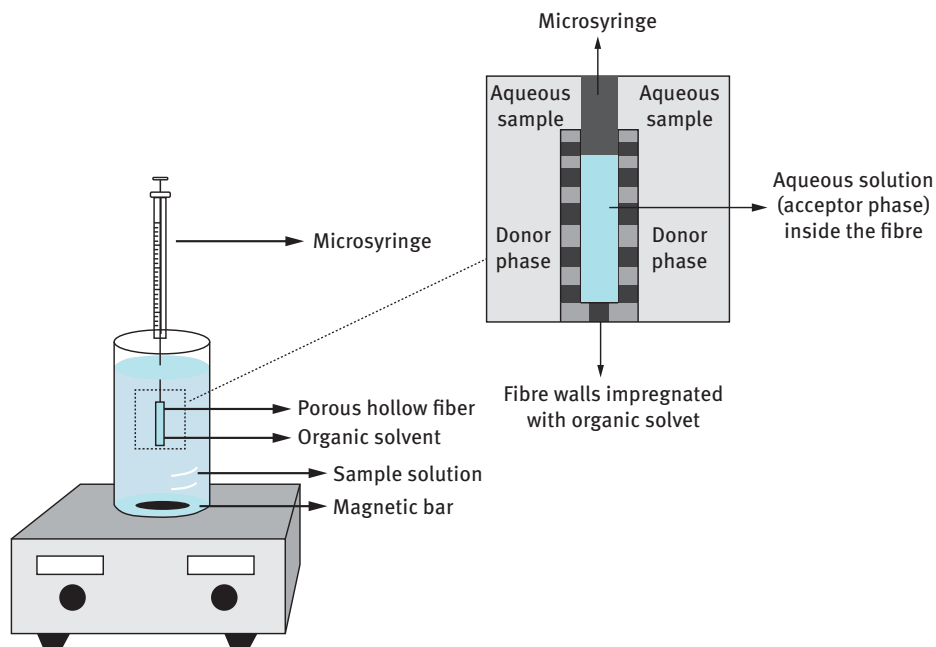
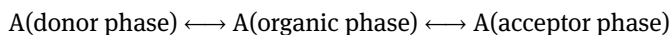


Figure 3.7: Schematic diagram of three-phase HF-LPME.

of organic solvent inside the lumen of the pores of a polypropylene hollow fiber and finally into an acidic/alkaline acceptor solution inside the hollow fiber. Up to now, this extraction mode is limited to basic or acidic analytes whose solubility can be adjusted in the donor and acceptor solution, without application on the analysis of REEs. For example, in order to extract basic compounds, pH of the sample has to be adjusted into the alkaline region to suppress the solubility of the analyte in aqueous sample solution (donor phase), whereas pH in the acceptor solution should be low to promote the solubility of analyte in the acceptor phase. In this manner, the basic compounds may easily be extracted into the organic phase and further into the acceptor phase. And for acidic analytes, the pH adjustment is just reversed. Following extraction, the aqueous acceptor solution is directly injected into CE, HPLC/LC-MS or other detection techniques for subsequent analysis. In this three-phase system, the acceptor phase is aqueous, which is compatible with HPLC or CE analysis. The acceptor phase in three-phase HF-LPME can also be organic, involving two immiscible organic solvents immobilized in the pores of the HF and filled in its lumen, respectively.

In three-phase HF-LPME, the extraction process of analyte (A) can be specified as follows [40]:



The distribution coefficient of A between organic phase and donor phase ($K_{\text{org/d}}$) and that between acceptor phase and organic phase ($K_{\text{a/org}}$) can be expressed as:

$$K_{\text{org/d}} = \frac{C_{\text{eq,ord}}}{C_{\text{eq,d}}} \quad (3.12)$$

$$K_{\text{a/org}} = \frac{C_{\text{eq,a}}}{C_{\text{eq,ord}}} \quad (3.13)$$

where $C_{\text{eq,a}}$ is the concentration of A in acceptor phase under equilibrium, and the total distribution coefficient of A between acceptor phase and donor phase ($K_{\text{a/d}}$) can be expressed as

$$K_{\text{a/d}} = \frac{C_{\text{eq,a}}}{C_{\text{eq,d}}} = K_{\text{org/d}} K_{\text{a/org}} \quad (3.14)$$

In the three-phase HF-LPME system, the extraction efficiency is not only affected by $K_{\text{org/d}}$, but also $K_{\text{a/org}}$, both of which determine the whole extraction process.

Under equilibrium, the concentration of A in acceptor phase ($C_{\text{eq,a}}$) can be calculated by

$$C_{\text{eq,a}} = \frac{K_{\text{a/d}} C_i V_d}{K_{\text{a/d}} V_a + K_{\text{org/d}} V_{\text{org}} + V_d} \quad (3.15)$$

where C_i is the initial concentration of A in sample solution (donor phase), and V_d , V_a and V_{org} are the volume of sample solution, acceptor phase and organic solvent, respectively.

3.4.6 Dispersive liquid–liquid microextraction

Based on ternary component solvent system, DLLME was introduced by Assadi and co-workers in 2006 [46]. The operation mode and required apparatus of DLLME are quite different from SDME and HF-LPME. Briefly, a mixture of a water-immiscible extraction solvent and a so-called dispersing solvent, miscible in both phases, is rapidly injected into the aqueous sample solution by a microsyringe, resulting in a cloudy solution which consists of fine particles of the extraction solvent dispersed in the aqueous phase. In this step, the disperser solvent could help the extraction solvent distributed homogeneously in the whole aqueous solution in a short time, resulting in a large contact area between extraction solvent and aqueous sample, and a consequent rapid attainment of extraction equilibrium. By centrifugation, a small volume of extraction solvent (containing the extracted target analytes) sedimented in the bottom of the conical test tube was obtained and then transferred for subsequent analysis (Figure 3.8).

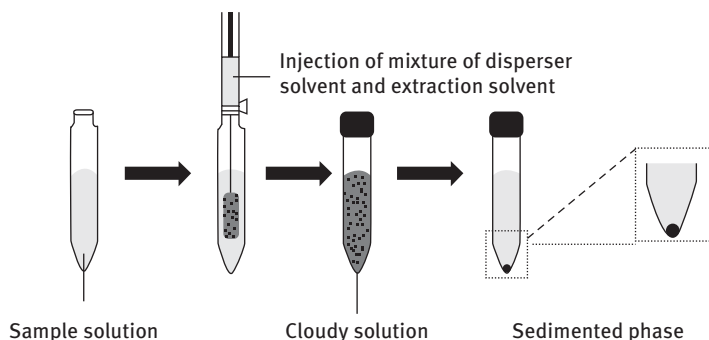


Figure 3.8: Schematic diagram of DLLME.

For DLLME, the extraction time is defined as the time from the injection of dispersant solution into the sample to centrifugation. Since the contact area between the extractants and the sample solution is quite large, the phase transition from water to the extraction phase is very fast. In DLLME, the EF is defined as the ratio of analyte concentration in the aqueous phase and extraction phase, and extraction recovery (R) (or extraction efficiency) is defined as the ratio of the total amount of analyte in the extraction phase and the aqueous solution. It can be expressed as

$$EF = \frac{C_{\text{sed}}}{C_0} \quad (3.16)$$

$$R = \frac{C_{\text{sed}} \times V_{\text{sed}}}{C_0 \times V_{\text{aq}}} \quad (3.17)$$

$$R = \frac{V_{\text{sed}}}{V_{\text{aq}}} \times EF \quad (3.18)$$

where C_{sed} is the concentration of analyte in the extraction phase, V_{sed} is the volume of extraction phase, C_0 is the initial concentration of analyte in sample solution, V_{aq} is the volume of sample solution and R is extraction recovery (efficiency).

DLLME is a modified solvent extraction method, in which the extraction time is greatly reduced comparing with the other two methods mentioned above. The apparatus involved in the DLLME operation procedure just includes a microsyringe, a centrifuge and some conical test tubes. There is no need for magnetic stirrer, magneton for agitation, hollow fiber and no trouble in the possibility of extraction drop dislodgment. DLLME has some advantages such as simplicity of the operation, rapidity, low sample consumption, low cost, high recovery and high EF. Nevertheless, the reproducibility and anti-interference ability of DLLME are not very satisfactory.

The disperser solvent is required to be miscible with water and extractants, and acetone, methanol and acetonitrile are the mostly used disperser solvents. The extractants are usually required to be immiscible with water with higher density than water and good extraction capacity for target analytes.

Mallah et al. [47] used ionic liquids, 1-hydroxy-2,5-pyrrolidinedione (HYD), in a DLLME for determination of trace REEs in uranium dioxide powder. In this process, an appropriate mixture of extraction solvent and disperser solvent is rapidly injected into an aqueous sample containing Sm, Eu, Gd and Dy complexes with HYD, and consequently a cloudy solution is formed. After centrifugation of this solution, the whole enriched phase was determined by ICP-OES. The experimental results indicate that the hexafluorophosphate anions with a partial ion exchange mechanism in ionic liquid solvents play a key role in the electrical neutralization of the lanthanoid complex in DLLME.

Chandrasekaran [48] developed a method based on DLLME and ICP-QMS for the simultaneous extraction and preconcentration of 14 REEs in groundwater. In this method, the REEs are complexed with 2,6-pyridinedicarboxylic acid (2,6-PDCA) in the presence of Aliquat-336 (tricaprylmethylammonium chloride), which enhanced the hydrophobicity of the ion-association complex, resulting in its improved extraction into chloroform. The extraction was carried out after adjusting the pH of the water sample to 4. The REE ions were back extracted from the chloroform layer with nitric acid for determination by ICP-QMS. Under optimum conditions, an average EF of 97 was obtained for 50 mL of water sample for ICP-QMS determination.

DLLME would provide relatively high EFs (e.g., 100-fold), while is generally suitable for water sample analysis due to limited anti-interference capability. Since SPE has excellent sample cleanup ability, DLLME has high EFs, and the desorption solvent of SPE matches the DLLME well, the coupling of SPE and DLLME will endow the dual extraction technique both excellent anti-interference ability and high EFs. Guo et al. [49] proposed a simple and efficient two-step method based on dispersive (D)-SPE and DLLME for the separation and preconcentration of 15 REEs from environmental water and sediment samples, followed by electrothermal vaporization (ETV)-ICP-MS detection. With Chelex 100 as the adsorbent of D-SPE, target REEs were first extracted and the retained REEs were then desorbed by 0.1 mol/L HNO_3 . After 125 mmol/L Tris and 40 mmol/L PMBP were added into the above elution solution, target REEs were further preconcentrated into CCl_4 by DLLME. The developed dual extraction technique exhibited high EFs (234–566-fold) and good anti-interference ability.

3.4.7 Solidified floating organic drop microextraction

SFODME is another new LPME technique introduced by Khalili Zanjani et al. [50], in which small volume of an organic solvent with a melting point near the room temperature (in the range of 10–30°C) is floated on the surface of aqueous solution. The aqueous phase is then stirred for a prescribed period of time, and the sample is transferred into an ice bath. When the organic solvent is solidified, it is transferred into a small conical vial and the melted organic solvent is used for subsequent determination (Figure 3.9). Compared with conventional solvent extraction, it also has the advantage

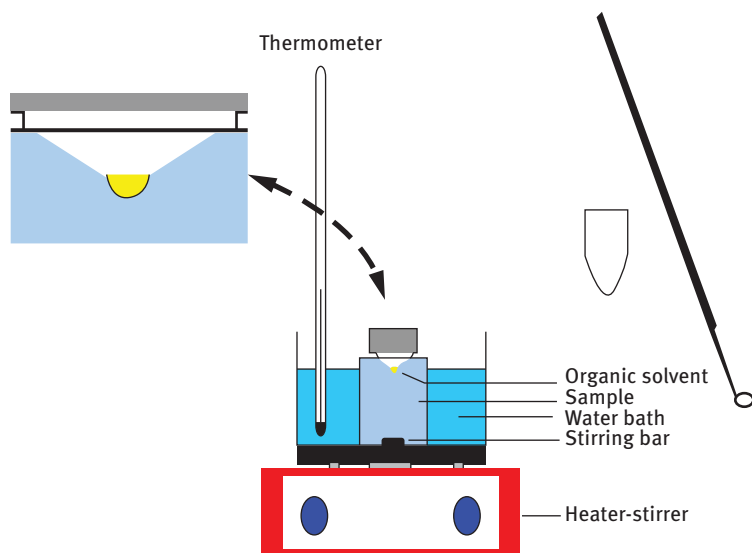


Figure 3.9: Schematic diagram of SFODME apparatus [50].

of great reduction in the amount of organic solvent and thus great enhancement of the EF. It is featured with simple operation, easy batch operation; high stirring rate sustainable, avoiding the problem of unstable drop in SDME and easy separation of organic phase and water phase after solidification.

SFODME is based on equilibrium extraction. The affecting factors found in eqs (3.19–3.21) present the calculation of EF [51].

$$C_{o,f} = KC_{aq,f} = \frac{KC_{aq,i}}{1 + K(V_o/V_{aq})} \quad (3.19)$$

$$\frac{dC_o}{dt} = \frac{A_i\beta \times (KC_{aq} - C_o)}{V_o} \quad (3.20)$$

$$EF = \frac{C_{o,f}}{C_{aq,i}} \quad (3.21)$$

where $C_{o,f}$ is the final concentration of analyte in organic phase, $C_{aq,f}$ and $C_{aq,i}$ are the final and initial concentration of analyte in sample solution (water phase), V_o and V_{aq} are the volume of organic phase and sample solution (water phase) at a certain time (t), A_i is the contact area between organic phase and water phase, β is the mass transfer coefficient, $C_{o,f}$ is the final concentration of analyte in organic phase obtained by the calibration.

In SFODME, the main affecting factor is the selection of organic extraction solvent. It should meet the following requirements: (1) immiscible with water; (2) melting point is around room temperature (10–30°C); (3) good extraction ability for target analytes; (4) the density is less than water; (5) compatible to the employed instruments (e.g., GC,

HPLC, AAS and ICP-OES). The suitable organic solvents include *n*-undecyl alcohol, *n*-dodecanol, 2-dodecanol, 1-bromo-hexadecane, 1,10-dichloro-decane and 1-chlorooctadecyl, and *n*-undecyl and *n*-dodecanol are the most commonly used organic solvents in SFODME.

Chen et al. [52] employed a SFODME-based method for the determination of trace Dy and Y in biological and environmental water samples followed by ETV-ICP-MS detection. 1-(2-Pyridylazo)-2-naphthol (PAN) was used as both chelating reagent in SFODME and chemical modifier in ETV for separation, preconcentration and volatilization of the REEs prior to their determination.

3.4.8 Affecting factors in LPME

The affecting factors are different in different LPME extraction modes. While the main affecting factors include extraction solvent, sample pH, stirring rate, extraction time, extraction temperature and ionic strength. For the extraction of REEs, the selection of chelating agent is very important, which refers to the section of “LLE of REEs”.

In general, the selection of extractants is mainly based on “like dissolves like” principle. And the following properties are preferred practically: (1) insoluble in water or very low solubility in water; (2) high boiling point and low saturated vapor pressure, to reduce the evaporation loss during extraction; (3) the distribution coefficient of analytes between the organic and aqueous phases is high. Table 3.22 lists the common organic solvents with corresponding properties.

Sample pH is usually adjusted to make target analytes existing in non-ionic form reducing their solubility in water and promoting the extraction. For the REEs extraction system which is mainly based on chelation or complexation reactions, pH mainly affect the stability of chelates or complexes, thus affecting the extraction.

Stirring rate is a dynamic factor affecting the extraction. In LPME process, the mass transfer of analytes is determined by the diffusion rate and the thickness of diffusion layer between sample solution and the organic solvent. Based on the theory of convection–diffusion, efficient stirring can accelerate the diffusion rate of the analyte and reduces the thickness of the diffusion layer. Thus, increasing the stirring rate would generally accelerate the extraction, and reduce the extraction time. While, when the stirring rate is too high, some negative impact would occur, e.g., extraction single drops is unstable, bubbles adhered on the surface of the hollow fiber membrane appear and impede extraction, or the dissolving loss of the organic extraction solvent is accelerated.

MIBK: 4-methyl-2-pentanone [C₆MIM][PF₆] 1-hexyl-3-methylimidazolium hexafluorophosphate. LPME of target analytes is a process based on their distribution between the sample solution and the extraction phase, and the maximum extraction efficiency would be obtained when the extraction equilibrium is reached. For the analytes with high distribution coefficient and fast mass transfer speed, the extraction equilibrium can be achieved in a short time, which is an incomplete extraction under

Table 3.22: Physical properties of the extractants used in LPME.

Extractant	Boiling point (°C)	Vapor pressure (T)	Water solubility (mg/L)	Density (g/cm ³)	Viscosity (cP)	Surface tension (dyn/cm)	Dipole moment (D)	Dielectric constant
Cyclohexane	80.7	97.8	55	0.78	0.9	24.65	0.00	2.02 (20°C)
<i>n</i> -Hexane	68.7	151.3	12	0.65	0.29	17.94	0.08	1.88
Octane	125.7	14.0	6.6 × 10 ⁻³	0.70	0.51	21.18	0.00	1.95 (20°C)
Iso-octane	99.2	49	2.4	0.69	0.50 (20°C)	18.8	0.00	1.94 (20°C)
Decane	174.2	1.3	0.05	0.73	0.86	23.37	0.00	1.99 (20°C)
Benzene	80.1	95.2	1,791	0.87	0.60	28.2	0.00	2.27
Toluene	110.6	28.5	515	0.86	0.55	27.92	0.31	2.38
<i>o</i> -Xylene	144.4	6.6	175	0.88	0.76	29.49	0.45	2.57 (20°C)
<i>m</i> -Xylene	139.1	8.3	146	0.86	0.58	28.10	0.30	2.37 (20°C)
<i>p</i> -Xylene	138.4	8.7	156	0.86	0.60	27.76	0.02	2.27 (20°C)
Ethylbenzene	136.2	9.6	152	0.86	0.64	28.48	0.37	2.40 (20°C)
1-Octanol	195.2	0.08	5.38	0.82	7.36	26.92	1.76	10.34 (20°C)
Benzyl alcohol	205.4	0.11	800	1.04	4.65 (30°C)	39.44	1.66	13.1 (20°C)
MIBK	117.4	18.8	1,700	0.80	0.55	23.64 (20°C)	-	13.11 (20°C)
Chlorobenzene	131.7	11.7	327	1.10 (20°C)	0.72 (20°C)	31.98 (30°C)	1.62	5.62
Phenetole	172	1.28	-	0.97 (20°C)	1.16 (25°C)	32.85 (22°C)	3.33	4.22
Dichlorometane	39.6	435.8	1,990	1.32	0.39 (30°C)	26.54 (30°C)	1.14	8.93
Chloroform	61.2	194.8	8,500	1.48	0.54	26.53	1.15	4.81 (20°C)
Tetrachloroethene	76.6	115.2	770	1.58	0.90	26.13	0.00	2.23
1,2-Dichloro-ethane	83.5	83.3 (20°C)	8,100 (20°C)	1.25	0.73 (30°C)	30.84 (30°C)	1.83	10.37

Extractant	Boiling point (°C)	Vapor pressure (T)	Water solubility (mg/L)	Density (g/cm ³)	Viscosity (cP)	Surface tension (dyn/cm)	Dipole moment (D)	Dielectric constant
1,2-Dichloro-benzene	180.5	1.3	156	1.30	1.32	26.48 (20°C)	2.14	9.93
Tetrachloroethylene	121.1	18.5	150	1.61	0.80 (30°C)	31.30	0.00	2.28
Bromobenzene	155.9	4.2	424	1.48	1.01 (30°C)	35.09 (30°C)	1.55	5.40
Nitrobenzene	210.8	0.28	1,900 (20°C)	1.20	1.62 (30°C)	42.17 (30°C)	4.00	34.78
Carbon disulfide	46.2	361.6	2,100 (20°C)	1.29	0.36 (20°C)	32.25 (20°C)	0.06	2.64
[C ₆ MIM][PF ₆]	-	-	18,800	1.36-1.37	148-450	48.8-49.8	-	-
[C ₆ MIM][PF ₆]	-	-	7,500	1.29-1.31	560-586	-	-	-
[C ₈ MIM][PF ₆]	-	-	2,000	1.20-1.23	682-710	34.2-36.5	-	-
[C ₆ MIM][Tf ₂ N]	-	-	3,400	1.33	-	-	-	-
Water	100.0	23.8	∞	1.00	0.89	71.81	1.82	78.36

equilibrium. However, for analytes with relatively low distribution coefficient or low mass transfer speed, long time are needed to reach the extraction equilibrium, and in this case, the extraction is usually processed under non-equilibrium state, during which the extraction time is strictly controlled to ensure the reproducibility.

Extraction temperature has a double impact on the extraction process in terms of thermodynamics and kinetics. In general, increasing the sample temperature would increase molecular motion, the diffusion coefficient of the analyte, and the mass transfer rate of the analyte, thus speeding up the extraction. However, increasing the extraction temperature would reduce the partition coefficient of the analyte, increase the water solubility of the organic solvent, resulting in lower extraction efficiency. Moreover, when the temperature is too high, small bubbles would occur in the aqueous phase, which is attached to the surface of the extraction solvent, hindering the extraction.

The addition of some inorganic salt, e.g., NaCl, Na₂SO₄, would increase the ionic strength of the sample solution, decrease the solubility of analytes in sample solution due to salt-out effect, increasing the distribution of analytes in the extraction phase and thus the extraction efficiency. While sometimes the salt addition would inhibit the extraction which is explained by that the salt would change the physical property of the extraction film and thus the diffusion rate of target analyte in the extraction phase.

3.4.9 Cloud point extraction

Cloud point extraction (CPE) is a new LLE mode which is based on the fact that most nonionic surfactants can form micelles in aqueous solutions and become turbid when they are heated beyond a temperature called the cloud point temperature (CPT). Above the CPT the micellar solution separates into a small volume of surfactant-rich phase and a diluted aqueous phase, in which the surfactant concentration is close to the critical micellar concentration (CMC). Any analyte solubilized in the hydrophobic core of the micelles, will be separated and concentrated in the small volume (usually in the range of 50–250 μL) of the surfactant-rich phase. This process is reversible, and two phases would combine into one phase when the temperature is lower than CMC. When the temperature is increasing, the micelle size of the surfactant is increasing, causing the hydrogen bonding not strong enough to keep the water molecule connected to the O atom of ether.

3.4.9.1 Application of CPE for trace REEs analysis

REEs react with complexants and produce hydrophobic complexes that are entrapped into the micelles and then into the surfactant-rich phase. Due to the viscosity and organic content of the surfactant-rich phase, appropriate sample introduction systems or nebulizers are required, such as employment of a free-clogging nebulizer, chemical vapor generation and micronebulization/aerosol desolvation. Table 3.23 lists the REEs extraction systems by CPE, along with subsequent detection technique.

Table 3.23: Applications of CPE for trace REEs analysis.

Analytes	Surfactant	Complexant	Enrichment factor	Detection	LOD	Sample	Ref.
REEs	Triton X-114	8-HQ	7.9–9.2	ICP-OES	41.4 (Yb)–448 ng/L (Gd)	Tea leaves and mushroom	[53]
		No complexant	5.4–8.1		69.0 (Sc)–509.5 ng/L (Sm)		
REEs	Triton X-114	TTA	9–14	ICP-OES	2 (Pr)–103 (Lu) ng/L	River water	[54]
Dy, Er, Eu, Gd, Ho, La, Lu, Pr, Sm, Tb, Tm and Yb	PONPE-7.5	PAN	70	NAA	0.27 (Yb)–3.07 (Eu) ng/g		[55]
Eu(III)	Triton X-114	Alizarin red S	22	FAAS	6 ng/mL	Water	[56]
REEs	Triton X-114	(<i>i</i> -pr)DGA	140	ICP-MS	0.2–30 ng/L	Soil	[57]

8-HQ: 8-hydroquinolein; TTA: 1-(2-thenoyl)-3,3,3-trifluoroacetone; (*i*-pr)DGA: *N,N,N',N'*-tetraisopropyl diglycolamide.

3.4.9.2 Affecting factors

3.4.9.2.1 Surfactants

Surfactants generally consist of a hydrophobic and a hydrophilic moiety, and the CPT is related to the chain length of hydrophilic and hydrophobic moiety in the surfactants. With the same hydrophobic moiety, CPT would increase with the increase of hydrophilic chain length; on the contrary, CPT declines with the increase of the hydrophobic chain length. Besides nonionic surfactants, amphoteric ionic surfactant exhibits cloud point phenomenon. Some anionic surfactants (e.g., sodium dodecyl sulfate [SDS], sodium dodecyl benzene sulfonate [SDBS] and sodium dodecyl sulfonate [SDSA]) in aqueous high concentration HCl medium would also appear phase separation. Table 3.24 lists the frequently used surfactants in CPE, along with the structure, CMC and CPT.

Increasing the surfactant concentration would improve the extraction efficiency, increase the ratio of two-phase volume, and simultaneously reduce the EF and distribution coefficient. In order to increase EF, a low surfactant concentration is preferred, while too low surfactant concentration would lead to difficult separation of the sedimented phase from sample solution, deteriorating the accuracy and reproducibility.

3.4.9.2.2 Sample pH and chelating agent

For the extraction of REE ions, a chelating agent is necessary to transform REEs into a hydrophobic form, which is then extracted into the surfactants. pH should

Table 3.24: Surfactants commonly used in CPE.

Surfactants		CMC (mmol/L)	CPT (°C)
Chemical name	Commercial name in series		
Polyoxyethylene fatty alcohol	Brij 30	0.02–0.06	2–7
	Brij 35	0.06	>100
	Brij 56	0.0006	64–69
<i>P-tert</i> -octyl phenyl polyethylene glycol ether	Triton X-100	0.17–0.30	64–65
	Triton X-114	0.20–0.35	22–25
<i>N</i> -alkyl phenyl polyethylene glycol ether	PONPE-7.5	0.085	5–20
Amphoteric ionic surfactants	PONPE-10	0.07–0.085	62–65
	C ₉ APSO ₄	4.5	65
	C ₈ -lecithin		45

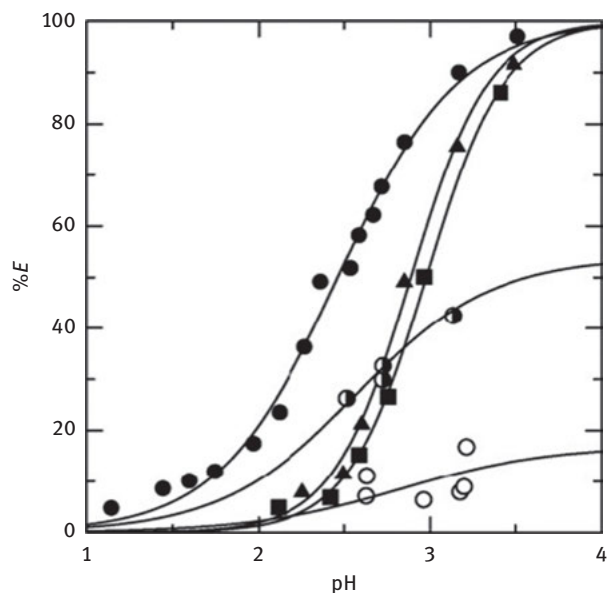


Figure 3.10: Extraction percentage of La(III), Eu(III) and Lu(III) vs. pH without chelating agents. Circle, La(III); triangle, Eu(III); square, Lu(III); closed, Aldrich (lot no. 13112LB); half closed, Aldrich (lot no. 03615HC); open, Nacalai Tesque; Ln(III), 3.6×10^{-5} mol/L; Triton X-100, 2.0 % (v/v); $I = 0.01$ mol/L (pH > 2.0) and 0.1 mol/L (pH < 2.0) with (H, Na)ClO₄ [58].

be appropriate for the formation of REEs complex. However, most of the complexation system for REEs occurs in slightly acidic pH (Figure 3.10), which is incompatible with digested solid samples which is generally strong acidic. Ohashi et al. [58] show good extraction in a more acidic media (pH = 3) for La, Eu and Lu(III), while higher

concentrations of surfactant were needed to counter the effect of the acidic media on the extraction. And the EF would be reduced and LOD would be deteriorated due to the low extraction efficiency.

The behaviors of La(III), Eu(III) and Lu(III) in CPE with and without di(2-ethylhexyl) phosphoric acid (HDEHP) as the complexant, Triton X-100 as the surfactant, were investigated [58]. It was suggested that the extraction of Ln(III) into the surfactant-rich phase without added chelating agent was caused by the impurities contained in Triton X-100. The extraction percentage more than 91 % for all test REEs was obtained using 3.0×10^{-5} mol/L HDEHP and 2.0 % (v/v) Triton X-100. From the equilibrium analysis, it was clarified that Ln(III) was extracted as Ln(DEHP)₃ into the surfactant-rich phase. Besides, Li et al. [53] proposed an on-line CPE system with ICP-OES detection with/without 8-HQ as complexant for trace analysis of REEs in biological samples. The experimental results indicated that: (1) the use of on-line CPE greatly simplifies the extraction procedure; (2) LODs for REEs obtained by on-line CPE-ICP-OES with 8-Ox as chelating agent were slightly better than that obtained by on-line CPE-ICP-OES without 8-Ox as chelating agent, and the RSDs of the two methods were comparable; (3) both on-line CPE-ICP-OES systems had good selectivity and could be used for the biological sample analysis.

3.4.9.2.3 Extraction temperature and time and centrifugation time

The extraction temperature and time are determined by the properties of surfactants and the extracted compounds. Generally, the extraction temperature is 15–20°C higher than the CPT of the employed surfactant. Increasing extraction time would increase the extraction efficiency, while too long extraction time hardly affect the extraction efficiency, and 30 min extraction is commonly used for a good extraction efficiency.

Increasing the centrifugation time would initially increase the extraction efficiency and distribution coefficient, which will be constant after a long extraction time. For a CPE system with relative high CPT, too long centrifugation would lead to the reversion of phase separation, decreasing the extraction efficiency.

3.4.9.2.4 Ionic strength

The ionic strength hardly affects the extraction efficiency and distribution coefficient. The addition of some inert salt would change the cloud point of the surfactant, favoring the separation of two phases.

3.5 Solid phase extraction

SPE is currently the most frequently used sample pretreatment technique in real sample analysis [59], featuring with high EFs, rapid phase separation, low organic solvent consumption, simple operation, as well as easy-to-automate. The principal

goals of SPE are trace enrichment (concentration), matrix simplification (sample clean-up) and medium exchange (transfer from the sample matrix to a different solvent or to the gas phase) [60]. Usually, the analytes are transferred from a mobile phase (gas, fluid or liquid) [61] to the solid phase where they are retained for the duration of the sampling process. The solid phase is then isolated from the sample and the analytes are recovered by elution using a liquid or fluid, or by thermal desorption into the gas phase. The adsorption process of target analytes on the adsorbents depends on the physical/chemical form of analytes, specific surface properties of the adsorbent and the experimental conditions, such as pH, temperature and analytes concentration. The adsorption involves interactions between the analytes and sorbents with various functional groups and ion exchange processes.

The adsorbent plays a key role in SPE-based methodology because it determines the selectivity, affinity and capacity. The ideal SPE adsorbents are expected to feature with the following characteristics: (1) porosity, having a large specific surface area; (2) low blank; (3) high chemical and mechanical stability; (4) fast kinetics of adsorption and desorption; (5) reversible adsorption; (6) high selectivity; (7) high recovery rate. Besides the conventional materials such as organic chelate resin [62], activated carbon [63], activated alumina [64] and microcrystalline material [65], a variety of novel materials including carbonaceous materials [66–68], molecular/ion imprinted polymers [69, 70], nanostructured materials [71–74], mesoporous materials [75–77], restricted access materials (RAM) [78, 79], monolithic materials [80, 81], magnetic materials and metal-organic frameworks (MOFs) [82–84], have been employed in SPE. The application of various SPE adsorbents in trace REEs analysis is listed in Table 3.25.

3.5.1 Carbon nanotubes and graphene oxide

Carbon nanotubes (CNTs), which were first discovered by Iijima [123], have led research to new area in many interdisciplinary investigations as the advantages of CNTs are unique structural, electronic, optoelectronic, semiconductor, mechanical, chemical and physical properties. CNTs can be described as a graphite sheet rolled up into a nanoscale-tube (which are single-wall carbon nanotubes [SWCNTs]), or with additional graphene tubes around the core of an SWCNT (which are multi-wall CNTs (MWCNTs)). These CNTs have diameters in the range between fractions of nanometers and tens of nanometers and lengths up to several centimeters with both their ends normally capped by fullerene-like structures.

Although raw CNTs walls are not reactive, oxidation of CNTs (by using such as HNO₃, NaOCl and KMnO₄ solutions) can lead to surface functionalization with oxygen-containing groups (e.g., carboxylic, carbonyl and hydroxyl group), allowing retention of cations [124]. These functional groups cause a rise in negative charge on carbon surface and the oxygen atoms in functional groups donate single pair of electrons to metal ions, consequently increasing their cation exchange capacity [125].

Table 3.25: Application of various SPE adsorbents in trace REEs analysis.

Materials	Elements	Detection	LOD (ng/L)	Adsorption capacity (mg/g)	Samples	Ref.
C ₁₈ silica cartridge modified with PAN	Ce, Dy, La, Sm and Y	ICP-OES	11–37		Spring, well, tap water and seawater	[85]
Silica gel column	La, Eu and Yb (PMBP complex)	ICP-OES	34–82		GBW07603, lake water and synthetic seawater	[86]
Microcolumn packed with MWNTs	La, Sm, Eu, Gd, Tb, Ho and Yb	ICP-OES	3–57	7.23–9.93	GBW07605, lake water and synthetic seawater	[87]
Ion-imprinted polystyrene resins	Y, La, Nd, Eu, Gd, Tb and Yb	FAAS, ICP-OES		8.9 ± 0.2 (Y)		[88]
Maleic acid grafted PTFE fibers	All lanthanides except Pm	ICP-MS	0.001–0.02	0.31 mmol/g (La)	GBW07312, GBW07313, GBW07405, seawater and river water	[89]
Fullerene derivatives poly(<i>b</i> -styryl)-(12-methanofullerene-C60)-61-formo hydroxamic acid	Ce, La, Pr, Nd, Sm and Gd	ICP-MS	0.9–3.5	1.25–2.15 mmol/g	Standard reference material (BCR-1, SO-Z, NBS 163), seawater	[66]
Carbon nanofibers	La, Eu, Gd and Yb	ICP-MS	0.36–0.6	14.2–19.1 GBW07605	Tea leaves	[90]
Mesoporous TiO ₂	V, Ce, Dy, Eu, La and Yb	ICP-OES	30–350	GBW08571 13.1–26.5	coal fly ash, water samples (river, pond, well and lake)	[91]
Tulsion CH-90 resin	^{152,154} Eu	NaI (Tl) gamma scintillation detector		GBW07401 0.31 mmol/g		[92]

Materials	Elements	Detection	LOD (ng/L)	Adsorption capacity (mg/g)	Samples	Ref.
Chitosan-based chelating resin functionalized with EDTA	All REEs except Pm	ICP-MS	0.12–5.6		Seawater	[93]
Nano-pore samarium (III)-imprinted polymer	Sm	ICP-OES				[94]
Silica gel modified with MTPB	Sc	ICP-OES	85 ng/g	0.6 mmol/g	Shrubbery leaves, Tibet soil, balsam pear leaves and lotus leaves	[95]
Octadecyl silica minicolumn	Ce, Dy, La, Sm, Y and Yb	ICP-OES	90–400		Seawater, tap water and well	[96]
Microcartridge containing C18-derivatized silica particles	La and Gd	CZE with diode array detector	0.02 (La) 0.08 (Gd)		Tap water	[97]
Syringe-driven chelating columns	All lanthanides except Pm	ICP-MS	0.005–0.09		Seawater	[98]
Amberlite XAD-4 resin with monoaza dibenzo 18-crown-6	La, Nd and Sm	ICP-OES	3,900–7,400	0.055–0.066 mmol/g		[99]
Bis-(2-ethylhexyl)-phosphate (HDEHP) coated reverse phase C18	Gd and Gd-based MRI contrast agents	ICP-MS	22–38		Surface water and waste water	[100]
Bentonite modified with <i>N</i> -(2-hydroxyethyl) ethylenediamine	Sm	ICP-OES	600	17.7	GBW07602, waste water	[101]
MWNTs with tannic acid	La, Tb and Lu	MPT-AES		3.97–8.55		[102]
Activated carbon modified with benzoyl hydrazine	Eu	ICP-OES	73 ng/g	59.8	GBW07402 GBW07308	[103]
					Yellow River sediments, orange leaves, balsam pear leaves	

Materials	Elements	Detection	LOD (ng/L)	Adsorption capacity (mg/g)	Samples	Ref.
TiO ₂ -graphene composite	La, Tb and Ho	MPT-AES	1,600–2,800		GBW07313	[104]
Nanoporous silica functionalized with <i>N'</i> -(2-hydroxy phenyl)methylene benzohydrazide	Dy	ICP-OES	50	47	REE oxide samples Tap water, seawater and river water	[105]
High-dispersion-type MW-CNTs attached to polymerbeads (TSK™)	All REEs except Sc and Pm	ICP-MS	0.016–0.159	70.0 ± 5.1 (La)	Seawater	[106]
Walnut shell packed microcolumn	All REEs except Sc and Pm	ICP-MS	0.01–0.17		Sediment, copper ore, tea leaf, human hair and food and agricultural products	[107]
Eu-imprinted polymer nanoparticles	Eu	Electro-chemistry	23,000		Synthetic water, river water, tap water	[108]
TiO ₂ nanotube packed microcolumn	La, Ce, Eu, Gd, Lu and Yb	ICP-MS	10.1–14.7	0.19–1.2	GBW07605 (tea leaves) natural water	[109]
Carbon-ferrite magnetic nanocomposite	La, Sm, Nd and Pr	ICP-OES	500–10,000		IAEA-soil-7	[110]
4-(2-Thiazolyazo) resorcinol immobilized	All lanthanides except La and Pm	ICP-MS	0.06–0.31	0.081–0.108 mmol/g	Estuarine water, Coastal seawater	[111]
Chromosorb 106	Pr ³⁺	UV-vis (with EDTA titration)		0.013 mmol/g		[112]
HQ-PHEMA/SiO ₂		ICP-OES	4		Acid mine drainage	[113]
Oxidized multiwalled carbon nanotubes packed microcolumn	Sc					

Materials	Elements	Detection	LOD (ng/L)	Adsorption capacity (mg/g)	Samples	Ref.
2,6-Pyridinedicarboxaldehyde-functionalized Amberlite XAD-4 resin	Nd, Sm, Eu, Gd, Tb, Dy, Ho, Yb, Lu and Ce	ICP-OES	7–150	0.0490–0.0667 mmol/g	SPS-SW2 Batch 127 seawater, tap water	[114]
8-Hydroxy-2-quinolinecarboxaldehyde functionalized Amberlite XAD-4 resin	Pr, Sm, Eu, Gd, Tb, Dy, Ho, Tm, Yb and Lu	ICP-OES	10–420	0.0496–0.112	SPS-SW2 Batch 127 seawater, tap water	[115]
Amberlite XAD-4 resin paced minicolumn	La	ICP-OES	270	16.6 mg for 0.25 g C versicolor immobilized on 1.0 g of Amberlite XAD-4	Tap water, river water	[116]
Coriolus versicolor immobilized Amberlite XAD-4						
Y(III) imprinted polymer	Y	ICP-OES	900	18.5	Standard rock reference material, radiotritium	[117]
Fe ₃ O ₄ @SiO ₂ @polyaniline-graphene oxide composite	All REEs except Sc and Prm	ICP-MS	0.04–1.49	7.7–16.3	GBW07605, tea leaves, lake water, river water	[118]
Fe ₃ O ₄ @SiO ₂ -(CH ₂) ₃ -S-cinchonidine	Eu	ICP-OES	40	26.5	Mineral water, agricultural water, tap water and spring water	[119]
Double-ion imprinted polymer @magnetic nanoparticles	Ce and Gd	Electro-chemistry	70 (Ce)			[120]
Transcarpathian clinoptilolite (thermally activated at 350 °C)	Tb	UV-vis	190 (Gd)	≈6.0	Synthetic water	[121]
Graphene oxide-TiO ₂ composite	La, Ce, Eu, Dy and Yb	ICP-OES	130–410	16.6–28.7	River water, lake water, seawater and sediment	[122]

It is commonly believed that the chemical interaction between the metal ions and the surface functional groups of CNTs is the major sorption mechanism.

The oxidation of MWCNTs with concentrated nitric acid lead to the surface functionalization with oxygen-containing groups, and the isoelectric point (IEP) of MWCNTs shifts to the lower pH values. When the pH of the solution is higher than the IEP of the oxidized MWCNTs, the negative charge on the surface provides electrostatic attractions that are favorable for adsorbing cations. The decrease of pH leads to the neutralization of surface charge, so the adsorption of cations onto MWCNTs decreases quickly. Liang et al. [126] investigated the adsorption behavior of REEs on MWCNTs and found that quantitative adsorption (>95 %) for the target REEs ions was obtained when the pH exceed 3.0, and pH 4.0 was selected as the optimum condition for the SPE of REE ions, followed by elution with 1.0 mol/L HNO₃ and ICP-OES detection. The detection limits of this method for REEs was between 3 and 57 ng/L, and the relative standard deviations for the determination of REEs at 10 µg/L level were found to be less than 6 % when processing 100-mL sample solution.

Su et al. [118] prepared a Fe₃O₄@SiO₂@polyaniline–graphene oxide composite (MPANI-GO) through a simple non-covalent method and applied it to magnetic solid phase extraction (MSPE) of trace REEs in tea leaves and environmental water samples followed by ICP-MS determination. The GO plays a key role in the adsorption of REEs on MPANI-GO and the function of MPANI was mainly to anchor and magnetically functionalize GO. The adsorption mechanism of the REEs on the MPANI-GO could be attributed to the chelation of the functional groups of GO containing hydroxyl, epoxide, carboxyl, and carbonyl groups with REEs. When 0.5 mol/L HNO₃ was used as the eluting agent, the MPANI-GO can be reused for more than 30 times without obvious decrease of the recoveries of REEs. It should be also noted that the prepared magnetic nanoparticles are superparamagnetic, which could be attracted to a magnetic field but retain no residual magnetism after the field is removed. During the extraction, the suspended superparamagnetic nanoparticles adhered to the target REEs can be removed very fast from a matrix using a magnetic field, and they do not agglomerate after removal of the field.

3.5.2 Silica-based materials

Modified silica gel merits good selectivity, high mass-exchange characteristics and good mechanical stability. Immobilization of organic functional groups on a siliceous surface has been successfully employed to produce varieties of modified silica gel. In this process, an organic reagent or a synthesized organic molecule containing the desired functional group is directly attached to the support, or to the original chain bonded to the support *via* a sequence of reactions to increase the main chain, where other basic centers can be added to ensure the enhancement of a specific adsorption.

Based on the hard–soft acid–base theory, chemically stable metal chelates can be formed between REEs and β-diketone reagents (e.g., acetylacetone,

trifluoroacetylacetone and hexafluoroacetylacetone) under suitable experimental conditions. These reagents, as derivatization reagents, have been successfully applied in GC analytical systems. Zhang et al. [127] prepared an acetylacetone-modified silica gel (ACACSG) for the preconcentration of trace REEs in environmental and biological samples. The maximum adsorption percentages for target REEs were obtained at pH 6.0–8.0. Two possible mechanisms could be used for the explanation of the adsorption of the REEs on ACACSG. First, REEs were adsorbed through the affinity of =O of acetylacetone. Second, the REEs were adsorbed on ACACSG by electrostatic action between REEs and the charge on silica gel surface. In the acidic medium, the first mechanism plays a dominating role. When the pH increases, the –OH on the surface of silica gel provides the ability of binding cation. Both mechanisms work, so the adsorption of REEs onto ACACSG increases quickly.

3.5.3 Chelating resin and ionic-exchange resin

Various chelating agents have been immobilized on polymeric supports to produce chelating sorbents for determination of REEs by SPE in natural water samples. These functional groups include 8-HQ [128], iminodiacetate (IDA) [129, 130], hydroxamic acid [131], 2-amino-5-hydroxy benzoic acid [132], 2,6-diacetylpyridine [133] and fluorinated β -diketone [134]. Chemical immobilization offers the ability to customize the sorption medium with different functional groups to improve selectivity, sorption capacity and reusability.

Fu et al. [135] synthesized alkyl phosphinic acid resin (APAR) for on-line preconcentration of trace REEs, followed by ICP-MS determination. REEs in seawater could be on-line concentrated on the APAR packed column, and eluted from the column with 0.5 mL 0.1 mol/L HNO_3 within 30 s. An EF of nearly 400 can be achieved for all REEs when the seawater sample volume was 200 mL, while the matrix and coexisting spectrally interfering ions such as Ba, Sn and Sb could be simultaneously separated. Zeereen et al. [111] prepared a new chelating resin by immobilizing 4-(2-thiazolylazo) resorcinol (TAR) on Chromosorb 106 and investigated the adsorption behavior of REEs on it. It was found that the REEs were quantitatively retained from saline solutions on the Chromosorb 106-TAR resin at pH 5.0 and can be eluted with 1 % (v/v) HNO_3 . The resin possesses large sorption capacity for REEs ranging from 81.1 $\mu\text{mol/g}$ for Lu and 108 $\mu\text{mol/g}$ for Nd. Gupte et al. [136] employed resorcin [4]calixpyrrole and its azo derivative impregnated Amberlite XAD-2 resin for the preconcentration of La^{3+} and Ce^{3+} . The resin was found to be highly selective for these two REE ions in the presence of various electrolytes at a particular pH. Table 3.26 presents some adsorption capacity for La^{3+} and Ce^{3+} .

Separation of REEs by ion chromatography on a Dionex Ion Pac CS3 column (sulfonic acid type) has been achieved by both isocratic and gradient elution with HIBA as the mobile phase [137]. It was shown that the plate height for Y was distinctly smaller than those for REEs with similar ionic radii. An improved combined

Table 3.26: Adsorption capacity (mg/g) of La^{3+} and Ce^{3+} on some chelating resin [136].

Adsorbents	La^{3+}	Ce^{3+}
Aliquat-336–Amberlite XAD-4	4.73	
Amberlite XAD-4 resin–bicine ligands	48.6	
Calix [4]arene- <i>o</i> -vanillinsemicarbazone–merrifield resin	25.2	28.1
Amberlite XAD-16 (AXAD-16)- <i>N,N</i> -dihexylcarbamoymethyl	188	–
Phosphonic acid, Amberlite XAD-4-(<i>o</i> -vanillinsemicarbazone)	2.30	2.48
Calix [4]arene-semicarbazone–merrifield’s peptide resin	1.88	1.44
Merrifield chloromethylated resin–(dimethyl amino-phosphonomethyl)-phosphonic acid (MCM–DAPPA)	169	
Azocalix [4]pyrrole Amberlite XAD-2 polymeric chelating resin	107, 111	88.2, 89.9

isocratic-gradient elution procedure was devised for separation of Sc, Y, La and the lanthanides in one run. By using strongly basic anion-exchanger (QAE-SephadexA-25), Gd complexed with negatively charged humic substances (humic and fulvic acids) was collected from sample solution [138]. A Gd-based MRI contrast agent (diethylenetriamine-*N,N,N',N'',N'''*-pentaacetato aquo gadolinium(III), Gd–DTPA²⁻) was simultaneously collected on the same column. The Gd–DTPA complex was desorbed by anion-exchange with 50-mM tetramethyl ammonium sulfate, leaving the Gd–humic complexes on the column. The Gd–humic complexes were subsequently dissociated with 1 M nitric acid to desorb the humic fraction of Gd. The 2-step desorption with small volumes of the eluting agents allowed 100-fold preconcentration for the fractionation analysis of Gd at low ng/L levels by ICP-MS. On the other hand, Gd(III) neither complexed with humic substances nor DTPA, i.e., free species, was not adsorbed on the column.

The details on relevant chromatographic separation of REEs can be referred from the section of “Liquid chromatographic separations of REEs”.

3.5.4 Metal oxide nanostructured materials

Nanoparticles are often defined as particles of less than 100 nm in diameter. The nanoparticles exhibit new or enhanced size-dependent properties compared with larger particles of the same material. Depending on the chemistry of the constituent atoms, nanoparticles are known to exhibit remarkable adsorption properties due to their enhanced surface area and large interface volume. Nano-sized inorganic oxides are widely used in SPE for the preconcentration/separation of metal ions because it can adsorb metal ions with high adsorption capacity. Different types of nanoparticles, such as nanometer-sized powder materials, mesoporous nanoparticles and magnetic nanoparticles, have been applied in SPE of REE ions.

The effect of pH on the adsorption characteristics of La^{3+} and La complexes of citric acid, 2-hydroxyisobutyric acid (HIBA), and humic acid on nanometer-sized TiO_2

was investigated [139]. It was found that there is an obvious difference between the adsorption of free La^{3+} and La complexes on nanometer-sized TiO_2 with pH changing from 4.0 to 6.5. Quantitative adsorption of lanthanum citrate, lanthanum HIBA and lanthanum humic complexes were achieved in a pH ranging from 4.0 to 8.0, whereas free La^{3+} cannot be quantitatively adsorbed until the pH value is up to 6.5. However, if the pH value was lower than 4.0 (pH 3.5 for lanthanum citrate), the adsorption of lanthanum citrate and lanthanum humate complexes declined remarkably due to incomplete complexing between La^{3+} and the organic ligands (the first acid dissociation constants [pKa] of the citric acid and the 2-hydroxyisobutyric acid are 3.13 and 3.72, respectively).

These nanometer-sized metal oxides are not selective and not suitable for samples with complicated matrices. In order to improve selectivity of the nanoparticles, the modification of the adsorption material is usually required. The most often used method is to load a kind of specific chelate reagent by physical or chemical procedure on the surface of this material. The former method is simple but the loaded reagent is prone to leakage. PAN, PMBP, 8-HQ and dithizone were commonly used as modifiers on metal oxides nanoparticles. Due to the chelating ability of the loaded reagent with the target analytes, selectivity of the nanoparticles could be improved. Jon et al. [140] employed PMBP physically immobilized nanometer Al_2O_3 as the adsorbents for the extraction of REE ions Sc^{3+} , Y^{3+} and La^{3+} . The interesting ions can be adsorbed quantitatively on the above material at pH = 4.5 and the analytes adsorbed on the column can be eluted with 0.5 mol/L HCl. The dynamic adsorption capacity of target REEs on the modified nanometer Al_2O_3 are 5.7 (Sc), 13.1 (Y) and 15.5 (La) mg/g, respectively. However, these materials prepared by the physical method are not stable, and the chemically bonded materials are more stable and could be used repeatedly.

Mesoporous nanoparticles are special kind of mesoporous materials. The particle size of the material was less than 100 nm, while it has mesoporous on the particles. The application of the material as adsorbent has been viewed in three perspectives: (1) As a new nanometer material with unsaturated surface atoms that can bind with other atoms, it possess highly chemical activity, very high adsorption capacity and selective adsorption of metal ions. (2) Due to its large surface area, mesoporous material provides more active sites, this results in achieving equilibrium adsorption in short time. (3) By virtue of mesoporous structure, fast adsorption and desorption has been obtained. Huang et al. [77] employed mesoporous TiO_2 nanoparticles as column packing sorbent for flow injection micro-column preconcentration on-line coupled with ICP-OES determination of trace metals (including REEs) in environmental samples. The results showed mesoporous TiO_2 possesses a high adsorption capacity toward the metal ions and the adsorbent was suitable for the preconcentration of trace metal ions in samples with complicated matrix, and is highly stable with long column life time, enabling more than one hundred of load and elution cycles to be performed without loss of analytical performance.

3.5.5 Ion-imprinted materials

Ion-imprinted polymers (IIPs) are similar to molecular-imprinted polymers (MIPs), but they can recognize metal ions after imprinting and retain all the virtues of MIPs. IIPs have outstanding advantages such as predetermined selectivity in addition to being simple and convenient to prepare. Traditional IIP exhibits poor site accessibility to the target ions because the functionality is totally embedded by high cross-linking density in the polymer matrices. In order to obtain IIP with high selectivity and easy site accessibility for target ions, efforts have been made to deal with the issue of accessibility by imprinting on the matrix surfaces. Recently, surface imprinting technique attracted extensive research interest due to good accessibility to the target species, low mass-transfer resistance, and completed removal of templates, fast adsorption kinetics and ease of preparation.

Meng et al. [141] prepared a novel Ce^{3+} ion imprinted silica based on the supported material of ordered mesoporous silica SBA-15 by surface imprinting technique via reversible addition-fragmentation chain transfer polymerization. The results showed that the synthesized material possessed high-ordered mesoporous structure and showed high selectivity and satisfied adsorption capacity for adsorption of Ce^{3+} . Zhang et al. [142] synthesized Dy^{3+} -imprinted TTA modified silica gel sorbent by surface imprinting technique and employed it as a selective SPE sorbent for on-line extraction and subsequent ICP-OES determination of Dy^{3+} . The largest selectivity coefficient for Dy^{3+} in the presence of competitive ions such as La^{3+} , Nd^{3+} and Gd^{3+} was above 350. The static adsorption capacity and selectivity coefficient of the imprinted sorbent are higher than those of the non-imprinted sorbent and the imprinted TTA modified silica gel sorbent offered a fast kinetics for the adsorption and desorption of Dy^{3+} . With a sample loading flow rate of 2.5 mL/min for 48 s preconcentration and elution flow rate of 1.5 mL/min for 8 s elution, an EF of 10 and the sample frequency of 40 samples/h were obtained.

3.5.6 Metal-organic frameworks (MOFs)

MOFs are a new class of hybrid inorganic–organic microporous crystalline materials self-assembled straightforwardly from metal ions with organic linkers via coordination bonds. Due to their unique physical and chemical properties, (e.g., permanent nanoscale pore structure, uniform pore size, large specific surface area and good thermal stability), MOFs demonstrated great application prospect in hydrogen storage, gas separation, the catalytic, sensors and biological imaging. The inherent high-specific surface area (appr. 5,000 m^2/g) indicates a large adsorption capacity; the uniform pore structure with certain pore size allows a selective adsorption of molecular with less pore size; the functionalization in their pores or outer surface can be achieved easily. While the application of MOFs-based sorbents is mainly limited in simple water samples or simulated samples (in organic solvents) presently.

Ln^{3+} @bio-MOF-1 were synthesized via postsynthetic cation exchange of bio-MOF-1 with Tb^{3+} , Sm^{3+} , Eu^{3+} or Yb^{3+} , and their photophysical properties were studied [143]. It is demonstrated that bio-MOF-1 encapsulates and sensitizes visible and near-infrared emitting lanthanide cations in aqueous solution. The development and application of MOFs in trace REEs is greatly expected although it is relatively scarce presently.

3.5.7 Restricted access materials

RAMs are a class of biocompatible adsorbent particles enabling the direct extraction of analytes from biological fluid (e.g., plasma and urine). The separation mechanism is based on the hydrophilic effect and size exclusion. To be brief, a hydrophilic barrier enables the small molecules to permeate through the inner part of the material; meanwhile, it excludes the macromolecules by physical or chemical means on the surface of the material. They have been successfully used as separation media for the analysis of environmental and biological samples in recent years. In LC pre-column, the commercialized alkyl-diol silica (ADS) was frequently applied as RAM for the clean-up of complex biological samples, such as blood, serum, urine and milk. And the mechanism was explained by that the outer surface (hydrophilic diol group) repelled macromolecules (such as proteins, nucleic acids), while the internal surface, comprising hydrophobic reversed-phase (C_4 , C_8 or C_{18}), retained analytes that penetrate through the porous layer.

Yan et al. [144] prepared restricted accessed magnetic nanoparticles by self-assembly of a nonionic surfactant (Tween-20) onto the PAR functionalized magnetic nanoparticles (MNPs). It was found that the as-prepared restricted accessed Fe_3O_4 @ SiO_2 @PAR nanoparticles have a porous structure with BET surface area of around $99.4 \text{ m}^2/\text{g}$, average pore size of about 6.14 nm and pore volume of $0.47 \text{ cm}^3/\text{g}$, respectively. Besides, the prepared restricted accessed Fe_3O_4 @ SiO_2 @PAR showed a good size exclusion property toward protein, providing an application potential for the direct analysis of biological samples. Based on it, a novel method of restricted accessed MSPE combined with ICP-MS was developed for the direct determination of trace metal ions in human fluids. Under the optimum conditions, the adsorption capacity of La(III) and Nd(III) on the as-prepared restricted accessed Fe_3O_4 @ SiO_2 @PAR were 33.7 and 36.9 mg/g , respectively.

3.5.8 Capillary microextraction

In 1990, Pawliszyn et al. proposed solid phase microextraction (SPME) [145] as a new pretreatment technique. It integrates extraction, preconcentration and sampling into one step, featuring with simple operation, low consumption of solvents/sample, good reproducibility, high efficiency and can be hyphenated with various detection techniques. It was commercialized by Supelco Corporation in 1993 and has been applied

extensively in a variety of fields [146–148]. While the application of SPME in the analysis of trace elements and their species is relatively scarce [149].

Eisert and Pawliszyn [150] proposed another operation mode for fiber-SPME in 1997 – capillary microextraction (CME) – also called in-tube SPME. Figure 3.11 presents a schematic diagram of in-tube SPME combined with LC–MS system [151].

The main difference between fiber-SPME and CME is the coating which is coated on the surface of the fiber for the former one while on the inside surface in the capillary

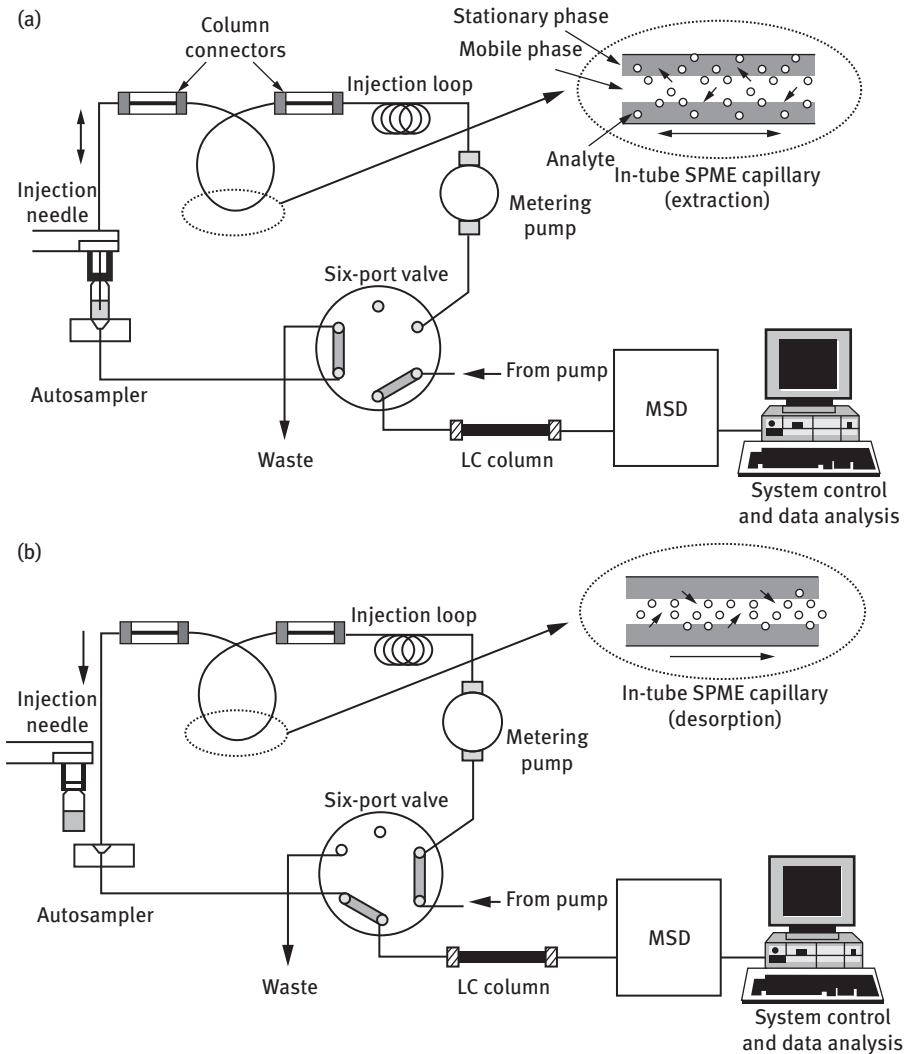


Figure 3.11: Schematic diagram of the in-tube SPME/LC/MS system [151]. (A) load position (extraction phase) and (B) injection position (desorption phase).

for the latter. Compared with fiber-SPME, CME can be easily online combined with HPLC or CE, improving the producibility; the problem of coating easily swelling or falling off in some organic solvents is overcome, lowering the analytical cost; it can be used for strong polar analytes analysis, widening the application field; the thickness of the extraction coating in CME (0.1–1.5 μm) is far less than that in fiber-SPME (10–100 μm), and the contacting surface between the coating and analytes is larger than that in fiber-SPME, shortening the required time to attain the equilibrium. CME needs that the sample solution should be clean, otherwise the particles would block the capillary column or the flow channel.

CME can be divided into three operation modes [152], which include open-tubular CME, packed CME and monolithic CME. The application of CME in trace REEs analysis is scarce presently.

Wu et al. [153] prepared a Congo red (CR) modified SWCNTs coated fused-silica capillary for CME of trace La, Eu, Dy and Y in human hair followed by fluorinating assisted (F)ETV-ICP-OES determination. The maximum adsorption capacities of the CR-SWCNTs coated capillary evaluated from the breakthrough curve were 0.8, 0.7, 0.7 and 0.7 $\mu\text{g}/\text{m}$ for La, Eu, Dy and Y, respectively. The proposed method was applied to the analysis of real-world human hair sample, featuring with simplicity, high sensitivity and less sample/reagents consumption. Zhang et al. [154] synthesized an IDA modified poly(glycidyl methacrylate-trimethylolpropane trimethacrylate) [poly(IDAGMA-TRIM)] monolithic capillary and used it for the selective extraction and preconcentration of REEs. Based on it, a novel method of poly(IDA-GMA-TRIM)-based CME on-line coupled to microconcentric nebulization (MCN)-ICP-MS was developed for the determination of ultra-trace REEs in biological samples (urine and serum). Under the optimal conditions, the LODs for REEs were in the range of 0.08 (Er)–0.97 ng/L (Nd) with a sampling frequency of 8.5/h. The method is featured with high sensitivity and sample throughput, low sample consumption and contamination risks, easy operation, wide pH application range and good tolerance to the matrix interferences.

A novel method of TiO_2 nanoparticles (NPs) functionalized monolithic CME on-line coupling with ICP-MS was developed for the sequential determination of Gd^{3+} and Gd-based contrast agents in human urine samples [155]. The monolithic capillary was prepared by embedding anatase TiO_2 NP_s in the poly(methacrylic acid–ethylene glycol dimethacrylate) (MAA–EDMA) framework. The Gd^{3+} and Gd-based contrast agents (such as gadolinium–diethylene triamine pentaacetic acid (Gd–DTPA) and Gd–DTPA–bismethylamide (Gd–DTPA–BMA)) display different adsorption behaviors on the prepared monolithic capillary which possesses the adsorption properties of both anatase TiO_2 NP_s and poly(MAA–EDMA) monolith. As shown in Figure 3.12, in the presence of PBS, Gd^{3+} was adsorbed completely on the poly(MAA–EDMA– TiO_2 NPs) monolithic capillary in a relatively wide pH range (2–9), whereas Gd–DTPA could be retained quantitatively on the monolith in the pH range of 2–3 and a sharp decrease of adsorption percentage of Gd–DTPA was observed when pH was higher than 4. It was speculated that in the presence of PBS, Gd–DTPA first reacted with PO_4^{3-} to form

a ternary complex (structure shown in Figure 3.12) because the interaction between Gd–DTPA and phosphate is stronger than that between Gd–DTPA and TiO₂ NPs. This ternary complex could be easily adsorbed by the prepared poly(MAA–EDMA TiO₂ NPs) monolithic capillary due to the good affinity of TiO₂ NPs to phosphate group at pH 2–3.

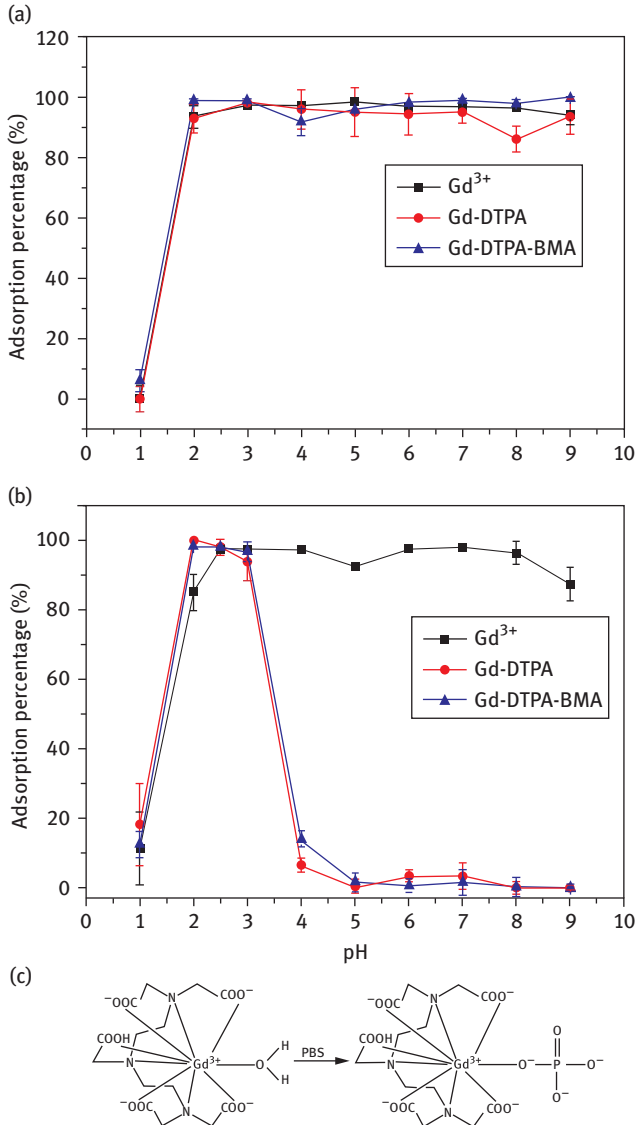


Figure 3.12: Effect of pH on the adsorption behavior of Gd³⁺, Gd–DTPA and Gd–DTPA–BMA in the absence (a) or presence (b) of PBS, and the formation of the deduced ternary complex (c) [155].

References

- [1] Jiang, ZC, Cai RX, Zhang HS. *Rare Earth Elements Analytical Chemistry*. Beijing, PRC, Science Press, 2000.
- [2] Zhang DL. Rapid determination of rare earth elements in water-soil-plant samples by ICP-AES. *Chin J Anal Lab* 1988, 3, 7, 61–62.
- [3] Roychowdhury P, Roy NK, Das DK, Das AK. Determination of rare-earth elements and Yttrium in silicate rocks by sequential inductively-coupled plasma emission spectrometry. *Talanta* 1989, 36, 12, 1183–6.
- [4] Iwasaki K, Haraguchi H. Determination of rare earth elements in geological samples by inductively-coupled plasma atomic emission spectrometry after oxalate coprecipitation and cation-exchange column separation. *Anal Chim Acta* 1988, 208, 163–72.
- [5] Duan TC, Chen HT, Zeng XJ. Determination of rare and rare earth elements in soils and sediments by ICP-MS using $\text{Ti}(\text{OH})_4$ - $\text{Fe}(\text{OH})_3$ co-precipitation preconcentration. *J Anal At Spectrom* 2002, 17, 4, 410–3.
- [6] Freslon N, Bayon G, Birot D, Bollinger C, Barrat JA. Determination of rare earth elements and other trace elements (Y, Mn, Co, Cr) in seawater using Tm addition and $\text{Mg}(\text{OH})_2$ co-precipitation. *Talanta* 2011, 85, 1, 582–7.
- [7] Xu GX, Yuan CY. *Solvent Extraction of Rare Earth*. Beijing, PRC, Science Press, 1987.
- [8] Hunan Metallurgical Research Institut. *Rare Earth Metallurgical Analysis*, 1973.
- [9] Yuan CY, Ye WZ, Ma HL et al. The synthesis and chemical structures of acidic phosphorus (Phosphine) and the extraction performance for Neodymium, Samarium, Ytterbium and Yttrium. *Sci Chin, Ser B*, 1982, 27, 3, 193–203.
- [10] Li DQ, Ji ER, Xu W, Yu DY, Zeng GF, Ni JZ. Extraction mechanism of rare earth elements (III), iron (III) and thorium (IV) from sulfuric acid solutions by primary amine N1923. *Chin J Appl Chem* 1987, 4, 2, 36–41.
- [11] Ni ZA, Li YX. Extraction mechanism for the extraction of perchloric acid rare earth by N1923. *Rare Earth Elem* 1991, 12, 1, 49–52.
- [12] Green H. Uses of liquid ion-exchangers in inorganic analysis. *Talanta* 1973, 20, 2, 139–61.
- [13] Stary J. *The Solvent Extraction of Metal Chelates*. New York, Pergamon Press New York, 1964.
- [14] Haraguchi K, Yamazaki Y, Saitoh T, Kamidate T, Watanabe H. Solvent-extraction of lanthanoids(III) with N-alkylcarbonyl-substituted N-phenylhydroxylamines. *Anal Sci* 1990, 6, 6, 877–82.
- [15] Inoue S. Solvent-extraction of lanthanoids with N-p-methoxybenzoyl- and N-p-octyloxybenzoyl-N-phenylhydroxylamine. *Anal Sci* 1991, 7, 1, 125–8.
- [16] Inoue S. Solvent-extraction of lanthanides with N-m-nitrobenzoyl- and N-m-cyanobenzoyl-N-phenylhydroxylamine. *Solvent Extr Ion Exch* 1995, 13, 2, 313–22.
- [17] Inoue S. Solvent-extraction of lanthanoids(III) with dinitrobenzoyl-N-phenylhydroxylamine. *Anal Sci* 1994, 10, 2, 315–30.
- [18] Inoue S, Zhang QB, Uto M. Steric Effect of substituents on the extraction of lanthanoids(III) with N-p-(n-, iso- and tert-)butylbenzoyl-N-phenylhydroxylamine. *Talanta* 1997, 44, 8, 1455–62.
- [19] Nakagawa K, Okada S, Inoue Y, Tai A, Hakushi T. Solvent-extraction of lanthanoid picrates with crown ethers – preferential sandwich complexation and unique cation selectivities. *Anal Chem* 1988, 60, 22, 2527–31.
- [20] Kitatsuji K, Meguro Y, Yoshida Z, Yamamoto T, Nishizawa K. Synergistic Ion-Pair Extraction of lanthanide(III) with thenoyltrifluoroacetone and crown-ether into 1,2-dichloroethane, *Solv Extr Ion Exch* 1995, 13, 2, 289–300.
- [21] Inoue Y, Nakagawa K, Hakushi T. Solvent-extraction of lanthanoid(III) picrates with a Bis(crown ether)-enhanced extractability through double-sandwich complexation. *J Chem SocDalton Trans* 1993, 15, 2279–81.

- [22] Beer PD, Drew MGB, Grieve A, Ogden MI. Lanthanide picrate complexes and picric acid adduct of a Calix[4]arene diamide. syntheses and structures of $Tm[(LH_{-2})_2A]$, $[Ce(LH_{-2})(MeOH)_2A] \cdot HA$, $[PrLa_3]$ and $L \cdot 2HA$ ($L = 5,11,17,23$ -tetra-tert-butyl-25,27-bis(diethylcarbamoylmethoxy)-26,28-dihydroxycalix[4]arene, $HA = \text{picric acid}$). *J Chem Soc Dalton Trans* 1995, 21, 3455–66
- [23] Inoue Y, Nakagawa K, Hakushi T. Solvent isotope effect in ion-pair extraction of aqueous lanthanoid(III) picrates with a crown-ether. *J Chem Soc Dalton Trans* 1993, 8, 1333–6.
- [24] Beer PD, Drew MG, Kann M, Leeson PB, Ogden MI, Williams G. Lanthanide structures, coordination, and extraction investigations of a 1,3-bis(diethyl amide)-substituted Calix[4]arene ligand. *Inorg Chem* 1996, 35, 8, 2202–11.
- [25] Daitch CE, Hampton PD, Duesler EN. Selective binding of group IIIA and lanthanide metals by hexahomotrioxacalix[3]arene macrocycles. *J Am Chem Soc* 1996, 118, 33, 7769–73.
- [26] Frazier R, Wai CM. The effect of solvents on the extraction of lanthanoids with 18-crown-6 and trichloroacetate. *J Radio Nucl Chem* 1992, 159, 1, 63–9.
- [27] Mathur JN, Choppin GR. The interaction of crown ethers with beta-diketonate complexes of f-elements. *Solvent Extr Ion Exch* 1993, 11, 1, 1–18.
- [28] Imura H, Mito H. Selective extraction of light lanthanides(III) with 18-crown-6 and perfluorooctanoate. *J Radioanal Nucl Chem Art* 1995, 189, 2, 229–35.
- [29] Fidelis I. Temperature Effect on the extraction of lanthanides in the TBP- HNO_3 system. *J Inorg Nucl Chem* 1970, 32, 3, 997–1003.
- [30] Peng CL. Separation and determination of trace rare earth elements in nickel-based high-temperature alloy and aluminium alloy. *Chin Sci Bulletin* 1973, 4, 170–3.
- [31] Sreelatha S, Prasada Rao T, Narayanan CS, Damodaran AD. Extraction equilibria of rare earths by a new reagent (2-ethylhexyl-3-pentadecylphenyl) phosphoric acid. *Talanta* 1994, 41, 3, 433–8.
- [32] Yoshizuka K, Kosaka H, Shinohara T, Ohto K, Inoue K. Structural Effect of phosphoric esters having bulky substituents on the extraction of rare earth elements. *Bull Chem Soc Japan* 1996, 69, 3, 589–96.
- [33] Takayanagi T, Yotsuyanagi T. Ion-associate solvent-extraction and separation of lanthanides(III) with 2,3-naphthalenediol and benzyldimethyltetradecylammonium chloride. *Bull Chem Soc Japan* 1994, 67, 7, 1835–9.
- [34] Korotkin YS. Use of synergistic effects in extraction chromatography. I. Behavior of Americium and Europium in the system TTA-TBP. *Sov Radiochem* 1981, 23, 2, 140–5.
- [35] Qin GR, Li SX. Synergistic extraction of uranium and rare earth elements with different synergistic extraction system involving PMBP. *Chinese Journal of Analysis Laboratory* 1983, (5), 19–22
- [36] Noro J, Sekine T. Solvent-extraction of lanthanum(III), europium(III), and lutetium(III) with 5,7-dichloro-8-quinolinol into chloroform in the absence and presence of tetrabutylammonium ions or triocetylphosphine oxide. *Bull Chem Soc Japan* 1993, 66, 9, 2564–9.
- [37] Jeannot MA, Cantwell FF. Solvent microextraction into a single drop. *Anal Chem* 1996, 68, 13, 2236–40.
- [38] Liu H, Dasgupta PK. Analytical chemistry in a drop. Solvent extraction in a microdrop. *Anal Chem* 1996, 68, 11, 1817–21.
- [39] Jeannot MA, Cantwell FF. Mass transfer characteristics of solvent extraction into a single drop at the tip of a syringe needle. *Anal Chem* 1997, 69, 235–9.
- [40] Ho TS, Pedersen-Bjergaard S, Rasmussen KE. Recovery, enrichment and Selectivity in liquid-phase microextraction-comparison with conventional liquid-liquid extraction. *J Chrom A* 2002, 963, 1–2, 3–17.
- [41] Wu YL, Jiang ZC, Hu B. A Novel micro drop solvent extraction technique combined with low temperature electrothermal vaporization ICP-AES for ultra trace element analysis. *Chem J Chin Univ Chin* 2003, 24, 10, 1793–4.

- [42] Xia LB, Hu B, Jiang ZC, Wu YL, Liang Y. Single-drop microextraction combined with low-temperature electrothermal vaporization ICPMS for the determination of trace Be, Co, Pd, and Cd in biological samples. *Anal Chem* 2004, 76, 10, 2910–5.
- [43] Ma MH, Cantwell FF. Solvent microextraction with simultaneous back-extraction for sample cleanup and preconcentration: Preconcentration into a single microdrop. *Anal Chem* 1999, 71, 2, 388–93.
- [44] Liu XJ, Fan ZF. Liquid-liquid-liquid micro extraction combined with CE for the determination of rare earth elements in water samples. *Chromatographia* 2009, 70, 3–4, 481–7.
- [45] Pedersen-Bjergaard S, Rasmussen KE. Liquid-liquid-liquid microextraction for sample preparation of biological fluids prior to capillary electrophoresis. *Anal Chem* 1999, 71, 14, 2650–6.
- [46] Rezaee M, Assadi Y, Hosseini MRM, Aghaee E, Ahmadi F, Berijani S. Determination of organic compounds in water using dispersive liquid-liquid microextraction. *J Chromatogr A* 2006, 1116(1–2), 1–9.
- [47] Mallah MH, Shemirani F, Maragheh MG. Ionic liquids for simultaneous preconcentration of some lanthanoids using dispersive liquid-liquid microextraction technique in uranium dioxide powder. *Environ Sci Technol* 2009, 43, 6, 1947–51.
- [48] Chandrasekaran K, Karunasagar D, Arunachalam J. Dispersive liquid-liquid micro-extraction for simultaneous preconcentration of 14 lanthanides at parts per trillion levels from groundwater and determination using a micro-flow nebulizer in inductively coupled plasma-quadrupole mass spectrometry. *J Anal At Spectrom* 2012, 27, 6, 1024–31.
- [49] Guo XQ, Tang XT, He M, et al. Dual dispersive extraction combined with electrothermal vaporization inductively coupled plasma mass spectrometry for determination of trace REEs in water and sediment samples. *RSC Adv* 2014, 4, 38, 19960–9.
- [50] Zanjani MRK, Yamini Y, Shariati S, Jonsson JA. A New liquid-phase microextraction method based on solidification of floating organic drop. *Anal Chim Acta* 2007, 585, 2, 286–93.
- [51] Ganjali MR, Sobhi HR, Farahani H, Norouzi P, Dinarvand R, Kashtiaray A. Solid drop based liquid-phase microextraction. *J Chromatogr A* 2010, 1217, 16, 2337–41.
- [52] Chen SZ, Zhu SP, Lu DB. Solidified floating organic drop microextraction for the determination of trace Dy and Y by electrothermal vaporization inductively coupled plasma mass spectrometry. *At Spectrosc* 2014, 35, 1, 1–6.
- [53] Li YJ, Hu B. Cloud Point Extraction with/without chelating agent on-line coupled with inductively coupled plasma optical emission spectrometry for the determination of trace rare earth elements in biological samples. *J Hazard Mater* 2010, 174, 1–3, 534–40.
- [54] Depoi FD, Bentlin FR, Ferrao MF, Pozebon D. Multivariate optimization for cloud point extraction and determination of lanthanides. *Anal Methods* 2012, 4, 9, 2809–14.
- [55] Perez-Gramatges A, Chatt A. Preconcentration neutron activation analysis of lanthanides by cloud point extraction using PAN. *J Radioanal Nucl Chem* 2006, 269, 2, 491–7.
- [56] Nouh EA. Micelle mediated extraction for preconcentration of Eu(III) prior to determination by flame atomic absorption spectrometry. *J Ind Eng Chem* 2015, 24, 87–91.
- [57] Labrecque C, Larivière D. Quantification of rare earth elements using cloud point extraction with diglycolamide and ICP-MS for environmental analysis. *Anal Methods* 2014, 6, 23, 9291–8.
- [58] Ohashi A, Hashimoto T, Imura H, Ohashi K. Cloud point extraction equilibrium of lanthanum(III), europium(III) and lutetium(III) using Di(2-ethylhexyl)phosphoric acid and triton X-100. *Talanta* 2007, 73, 5, 893–8.
- [59] Camel V. Solid phase extraction of trace elements. *Spectrochim Acta Part B: At Spectrosc* 2003, 58 7, 1177–233.
- [60] Poole CF. New trends in solid-phase extraction. *TRAC Trends Anal Chem* 2003, 22, 6, 362–73.

- [61] Melo LFC, Collins CH, Jardim ICSF. New materials for solid-phase extraction and multiclass high-performance liquid chromatographic analysis of pesticides in grapes. *J Chromatogr A* 2004, 1032, 1–2, 51–8
- [62] Kumar M, Rathore DPS, Singh AK. Pyrogallol immobilized amberlite XAD-2: A newly designed collector for enrichment of metal ions prior to their determination by flame atomic absorption spectrometry. *Mikrochim Acta* 2001, 137, 3–4, 127–34.
- [63] Strelko V, Malik DJ, Streat M. Interpretation of transition metal sorption behavior by oxidized active carbons and other adsorbents. *Sep Sci Technol* 2004, 39, 8, 1885–905.
- [64] Marques MJ, Morales-Rubio A, Salvador A, de la Guardia M. Chromium speciation using activated alumina microcolumns and sequential injection analysis-flame atomic absorption spectrometry. *Talanta* 2001, 53, 6, 1229–39.
- [65] Wie ZG, Hong FS, Yin M, et al. Off-line separation and determination of rare earth elements associated with chloroplast pigments of hyperaccumulator *dicranopteris dichotoma* by normal-phase liquid chromatography and ICP-MS. *Anal Bioanal Chem* 2004, 380, 4, 677–82.
- [66] Agrawal YK. Poly(Beta-Styryl)-(1,2-methanofullerene-C60)-61-formo, hydroxamic acid for the solid phase extraction. *Sep Preconcentration Rare Earth Elem Fullerenes Nanotubes Carbon Nanostruct* 2007, 15, 5, 353–65.
- [67] Li YH, Wang SG, Wie JQ, et al. Lead adsorption on carbon nanotubes. *Chem Phys Lett* 2002, 357, 3–4, 263–6.
- [68] Di ZC, Ding J, Peng XJ, Li YH, Luan ZK, Liang J. Chromium Adsorption by aligned carbon nanotubes supported ceria nanoparticles. *Chemosphere* 2006, 62, 5, 861–5.
- [69] Lv YK, Wang LM, Yang L, Zhao CX, Sun HW. Synthesis and application of molecularly imprinted poly(methacrylic acid)-silica hybrid composite material for selective solid-phase extraction and high-performance liquid chromatography determination of oxytetracycline residues in milk. *J Chromatogr A* 2012, 1227, 48–53.
- [70] Zambrzycka E, Roszko D, Leśniewska B, Wilczewska AZ, Godlewska-Żyłkiewicz B. Studies of ion-imprinted polymers for solid-phase extraction of ruthenium from environmental samples before its determination by electrothermal atomic absorption spectrometry. *Spectrochim Acta Part B: At Spectrosc* 2011, 66, 7, 508–16.
- [71] Pu XL, Hu B, Jiang ZC, Huang CZ. Speciation of dissolved iron(ii) and iron(iii) in environmental water samples by gallic acid-modified nanometer-sized alumina micro-column separation and ICP-MS Determination. *Anal* 2005, 130, 8, 1175–81.
- [72] Liang P, Qin YC, Hu B, Li CX, Peng TY, Jiang ZC. Study of the adsorption behavior of heavy metal ions on nanometer-size titanium dioxide with ICP-AES. *Fresenius J Anal Chem* 2000, 368, 6, 638–40.
- [73] Liang P, Shi TQ, Lu HB, Jiang ZC, Hu B. Speciation of Cr(III) and Cr(VI) by nanometer titanium dioxide micro-column and inductively coupled plasma atomic emission spectrometry. *Spectrochim Acta Part B At Spectrosc* 2003, 58, 9, 1709–14.
- [74] Yin J, Jiang ZC, Chang G, Hu B. Simultaneous on-line preconcentration and determination of trace metals in environmental samples by flow injection combined with inductively coupled plasma mass spectrometry using a nanometer-sized alumina packed micro-column. *Anal Chim Acta* 2005, 540, 2, 333–9.
- [75] Sawicki R, Mercier L. Evaluation of mesoporous cyclodextrin-silica nanocomposites for the removal of pesticides from aqueous media. *Environ Sci Technol* 2006, 40, 6, 1978–83.
- [76] Tian RJ, Ye ML, Hu LH, Li X, Zou HF. Selective extraction of peptides in acidic human plasma by porous silica nanoparticles for peptidome analysis with 2-D LC-MS/MS. *J Sep Sci* 2007, 30, 14, 2204–9.

- [77] Huang CZ, Jiang ZC, Hu B. Mesoporous Titanium Dioxide as a novel solid-phase extraction material for flow injection micro-column preconcentration on-line coupled with ICP-OES determination of trace metals in environmental samples. *Talanta* 2007, 73, 2, 274–81.
- [78] Jiang HM, Hu B, Chen BB, Xia LB. Hollow fiber liquid phase microextraction combined with electrothermal atomic absorption spectrometry for the speciation of arsenic (III) and arsenic (V) in fresh waters and human hair extracts. *Anal Chim Acta* 2009, 634, 1, 15–21.
- [79] Wang F, Guan YF, Zhang S, Xia Y. Hydrophilic Modification of silica–titania mesoporous materials as restricted-access matrix adsorbents for enrichment of phosphopeptides. *J Chromatogr A* 2012, 1246, 76–83.
- [80] Zhang Y, Liu HY, Zhang XY, Lei H, Bai LG, Yang GL. On-line solid phase extraction using organic-inorganic hybrid monolithic columns for the determination of trace B-lactam antibiotics in milk and water samples. *Talanta* 2013, 104, 17–21.
- [81] Choi K, Ng AHC, Fobel R, et al. Automated digital microfluidic platform for magnetic-particle-based immunoassays with optimization by design of experiments. *Anal Chem* 2013, 85, 20, 9638–46.
- [82] Gu ZY, Chen YJ, Jiang JQ, Yan XP. Metal-organic frameworks for efficient enrichment of peptides with simultaneous exclusion of proteins from complex biological samples. *Chem Commun* 2011, 47, 16, 4787–9.
- [83] Ni Z, Jerrell JP, Cadwallader KR, Masel RI. Metal-organic frameworks as adsorbents for trapping and preconcentration of organic phosphonates. *Anal Chem* 2007, 79, 4, 1290–3.
- [84] Zhou YY, Yan XP, Kim KN, Wang SW, Liu MG. Exploration of coordination polymer as sorbent for flow injection solid-phase extraction on-line coupled with high-performance liquid chromatography for determination of polycyclic aromatic hydrocarbons in environmental materials. *J Chromatogr A* 2006, 1116, 1–2, 172–8.
- [85] Bahramifar N, Yamini Y. On-line preconcentration of some rare earth elements in water samples using C-18-cartridge modified with 1-(2-pyridylazo) 2-naphtol (PAN) prior to simultaneous determination by inductively coupled plasma optical emission spectrometry (ICP-OES). *Anal Chim Acta* 2005, 540, 2, 325–32.
- [86] Liang P, Fa WJ. Determination of La, Eu and Yb in water samples by inductively coupled plasma atomic emission spectrometry after solid phase extraction of their 1-phenyl-3-methyl-4-benzoylpyrazol-5-One complexes on silica gel column. *Microchim Acta* 2005, 150, 1, 15–9.
- [87] Liang P, Liu Y, Guo L. Determination of trace rare earth elements by inductively coupled plasma atomic emission spectrometry after preconcentration with multiwalled carbon nanotubes. *Spectrochim Acta Part B At Spectrosc* 2005, 60, 1, 125–9.
- [88] Chauvin AS, Bunzli JCG, Bochud F, Scopelliti R, Froidevaux P. Use of dipicolinate-based complexes for producing ion-imprinted polystyrene resins for the extraction of Yttrium-90 and heavy lanthanide cations. *Chem Eur J* 2006, 12, 26, 6852–64.
- [89] Wang ZH, Yan XP, Wang ZP, Zhang ZP, Liu LW. Flow injection on-line solid phase extraction coupled with inductively coupled plasma mass spectrometry for determination of (ultra)trace rare earth elements in environmental materials using maleic acid grafted polytetrafluoroethylene fibers as sorbent. *J Am Soc Mass Spectrom* 2006, 17, 9, 1258–64.
- [90] Chen SZ, Xiao MF, Lu DB, Zhan XL. Carbon nanofibers as solid-phase extraction adsorbent for the preconcentration of trace rare earth elements and their determination by inductively coupled plasma mass spectrometry. *Anal Lett* 2007, 40, 11, 2105–15.
- [91] Huang CZ, Jiang ZC, Hu B. Mesoporous titanium dioxide as a novel solid-phase extraction material for flow injection micro-column preconcentration on-line coupled with ICP-OES determination of trace metals in environmental samples. *Talanta* 2007, 73, 2, 274–81.
- [92] Dutta S, Mohapatra PK, Dhekane GD, Das AK, Manchanda VK. Solid phase extraction of europium and uranium using tulsion CH-90 Resin. *Desalination* 2008, 232, 1–3, 216–24.

- [93] Katarina RK, Takayanagi T, Oshita K, Oshima M, Motomizu S. Sample pretreatment Using chitosan-based chelating resin for the determination of trace metals in seawater samples by inductively coupled plasma-mass spectrometry. *Anal Sci* 2008, 24, 12, 1537–44.
- [94] Shirvani-Arani S, Ahmadi SJ, Bahrami-Samani A, Ghannadi-Maragheh M. Synthesis of nano-pore samarium (III)-imprinted polymer for preconcentrative separation of samarium ions from other lanthanide ions via solid phase extraction. *Anal Chim Acta* 2008, 623, 1, 82–8.
- [95] Zhang LL, Chang XJ, Zhai YH, et al. Selective solid phase extraction of trace Sc(III) from environmental samples using silica gel modified with 4-(2-morinyldiazanyl)-N-(3-(trimethylsilyl)propyl)benzamide. *Anal Chim Acta* 2008, 629, 1–2, 84–91.
- [96] Shariati S, Yamini Y, Faraji M, Saleh A. On-line solid phase extraction coupled to ICP-OES for simultaneous preconcentration and determination of some transition elements. *Microchim Acta* 2009, 165, 1–2, 65–72.
- [97] Vizioli N, Gil R, Martinez LD, Silva MF. On-line solid phase extraction CZE for the simultaneous determination of lanthanum and gadolinium at picogram per liter levels. *Electrophoresis* 2009, 30, 15, 2681–7.
- [98] Zhu YB, Umemura T, Haraguchi H, Inagaki K, Chiba K. Determination of REEs in seawater by ICP-MS after on-line preconcentration using a syringe-driven chelating column. *Talanta* 2009, 78, 3, 891–5.
- [99] Dave SR, Kaur H, Menon SK. Selective solid-phase extraction of rare earth elements by the chemically modified amberlite XAD-4 resin with azacrown ether. *React Funct Polym* 2010, 70, 9, 692–8.
- [100] Raju CSK, Lueck D, Scharf H, Jakubowski N, Panne U. A Novel solid phase extraction method for pre-concentration of gadolinium and gadolinium based MRI contrast agents from the environment. *J Anal At Spectrom* 2010, 25, 10, 1573–80.
- [101] Li DD, Chang XJ, Hu Z, Wang QH, Li RJ, Chai XL. Samarium (III) adsorption on bentonite modified with N-(2-hydroxyethyl) ethylenediamine. *Talanta* 2011, 83, 5, 1742–7.
- [102] Tong SS, Zhao SJ, Zhou WH, Li RG, Jia Q. Modification of multi-walled carbon nanotubes with tannic acid for the adsorption of La, Tb and Lu ions. *Microchim Acta* 2011, 174, 3–4, 257–64.
- [103] Wang QH, Chang XJ, Hu Z, Li DD, Li RJ, Chai XL. Preconcentration of Erbium(III) ions from environmental samples using activated carbon modified with benzoyl hydrazine. *Microchim Acta* 2011, 172, 3–4, 395–402.
- [104] Zhang JL, Cheng RM, Tong SS, et al. Microwave plasma torch-atomic emission spectrometry for the on-line determination of rare earth elements based on flow injection preconcentration by TiO₂-graphene composite. *Talanta* 2011, 86, 114–20.
- [105] Berijani S, Ganjali MR, Sereshti H, Norouzi P. A selective modified nanoporous silica as sorbent for separation and preconcentration of dysprosium in water samples prior to ICP-OES determination. *Int J Environ Anal Chem* 2012, 92, 3, 355–65.
- [106] Cho J, Chung K, Choi MS, Kim H. Analysis of rare earth elements in seawater by inductively coupled plasma mass spectrometry after pre-concentration using TSKTM-HD-MW-CNTs (highly dispersive multi-walled carbon nanotubes). *Talanta* 2012, 99, 369–74.
- [107] Li Y, Yang JL, Jiang Y. Trace Rare Earth element detection in food and agricultural products based on flow injection walnut shell packed microcolumn preconcentration coupled with inductively coupled plasma mass spectrometry. *J Agric Food Chem* 2012, 60, 12, 3033–41.
- [108] Alizadeh T, Amjadi S. Synthesis of nano-sized Eu³⁺-imprinted polymer and its application for indirect voltammetric determination of europium. *Talanta* 2013, 106, 431–9.
- [109] Chen SZ, Zhu SP, Lu DB. Titanium dioxide nanotubes as solid-phase extraction adsorbent for on-line preconcentration and determination of trace rare earth elements by inductively coupled plasma mass spectrometry. *Microchem J* 2013, 110, 89–93.

- [110] Tajabadi F, Yamini Y, Sovizi MR. Carbon-based magnetic nanocomposites in solid phase dispersion for the preconcentration some of lanthanides, followed by their quantitation via ICP-OES. *Microchim Acta* 2013, 180, 1–2, 65–73.
- [111] Zereen F, Yilmaz V, Arslan Z. Solid phase extraction of rare earth elements in seawater and estuarine water with 4-(2-Thiazolylazo) resorcinol immobilized chromosorb 106 for determination by inductively coupled plasma mass spectrometry. *Microchem J* 2013, 110, 178–84.
- [112] Gao BJ, Zhang QJ, Xu Y. Study on recognition and separation of rare earth ions at picometre scale by using efficient ion-surface imprinted polymer materials. *Hydrometall* 2014, 150, 83–91.
- [113] Jerez J, Isaguirre AC, Bazán C, Martínez LD, Cerutti S. Determination of scandium in acid mine drainage by ICP-OES with flow injection on-line preconcentration using oxidized multiwalled carbon nanotubes. *Talanta* 2014, 124, 89–94.
- [114] Karadas C, Kara D. Preconcentration of rare earth elements using amberlite XAD-4 modified with 2,6-pyridinedicarboxaldehyde and their determination by inductively coupled plasma optical emission spectrometry. *Water Air Soil Poll* 2014, 225, 5, 1972–81.
- [115] Karadas C, Kara D. Determination of rare earth elements by solid phase extraction using chemically modified amberlite XAD-4 resin and inductively coupled plasma-optical emission spectrometry. *Water Air Soil Poll* 2014, 225, 11, 2192–201.
- [116] Ozdemir S, Okumus V, Dundar A, Celik KS, Yuksel U, Kilinc E. Selective preconcentration of lanthanum(III) by coriolus versicolor immobilised on amberlite XAD-4 and its determination by ICP-OES. *Int J Environ Anal Chem* 2014, 94, 6, 533–45.
- [117] Sarabadani P, Sadeghi M, Payehghadr M, Es'haghi Z. Synthesis and characterization of a novel nanostructured ion-imprinted polymer for pre-concentration of Y(III) ions. *Anal Methods* 2014, 6, 3, 741–9.
- [118] Su SW, Chen BB, He M, Hu B, Xiao ZW. Determination of trace/ultra-trace rare earth elements in environmental samples by ICP-MS after magnetic solid phase extraction with $\text{Fe}_3\text{O}_4@ \text{SiO}_2@ \text{polyaniline-graphene oxide}$ composite. *Talanta* 2014, 119, 458–66.
- [119] Berijani S, Ganjali MR, Sereshti H, Tabatabaei SH, Norouzi P. Application of a new modified magnetic nanoparticle as a selective sorbent for preconcentration and extraction of Europium in environmental water samples prior to ICP-OES determination. *J Iran Chem Soc* 2015, 12, 4, 737–42.
- [120] Prasad BB, Jauhari D. Double-Ion Imprinted Polymer @magnetic nanoparticles modified screen printed carbon electrode for simultaneous analysis of cerium and gadolinium ions. *Anal Chim Acta* 2015, 875, 83–91.
- [121] Vasylechko VO, Gryshchouk GV, Zakordonskiy VP, Vyviurska O, Pashuk AV. A Solid-phase extraction method using transcarpathian clinoptilolite for preconcentration of trace amounts of terbium in water samples. *Chem Cent J* 2015, 9, 1, 1–7.
- [122] Zhang YN, Zhong C, Zhang QY, Chen BB, He M, Hu B. Graphene oxide-TiO₂ composite as a novel adsorbent for the preconcentration of heavy metals and rare earth elements in environmental samples followed by on-line inductively coupled plasma optical emission spectrometry detection. *RSC Adv* 2015, 5, 8, 5996–6005.
- [123] Iijima S. Helical microtubules of graphitic carbon. *Nature* 1991, 354, 56–58.
- [124] Trojanowicz M. Analytical applications of carbon nanotubes: A review. *TRAC Trends Anal Chem* 2006, 25, 5, 480–9.
- [125] Lu CY, Liu CT. Removal of nickel(II) from aqueous solution by carbon nanotubes. *J Chem Technol Biotechnol* 2006, 81, 12, 1932–40.
- [126] Liang P, Liu Y, Guo L. Determination of trace rare earth elements by inductively coupled plasma atomic emission spectrometry after preconcentration with multiwalled carbon nanotubes. *Spectrochim Acta Part B: At Spectrosc* 2005, 60, 1, 125–9.

- [127] Zhang N, Huang C, Hu B. ICP-AES Determination of trace rare earth elements in environmental and food samples by on-line separation and preconcentration with acetylacetone-modified silica gel using microcolumn. *Anal Sci* 2007, 23, 8, 997–1002.
- [128] Kajiya T, Aihara M, Hirata S. Determination of rare earth elements in seawater by inductively coupled plasma mass spectrometry with on-line column pre-concentration using 8-quinolinole-immobilized fluorinated metal alkoxide glass. *Spectrochim Acta Part B At Spectrosc* 2004, 59, 4, 543–50.
- [129] Willie SN, Sturgeon RE. Determination of transition and rare earth elements in seawater by flow injection inductively coupled plasma time-of-flight mass spectrometry. *Spectrochim Acta Part B At Spectrosc* 2001, 56, 9, 1707–16.
- [130] Hirata S, Kajiya T, Aihara M, Honda K, Shikino O. Determination of rare earth elements in seawater by on-line column preconcentration inductively coupled plasma mass spectrometry. *Talanta* 2002, 58, 6, 1185–94.
- [131] Kumar SA, Pandey SP, Shenoy NS, Kumar SD. Matrix separation and preconcentration of rare earth elements from seawater by poly hydroxamic acid cartridge followed by determination using ICP-MS. *Desalination* 2011, 281, 49–54.
- [132] Sabarudin A, Lenghor N, Oshima M, et al. Sequential-injection on-line preconcentration using chitosan resin functionalized with 2-amino-5-hydroxy benzoic acid for the determination of trace elements in environmental water samples by inductively coupled plasma-atomic emission spectrometry. *Talanta* 2007, 72, 5, 1609–17.
- [133] Karadas C, Kara D, Fisher A. Determination of rare earth elements in seawater by inductively coupled plasma mass spectrometry with off-line column preconcentration using 2,6-diacetylpyridine functionalized amber lite XAD-4. *Anal Chim Acta* 2011, 689, 2, 184–9.
- [134] Waqar F, Jan S, Mohammad B, Hakim M, Alam S, Yawar W. Preconcentration of rare earth elements in seawater with chelating resin having fluorinated beta-diketone immobilized on styrene divinyl benzene for their determination by ICP-OES. *J Chin Chem Soc* 2009, 56(2), 335–40.
- [135] Fu Q, Yang LM, Wang QQ. On-line preconcentration with a novel alkyl phosphinic acid extraction resin coupled with inductively coupled plasma mass spectrometry for determination of trace rare earth elements in seawater. *Talanta* 2007, 72, 4, 1248–54.
- [136] Gupte HS, Bhatt KD, Jain VK, Vyas DJ, Makwana BA. Azo resorcin[4] calixpyrrole grafted amberlite XAD-2 polymer: An efficient solid phase extractant for separation and preconcentration of La(III) and Ce(III) from natural geological samples. *J Inclusion Phenom Macrocyclic Chem* 2015, 81, 3–4, 409–22.
- [137] Dybczynski R, Kulisa K. Effect of temperature and the mechanism of zone spreading during cation-exchange separation of rare earth elements by ion chromatography. *Chromatographia* 2005, 61, 11–12, 573–80.
- [138] Matsumiya H, Inoue H, Hiraide M. Separation of Gd-humic complexes and Gd-based magnetic resonance imaging contrast agent in river water with QAE-sephadex A-25 for the fractionation analysis. *Talanta* 2014, 128, 500–4.
- [139] Li SQ, Hu B, Jiang ZC, Liang P, Li X, Xia LB. Selective separation of La³⁺ and lanthanum organic complexes with nanometer-sized titanium dioxide and their detection by using fluorination-assisted electrothermal vaporization ICP-AES with in-situ matrix removal. *Environ Sci Technol* 2004, 38, 7, 2248–51.
- [140] Jon GG, Pu XL, Jiang ZC, Hu B. Separation/preconcentration of trace rare earth elements by micro-column packed with immobilized 1-phenyl-3-methyl-4-bonzoil-5-pyrazone on nanometer Al₂O₃ and their determination by inductively coupled plasma-atomic emission spectrometry. *Chin J Anal Chem* 2005, 33, 2, 207–10.

- [141] Meng MJ, Meng XG, Liu Y, et al. An ion-imprinted functionalized SBA-15 adsorbent synthesized by surface imprinting technique via reversible addition-fragmentation chain transfer polymerization for selective removal of Ce(III) from aqueous solution. *J Hazard Mater* 2014, 278, 134–43.
- [142] Zhang N, Hu B, Huang CZ. A New ion-imprinted silica gel sorbent for on-line selective solid-phase extraction of Dysprosium(III) with detection by inductively coupled plasma-atomic emission spectrometry. *Anal Chim Acta* 2007, 597, 1, 12–8.
- [143] An J, Shade CM, Chengelis-Czegan DA, Petoud S, Rosi NL. Zinc-adeninate metal-organic framework for aqueous encapsulation and sensitization of near-infrared and visible emitting lanthanide cations. *J Am Chem Soc* 2011, 133, 5, 1220–3.
- [144] Yan P, He M, Chen BB, Hu B. Restricted accessed nanoparticles for direct magnetic solid phase extraction of trace metal ions from human fluids followed by inductively coupled plasma mass spectrometry detection. *Analyst* 2015, 140, 12, 4298–306.
- [145] Arthur CL, Pawliszyn J. Solid Phase Microextraction with thermal desorption using fused silica optical fibers. *Anal Chem* 1990, 62, 2145–8.
- [146] Kumar A, Gaurav Malik AK, Tewary DK, Singh B A Review on development of solid phase microextraction fibers by sol-gel methods and their applications. *Anal Chim Acta* 2008, 610, 1, 1–14.
- [147] Ouyang G, Pawliszyn J. A Critical review in calibration methods for solid-phase microextraction. *Anal Chim Acta* 2008, 627, 2, 184–97.
- [148] Kumar A, Malik AK. A review on the hyphenation of solid phase microextraction with capillary electrophoresis and mass spectrometry, *Crit Rev Anal Chem* 2009, 39, 2, 81–8.
- [149] Musteata FM, Pawliszyn J. Bioanalytical Applications of solid-phase microextraction. *TRAC Trends Anal Chem* 2007, 26, 1, 36–45.
- [150] Eisert R, Pawliszyn J. Automated In-tube Solid-phase microextraction coupled to high-performance liquid chromatography. *Anal Chem* 1997, 69, 3140–7.
- [151] Kataoka H, Narimatsu S, Lord HL, Pawliszyn J. Automated in tube solid-phase microextraction coupled with liquid chromatography/electrospray ionization mass spectrometry for the determination of beta-blockers and metabolites in urine and serum samples. *Anal Chem* 1999, 71, 19, 4237–44.
- [152] Li W, Fries DP, Malik A. Sol-gel stationary phases for capillary electrochromatography. *J Chromatogr A* 2004, 1044, 1–2, 23–52.
- [153] Wu SW, Hu CG, He M, Chen BB, Hu B. Capillary microextraction combined with fluorinating assisted electrothermal vaporization inductively coupled plasma optical emission spectrometry for the determination of trace lanthanum, europium, dysprosium and yttrium in human hair. *Talanta* 2013, 115, 342–8.
- [154] Zhang L, Chen BB, He M, Hu B. Polymer Monolithic Capillary microextraction combined on-line with inductively coupled plasma mass spectrometry for the determination of trace rare earth elements in biological samples. *J Sep Sci* 2013, 36, 13, 2158–67.
- [155] Liu XL, Chen BB, Zhang L, et al. TiO₂ nanoparticles functionalized monolithic capillary microextraction online coupled with inductively coupled plasma mass spectrometry for the analysis of Gd ion and Gd-based contrast agents in human urine. *Anal Chem* 2015, 87, 17, 8949–56.

Beibei Chen, Man He, Huashan Zhang, Zucheng Jiang and Bin Hu

4 Chromatographic Techniques for Rare Earth Elements Analysis

Abstract: The present capability of rare earth element (REE) analysis has been achieved by the development of two instrumental techniques. The efficiency of spectroscopic methods was extraordinarily improved for the detection and determination of REE traces in various materials. On the other hand, the determination of REEs very often depends on the preconcentration and separation of REEs, and chromatographic techniques are very powerful tools for the separation of REEs. By coupling with sensitive detectors, many ambitious analytical tasks can be fulfilled.

Liquid chromatography is the most widely used technique. Different combinations of stationary phases and mobile phases could be used in ion exchange chromatography, ion chromatography, ion-pair reverse-phase chromatography and some other techniques. The application of gas chromatography is limited because only volatile compounds of REEs can be separated. Thin-layer and paper chromatography are techniques that cannot be directly coupled with suitable detectors, which limit their applications. For special demands, separations can be performed by capillary electrophoresis, which has very high separation efficiency.

4.1 Introduction

Separation of rare earth elements (REEs) is essential to promote the development of REEs industry. Due to the similar properties of REEs, conventional separation methods such as extraction and coprecipitation cannot achieve the separation of single REE. Chromatography (including liquid chromatography (LC) and gas chromatography (GC)) and capillary electrophoresis (CE) techniques are powerful separation techniques with high separation resolution and have been successfully applied in separation of REEs. Among them, LC is the most widely used technique because it has the advantages of various separation modes, robustness, fast separation and so on. Ion exchange chromatography (IEC) is the most suitable LC separation mode for REE ions. Besides IEC, ion chromatography (IC), ion-pair reverse-phase chromatography (RPC), extraction chromatography and centrifugal partition chromatography have also been used for the separation of REEs. GC is only suitable for the separation of volatile or semi-volatile compounds. Therefore, it is not an optional separation technique for the separation of REE ions. CE is a good choice for the separation of charged REE ions. Compared with LC, CE presents better separation resolution, but it is less robust and the absolute limits of detection are relatively high. Therefore, the application of CE on separation of REEs is not as wide as that of LC. In this chapter, the state of art about the

applications of chromatography and CE to the separation of REEs will be introduced, and the emphasis is laid on the applications of LC.

4.2 Liquid chromatography

LC method is the dominant method in the separation of REEs with high separation resolution. Modern LC methods can be classified into two types: column chromatography and planar chromatography. The representative for former one is high-performance liquid chromatography (HPLC), which was the most important development in LC during 1960s and was first applied to the separation of REEs in 1972 utilizing an ion exchange mode [1]. In addition to ion exchange mode, other LC separation modes, including IC, ion pair chromatography (IPC), normal and reverse-phase (RP) LC, extraction chromatography and centrifugal partition chromatography, have also been used for separation and determination of REEs, which greatly promoted the development of rare earth industry. Thin-layer chromatography (TLC) and paper chromatography (PC) are assigned to planar chromatography. These methods used to be important means for the separation of REEs before 1960s, while their application gradually decreased since the introduction of HPLC. When compared with planar chromatography methods, HPLC effectively shortens the analytical time. Moreover, HPLC can be easily combined with various detection techniques such as photometry, fluorescence spectrometry, inductively coupled plasma-optical emission spectrometry/mass spectrometry (ICP-OES/MS) and electrochemical detection, and the detection sensitivity toward REEs can be greatly improved. Thus, HPLC is widely used in the separation and analysis of REEs. Among all the HPLC methods, IEC and RP ion pair chromatography (RPIP) are the most widely used methods.

4.2.1 Ion-exchange chromatography

With ion-exchange resin as stationary phase, IEC is the main method for the analysis of REEs. It is mainly used for the separation of rare earth impurities from single rare earth matrix. Since Sisson et al. [1] successfully realized the HPLC separation of REEs with ion-exchange resin as stationary phase in 1972, IEC is more and more widely used in the separation of REEs.

4.2.1.1 Ion exchanger

The stationary phase used in IEC is the ion exchanger, mainly strong acidic cation exchange resin (such as styrene–divinylbenzene copolymer) and strong basic anion exchange resin (organic resin). According to the physical structure of resin, the ion exchanger can be divided into micro-reticular resin, macro-reticular resin, thin-shell mold resin, porous covering resin, directly synthesized chelating resin and

supported resin. Micro-reticular resin and macro-reticular resin are often used in classical IEC separation of REE, whereas the thin-shell mold resin, macro-reticular resin and bonded-phase porous ion exchanger are usually applied in high-performance IEC separation of REE.

Organic resin

Micro-reticular and macro-reticular ion exchange resin.

Micro-reticular ion exchange resin, also known as gel resin, is a kind of traditional common resin. This resin is full of micropores with small porosity and pore size uniformity. The pore size is determined by the cross-linking degree. When the cross-linking degree is more than 8 %, the pore size is less than 50 Å and a high exchange capacity is achieved (4.5–5.0 mmol/g for cation resin and 3.5–4.0 mmol/g for anion resin).

Macro-reticular ion exchange resin has large pore size and high surface area. Not only the gel pores but also the tunnel macropores (pore size larger than 200–1,000 Å) exist in the skeleton structure of this kind of resin. The macroporous resin shows cavities under dry or swelling state, while the cavities of microporous resin only appear under the swelling state. Although the surface area of macroporous resin is large, the exchange capacity is low. With high permeability for large organic ions and stable swell-shrinking property in different eluents, the macroporous resin is quite suitable for ion exchange separation in organic solvent. Hoehlein et al. [2] employed macroporous resin Aminex A-5 and common resin Dowex AG-X8 for separation of La, Ce, Pr, Nd, Pm, Sm and Eu. The results showed that the theoretical plate number of macroporous resin is dozen times of common resin, and both the separation efficiency and the purity of obtained rare earths are relatively high. Dowex 50W-X8 and AG 50W-X were also successfully used for the separation of REEs [3, 4].

Exchange resin with thin shell

It is a type of ion exchange resin with core-shell structures. The core is a polystyrene rigid particle with low cross-linking degree (2–5 %) and a diameter of 10–30 µm, which is a hydrophobic inert nuclei without any exchange groups. The coating is a thin sulfonated or aminated resin film. Since the exchange groups are on the surface of resin, it has good permeability, high exchange speed and high resolution. Besides, due to the rigidity of the inside core, swelling or shrinkage deformation of the resin is limited and the resin can be used in a wide pH range. Thus, the exchange resin with thin shell is an appropriate alternative for the carrier of high-performance IEC stationary phase. The limitation of exchange resin with thin shell is that the exchange capacity is low. In order to avoid the ion diffusion toward resin center, the layer of ion exchange resin such as HC-Pellionex-SCX and AS-Pellionex-SAX [5] was coated on the surface of small glass beads or silicon dioxide particles.

Silica gel-based ion exchanger

Total porous silica gel and surface-covered silica gel are the two main kinds of silica gel used as carrier of ion exchanger. They belong to bonded-phase porous ion exchanger. To form silica gel-based ion exchanger, the porous silica gel was covalently bound with alkyl or aryl and then grafted with quaternary amine or sulfonic acid group. With small particles (5–10 μm) of silica gel as carrier, the ion exchanger has a good chromatographic performance and high exchange capacity. This kind of ion exchanger could bear high column pressure and achieve rapid analysis; its physical and chemical parameters are easy to control, but it only can be used in acidic pH range. With α -hydroxyisobutyric acid (α -HIBA) as the eluent, a separation of REEs was realized on Nucleosil SA series of silica gel (10 μm particle size) based sulfonic acid cation exchanger [6].

The above-mentioned resins can be chosen according to different target analytes. Resin with thin shell is the primary choice for the separation of simple mixtures. For the samples that are difficult to separate or large sample injection dosage is required, bonded-phase porous ion exchanger with particle size of 5–10 μm is a better choice. In some REEs separation, high stability of columns is required and the common ion exchange resin with diameter of 10 μm is generally used. Table 4.1 lists the characteristics of the above-mentioned ion exchange resins.

Chelating agent-loaded resin

Chelating agent-loaded resin, also known as chelate-forming resin or modified chelating resin, is a novel selective ion exchange resin. The selectivity of chelating

Table 4.1: The characteristics of several ion exchangers.

Characteristic	Thin-shell mold resin	Bonded-phase porous resin	Polystyrene-divinylbenzene resin
Diameter (μm)	30–40	5–10	7–10
Exchange capacity (mmol/g)	0.01–0.1	0.5–2	3–5
Anti-deformability and anti-pressure capability	Best	Good	Poor ^a
Shape	Spherical	Spherical or amorphous	Spherical
Pressure drop	Low	High	Highest
Separation efficiency	Moderate	High	Low
Packing way	Dry-type filling	Homogenization	Homogenization
pH range	2–7.5	2–7.5	0–12 (anionic) 0–14 (cationic)
Regenerative speed	Fast	Moderate	Slow

^aDepends on the difference of cross-linking degree.

agent-loaded resin is similar to that of the chelating agent when using for the enrichment of metal ions. Besides, it is easy to prepare. The reported chelating agent-loaded resins are divided into strong basic anion exchange resin and nonpolar adsorption resin based on the resin matrix. And the chelating agents loaded on the two types of resins were water-soluble and hydrophobic agents, respectively.

There are mainly two kinds of mechanism for the adsorption of chelating agent on resin: anion exchange [7] and surface adsorption [8]. Besides anion exchange contributing to the adsorption of chelating agent on anion exchange resin, molecular adsorption between the chelating agent and the resin is another important factor for the adsorption which is highly related to the molecular structure.

The stability of chelating agent-loaded resin is one of the most important factors to evaluate the performance of resin, and it directly affects the separation and detection of REEs and the regeneration of resin. The stability is dependent on the structure of chelating agents. To obtain a stable chelating agent-loaded resin, the chelating agent should have anionic groups and big conjugate system. In addition, different types of anion exchange resin as the carrier also have an influence on the stability. Generally, the stability of a strong base anion resin is better than a weak base anion resin. Moreover, the common anions such as NO_3^- , Cl^- , SO_4^{2-} , ClO_4^- and Ac^- and their concentration also affect the stability of loaded resin. The order of the effect of these anions corresponds to their order in affinity to the resin [9]. Trichloroarsenazo- and tribromoarsenazo-loaded resins have good stability and have been used in the separation of REEs.

The mixture of di(2-ethylhexyl)phosphoric acid (P204) and 2-ethylhexyl hydrogen 2-ethylhexylphosphonate (P507) is a very strong complexing agent and can be used in acidic solution. After loading on C18 silica gel, the resin was packed in a column and applied for the preconcentration and separation of REEs from the seawater followed by the ICP-MS detection [10].

Chelating resin

Chelating resin is usually synthesized by chemical bonding of the chelating agent or the functional groups on the polymers, resulting in good selectivity. For example, polystyrene–divinylbenzene (PS-DVB)-based Amberlite XAD-2 resin functionalized with *ortho*-vanillin thiosemicarbazone [11] exhibits good chemical stability, selectivity, reusability and fast equilibration rate for Th and U.

4.2.1.2 Basic properties of ion exchange resins

Cross-linking degree

The cross-linking degree of PS-DVB-based ion exchange resin was expressed by the percentage of divinylbenzene, which is the cross-linking agent of resin. A stereoscopic network structure could be formed in the long chain of polystyrene by adding the cross-linking agent. The cross-linking degree of polymeric ion exchange resin is usually ranging from 4 % to 12 %, while it is 8 % for the commonly used ion exchanger

in typical separation process. The property of resin is greatly affected by the cross-linking degree: the resin is tough and the mass transfer is slow for REE ions at high cross-linking degree (12–16 %), while the opposite phenomenon is observed at low cross-linking degree (1–4 %). In HPLC, ion exchange resin with small particle size (5–10 μm) and 8–12 % of cross-linking degree have a relatively good separation result.

Swelling degree and thermal stability

When water is used as the mobile phase, the polymer-based ion exchange resin as stationary phase will absorb moisture and swell. The swelling degree of the ion exchanger is determined by the cross-linking degree. When the cross-linking degree is higher, the swelling degree is lower. In solution with high ionic concentration, the swelling degree is low; on the contrary, the swelling degree is high and the maximum swelling would occur in pure water. A high swelling degree is along with a large exchange capacity for the same type resin. The swelling degree of strong acid cation exchange resin is in the order of $\text{H}^+ > \text{Na}^+ > \text{NH}_4^+ > \text{K}^+ > \text{Cs}^+$; and it is in the order of $\text{F}^- > \text{OH}^- > \text{HCO}_3^- > \text{SO}_4^{2-} > \text{Cl}^- > \text{NO}_3^- > \text{Br}^- > \text{I}^-$ for the swelling degree of strong basic anion exchange resin. Furthermore, the swelling is relevant to solvent polarity, and the resin swells slightly in nonpolar solvent.

The optimal performance of resin is also limited by the temperature. Sulfonic acid resin would react slowly with water and lose the sulfonic acid at 100 °C, while sulfonate resin would be stable at 200 °C. The hydroxyl type of anion exchange resin containing quaternary ammonium group begins to decompose at 50 °C, while the ammonium type of anion exchange resin is stable at 100 °C.

Exchange capacity

Ion exchange capacity reflects the exchange ability of resin, which is equal to the concentration of measured (titrated) exchangeable groups among the network structure inside the resin, and it would change along with pH value. The relative retention value and maximum sample volume of column is also increasing with the increase of the exchange capacity of anion exchange resin. In addition, capacity factor (k') of sample is directly proportional to the ion exchange capacity that usually depends on the employed type of resin.

4.2.1.3 Mobile phase

Generally, the mobile phase of IEC should meet the following requirements: (1) it is able to dissolve various kinds of salt and acid adequately and act as buffer solution for ion exchanging at the same time; (2) it merits good selectivity for interest analytes and good separation can be achieved with a proper solvent strength. Aqueous solutions with the addition of salt are usually used as the mobile phase in IEC, such

as buffer solution and sometimes spiked with organic solvent (methanol, ethanol and acetonitrile)/water mixtures. The strength and selectivity of the mobile phase are often related to the buffer type, concentration and pH, as well as the type and quantity of organic solvent added.

Effect of ionic strength

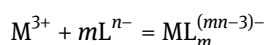
The ionic strength of the mobile phase would be increased by changing the buffer concentration (under fixed pH value) or mixing with another acid, and the solvent strength is often increased with the increase of the ionic strength. With the increase of the ions concentration in the mobile phase, competitive exchanging between ionic exchange groups and mobile phase would be increased and the sample retention is decreased accordingly.

Effect of pH value

The retention of interest analytes in IEC could also be altered by varying the pH value of mobile phase or concentration of hydrogen ions. With the increase of pH value, the retention of target analyte would decrease in cation exchange chromatography, while the retention of target analyte would increase in anion exchange chromatography. Therefore, it is a very useful means to optimize the retention performance of analytes and separation selectivity in IEC by altering pH value and H^+ concentration of mobile phase.

Selection of complexing agent in mobile phase

In a simple ion exchange system for the separation of cation or anion, the separation of ions is dominated by the retention affinity difference between ions. For REEs with similar properties, the difference between their retention affinity is not enough for their separation on the resin. In order to improve the retention difference of adjacent REEs, complexing agent (H_nL) is added into mobile phase. It could broaden the retention value of target REEs and increase the separating factor (α) by utilizing the differences of stability constant (β) of rare earth complex anions (ML^{3-n}), resulting in the separation of adjacent REEs eventually. The formation of rare earth complex anions and stability constant (β) is expressed by the following formulas:



$$\beta = \frac{[ML_m^{(mn-3)-}]}{[M^{3+}][L^{n-}]^m}$$

Distribution coefficient (K'_d) of rare earth ions in resin is as follows:

$$K'_d = \frac{[M']}{[M^{3+}] + [ML_m^{(mn-3)-}]}$$

where $[M']$ is the concentration of rare earth ions in resin. It can be obtained by combining the above formulas:

$$K'_d = \frac{[M']}{[M^{3+}]} \cdot \frac{1}{(1 + \beta[L^{n-1}]^m)}$$

There are no complex anion $ML_m^{(mn-3)-}$ if no complexing agent is added into mobile phase. In this case, distribution coefficient (K_d) shall be

$$K_d = \frac{[M']}{[M^{3+}]}$$

so that K'_d can be expressed by the following formulas:

$$K'_d = K_d \cdot \frac{1}{1 + \beta[L^{n-1}]^m}$$

From above we can see that distribution coefficient changes with formation of rare earth complex anions by adding complexing agent into mobile phase, and the separation factor (α) shall be measured by

$$\alpha' = \frac{K'_d d_2}{K'_d d_1} = \frac{K d_2}{K d_1} \cdot \frac{1 + \beta_1[L^{n-1}]^m}{1 + \beta_2[L^{n-1}]^m}$$

$$\alpha' = \alpha \cdot \frac{1 + \beta_1[L^{n-1}]^m}{1 + \beta_2[L^{n-1}]^m}$$

where α and α' refer to the rare earth separation factor without and with the addition of complexing agent. As can be seen, the separation factor will change with the variation of complexing constant. Hence, adding appropriate complexing agent into mobile phase can increase the separation factor according to the following formula:

$$R_s = \frac{1}{4} \frac{\alpha - 1}{\alpha} \frac{k}{k - 1} \sqrt{N}$$

where N refers column plate number, k refers capacity factor and R_s refers resolution. As can be seen, R_s would vary significantly with a minor variation of the separation factor, thus affecting the retention properties of REEs remarkably. Therefore, it is important to select a proper complexing agent.

In the selection of complexing agent, big difference in stability constants between different REEs is needed. Besides, the complexing agent should be of low cost and be featured with proper solubility in the mobile phase. For separating REEs in cation exchange chromatography, complexing agent in mobile phase can be carboxylic acid, hydroxycarboxylic acid, aminocarboxyl chelating agent and so on.

Hydroxy carboxylic complexing agent

Hydroxy carboxylic acid includes α -HIBA, α -hydroxy- α -methylbutyric acid (α -H- α -MBA), lactic acid, malic acid and glycolic acid. The first three were the most frequently used complexing agents. The separation factors for adjacent REEs in cation exchange chromatography by using hydroxy carboxylic acid as eluent are shown in Table 4.2.

α -HIBA is also named as α -hydroxy- α -methylpropionic acid. As early as 1956, Choppin et al. [12] used α -HIBA as eluent in cation exchange chromatography to separate actinide and lanthanide elements. It could be complexed with rare earth ions rapidly with many advantages such as small temperature coefficient, large separation factor and good separation uniformity. α -HIBA can separate adjacent REEs effectively at room temperature and it is the most effective and widely used eluent [13, 14]. But it was difficult to separate Y and Dy because of their small separation factor. The slight change of concentration and acidity of α -HIBA elution has a great influence on the separation effect of REEs; thus, these influencing factors should be controlled strictly.

Table 4.2: The separation factors of cation exchange chromatography for the separation of adjacent REEs by using hydroxy carboxylic acid as eluent [26, 27].

Adjacent REEs	α -HIBA		α -H- α -MBA	Lactic acid	
	25 °C	87 °C	87 °C	25 °C	87 °C
La–Ce	2.1	2.1	3.0	2.10	1.83
Ce–Pr	1.7	1.7	1.6	2.04	1.73
Pr–Nd	1.4	1.5	1.4	1.38	1.36
Nd–Pm	1.6	1.5	1.4	1.38	1.36
Pm–Sm	1.7	1.7	1.8	1.32	1.32
Sm–Eu	1.9	1.7	2.0	1.20	1.28
Eu–Gd	1.5	1.4	1.4	1.04	1.22
Gd–Tb	1.9	1.9	1.9	1.50	1.73
Tb–Dy	1.8	1.8	1.8	1.65	1.56
Dy–Ho	2.0	1.6	1.8	1.45	1.38
Ho–Er	1.4	1.3	1.3	1.60	1.52
Er–Tm	1.6	1.4	1.7	1.55	1.47
Tm–Yb	1.5	1.4	1.4	1.54	1.43
Yb–Lu	1.4	1.3	2.4	1.40	1.31
Y–Ho	1.77	1.56	1.67		
Y–Dy	1.10	1.04	1.10		

The melting point of α -H- α -MBA is 675 °C, the dissociation constant is 1.87×10^{-4} (30 °C), the solubility is 1.679 g/L in water and the solubility of its sodium salt is 61.9 g/L (30 °C). As shown in Table 4.2, α -H- α -MBA has a better separation effect. It has been used as eluent for the separation of heavy REEs in cation exchange chromatography.

Lactic acid is also named as 2-hydroxypropionic acid. The melting point of lactic acid is 16.8 °C. With large temperature coefficient, lactic acid should be used at higher temperature (70–95 °C) and its separation factor is smaller than α -HIBA as shown in Table 4.2. Due to its self-polymerization, the separation repeatability of lactic acid is poor.

Complexing agents other than α -HIBA may be superior for certain separations (e.g., a particular detection system) or, indeed, for the separation of a particular combination of lanthanides. In the determination of individual lanthanides in rare earth ores and high-purity lanthanide reagents by HPLC-ICP-OES, using an IEX-210 SC cation exchanger, a concentration gradient of aqueous ammonium lactate was chosen [15] as the mobile phase. This eluent was preferred to be the common aqueous solutions of α -HIBA (or citrate, or EDTA) as the latter clogged the ICP torch. The ammonium lactate eluent produced efficient separations of the lanthanides. The mobile phase flow rate was adjusted to achieve a compromise between the requirements of HPLC for low flow rates for maximum column efficiency and that of ICP for high flow rates for strongest emission intensities. Comparative evaluation of three hydroxycarboxylic acids for the separation of lanthanides has been tested by Raut et al. [16]. α -HIBA was found to be the best for separation of heavier lanthanides (Tb to Lu), while α -H- α -MBA led to a better separation for lighter lanthanides (La to Eu). All the 14 lanthanides were separated by gradient HPLC employing both α -HIBA and α -H- α -MBA.

Aminocarboxyl chelating agent

Aminocarboxyl chelating agent such as ethylenediaminetetraacetic acid (EDTA), hydroxyethyl ethylenediamine triacetic acid, diethylenetriaminepentacetic acid (DTPA) and nitrilotriacetic acid (NTA) have been used as eluent in ion exchange separation of REEs. The complex of aminocarboxyl chelating agent with REEs is stable and the separation factor between adjacent REEs is relatively large, which is beneficial to the separation. Separation and analysis of the europium–gadolinium couple was achieved by adding EDTA into mobile phase of IEC [17]. However, both the formation speed and the dissociation speed of the complex are slow, which affect the speed of ion exchange and lead longer elution time, so the application of aminocarboxyl chelating agent on the separation of REEs is rare.

On the other hand, oxalic acid has been also used as chelating agent in the mobile phase with anion exchangers [18]. Oxalic acid forms negatively charged complexes with REEs that are separated by anion exchange chromatography. In this case, a reverse order of elution was produced, since La forms a weaker complex than Ce or Lu. The order of elution in this case is $La < Ce \ll Lu$.

4.2.1.4 Application of IEC in separation of REEs

In 1972, Sisson et al. [1] used AG 50W ion exchange resin as stationary phase and α -HIBA as mobile phase and realized the HPLC separation of REEs. From then on, IEC is widely used in separation of REEs.

IEC can be used to separate the rare earth samples in meso- to micro-analysis, and also the purification of single rare earth sample. It is a main method for the analysis of REEs and mainly used for the separation of rare earth impurities from single rare earth matrix. Table 4.3 lists the applications of IEC in separation of REEs.

In separation of REEs, cation exchange chromatography has been used more extensively. Anion exchange has not been as popular as cation exchange for REE separations because column performance is generally poorer than for separations based on cation exchange chromatography.

Rollin et al. [19] used IonPac CS10 column as stationary phase, 1 mol/L HCl and α -HIBA as mobile phase with gradient elution and post-column derivatization with Arsenazo III, and realized the separation of uranium, thorium and lanthanide elements by the detection of ultraviolet (UV) at 650 nm. This method could be used for the determination of lanthanide and actinide elements in nuclear materials. Schwantes et al. [20] used CS-3 cation exchange resin as stationary phase and α -HIBA with different concentration and pH as mobile phase, realized the separation of five pair of lanthanide elements (Tm/Er, Gd/Eu, Eu/Sm, Sm/Pm and Pm/Nd) in 15 min and the separation factor was more than 2.8. Recently, Borai et al. [21] developed a new method for group separation of some heavy metals from REEs followed by online sequential individual separation of REEs with a combination of chelation chromatography and ICP-OES. In this study, various chelating agents such as DTPA, PDCA (2,6-pyridinedicarboxylic acid), NTA, α -HIBA and oxalic acid were used as mobile phases, and the elution capability and separation efficiency of the investigated eluents are mainly dependent on the number of carboxylic acid and geometrical structures. The results showed that heavy REEs and intermediate REEs could be efficiently separated by using 0.001 mol/L NTA at pH 3, while light REEs were separated by using 0.005 mol/L α -HIBA at pH 4 followed by 0.001 mol/L PDCA at pH 2.

The separation of the same type of metal chelates on dynamically coated cation or anion exchange columns introduces additional possibilities for improving the resolution. In the ion interaction technique, the exchange sites are dynamically coated on an RP C18 column using oxalate tetrabutylammonium [22] as mobile phase and the separation is performed by an ion pair mechanism. The cation or anion exchange sites in the ion interaction method are similar to cation or anion exchange mode. However, the sulfonic acid or ammonium exchange sites functionality is achieved by the octanesulfonate or tetrabutylammonium added together with the eluent.

On the other hand, a reversed chromatographic system where chelation takes place at the surface of the stationary phase or the so-called high-performance chelation IC has attracted attention over the last decade, mainly due to the development of new efficient chelating exchange substrates. The chelating exchangers, as iminodiacetate functional groups [23], usually exhibit the opposite effect to cation exchange

Table 4.3: Application of IEC in separation of REEs.

Target analytes	Exchange materials or chromatographic column	Mobile phase	Comments	Ref.
REEs	Shimadzu model LC-3A stainless steel column pack with strong cation exchange resin (IEX-210SC)	0.4–1.0 mol/L ammonium lactate (pH 4.22)	HPLC coupled with ICP-OES detection	[15]
Lanthanide and actinide elements	IonPac CS10 cation exchange column	1 mol/L HCl and α -HIBA	Post-column derivatization with Arsenazo III and spectrophotometric detection at 650 nm	[19]
Neighboring lanthanide elements	CS-3 Dionex cation exchange column	α -HIBA with different concentration and pH	Dionex IC-2500 HPLC, post-column derivatization with 4-(2-pyridylazo)resorcinol (PAR)	[20]
REEs	Dowex 50W-X8 cation exchange	0.001 mol/L NTA at pH 3 (heavy REEs and intermediate REEs); 0.005 mol/L α -HIBA at pH 4.5 followed by 0.001 mol/L PDCA at pH 2 (light REEs)	Group separation of heavy metals from REEs followed by online individual separation of REEs	[21]
REEs	Hydrophilic polymer-based NTA gel	16–80 mmol/L HNO ₃	Post-column derivatization with Arsenazo III and spectrophotometric detection at 658 nm; ICP-MS detection	[23]
Separation of Y from REEs	Kromasil 100 C18 reversed-phase column	0.5–4 mmol/L NTA + 0.8–16 mmol/L TBAOH + 2–130 mmol/L NaCl pH = 2.3–6.0	Post-column derivatization with Arsenazo III and spectrophotometric detection at 658 nm	[24]
REEs	Conventional anion exchange chromatographic column (IonPac AS9-HC)	5 mmol/L EDTA (pH 5.5–7.5)	ICP-MS detection	[25]
Lu, Tb, Tm, Er, Ho, Dy and Tb	Modified silica gel with chemically bound phosphonic acid	80 mmol/L α -HIBA, 5 mmol/L SDS (pH 3.5)	HPLC (flow rate, 0.75 mL/min); post-column derivatization with Arsenazo III and spectrophotometric detection at 660 nm	[26]

affinity for the REEs and give rise to the possibility of isocratic separation. Dybczynski et al. [24] developed a new RP-HPLC method for selective separation of yttrium from all REEs by employing NTA as a complexing agent in anion exchange mode. In the new RP-HPLC system with C18 column, tetra-*n*-butyl ammonium hydroxide (TBAOH) as an ion interaction reagent and NTA as a complexing agent enable baseline separation of yttrium from light and heavy REEs.

Traditionally, REEs are detected by post-column spectrophotometric reaction with strongly absorbing chromophores such as 4-(2-pyridylazo)resorcinol (PAR) or Arsenazo III, but the use of ICP-OES [15] and ICP-MS [25] detection has been increased in the recent years.

4.2.2 Ion chromatography

Since its commercial introduction in 1975 [27], IC has been recognized as a very useful tool for analyzing a broad range of cations and anions with excellent speed and sensitivity. The IC system usually consists of two ion exchange columns (separating column and suppressor column) and electric conductivity detector; the separation of the analytes is achieved in the separating column; and the suppressor column absorbs counterions that interfere with the conductivity detection system. However, it was not particularly suitable for many metal ions including REEs because the hydroxide-type suppressor column precipitated the metal hydroxides. With the development of non-suppressed IC, the suppressor column is eliminated from the system by carefully choosing the ion exchanger and eluent solution of low ionic strength as the mobile phase. This modification made the IC determination of REEs available. And then IC can be divided into two types: double-column IC (suppressed IC) and single-column IC (non-suppressed IC) system.

4.2.2.1 Principle of the method

Taking the detection of the cation (such as monovalent cation) as an example, the eluent is diluted HCl or HNO₃, the separation column is packed with H⁺-type cationic exchange resin (R-SO₃⁻H⁺) with low exchange capacity and the suppression column is packed with strong basic anionic exchange resin (R-N⁺OH⁻) with high exchange capacity. The reaction on the separation column is $\text{RSO}_3^- \text{H}^+ + \text{Y}^+ \text{Cl}^- \rightarrow \text{RSO}_3^- \text{Y}^+ + \text{H}^+ \text{Cl}^-$, then all kinds of cations are separated based on the different affinity with the resin; the reaction of elution on the suppression column is $\text{R-N}^+ \text{OH}^- + \text{H}^+ \text{Cl}^- \rightarrow \text{R-N}^+ \text{Cl}^- + \text{H}_2\text{O}$, and water of low conductivity is eluted from the column; then the reaction of the determined cation (Y⁺) is $\text{R-N}^+ \text{OH}^- + \text{Y}^+ \text{Cl}^- \rightarrow \text{R-N}^+ \text{Cl}^- + \text{Y}^+ \text{OH}^-$. Therefore, the determined cation turns into hydroxide that dissolves in water and then was eluted from the column. Compared with water, the hydroxide has higher conductivity. The different hydroxides produce different response signals when they enter the electric conductivity detector and then a cationic chromatogram is obtained.

For anion (such as Cl^- and NO_3^-) detection, the eluent is diluted sodium hydroxide, and the separation column is loaded with OH^- -type cationic exchange resin with low exchange capacity. The reaction of the determined anion (X^-) in the separation column is $\text{R}\cdot\text{N}^+\text{OH}^- + \text{Na}^+\text{X}^- \rightarrow \text{R}\cdot\text{N}^+\text{X}^- + \text{Na}^+\text{OH}^-$. The suppression column is loaded with cationic resin (RSO_3^-H^+) with high exchange capacity, which reacts with the elution containing separated anions: $\text{RSO}_3^-\text{H}^+ + \text{Na}^+\text{OH}^- \rightarrow \text{RSO}_3^-\text{Na}^+ + \text{H}_2\text{O}$; $\text{RSO}_3^-\text{H}^+ + \text{Y}^+\text{Cl}^- \rightarrow \text{RSO}_3^-\text{Na}^+ + \text{H}^+\text{X}^-$. In this case, the determined anions turn into acid and enter the electric conductivity detector together with water, then different response signal is produced and an anionic chromatogram is obtained.

In IC, both the separation column and the suppressor column are packed with ion exchange resin. According to the features of this method such as narrow range of target concentration (10^{-9} – 10^{-6}), small inject volume (<100 μL) and short analytical time, the ion exchange resin should meet these requirements: small-sized spherical particle, high stability under the high pressure, good mass transfer effect and fast equilibrium; sharp peak would be obtained after fast ion exchanging in the mobile phase; low degree of swelling and shrinkage, good chemical stability and thermo-stability; properly lowering exchange capacity that makes good resolution and short separating time. Table 4.4 shows the comparison of the resin used in IC and IEC.

4.2.2.2 Double-column IC

Double-column IC is also named suppressed IC. It consists of the separation column, the suppression column and the electric conductivity detector. According to the interest, analytes with different charges can be classified into anion chromatography and cation chromatography.

In double-column anion chromatography, the packing materials in the separation column are usually a covered type of aminated anion exchange resin, and the packing materials in the suppression column are strong acidic cation exchange resin with high capacity (hollow fiber membrane suppressor and tablet micro-membrane suppressor were employed later). The elution is a strong base–weak acid salt with low concentration, such as Na_2CO_3 , NaHCO_3 , NaB_4O_7 and sodium phenoxide.

Table 4.4: The comparison of the resin used in IC and IEC.

The resin used in IEC	The resin used in IC
Capacity is 3–5 mmol/g	Capacity is 0.02 mmol/g
Large swelling	Small swelling
More diffusion paths	Less diffusion paths
High sample concentration	Low sample concentration
High elution concentration	Low elution concentration
Wide peak	Narrow peak

As for double-column cation chromatography, the separation column is packed with sulfonated styrene–divinylbenzene copolymer-coated thin-shell cation exchange resin with low exchange capacity, and the suppression column is packed with strong base anion exchange resin with high exchange capacity. The strong acid solution (such as HCl and HNO₃) at low concentration is often used as the eluent and assisted by low-concentration appropriate salt solution. However, this method is only applicable to alkali metal, ammonium, alkaline earth metal and organic amine. Cations that have precipitation reaction in the alkaline suppression column, for example, heavy metal, transition elements and REEs, are not suitable for this method.

4.2.2.3 Single-column IC

Single-column IC, also called non-suppressed IC, can be divided into single-column anion chromatography and single-column cation chromatography. In this method, there is no suppression column, but one separation column is used throughout the process. Ion to be detected is introduced into the electric conductivity detector directly after separation. The instrument of single-column method is simple, and sharp peaks and excellent resolution can be obtained.

In single-column anion chromatography based on reducing the exchange capacity of the ion exchange resin and the eluent concentration and maintaining the retention value of the separated ion, the anion exchanger with low exchange capacity (0.007–0.04 mmol/g), small size (5–25 μm) and large aperture is employed. The eluent of this method is aromatic organic weak acid or its salt solution with low background conductance and low concentration, such as benzoic acid, citric acid, phthalate and so on. The type, concentration and pH value of the eluent will affect the separation of anion.

Single-column cation chromatography not only can separate and detect cations that can be detected by double-column method, but also can separate and detect the cations that cannot be detected by double-column method such as heavy metal, transition elements and REEs. The packing materials are mild sulfonated styrene–divinylbenzene copolymer with low exchange capacity or the silica gel bonded with sulfonated organic groups. The exchange capacity is not higher than 0.02 mmol/g and the particle size is less than 5 μm. Table 4.5 lists some commercial single-column cation chromatography column.

4.2.2.4 Application of IC in separation of REEs

Single-column method has been used for the separation of REEs and a low-capacity ion-exchange column is commonly used with an electrolyte solution of low ionic strength as the mobile phase. Sevenich et al. [28] developed a single-column method for lanthanide separation using a conductivity detector and ethylenediammonium/tartrate as eluent. The substitution of tartrate with α-HIBA improved the separation slightly and elution times, predictably, decreased with increasing atomic

Table 4.5: Some commercial single-column cation chromatography column.

Type	Particle size (μm)	Exchange material	Exchange capacity (mmol/g)	Column dimension (mm)
TSKgel IC-Cation	10	PS/SVB, thin-shell mold resin-SO ₃ groups	0.012	50 × 4.6
TSKgel IC-Cation SW	5	Silica particles, surface-SO ₃ groups	0.45	50 × 4.6
Wescan-Cation	15	PS/SVB, thin-shell mold resin-SO ₃ groups	0.02	300 × 4.6
IC-PAK Cation (waters)	15	PS/SVB, thin-shell mold resin-SO ₃ groups	0.02	300 × 4.6
YSC-2	14	PS/SVB, thin-shell mold resin-SO ₃ groups	0.017	100 × 5

Note: PS/SVB is polystyrene–divinylbenzene copolymer.

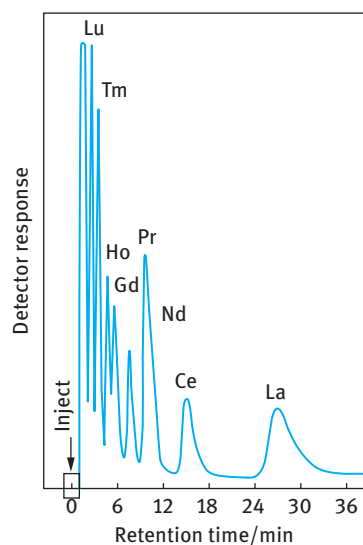


Figure 4.1: Separation of selected lanthanides (20 mg/L) on a sulfonated gel-type resin using 2 mmol/L ethylenediammonium and 2 mmol/L tartrate (pH 4.5) as eluent. Conductivity detection [28].

number (Figure 4.1). The utilization of conductivity detection necessitated an isocratic elution system, which prevented efficient separation (Figure 4.1). Unfortunately, gradient elution in this system would dramatically alter the baseline and complicate detection. Wang et al. [6] also employed non-suppressed IC for separation of the lanthanides. The system, consisting of a bonded-phase cation-exchange resin with

2-methylactic acid as eluent, was distinguished from normal cation exchange by the low ionic strength (0.01–0.04 mol/L) of the eluent. The determination is completed after post-column derivatization and detection at 600 nm.

Nesterenko and Jones [29] achieved the isocratic separation of lanthanides and yttrium by using high-performance chelation IC on iminodiacetic acid-bonded silica. The obvious advantage of this approach is the possibility of prediction of elution order of lanthanides by utilizing a large amount of published values of stability constants of different complexes for selecting a proper chelating exchanger to achieve a reasonable separation. This work also shows the high-performance chelation separations of complex metal mixtures such as the lanthanides and yttrium.

IC can be taken full advantage of in combination with element-selective detection techniques such as ICP-OES [30, 31] or ICP-MS [32–36]. In such applications, the eluent from the column is injected directly into the detection system. High sensitivity and anti-interference ability would be obtained. Neutron activation analysis (NAA) is also a reliable determination of individual REE at trace and ultra-trace levels. Dybczynski et al. [37] compared the performance of purely instrumental normal activation analysis (INAA) and radiochemical mode (RNAA) with pre- and post-irradiation group separation for the determination of individual lanthanides with the special emphasis on Gd, Ho, Er, Tm and Lu. The results showed that RNAA is able to determine all or nearly all lanthanides from one sample with reasonable accuracy in a variety of materials, while INAA is able to determine only certain members of the lanthanide series. In this work the same separation scheme was also combined with IC yielding very good results for all lanthanides and yttrium except of materials containing extremely low concentrations of REEs [38]. Earlier, they investigated the effect of temperature and the mechanism of zone spreading during cation exchange separation of REEs by IC [39], and effect of carboxylic α -hydroxyacid and temperature was also studied afterward.

IC has wide applications in the analysis of REEs and the application of high-performance IC (HPIC) to the analysis of REEs has been reviewed [40]. Automation is also a trend for IC separation of REEs. Haley and Klinkhammer [41] realized the complete separation of REEs from small volume (5 mL) seawater samples by automated IC coupled with ICP-MS detection. Meynadier et al. [42] developed an automated separation of Sr prior to isotopic analysis from liquid samples (river water, seawater or solutions resulting from natural carbonate dissolution) by using HPIC technique. Table 4.6 is the application of IC in the separation and determination of REEs.

4.2.3 Reverse-phase ion pair chromatography (RPICP)

Ion pair extraction has become a valuable liquid–liquid separation technique for isolating water-soluble ionic compounds by partitioning them between water and an immiscible liquid. The principle was extended to chromatography [44] during the

Table 4.6: Application of IC in the separation and determination of REEs.

Target analytes	Exchange materials or chromatographic column	Mobile phase	Comments	Ref.
Lanthanide elements	Bonded-phase cation-exchange resin Nucleosil SA	0.01–0.04 mol/L 2-methylactic acid	Post-column derivatization with Arsenazo I and spectrophotometric detection at 600 nm	[6]
La, Nd, Gd, Ho, Tm, Yb, Lu	Gel-type cation-exchange resins	4 mmol/L ethylenediamine and 3 mmol/L α -HIBA (pH 4.5)	Use of a masking agent EDTA and a conductimetric detector	[28]
REEs	IonPac CS5A column	Gradient elution containing oxalic acid and α -HIBA	Comparative evaluation of ICP-AES detection and UV-VIS spectrophotometric detection after post-column derivatization with PAR	[30]
REEs	Excelpak ICS-C15 column or Excelpak ICS-C35 column	α -HIBA or lactic acid	ICP-MS detection	[32]
Lanthanides and Y	Dionex IonPac CS3 column	α -HIBA	ICP-MS detection compared with neutron activation analysis (NAA) as well as IC	[34]
REEs, Am, Cs, Ce	LUNA CSX	0.13 mol/L α -H- α -MBA (pH 3.6) during 20 min; then 0.22 mol/L α -H- α -MBA (pH 4.5)	Post-column derivatization with Arsenazo III and spectrophotometric detection at 654 nm (for REEs) ICP-MS detection (for Cs)	[36]
REEs	IonPac TMC-1 column	A gradient mixture of oxalic acid and diglycolic acid	Automated HPIC coupled with ICP-MS detection	[41]
Sr	Cation exchange columns CS16 and GS16	40 mmol/L methanesulfonic acid	Automated HPIC coupled with thermal ionization mass spectrometry (TIMS) detection	[42]
Lanthanide elements	IonPac CS5 column	8–25 mmol/L oxalic acid/0–23 mmol/L diglycolic acid (pH = 3.0–5.5)	Post-column spectrophotometric detection with PAR at 520 nm, separation of 13 REEs	[43]

1970s and has been used in both the liquid–solid (adsorption) and liquid–liquid (partition) modes. Prior to 1980, normal-phase ion-pair chromatography (NPIPC) was commonly used with silica or cellulose micro-particles coated with polar stationary phases and nonpolar mobile phases containing an ion pair reagent. However, the stability of NPIPC is poor and its application is limited. The current wide popularity of IPC stems from the use of bonded micro-particulate alkyl silica as nonpolar stationary phases associated with aqueous buffers containing low concentration of the ion-pairing reagent. The latter form of IPC has shown promise for lanthanide separations, which is named RPIPC. RPIPC is developed on the basis of RPC; by the addition of ion pair reagent in mobile phase, analyte ions form weak polar ion pair with ion pair reagent and the retention value would be increased. Compared with general RPC, the retention of solute is increased and the separation selectivity and detection sensitivity are improved, which is greatly attributed to the addition of ion pair reagent.

4.2.3.1 Ion pair reagent

In RPIPC, the capacity factor of the sample is affected by the mobile phase composition, pH and the ion pair reagent. In other words, the species, concentration and property of the ion pair reagent in the mobile phase are the main factors for solute retention and isolation. The ion pair reagent includes cationic and anionic reagents. Some ion pair reagents that commonly used in rare earth separation are listed in Table 4.7.

In the analysis of REEs by RPIPC, alkyl sodium sulfonate and alkyl sodium sulfate are widely used ion pair reagents. IPC of the 2-hydroxy-2-methylpropionic acid and ammonium 2-hydroxy-2-methylpropionate complexes with a C18 phase pretreated with sodium eicosyl sulfate, ammonium dodecyl sulfate and ammonium octanesulfonate has been used for REE separation, respectively.

Table 4.7: Ion pair reagents commonly used for rare earth separation.

	Name	Molecular formula	Number of carbon atoms
Anions	1-Butyl sulfonate	$1\text{-CH}_3(\text{CH}_2)_4\text{SO}_3^-$	4
	1-Hexyl sulfonate	$1\text{-CH}_3(\text{CH}_2)_5\text{SO}_3^-$	6
	1-Octyl sulfonate	$1\text{-CH}_3(\text{CH}_2)_7\text{SO}_3^-$	8
	1-Dodecyl sulfonate	$1\text{-CH}_3(\text{CH}_2)_{11}\text{SO}_3^-$	12
	1-Eicosyl sulfonate	$1\text{-CH}_3(\text{CH}_2)_{19}\text{SO}_3^-$	20
Cations	Tetramethyl ammonium	$(\text{CH}_3)_4\text{N}^+$	4
	Tetraethyl ammonium	$(\text{CH}_3\text{CH}_2)_4\text{N}^+$	8
	Tetraethyl ammonium	$(\text{CH}_3(\text{CH}_2)_3)_4\text{N}^+$	16
	Tetrahexyl ammonium	$(\text{CH}_3(\text{CH}_2)_5)_4\text{N}^+$	24
	Trioctyl methyl ammonium	$\text{CH}_3(\text{CH}_3(\text{CH}_2)_5)_3\text{N}^+$	25
	Tetraoctyl ammonium	$(\text{CH}_3(\text{CH}_2)_7)_4\text{N}^+$	32
	Tridecyl methyl ammonium	$\text{CH}_3(\text{CH}_3(\text{CH}_2)_9)_3\text{N}^+$	31

Knight et al. [45] used α -HIBA and octane sulfonic ion pair reagent as mobile phase in C18 RP column and achieved analysis of REEs in samples of hydrometallurgy uranium mine. Götze et al. [46] used C18 RP column as stationary phase, and tetrabutyl ammonium bromide and tetrahexyl ammonium bromide (water–methyl alcohol) as mobile phase, realizing the separation of heavy REE by the detection of REEs–EDTA complex at 220 nm. Saraswati et al. [47] used 4-(2-thiazolylazo)resorcinol as a chelating reagent in the RP-HPLC separation of transition metals from REEs in low-alloy steels by increasing the concentration of the eluent (octane-1-sulfonate-tartaric acid). Zhang et al. [48] used C18 RP column as stationary phase, and 100 mmol/L HAc and 200 mmol/L triethanolamine (methanol/water = 85/15) as mobile phase, realizing the separation of REE–tetra-kis(4-methoxyphenyl)porphyrin (TMOPP)–Cl complex, and this method is convenient and efficient.

Tsakanika et al. [49] used α -HIBA and octane sulfonic ion pair reagent as mobile phase with gradient elution and derivatization with 4-(2-pyridylazo)resorcinol post-column, realizing the separation of scandium from other REEs in laterite samples under the detection at 520 nm. Raut et al. [50] used α -HIBA and octane sulfonic natrium as mobile phase, and separated REEs from uranium and thorium in 11 min, by eliminating the interference of uranium and thorium; this method was used in the analysis of REEs in rock samples. Santoyo and Verma [51] used C18 RP column as stationary phase, and α -HIBA and octane sulfonic natrium as mobile phase with gradient elution and derivatization with Arsenazo III post-column, realizing the separation of REEs in synthesized samples in 15 min under the detection at 658 nm. Jaison et al. [52] investigated the separation of REEs in different RPC columns (C18 and C8) and with different ion pair reagents (octane sulfonate, octane sulfate, nonane sulfonate, octadecylbenzene sulfonate and eicosyl sulfate), and then used C18 RP column as stationary phase, α -HIBA as mobile phase with gradient elution and derivatization with Arsenazo III post-column, realizing the separation and detection of 14 lanthanide elements and iron, thorium and uranium.

It should be mentioned that the concentration of ion pair agent in mobile phase should not be high, or the precipitation from ion pair agent might block up the column. So the concentration of ion pair agent should be as low as possible in an appropriate range.

4.2.3.2 Application of RPIPC in the separation of REEs

RPIPC always need a certain period of time to equilibrate the column because of the addition of ion pair reagent, and the column efficiency would decrease due to long-time service. However, the utilization of RPIPC has been gradually increased because it is easy to operate and the separation efficiency is excellent.

Figure 4.2 shows the anionic chromatogram of separating REE-oxalate complexes by RPIPC [22], which was successfully employed for the determination of trace rare earth impurity in HNO_3 solution or reference material. In Supelcosil LC-18 column, 1-octanesulfonate ion pair agent was used as mobile phase of α -HIBA, which exhibits

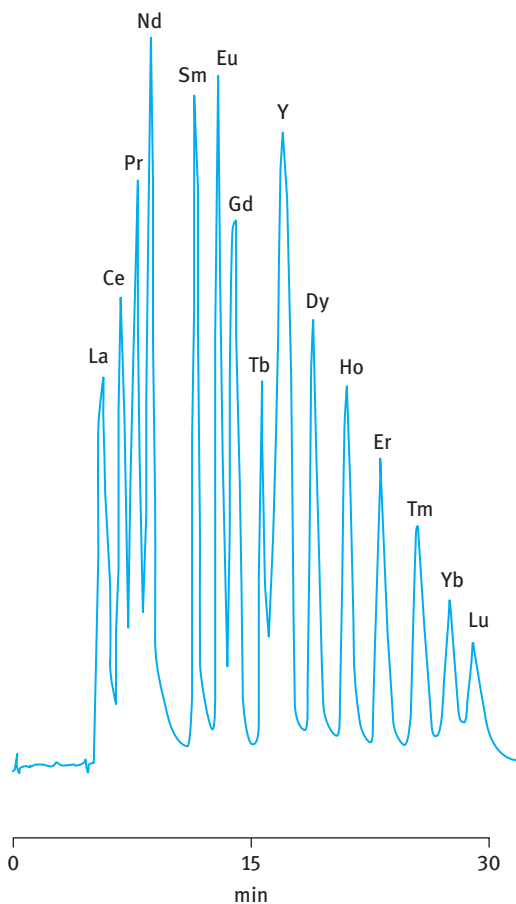


Figure 4.2: Chromatograms of separating REE-oxalate complexes by ion pair chromatography [22]. Column: Supelcosil LC-18 (5 μm , 150 \times 4.6 mm); mobile phase: 0.5 mmol/L oxalic acid–2.5 mmol/L tetrabutylammonium hydroxide (pH 4.6; detection at 658 nm following post-column derivation with Arsenazo III).

good separation performance for all REEs (Figure 4.3) [45]. This method was used for the analysis of REEs in samples of hydrometallurgy uranium mine.

By coupling RP-HPLC with ICP-MS detection, Pedreira et al. [53–56] have completed a series of work on determination of trace REE impurities in highly pure rare earth matrix. One of the major difficulties in the REEs separation is purification of yttrium from heavy REEs. With acetic acid as a novel eluent, Kifle and Wibetoe [57] realized selective separation of yttrium from the other REEs. The method is capable of baseline separation of adjacent lighter and medium lanthanide as well as yttrium. However, the separation of heavier Ln remains unsatisfactory. The method can be particularly important in preparative purification of yttrium from heavier lanthanides and

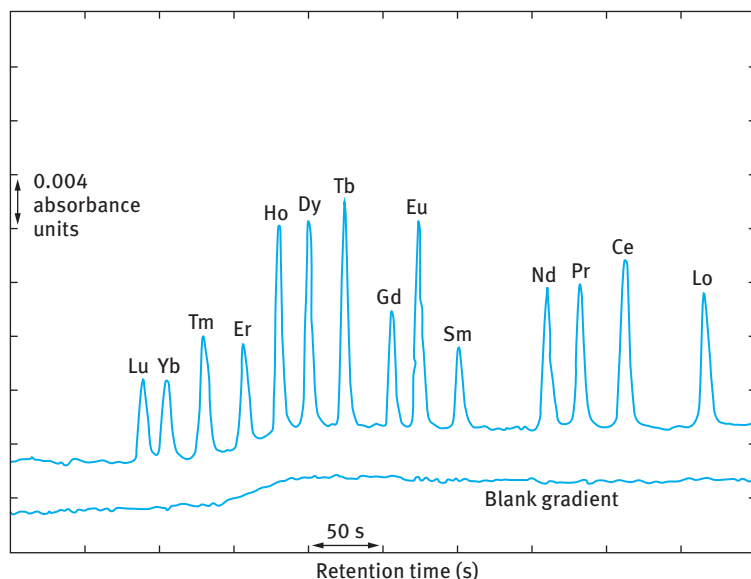


Figure 4.3: Gradient separation of the lanthanides: Supelcosil LC18 column; linear program at pH 4.6 from 0.05 mol/L HIBA to 0.40 mol/L HIBA over 10 min at 2.0 mL/min; modifier, *l*-octanesulfonate at 0.01 mol/L; detection at 653 nm after post-column reaction with Arsenazo III; sample, 5 μ L of solution containing 10 μ g/mL of each lanthanide [45].

it may also be employed for separating REEs in several subgroups as lighter, medium and heavy fractions.

Santoyo and Verma [51] proposed an RPIPC method for determining lanthanides in synthetic standards by using a linear gradient program of α -HIBA eluent (0.05–0.5 mol/L, pH at 3.8) mixed with 0.01 mol/L sodium *n*-octanesulfonate. With the aid of a weighted least-squares (WLS) regression model, the sensitivity and detection limits were estimated. It was found that the WLS method was able to compute the straight-line slopes and intercepts with considerably smaller errors than the conventional ordinary least-squares (OLS) regression method, and hence, to obtain a much better estimation of the limit of detection (LODs). They also achieved the determination of lanthanides in international geochemical reference materials by RPIPC using error propagation theory to estimate total analysis uncertainties [58].

Table 4.8 shows the application of RPIPC in REE separation. REE separation by RPIPC has attracted lots of attention due to its easily controlled separation condition, large theoretical plate number and high separation efficiency. Normally, REE complex can be hardly determined in the UV and visible regions. Thus, derivatization by chromogenic agent was used in post-column derivation. Due to the uncertainty of the retention process, IPC was described by several different proliferations of names as the following: paired ion, soap, solvent-generated ion exchange, ion association and ion interaction chromatography and dynamic ion exchange.

Table 4.8: Application of RPIPC in the separation of REEs.

Target analytes	Column	Mobile phase	Comments	Ref.
Selective separation of Y from all REEs	Kromasil 100 C18	0.5–4 mmol/L NTA + 0.8–16 mmol/L TBAOH (tetra- <i>n</i> -butyl ammonium hydroxide) + 2–130 mmol/L NaCl (pH = 2.3–6.0)	Detection after post-column derivatization with Arsenazo III	[24]
Number of fissions in thorium–uranium dioxide Fuels	Supelcosil LC-18 column	0.05–0.40 mol/L α -HIBA with 0.01 mol/L L-octane sulfonate (pH 4.6)	Detection at 653 nm after post-column reaction with Arsenazo III	[45]
Er, Dy, Eu	Silica gel 60 C8-RP	5 mmol/L phosphate buffer solution (pH 6.5) and 7.5 mmol/L (C ₄ H ₉)NCl water and methanol (99 + 1)	RP ion pair HPLC with EDTA complex	[46]
Transition and REEs	Spherisorb S-5 ODS-1 column	0.001 mol/L sodium octane–0.023 mol/L L-sulfonate-tartaric acid (pH 6.0)	Detection at 580 nm after post-column reaction with 4-(2-thiazolyazo) resorcinol (TAR)	[47]
Y, Er, Tm and Yb	YWG-C18 ODS	Methanol/water (85/15, V/V) containing 100 mmol/L HAC and 200 mmol/L triethanolamine	SPD-10AV UV-Vis detector (428 nm)	[48]
Sc and REES	Vydac 201TP5415 RP C18	0.06–0.4 mol/L α -HIBA with 0.01 mol/L sodium 1-octane sulfonate (pH 3.7)	Detection at 520 nm after post-column derivatization with PAR	[49]
Th, U	C18-RP	Dual gradient elutions of α -HIBA and sodium 1-octane sulfonate	Detection at 650 nm after post-column derivatization using Arsenazo III	[50]
Lanthanide elements in synthetic standards	C18 RP column	0.05–0.5 mol/L α -HIBA, with 0.01 mol/L sodium <i>n</i> -octanesulfonate (pH = 3.8)	Detection at 658 nm after post-column reaction with Arsenazo III	[51]
Lanthanide elements and iron, thorium, uranium	C8, C18 RP column	7 % (v/v) (0.007 mol/L) of different ion pair reagents with α -HIBA as gradient elution	Detection after post-column derivatization with Arsenazo III	[52]
Trace REEs in highly pure neodymium oxide	Shim-pack CLC-ODS column	0.7 mol/L lactic acid (pH 2.9) modified with 0.01 mol/L sodium laurylsulfonate	Detection at 655 nm after post-column reaction with Arsenazo III.	[55]
Separation of yttrium from the other REEs	0.3 mmol/L HDEHP-coated C-18 column	Isocratic elution with 0.3 mol/L CH ₃ COOH and 20 mmol/L <i>n</i> -octane sulfonate at pH 4.75	Detection at 658 nm after post-column reaction with Arsenazo III	[57]

4.2.4 Extraction chromatography

Extraction chromatography is a liquid–liquid partition chromatography that is combining solvent extraction principles with chromatographic separation technology, which is known as RP partition chromatography. It is a novel technology for the separation of REEs, which makes a great progress in separation and preparation of high-purity rare earth oxides. In this section, the extraction chromatography is focused on the reverse extraction chromatography.

In this method, the stationary phase is an organic extractant which is adsorbed on to a porous hydrophobic support and the mobile phase is a suitable solution of an acid, base or salt. The separation mechanism is unclear, which involves ion pairing, ion exchange, coordination, simple partitioning or any combination of them [13].

In 1961, Fidelis and Siekierski [59] studied extraction chromatography separation of REEs systematically both in theory and in application, which realized a complete separation for all REEs in a short time. In recent years, the separation of REEs by using extraction chromatography became less.

4.2.4.1 Support material and stationary phase

In the extraction chromatography, the support material is applied to adsorb stationary phase. Normally, solid particles are used as the support material, which have many merits such as porous, uniform pore distribution, large specific surfaces, no expansion in mobile phase and no adsorption with ions in solution. Diatomite, silica gel, poly(tetrafluoroethylene) (PTFE) and polyethylene–vinyl acetate copolymer have been used as the stationary phase supports.

Stationary phase employed mostly in extraction chromatography is organic extractant, including acidic, neutral and basic extractant. The former is mainly represented by acidic organophosphorus extractant, such as P204, P507, P215 and so on. The neutral extractant is principally neutral phosphorus extractant or sulfoxide extractant, and the basic extractant is mostly polymeric amine, also known as liquid anion exchanger. Selective separation of REEs can be attributed to studies of acidic phosphorus-based cation extractants and long-chain tertiary and quaternary amines as anion extractants. The acidic extractant has been used most frequently. An acidic extractant is preferred to a neutral extractant [e.g., trioctyl-phosphine oxide (TOPO) and tributyl phosphate (TBP)] because of larger separation factors and the need for a lower acid concentration in the mobile phase. Separations of REEs with acidic extractants are more numerous than those with neutral or basic amine extractants.

4.2.4.2 Effect of mobile phase and other conditions on separation

Inorganic acid solution is often used as mobile phase in extraction chromatography, and the selection of acid in mobile phase is crucial for accurate separation because separation factors can vary with the type of acid. HNO_3 , HCl and H_2SO_4 and the

mixture of these acids and some inorganic salt solution are commonly utilized as mobile phase.

The general conditions of LC on the separation effect are also suitable for extraction chromatography. Amount and uniformity of stationary liquid (extractant) can affect the efficiency of the chromatographic column. Vermont [60] and Horwitz and Bloomquist [61] had proposed a way to coat the extractant firmly, which improved the stability and reproducibility of chromatographic column. In general, the amount of extractant coating is greater, the theoretical plate height is higher and the column efficiency is lower. The means of elevating column temperature is usually employed to improve the column efficiency.

4.2.4.3 Application of extraction chromatography on the separation of REEs

The acidic organophosphorus extractant (such as P204, P507, P215, P229 and so on) as stationary phase of extraction chromatographic system is most commonly used for separating REEs. Acidic organophosphorus extractants (P204 and P507) have paid great attention for REEs separation. Tsuyoshi and Akiba [62] realized the separation and determination of Sm in the presence of a large amount of Nd by HPLC using RP stationary phase dynamically modified with P204. Miranda et al. [63] studied the REEs fractionation by solvent extraction by use of HPLC as an analytical control technique with P204 as the extractant. Knutson et al. [64] accomplished an overloaded one-step separation of REEs through preparative ion exchange HPLC with a P204-impregnated column and nitric acid as eluent. An ICP-MS system was used for post-column element detection.

The separation of rare earth impurities in high-purity rare earth oxides and preparation of high-purity REEs were achieved with P507 leventrel resin as stationary phase and inorganic acid solution as mobile phase to separate matrix and other rare earth impurities. Qin et al. [65] proposed a new method to determine trace rare earth impurities in high-purity CeO_2 by using electrothermal vaporization (ETV) ICP-OES after HPLC separation with P507 resin as the stationary phase. They also developed a new method for the determination of trace rare earth impurities in high-purity La_2O_3 by HPLC combined with ICP-MS [66]. The chromatographic retention behavior of La and impurities in HPLC was studied with P507 resin as the stationary phase and HNO_3 as the mobile phase. Compared with the conventional open-column method, the proposed separation system shows a good performance with regard to short separation time, low reagent consumption and simple operation. The method has been applied to the analysis of real samples of high-purity La_2O_3 with satisfactory results. Shuai et al. [67] proposed a rapid and effective method for separation and determination of trace rare earth impurities in high-purity La_2O_3 by combination of P507/HPLC separation with high-sensitive ETV-ICP-OES determination. The results showed that a selective separation of La matrix can be obtained by using P507 resin as the stationary phase and the diluted HNO_3 as the mobile phase. This HPLC system possessed a series of outstanding characteristics in rapid speed, simple operation and low

amounts of reagents consumed. Li et al. [68] adopted a single-step extraction chromatography separation method for Sm–Nd isotope analysis of micro-samples of silicate rocks by high-sensitivity thermal ionization mass spectrometry (TIMS) detection. The combination of single-stage separation with NdO^+ TIMS technique greatly improves sample throughput and reduces sample consumption. Thus, the method provides a straightforward and time-efficient way for the Nd isotope analysis in limited amount samples.

4.2.4.4 Centrifugal Partition Chromatography

Centrifugal partition chromatography is also called centrifugal countercurrent chromatography (CCC) or high-speed countercurrent chromatography (HSCCC), which is a kind of liquid–liquid extraction chromatography without the stationary phase support. On the basis of classic reflux chromatography, Murayama et al. [69] proposed a new method of centrifugal countercurrent chromatography with a rotary seal joint. The key of the method is the rotating sealing device (Figure 4.4), which is simple and applicable to the preparative separation in a short time.

Centrifugal partition chromatography is used for the separation of 2,4-dinitrobenzene derivatives of amino acids at first. Araki et al. [70] and Akiba et al. [71] separated REEs with suitable concentration of acid solution as mobile phase and P204 and P507 as stationary phase, respectively. The former separated Pr, Nd, and Er, Yb; the later realized the separation and detection of the adjacent REEs using post-column derivatization with Arsenazo III. Nakamura et al. [72] realized the mutual separation of heavy REEs by using HSCCC provided with a multilayer coiled column containing a toluene solution of 2-ethylhexylphosphonic acid (EHPA). The REEs were chromatographically eluted by a mobile phase with a stepwise pH gradient, as shown in Figure 4.5. By using CCC, they also realized the separation of yttrium from lanthanoid elements [73] and purification of yttrium [74]. Tsuyoshi et al. achieved separation of praseodymium and neodymium [75] and purification of yttrium from xenotime [76] by using HSCCC with a toluene solution containing 2-ethylhexylphosphonic acid mono-2-ethylhexyl ester (EHPA) or di(2,4,4-trimethylpentyl) phosphinic acid as stationary phase.

Wu et al. [77] investigated the effects of concentration of extractant, pH and the flow rate of mobile phase on the separation efficiency of Am and Eu by HSCCC with dichlorophenyldithiophosphinic acid in xylene as the stationary phase and 0.1 mol/L NaClO_4 as mobile phase. The results show that the separation factor increases with the increasing concentration of extractant and the pH value of the mobile phase; furthermore, decreasing the flow rate of the mobile phase can also improve the separation efficiency between Am and Eu. Mutual separation between Am^{3+} and Eu^{3+} can be accomplished by optimizing the separation condition, and the separation factor and separation efficiency between Am^{3+} and Eu^{3+} can reach 2.87 and 0.74, respectively. Hennebrüder et al. [78] developed an analytical scheme for the determination of REEs and Gd-DTPA in river water based on the preconcentration by means of CCC followed

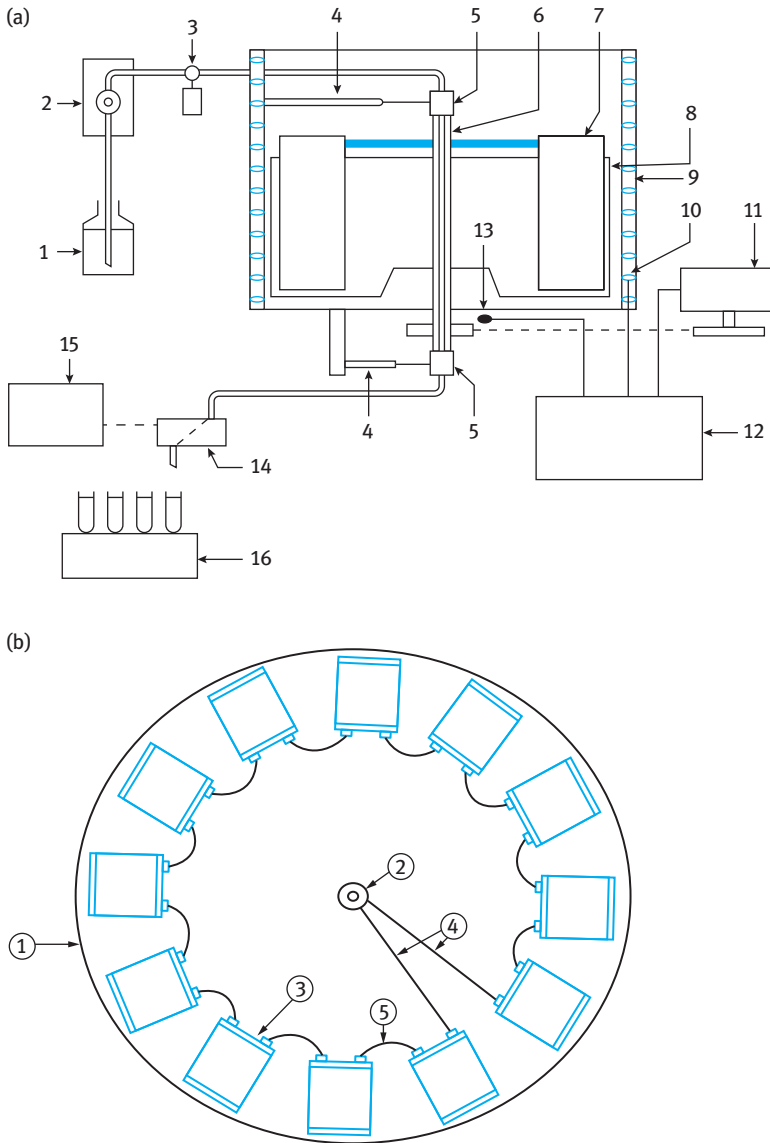


Figure 4.4: (a) The system of centrifugal partition chromatography [4]. 1, the solvent reservoir; 2, high-pressure constant flow pump; 3, sample injector; 4, the joint of sealed rotating connection device; 5, the sealed rotating connection device; 6, rotation axis; 7, column storage chamber; 8, rotator; 9, heating and cooling device; 11, motor; 12, controller of temperature and speed; 13, speed-controlled sensor; 14, monitor; 15, recorder; 16, collector. (b) The rotator of centrifugation distribution chromatography [4]. 1, centrifugal rotator; 2, the sealed rotating device; 3, column storage chamber; 4, connecting pipe; 5, column storage chamber connecting pipe.

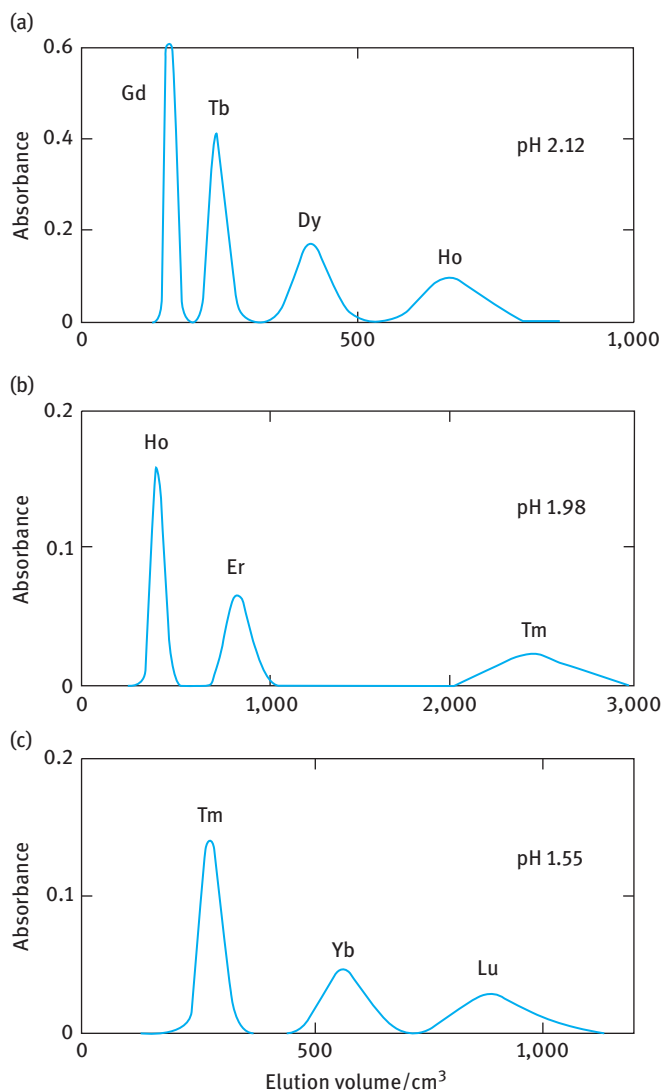


Figure 4.5: Chromatographic separation of heavy REEs. Stationary phase: 0.02 mol/L (EHPA)₂ in toluene; mobile phase: 0.1 mol/L (H,Na)Cl₂CHCOO; sample: 5×10^{-4} mol/L lanthanoid in 10^{-3} mol/L HNO₃ [72].

by ICP-MS detection. The analytical results obtained were compared with the preconcentration using SPE. It could be demonstrated that CCC results are comparable with those employing SPE. By employing the optimized conditions of CCC, the times for the enrichment of REEs (25 min) could be substantially shortened compared with the SPE procedure (120 min) for a single sample.

The literatures about centrifugal partition chromatography for the separation of REEs are listed in Table 4.9.

Table 4.9: Centrifugal partition chromatography for separation of REEs.

Target analytes	Stationary phase.	Mobile phase	Comments	Ref.
Rare earth	0.1 mol/L P204 in heptane; 0.1 mol/L P204 in dichloromethane	0.06 mol/L HCl (Ce, Pr); 0.07 mol/L HCl (Pr, Nd); 0.1 mol/L HCl (Er, Yb)	Detected after post-column reaction with Arsenazo III	[70]
Lanthanoid elements	0.02 mol/L P507 in kerosene	20 % ethylene glycolchlorine acetate buffer solution (pH 1.27–2.94)	Detected after post-column reaction with Arsenazo III	[71]
Heavy REEs and Y	0.02 mol/L EHPA in toluene	0.1 mol/L (H, Na) Cl ₂ CHCOOH	Detected after post-column reaction with Arsenazo III	[72]
Separation of Y from La	0.02 mol/L P204 in toluene (primary stationary phase), 0.25 mol/L Versatic 10 in toluene (secondary stationary phase)	0.1 mol/L chloroacetic acid; 0.01 mol/L CH ₃ COONa (in 0.1 mol/L NaNO ₃)	Detected after post-column reaction with Arsenazo III	[73]
REEs and Gd-DTPA	0.5 mol/L P204 in <i>n</i> -decane	0.01 mol/L HNO ₃	ICP-MS detection	[78]
Rare earth	Three-tier-connected spiral PTFE tube (300 m × 1.07 mm), 0.003 mol/L P204 in <i>n</i> -heptane	0–0.3 mol/L HCl gradient elution	Detected after post-column reaction with Arsenazo III	[79]
Lanthanide elements	P204: <i>n</i> -pentadecane: carbon tetrachloride (6:11:3)	0.5 mol/L HNO ₃	ICP-MS detection	[80]
Light REEs (Pr and Eu)	TBP: decane; carbon tetrachloride (6:7:7)	5 mol/L LiNO ₃ –1 mol/L HNO ₃	ICP-MS detection	[81]

4.2.5 Thin layer chromatography (TLC) and Paper chromatography (PC)

TLC and PC can be called as planar chromatography. These two methods used to be important means of REE separation, especially for the separation of adjacent REE. Since the introduction of HPLC in separation of REEs, application of planar chromatography especially PC is decreasing.

In TLC and PC, the movement of target analytes (REEs) is usually expressed in rate of flow (R_f), which is defined as the ratio of the distance between the origin point of sample and the center point of target analytes and the distance between the origin point of sample and the front of mobile phase. The R_f value is always less than 1 and it

is associated with the distribution coefficient of target analytes. When the distribution coefficient is larger, the distance of target analytes moved in the plane is smaller, so the R_f value is also smaller. R_f value is determined by the distribution coefficient. Besides, the property of the adsorbent, the thickness of the paper or thin layer, the composition and proportion of mobile phase, temperature, humidity and the degree of saturation vapor pressure also have effect on the R_f value. For example, temperature can affect the distribution coefficient and the composition of developing solvent. To ensure the stability of the R_f value, it is better to do the operation under the condition of constant temperature, humidity and vapor pressure of mobile phase. Generally, the separation is operated in a chromatographic cylinder or chromatographic box.

4.2.5.1 Paper chromatography

With paper as the carrier, the separation mechanism of PC is assigned to distribution behavior. PC is usually a normal-phase chromatography with less polar organic solvent as the mobile phase and the absorbed water on the supporting matrix (paper) as the stationary phase. The supporting matrix of PC for separation of REEs include cellulose, inorganic or organic ions infiltrated cellulose, ion exchanger (polymeric amine and acidic phosphate ester) infiltrated cellulose and chelating agent (such as 8-hydroxyquinoline) infiltrated cellulose. For the separation of REEs by using PC, inorganic acid aqueous solution or its mixture with organic solvent were used as mobile phase at times. And some complexing agents such as lactic acid [82] and EDTA [83] can be introduced into the mobile phase to improve the distribution property of REEs.

PC needs no expensive equipment and is suitable for the routine analysis of large numbers of samples. It was applied in REEs as early as 1955, and Lederer [84] employed ethanol 2 mol/L $^{-1}$ HCl (9:1, V/V) as mobile phase for the separation of La, Ce, Pm, Eu, Dy and so on. Few years later, Dubuquoy et al. [85] adopted a SA-2 ion exchange paper with ammonium α -HIBA as developing solvent for separation of La, Ce, Pr, Nd, Pm and Sm from U fission. They also separated Lu, Yb, Tm, Y, Tb and Eu by using SA-2 ion exchange paper with different developing solvent [82] and a review about the separation of REEs by using SA-2 paper IEC was reported later [86]. In 1986, Chen and Yuan [83] used N_{1923} as stationary phase and 0.01 mol/L EDTA (pH = 5) as developing solvent for the separation of light REEs and heavy REEs with their associated element Zr and U. Kostyuk [87] investigated the possibility of the separation of seven REEs (Pr, Nd, Sm, Eu, Gd, Er and Yb) by PC and optimized the separation conditions. The impregnation of PC by ammonium nitrate had given most successful results. The acetone–ether mix with the rhodanide acid (1 %) as the eluent.

PC has been applied to the separation of lanthanides from other ions (such as main group, transition and actinide ions) and for group separation of the rare earths. Complete separation of all lanthanides by PC has apparently not yet been achieved although separation of the light rare earths (La, Ce, Pm, Nd, Sm and Eu) and other combinations has been successful [88]. Limitations imposed by the low intrinsic efficiency of PC may be overcome by utilizing a two-dimensional development, although

it is generally easier to use TLC or paper electrophoresis instead. PC can be combined usefully with coprecipitation, solvent extraction and IEC on columns for the selective determination of lanthanide mixtures. The detection of lanthanides separated by PC usually relies on spray reagents containing chromogenic complexing reagents such as Alizarin Red, 8-hydroxyquinoline, Arsenazo I, II or III and pyridylazoresorcinol.

A disadvantage of PC is the relatively long developing time required (2–20 h). Moreover, the separation effect among REEs by using PC is not satisfactory, so the application of PC on REEs is rare.

4.2.5.2 Thin-layer chromatography

TLC as an important branch of chromatographic analysis can get good separation effect without any sample pretreatment and its overall performance exceeded the PC and atmospheric column chromatography.

Stationary phase

According to the separation mechanism of TLC, the support material (sorbent) is divided into adsorptive carrier and distributive carrier. The main types of sorbent include silica gel, cellulose, alumina, organic Teflon40, Corvic and so on. Among them, silica gel is the most common used carrier, and cellulose is suitable for the light rare earth separation. The requirements for the sorbent are as follows: (1) it has huge surface area and sufficient adsorption capacity, different adsorption capacity for different components; (2) it is not dissolved in the solvent and developing agent and do not have chemical reaction with solvent or developing solvent or chemical composition in the sample; (3) the particles are uniform and wouldn't be broken during use.

Developing solvent

TLC for separation of REEs includes adsorption thin layer, distribution thin layer, ion exchange thin layer, gel thin layer and so on. Due to the different separation mechanism, the choice of developing solvent is a key factor for a successful TLC separation. The appropriate developing solvent was selected by considering the polarity of separated components, the type and activity of thin layer, and the polarity (elution force) of developing solvent. The first two factors determine the polarity of developing solvent and the elution capacity. Touchstone et al. [89] pointed out that the elution ability of the solvent is proportional to the dielectric constant, and a large dielectric constant of the solvent would reduce the separation ability and increase the R_f value; on the contrary, the separation ability would be increasing and the R_f value would be decreasing. When the R_f value is too high, developing solvent with low dielectric constant should be chosen.

Generally, the developing solvent system for normal-phase thin-layer analysis of REEs is extractant–organic solvent–acid, for example, P204–ether–HNO₃ and

TBP–hydrocarbon–HNO₃ are preferable. As for RP thin layer, the layer is usually impregnated by extraction agents such as P204, TBP and TOPO; of which P204 is the best, TBP ranks second and TOPO is the worst. The commonly used developing solvent is inorganic acids, and nitric acid is the most widely used.

Table 4.10: Application of TLC in separation of REEs.

Elements	Stationary phase	Mobile phase/developing solvent	Comments	Ref.
Adjacent lanthanides	Silica gel (pH 7.0) pretreated with 0.1 mol /L Tris(hydroxymethyl)-aminomethane and 0.1 mol /L HCl	Nitrate solution of alkaline earth metal	RF values of the lanthanides varied in a regular and characteristic way accompanied by the tetrad effect with increasing atomic number	[90]
REEs	Silica gel H and silica gel H impregnated with NH ₄ NO ₃	Et Me ketone-THF -di(2-ethylhexyl) dithiophosphoric acid (1 mol/L), 6.8/3.2 /0.4 (v/v/v)	–	[91]
REEs	Silica gel	Aqueous nitrate solutions of alkali metals	Spraying with aqueous 0.02 % Arsenazo III and then 1 mol/L CH ₃ COOH	[92]
REEs	Whatman KC 18 reversed-phase thin-layer chromatography plates	1 mol/L lactate in 50 % methanol	Reversed-phase TLC with spraying aqueous 0.1 % Arsenazo III or 0.1 % xylenol orange	[93]
REEs	Silica gel without binder	0.1–2 mol/L ammonium sulfate solution (pH = 5.4 ± 0.1)	Spraying with aqueous 0.02 % Arsenazo III and then an aqueous NH ₃ , followed by gentle heating	[94]
REEs	DC-Trennung	Diethyl ether/HDEHP/HNO ₃ (100: 1:3.5)	Increase the R _f differences between the heavy and the light rare earths by variation of HDEHP and HNO ₃	[95]
REEs and Y	Fixion 50-X8 sheet material with a layer of Dowex 50-X8 cation exchanger on the polymer base	0.1 mol/L oxalic acid– 2 mol/L NH ₄ Cl at pH 7.5–8.5	Desorption of the REE group with 5 mol/L HCl followed by dilution and then determination by ICP-OES	[96]

TLC separation of REEs

With high-performance TLC, it is possible to separate all the REE in a single step [97]. TLC has replaced PC as the preferred method for separating REEs. A wide variety of stationary phases, mobile phase and detection methods have been investigated for TLC (as shown in Table 4.10).

TLC is divided into normal and RP TLC. The developing system in normal-phase TLC is generally extractant–organic solvent–acid, for example, P204–ether–HNO₃. Specker and Hufnagel [97] and Specker [98] investigated different developing system for the separation of all REEs by TLC with employing silylanization silica as stationary phase; they finally chose P204–diethyl ether–tetrahydrofuran–HNO₃ as the developing system [97] (as shown in Figure 4.6). Ishida et al. [99] used silica as stationary phase and NH₄NO₃ solution as mobile phase to separate REEs. They got a poor separation for the REEs. And then they used gradient elution with NH₄NO₃ and double-phase TLC to realize the complete separation.

The separation of single REE by normal-phase TLC is not good, and the application area of RP TLC is more widely used. As early as 1964, Pierce and Flint [100] adopted RP TLC for the separation of REEs, and since then a lot of works on the separation of REEs by this method were reported. For example, Takeda and Ishida [90] used 0.1 mol/L trihydroxymethylamine and 0.1 mol/L HCl-impregnated silica (pH = 7) as stationary phase, and different alkali metal nitrate solutions as mobile phase to separate all the REEs except Po. Later on, they used both carboxymethylcellulose–aqueous sodium nitrate systems [101] and carboxymethylcellulose–aqueous sodium chloride systems [102] for the separation of REEs, and Y has been separated from all of the REEs, except for La, which provides *R_f* values similar to those of Y.

Soran et al. [103] studied the separation of REEs by TLC using silica H and ammonium nitrate-impregnated saturated silica H as stationary phase, and di(2-ethylhexyl)dithiophosphoric acid as complexing agent in the mobile phase. They

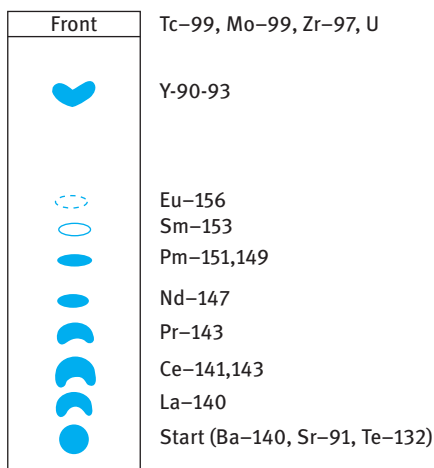


Figure 4.6: Thin-layer chromatograms of REEs: (a) the mixture of REEs; (b) uranium and nuclear fission products. Stationary phase: silylanization diatomite; mobile phase: diethyl ether/tetrahydrofuran/P204/nitric acid [97].

found that the best results were obtained by the use of ethyl methyl ketone-tetrahydrofuran-di(2-ethylhexyl)dithiophosphoric acid (1 mol/L), 6.8 + 3.2 + 0.4 (v/v), as mobile phase. In another work, they also used mobile phase containing di(2-ethylhexyl) disulfophosphate and di(isobutyl) disulfophosphate to separate Ur, Th and REEs and demonstrated that disulfophosphate played a great role in the separation of lanthanide and actinide [91].

Due to the limitation of the subsequent detection methods, TLC is difficult to be applied to the determination of REEs. However, it can be used in the initial separation analysis of REEs to provide reference information for further research. Table 4.10 shows the application of TLC in separation of REEs.

4.3 Gas chromatography

GC is a simply operated and widely used separation and analysis method, which is highly selective, sensitive and effective. GC is suitable for the analysis of volatile and thermally stable analytes. This technique was first used in the separation of lanthanide elements – methylene pivalic acyl clathrates by Eisentrunk et al. [104].

Table 4.11: The separation and determination of REEs by GC.

REEs	Chelates	Stationary phase	Column temperature	Ref.
Sc, Lu, Er	Isobutyrylpivalylmethane	Silicone	210~280 °C	[105]
Nd, Gd, Er	Isobutyrylpivalylmethane, trifluoroacetylacetone	Silicone E-30	160~280 °C	[106]
Y, La–Nd, Sm–Tb, Yb	Hexafluoroacetylacetone + tributyl phosphate (TBP)	Dexsil 300GC	150~210 °C	[107]
Y, lanthanides	Fluorinated β -diketones + organic neutral donors	SE-3, QF-1	185~215 °C	[108]
Yttrium group lanthanides	Polyfluorinated β -diketones + DBSO	Dexsil 300GC	140~215 °C	[109]
Y, lanthanides	Hexafluoroacetylacetone + TBP	1.0 % Silicone SE-30	250~275 °C	[110]
Sm, Eu, Gd, Tb, Dy, Ho, Er, Yb, Tm, Lu, Y	Trifluoroacetyl pivaloyl methane	SE-30	200 °C	[111]
Ho, Dy, Tb, Gd	Trifluoroacetylacetone	PEG-20M, OV-17	240 °C	[112]
Sc, Y, REEs	Pivaloyltrifluoroacetone	Silicone	170~270 °C	[113, 114]
Cerium group lanthanides	Polyfluorinated β -diketone + DBSO	Dexsil 300GC	172–215 °C	[115]
Lanthanides	β -Diketone + DBSO	DB-5 HT capillary	50–300 °C	[116]

In the later study of GC separation for REEs, β -diketonates as ligand account for the largest proportion. The separation and determination of REEs by GC are summarized in Table 4.11.

Problems such as adsorption and low resolution of lanthanide β -diketonates have not been effectively solved through changing stationary phase, so the research works on GC separation of REEs decreased gradually, and there is almost no research on this aspect in recent years.

4.4 Capillary Electrophoresis (CE)

CE is a kind of electrokinetic separation method performed in capillaries. In CE methods, analytes migrate through electrolyte solutions under the influence of an electric field. The separation is based on the ionic mobility. CE techniques include capillary zone electrophoresis (CZE), micellar electrokinetic chromatography, capillary gel electrophoresis, capillary isoelectric focusing and capillary isotachopheresis (CITP). Among them, CZE and CITP are the most widely used CE modes in REEs separation and analysis.

4.4.1 Basic knowledge and principle

4.4.1.1 Zeta potential

The directional migration of the analytes in capillary is not only affected by the applied voltage but also influenced by the charge on the inner surface of the capillary. When the electrolyte contacts with the inner surface of the capillary, a double electrode layer is formed. One layer next to the inner surface is the Stern layer, and the other one in a free state is the diffusion layer. The potential between the Stern layer and the starting edge of the diffusion layer is the zeta potential (ζ_i) of the capillary wall. In fused silica capillary, when the pH of the solution is higher than 2.5, the Si-OH on the inner surface of the capillary is ionized as SiO^- , making the inner surface of the capillary negative charged. Next to this negative charged surface, ions with opposite charges agglomerate forming the double electrode layer. The relationship between the zeta potential and the thickness of the diffusion layer (δ) can be expressed as

$$\zeta_i = \frac{4\pi\delta e}{\varepsilon}$$

where ε is the dielectric constant and e is the total excess charge per unit area in the solution. The zeta potential is proportional to the product of the charge numbers on the inner surface and the thickness of the diffusion layer, which is affected by the property of the ions with opposite charges, pH of the buffer solution, the equilibrium between the cations in the solution and the negative charged surface of the fused silica capillary, and so on.

4.4.1.2 Electrophoresis

The electrophoresis is the directional migration of the charged analytes under the influence of an electric field. The migration velocity (U_{ep}) is expressed as

$$U_{ep} = \mu_{ep} \cdot E \quad (4.1)$$

where E is the electric field intensity and μ_{ep} is the mobility of the analytes. The ion mobility is the migration distance in a given buffer solution per unit time and per unit electric field intensity, which is

$$\mu_{ep} = \frac{\varepsilon \zeta_i}{4\pi\eta}$$

where η is the viscosity of the medium, ζ_i is the zeta potential of the target ion. ζ_i is related to the surface electric density of the target ion. If the charged number of the target ion is fixed, the larger the mass, the lower the zeta potential. Different ions migrate in the electrolyte with the different mobility according to their specific mass and surface electric density, which is the separation base of the electrophoresis.

4.4.1.3 Electroosmotic flow

Electroosmotic flow (EOF) is an electrokinetic phenomenon generated along with the electrophoresis. Under the influence of an electric field, the electrolyte will directionally move relative to a stationary charged boundary. The mobility of EOF (μ_{eo}) is expressed as

$$\mu_{eo} = \frac{\varepsilon \zeta_w}{4\pi\eta}$$

where ζ_w is the zeta potential of the capillary wall. The formation of EOF is related to the double electric layer, which is mainly controlled by the SiO^- on the surface of fused silica capillary, or the adsorption on the surface of nonionic capillary material (e.g., PTFE). EOF plays a great role in CE separation. The adjusting of the mobility and direction of EOF are important to improve the separation efficiency, selectivity and resolution. Usually, the mobility of EOF is five- to sevenfold faster than the mobility of the charged ions, and the direction of EOF is from anode to cathode. Therefore, all the particles (cations, anions and neutral particles) will migrate from anode to cathode with the appeared mobility (μ_{ap}), which is the vector sum of μ_{eo} and μ_{ep} and can be calculated as

$$\mu_{ap} = \mu_{eo} + \mu_{ep} = \frac{l}{t} \cdot \frac{L}{V}$$

where l is the distance between the injector and the detection window, t is the migration time, L is the length of the capillary and V is the applied voltage.

4.4.1.4 Separation efficiency and resolution

In CE separation, the separation efficiency can be expressed as the theoretical plate numbers (N), which is calculated as

$$N = \frac{Vl}{2DL} \mu_{ap}$$

where D is the diffusion coefficient of the solute. The higher the electric field, the higher the separation efficiency; the higher the appeared mobility, the higher the separation efficiency; the lower the diffusion coefficient, the higher the separation efficiency.

The plate numbers can also be determined by experiments, which is calculated as

$$N = 5.54 \left(\frac{t}{W_{h1/2}} \right)^2 \quad (4.2)$$

where $W_{h1/2}$ is the peak width at half peak height.

Resolution (R_s) is another factor to evaluate the separation degree in CE. For two analytes (1 and 2) next to each other, according to Giddings equation, R_s can be calculated as

$$R_s = \frac{\sqrt{N}}{4} \left(\frac{\mu_{ap,2} - \mu_{ap,1}}{\mu_{ap,2} + \mu_{ap,1}} \right)$$

It can be seen that the difference in the appeared mobility of two analytes is the main factor that affects the resolution.

4.4.2 Influencing factors on CE separation

There are many factors that would affect CE separation, including voltage, buffer solution composition and pH, adducts and temperature, and so on.

4.4.2.1 Voltage

Increasing voltage would result in improvement of separation efficiency and resolution; however, it would also cause the increase of Joule heat which is not beneficial for CE separation.

4.4.2.2 Buffer composition

Since CE is processed in buffer solution as background electrolyte, the selection of electrolyte has great influence on the migration and separation of analytes. There are some criteria for choosing the buffer solution: the buffer solution should have large buffering capacity in a certain pH range; the mobility of the electrolyte should be

small, indicating large molecule and small charge to reduce the current; the influence of the electrolyte on the detection can be ignored.

4.4.2.3 Buffer pH

The buffer pH has great influence on EOF. At high pH, the Si–OH on the inner surface of capillary is ionized at a great degree, resulting in a high EOF; at low pH, the ionization of Si–OH was restricted, resulting in reduced EOF. The highly dependent of EOF on pH determined that the migration time of analytes is highly related to the buffer pH. Therefore, optimization of buffer pH is important to obtain an optimal CE separation of REEs.

4.4.2.4 Adducts

Adducts is another important factor for the separation of interest analytes in CE. The addition of an appropriate adduct can change the physical and chemical properties of capillary wall and the solutes via their interactions. The CE separation of metal cations is greatly dependent on the molar conductance of target cations. Since REE cations have similar molar conductance, the CE separation of REE cations usually involves the addition of complexes to improve the separation resolution. Commonly used complexes include oxalate, citrate, lactate, tartrate, NTA, EDTA, α -hydroxyisobutyrate (α -HIBA), 8-hydroxyquinoline-5-sulfonic acid and so on. Among them, α -HIBA is the most frequently used adduct.

4.4.2.5 Temperature

The increase of temperature leads to the decrease of the solution viscosity and the increase of current, which cause the variation of EOF. Normally, increase in temperature would result in the reduction of the migration time.

4.4.3 Applications in REEs analysis

In CE separation of REEs, the migration direction of REEs is the same as the EOF. The tiny difference in charge and radius of REEs leads to a slight difference in mobility. For instance, the mobility of trivalent REE cations varies from $72.3 \times 10^5 \text{ cm}^2/\text{V}$ (La) to $67.5 \times 10^5 \text{ cm}^2/\text{V}$ (Yb). Therefore, these REE cations cannot be well separated in conventional CE. The addition of complex in separation system would enlarge the difference in mobility of REEs, leading to an effective separation. Besides adducts, electrolyte composition, buffer pH and the property of capillary wall will also influence the separation of REEs. Janos [117] provided a review on separation of lanthanides by CE in 2003.

As early as 1970, the CE separation has shown its advantages of fast and high resolution in REE separation. The applications of CE in separation of REEs are listed in Table 4.12. In 1970, Korchemmaya [118] achieved a CE separation of all the REEs in

Table 4.12: The applications of CE in separation of REEs.

REEs	CE methods	Separation condition	Time (min)	LODs	Ref.
Ln, Y, Sc	CZE-UV (fused silica 50 cm × 75 μm)	Borate buffer (20 mM, pH 11.0) + 1 mM CDTA	12	2–5 μM (Ln), 10 μM (Sc)	[119]
Ln	CZE-UV (fused silica 40 cm × 100 μm)	30 mM creatine + 7 mM α-HIBA + 30 mM acetate acid, pH 4.8	–	–	[120]
La, Ce, Tb, Gd	CZE-UV (fused silica 52 cm × 75 μm)	10 mM creatine + 2 mM α-HIBA + acetate buffer, pH 4.1	3.5	40 μg/L	[121]
La–Yb, alkalis, Ca, Mg	CZE-UV (fused silica 36.5 cm × 75 μm)	4 mM α-HIBA, pH 4.4	8	77–199 mg/mL	[122]
Ln	ITP (PTFE 20 cm × 0.05 mm)	0.027 M KOH + 0.015 M α-HIBA + acetate buffer + 0.0025 % PVA, pH 4.92	20	5 nmol	[123]
La–Tm	CZE-UV (fused silica 50 cm × 50 μm)	30 mM creatine + 0.4 mM α-HIBA, acetate buffer, pH 4.0	11	–	[124]
Ln	CZE-UV (fused silica 57 cm × 75 μm)	4.25 mM α-HIBA, 8 mM acetate buffer, pH 4.4	10	0.03 nmol	[125]
Ln	CZE-UV (fused silica 35 cm × 50 μm)	0.02 M imidazole + 6 μM lactic acid, pH 3.4	6	5 μM	[126]
Ln	CZE-UV (fused silica 40 cm × 75 μm)	8 mM α-HIBA + 0.9 mM malonic acid + 30 mM creatine, ethylbutyric acid buffer, pH 4.8	5	–	[127]
Y, Ln except Pm	ITP (PTFE 25 cm × 0.32 mm)	Leading: 20 mM ammonia; BGE: 7.5 mM α-HIBA + 2 mM malonic acid + 2-ethylbutyric acid, pH 4.8; trailing: 20 mM carnitine hydrochloride; all with 0.1 % (w/w) HPC	–	–	[128]
La, Ce, Pr, Nd, Sm, Eu	ITP-UV (fused silica 50 cm × 50 μm)	Leading: 10 mM H ₂ SO ₄ ; BGE: 0.4 mM quinine sulfate + 8 mM α-HIBA; trailing: 80 mM TRIS	3	6–11 nM	[129]

Table 4.12: (continued)

REEs	CE methods	Separation condition	Time (min)	LODs	Ref.
RE, Th, U (as DBCAs chelate)	CZE-Vis (fused silica 70 cm × 75 μm)	20 mM NaAc-HCl buffer + 0.2 mM DBCAs, pH 3.0,	10	48.1–72.3 nM	[130]
14 REEs	CZE-UV (fused silica 35 cm × 50 μm)	20 mM imidazole + 8 mM α-HIBA, pH 3.4 with HCl	10	5 nM	[131]
14 REEs	CZE-UV (fused silica 65 cm × 50 μm)	0.1 mM cupferron + 15 mM α-HIBA, pH 4.9	7	0.24–0.47 μg/mL	[132]
La-Lu	CZE-UV (fused silica 36.5 cm × 50 μm)	4 mM α-HIBA + 10 mM UVCat-1, pH 4.4 with HAC	<1	<0.1 ng	[133]
Ln	CZE-UV (fused silica 71 cm × 50 μm)	0.8 mM picolinic acid + 10 mM α-HIBA + 25 mM formic acid, pH 4.7	9	0.53–0.96 μg/mL	[134]
Ln (xenotime, monazite)	EKS-CZE-UV (fused silica 100 cm × 75 μm)	Leading: 100 mM ammonia + 7.5 mM α-HIBA + 2.0 mM malonic acid, 2-ethylbutyric acid, pH 4.8 Supporting: 10 mM 4-methylbenzylamine + 4 mM α-HIBA + 0.4 mM malonic acid, 2-ethylbutyric acid, pH 4.8 Tailing: 1 M HCl	<5 min	–	[135]
Ln (as ABEDTA chelate)	CZE-UV (fused silica 50 cm × 50 μm)	50 mM borate + 20 mM carbonate, pH 12.35 with NaOH	35	0.94 μM	[136]
16 REEs	CZE-UV (fused silica 50 cm × 75 μm)	17 mM creatinine + 7.8 mM α-HIBA + 175 mM HAC	12	–	[137]
Eu, Gd species	CZE-ICP-MS (fused silica 80 cm × 74 μm)	100 mM HAC + 10 mM NaAc, pH 3.7	<8	125 (Eu), 250 (Gd) ng/L	[138]
Ln (as NBD-ABEDTA chelate)	CZE-UV (fused silica 60 cm × 50 μm)	9.5 mM borate + 33.5 mM IDA, pH 9.45	20	0.42 μM	[139]
REEs (geological samples)	CZE-UV (fused silica 60 cm × 75 μm)	17 mM creatinine + 7 mM α-HIBA + 140 mM HAC + 6.5 mM HCl	13	~10(Y), ~20 (other REEs) μg/L	[140]

REEs	CE methods	Separation condition	Time (min)	LODs	Ref.
Ln-humic acid	CZE-ICP-MS (fused silica 80 cm × 74 μm)	100 mM HAC + 10 mM NaAc, pH 3.7		0.8–1.6 nM	[141]
Ln (as FTC-ABEDTA chelate)	CZE-LIF (fused silica 80 cm × 74 μm)	12 mM borate + 5.5 mM IDA + 9.0 mM citrate + 25 μM CyDTA, pH 9.60	23	91 pM	[142]
Ln	CZE-UV (fused silica 35.5 cm × 75 μm)	4 mM α-HIBA + 10 mM UVCat-1, pH 4.4	~3	0.67–16 ng (“odd–even” pattern)	[143]
Ln-humic acid	CZE-ICP-MS (fused silica 80 cm × 74 μm)	100 mM HAC + 10 mM NaAc, pH 3.7	–	–	[144]
Ln	CZE-ESI-MS (fused silica 120 cm × 50 μm)	0.8 mM picolinic acid + 10 mM α-HIBA + 25 mM formic acid, pH 4.7 with TRIS	<30	Low mg/L	[145]
Ln	LLME + CZE-UV (fused silica 50 cm × 75 μm)	28 mM creatinine + 11.5 mM α-HIBA + 0.26 M HAC	20	0.19–0.70 μg/L	[146]
Nd (as FTC-ABEDTA chelate)	CZE-LIF (fused silica 80 cm × 74 μm)	12 mM borate + 25 μM CyDTA, pH 9.60	12	22 pM	[147]
Ln	ITP-CD/ICP-MS (fused silica or PVA-coated 56 cm × 30 μm)	Leading: 14 mM HMBA + 10 mM HAC, pH 4.5 with ammonia Terminating: 15 mM HAC	~30	–	[148]
Ln, Th, UO ₂ ²⁺	CZE-UV (fused silica 57 cm × 75 μm)	1 mM HTTA + 50 mM α-HIBA + 5 mM NaNO ₃ + 5 % methanol, pH 5.2	12	–	[149]

CDTA, cyclohexane-1,2-diaminetetraacetic acid; PVA, polyvinyl alcohol; HPC, hydroxypropyl cellulose; TRIS, Tris(hydroxymethyl)aminomethane; DBC-As, 2-(2-arsenophenylazo)-1,8-dihydroxy-7-(4-chloro-2,6-dibromophenylazo)-naphthalene-3,6-disulfonic acid; EKS, electrokinetic supercharging; ABEDTA, 1-(4-aminobenzyl) ethylenediamine-*N,N,N',N'*-tetraacetate; NBD, nitrobenzofurazan; IDA, iminodiacetate; LIF, laser-induced fluorescent; FTC, fluorescein-thiocarbamyl; CyDTA, *trans*-1,2-diaminocyclohexane-*N,N,N',N'*-tetraacetic acid; LLLME, liquid liquid microextraction; HMBA, 2-hydroxy-2-methylbutyric acid; CD, conductivity detection; HTTA, 2-thenoyltrifluoroacetone.

15–20 min. Then, Foret et al. [150] separated 19 metal ions including 14 REEs in 5 min by using CZE. Later on, Jandick et al. [151] separated 24 elements, including REEs in 5 min. Chen and Cassidy [152] compared the CE separation of REEs with different capillary coatings. With benzylamine aminotoluene and α -HIBA as complexes, 14 REEs could be separated in 6 min by using C1-coated capillary, while the separation time is 8 min when using C18-coated capillary. A comparison of CZE and ITP demonstrated that the selection of electrolyte and the optimization of CE conditions in ITP are much more complicated than that in CZE. In ITP, the leading catholyte should be acids with high mobility, and the trailing anodolyte should be weak acids [127]. The optimization of CZE conditions without such limitations is more convenient.

UV (with indirect or direct UV mode) is the most widely used detector in CE analysis of REEs. To obtain higher sensitivity than UV detection, Saito et al. [142, 147] employed laser-induced fluorescence (LIF) as CE detector for the detection of the complexes of lanthanides with fluorescein-thiocarbamyl-1-(4-aminobenzyl) ethylenediamine-*N,N,N',N'*-tetraacetate (FTC-ABEDTA). The LODs were decreased to dozens of pM level. Elemental-specific ICP-MS is one of the most sensitive methods for the determination of REEs. A combination of CE-ICP-MS is capable for the speciation of Ln and Ln-humic acids [138, 141, 144]. However, an interface with small dead volume and high transport efficiency between CE and ICP-MS is necessary. ESI-MS is a method of choice for elemental and molecular analysis of lanthanides, and has also been employed as CE detector [145]. However, the LOD of Ln obtained by CE-ESI-MS is much higher than that by CE-ICP-MS.

4.5 Supercritical fluid chromatography

Supercritical fluid chromatography (SFC) [153] was called high-pressure GC in the early time, which utilizes supercritical fluid as mobile phase. Lanthanide chelate is one of the first metal chelates that was separated by SFC. In 1968, Karayannis et al. [154] separated lanthanide β -diketonates by utilizing supercritical CCl_2F_2 as mobile phase under the temperature lower than that used in GC. So SFC solves the problem of thermal instability of compounds that exists in GC. A few years later, the separation of lanthanide chelates of acetylacetone (ACAC), trifluoroacetylacetone, thenoyltrifluoroacetone, dipivaloylmethane, and 6,6,7,7,8,8,8-heptafluoro-2,2-dimethyl-3,5-octanedione with ethanol-modified inert silylated column were investigated by Laintz et al. [155]. Mobile phases consisting of supercritical CO_2 were used and all of the compounds were shown to have good chromatographic performance. Furthermore, Wu et al. [156, 157] separated and analyzed lanthanide β -diketonates with good performance. However, due to supercritical chromatography, instruments are relatively complex, difficult to popularize and show no obvious advantages when compared with HPLC, limiting the development of this technology in the separation and analysis of REEs. With the gradual improvement of HPLC technology, SFC has gradually been replaced by HPLC; actually it is rarely used now.

References

- [1] Sisson DH, Mode VA, Campbell DO. High-speed separation of rare earths by ion exchange. *J Chromatogr A* 1972, 66, 129–35.
- [2] Hoehlein G, Voeller H, Weinlaender W. Use of aminex for separation of actinides and lanthanides. *Radiochim Acta* 1969, 11, 172–5.
- [3] Iwasaki, K, Haraguchi H. Determination of rare earth elements in geological samples by inductively-coupled plasma atomic emission spectrometry after oxalate coprecipitation and cation-exchange column separation. *Anal Chim Acta* 1988, 208, 163–72.
- [4] Hirata T, et al. Precise determination of rare earth elements in geological standard rocks by inductively coupled plasma source mass spectrometry. *Anal Sci* 1988, 4, 637–43.
- [5] Pierce TB, Hobbs RS. The separation of the rare earths by partition chromatography with reversed phases. *J Chromatogr A* 1963, 12, 74–80.
- [6] Wang WN, Chen YJ, Wu MT. Complementary analytical methods for cyanide, sulphide, certain transition metals and lanthanides in ion chromatography. *Analyst* 1984, 109, 281–6.
- [7] Chikuma M, et al. Chelate-forming resins prepared by modification of anion-exchange resins. *Talanta* 1980, 27, 807–10.
- [8] Lundgren JL, Schilt AA. Analytical studies and applications of ferroin type chromogens immobilized by adsorption on a styrene-divinylbenzene copolymer. *Anal Chem* 1977, 49, 974–80.
- [9] Chao HE, Suzuki N. Adsorption behaviour of scandium, yttrium, cerium and uranium from xylene orange solutions onto anion exchange resins. *Anal Chim Acta* 1981, 125, 139–47.
- [10] Shabani MB, Akagi T, Masuda A. Preconcentration of trace rare-earth elements in seawater by complexation with bis(2-ethylhexyl) hydrogen phosphate and 2-ethylhexyl dihydrogen phosphate adsorbed on a C18 cartridge and determination by inductively coupled plasma mass spectrometry. *Anal Chem* 1992, 64, 737–43.
- [11] Jain, VK, et al. Sequential separation and trace enrichment of thorium(IV) and uranium(VI) on chelating resin amberlite XAD-2-ortho-vanillinthiosemicarbazone (o-VTSC). *Separ Sci Technol* 1998, 33, 1803–18.
- [12] Choppin GR, Harvey BG, Thompson SG. A new eluant for the separation of the actinide elements. *J Inorg Nucl Chem* 1956, 2, 66–8.
- [13] Robards K, Clarke S, Patsalides E. Advances in the analytical chromatography of the lanthanides. A review. *Analyst (London)* 1988, 113, 1757–79.
- [14] Kumar M. Recent trends in chromatographic procedures for separation and determination of rare-earth elements – A review. *Analyst* 1994, 119, 2013–24.
- [15] Yoshida K, Haraguchi H. Determination of rare earth elements by liquid chromatography/inductively coupled plasma atomic emission. *Anal Chem* 1984, 56, 2580–5.
- [16] Raut NM, Jaison PG, Aggarwal SK. Comparative evaluation of three alpha-hydroxycarboxylic acids for the separation of lanthanides by dynamically modified reversed-phase high-performance liquid chromatography. *J Chromatogr A* 2002, 959, 163–72.
- [17] Brunisholz G, Roulet R. Separation of rare earth elements by ion exchange chromatography. II. Separation and analysis of the europium-gadolinium couple. *Helv Chim Acta* 1970, 53, 126–30.
- [18] Bruzzoniti MC, Mentasti E, Sarzanini C. Determination of lanthanides by ion chromatography. Separation and retention mechanism. *Anal Chim Acta* 1997, 353, 239–44.
- [19] Rollin S, et al. Determination of lanthanides and actinides in uranium materials by high-performance liquid chromatography with inductively coupled plasma mass spectrometric detection. *J Chromatogr A* 1996, 739, 139–49.
- [20] Schwantes JM, et al. Rapid, high-purity, lanthanide separations using HPLC. *J Alloys Compd* 2006, 418, 189–94.

- [21] Borai E, Eklhom P, Harjula R. Group Separation of heavy metals followed by subsequent and individual separation of lanthanides by chelation chromatography. *J Liq Chromatogr Related Technol* 2014, 37, 1614–31.
- [22] Jones EA, Bezuidenhout HS, Van Staden JF. Separation of lanthanides and yttrium as anionic complexes by isocratic ion-interaction chromatography. *J Chromatogr A* 1991, 537, 277–86.
- [23] Inoue Y, et al. Ion Chromatographic separation of rare-earth elements using a nitrilotriacetate-type chelating resin as the stationary phase. *Anal Chem* 1996, 68, 1517–20.
- [24] Dybczynski RS, et al. New reversed phase-high performance liquid chromatographic method for selective separation of yttrium from all rare earth elements employing nitrilotriacetate complexes in anion exchange mode. *J Chromatogr A* 2015, 1386, 74–80.
- [25] Fernandez RG, Garcia Alonso JI, Separation of rare earth elements by anion-exchange chromatography using ethylenediaminetetraacetic acid as mobile phase. *J Chromatogr A* 2008, 1180, 59–65.
- [26] Garcia-Valls R, et al. Separation of rare earth elements by high performance liquid chromatography using a covalent modified silica gel column. *Anal Chim Acta* 2001, 439, 247–53.
- [27] Small H, Stevens TS, Bauman WC. Novel ion exchange chromatographic method using conductimetric detection. *Anal Chem* 1975, 47, 1801–9.
- [28] Sevenich GJ, Fritz JS. Addition of complexing agents in ion chromatography for separation of polyvalent metal ions. *Anal Chem* 1983, 55, 12–6.
- [29] Nesterenko PN, Jones P. Isocratic separation of lanthanides and yttrium by high-performance chelation ion chromatography on iminodiacetic acid bonded to silica. *J Chromatogr A* 1998, 804, 223–31.
- [30] Borai EH, Eid MA, Aly HF. Determination of REEs distribution in monazite and xenotime minerals by ion chromatography and ICP-AES. *Anal Bioanal Chem* 2002, 372, 537–41.
- [31] Farinas JC, Cabrera HP, Larrea MT. Improvement in the ion exchange chromatographic separation of rare earth elements in geological materials for their determination by inductively coupled plasma atomic emission spectrometry. *J Anal At Spectrom* 1995, 10, 511–6.
- [32] Kawabata K, et al. Determination of rare-earth elements by inductively coupled plasma mass spectrometry with ion chromatography. *Anal Chem* 1991, 63, 2137–40.
- [33] Kishi Y, et al. Determination of rare earth elements by IC-ICP-MS (inductively coupled plasma mass spectrometer). *Kidorui* 1990, 16, 134–5.
- [34] Bulska E, et al. Inductively coupled plasma mass spectrometry in comparison with neutron activation and ion chromatography with UV/VIS detection for the determination of lanthanides in plant materials. *Talanta* 2012, 97, 303–11.
- [35] Künemeyer J, et al. Speciation analysis of gadolinium chelates in hospital effluents and wastewater treatment plant sewage by a novel HILIC/ICP-MS method. *Environ Sci Technol* 2009, 43, 2884–90.
- [36] Goutelard F, et al. Optimization conditions for the separation of rare earth elements, americium, curium and cesium with HPLC technique. *J Radioanal Nucl Chem* 2009, 282, 669–75.
- [37] Dybczynski RS, et al. Comparison of performance of INAA, RNAA and ion chromatography for the determination of individual lanthanides. *Appl Radiat Isot* 2010, 68, 23–7.
- [38] Dybczynski RS, et al. Accurate determination of trace amounts of lanthanum, yttrium and all stable lanthanides in biological materials by ion chromatography. *Chem Anal* 2007, 52, 549–64.
- [39] Dybczynski RS, Kulisa K. Effect of temperature and the mechanism of zone spreading during cation-exchange separation of rare earth elements by ion chromatography. *Chromatographia* 2005, 61, 573–80.

- [40] Verma SP, Santoyo E. High-performance liquid and ion chromatography: Separation and quantification analytical techniques for rare earth elements. *Geostand Geoanal Res* 2007, 31, 161–84.
- [41] Haley BA, Klinkhammer GP. Complete separation of rare earth elements from small volume seawater samples by automated ion chromatography: method development and application to benthic flux. *Mar Chem* 2003, 82, 197–20.
- [42] Meynadier L, et al. Automated separation of Sr from natural water samples or carbonate rocks by high performance ion chromatography. *Chem Geol* 2006, 227, 26–36.
- [43] Bruzzoniti MC, et al. Determination of rare earth elements by ion chromatography. Separation procedure optimization. *Anal Chim Acta* 1996, 322, 49–54.
- [44] Cassidy RM, et al. Dynamic ion exchange chromatography for the determination of number of fissions in uranium dioxide fuels. *Anal Chem* 1986, 58, 1181–6.
- [45] Knight CH, et al. Dynamic ion exchange chromatography for determination of number of fissions in thorium-uranium dioxide fuels. *Anal Chem* 1984, 56, 474–8.
- [46] Götzte HJ, Bialkowski D. Separation of some rare earths EDTA complexes by ion-pair chromatography. *Fresenius' Z Anal Chem* 1985, 320, 370.
- [47] Saraswati R, Desikan NR, Rao TH. Determination of transition and rare earth elements in low-alloy steels as chelates with 4-(2-Thiazolylazo)resorcinol by reversed-phase high performance liquid chromatography. *Microchim Acta* 1992, 109, 253–60.
- [48] Zhang JF, et al. Behavior of new complexes of tetrakis(4-methoxyphenyl)porphyrin with heavy rare earth elements in reversed-phase high performance liquid chromatography. *J Separ Sci* 2004, 27, 1037–41.
- [49] Tsakanika LV, Ochsenuhn-Petropoulou MT, Mendrinou LN. Investigation of the separation of scandium and rare earth elements from red mud by use of reversed-phase HPLC. *Anal Bioanal Chem* 2004, 379, 796–802.
- [50] Raut NM, Jaisan PG, Aggarwal SK. Separation and determination of lanthanides, thorium and uranium using a dual gradient in reversed-phase liquid chromatography. *J Chromatogr A* 2004, 1052, 131–6.
- [51] Santoyo E, Verma SP. Determination of lanthanides in synthetic standards by reversed phase high-performance liquid chromatography with the aid of a weighted least-squares regression model – Estimation of method sensitivities and detection limits. *J Chromatogr A* 2003, 997, 171–82.
- [52] Jaisan PG, et al. Comparative study of ion interaction reagents for the separation of lanthanides by reversed-phase high performance liquid chromatography (RP-HPLC). *J Liq Chromatogr Related Technol* 2009, 32, 2146–63.
- [53] Pedreira WR, et al. Determination of trace amounts of rare earth elements in highly pure praseodymium oxide by double focusing inductively coupled plasma mass spectrometry and high-performance liquid chromatography. *J Alloys Compd* 2001, 323, 49–52.
- [54] Pedreira WR, et al. Determination of trace amounts of rare earth elements in high pure lanthanum oxide by sector field inductively coupled plasma mass spectrometry (HR ICP-MS) and high-performance liquid chromatography (HPLC) techniques. *J Alloys Compd* 2002, 344, 17–20.
- [55] Pedreira WR, et al. Determination of trace amounts of rare-earth elements in highly pure neodymium oxide by sector field inductively coupled plasma mass spectrometry (ICP-SFMS) and high-performance liquid chromatography (HPLC) techniques. *J Solid State Chem* 2003, 171, 3–6.
- [56] Pedreira WR, et al. Trace amounts of rare earth elements in high purity samarium oxide by sector field inductively coupled plasma mass spectrometry after separation by HPLC. *J Alloys Compd* 2006, 418, 247–50.

- [57] Kifle D, Wibetoe G. Selective liquid chromatographic separation of yttrium from heavier rare earth elements using acetic acid as a novel eluent. *J Chromatogr A* 2013, 1307, 86–90.
- [58] Santoyo E, Guevara M, Verma SP. Determination of lanthanides in international geochemical reference materials by reversed-phase high-performance liquid chromatography using error propagation theory to estimate total analysis uncertainties. *J Chromatogr A* 2006, 1118, 73–81.
- [59] Fidelis I, Siekierski S. Separation of heavy rare earths by reversed-phase partition chromatography. *J Chromatogr A* 1961, 5, 161–5.
- [60] Vermont J, et al. Modern liquid chromatography on Spherosil. *Anal Chem* 1975, 47, 1329–37.
- [61] Horwitz EP, Bloomquist CAA. The preparation, performance and factors affecting band spreading of high efficiency extraction chromatographic columns for actinide separations. *J Inorg Nucl Chem* 1972, 34, 3851–71.
- [62] Tsuyoshi A, Akiba K. High-performance liquid chromatography using reversed-phase stationary phases dynamically modified with organophosphorus compound for the separation and determination of lanthanoid elements. *Anal Sci* 2000, 16, 843–6.
- [63] Miranda P, et al. Study of the rare earth elements fractionation by solvent extraction: Use of HPLC as an analytical control technique. *J Alloys Compd* 2002, 344, 46–50.
- [64] Knutson HK, et al. Experimental productivity rate optimization of rare earth element separation through preparative solid phase extraction chromatography. *J Chromatogr A* 2014, 1348, 47–51.
- [65] Qin S, et al. Determination of trace rare earth impurities in high-purity cerium oxide by using electrothermal vaporization ICP-AES after HPLC separation with 2-ethylhexylhydrogen 2-ethylhexylphosphonate resin as the stationary phase. *J Anal At Spectrom* 2000, 15, 1413–6.
- [66] Qin S, et al. HPLC combined with ICP-MS for the determination of trace amounts of rare earth impurities in high-purity La_2O_3 by using 2-ethylhexyl hydrogen-2-ethylhexylphosphonate resin as a stationary phase. *Fresenius J Anal Chem* 2000, 367, 250–3.
- [67] Shuai Q, et al. Determination of rare earth impurities in high-purity lanthanum oxide using electrothermal vaporization/ICP-AES after HPLC separation. *Anal Sci* 2000, 16, 957–61.
- [68] Li CF, et al. An evaluation of a single-step extraction chromatography separation method for Sm-Nd isotope analysis of micro-samples of silicate rocks by high-sensitivity thermal ionization mass spectrometry. *Anal Chim Acta* 2011, 706, 297–304.
- [69] Murayama W, et al. A new centrifugal counter-current chromatograph and its application. *J Chromatogr A* 1982, 239, 643–9.
- [70] Araki T, et al. Further results on behaviors of rare earth metal ions in centrifugal partition chromatography with DI(2-ethylhexyl) phosphoric acid. *J Liq Chromatogr* 1988, 11, 2473–85.
- [71] Akiba K, et al. Mutual separation of lanthanoid elements by centrifugal partition chromatography. *J Liq Chromatogr* 1988, 11, 2517–36.
- [72] Nakamura S, et al. Mutual separation of heavy lanthanoid elements and yttrium by high-speed countercurrent chromatography. *Anal Sci* 1997, 13, 525–9.
- [73] Nakamura S, Watanabe M, Akiba K. Separation of yttrium from lanthanoid elements by centrifugal partition chromatography. *J Liq Chromatogr* 1995, 18, 377–94.
- [74] Nakamura S, Hashimoto H, Akiba K. Purification of yttrium by high-speed countercurrent chromatography. *J Liq Chromatogr Related Technol* 1999, 22, 451–61.
- [75] Tsuyoshi A, et al. Separation of praseodymium and neodymium by high-speed countercurrent chromatography using a stationary phase of organophosphonic acid ester. *Solvent Extr Res Dev Japan* 2000, 7, 127–38.
- [76] Tsuyoshi A., Akiba K, Nakamura S. Purification of a yttrium concentrate from xenotime by high-speed countercurrent chromatography using an organophosphonic acid stationary phase. *Solvent Extr Res Dev Japan* 2002, 9, 39–49.
- [77] Wu JF, et al. Separation of americium and europium by high speed countercurrent chromatography. *Chin J Anal Chem* 2006, 34, 1311–4.

- [78] Hennebrüder K, et al. Enrichment of rare-earth elements (REE) and Gd-DTPA in surface water samples by means of countercurrent chromatography (CCC). *Anal Chim Acta* 2005, 542, 216–21.
- [79] Kitazume E, Bhatnagar M, Ito Y. Separation of rare earth elements by high-speed counter-current chromatography. *J Chromatogr A* 1991, 538, 133–40.
- [80] Abe H, Usuda S, Tachemori S. Characteristics of centrifugal partition chromatography for lanthanoid separation in HDEHP extraction system. *J Liq Chromatogr* 1994, 17, 1821–35.
- [81] Abe H, et al. Separation of light lanthanoids by centrifugal partition chromatography in 30 % TBP extraction system. *J Liq Chromatogr* 1993, 16, 2661–72.
- [82] Dubuquoy C, Gusmini S, Poupard D. Separation of lanthanides by SA-2 ion-exchange paper chromatography. III. Separation of yttrium rare earths. *J Chromatogr* 1972, 70, 216–9.
- [83] Chen L, Yuan B. Reversed-phase paper chromatography for the separation of rare earth elements by primary amine N 1923 as a stationary phase. *Nat Sci J Xiangtan Univ* 1986, 32, 81–5.
- [84] Lederer M. Separation of rare-earth elements. *Nature* 1955, 176, 462–3.
- [85] Dubuquoy C, et al. Separation of the lanthanides by ion-exchange paper chromatography on SA-2. *J Chromatogr* 1971, 57, 455–9.
- [86] Dubuquoy C, et al. Separation of lanthanides using SA-2 paper ion exchanger chromatography studies and applications 1973, Commis Energ At Report Nr.CEA-R-4440, p. 43
- [87] Kostyuk NN. Selection of optimal conditions for separation of seven rare earth elements by paper chromatography. *Vestn Beloruss Gos Univ Ser* 2005, 2(1),7–12.
- [88] Fenyo JC, et al. Separation of lanthanides by chromatography on ion-exchange paper SA-2 in α -Hydroxyisobutyrate medium. *J Chromatogr* 1970, 49, 269–77.
- [89] Touchstone JC, Dobbins MF, *Practice of Thin Layer Chromatography*. John Wiley & Sons, New York, 1983, 2nd Edition (ISBN 0471097667), p. 103–26
- [90] Takeda Y, Ishida K. Thin-layer chromatographic behavior of rare earths on silica gel with aqueous alkaline earth metal nitrate solutions as mobile phases. *Fresenius J Anal Chem* 2001, 370, 371–6.
- [91] Soran M-L, et al. TLC separation of rare earths using di(2-ethylhexyl)dithiophosphoric acid as complexing reagent. *J. Planar Chromatogr.-Mod. TLC* 2005, 18, 160–3.
- [92] Ninomiya S, Takeda N, Ishida K. Thin-layer chromatographic behavior and separation of rare earths in silica gel-aqueous alkali metal nitrate systems. *Fresenius' Z Anal Chem* 1988, 332, 798–801.
- [93] Kuroda R, Adachi M, Oguma K. Reversed-phase thin-layer chromatography of the rare-earth elements. *Chromatographia* 1988, 25, 989–92.
- [94] Ishida K, Ninomiya S, Osawa M. Thin-layer chromatographic behavior and separation of rare earths on silica gel in aqueous ammonium sulfate solution. *Fresenius' Z Anal Chem* 1987, 328, 228–31.
- [95] Jung K, et al. Studies on the quantitative determination of rare earths after thin layer chromatographic separation with known and new eluents. *Fresenius' Z Anal Chem* 1978, 291, 328–31.
- [96] Safronova NS, et al. Inductively-coupled plasma-atomic emission spectrometric determination of rare earth elements in granites and greisens using thin-layer chromatographic preconcentration. *Analyst* 1995, 120, 1427–32.
- [97] Specker H, Hufnagel A. Thin-layer chromatography-liquid column chromatography, an ideal supplement demonstrated by the lanthanides. *Fresenius' Z Anal Chem* 1984, 318, 198–200.
- [98] Specker H. Chromatographic separation and determination of rare earths. *Chem Labor Betr* 1981, 32, 519–24.

- [99] Ishida K, et al. Thin-layer chromatographic behaviour and separation of rare earths on silica gel in aqueous ammonium nitrate solution. *J Chromatogr A* 1986, 351, 489–94.
- [100] Pierce TB, Flint RF. The rapid separation of rare earth mixtures by thin-layer chromatography. *Anal Chim Acta* 1964, 31, 595–7.
- [101] Takeda Y, Ishida K. Thin-layer chromatography of rare earths in a carboxymethyl cellulose-aqueous sodium nitrate system, and the separation of yttrium. *Bunseki Kagaku* 2004, 53, 1325–8.
- [102] Takeda Y, Ishida K. Thin-layer chromatography of rare earth elements in carboxymethyl cellulose-aqueous sodium chloride systems and the specific separation of yttrium. *Bunseki Kagaku* 2004, 53, 729–34.
- [103] Soran ML, Curtui M, Marutoiu C. Separation of U(VI) and Th(IV) from some rare earths by thin layer chromatography with di-(2-ethylhexyl)-dithiophosphoric acid on silica gel. *J Liq Chromatogr Related Technol* 2005, 28, 2515–24.
- [104] Eisentraut KJ, Siever RE. Volatile rare earth chelates, *J Am Chem Soc*, 1965, 87, 5254–6.
- [105] Utsunomiya K. Gas chromatography of rare earth chelates of isobutyrylpivalylmethane. *Anal Chim Acta* 1972, 59, 147–51.
- [106] Hicks JE, McPherson RT, Salyer JW. The effect of low concentrations of miscible organic solvents on the determination of trace metals in water samples by atomic absorption spectrometry. *Anal Chim Acta* 1972, 61, 441–8.
- [107] Greulich N, et al. Fast preparation and gas-chromatographic separation of lanthanide and actinide hexafluoroacetylacetonates. *Fresenius' Z Anal Chem* 1986, 323, 839–45.
- [108] Sieck RF, Banks CV. Gas chromatography of volatile mixed-ligand complexes of the lanthanides. *Anal Chem* 1972, 44, 2307–12.
- [109] Burgett CA, Fritz JS. Separation and quantitative determination of the yttrium group lanthanides by gas-liquid chromatography. *Anal Chem* 1972, 44, 1738–42.
- [110] Butts WC, Banks CV. Solvent extraction and gas chromatography of the rare earth mixed-ligand complexes of hexafluoroacetylacetone and tributyl phosphate. *Anal Chem* 1970, 42, 133–6.
- [111] Tanaka M. Thermogravimetric analysis and gas chromatography of rare earth chelates of trifluoroacetyl-pivaloylmethane. *Anal Chim Acta* 1968, 43, 157–8.
- [112] Fujinaga T, Kuwamoto T, Kimoto T. The rapid separation and determination of rare earth elements by use of the ligand vapour gas-chromatographic method 11 Patent pending. *Talanta* 1976, 23, 753.
- [113] Shigematsu T, Matsui M, Utsunomiya K. Gas chromatography of rare earth chelates of pivaloyltrifluoroacetone. *Bull Chem Soc Japan* 1968, 41, 763.
- [114] Shigematsu T, Matsui M, Utsunomiya K. Gas chromatography of rare earth chelates of pivaloyltrifluoroacetone. *Bull Chem Soc Japan* 1969, 42, 1278–81.
- [115] Burgett CA, Fritz JS. Separation and quantitative determination of the cerium group lanthanides by gas – liquid chromatography. *Talanta* 1973, 20, 363–9.
- [116] Harvey SD, Lucke RB, Douglas M. Rapid separation of beryllium and lanthanide derivatives by capillary gas chromatography. *J Separ Sci* 2012, 35, 2750–5.
- [117] Janos P. Analytical separations of lanthanides and actinides by capillary electrophoresis. *Electrophoresis* 2003, 24, 1982–92.
- [118] Korchemmaya EK. Separation of rare earth elements by electrophoresis. *Zh Anal Khim* 1970, 25, 705.
- [119] Timerbaev AR, Semenova OP, Bonn GK. Capillary zone electrophoresis of lanthanoid elements after complexation with aminopolycarboxylic acids. *Analyst* 1994, 119, 2795–9.
- [120] Vogt C, Conradi S. Complex equilibria in capillary zone electrophoresis and their use for the separation of rare-earth-metal ions. *Anal Chim Acta* 1994, 294, 145–53.

- [121] Jimidar M, et al. Method development and optimization for the determination of rare-earth-metal ions by capillary zone electrophoresis. *Anal Chim Acta* 1993, 284, 217–25.
- [122] Weston A, et al. Factors affecting the separation of inorganic metal-cations by capillary zone electrophoresis. *J Chromatogr* 1992, 593, 289–95.
- [123] Nukatsuka I, Taga M, Yoshida H. Separation of lanthanides by capillary-tube isotachopheresis using complex-forming equilibria. *J Chromatogr* 1981, 205, 95–102.
- [124] Wu J, et al. High performance capillary zone electrophoresis for the determination of rare earth elements. *Chin J Anal Chem* 1994, 22, 341–5.
- [125] Zhang Y, et al. Separation of lanthanides and quantification of hydronium ion by capillary zone electrophoresis. *J Liq Chromatogr Related Technol* 1996, 19, 3315–32.
- [126] Yang Y, et al. Separation and determination of rare earth metal ions with capillary ion electrophoresis. *Chin J Anal Chem* 1997, 25, 947–50.
- [127] Mao Q, et al. Separation of rare-earth ions by isotachopheresis and capillary zone electrophoresis. *J Chromatogr A* 1998, 802, 203–10.
- [128] Hirokawa T, Hashimoto Y. Simultaneous separation of yttrium and lanthanide ions by isotachopheresis. *J Chromatogr A* 1997, 772, 357–67.
- [129] Church MN, et al. Transient isotachopheretic-electrophoretic separations of lanthanides with indirect laser-induced fluorescence detection. *Anal Chem* 1998, 70, 2475–80.
- [130] Liu BF, Liu LB, Cheng JK. Separation and determination of thorium, uranium and mixed rare-earth elements as their UV/Vis absorbing complexes by capillary zone electrophoresis. *Talanta* 1998, 47, 291–9.
- [131] Yang Y, et al. Improved separation and determination of rare earth metal ions in real samples by capillary electrophoresis with indirect UV detection. *Anal Lett* 1998, 31, 1955–64.
- [132] Oztekin N, Erim FB. Separation and direct UV detection of lanthanides complexed with cupferron by capillary electrophoresis. *J Chromatogr A* 2000, 895, 263–8.
- [133] Verma SP, et al. Improved capillary electrophoresis method for measuring rare-earth elements in synthetic geochemical standards. *J Chromatogr A* 2000, 884, 317–28.
- [134] Öztekin N, Erim FB. Separation and direct UV detection of lanthanides complexed with pyridine-2-carboxylic acid by capillary electrophoresis. *J Chromatogr A* 2001, 924, 541–6.
- [135] Okamoto H., Hirokawa T. Application of electrokinetic supercharging capillary zone electrophoresis to rare-earth ore samples. *J Chromatogr A* 2003, 990, 335–41.
- [136] Saito S, Hoshino H. Highly-sensitive simultaneous detection of lanthanide(III) ions as kinetically stable aromatic polyaminocarboxylato complexes via capillary electrophoresis using resolution enhancement with carbonate ion. *Anal Bioanal Chem* 2004, 378, 1644–7.
- [137] Sun Y, Detailed study on simultaneous separation of rare earth elements by capillary electrophoresis. *J Chromatogr A* 2004, 1048, 245–51.
- [138] Kautenburger R, Nowotka K, Beck HP. Online analysis of europium and gadolinium species complexed or uncomplexed with humic acid by capillary electrophoresis-inductively coupled plasma mass spectrometry. *Anal Bioanal Chem* 2006, 384, 1416–22.
- [139] Saito S, Danzaka N, Hoshi S. Highly sensitive determination of lanthanides by capillary electrophoresis with direct visible detection after precapillary complexation with aromatic polyaminocarboxylate and additionally applying dynamic ternary complexation with nitrilotriacetic acid. *Electrophoresis* 2006, 27, 3093–100.
- [140] Sun YL, Sun M, Zhao GC. Applicability of capillary electrophoresis to the analysis of trace rare earth elements in geological samples. *Anal Sci* 2006, 22, 551–5.
- [141] Kautenburger R, Beck HP. Complexation studies with lanthanides and humic acid analyzed by ultrafiltration and capillary electrophoresis-inductively coupled plasma mass spectrometry. *J Chromatogr A* 2007, 1159, 75–80.

- [142] Saito S, et al. Direct fluorescence detection of ultratrace lanthanide(III) ions complexed with aromatic polyaminocarboxylate, avoiding quenching of ligand-centered emission, using capillary zone electrophoresis with a ternary complexing technique. *Analyst* 2007, 132, 237–41.
- [143] Santoyo E, et al. Separation and quantification of lanthanides in synthetic standards by capillary electrophoresis: a new experimental evidence of the systematic “odd-even” pattern observed in sensitivities and detection limits. *J Chromatogr A* 2007, 1149, 12–19.
- [144] Stern JC, Sonke JE, Salters VJM. A capillary electrophoresis-ICP-MS study of rare earth element complexation by humic acids. *Chem Geol* 2007, 246, 170–80.
- [145] Pitois A, Heras LAdL, Betti M. Multi-component elemental and molecular analysis of lanthanides by capillary electrophoresis–electrospray mass spectrometry (CE–ESI-MS). *Int J Mass Spectrom* 2008, 273, 95–104.
- [146] Xuejuan L, Zhefeng F. Liquid–liquid–liquid micro extraction combined with CE for the determination of rare earth elements in water samples. *Chromatographia* 2009, 70, 481–7.
- [147] Saito S, et al. Highly sensitive detection of neodymium ion in small amount of spent nuclear fuel samples using novel fluorescent macrocyclic hexadentate polyaminocarboxylate probe in capillary electrophoresis-laser-induced fluorescence detection. *J Chromatogr A* 2012, 1232, 152–7.
- [148] Vio L, et al. Separation and analysis of lanthanides by isotachopheresis coupled with inductively coupled plasma mass spectrometry. *Talanta* 2012, 99, 586–93.
- [149] Shiri-Yekta Z, et al. Separation and direct UV detection of complexed lanthanides, thorium and uranyl ions with 2-thenoyltrifluoroacetone by using capillary zone electrophoresis. *J Radioanal Nucl Chem* 2014, 302, 1143–50.
- [150] Foret F, et al. Capillary zone electrophoresis of rare-earth-metals with indirect UV absorbency detection. *Electrophoresis* 1990, 11, 780–3.
- [151] Jandick P, et al. Electrophoretic capillary ion analysis: origins, principle, and applications. *LC-GC* 1991, 9, 634–45.
- [152] Chen M, Cassidy RM. Bonded-phase capillaries and the separation of inorganic-ions by high-voltage capillary electrophoresis. *J Chromatogr* 1992, 602, 227–34.
- [153] Sethi N, et al. Supercritical fluid chromatography-a hybrid of GC and LC. *Chron Young Sci* 2010, 1, 12–22.
- [154] Karayannis NM, et al. Apparatus and materials for hyperpressure gas chromatography of nonvolatile compounds. *Anal Chem* 1968, 40, 1736–9.
- [155] Laintz KE, et al. A brief study of the supercritical fluid chromatographic behavior of lanthanide β -diketonates. *J High Res Chromatogr* 1994, 17, 603–6.
- [156] Wu H, et al. Separation of lanthanide β -diketonates via organophosphorus adduct formation by supercritical fluid chromatography. *Anal Chem* 1996, 68, 4072–5.
- [157] Lin Y, et al. Investigation of adducts of lanthanide and uranium β -diketonates with organophosphorus Lewis bases by supercritical fluid chromatography. *J Chromatogr* 1998, 793, 107–13.

Lena Telgmann, Uwe Lindner, Jana Lingott and Norbert Jakubowski

5 Analysis and Speciation of Lanthanoides by ICP-MS

Abstract: Inductively coupled plasma mass spectrometry (ICP-MS) is based on formation of positively charged atomic ions in a high-frequency inductively coupled Argon plasma at atmospheric pressure. The ions are extracted and transferred from the plasma source into a mass analyzer operated at high vacuum via an interface equipped with a sampling and a skimmer cone. The ions are separated in the mass analyzer according to their charge to mass ratio. The ions are converted at a conversion dynode and are detected by use of a secondary electron multiplier or a Faraday cup.

From an analytical point of view, ICP-MS is a well-established method for multi-elemental analysis in particular for elements at trace- and ultra-trace levels. Furthermore, methods based on ICP-MS offer simple quantification concepts, for which usually (liquid) standards are applied, low matrix effects compared to other conventional analytical techniques, and relative limits of detection (LODs) in the low pg g^{-1} range and absolute LODs down to the attomol range. For these applications, ICP-MS excels by a high sensitivity which is independent of the molecular structure and a wide linear dynamic range. It has found acceptance in various application areas and during the last decade ICP-MS is also more and more applied for detection of rare earth elements particularly in the life sciences.

Due to the fact that all molecules introduced into the high temperature of the plasma in the ion source were completely dissociated and broken down into atoms, which are subsequently ionized, all elemental species information is completely lost. However, if the different species are separated before they enter the plasma by using adequate fractionation or separation techniques, then ICP-MS can be used as a very sensitive element-specific detector. We will discuss this feature of ICP-MS in this chapter in more detail at hand of the speciation of gadolinium-containing contrast agents.

5.1 Introduction

Inductively coupled plasma mass spectrometry (ICP-MS) is one of the most successful analytical methods in atomic spectroscopy. It has found widespread acceptance in various application areas including environmental (e.g. drinking, river, sea and waste water) [1, 2], geological (e.g. trace element patterning), clinical (e.g. determination of trace metals in blood, serum and urine) [3] and industrial [4] analysis. ICP-MS is a multi-element detection method which offers simple calibration and quantification most often by liquid samples and excels by limits of detection (LODs) in the sub pg mL^{-1} range.

5.2 Fundamentals of ICP-MS

In MS, the fundamental properties of electric, magnetic and radio frequency (Rf) fields are used to separate ions with different mass to charge ratios. The ions to be separated are generated in an ion source which is the inductively coupled high-frequency plasma in case of ICP-MS. Therefore, most ICP-MS instruments consist of the following components which are schematically shown in Figure 5.1.

- A sample introduction system where the sample is converted to a physical state which is optimized for the function of the ion source. In case of ICP-MS, sample introduction is most often realized by pneumatic nebulization of a liquid sample.
- A plasma ion source, where ions are generated from atoms by use of external energies from an inductively coupled high-frequency electromagnetic field. In the plasma source, the aerosol is dried, decomposed, dissociated and atomized, excited and finally positively ionized.
- An interface system, which consists of a sampling and a skimming cone and a vacuum fore pump, by which the ions are extracted from the plasma. This device is also needed to reduce the pressure from the ion source to the vacuum needed in the mass analyzer region.
- A lens system to focus the ions into the mass analyzer.
- The mass analyzer (quadrupole [ICP-QMS], magnetic sector field [ICP-SFMS], time-of-flight analyzer [ICP-TOFMS]) where the ions are separated due to their mass to charge ratio.
- A unit by which the ions are detected (secondary electron multiplier or Faraday cup).
- A computer which controls all functions of the mass spectrometer, acquires data and delivers the mass spectrum, where the mass to charge ratios of the ions are represented with their measured intensities.

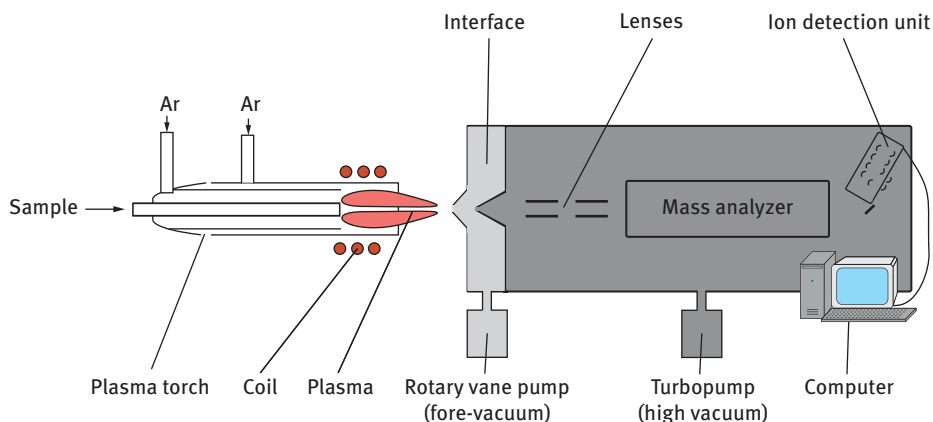


Figure 5.1: Schematic view of an ICP-MS instrument (with courtesy of Frank Bierkandt).

5.2.1 Sample preparation

ICP-MS is a method which conventionally is used for liquid analysis. For this purpose, the sample, in particular solid or particulate materials, has to be converted into a solution from which an aerosol is generated by a pneumatic nebulizer (see Section 5.2.2). The aerosol is transported continuously by a transport gas (most often Argon (Ar)) and a tubing to the plasma ion source, which is operated at atmospheric pressure.

Most often, digestion by use of mineral acids at high temperatures and high pressures is required to get solids and medical samples such as body fluids, tissues and bones into solutions. These mineral acids are often combined with oxidizing reagents in particular if carbon-rich materials have to be digested. Microwave-assisted digestions are generally sufficient to get many environmental and medical relevant materials into clear solution, which are compatible with the needs of ICP-MS (for more details see Ref. [5]).

Analyte quantification is commonly carried out by calibration with external single or multi-element standards and concerning sample handling usually an auto-sampler is applied to measure up to hundred samples a day and in some routine analytical labs the ICP-MS instruments are even working overnight. When instrumental drift or matrix effects are expected, an internal standard can be added in liquid form to compensate for intensity drift, as well as transport and ionization effects. The matrix load of an ICP-MS is usually limited to less than $1,000 \mu\text{g mL}^{-1}$ and even at low $\mu\text{g mL}^{-1}$ levels matrix effects have to be compensated. Alternatively to internal standards, matrix addition is a laborious but sensible approach if accurate data are needed and higher salt loads can be tolerated, which is the case for REE. They have to be analyzed in geological or environmental samples at ultra-trace levels due to the very low natural abundances of all these elements and thus dilution most often should be avoided.

Special care is needed in case of a speciation analysis of gadolinium (Gd)-containing contrast agents. To preserve the original species during all sample preparation steps, the common addition of nitric or hydrochloric acids to the samples has to be avoided to prevent the degradation of the chelates.

5.2.2 Sample introduction

The robustness of the ion source and the fact that the ion source is operated at atmospheric pressure enables a large variety of sample introduction systems to be used. The most common samples are in a liquid form and have to be converted into an aerosol. The aerosol is tolerated by the plasma if the droplets are small enough to be vaporized and the water load is not getting too high to effect the plasma properties. Commonly, pneumatic and, in particular, concentric nebulizers are used for aerosol generation (for a more detailed description and additional references see Refs. [6, 7]).

The most common pneumatic nebulizer consists of a nozzle in front of a concentrically centered capillary containing the analyte solution in which the liquid is accelerated by the Venturi effect using a pressurized nebulizer gas (Argon). By the turbulences generated in front of the nozzle, the liquid surface is disrupted and the liquid is dispersed into small droplets which are transported by the nebulizer gas via tubing to the plasma ion source.

Pneumatic nebulizers are typically combined with a spray chamber for removal of the larger droplets [6–8]. Additionally, cooling of the spray chamber significantly reduces the solvent load of the plasma and as a result water- and acid-based interferences. An alternative way to reduce the solvent load, which is particularly important if organic solvents are nebulized, is the use of a desolvation system. The desolvation system in most cases consists of a heated selective membrane, through which the gaseous solvent molecules are transported, whereas the dried aerosol is retained in the gas stream and transported to the plasma.

The main drawback of conventional nebulizer is their low efficiency (most often less than 5 %), which means that only a few percent of the sample liquid is injected into the plasma. This limitation can be overcome by application of high-efficiency nebulizers among which the ultrasonic nebulizer is one of the most successful ones. Micro-concentric pneumatic nebulizers working at extremely low sample introduction rates also achieve a higher efficiency. They are most often combined with separation systems requiring low mobile phase flow rates (capillary electrophoresis [CE], nano-high-performance liquid chromatography [HPLC]).

Nebulizers and spray chambers manufactured from inert polymers (such as Teflon or PFA) have to be used when aggressive chemicals, such as HF are applied. In this context, these nebulizers are most often combined with a torch injector tube manufactured from sapphire and cones made from Pt.

Many alternative sample introduction systems have been investigated with the aim of improving the sensitivity, reducing spectral interferences or handling small volumes of sample. Other sample introductions systems are used in the context of speciation (e.g. chromatographic systems) or for direct analysis of solids (e.g. laser ablation, electro-thermal vaporization).

5.2.3 The ion source

The ICP is one of the most successful analytical ion sources in atomic MS. This plasma is generated electrodeless in an atmospheric pressure discharge gas (Argon) by application of high-frequency voltages to an induction coil located at the top of a torch consisting of three concentric quartz tubes. Usually three different Argon flows are used. A relatively low gas flow rate (called inner gas, nebulizer gas, transport or carrier gas) of about 1 L min^{-1} is used for aerosol production of the liquid sample and to transport and inject the aerosol into the hot core of the plasma plume. A much higher

flow rate (10–15 L min⁻¹) (called outer gas, plasma gas or coolant gas) is introduced tangentially. This flow of Argon thermally isolates the plasma from the outer quartz tube and thus prevents melting. The third flow (Argon support gas, intermediate gas, auxiliary gas) is optionally used for alignment of the plasma in the torch. The outer quartz tube is surrounded by a water-cooled induction coil connected to an Rf generator power supply with a frequency of 27 MHz. An oscillating magnetic field induces high-frequency oscillating electrons and an ion current in a closed circular path, by which the plasma gas is heated to high temperatures (gas-kinetic temperature of 6,000–8,000 K, ionization temperature ca. 7,500 K, excitation temperature of 6,500–7,000 K, electron temperature ca. 10,000 K). The plasma is ignited by a high-voltage spark.

The ICP is thus maintained by inductive heating in the high-frequency electromagnetic field, but an electrical power of up to 1,500 W is required for continuous operation. The injected aerosol travels through a narrow axial channel, surrounded by the high-temperature plasma core forming a donut-shaped structure, where volatilization, atomization, excitation and ionization of the sample components take place. Predominantly positively singly charged ions are generated from most elements of the periodic table. The fraction of ionization of a given element is usually calculated by use of the so-called Saha–Eggert equation if the electron densities and electron temperatures are known. From this formula, it can be estimated that most elements with first ionization potentials below 8 eV are completely ionized and elements with potentials in a range between 8 and 12 eV are partly ionized. Thus, the mass spectrum acquired during a mass scan consists mainly of isotopes of singly charged elemental ions.

Due to the high temperatures and the high electron densities the ICP is a very robust electrical flame, which shows only little matrix effects. The fundamental plasma properties and analytical figures of merit are not significantly affected when the sample composition is altered. This is a tremendous advantage over many other analytical methods. Therefore, these plasmas are operated in ICP-optical emission spectrometry (ICP-OES) with quite high concentrations in the percent range; however, due to space charge effects in ICP-MS the maximum concentration tolerated is limited (see Section 5.2.1).

5.2.4 Interface

As mentioned before, the plasma of the ion source is operated at atmospheric pressure, whereas the mass spectrometer has to be operated under high vacuum conditions. Thus, an interface is required to extract the ions from the plasma and to stepwise reduce the pressure on the way to the mass analyzer. Due to the fact that the interface is in direct contact with the hot plasma, it is usually water-cooled and made of materials with high thermal conductivity and sufficient chemical resistance. It generally consists of two cones, both often made of Nickel (Ni): the sampler, which

is in direct contact with the plasma and the skimmer cone, which separates the first pumping stage from the second one. In the center of the metallic conus, an orifice (0.8–1.2 mm) is used for extraction of the ions from the plasma. The second cone (skimmer) is typically pointed and has a smaller orifice. The cones are placed coaxially in a distance of a few millimeters allowing a sequential pressure decrease. When analyzing corrosive solutions or measuring low Ni concentrations, platinum cones are preferred in order to avoid abrasion of the cone metal and Ni background, respectively. In order to reduce effects of electrostatic coupling between the load coil and the plasma discharge – resulting in an electrical discharge between plasma and sampler cone – the load coil is usually grounded at the side facing the sampler cone.

The ions generated in the plasma are sucked into the sampler orifice by the pressure drop between the atmospheric plasma and low pressure of a few mbar in the first vacuum stage. The ions are accelerated in this first pumping stage to ultrasonic velocities and are picked up by the skimmer by the flow dynamics of the hot expanding argon gas. Behind the skimmer cone a lens system is arranged for ion focusing.

5.2.5 Lens system

Behind the skimmer an additional pressure drop is generated by turbo-molecular pumps. Electrostatic fields can then be applied to an electrostatic lens system to accelerate the ions and focus them into the mass analyzer region. For reduction of the noise coming from neutrals and photons, different technical means (ion mirrors, photon stops, Omega-lenses, bended geometries in case of sector field and time-of-flight instruments) are applied to hinder them from reaching the detector.

5.2.6 Mass analyzers

Ions are separated in the mass analyzer due to their mass to charge ratio by using the fundamental properties of electric, magnetic or Rf fields. The most commonly used mass analyzer in ICP-MS is the ICP-QMS. Historically, it was first coupled to an ICP by Robert Samuel Houk in 1980 (for more details see the famous publication [5]) and was already commercially available a few years later in 1983. Since then, it had become one of the most successful multi-element techniques in atomic spectrometry.

5.2.6.1 Quadrupole analyzer

The quadrupole analyzer usually consists of four cylindrical metallic rods arranged symmetrically around a central axis. The pair of facing rods is supplied by a positive Rf and a direct current (DC) voltage, whereas the second pair is supplied by negative Rf and DC voltages. For a given combination of these voltages, only ions of a given single mass to charge value have a stable trajectory and are transmitted through the rod system whereas all others hit the wall or the rods and thus are removed from the

ion beam. Ramping the ratio between the Rf and the DC voltage offset allows fast scanning across the whole analytical mass range sequentially. ICP-QMS provide a unit mass resolution all over the mass range, which means that one peak (isotope) is separated from the neighboring peak (isotope) only. They do not reach high-resolution mode, and thus spectral interferences can limit applications of ICP-QMS.

Among spectral interferences polyatomic species are most problematic, because they are less predictable and depend on the sample composition and the operational parameters of the ICP-MS system. The formation of cluster ions from the most dominant species in the plasma (Ar, H, O, C, N) and the matrix solution (water, mineral acids, salts, etc.) is a major source of polyatomic interferences in ICP-MS.

Other technical means are therefore required to overcome these limitations by spectral interferences. Reaction and collision cells as well as double focusing sector field devices are used to overcome this limitation.

5.2.6.2 ICP-QMS combined with reaction and collision cells

Collision and reaction cells can be used in quadrupole instruments exclusively. In this approach, a pressurized cell usually is located behind the skimmer cone. Two types of gases are used in the cell: inert buffer gases (collision cell) and chemically reactive (reaction cell) gases. In the first case, the buffer gas collides with the ions from the plasma. Big molecular ions, in particular polyatomic molecular species, collide more often with the buffer gas than atomic ions due to the higher impact cross section. This results in a higher energy loss. At the exit of the collision cell, a retarding field is applied where only the atomic ions have sufficient kinetic energy to overcome the barrier. In the second approach, a reaction gas is applied that either reacts with the analyte element to shift to an un-interfered mass range, or with the polyatomic species to a product molecular ion with a significant shift of the mass. Also, charge transfer reactions are often applied to neutralize the interfering species directly. In modern instrumentation both approaches are accessible. Recently, a new technology was launched to the market, where a quadrupole mass filter is arranged in front of the reaction cell so that only preselected ions can enter the cell for reactions. This approach significantly reduces the number of unwanted reactions in the cell. Due to its similarity to organic mass spectrometers, this new approach is also known as MS/MS approach, because two quadrupoles are used synchronized to each other.

Although very powerful and quite often used, collision and reaction cell devices have a significant disadvantage: the loss in multi-element capability.

5.2.6.3 ICP-sector field mass analyzer

Most of the hardware items of a sector field device are identical to quadrupole devices. This holds true for the sample introduction, the ICP, the interface, as well as the detector and computer system. However, they contain a more complex lens system,

an entrance and an exit slit and a magnetic and an electric sector field. The lens system is needed for acceleration of all ions to high energies >8,000 electron volts (eV) and for beam shaping to adopt the circular geometry of the ion beam behind the skimmer to a more linear geometry which fits to the shape of the entrance and exit slit (for more details see Ref. [9]). The high energies are required for optimal function of the magnetic sector, which is used to separate the ions due to their mass to charge ratio. The electric sector is needed to compensate differences of the ion energy, which otherwise can compromise the resolving power of the magnetic field.

In general, sector field instruments (for more details see Ref. [9]) are equipped with up to two single detectors (Faraday cup, secondary electron multiplier or channeltron detectors) and are usually operated in scanning mode for multi-element analysis. In contrast to this type of sector field instruments, a multi-collector (MC)-ICP-MS is operated in static mode and is equipped with multiple detectors (Faraday cups, multiple ion counting systems or channel plates). The latter configuration has the advantage that all isotopes of an element are measured at the same time, which improves the precision of signal intensity measurements by orders of magnitude in comparison to all scanning devices. Due to the fact that MC-ICP-SFMS instruments are mainly applied for isotope ratio measurements, so far they are not yet applied for REE analysis and thus will be discussed elsewhere in more detail [9–11].

Compared to quadrupole devices, sector field instruments show a higher sensitivity (slope of the calibration graph) at a low resolving power and significantly reduced background due to their bended geometry (less than 1 count per second (cps) in the mass range above 100 Da) and thus lower detection limits are achieved. The main advantage of sector field instruments is the capability to apply a high mass resolving power that separates the spectroscopic interferences from the signal of the isotope of interest by variation of the slit width of the entrance and exit slit.

The resolution of the ICP-SFMS instrument is defined by

$$R = (m/z)/\Delta(m/z)$$

R: mass resolution [without units].

m: nominal mass of measured signal (peak) [should be given as a reference, because the mass resolution of an sector field instrument is constant over the mass range, and thus the peak width (Δm) of a signal increases proportional to mass. This is quite opposite to a quadrupole machine, where the peak width is constant over the whole mass range and thus the resolution increases with increasing mass].

Δm : mass difference between a peak at the nominal mass *m* and a peak at *m* + Δm .

z: absolute charge number of the isotope of interest.

Commercial instruments provide a resolution *R* of up to 10,000 by which most of the common spectral interferences originating from polyatomic species can be resolved from the isotope of interest. However, it should be mentioned that the sensitivity

Table 5.1: Mass resolution (*R*) necessary to separate typical interferences.

Nominal mass (<i>m/z</i>)	Polyatomic species	Analyte isotope	Resolution <i>R</i>
	Solvent H₂O and HNO₃		
31	¹⁴ N ¹⁶ O ¹ H ⁺	³¹ P ⁺	968
	¹⁵ N ¹⁶ O ⁺	³¹ P ⁺	1,458
54	⁴⁰ Ar ¹⁴ N ⁺	⁵⁴ Cr ⁺	2,031
	⁴⁰ Ar ¹⁴ N ⁺	⁵⁴ Fe ⁺	2,088
	Solvent HCl		
51	³⁵ Cl ¹⁶ O ⁺	⁵¹ V ⁺	2,572
52	³⁵ Cl ¹⁶ O ¹ H ⁺	⁵² Cr ⁺	1,671
75	⁴⁰ Ar ³⁵ Cl ⁺	⁷⁵ As ⁺	7,775
	Solvent H₂SO₄		
48	³² S ¹⁶ O ⁺	⁴⁸ Ti ⁺	2,519
64	³² S ₂ ⁺	⁶⁴ Zn ⁺	4,261
64	³² S ¹⁶ O ₂ ⁺	⁶⁴ Zn ⁺	1,952
65	³² S ³³ S ⁺	⁶⁵ Cu ⁺	1,939

is indirectly proportional to the resolution: higher resolutions are paid by a loss in sensitivity.

In Table 5.1, typical spectral interferences and the respective theoretical resolution for separation from the analyte isotopes are compiled.

From Table 5.1, it can be seen that a resolution of about 4,000 is already sufficient to separate most isotopes from polyatomic species. However, the resolution of commercial instruments is often not sufficient to overcome isobaric interferences from isotopes of different elements located at the same nominal mass (e.g. ⁵⁴Cr and ⁵⁴Fe) for which a resolution of more than 100,000 (73,900 to separate ⁵⁴Cr from ⁵⁴Fe) is required.

5.2.6.4 Time-of-flight mass analyzer

In a “time-of-flight” mass analyzer (ICP-TOFMS), the ions are accelerated in an electric field by a voltage applied to a grounded plate and an ion transparent grid. All ions in the electric field receive the same energy. They are separated according to the difference in time that they need to reach the detector in a fixed distance. After passing the grid the ions travel in a field-free region with velocities dependent on their mass. Low-mass ions hit the detector first, followed by heavier ions. Thus, the detector registers ion signals with μs time resolution. Depending on manufacturer up to 30,000 full mass spectra can be recorded per second. These instruments are therefore very useful for measurement of very short transient signals.

A specialized ICP-TOFMS – well known under the name “mass cytometer” – is schematically shown in Figure 5.2. This instrument [12] was introduced to the market as a trademark “CyTOF™” by the company DVS Sciences Inc. (now Fluidigm, CA, USA). The instrument addresses the challenges of a special detector for biological and medical cell flow cytometry.

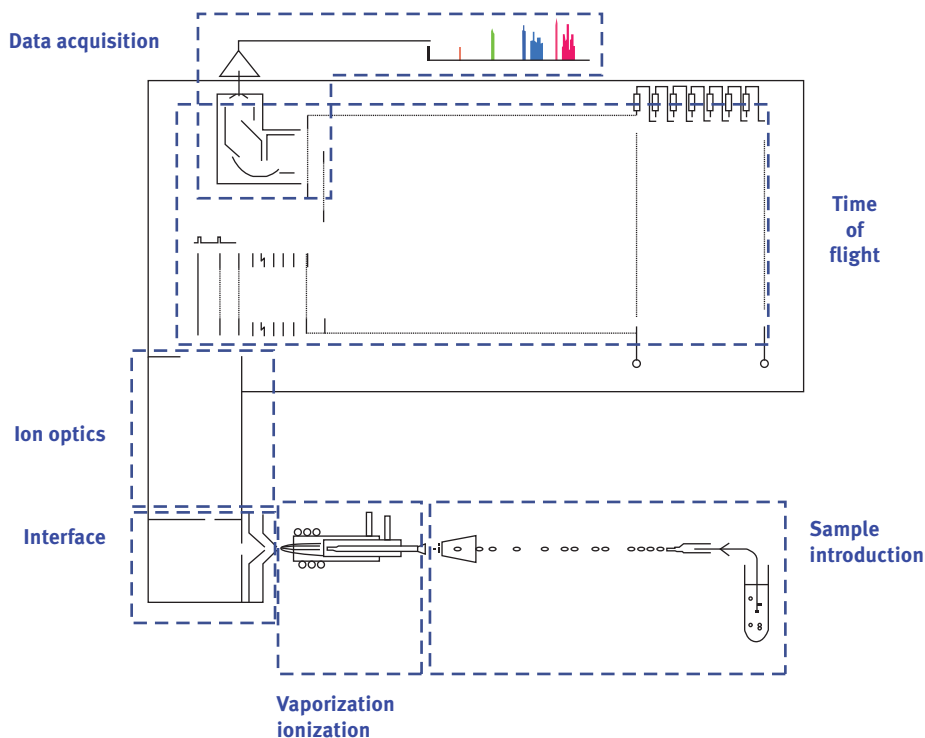


Figure 5.2: Schematic set-up of a mass cytometer (see Ref. [12]).

It employs a fast ICP-TOFMS with an integral electrostatic quadrupole deflector minimizing the exposure of ion optics and detector to unionized particles and an RF-quadrupole ion guide is used as a low-mass cut-off filter ($m/z < \text{approx.}82$) rejecting abundant interfering plasma species (for instance Ar^+ , ArO^+ , Ar_2^+). But this mass cut off also limits the range of detectable masses to >82 Da with a mass resolution $R = 600$. The sample introduction of the CyTOFTM is based on a concentric nebulizer designed and used to nebulize a cell suspension with a sample uptake rate of $<60 \mu\text{L min}^{-1}$. The nebulizer is connected to a heated spray chamber, to which a make-up argon gas flow (typically at 0.7 L min^{-1}) is supplied via a mass flow controller. In the spray chamber, the droplets with imbedded cells are dried (all water and droplets without cells are vaporized) and transported to the ICP in a laminar flow. The instrument allows multi-element analysis of a few thousand single cells just in the time frame of a second.

This instrument opens a new door for application of lanthanoid elements. A whole article (see: Novel Applications of Lanthanoides as Analytical or Diagnostic Tools in the Life Sciences by ICP-MS-based Techniques) is dedicated to this new technology, because lanthanoides are applied in this application for tagging of antibodies to detect biomarkers in highly multiplexed immune-assays, and is therefore of high interest in clinical diagnosis and cell biology.

5.2.7 Detector and computer

Most ICP-MS instruments are equipped with an ion-to-electron conversion dynode and an electron multiplier (discrete dynode detector or channeltron), which can be operated in analogue or counting mode. That allows to cope with a large variation in the number of ions that reach the detector per unit of time (cps) so that a linear dynamic range of up to 9 orders of magnitude can be achieved. For sector field instruments, an additional detector, a Faraday cup, is optional which allows extending the linear dynamic range even to 12 orders of magnitude.

Finally a computer, which controls all functions of the mass spectrometer, the generator and the vacuum system, acquires data and delivers the mass spectrum, where the mass to charge ratios of all measured isotopes are represented by their intensities. Most instruments provide all software needed for calculation of mean and integrated intensity values and standard deviations of the measured intensities. From these values, calibration, drift correction and quantification of specific elements can be performed. The operator selects all isotopes needed for analysis and arranges the samples in a given sequence defined in the software and finally evaluates the results of the whole sequence with the software.

Specialized software for peripherals, in particular special sample introduction systems, as well as for performing time resolved measurements, for instance in hyphenated techniques, is also usually provided by the instrument manufacturers.

5.3 Analytical figures of merit

All multi-element methods in atomic spectrometry are in principal suited for analysis of lanthanoides. However, analysis by ICP-OES of lanthanoides in particular REE can be problematic due to very line-rich emission spectra causing significant spectral interferences. In comparison, the mass spectrum in ICP-MS is quite simple and consists only of peaks of all isotopes of the element of interest. In the mass range of the REE, polyatomic molecules are not observed and thus ICP-MS is often applied in industry, geology and in the life sciences. Concerning spectral interferences, the main limitation of REE analysis is oxide formation which is rather a big problem compared to other elements. Careful tuning allows reducing this value below 1 %, but if all REE are present at similar concentrations, as it is the case for many geological applications, than this problem can become an important issue.

For most of the applications, in particular for industrial quality and purity control of starting products, the oxide problem can be neglected. The LODs are quite low for lanthanoides, because their natural background is rather low. However, the LODs strongly depend on the application and thus will be discussed in more details in the application section of this book.

The analysis of lanthanoides, and in particular of REE, is a general topic of this book, thus different applications will be presented where different analytical

methods are applied for multi-element analysis in different matrices (environment, geological samples, new materials) and of course ICP-MS can be applied for all these applications – a critical review is presented elsewhere [13].

In the next sections, we want to focus on a quite new application of ICP-MS where this method is used for a speciation analysis mainly of Gd-containing contrast agents in environmental waters [14].

5.4 Speciation of Gd-based contrast agents

Speciation has been defined by the International Union for Pure and Applied Chemistry as “speciation analysis is the analytical activity of identifying and/or measuring the quantities of one or more individual chemical species in a sample; the chemical species are specific forms of an element defined as to isotopic composition, electronic or oxidation state, and/or complex or molecular structure; the speciation of an element is the distribution of an element amongst defined chemical species in a system.” [15].

The most important tool for speciation studies of metals is the combination of a separation and/or a fractionation technique with ICP-MS, and most often the ICP-MS instrument is only used as a metal-specific detector, which provides a time-resolved intensity measurement for the isotope of interest. The compound of interest then is identified by standards having the same retention time and if standards are available they also can be used for calibration, just to get quantitative results.

Different separation and fractionation techniques are described in literature, and their selection depends strongly on the compounds of interest. So far, the most common separation techniques applied in ICP-MS couplings are HPLC, GC and CE. They allow speciation analysis aiming to solve analytical problems in the life sciences and in environmental research.

ICP-MS, by itself or hyphenated to separation techniques, is a powerful tool for the analysis of contrast agents for magnetic resonance imaging (MRI). The mechanism of these compounds is based on the magnetic characteristics of Gd. In ionic form, Gd enhances the MRI signals. Since the Gd ion is highly toxic for humans, it is complexed with polyaminocarboxylates for a safe application and fast excretion.

Several Gd chelates are on the market as contrast media. Chelating agents can be macrocyclic or open chains as shown in Figure 5.3. According to the number of carboxylic groups, ionic or non-ionic complexes are formed. Because of their similar extracellular distribution, administration of any of the contrast agents results in the same diagnostic information. The only exception is cartilage; here the distribution of anionic agents is lower than neutral agents because of repulsion from the negatively charged glycosaminoglycans.

Gd-based MRI contrast agents are administered intravenously eliminated rapidly by the kidneys and excreted unchanged in the urine. Due to the concentration level in which the contrast agents are administered (about 1 g/kg body weight) and the

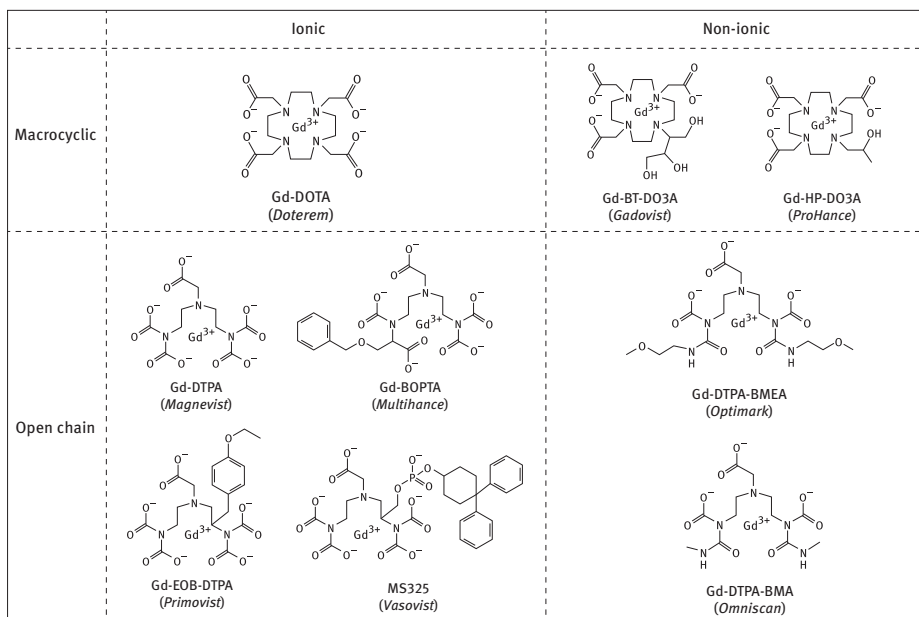


Figure 5.3: Structures of the Gd complexes employed as MRI contrast agents. The chelates can be separated in ionic and nonionic complexes and in complexes with linear or macrocyclic ligands.

demand of detailed information even in low concentrations, an analytical method with low detection limits is required for the analysis of Gd in human body fluids. ICP-MS is often used for this kind of studies.

As described in Section 5.2.1 sample preparation is necessary for most ICP-MS applications, especially for samples with a high matrix content such as human body fluids. Many studies in the past included an acid-based digestion step in their procedure in order to free samples from unwanted organic compounds. Although Gd is not normally considered as a contaminant easily picked up from the environment, sample preparation has to be carried out with care. Analysis of blood and urine samples for Gd with ICP-MS has in the past been shown to be reproducible with a high precision. Many studies investigating the excretion and pharmacokinetics of the contrast agents have been successfully employed ICP-MS.

The Gd chelates have in clinical studies been shown to be excreted unchanged. However, the discovery of the cutaneous disease nephrogenic systemic fibrosis, a rare but fatal condition that has been linked to these compounds, demonstrated the need of further investigations. Especially potential species transformations within the patient's body came into focus. Because analytes are ionized completely in the plasma, ICP-MS only detects Gd signals without molecular information. The analysis strategy needed to be extended for the characterization of the respective Gd species.

Hyphenation to a separation system is commonly the method of choice. The coupling of HPLC to mass spectrometers has in particular been the focus of researchers for speciation analysis.

All Gd chelates that are being used as active ingredient in contrast agent formulations can be separated on a range of HPLC columns. As the complexes are highly polar or even ionic, finding a suitable column is crucial. The type of stationary phase determines its ability to separate analytes of different nature. Hydrophilic interaction chromatographic (HILIC) stationary phases have been applied for the separation of the complexes with great success.

HILIC columns can consist of any polar material and several surfaces, including for example amide- or silanol-bonded phases. The Gd chelates have been separated on zwitterionic bonded phases with great efficiency. The separation mechanism is described as a hydrophilic partitioning combined with ionic interactions. Eluents are similar to reversed-phase chromatography, often based on acetonitrile or methanol.

Other stationary phases that have been used in the past for contrast agent separation are porous graphitic carbon, C₁₈, as well as silica-based gel-filtration columns and size-exclusion columns. Many of these columns, however, were generally not suitable for the simultaneous separation of all available Gd complexes, but only for two or three of the complexes.

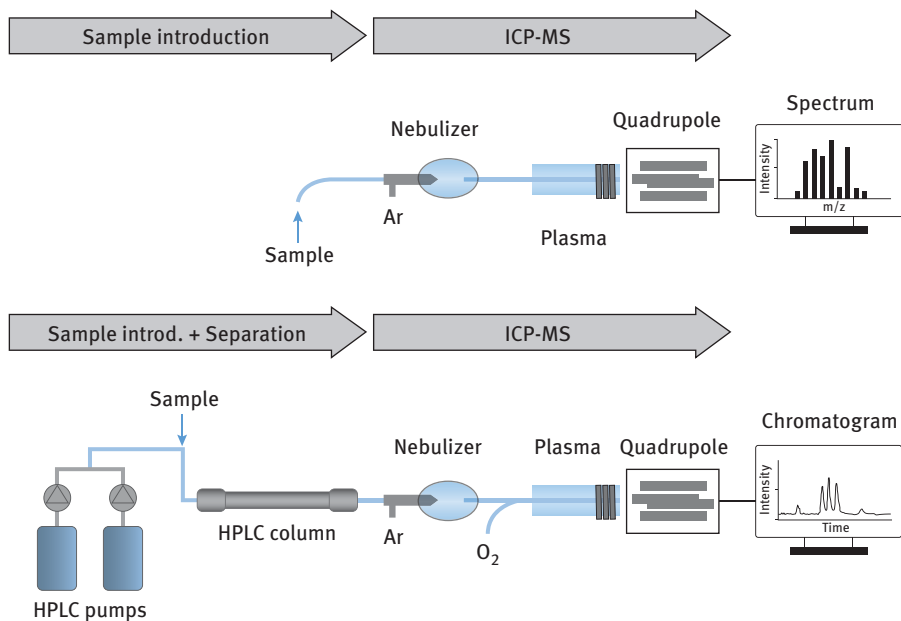


Figure 5.4: Schematic of direct sample introduction into an ICP-QMS (top) and hyphenation of an HPLC system to an ICP-QMS (bottom).

Hyphenation of HPLC systems to an ICP-MS requires an interface. In the simplest case fitting tubing for the transfer of the HPLC outflow directly into the nebulizer of the ICP-MS is sufficient. When the flow is very high, a splitting might be necessary. Often, the addition of oxygen is necessary after nebulization. Common ICP-MS instruments tolerate about 2 % organic solvent. Higher percentages overburden the plasma and the plasma extinguishes or carbon depositions on skimmer and sampler cones can cause signal drift effects. The addition of oxygen results in the reaction of the organic content to carbon dioxide. The use of common organic solvents like acetonitrile or methanol in HPLC characteristic percentages is possible.

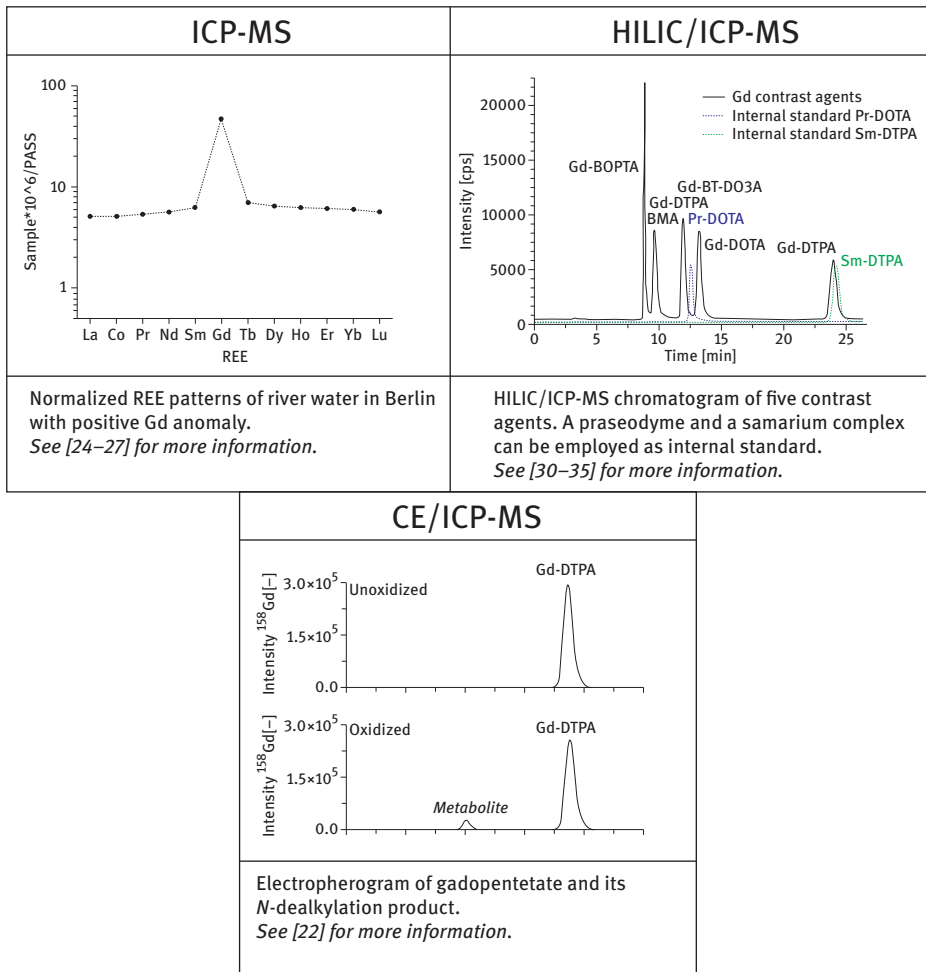


Figure 5.5: ICP-MS was employed for the determination of rare earth element concentration in river water. A chromatogram and an electropherogram show the power of separation techniques hyphenated to ICP-MS for Gd species analysis.

Figure 5.4 shows the difference between a common ICP-QMS set-up for the analysis of Gd concentrations in directly introduced samples as described in Section 5.2.2 and an HPLC system hyphenated to an ICP-QMS. When the sample is introduced directly into the plasma, a spectrum is recorded and the intensity documented. The concentration of the analyte can be determined with the intensity of the selected isotope and respective calibration measurements as described in Section 5.3.

In the HPLC system, two pumps provide a mixture of two solvents for the chromatographic separation. The sample is introduced into the flow which then enters the column. On the column, the analytes are separated. After their respective retention time, the analytes exit the column and are being transferred with the HPLC flow into the nebulizer and subsequently into the plasma. The plasma ionizes all analytes, but due to the distinct retention time and transient signal recording, the chromatographic peaks can be assigned to the respective substance. This is done by comparing the chromatogram of the sample with chromatograms of standard solutions with known analyte composition and concentration that were run under the same conditions. Analytes in the samples can then be identified by comparing retention times which are specific for individual molecules.

Figure 5.5 gives an overview on different analytical methods for Gd quantification and speciation, respectively.

5.5 Analysis of Gd-based contrast agents in medical samples

The contrast agents are excreted rapidly and especially fast in the first few hours after application. Excretion monitoring and the assessment of pharmacokinetics were the first studies carried out with ICP-MS. The excretion can be monitored well with the procedure mentioned above. Elimination rates can be determined and total excretion from the patient's body could be confirmed. In comparison to other analytical methods such as ICP optical emission spectroscopy or total reflection X-ray spectroscopy, ICP-MS exhibits the necessary low detection limits for a full monitoring of Gd concentrations.

ICP-QMS has also been applied for the analysis of Gd in tissue, fingernail and hair. The high sensitivity of the method showed great potential for accurate pharmacokinetic studies down to very low concentration levels in a wide range of sample matrix [16–18].

With the ability for speciation analysis and therefore the distinction between different Gd species, several studies concerning the potential of contrast agent transformation were carried out. The first analysis of urine samples of an MRI patient by means of HPLC/ICP-QMS showed that the injected Gd-based contrast agent was excreted fast, undissociated and almost quantitatively (>99 %). The separation of free Gd ions and gadopentetate was carried out with a size-exclusion chromatographic column [19]. The assessment of complex stability identified a difference between linear and macrocyclic ligands. HPLC/ICP-QMS analysis detected Gd ions in human

serum samples of chelates with linear ligands, indicating their release from the complex [20]. Similar results were found in a study concerning potential transmetalation of the complexes with iron ions. Transmetalation and the associated release of toxic Gd ions was shown to take place in samples with Gd complexes with linear ligands but not in samples with macrocyclic ligands. These results were shown by the complementary employment of HILIC/ICP-QMS and HILIC hyphenated to electrospray ionization (ESI)-MS [21]. The combination of the two analytical methods was also successfully employed for the investigation of metabolic reactions of the contrast agents. Electrochemical simulation of the oxidative metabolism and subsequent analysis of the respective samples by means of HILIC/ICP-MS and HILIC/ESI-MS indicated a ligand dealkylation and therefore destabilization of the complex. The same study employed another separation technique hyphenated to ICP-QMS in order to achieve more information: ionic reaction products, especially Gd ions, were investigated by means of CE/ICP-QMS [22].

The analysis of a skin biopsy sample from a suspected nephrogenic systemic fibrosis patient was carried out complementary by laser ablation ICP-QMS and HILIC/ICP-QMS. It revealed the presence of the intact Gd complex that had been administered 8 years before the analysis [23].

As can be seen from the presented studies, ICP-MS is a powerful tool for the investigation of contrast agents and their behavior in the human body. It is very important, however, to choose the appropriate analytical strategy corresponding to the objective of the study. The hyphenation of separation techniques to ICP-MS is most often necessary for species identification.

HPLC/ICP-MS will without question continue to be one of the most important analytical techniques for the detailed investigation of contrast agents as well as a whole range of other (metallo-)drugs. The constant development of new stationary phases as well as the constant improvement of ICP-MS detection limits will encourage speciation analysis of pharmaceuticals in the future.

5.6 Analysis of Gd-based contrast agents in environmental samples

A second challenge concerning Gd-based MRI contrast agents was the discovery of high Gd concentrations in surface waters. In an extensive study, rivers, tap water, sea water as well as the effluent of a wastewater-treatment plant and a hospital were sampled. The concentrations of REEs, determined by ICP-QMS, were normalized to post-Archaeon Australian Shale and showed a distinct Gd anomaly that indicated its anthropogenic nature [24]. Many studies were carried out since, all with ICP-QMS, all showing a similar pattern. Positive Gd anomalies ranging between 1.5 and 240 were exposed in many rivers that run through populated areas [25–27]. In sharp contrast, rivers in thinly populated areas did not show Gd anomalies [24]. The Gd source was

soon to be traced back to the employment of MRI contrast agents [24]. Effluents of wastewater treatment plants were analyzed with ICP-SFMS and a significant output of Gd by the plants was proven. A balancing of Gd input and output with ICP-SFMS, employing isotope dilution analysis in order to avoid matrix effects, showed that only about 10 % Gd is removed during treatment [28, 29].

In most studies, sample preparation consisted of filtration and acidification before ICP-QMS analysis. For an even more efficient determination of trace levels of Gd in natural water samples, a pre-concentration method based on solid phase extraction was developed by Raju et al. A C18 phase coated with bis-(2-ethylhexyl)-phosphate yielded in hundredfold-Gd enrichment. Recovery for several Gd complexes was >95 % [30].

Due to the toxicity of the un-complexed Gd ion, studies soon focused on the investigation of the present Gd species. Wastewater treatment plant effluent was analyzed complementary with ICP-QMS and HILIC/ICP-QMS. The results showed that the complexes are mostly intact. However, total concentrations determined by ICP-QMS were higher than the concentration of complexed Gd determined with HILIC/ICP-QMS, indicating species transformation [31].

The dilution of Gd discharged by a wastewater-treatment plant into the adjacent channel was monitored by means of ICP-QMS. The highest concentration was found close to the plant outlet as expected. Already after 2 km, the Gd concentration was constant [32]. Samples from a nature reserve into which the effluent from a wastewater-treatment plant enters the environment were examined by HILIC/ICP-SFMS. Samples were introduced as dry aerosol generated by desolvation, a process that improved detection limits for all major Gd complexes to well below 0.1 nmol L^{-1} . Several contrast agents were determined and the mass balancing showed that the contrast agent concentration accounts for about 80 % of the total Gd concentration [33]. The analyte enrichment by means of surface evaporation enhanced the ability to analyze sample with very low Gd concentrations. Lake water samples were gently heated by infrared light by Raju et al. HILIC/ICP-QMS analysis of the samples detected Gd complex concentrations in the ng L^{-1} range [34].

Gd complexes cannot only be found in surface waters; the analysis of tap water samples with HILIC/ICP-QMS proved the presence of several of the chelates in river bank filtration water. The application of a praseodymium complex as internal standard successfully corrected intensity drifts as well as changes in sample volume and matrix effects [35].

HILIC/ICP-QMS was also an appropriate analytical technique for the investigation of the uptake of Gd-based contrast agents by plants. The complexes could be extracted from cress plants that were exposed to the contrast agents. The highest Gd concentration relative to the concentration in the growing solution was observed in the leaves. Lower concentration where determined in stem and roots, indicating a concentration gradient. Speciation analysis was important for these experiments to demonstrate that Gd is transported from the roots to the leaves in complexed form [32]. An overview of studies employing different HPLC columns for separation of Gd complexes is presented in Table 5.2.

Table 5.2: Overview of different studies employing different HPLC columns for the separation of Gd complexes as well as different ICP-MS systems. The detection limit (LOD) is presented for five of the most used and most investigated Gd contrast agents [35].

	Method	LOD in pmol L ⁻¹ (absolute mass in fmol)				
		Gd-BOPTA	Gd-DTPA	Gd-DOTA	Gd-DTPA-BMA	Gd-BT-DO3A
Lindner et al. [35]	ZIC-cHILIC – ICP-QMS	14 (0.14)	13 (0.13)	14 (0.14)	22 (0.22)	19 (0.19)
Lindner et al. [32]	ZIC-HILIC – ICP-QMS	400 (2.00)	250 (1.25)	310 (1.55)	260 (1.30)	390 (1.95)
Birka et al. [23]	HILIC – ICP-SFMS (desolvation nebulizer)		90 (0.18)	100 (0.20)		80 (0.16)
Telgmann et al. [21]	HILIC – ICP-SFMS	830 (1.66)	830 (1.66)	830 (1.66)	830 (1.66)	830 (1.66)
Raju et al. [34]	ZIC-HILIC – ICP-QMS	130 (0.65)	170 (0.85)	110 (0.55)	120 (0.60)	150 (0.75)
Künemeyer et al. [31]	ZIC-HILIC – ICP-QMS	1,000 (4.00)	1,000 (4.00)	1,000 (4.00)	1,000 (4.00)	1,000 (4.00)

5.7 Summary and outlook

ICP-MS is a powerful tool for analysis of lanthanoides in various matrices. This method will always be applied if multi-element analysis of as many as possible lanthanoides is required with lowest limit of detection.

Concerning speciation the determination of Gd concentrations in environmental samples will remain a focus for future research in analytical chemistry. In particular the question how far a bio-enrichment can occur in the biosphere of aquatic compartments has to be answered. The application of MRI contrast agents based on Gd will continue and no sewage treatment stage is in sight to prevent Gd from reaching surface waters. The improvement of ICP-MS detection limits, be it through instrument upgrades, advanced pre-concentration methods or enhanced sample introduction systems, will be of major interest for environmental studies because of the low Gd concentration in many samples. This will be especially important for speciation analysis in order to give a detailed overview of the contrast agent behavior during and after wastewater treatment.

References

- [1] Moldovan M, Krupp EM, Holliday AE, Donard OF. High resolution sector field ICP-MS and multi-collector ICP-MS as tools for trace metal speciation in environmental studies: A review. *J Anal At Spectrom* 2004, 19, 815–22.

- [2] Krachler M. Environmental applications of single collector high resolution ICP-MS. *J Environ Monitor* 2007, 9, 790–804.
- [3] Taylor A, Branch S, Day MP, Patriarca M, White M. Atomic spectrometry update. Clinical and biological materials, foods and beverages. *J Anal At Spectrom* 2011, 26, 653–92.
- [4] Lange B, Recknagel S, Czerwensky M, et al. Analysis of pure copper – a comparison of analytical methods. *Microchim Acta* 2008, 160, 97–107.
- [5] Houk RS, Fassel VA, Flesch GD, Svec HJ, Gray AL, Taylor CE. Inductively coupled argon plasma as an ion source for mass spectrometric determination of trace elements. *Anal Chem* 1980, 52, 2283–9.
- [6] Montaser A. *Inductively Coupled Plasma Mass Spectrometry*. New York, NY, Wiley-VCH, 1998.
- [7] Nelms S. *Inductively Coupled Plasma Mass Spectrometry Handbook*. Oxford, Blackwell Publishing Ltd., 2005.
- [8] Thomas R. *Practical Guide to ICP-MS*. New York, NY, Marcel Dekker, Inc., 2004.
- [9] Prohaska T, Irrgeher J, Zitek A, Jakubowski N. *Sector Field Mass Spectrometry for Elemental and Isotopic Analysis*. Cambridge, Royal Society of Chemistry, 2015.
- [10] Vanhaecke F, Degryse P. *Isotopic Analysis: Fundamentals and Applications Using ICP-MS*. Weinheim, Germany, John Wiley & Sons, 2012.
- [11] Alonso J, González. *Isotope Dilution Mass Spectrometry*. Cambridge, Royal Society of Chemistry, 2013.
- [12] Bandura DR, Baranov VI, Ornatsky OI, et al. Mass cytometry: Technique for real time single cell multitarget immunoassay based on inductively coupled plasma time-of-flight mass spectrometry. *Anal Chem* 2009, 81, 6813–22.
- [13] Zawisza B, Pytlakowska K, Feist B, Polowniak M, Kita A, Sitko R. Determination of rare earth elements by spectroscopic techniques: A review. *J Anal At Spectrom* 2011, 26, 2373–90.
- [14] Szpunar J. Trace element speciation analysis of biomaterials by high-performance liquid chromatography with inductively coupled plasma mass spectrometric detection. *Trends Anal Chem* 2000, 19, 127–37.
- [15] Templeton DM, Ariese F, Cornelis R, et al. Guidelines for terms related to chemical speciation and fractionation of elements. Definitions, structural aspects, and methodological approaches (IUPAC Recommendations 2000). *Pure Appl Chem* 2000, 72, 1453–70.
- [16] Frame EMS, Uzgiris EE. Gadolinium determination in tissue samples by inductively coupled plasma mass spectrometry and inductively coupled plasma atomic emission spectrometry in evaluation of the action of magnetic resonance imaging contrast agents. *Analyst* 1998, 123, 675–9.
- [17] Saussereau E, Lacroix C, Cattaneo A, Mahieu L, Goulle JP. Hair and fingernail gadolinium ICP-MS contents in an overdose case associated with nephrogenic systemic fibrosis. *Forensic Sci Int* 2008, 176, 54–57.
- [18] Sato T, Ito K, Tamada T, Kanki A, et al. Tissue gadolinium deposit in renally impaired rats exposed to different gadolinium-based MRI contrast agents: Evaluation with inductively coupled plasma mass spectrometry (ICP-MS). *Magn Reson Imaging* 2013, 1412–17.
- [19] Loreti V, Bettmer J. Determination of the MRI contrast agent Gd-DTPA by SEC-ICP-MS. *Anal Bioanal Chem* 2004, 379, 1050–4.
- [20] Frenzel T, Lengsfeld P, Schirmer H, Hutter J, Weinmann HJ. Stability of gadolinium-based magnetic resonance imaging contrast agents in human serum at 37°C. *Invest Radiol* 2008, 43, 817–28.
- [21] Telgmann L, Wehe CA, Künemeyer J, Bülter AC, Sperling M, Karst U. Speciation of Gd-based MRI contrast agents and potential products of transmetalation with iron ions or parenteral iron supplements. *Anal Bioanal Chem* 2012, 404, 2133–41.

- [22] Telgmann L, Faber H, Jahn S, et al. Identification and quantification of potential metabolites of Gd-based contrast agents by electrochemistry/separations/mass spectrometry. *J Chromatogr A* 2012, 1240, 147–55.
- [23] Birka M, Wentker KS, Lusmüller E, et al. Diagnosis of Nephrogenic Systemic Fibrosis by means of elemental bioimaging and speciation analysis. *Anal Chem* 2015, 87, 3321–8.
- [24] Bau M, Dulski P. Anthropogenic origin of positive gadolinium anomalies in river waters. *Earth Planet Sc Lett* 1996, 143, 245–55.
- [25] Nozaki Y, Lerche D, Alibo DS, Tsutsumi M. Dissolved indium and rare earth elements in three Japanese rivers and Tokyo Bay: Evidence for anthropogenic Gd and In. *Geochim Cosmochim Acta* 2000, 64, 3975–82.
- [26] Elbaz-Poulichet F, Seidel JL, Othoniel C. Occurrence of an anthropogenic gadolinium anomaly in river and coastal waters of southern France. *Water Res* 2002, 36, 1102–5.
- [27] Zhu Y, Hoshino M, Yamada H, Itoh A, Haraguchi H. Gadolinium anomaly in the distributions of rare earth elements observed for coastal seawater and river waters around Nagoya city. *B Chem Soc Jpn* 2004, 77, 1835–42.
- [28] Telgmann L, Wehe CA, Birka M, et al. Speciation and isotope dilution analysis of Gadolinium-based contrast agents in wastewater. *Environ Sci Technol* 2012, 46, 11929–36.
- [29] Verplanck PL, Furlong ET, Gray JL, Phillips PJ, Wolf RE, Esposito K. Aqueous stability of gadolinium in surface waters receiving sewage treatment plant effluent, Boulder Creek, Colorado. *Environ Sci Technol* 2010, 44, 3876–82.
- [30] Raju CSK, Lück D, Scharf H, Jakubowski N, Panne U. A novel solid phase extraction method for pre-concentration of gadolinium and gadolinium based MRI contrast agents from the environment. *J Anal Atom Spectrom* 2010, 25, 1573–80.
- [31] Künemeyer J, Terborg L, Meermann B, Brauckmann C, Möller I, Scheffer A, Karst U. Speciation analysis of gadolinium chelates in hospital effluents and wastewater treatment plant sewage by a novel HILIC/ICP-MS method. *Environ Sci Technol* 2009, 43, 2884–90.
- [32] Lindner U, Lingott J, Richter S, Jakubowski N, Panne U. Speciation of gadolinium in surface water samples and plants by hydrophilic interaction chromatography hyphenated with inductively coupled plasma mass spectrometry. *Anal Bioanal Chem* 2013, 405, 1865–73.
- [33] Birka M, Wehe CA, Telgmann L, Sperling M, Karst U. Sensitive quantification of gadolinium-based magnetic resonance imaging contrast agents in surface waters using hydrophilic interaction liquid chromatography and inductively coupled plasma sector field mass spectrometry. *J Chromatogr A* 2013, 1308, 125–31.
- [34] Raju CSK, Cossmer A, Scharf H, Panne U, Luck D. Speciation of gadolinium based MRI contrast agents in environmental water samples using hydrophilic interaction chromatography hyphenated with inductively coupled plasma mass spectrometry. *J Anal Atom Spectrom* 2010, 25, 55–61.
- [35] Lindner U, Lingott J, Richter S, Jiang W, Jakubowski N, Panne U. Analysis of gadolinium-based contrast agents in tap water with a new hydrophilic interaction chromatography (ZIC-cHILIC) hyphenated with inductively coupled plasma mass spectrometry. *Anal Bioanal Chem* 2015, 407, 2415–22.

Man He, Bin Hu, Beibei Chen and Zucheng Jiang

6 Inductively Coupled Plasma Optical Emission Spectrometry for Rare Earth Elements Analysis

Abstract: Inductively coupled plasma optical emission spectrometry (ICP-OES) merits multielements capability, high sensitivity, good reproducibility, low matrix effect and wide dynamic linear range for rare earth elements (REEs) analysis. But the spectral interference in trace REEs analysis by ICP-OES is a serious problem due to the complicated emission spectra of REEs, which demands some correction technology including interference factor method, derivative spectrum, Kalman filtering algorithm and partial least-squares (PLS) method. Matrix-matching calibration, internal standard, correction factor and sample dilution are usually employed to overcome or decrease the matrix effect. Coupled with various sample introduction techniques, the analytical performance of ICP-OES for REEs analysis would be improved. Compared with conventional pneumatic nebulization (PN), acid effect and matrix effect are decreased to some extent in flow injection ICP-OES, with higher tolerable matrix concentration and better reproducibility. By using electrothermal vaporization as sample introduction system, direct analysis of solid samples by ICP-OES is achieved and the vaporization behavior of refractory REEs with high boiling point, which can easily form involatile carbides in the graphite tube, could be improved by using chemical modifier, such as polytetrafluoroethylene and 1-phenyl-3-methyl-4-benzoyl-5-pyrazone. Laser ablation-ICP-OES is suitable for the analysis of both conductive and nonconductive solid samples, with the absolute detection limit of ng-pg level and extremely low sample consumption (0.2 % of that in conventional PN introduction). ICP-OES has been extensively employed for trace REEs analysis in high-purity materials, and environmental and biological samples.

6.1 Introduction

Atomic emission spectrometry is a methodology for elemental qualitative, semi-quantitative and quantitative analysis, which is based on the characteristic electromagnetic radiation emitted from atoms/ions under heat/electrical excitation. Atomic emission spectrometry involves three steps: (1) The sample is vaporized, atom generation in the gas phase occurs, the atoms are excited and optical radiation under the action of the energy source is emitted. (2) The compound radiation emitted by the optical source is dispersed according to the wavelength order by the monochromator, forming a spectrum. (3) The wavelength and the intensity of the spectral lines are detected by the detector. The qualification depends on the wavelength of characteristic resonance emission line and quantification depends on the proportional relation between the signal intensity and analytes concentration.

Inductively coupled plasma (ICP) is a partially ionized gas, which is formed by the working gas in a high-frequency electromagnetic field when high-frequency current flows through the induction coil. The generated flame-shaped discharge (plasma torch) presents high temperature of around 10,000 K, which is an excellent radiation source/energy source with good performance in terms of vaporization, atomization, excitation and ionization in atomic emission spectrometry.

The plasma torch is in a cyclic structure, favoring the sample introduction from the center channel of plasma and maintaining a stable flame; carrier gas with low flow rate (less than 1 L/min) can easily penetrate the ICP, making the residence time for sample at the center channel of around 2–3 ms, complete evaporation and atomization of the sample; the high temperature provided by ICP is higher than that provided by any flame favoring the excitation of atoms and ions; samples are heated indirectly in the center channel, causing little influence on the properties of ICP discharge; ICP is a thin light source with low self-absorption phenomena, and it's an electrodeless discharge without electrode contamination.

By using ICP as the light/energy source for atomic emission spectrometry, inductively coupled plasma atomic emission spectrometry (ICP-AES), also termed inductively coupled plasma optical emission spectrometry (ICP-OES), was proposed in 1960s and developed rapidly since 1970s. ICP-OES has been demonstrated to feature multielemental analysis ability, wide dynamic linear range, low chemical interference/matrix effect, good stability and reproducibility, low detection limit, and various sample introduction techniques available for different demands in real sample analysis.

As the light source of atomic emission spectrometry, ICP can provide high temperature for the sufficient dissociation, atomization, excitation and ionization of target analytes, low background and relatively high signal-to-background ratio due to the long residence time of analytes in it. The detection limit is mainly determined by standard deviation of background signal and background equivalent concentration (BEC), and Table 6.1 lists BEC and detection limits of REEs in ICP-OES.

The merits of ICP-OES in trace REEs analysis can be specified as follows:

- (1) Low detection limits
In general, ICP-OES provides excellent detection capability for REEs with the detection limit of ng/mL level. For the elements with single oxide dissociation energy of above 7 eV (e.g., REEs, Nb, Zr), the detection limit obtained by ICP-OES is 1–2 magnitudes lower than that obtained by flame atomic absorption spectrometry (FAAS) and atomic fluorescence spectrometry (AFS). Table 6.2 lists the detection limits of REEs obtained by ICP-OES for their sensitive lines.
- (2) Good reproducibility
Without internal standard, the relative standard deviation (RSD) can be maintained at around 1–2 %.
- (3) Low matrix effect
Compared with FAAS and AFS, ICP-OES exhibits low matrix effect.
- (4) Wide linear range

Table 6.1: The analytical lines, background equivalent concentration (BEC) and detection limits (C_L) of REEs [1].

Analytical lines (nm)	BEC ($\mu\text{g/mL}$)	C_L (ng/mL)
Sc II 361.384	0.035	1.0
Sc II 357.253	0.16	4.5
Sc II 337.215	0.22	6.2
Y II 371.030	0.042	1.2
Y II 324.228	0.084	2.4
Y II 377.433	0.14	4.0
Y II 437.494	0.15	4.2
Y II 224.306	0.25	7.0
La II 333.749	0.27	7.6
La II 412.323	0.27	7.6
La II 398.852	0.30	8.5
Ce II 413.765	0.60	17.0
Ce II 413.380	0.60	17.0
Ce II 395.254	0.60	17.0
Ce II 418.660	0.60	17.0
Ce II 399.924	0.71	20.0
Ce II 446.021	0.81	23.0
Ce II 429.667	0.81	23.0
Pr II 390.844	0.53	15.0
Pr II 414.311	0.53	15.0
Pr II 417.939	0.53	15.0
Pr II 422.535	0.71	20.0
Pr II 411.846	1.41	40.0
Nd II 401.225	1.41	40.0
Nd II 430.358	1.77	50.0
Nd II 406.109	1.77	50.0
Nd II 386.340	3.54	100.0
Sm II 359.260	0.32	9.0
Sm II 442.435	0.64	18.0
Sm II 360.949	0.64	18.0
Sm II 363.429	0.71	20.0
Sm II 428.079	0.78	22.0
Sm II 446.734	0.78	22.0
Sm II 356.827	0.78	22.0
Eu II 381.967	0.025	0.7
Eu II 420.505	0.071	2.0
Eu II 272.778	0.46	13.0
Eu II 443.556	0.54	15.0
Eu II 281.294	0.71	20.0
Gd II 342.247	0.24	6.7
Gd II 336.223	0.35	10.0
Gd II 335.047	0.35	10.0
Gd II 310.050	0.53	15.0
Gd II 354.936	0.53	15.0

Table 6.1: (continued)

Analytical lines (nm)	BEC $\mu\text{g/mL}$	C_L (ng/mL)
Tb II 350.917	0.46	13.0
Tb II 367.653	0.78	22.0
Tb II 387.417	0.78	22.0
Tb II 332.440	2.12	60.0
Tb II 374.725	2.12	60.0
Dy II 353.170	0.23	6.5
Dy II 340.780	0.96	27.0
Dy II 338.502	1.27	36.0
Ho II 345.600	0.25	7.0
Ho II 339.898	0.35	10.0
Er II 337.271	0.11	3.0
Er II 349.910	0.13	3.7
Er II 326.478	0.14	4.0
Tm II 313.126	0.14	4.0
Tm II 346.220	0.25	7.0
Tm II 376.133	0.35	10.0
Tm II 336.261	0.35	10.0
Tm II 376.192	0.42	12.0
Tm II 250.908	0.71	20.0
Yb II 328.937	0.071	2.0
Yb II 369.119	0.11	3.0
Yb II 289.138	0.22	6.0
Lu II 261.542	0.026	0.74
Lu II 291.139	0.21	6.0

Note: II is the primary ionization ion line.

The linear range for REEs analysis by ICP-OES can achieve 5 magnitudes. For example, a good linear relationship can be obtained in the concentration range of 0.01–100 mg/L for the calibration standard of Yb and Tm.

6.1.1 Spectral interference

The ICP-OES spectra of REEs are complex in ICP-OES detection, and Table 6.3 lists the commonly used spectral lines for REEs analysis. As can be seen, the spectral interferences among REEs are obvious, and the spectral interferences in the determination of trace REEs, especially REEs impurities in rare earth matrix, have become a prominent and challenging issue. Taking the analysis of other 14 REEs (except Sc) impurities in Eu or Gd matrix as an example, 113 emission spectral interference lines in MIT Table [2] can be found for Eu in the range of analytical line ± 0.1 nm, and 57 emission spectral interference lines can be found for Gd.

Table 6.2: Sensitive lines and detection limits of REEs in ICP-OES.

Serial number	Element	Wavelength (nm)	Detection limits (ng/mL)	Serial number	Element	Wavelength (nm)	Detection limits (ng/mL)
1	Ce II	413.77	32	1	Eu II	381.97	1.8
2		413.38	33	2		412.97	2.9
3		395.25	35	3		420.51	2.9
4		418.66	35	4		393.04	3.8
5		399.92	39	5		390.71	5.1
6		393.11	40	6		272.78	5.4
7		446.02	41	7		372.49	5.9
8		394.28	45	8		397.20	6.3
9		429.67	46	9		443.56	8.0
10		407.58	47	10		281.39	8.7
1	Dy II	353.17	6.7	1	Gd II	342.25	9.3
2		364.54	15	2		336.22	13
3		340.28	18	3		335.05	14
4		353.60	20	4		335.86	14
5		394.47	21	5		310.05	15
6		396.84	21	6		376.84	17
7		338.50	22	7		303.28	18
8		400.05	23	8		344.00	20
9		387.21	24	9		358.50	20
10		407.80	27	10		364.62	20
1	Er II	337.27	6.7	1	Ho II	345.60	3.3
2		349.91	11	2		339.90	8.7
3		323.06	12	3		389.10	11
4		326.48	12	4		347.43	12
5		369.27	12	5		341.65	12
6		390.63	14	6		381.07	13
7		291.04	18	7		348.48	13
8		296.45	18	8		379.68	17
9		331.24	20	9		351.56	18
10		339.20	21	10		345.31	20
1	La II	333.75	6.7	1	Pr II	390.84	25
2		379.48	6.7	2		414.31	25
3		408.67	6.7	3		417.94	27
4		412.32	6.7	4		422.54	28
5		398.85	7.3	5		422.29	31
6		379.08	7.3	6		406.28	31
7		399.58	8.7	7		411.85	33
8		407.74	9.3	8		418.95	40
9		387.16	10	9		440.88	41
10		375.91	10	10		400.86	43
1	Lu II	261.54	0.67	1	Sc II	361.38	1.0
2		291.14	4.1	2		357.25	1.3
3		219.55	5.5	3		363.08	1.4

Table 6.2: (continued)

Serial number	Element	Wavelength (nm)	Detection limits (ng/mL)	Serial number	Element	Wavelength (nm)	Detection limits (ng/mL)
4		307.76	5.9	4		364.28	1.8
5		289.48	6.7	5		424.68	1.8
6		339.71	6.7	6		357.64	2.5
7		350.74	7.3	7		335.37	2.5
8		270.17	8.0	8		337.22	2.9
9		290.03	8.0	9		358.09	3.0
10		275.47	8.0	10		255.24	3.1
1	Nd II	401.23	33	1	Sm II	359.26	29
2		430.36	50	2		442.43	36
3		406.11	64	3		360.95	38
4		415.61	71	4		363.43	44
5		410.95	77	5		428.08	46
6		386.34	87	6		446.73	49
7		404.08	87	7		367.08	50
8		417.73	91	8		356.83	51
9		385.37	100	9		373.13	52
10		394.15	100	10		443.43	55
1	Tb II	350.92	15	1	Y II	371.03	2.3
2		384.87	37	2		324.23	3.0
3		367.64	40	3		360.07	3.2
4		387.42	41	4		371.43	3.5
5		356.17	42	5		437.49	4.3
6		356.85	43	6		378.87	5.0
7		370.29	43	7		361.11	5.0
8		332.44	57	8		321.67	5.3
9		389.92	64	9		363.31	5.5
10		374.73	67	10		224.31	6.1
1	Tm II	313.13	3.5	1	Yb II	328.94	1.2
2		346.22	5.4	2		369.42	2.0
3		386.80	6.5	3		289.14	5.7
4		342.51	6.7	4		222.45	5.9
5		376.13	7.3	5		211.67	6.3
6		379.58	7.3	6		212.67	6.3
7		336.26	7.3	7		218.57	8.7
8		317.28	8.7	8		275.05	11
9		376.19	8.7	9		297.06	11
10		313.39	8.7	10		365.38	14

The spectral interferences observed in ICP-OES are induced by overlapping of spectral lines, partial overlapping, molecular spectra and continuous background. There are three cases for the spectral interferences of REEs: (1) the analytical line is completely overlapped by the matrix line; (2) a strong matrix line appears on one side of

Table 6.3: Commonly used spectral lines (nm) for REEs analysis.

Sc	Y	La	Ce	Pr	Nd	Sm	Eu	Gd	Tb	Dy	Ho	Er	Tm	Yb	Lu
335.37	319.56	324.51	306.30	390.84	383.65	356.83	281.39	310.05	329.31	330.31	339.90	323.26	313.13	289.14	261.54
361.38	324.23	333.75	380.15	400.87	392.10	360.95	381.97	335.05	332.44	340.78	345.31	326.48	313.39	297.06	291.14
390.75	332.79	338.09	394.21	405.65	394.15	363.43	390.71	335.86	350.92	353.17	345.60	331.24	325.80	303.11	307.76
391.18	344.88	392.76	401.24	410.07	401.22	366.14	393.05	336.22	356.17	353.60	347.43	337.27	329.10	328.94	327.90
402.04	360.07	392.92	413.76	417.94	406.11	367.08	397.20	342.25	367.63	364.54	389.10	349.91	336.26	346.44	329.17
424.68	361.10	394.91	418.66	420.67	424.74	373.91	412.97	344.00	370.39	389.85	405.39	369.26	342.51	347.88	331.21
	362.09	398.85	422.26	422.30	430.36	388.53	459.40	365.46	384.87	400.05	410.38	390.63	344.15	369.42	347.25
	363.32	399.57	446.02	422.53	445.16	425.64	462.72	367.12	431.88	404.60	416.30	400.80	346.22	398.80	451.86
	321.03	403.17	456.24	430.58	463.42	427.97	466.19	368.41	432.64	410.39			371.79		513.51
	328.26	408.67	569.92	440.88	489.69	428.08		371.27	433.84	418.68			379.57		
	407.74	433.37		446.87	492.45	429.67		376.84		421.17			388.31		
	410.24	452.61		449.65	495.48	442.05		396.63					409.42		
	437.49	550.13		493.97		442.43		422.58							
				495.14		443.39		440.19							
						443.43									
						446.73									
						476.03									
						478.31									
						488.40									

the analytical line, causing partial overlapping; (3) the analytical line locates between two weak matrix lines or a weak matrix line appears on one side of the analytical line. The analytical line of the first two cases should not be chosen and it's better to select another analytical line. For the third case, the spectral interference depends on the matrix concentration to a great extent. If the concentration of matrix is high, the effect of spectral interference is very serious; while if the concentration of matrix is low, the spectral interference is not distinct and can be ignored when the content of target REEs is high, and the interference effect is serious and it is difficult to distinguish and recognize the analytical line accurately when the signal of target REEs is very weak.

Even if a spectrometer with high resolution is adopted, it is still difficult to completely overcome the spectral interferences for the analysis of a complex RE system. The severity of the spectral interferences is determined by not only the complex spectrum of REE matrix, but also the concentration of REE matrix. The higher the matrix concentration is, the spectral interference is more serious. Based on it, high dilution is expected to be a simple and feasible approach to reduce the spectral interferences with a premise that the analytical sensitivity is enough.

Although commercial spectrometry instrument can easily process the correction of background interference, it cannot automatically deduct the spectral interference caused by spectral overlap or partial overlap. How to judge the existence of the spectral interference and how to effectively correct the interference have become a challenge in REEs analysis. Fortunately, the prediction and correction of spectral interference between REEs spectral lines can be achieved based on the established database of REEs spectral lines. And some spectral correction technologies have been employed in trace REEs analysis by ICP-OES, including interference coefficient method, derivative spectrometry, Kalman filtering method, self-modeling curve resolution method (SMCRM) and partial least-squares method (PLS).

Interference coefficient method (or interference factor method) is the simplest method which has been widely used in spectral correction, possessing the ability of simultaneous correction of spectral interference and background interference. The Interference coefficient is obtained by the ratio of interference equivalent concentration (IEC) and the concentration of interference compounds. The limitation of the method is that it's unsuitable for the analysis of samples with changing matrix composition.

Derivative spectrometry was widely used in molecular absorption spectrometry and then introduced for spectral interference correction in ICP-OES analysis. Compared with interference factor method, derivative spectrometry exhibits more adaptability, which not only can correct the spectral interference but also can reduce IEC and improve the resolution. Kalman filtering is a more effective way to resolve serious spectral interference than derivative spectrophotometry. It can be used to correct the spectral interference of almost completely overlapping lines of Er 324.750/Cu324.754 (nm) and Nd 359.259/Sm359.260 (nm) in synthetic samples [3].

SMCRM is a mathematical method based on the resolution factor. By using SMCRM, the overlapping peaks can be decomposed into the original real shape without the need of firstly assuming the parameter and distribution function of the peaks. PLS is a stoichiometry method and is especially effective for the complex multicomponent system that can interact with each other.

It should be pointed out that these spectral interference correction technologies mentioned above are based on mathematical model and can only be used to correct spectral interference in simple matrix sample, with not enough application potential in real complex sample analysis.

To effectively resolve the spectral interference problem in trace REE analysis, some appropriate and effective measures are considered: (1) selecting another analytical line when the detection sensitivity is enough is an ideal choice, reflecting the high selectivity of atomic emission spectrometry; (2) adoption of spectrometer with high resolution and dispersive power, which is essential for analysis REEs in complex matrix; (3) using properly diluted sample solution for detection under the premise that the detection sensitivity can meet the analytical requirements; (4) using a chemical separation technology to remove REE matrix; (5) resolving the spectral interference by correction techniques.

The existence of REEs matrix has obvious effects on the spectral background. As can be seen from Figure 6.1, the intensity of the background is increased with the increase of matrix concentration. But the impact is not the same for different spectrum regions. The emission intensity of background is affected by many factors including operating parameters of ICP, apparatus properties such as dispersive power and stray light, and the spectral complexity and concentration of sample matrix. Under a certain operation condition of the instrument, the emission intensity of background mainly depends on the spectral complexity and concentration of the matrix. The emission intensity of background caused by REEs matrix (e.g., Ce, Nd, Tb) with abundant spectral lines is much stronger than that caused by REEs matrix (e.g., La, Eu) with simple spectral lines. In addition, the intensity of the background also depends on the concentration of the matrix. Taking high-purity terbium oxide as an example, when the concentration of Tb_4O_7 is 10 mg/mL, the spectrum of the matrix is very complex. Even a spectrometer with high dispersion rate (36,000/mm optical grating, 0.26 nm/mm reciprocal linear dispersion power) is unable to overcome such serious spectral interference and strong background interference, which makes quantitative determination impossible. However, the detection limit of 0.31–30 $\mu\text{g/g}$ for REEs impurity by ICP-OES detection is still achieved when the concentration of Tb matrix is reduced to 1 mg/mL [4]. When the trace REEs impurities in 99 % purity Tb_4O_7 is analyzed by a spectrometer with a moderate dispersion rate, the adopted matrix concentration was only 0.2 mg/mL.

The background interference caused by continuous spectrum or stray light can be easily deducted by the off-peak method. Presently, most of the instruments have been allocated with the function of automatic background correction. Sometimes

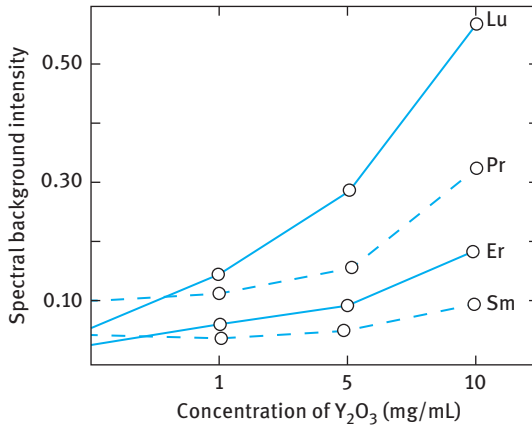


Figure 6.1: The effect of matrix concentration on the spectral background intensity [5].

the on-peak method is also employed for correction, during which matrix blank is detected immediately after each sample analysis to ensure the consistency of matrix interference value.

To understand the impact of the existence of matrix on the increase of background, background factor is proposed, which refers to the background intensity ratio between the mixed solution of 1 mg/mL matrix and corresponding analyte and the solution containing only the analytes with same concentration. Table 6.4 lists the background factors and corresponding detection limits obtained from the analysis of high-purity Tb₄O₇ samples. As can be seen from Table 6.4, the existence of matrix increases the detection limit, and the increase of background clearly makes a contribution to the increase of detection limit.

Table 6.4: Background factors and corresponding detection limits (Tb matrix concentration: 1 mg/mL) [6].

Element	Line (nm)	Background factors	Detection limits (ng/mL)	
			In water solution	In matrix solution
Y	371.030	3.62	0.4	1.2
Sm	466.734	1.80	4.0	3.0
Eu	393.048	5.85	0.7	6.0
Gd	310.050	3.67	3.0	12.0
Dy	387.211	2.53	3.0	7.0
Er	390.631	1.83	6.0	8.0

6.1.2 Matrix effect

In general, matrix effects include spectral interferences and non-spectral interferences. Non-spectral interferences are mainly caused by sample atomization, transmission, desolvation and the variation of the spectral excitation parameters. The combined influences lead to the variation of analytes' spectral intensity.

In the ICP-OES analysis of high-purity REEs, matrix effect generally exhibits an inhibition effect on the analytical signal (Figure 6.2). In other words, when RE matrix concentration exceeds a certain value in the solution, the normalized intensity of the analytes ($I_{\text{matrix}}/I_{\text{no matrix}}$) values should be less than 1. However, due to the excellent properties of ICP light source, when RE matrix concentration is less than 1.0 mg/mL, the existence of the matrix has no significant impact on the signal intensity of target analytes [7]. Besides, the severity of the REEs matrix effects is related to the medium and sample injection mode. It is reported that in contrast with the sample injection mode of water/non-desolvation, the matrix effect is more serious when the sample solution containing ethanol was introduced into the ICP with desolvation. Moreover, as the desolvation temperature increases, matrix effect is further increased [8].

Table 6.5 lists the detection limit of REEs with and without the existence of RE matrix. It shows that the existence of the matrix deteriorates the detection limit.

Signal inhibition caused by matrix effect has been discussed. Although the mechanism is still not very clear, there are some tendentious opinions.

The influence on sampling efficiency: The existence of a large number of REE matrix results in a decrease of sampling efficiency of target REEs, which is considered as an important factor.

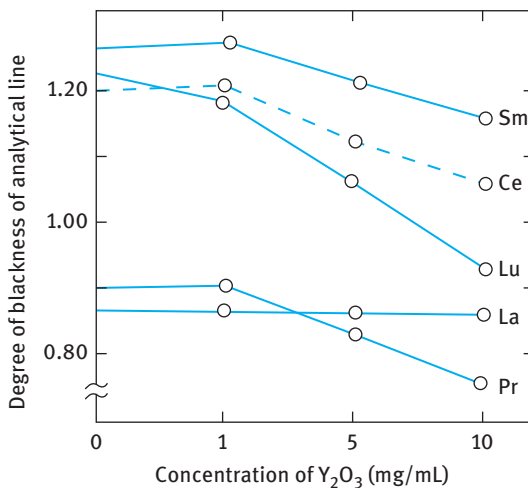


Figure 6.2: The effect of Y₂O₃ matrix concentration on target REE signals

Table 6.5: The influence of REE matrix on the detection limit of trace REEs.

Elements	Detection limit ($\mu\text{g/mL}$)		Elements	Detection limit ($\mu\text{g/mL}$)	
	Without matrix	With matrix*		Without matrix	With matrix*
La	0.025	0.04	Tb	0.20	0.40
Ce	2.5	1.0	Dy	0.10	0.80
Pr	0.25	0.80	Ho	0.10	0.40
Nd	0.05	0.06	Er	0.05	0.20
Sm	0.10	0.60	Yb	0.50	1.2
Eu	0.005	0.01	Lu	0.05	0.06
Gd	0.025	0.10	Y	0.02	0.02

Note: *Matrix (Ti_2O_3) concentration: 10 mg/mL.

The influence on excitation temperature of ICP: The existence of matrix leads to the decrease of the excitation temperature of ICP, because the evaporation and dissociation process consume a portion of energy of the ICP excitation source when the matrix is introduced into ICP.

The influence on ionization process of analytes: Based on the investigation of intensity ratio of spectral line in different types for target elements, it is found that the introduction of the matrix decreases the ionization degree of analytes in ICP.

Elastic collisions happen between analytes particles in the excited states and matrix particles in the ground state, which leads to the transfer of excitation energy.

To overcome matrix effects in REEs analysis, we can take the following measures:

(1) Matrix matching

This is the most commonly used method, processing matrix matching between the tested sample solution and standard series to eliminate the matrix effect. The main problem is that higher-purity matrix is very expensive and sometimes unavailable. In general, in the analysis of high-purity rare earth with purity of 99.99 %, we should use high-purity rare earth with purity of 99.999–99.9999 % as the matrix for matching at least. Otherwise, the blank value generated by the matching matrix cannot be ignored.

(2) Internal standard compensation

To overcome the problem of the matrix-matching method, internal standard is another effective way to eliminate the matrix effect. In high-purity REEs analysis, internal standard is the spiked elements, which has similar physical and chemical properties with target elements. Internal standard method is based on the similarity of the matrix effects on internal standard lines and analytical lines, the spectral line intensity ratio of which is irrelevant or insensitive to the existence/concentration of the matrix. Therefore, internal standard can be used to compensate for the influences of matrix. Table 6.6 lists the application of the internal standard method in high-purity REEs analysis. As can be seen, when Sc is used as the internal standard for the determination of trace REEs impurities

Table 6.6: The results of trace REEs impurities in high-purity yttrium oxide using internal standard method and matrix-matching method.

Method	Measured value ($\mu\text{g/g}$)						
	La	Ce	Pr	Nd	Sm	Gd	Dy
Internal standard method	16.0	160	<8	160	4.9	9.0	7.4
Matrix-matching method	17.0	180	<8	150	6.0	8.0	7.0

Note: Internal standard lines (nm): Sc 432.501 or Sc 337.215.

in high-purity yttrium oxide, the analysis results obtained by internal standard method are generally consistent to that obtained by matrix-matching method.

(3) Correction factor

Based on the single matrix and controllable concentration of high-purity REEs analysis, the correction factor method provides an alternative way for the compensation of matrix effect. The correction factor method is based on the fact that under a certain working conditions of ICP, the intensity of the analytical lines is mainly dominated by the properties and concentrations of REE matrix; in other words, the matrix effect is constant or nearly constant. Therefore, we can use a correction factor to compensate the matrix effect. Table 6.7 lists the analytical results obtained by correction factor and matrix-matching method. As can be seen, although the matrix effect can be corrected with the correction factor method to a certain extent, the real application of this method still requires further investigation. The limitation of the correction factor method is that it is unsuitable to the situation in which matrix composition is varied.

Table 6.7: The application of the correction factor method in high-purity yttrium oxide analysis.

Elements	Spiked amount ($\mu\text{g/mL}$)	Measured value ($\mu\text{g/mL}$)		
		Non-correction	Correction factor method	Matrix-matching method
La	0.05	0.038	0.046	0.051
Ce	0.05	0.036	0.047	0.049
Pr	0.10	0.085	0.120	0.097
Nd	0.10	0.062	0.080	0.095
Eu	0.05	0.036	0.049	0.043
Gd	0.05	0.038	0.042	0.038
Tb	0.05	0.034	0.043	0.065
Dy	0.10	0.062	0.080	0.095
Er	0.10	0.065	0.091	0.10
Lu	0.10	0.082	0.10	0.11

(4) Dilution method

When the matrix spectrum is very complex, highly diluted samples can be adopted for instrumental analysis. For instance, when the matrix is diluted to 1 mg/mL in the determination of REEs impurities in Dy₂O₃, the sample solution can be directly analyzed, and the non-spectral interference effect has been reduced to a negligible degree. Thus, the quantification can be performed without matrix matching. There are other similar reports, such as Ref. [4]. When the matrix (Tb) is diluted to 0.2 mg/mL, spectral interferences and non-spectral interferences are reduced greatly and can be ignored, and the sensitivity of the method can still meet the analysis requirements of Tb₄O₇ with purity of 99 %. Therefore, the dilution method is a simple way to reduce the matrix effects. The shortcoming of this method is that the sensitivity will be reduced.

6.1.3 Acid effect

Acid effect in ICP-OES is a kind of non-spectral interference. The presence of HNO₃, HCl, HClO₄, H₂SO₄ or H₃PO₄ would reduce the uptake amount of the solution and decrease the signal intensity of interest analytes. The effect is increasing with the order of HNO₃ < HCl < HClO₄ < H₂SO₄ < H₃PO₄, and no difference to atomic lines and ionic lines. This interference can be greatly reduced by employing peristaltic pump for sample introduction, indicating that the uptake rate variation caused by nebulization interference is the main reason.

To overcome the acid effect, some strategies can be taken:

Improvement of the working conditions of sample introduction system. Inorganic acid would lead to variation of the aerosol transportation, resulting in matrix interference. Therefore, improved nebulizer has become one of the effective ways to overcome the acid effects, such as micro-concentric nebulizer, high-efficient nebulizer, and the desolvation system has been demonstrated to be effective.

Use of high RF power and low carrier gas flow rate. Acid effect would decrease the energy transfer in the plasma, especially those acids featuring with low viscosity and low density (hydrochloric acid, nitric acid, perchloric acid) which would affect the excitation temperature and electron density of the plasma, and this influencing is much more serious than that caused by sample introduction system. Thereby increasing the RF power of the plasma (>1.2 kW) and prolonging the retention time of the analyte in the central channel of the plasma would strengthen the plasma state, and the signal intensity variation would be maintained constant as possible with the introduction of different amount of matrix.

Commonly used methods to overcome matrix interference. Matrix-matching, standard addition and internal standard methods could be used to decrease the acid effect.

6.1.4 Sensitivity-enhancing effect of organic solvent

Since Fassel et al. directly introduced organic solvent to ICP for the first time in 1976, the reports on organic solvent have been increasing, and the investigation of organic solvent in ICP has become a hot topic in this field. The research on the application of organic solvent in ICP is mainly concentrated on three points: (1) the effects of enhanced sensitivity caused by organic solvent on spectral lines and its mechanism; (2) the hyphenation of solvent extraction with it; (3) the direct analysis of metal or metalloid elements in organic samples.

6.1.4.1 Affecting factors

The main factors that can influence the analytical functions of organic ICP are summarized as follows:

(1) Forward power

A high forward power must be provided to keep a steady discharge of organic ICP. When the solutions containing inorganic matter, organic matter, or both inorganic matter and organic matter are separately introduced to ICP, it is found that the incident power of organic ICP is about 0.5 kW higher than that of aqueous ICP on the same conditions. The possible reason is that the particles formed during organic molecular decomposition process give rise to the conductance and thermal conduction of aerosol tunnel.

Additionally, the analytical intensity of spectral line is increasing with an increase of the power, while the increasing rate of background intensity is lower, resulting in an improvement of the signal/noise ratio of spectral line. Besides, increasing the incident power would allow more uptake amount of samples with no quenching of the plasma.

(2) Gas flow rate and observation height

The increasing of cooling gas flow rate could weaken the emittance of cyanogen molecular band and has no obvious influence on the intensity of spectral line. When organic solvents are introduced into the plasma, auxiliary gas would not be shut down in order to prevent the deposition of carbon particles on the wall of middle and inside tube of torch. Carrier gas flow rate affects the intensity of spectral line seriously, which varies with the properties of spectral line, namely hard line or soft line. Generally, the best observation height for the analysis of organic solutions is lower than that for the analysis of aqueous solutions.

(3) Uptake rate of solutions and ICP tolerance

It is found that the solvent with higher vapor pressure, such as methanol, acetone, benzene and cyclohexane, is difficult to be introduced, but for the solvent with lower vapor pressure the situation is contrary. One of the reasons for ICP quenching is the unstability of the plasma and impedance unmatching which is caused by the sudden entering of too much organic solvent with higher vapor pressure.

There are two ways to improve the tolerance capacity of ICP for organic solvents. One is to increase the incident power, and the other is to control the uptake rate of the solvent. Generally speaking, the higher the evaporation factor of solvent is, the slower the ultimate uptake rate is.

6.1.4.2 Enhanced sensitivity caused by organic solvents in REEs analysis

It has been long observed that the introduction of organic solvent could enhance the spectral line intensity of REEs and improve the detection sensitivity of ICP-OES for REEs.

6.1.4.2.1 Enhanced sensitivity by ethanol

By using the conventional pneumatic nebulization (PN) sample introduction system, 15–30 % (v/v) ethanol solution are found to effectively improve the spectral line detection for most elements in ICP-OES. Based on the investigation of the effects of ethanol on the spectral line intensity of REEs, it is found that the spectral line intensity of REEs is increased, and the background intensity decreases with the increase of ethanol concentration. What's more, the sensitivity-enhancing effect on the ionic spectral line is higher than that on the atomic spectral line. Thus, the introduction of ethanol is beneficial to improve the detection limit of REEs (Table 6.8).

The introduction of ethanol also affects the stability of ICP discharge, especially when the working power of ICP is relatively low. The lower the working power is, the less the amount of ethanol the plasma can tolerate. So a higher working power should be employed when ethanol is introduced to ICP compared with aqueous solution.

Introducing ethanol to ICP would cause some negative effects, such as the instability of ICP discharging, the deposition of carbon particles formed during the decomposition of organic matter at high temperature and the resulting molecular spectrum of cyano group, which would cover the corresponding band of light spectrum.

Table 6.8: The effect of ethanol on the detection limit of REEs.

Element	Wavelength (nm)	Detection limit (ng/mL)		Element	Wavelength (nm)	Detection limit (ng/mL)	
		Ethanol	Water			Ethanol	Water
La	333.749	14	29	Dy	364.540	25	33
Ce	418.963	71	90	Ho	339.898	14	19
Pr	422.293	95	120	Er	337.271	2.3	3
Nd	401.225	52	146	Tm	313.126	4.7	8.7
Sm	442.434	99	190	Yb	328.937	0.78	0.87
Eu	381.967	8	12	Lu	261.542	17	3
Gd	303.285	56	71	Y	324.228	30	5.4
Tb	387.417	230	570				

6.1.4.2.2 Mechanism for sensitivity-enhancing effect of ethanol

Some research showed that the enhanced sensitivity caused by ethanol on the spectral line of REEs can be attributed to the improved nebulization efficiency and atomization efficiency based on the introduction of ethanol.

In order to investigate the influence of ethanol on nebulization efficiency, Chen et al. [9] compared two mixing situations, mixing ethanol with water in solutions and mixing two aerosols of ethanol with water. The results show that the sensitivity-enhancing effect caused by mixing ethanol with water in solutions is obviously higher than that by mixing aerosols, indicating that the sensitivity-enhancing effect of ethanol depends on the improvement of sample nebulization and mass transfer process. Because the surface tension of ethanol is lower than that of water, ethanol is easier to form tiny droplet. Similar conclusion was obtained in some Refs [10, 11], and it is specified that the sensitivity enhancing of the REEs spectral line is caused by the decreasing of the droplet diameter and the increasing of the transition rate of target elements.

To investigate the effect of ethanol on the nebulization efficiency, the mixed aerosol of ethanol and water in different ratios are introduced into the plasma, and the results are shown in Figure 6.3. As can be seen, with the increase of ethanol concentration, the intensity of REE spectral line is increased obviously; when the concentration of ethanol is higher than 60 % (v/v), the increasing of the spectral line intensity is sharper. The results show that REE compounds may experience a process of first dissociating and then recombining, forming monoxide of REEs finally which is difficult to dissociate. While when the existence amount of ethanol is enough, the possibility of forming REEs monoxide is reduced because of the strong reducing property of carbon particles or carbon-containing free radicals which occur in high temperature, thus improving the atomization efficiency.

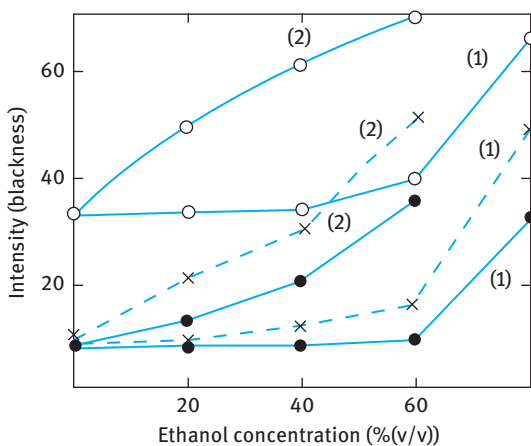


Figure 6.3: The effect of ethanol on nebulization and atomization efficiency (x, Ho; •, Tm; ◐, Y; (1) introduction after aerosol mixing; (2) introduction after solution mixing) [9].

6.1.4.2.3 Organic solvent and pre-desolvation

Yang et al. [12] proposed that the combination of the sensitivity-enhancing effects of organic solvent (ethanol) and desolvation would improve the detection sensitivity of REEs.

(1) Effect of desolvation temperature

As can be seen from Figure 6.4, the signal-to-noise ratio of REEs is gradually increased with the increasing of the desolvation temperature from 150 to 300 °C. And the detection limits of interest REEs are obviously improved when the desolvation temperature is 300 °C and the concentration of ethanol is 95 % (v/v). Compared with non-desolvation aqueous solution, the detection limits of REEs are decreased about one order of magnitude (Table 6.9).

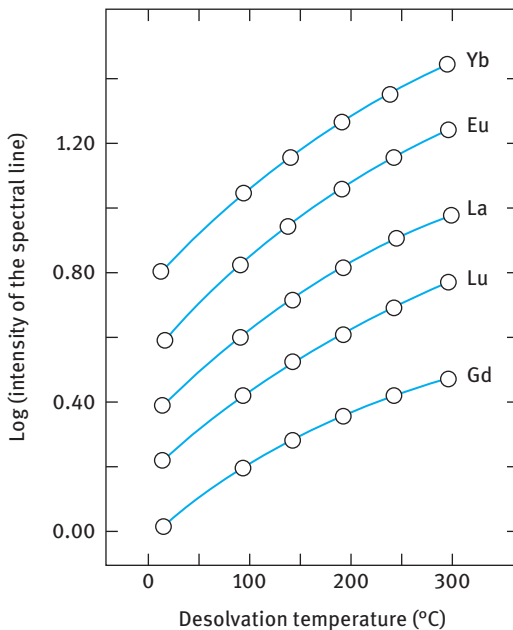


Figure 6.4: The effect of desolvation temperature on the spectral line intensity of REEs [12].

Table 6.9: The detection limit of REEs with/without desolvation [12].

Elements	Line (nm)	Detection limit (ng/mL)		
		Non-desolvation (Water)	Desolvation (Water)	Desolvation (95 % Ethanol)
La	399.575	49	28	5
Eu	281.395	41	22	3.7
Gd	342.247	23	13	2.5
Yb	289.139	21	14	3
Lu	347.148	53	21	4.9

It should be pointed out that (1) desolvation also depends on the concentration of matrix concentration. The improvement of the detection limits is obvious without the matrix existing, and the improvement is more and weaker when the concentration of matrix is increasing. Thus, there is a strict limit on the total salinity of the sample solution for desolvation sampling, generally less than 5 mg/mL. Otherwise, the high salinity not only affects the improvement of the detection limits but also causes torch blockage; (2) compared with non-desolvation, the matrix effect is obviously enhanced (Figure 6.5) when the sample is introduced into the plasma under desolvation. As can be seen, the spectral line intensity of the elements is decreased clearly when the concentration of Y matrix is up to 1 mg/mL. Moreover, the analytical signal is decreased by nearly 50 % when the concentration of Y matrix is up to 5 mg/mL; the matrix effect increases with the increasing of the desolvation temperature.

(2) The effect of ethanol concentration

Figure 6.6 shows the effect of the ethanol concentration on the spectral line intensity of REEs with the desolvation temperature of 300 °C. As can be seen, the signal of analyte is gradually raising with the increasing of ethanol concentration up to 95 % (v/v).

Based on the investigation of the effect of ethanol concentration and desolvation temperature on the sampling rate of the analytes into the plasma (the quantity of the analytes entering the plasma excitation area in unit time), it can be concluded that (1) the loss rate of analytes in transportation would drop

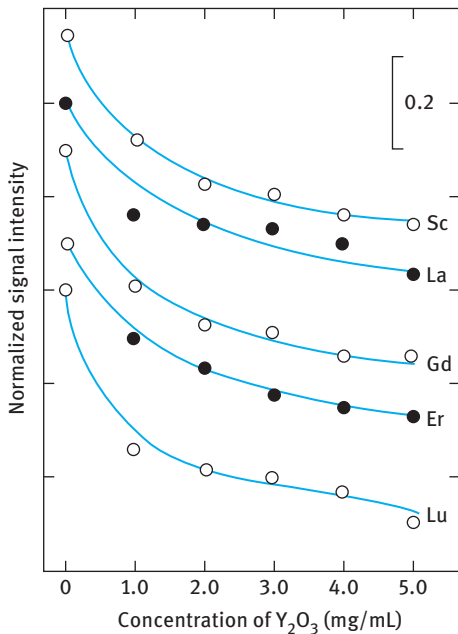


Figure 6.5: The effect of Y matrix on spectral line intensity of REEs under pre-desolvation [12].

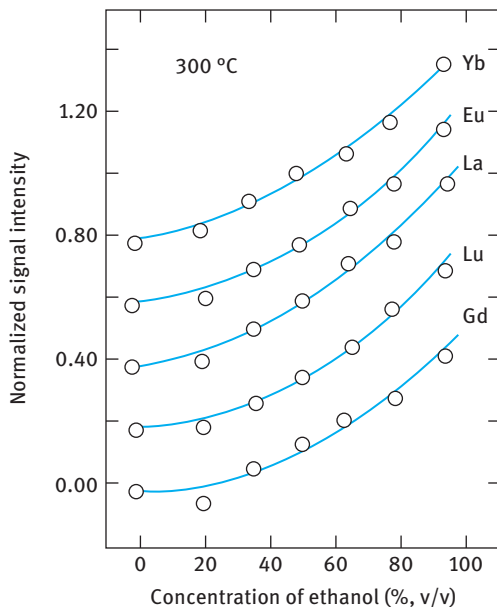


Figure 6.6: The effect of ethanol concentration on the signal intensity of REEs in ICP-OES.

to 50 % with the increase of ethanol concentration, specifically, 95 % loss of the analyte in aqueous solution to 50 % loss in 95 % ethanol. (2) The desolvation efficiency is increased from 32 to 73 % with the increase of the desolvation temperature, and the loss of analytes is further decreased. Above all, it can be assumed that the reason why it can improve the detection sensitivity of REEs through the combination of ethanol with desolvation is that the uptaking rate of analytes into the torch is enhanced and the effect of the solvent on the plasma is excluded or decreased during the process.

(3) Matrix effect in ethanol/desolvation system

Yang et al. [7, 12] systematically investigated the matrix effects in ethanol/desolvation system and compared it with normal non-desolvation system. It was found that the existence of 1 mg/mL Y matrix has no obvious effect on the normalization intensity of target analyte, while the spectral line intensity is obviously decreased with desolvation sampling under the same condition.

The performance of matrix effect observed under the condition of ethanol/desolvation can be described as follows: (1) The effect on the sampling efficiency: it showed that when the concentration of matrix is in the range of 1–5 mg/mL, the sampling efficiency of analytes is decreased nearly 40 % compared with that obtained under no matrix existence. (2) The effect on the excitation conditions of ICP: it was found that the ionizability of target element (Yb) is decreased when the matrix was introduced into ICP based on the investigation of

the intensity ratio of the spectral line in different types (atomic line and ionic line). Moreover, the ICP temperature was measured and it was found that the excitation temperature of the plasma is decreased with the introduction of matrix to the plasma, probably due to that the process of matrix evaporation and dissociation consumes a part of energy of ICP.

(4) Sensitivity-enhancing effects by other solvents for REEs analysis

Chen et al. [13] investigated the sensitivity-enhancing effects of five organic solvents, including butyl acetate, methylisobutylketone, chloroform xylene and phenoxin, and on target REEs, and combine it with liquid extraction technique. In this process, target REE ions formed organometallic chelates firstly with the organic agent PMBP, and the compound was extracted from aqueous solution to organic phase using appropriate organic solvents and then directly introduced into ICP. The sensitivity-enhancing factor obtained by five organic solvents for La and Y is listed in Table 6.10. It can be found that the introduction of all tested organic solvents exhibited sensitivity-enhancing effects in different degree, and the order is butyl acetate > MIBK > $\text{HCCl}_3 \approx \text{phenoxin} \approx \text{CCl}_4$. A comparison of the detection limit and RSD for La and Y obtained in different solvents is listed in Table 6.11.

Based on the distribution ratio difference of La in TBP- HNO_3 system with other REEs, the selective extraction and separation of REEs impurities (Eu-Lu and Y) from

Table 6.10: Sensitivity-enhancing factor of organic solvent on La and Y.

Solvent	Enhancing factor ($I_{\text{organic solution}}/I_{\text{aqueous solution}}$)			
	La 333.7 nm	La 338.0	Y 324.2 nm	Y 371.0 nm
Methylisobutylketone	2.7	2.7	6.8	7.8
Butyl acetate	6.3	4.9	14.2	16.4
Xylene	2.2	3.3	3.6	13.6
Chloroform	3.1	3.6	6.3	11.4
Phenoxin	2.0	2.4	3.0	4.7

Table 6.11: Detection limit and precision for La and Y in different solvents.

Solvent	La		Y	
	DL (ng/mL)	RSD (%)	DL (ng/mL)	RSD (%)
Water	26	1.2	2.6	3.6
Butyl acetate	2.9	2.4	0.18	1.0
Methylisobutylketone	6.3	3.5	0.31	2.1
Xylene	10.3	4.2	0.86	6.4
Chloroform	15.8	6.1	0.70	4.7
Phenoxin	19.4	2.9	2.6	3.1

La matrix were processed by using TBP as the extractant [14]. The organic phase was directly introduced into ICP for detection and the detection limit of the method is ranging from 0.34 to 9.3 ng/mL.

6.2 Sample introduction for ICP

The analytical performance of plasma source spectrometry is highly dependent on the employed sample introduction techniques. Therefore, the research on new sample introduction techniques has always received the greatest attention. An “ideal” sample introduction technique should meet these requirements: (1) high sample introduction efficiency; (2) low sample mass requirement and (3) powerful ability to analyze a wide variety of samples with complex matrix. However, it is difficult to realize the above-mentioned criteria even with a PN, which is the most popular sample introduction technique in ICP-OES.

6.2.1 Pneumatic nebulization and ultrasonic nebulization

Conventional PN sample introduction is characterized with several shortcomings including low transport efficiency (ca. 10 %), large sample mass requirement and possible risk of blockage in the nebulizer during the analysis of samples containing high concentration of dissolved salts or slurries. Although Babington nebulizer can be applied to the direct analysis of these samples, it was particle diameter dependent and severely suffered from the matrix effect.

By using an ultrasonic nebulizer coupled to a desolvation system the amount of solvent entering the plasma can be drastically reduced and sensitivity improved. Bentlin et al. [15] compared pneumatic and ultrasonic nebulization in terms of the detection limits for both radially and axially viewed plasma, by monitoring the most sensitive spectral lines when possible. It was found that the lowest detection limits were obtained by using ultrasonic nebulization and axially viewed plasma (Table 6.12). The best detection limits obtained with ultrasonic nebulization are mainly due to the greater aerosol output of the ultrasonic nebulizer (the sample uptake rate and aerosol transportation to the plasma are higher than those of the MicroMist nebulizer). The detection limits found using ultrasonic nebulization and axially viewed plasma are lower than those reported for La, Ce, Nd, Sm, Eu, Er and Yb, measured using ultrasonic nebulization ICP-OES and matrix removal [16]. For comparison purposes, the detection limits obtained by PN-ICP-MS [17] are also shown in Table 6.12. It can be seen that detection limits found using ultrasonic nebulization and axially viewed plasma are in general only one order of magnitude higher, or less, than those found by ICP-MS.

6.2.2 Flow injection

In 1975, Ruzicka and Hansen [18] published their research works, which marked the establishment of a new analytical technique – flow injection analysis (FIA). In 1981,

Table 6.12: Selected spectral lines of the lanthanides and respective detection limits (mg/L) by ICP-OES as a function of the nebulizer and plasma view [15].

Analyte	Pneumatic		Ultrasonic		ICP-OES [16]	ICP-MS [17]
	Axial	Radial	Axial	Radial		
La (II) 398.852	0.164	0.818	0.010	0.073	0.30	0.004
Ce (II) 413.380	1.436	4.799	0.069	0.272	0.93b	0.004
Pr (II) 414.311	1.114	2.767	0.036	0.237	–	0.003
Pr (II) 390.844a	0.834	3.401	0.041	0.205	–	–
Nd (II) 406.109	1.252	2.696	0.060	0.194	0.51c	0.018
Sm (II) 360.949	0.804	2.023	0.062	0.417	–	0.016
Sm (II) 359.260a	2.077	3.398	0.039	0.221	0.25	–
Eu (II) 381.967	0.034	0.140	0.003	0.019	0.045	0.011
Gd (II) 335.047	0.504	2.684	0.036	0.309	–	0.013
Gd (II) 342.247a	0.196	0.659	0.012	0.106	0.72	–
Tb (II) 350.917	0.349	1.942	0.023	0.211	–	0.004
Tb (II) 367.635a	1.354	4.610	0.039	0.239	–	–
Dy (II) 353.170	0.165	0.579	0.007	0.045	–	0.011
Ho (II) 345.600	0.167	0.512	0.008	0.065	–	0.004
Er (II) 349.910	0.160	0.922	0.013	0.137	0.12d	0.012
Tm (II) 384.802	0.433	1.050	0.009	0.080	–	0.003
Yb (II) 328.937	0.018	0.061	0.003	0.090	0.01	0.010
Lu (II) 261.542	0.017	0.124	0.003	0.014	0.006	0.003

Fang [19] introduced the instrument, principle and application of FIA in China for the first time. The application of FIA in atomic spectrometry is originated in atomic absorption analysis (AAS), and it was until 1980 when Ito et al. [20] introduced FIA into ICP-OES. From then on, FIA was applied widely in ICP-OES as an on-line/pretreatment technology for trace analysis. Fu et al. [21] reviewed the application of FIA in REEs analysis in China, which was mainly concentrated on the hyphenation of FIA with spectrophotometry, and electroanalysis and ICP-OES analysis were discussed as well. The hyphenation of FIA with ICP-OES merits low sample consumption, simple operation, rapidity, good reproducibility, low pollution and easy automation, demonstrating that it is a kind of promising sampling technique. The characteristics of FIA coupled with atomic spectroscopy can be summarized as follows:

- (1) Sample volume is usually 10–300 μL .
- (2) Sample throughput can be as high as 500 h^{-1} .
- (3) The absolute detection limit can be improved.
- (4) The clogging of nebulizer can be prevented effectively.
- (5) The impact caused by matrix or acidity variation can be reduced.
- (6) An improved reproducibility can be obtained over common continuous sampling.
- (7) Online dilution is available for the determination of target elements with different concentration.

- (8) The sensitivity-enhancing effect of organic solvent can be fully utilized, and the resistance for organic solvent in FIA-ICP-OES system is apparently higher than that in common ICP-OES system.

6.2.2.1 FIA coupled with ICP-OES for direct determination of trace REEs

Chen et al. [22] applied FIA-ICP-OES for the determination of 14 trace REEs in the high-purity Y_2O_3 directly. When the employed sample volume was 1 mL in which the matrix concentration was 40 mg/mL, detection limit for target REEs was in the range of 0.25–12.5 g/g, with RSD of 1.0–2.9 %. This method can be used for the rapid and accurate determination of trace REEs in Y_2O_3 with 99.99 % purity.

Compared with conventional PN, FIA-ICP-OES has the following obvious advantages:

- (1) Both of acid and matrix effects can be reduced to a certain extent, and these two interferences can be further reduced with the decrease of sample injection volume (Figure 6.7), which is probably due to the dilution effect of carrying flow on the sample and the sampling mode of peristaltic pump. Luo et al. [23] investigated the chemical/physical interference by using three injection modes, PN, peristaltic pump uptake and flow injection, and it was found that the acid effect was effectively eliminated or reduced in FIA system.

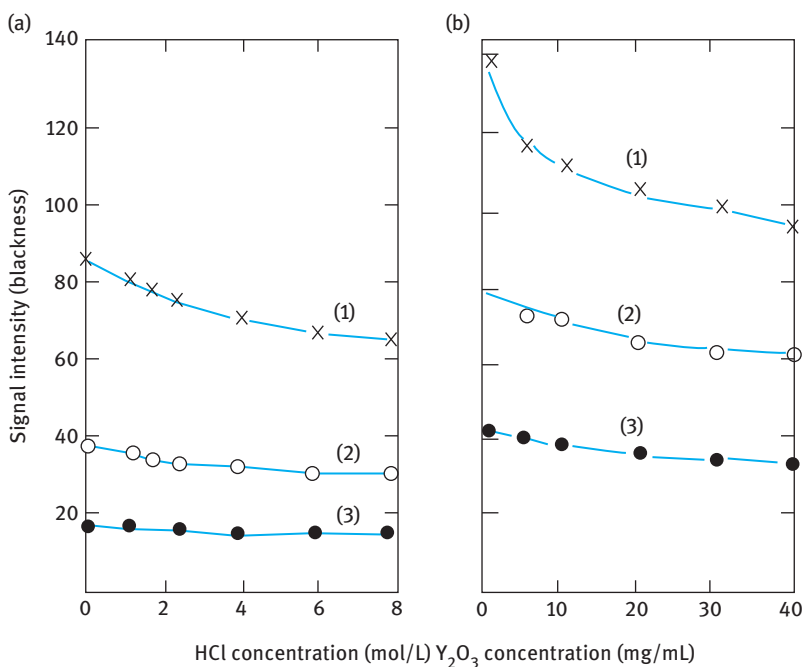


Figure 6.7: The effect of HCl and matrix concentration on the signal intensity of REEs [22]: (a) HCl, Gd 335.1 nm; (b) Y_2O_3 , Er 337.2 nm; (1) continuous pneumatic nebulization; (2) FIA, 1 mL; (3) FIA, 0.36 mL.

- (2) High concentration of matrix in sample solution is allowable. It was found in the experiment that no clogging happened in nebulizer or ICP center tube when 50 mg/mL Y_2O_3 matrix was introduced into the plasma by FIA system continuously for a long time. Apparently, it is closely related to the dilution effect of carrying flow and the rapid contact of sample solution with the nebulizer or central tube.
- (3) Reproducibility of the method can be further improved. Table 6.13 lists a comparison of analytical performance obtained by PN and FIA-ICP-OES for REEs.

6.2.2.2 Standard addition method in FIA

In this method, sample solution is used as the carrying flow, the standard solutions with different concentrations are successively injected into the carrying flow by the sampling valve, and they flow through a coil of a certain length to mix sufficiently, followed by introducing directly into the nebulization system and subsequent ICP-OES detection. The obtained curve is shown in Figure 6.8, and the cross point which is made by the working curve and the concentration axis is the determined concentration of target analyte in the sample solution. This standard addition method is called flow injection reverse standard addition method, also called interpolating standard addition method.

The reverse standard addition method was applied to the determination of single REE in the mixed REEs sample [24], featuring with simple operation, rapid analysis, good accuracy, and it is unsusceptible to the variation of sample composition. Yet a

Table 6.13: A comparison of analytical performance of REEs in Y_2O_3 matrix [22].

Analytes	LOD ($\mu\text{g/g}$)			RSD (%)	
	C (10 mg/mL)	F (20 mg/mL)	F (40 mg/mL)	FIA	PN
La	5	10	2.5	1.0	2.1
Ce	10	50	12.5	2.5	4.1
Pr	10	50	12.5	2.4	3.0
Nd	10	10	12.5	2.5	4.4
Sm	10	50	12.5	2.2	3.4
Eu	1	1	0.25	1.3	1.0
Gd	1	5	2.5	2.6	5.5
Tb	5	5	1.25	2.9	6.5
Dy	1	1	0.25	1.2	3.5
Ho	1	1	0.25	2.8	5.5
Er	1	1	0.25	1.8	3.3
Tm	5	5	1.25	2.2	5.5
Yb	1	1	0.25	1.0	1.6
Lu	10	10	2.5	2.2	6.5

Note: LOD, limit of detection; C, continuous nebulization; F, flow injection; (), matrix concentration.

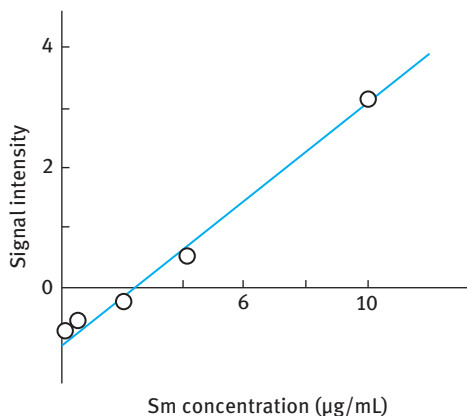


Figure 6.8: The curve of Sm concentration vs. signal intensity in flow injection reverse standard addition method (Sm 359.2 nm) [24].

large volume of sample solution is consumed in this method. The main influencing factors in this method include the length of mixing tube, injection volume, flow rate and signal integration interval. In order to obtain accurate results, the spiked amount of the standard series solutions should be closed to the concentration of target analytes in the real sample.

Three standard addition methods in FIA-ICP-OES analysis are compared in terms of the analytical performance, including (1) interpolating standard addition method (sample solution is the carrying flow), spiking standard series with fixed volume into the carrying flow; (2) gradient correction technology, spiking standard series with different concentration into sample solution; (3) the method in which water carrying flow is in front of the sample solution, which is followed by the standard series. The order for the precision is (1) > (3) > (2), (2) > (1) > (3) for the simplicity, and (2) > (1) > (3) in sample consumption.

6.2.2.3 Online separation/preconcentration ICP-OES for trace REEs analysis

Online flow injection (FI) combined with ICP-OES detection is widely used for the analysis of metals and metalloids. The advantages are summarized as follows: (1) high enrichment efficiency; (2) low sample/reagent consumption; (3) simple operation and high analytical efficiency. Yet the injection volume and sample throughput restrain mutually; the improvement of detection limit is limited; the separation device/operation is relatively complex. The commonly used online separation/preconcentration system is shown in Figure 6.9. And Table 6.14 lists the representative application of online FI separation/preconcentration ICP-OES for trace REEs analysis.

6.2.3 Laser ablation

As an inefficient solid sampling technique, laser ablation (LA) has been successfully employed in ICP-OES. Arrowsmith et al. [32] reported the strategy by using LA as

Table 6.14: Online FI separation/preconcentration ICP-OES for trace REEs analysis.

Sample	Analytes	Stationary phase	Elution	Enrichment factors	Sample throughput (h ⁻¹)	LOD	Ref.
Mineral	REEs	Chelate resin	1 mol/L HCl	99	–	sub-ng/mL	[25]
High-purity zinc	La, Nd, Eu, Gd, Tb, Dy, Ho, Lu	DSC-arsenazo loaded activated carbon	4 mol/L HCl	12	–	ng/mL	[26]
Water samples	La	P507 chelating resin	1 mol/L HCl	30	60	0.7 ng/mL	[27]
Mineral	14 REEs	P507 extraction-eluting resin	3.5 mol/L HNO ₃	8–15	14	0.05–0.5 µg/g	[28]
Natural water and coal fly ash	Co, Cd, Cr, Cu, Mn, Ni, V, Ce, Dy, Eu, La and Yb	Mesoporous TiO ₂	2 mol/L HCl	10	20	0.03–0.36 µg/L	[29]
Acid drainage	Sc	oxidized multi-walled carbon nanotubes	30 % (v/v) HNO ₃	225	10	4 ng/L	[30]
Environmental water	REEs	CCTS-AHBA resin	2 mol/L HNO ₃	21.1–30.8	–	1–18 ng/L	[31]
Urine samples	La	Amberlite XAD-7 resin	2 mol/L HNO ₃	100	–	90 ng/L	[31]

Note: CCTS-AHBA, functional moiety of 2-amino-5-hydroxy benzoic acid (AHBA) chemically bonded to amino group of cross-linked chitosan (CCTS).

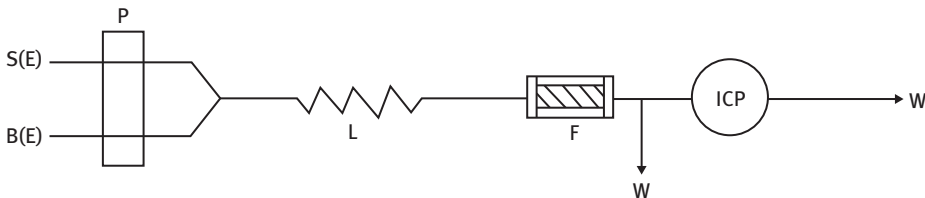


Figure 6.9: Online separation/preconcentration system combined with ICP [26] (P – pump; E – elution solution; S – sample; L – reaction/mixing coil; F – microcolumn; W – waste).

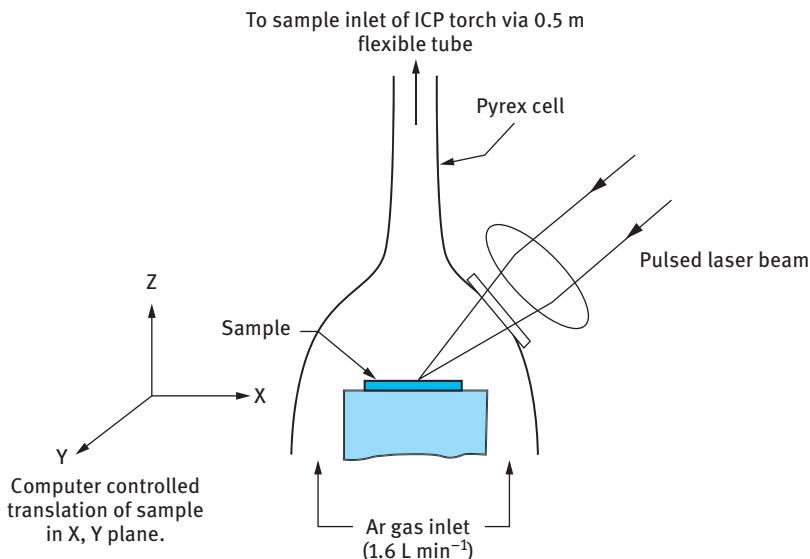


Figure 6.10: Schematic diagram of the laser ablation housing for 45° laser beam angle of incidence [32].

the sampling system and ICP as the excitation unit. The schematic diagram of the apparatus is presented in Figure 6.10.

LA-ICP-OES is featured with low absolute detection limit (ng to pg level); the ability for conductor and nonconductor analysis, especially those solid samples difficult to decompose (e.g., complicated minerals, ceramics); supplementary means of micro-analysis; non-destructive analytical techniques; and low sample consumption, just 0.2 % of that needed in conventional PN sampling.

Lin et al. [33] employed LA-ICP-OES for the direct determination of refractory elements (including REEs) in minerals without chemical separation, and relative detection limits of g/g or much lower were achieved. In the sample preparation, graphite, caprolactam and polychlorotrifluoroethylene (2:2:4) were used as the diluent, and the sample was mixed with the diluent with the ratio of 1:4. 6 mg mixed sample was pressed into discs (Ø25 mm × 1.5 mm) and used for direct detection. The obtained detection limit for the refractory elements is listed in Table 6.15.

The addition of a certain amount of organic fluorinating reagent benefits the improvement of the vaporization behavior of target analytes, decreasing the effect of existing form of matrix and target analytes on the vaporization process. If the concentrated analytes can be introduced into plasma completely, the detection limit will be decreased efficiently. Under a certain condition, trace REEs were selectively adsorbed on an ionic-exchange paper, which was then vaporized by continuous laser and introduced into ICP for detection. The detection limit of ng/g can be obtained (Table 6.16).

Table 6.15: The detection limits for refractory elements by LA-ICP-OES.

Element	Relative detection limit($\mu\text{g/g}$)	Absolute detection limit (ng)	Element	Relative detection limit($\mu\text{g/g}$)	Absolute detection limit (ng)
Ba	2.6	3.1	Ce	11	13
Cu	0.1	0.12	Cr	9.7	1.2
La	6.1	7.3	Mn	10	12
Nb	8.0	9.6	Sc	17	20
Sr	3.0	3.6	Ti	–	–
V	11	13	Y	4.5	5.4
Yb	0.62	0.74	Zr	4.5	5.4

Table 6.16: Trace REEs analysis by LA-ICP-OES combined with chemical separation/preconcentration technique.

Element	Wavelength (nm)	Detection limit (ng/g)	Element	Wavelength (nm)	Detection limit (ng/g)
La	379.1	1	Dy	353.1	0.1
Ce	371.1	30	Ho	345.6	0.6
Pr	390.8	10	Er	369.3	1
Nd	406.1	10	Tm	346.2	0.1
Sm	359.2	1	Yb	328.9	0.1
Eu	381.9	0.1	Lu	350.7	1
Gd	342.2	1	Y	371.0	0.1
Tb	350.9	1			

6.2.4 Electrothermal vaporization

This technique was developed from the atomizer source in graphite furnace atomic absorption spectrometry (GFAAS) and has gained renewed interest by the atomic spectroscopy community due to its outstanding characteristics compared with conventional PN. Firstly, ETV has high transport efficiency (approximately 80 %), which is useful to promote the detection limits for the analysis of real samples. Secondly, the ETV steps of sample vaporization and its excitation/ionization are separated spatiotemporally, which is helpful in removing the matrix and reducing non-spectroscopic or spectroscopic interferences from the matrix. Thirdly, the low sample mass requirement of ETV is favorable to some situations in which only a small amount of sample is available. Finally, ETV is quite suitable for direct analysis of solid samples, which leads to increasing applications in trace analysis.

Since the precursory reports of using a tantalum filament device as a vaporizer for ICP in 1974 [34] and employing a graphite furnace for sample introduction for ICP in 1978 [35], ETV-ICP-OES has been developed as an important tool for the determination

of trace elements. When ETV sample introduction devices were hyphenated to ICP-MS [36], the performance of high sensitivity and solid sample analysis potential of ETV-ICP-MS attracted great attention for the determination of elements at trace and ultra-trace levels. Nowadays, ETV-ICP-OES/MS has been considered as one of the most versatile methods with respect to its accommodation of different types of samples with complex matrices (non-aqueous solutions, high dissolved salt or acid concentrations, slurries, and solid samples), especially solid samples.

6.2.4.1 Analytical performance

ETV-ICP-OES merits wide linear range, simultaneous multielement detection ability and good anti-interference capability in comparison with GFAAS. ICP-OES equipped with an ETV device offers 1–2 orders of magnitude improvements in detection limits, compared with conventional pneumatic nebulizer as sample introduction for the determination of many elements. The absolute detection limits generally range from sub-nanogram to picogram level for ETV-ICP-OES and from picogram to femtogram level for ETV-ICP-MS. Table 6.17 compares the analytical performance of ETV/PN-ICP-OES with GFAAS.

6.2.4.2 ETV devices and operation parameters

The vaporizers used in ETV are usually modified from a metal coil atomizer (tungsten, platinum, tantalum, etc.) or a graphite furnace. The metal coil device has smaller size than the latter, which facilitates its use in some miniaturized analysis instruments. However, its inherent potential to interact with oxygen and evaporate at high temperature prevents its application as an atomizer. Consequently, the graphite furnace is employed most often, even though it suffers from “memory” effect at high temperature due to analyte transferring into the inner surface of graphite tube and formation of refractory carbides. The use of pyrolytic graphite-coated tube or metallic carbide-coated tube could improve the performance of graphite furnace ETV.

Many designs have been studied in order to obtain a high transport efficiency of analyte from ETV to ICP. One of the most used designs is the horizontal flow-through

Table 6.17: Analytical performance of ETV-ICP-OES, PN-ICP-OES and GFAAS.

Analytical performance	ETV-ICP-OES	GFAAS	PN-ICP-OES
Detection limit	+	+	–
Anti-interference	+	–	++
Multielement simultaneous determination	–	–	+
Linear range	–	–	+
Micro sample introduction	+	+	–
Analytical rate	+	+	+
Analytical cost	–	+	–

Note: + represents good performance; – represents bad or average performance.

type. The carrier gas flows through the longitudinally heated graphite tube from one end to the other toward the plasma. In order to form a stable aerosol, a finely designed cold gas flow was usually incorporated at the outlet of the graphite furnace. The bypass cold gas is favorable for minimizing aerosol condensation and deposition in the transferring tubing.

Some factors are usually considered in the design of the electrothermal vaporization (ETV) device: (1) avoiding the condensation and deposition of sample aerosol in the internal surface of evaporation chamber; (2) providing maximum vapor density for transmission; (3) reducing the pulse effect (piston effect) in the ICP to keep the stability; (4) achieving long retention time of analytes in the plasma and maximizing the atomization/excitation efficiency. A schematic diagram of ETV-ICP system by using a graphite furnace as the vaporizer is presented in Figure 6.11.

It should be noted that the role played by graphite furnace in GFAAS and in ETV-ICP-OES/MS is different. For GFAAS, the graphite furnace is used not only as

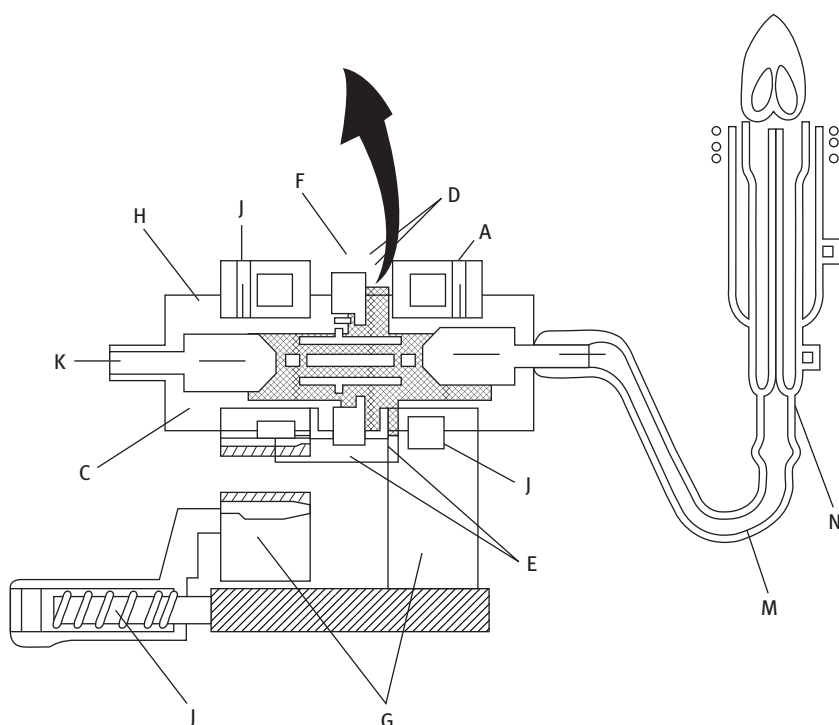


Figure 6.11: Schematic diagram of ETV-ICP system by using a graphite furnace as the vaporizer (A – graphite tube; B – sampling hole; C – graphite seat; D – seat cover; E – packing ring; F – filling plug; G – electrothermal unit; H – pipe connector; I – cooling water pipe; J – compression spring; K – carrier gas; L – outside flow air; M – PTFE tube; N – ICP torch) [37].

a vaporizer but also as an atomizer, in which the sample drying, ashing and atomization take place. Sometimes, it is difficult to achieve a complete atomization for refractory elements and carbide-forming elements, due to restricted maximum available temperature (2,800–3,000 °C) and the small size of space in the graphite furnace. However, for ETV-ICP-OES/MS, the graphite furnace is only used as a vaporizer, in which the sample undergoes drying, ashing and evaporation. In this case, a complete vaporization of the analyte and its efficient transportation into ICP, in which excitation/ionization of the analyte occurs, are only necessary for adjusting the graphite furnace as sample introduction device.

Good performance of ETV-ICP-OES/MS depends on its operation conditions. A higher flow rate of carrier gas would decrease the dilution effect on aerosol, whereas a lower gas flow rate would lead to a longer retention time of analyte in the plasma, which is favorable for multielement detection. Optimization of ICP-OES/MS should also be carried out usually with a conventional PN method, before its connection with ETV. Similarly to GFAAS, the temperature programs for ETV-ICP-OES/MS also consist of drying, ashing and vaporization steps. During the drying step, the sample overheating and plasma overloading should be prevented. Successful removal of matrix may be realized by proper usage of drying and ashing steps. The optimized vaporization temperature should be chosen for good signal profiles and the highest intensities of analytes of interest.

6.2.4.3 Limit of conventional ETV system

Low vaporization and transportation efficiency of interesting analytes sometimes occurred in conventional ETV-ICP-OES, which is mainly caused by the following situations: (1) the analytes vaporized out before vaporization step in the temperature programs, which is called ashing loss; (2) incomplete vaporization of interest analytes leads to a decrease in the transportation efficiency; (3) the deposition of analytes in the internal surface of ETV device and the transportation tubing result in a decreased transportation efficiency.

To achieve complete vaporization of refractory elements and those that can easily form nonvolatile carbides with graphite at high temperature, the following strategies can be adopted:

- (1) Employing refractory metal (e.g., Ta) as the vaporizer. The disadvantage of this vaporizer is that these metals can easily react with active substances in air and sample to become brittle at high temperature. Moreover, the vaporization of these metals at high temperature may cause spectral interferences.
- (2) Coating the graphite tube with metallic carbides. While it could improve the detection limits of several elements it led to worse detection limits of some others.
- (3) Use of chemical modifiers. Chemical modifiers could be spiked to react with interest analytes (or matrix), forming volatile compounds which can be vaporized out. It is proved to be efficient and effective to resolve this problem.

The most widespread and efficient type of chemical reaction is halogenating reaction, especially fluorination and chlorination reaction. The halogenating reaction can easily happen at high temperature to a great number of elements and the formed halide is more volatile than their oxide substances. Besides, metal chelating and alkylating reactions can also be employed.

The chemical modifiers can be divided into inorganic and organic chemical modifiers. Comparatively, organic chemical modifiers are more commonly used in ETV-ICP-OES system, probably due to the more degradability of organic reagents, which can easily release active substances.

The chemical modifiers can be spiked into ETV system in gaseous or solid form. Gaseous chemical modifier (e.g., Freon) is mixed into the carrier gas (Ar), and the reaction process is happening between gaseous chemical modifiers and solid samples; solid modifiers are mixed with the sample evenly or prepared into slurry solution, followed by introducing into the vaporizer. Slurry sample introduction inherits the advantages of direct solid sample introduction and liquid sample introduction.

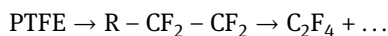
6.3 ETV-ICP-OES for REE analysis

When ETV-ICP-OES is used for the determination of refractory elements and easily forming carbides elements (e.g., REEs), incomplete vaporization of the analytes and memory effects are the major difficulties. The application of a suitable chemical modifier has been proved to be one of the most efficient methods.

6.3.1 Fluorination-assisted (F)ETV-ICP-OES for REEs analysis

Halogenation with halocarbon vapors (CCl_4 , CF_2Cl_2 , CHF_3 , etc.) has been successfully introduced into GFAAS and ETV-ICP-OES/MS for volatilization of refractory elements or for in situ removal of matrix. When polytetrafluoroethylene (PTFE) emulsion was used as a halogenating reagent in ETV, the vaporization of refractory elements and carbide-forming elements from the graphite tube and their transport into the plasma could be dramatically improved.

PTFE is high molecular polymer with a decomposition temperature of 415 °C and would decompose into a series of monomers of tetrafluoroethylene at temperature higher than its decomposition temperature.



At high temperature, the decomposition products of PTFE and C_2F_4 would react with the oxides of many elements, forming corresponding fluoride. Compared with other halogenating reagents, PTFE presents several advantages: (1) high fluorine content; (2) sufficient chemical activity of F; (3) suitable decomposition temperature (about

415 °C), favoring the elimination of organic matrix; (4) low amount of inorganic impurities; and (5) easy to use, and can be easily mixed with sample in any ratio.

FETV technique for sample introduction, using PTFE slurry as fluorinating reagent to promote the volatility of REEs, has been proved to be effective and efficient. By the use of PTFE as a fluorinating reagent, the vaporization and transport efficiency of trace REEs in ETV-ICP-OES are dramatically improved, which leads to the promotion of detection limits by one or two orders of magnitude in comparison with that obtained with an ETV technique without the use of PTFE.

6.3.1.1 Vaporization mechanism of REEs fluorination

REEs are refractory metals with high boiling points for the elements or their oxides. Besides, REEs would easily form very stable involatile carbide on the surface of graphite tube. Table 6.18 lists some physicochemical characteristics of REEs and related compounds.

Figure 6.12 presents the typical signal profiles of Yb in the absence and presence of PTFE. As can be seen, the signal of Yb obtained in the absence of PTFE is very weak, the peak is broad, and asymmetry with tailing and the memory signal is obvious. In the presence of PTFE, the signal peak of Yb is strong, sharp and symmetrical, and the memory signal is negligible. The results indicate that refractory RE oxides reacted with fluorinating reagent in the presence of PTFE and form fluorides with low boiling point which is vaporized and transported into ICP.

Table 6.18: Melting and boiling points (°C) for REEs and corresponding compounds.

Element	Metal		Oxide		Carbide		Fluoride	
	Melting points	Boiling points	Melting points	Boiling points	Melting points	Boiling points	Melting points	Boiling points
Sc	1,538	2,730	–	4,450	1,797	–	1,515	1,527
Y	1,530	3,304	–	4,300	1,950	–	1,152	2,230
La	920	3,470	2,217	4,200	2,360	–	1,493	2,327
Ce	795	3,475	2,397	3,300	2,290	–	1,430	2,327
Pr	919	3,130	2,042	–	2,160	–	1,395	2,327
Nd	1,019	3,127	2,211	–	–	–	1,374	2,327
Sm	1,072	1,803	2,262	–	–	–	1,306	2,327
Eu	826	1,440	2,002	–	2,265	–	1,276	2,327
Gd	1,306	3,000	2,322	–	2,097	–	1,231	2,277
Tb	1,360	2,800	2,337	–	2,245	–	1,172	2,280
Dy	1,500	2,600	2,352	–	–	–	1,154	2,230
Ho	1,461	2,600	2,367	–	2,280	–	1,143	2,230
Er	1,497	2,900	2,387	–	2,180	–	1,140	2,230
Tm	1,545	1,730	2,392	–	2,180	–	1,158	2,230
Yb	824	1,430	2,372	3,227	–	–	1,157	2,230
Lu	1,652	3,300	2,467	–	–	–	1,182	2,230

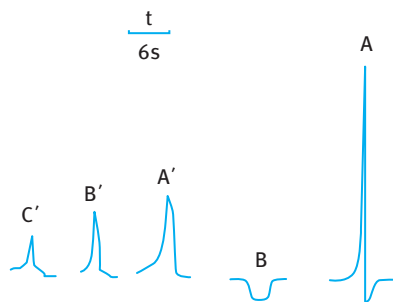


Figure 6.12: Signal profiles of Yb in the absence and presence of PTFE [38]: A, 0.5 mg/L Yb, 6 % PTFE; B, 10 mg/L Yb, 6 % PTFE cleaning signal; A', 2mg/L Yb, without PTFE; B' and C' are the 1st and 2nd cleaning signal, respectively.

Table 6.19: The deposition loss of analytes with and without the presence of PTFE.

Element	Deposition loss (%)	
	Without PTFE	With PTFE
La	19.2	15.7
Yb	24.6	14.9
Y	25.8	13.5

6.3.1.1.1 Transportation process

Deposition loss is usually employed for the evaluation of the transportation efficiency of analytes in the transportation process. Table 6.19 lists the deposition loss of analytes with and without the presence of PTFE. As can be seen, although the deposition loss is reduced under the presence of PTFE, it's not very much. And the deposition loss is mainly caused by rapid temperature decreasing.

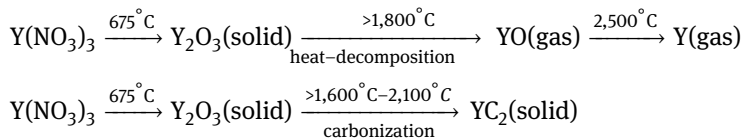
While the premise for evaluating the transportation efficiency with deposition loss is the complete vaporization of target analytes, this is not true in practical process. Thus, the relative deposition loss is proposed for a better understanding of the transportation efficiency, which is defined as the ratio of the deposition loss amount of target analytes to the vaporized amount of corresponding elements. Table 6.20 presents the relative deposition loss of target analytes with and without the presence of PTFE. It shows that the relative deposition loss with the presence of PTFE is reduced by two times (Yb) to five times (La) over that without the presence of PTFE, indicating that the introduction greatly improves the transportation of REEs in ETV system. The reason may be specified by two factors. (1) The formed fluoride is transported in the form of a molecule, whose transportation rate is higher than that of the conventional atom transportation form. (2) Besides the reactive small molecular decomposed from the PTFE under high temperature, other nonreactive small molecular and tiny particles are formed by the gas flow, and it can act as a “condensation nuclei” of gaseous fluorides in the condition of rapid ETV heating, improving the transportation efficiency of target analytes [39].

Table 6.20: The relative deposition loss of target analytes with and without the presence of PTFE.

Element	Relative deposition loss (%)	
	Without PTFE	With PTFE
La	63.0	16.0
Yb	32.5	15.6
Y	67.6	13.5

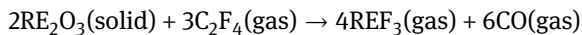
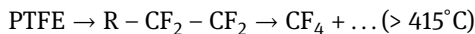
6.3.1.1.2 Vaporization process of REEs and the mechanisms

Without the presence of PTFE, REEs are vaporized in atomic vapor form in ETV-ICP-OES; the vaporization process can be described as follows by taking Y as the representative.



The formed YC_2 is very stable and cannot decompose during the ETV heating program. Yet $\text{Y}_2\text{O}_3(\text{solid}) \rightarrow 2\text{YO}(\text{gas}) + \text{O}(\text{gas})$ would happen from the thermodynamics' point of view. Thus, Y is vaporized in the form of gaseous atom and the vaporization is incomplete.

With the presence of PTFE, the situation is contrary. The target REEs are vaporized out under a relatively low temperature and the vaporization efficiency of above 98 % can be achieved. RE oxides react with PTFE as in the following process. The thermodynamics data listed in Table 6.21 can also prove the feasibility.

**Table 6.21:** ΔG (kJ) for the fluorinating reaction of La, Y and Yb with the presence of PTFE.

Reaction	1,000 K	1,500 K	2,000 K
$2\text{La}_2\text{O}_3(\text{s}) + \text{C}_2\text{F}_4(\text{g}) \rightarrow 4\text{LaF}_3(\text{g}) + 6\text{CO}(\text{g})$	–	–2,202	–
$2\text{Y}_2\text{O}_3(\text{s}) + \text{C}_2\text{F}_4(\text{g}) \rightarrow 4\text{YF}_3(\text{g}) + 6\text{CO}(\text{g})$	–1,172	–1,725	–2,203
$2\text{Yb}_2\text{O}_3(\text{s}) + \text{C}_2\text{F}_4(\text{g}) \rightarrow 4\text{YbF}_3(\text{g}) + 6\text{CO}(\text{g})$	–524	–983	–

6.3.1.2 Affecting factors for fluorination vaporization

The main factors influencing the formation and vaporization of fluorides include the amount of fluorinating reagents, ashing temperature, vaporization temperature and matrix concentration.

(1) Amount of fluorinating reagents (PTFE slurry)

The concentration of fluorinating reagents is one of the main impactors which influence the completion of fluorination reaction. Figure 6.13 represents the effect of PTFE concentration on the vaporization signal intensity of La. It indicates that the signal intensity is increased with the increase of the concentration of PTFE and maintains constant when the concentration of PTFE is above 4 % (m/V). Yet when the concentration of PTFE is increased further, the plasma is unstable and quenched sometimes, probably due to the rapid decomposition of PTFE in the plasma and the resulting unmatching impedance. Generally, 6 % PTFE is employed in the experiment.

(2) Ashing temperature

The selection of ashing temperature should consider the following factors. (1) It is beneficial to the removal of the matrix, especially organic matrix; (2) It helps the rapid formation of RE fluorides; (3) No loss of analytical signal. Figure 6.14 represents the effect of ashing temperature on the vaporization signal of La. An obvious ashing loss is observed when the temperature is higher than 1,800 °C. In other words, an ashing temperature up to 1,500 °C can be employed, and a lot of interference components (organic compounds and part of inorganic matrix) can be completely removed under this temperature. This temperature is much higher than the decomposition temperature of PTFE (415 °C), indicating that there is no

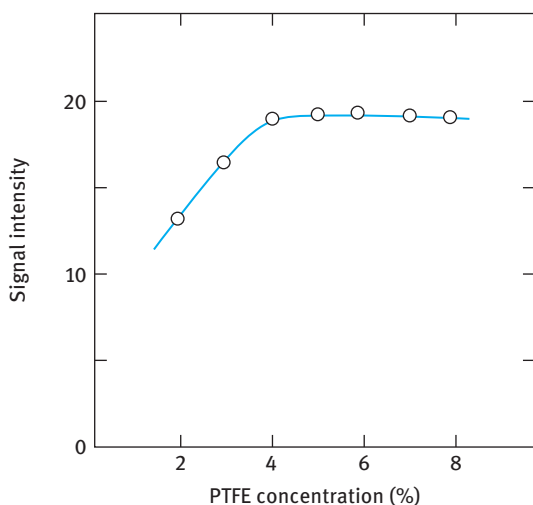


Figure 6.13: The effect of PTFE slurry concentration on the signal intensity of La [40].

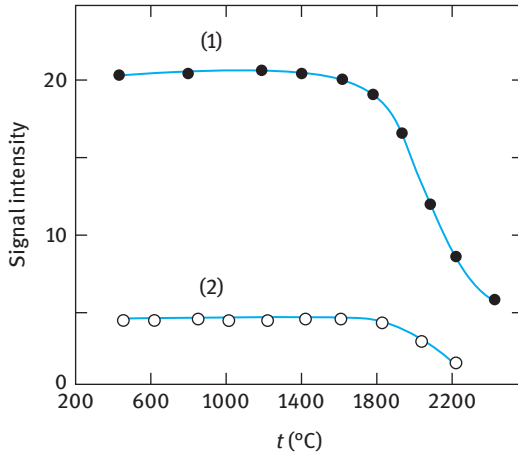


Figure 6.14: Ashing curve of La [40]: (1) 0.2 mg/L La, 6 % PTFE; (2) biological sample, 6 % PTFE.

obvious loss of the formed fluorides at such a high temperature. Thus, for the elements with boiling points higher than 415 °C for their fluorides (e.g., REEs), the selection of ashing temperature should refer to the boiling point of corresponding fluorides; for the elements with boiling points lower than 415 °C for their fluorides (e.g., Si), the selection of ashing temperature should refer to the decomposition temperature of PTFE, $T_{\text{ashing}} < 415$ °C. In general, the ashing time affects the extent of fluorination reaction to some extent.

(3) Vaporization temperature

Figure 6.15 provides the effect of vaporization temperature on the signal intensity of La. It shows that the vaporization efficiency is increased with the increase of the vaporization temperature, along with the increasing of the signal intensity. And the signal intensity maintains constant when the temperature is above a certain level (e.g., 2,400 °C). Compared with conventional ETV, the optimal vaporization temperature in fluorination-assisted ETV is lower.

(4) Matrix concentration

Matrix effect is one of the main factors evaluating the analytical performance of the method.

Alkali and alkaline earth metals are common matrix elements in many real-world samples. Table 6.22 lists the tolerance limit of alkali and alkaline earth metals in the determination of La and other refractory metals by FETV-ICP-OES. As can be seen, the highest tolerance limit of alkali and alkaline earth metals exceeds 5 mg/mL, which is approximately 10^4 – 10^5 times of the concentration of target element.

Table 6.23 lists the tolerance limit of transitional metals in the determination of La and other refractory metals by FETV-ICP-OES. As can be seen, the effect of

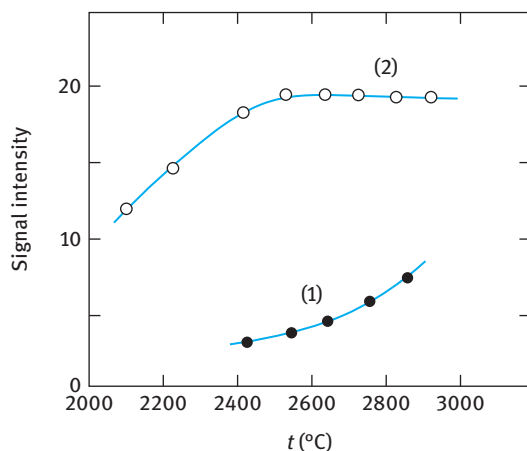


Figure 6.15: The effect of vaporization temperature on the signal intensity of La [40]: (1) 2 mg/L La; (2) 0.2 mg/L La, 6% PTFE.

Table 6.22: Matrix effect of alkali and alkaline earth metals.

Element and wavelength (nm)	Concentration of target element (mg/L)	Tolerance limit (mg/mL)			
		K	Na	Ca	Mg
La 333.749	0.5	5.0	5.0	5.0	5.0
Mo 202.030	0.1	5.0	5.0	5.0	5.0
Cr 267.716	0.4	5.0	5.0	5.0	5.0
B 249.678	0.3	5.0	5.0	5.0	5.0

Table 6.23: Matrix effect of transitional metals.

Element and wavelength (nm)	Concentration of target element (mg/L)	Tolerance limit (mg/mL)				
		Cu	Mn	Pb	Zn	Fe*
La 333.749	0.5	5.0	5.0	5.0	5.0	5.0
Mo 202.030	0.1	5.0	–	–	4.0	2.0
Cr 267.716	0.4	5.0	–	–	5.0	5.0
B 249.678	0.3	5.0	–	5.0	5.0	–

Note: *When the concentration of Fe is above 2 mg/mL, Fe 202.050 nm interferes with Mo 202.030 nm.

transitional metals on the fluorination-assisted vaporization of interest elements is not very obvious.

Figure 6.16 presents the effect of RE matrix (Y, Yb) on the signal intensity of La. No obvious variation of the signal intensity is observed when the concentration of matrix (Y, Yb) is below 2 mg/mL. When the concentration of matrix is above 2 mg/mL,

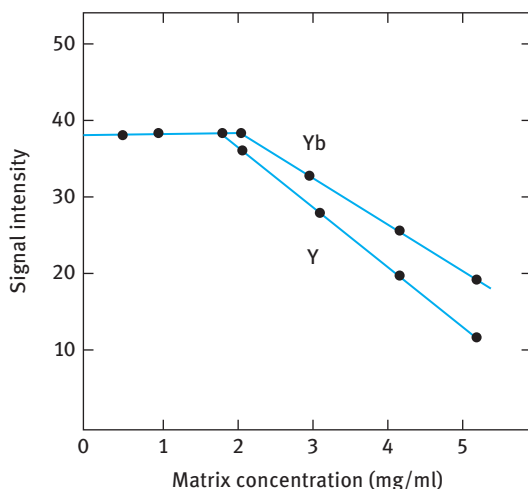


Figure 6.16: The effect of RE matrix (Y, Yb) on the signal intensity of La [38].

the signal intensity of La is decreased sharply, probably due to the two competition reactions. One happens between target analytes and fluorinating reagents, the other happens between the RE matrix and fluorinating reagents, and they may cause the incomplete vaporization of La or variation of the vaporization rate.

6.3.1.3 Analytical performance

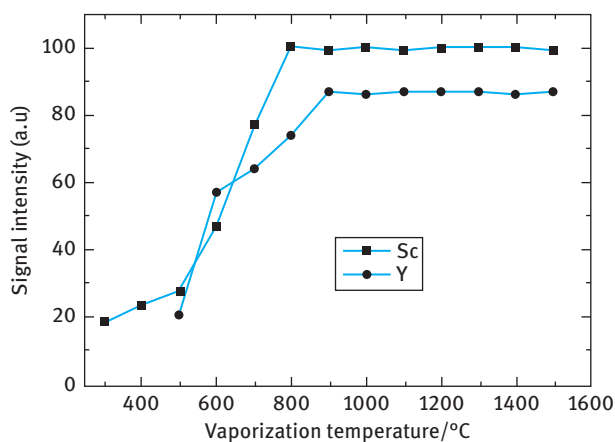
Table 6.24 presents the detection limits of REEs obtained by FETV-ICP-OES. As can be seen, the absolute detection limit of sub ng/pg is obtained for REEs by FETV-ICP-OES. Compared with conventional ETV-ICP-OES detection system, the detection is improved by about 2 orders of magnitude; the relative detection limit is comparable or superior to that obtained by PN-ICP-OES. RSD of less than 5 % can be achieved in FETV-ICP-OES, and the dynamic linear range covers 3–4 orders of magnitude. As mentioned above, the tolerance limit of coexisting ions is about 10^4 – 10^5 times of target REEs in FETV-ICP-OES measurement, which is one order of magnitude higher than that obtained in conventional ETV-ICP-OES.

6.3.2 Low-temperature ETV-ICP-OES for REEs analysis

The use of organic chelating reagents as chemical modifiers in the ETV-ICP-OES has some characteristics including the following: (1) refractory elements can be vaporized at lower temperatures, which is beneficial to prolong the lifetime of evaporator; and (2) organic chelating reagents can be used both as chemical modifiers and as extracting reagents; thus, the application potential and the determination sensitivity of the method can be further improved.

Table 6.24: Detection limits of REEs [41].

Element	Wavelength (nm)	PN-ICP-OES	Conventional ETV-ICP-OES		FETV-ICP-OES		
		ng/mL	ng/mL	ng	ng/mL	ng	ng [42]
La	333.7	263	500	5.0	4.0	0.08	
Ce	413.7	86			14	0.28	
Pr	401.2	83			17	0.34	
Nd	390.8	290			10	0.20	
Sm	359.3	52			9.6	0.19	
Eu	381.9	18			1.8	0.036	0.012
Gd	342.2	29			8.2	0.16	
Tb	350.9	30			8.7	0.17	
Dy	353.1	22			3.7	0.07	
Ho	345.6	15			2.5	0.05	
Er	337.2	21			3.0	0.06	0.034
Tm	313.3	46			1.6	0.03	
Yb	328.9	7			1.2	0.02	0.018
Lu	261.5	1.1			0.2	0.004	0.054
Y	371.0	23	621	12	0.6	0.012	0.025
Sc	361.3	7			0.2	0.004	0.017

**Figure 6.17:** The effect of vaporization temperature on the signal intensity of Sc and Y (Sc and Y, 2 ng; TTA, 0.8 mmol/L) [43].

A series of chelating reagents including EDTA, polyhydroxy compounds, 8-hydroxyquinoline, 1-phenyl-3-methyl-4-benzoyl-5-pyrazole (PMBP), acet-ylacetone, thenoyltrifluoroacetone (TTA), diethyldithiocarbamate and ammonium pyrrolidinedicarbodithioate have been tested as chemical modifiers for ETV-ICP-OES/MS determination of trace elements. Peng and Jiang [44] firstly attempted to use

the reaction of PMBP and REEs in ETV, which form volatile and chemically stable REEs chelates for the subsequent vaporization. It was found that PMBP chelates of La, Y, Eu and Sc could be vaporized from graphite tube at 1,000, 1,200, 1,200, and 900 °C, respectively. The proposed method was successfully employed for trace REEs (La, Eu, Y and Sc) analysis in environmental samples. By using PMBP as the chemical modifier in ETV-ICP-OES analysis of refractory REEs, the vaporization temperature (900–1,200 °C) of interest REEs is significantly decreased compared to that in conventional ETV system, the formation of RE carbides is effectively avoided, and the detection limit of REEs (ng/mL level) is comparable to that in FETV-ICP-OES. Fan et al. [43] developed a method of ETV-ICP-OES for the determination of trace Sc and Y, based on gaseous compound introduction into the plasma as their TTA complexes. As can be seen from Figure 6.17, a weaker signal intensity could be detected for Sc and Y at the temperature of 300 and 500 °C, respectively, indicating that the TTA complexes of Sc(III) and Y(III) formed and started to vaporize into ICP [43]. With the elevation of vaporization temperature, the signal intensity for both Sc and Y increased notably, and the maximum emission signal was obtained at 800 °C for Sc and 900 °C for Y. These maximum signals remained constant with further increases of vaporization temperature up to 1,500 °C.

Besides, low-temperature ETV-ICP-OES can be easily combined with sample pre-treatment techniques for further improvement in the detection limit of target REEs. Chen et al. [45] employed PBMP as both the extractant and chemical modifier and realized the quantification of trace Eu in high-purity ZrO₂ by ETV-ICP-OES.

Above all, compared with conventional ETV system, low-temperature (LT)ETV merits the following: (1) the vaporization of REEs can be performed at fairly low temperature in LT-ETV; (2) the lifetime of graphite tube can be prolonged; (3) the formation of refractory carbides is effectively prevented; (4) the sensitivity is improved significantly; (5) it's easy to combine with chemical separation/preconcentration technique.

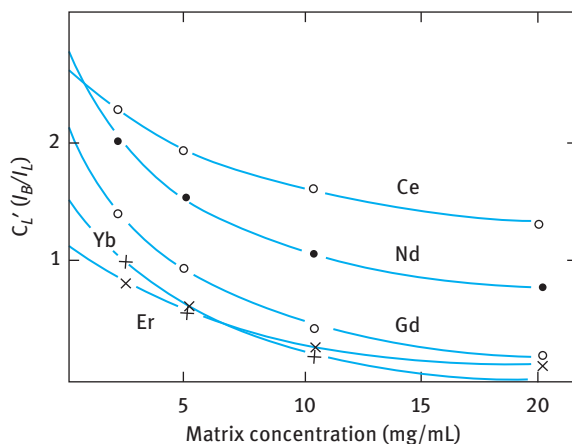


Figure 6.18: Relationship between the solid detection limit and matrix concentration [46].

6.4 Application of ICP-OES in the analysis of high-purity REE, alloys and ores

6.4.1 High-purity REE analysis by ICP-OES

High-purity REE refers to RE metals or oxides with the purity higher than 99.9 %, which are mainly used in optical, electric, magnetic and other functional materials. The metal impurities in these high-purity REE materials are in g/g level or much lower. ICP-OES can be employed for the analysis of high-purity REE (99.9–99.99 %) with good reproducibility – no need for complicated sample pretreatment process and multielement analysis ability. The application of ICP-OES for the analysis of high-purity REE is presented in Table 6.25.

Table 6.25: Application of ICP-OES in the determination of REEs impurities in high-purity REE.

Matrix	Determined elements	Instrument types	Reciprocal linear dispersion (nm/mm)	Limit of determination or purity	Ref.
Ce	La, Pr, Nd, Sm, Y	PGS-2/spectrographic	0.37	99.99 %	[47]
La	Part of the REEs	7502B/multichannel	0.55	99–99.9 %	[6]
Tb	Y, Sm, Eu, Gd, Dy, Ho, Er	JY38/scanning	0.26	10–100 µg/g	[5]
La	Ce, Pr, Nd, Sm	JY38/scanning	0.26	ng/mL grade	[48]
Pr	La, Ce, Nd, Sm, Y	JY38/scanning	0.26	99.95 %	[49]
Sm	14 REEs	ICPS-1000/scanning	–	99.95 %	[50]
Nd	14 REEs	WSP-1/spectrographic	0.46	high purity	[51]
Eu	14 REEs	PGS-2/spectrographic	0.37	0.5–30 µg/g	[46]
Eu	14 REEs	ICPS-1000/scanning	–	1–10 µg/g	[52]
Gd	14 REEs	WPG-100/ Spectrographic	0.8	1.3–36 µg/g	[53]
Tb	Ce, Pr, Nd, Sm, Eu, Gd, Dy, Ho, Er, Y	WSP-1/spectrographic	0.46	99.8 %	[54]
Tm	14 REEs	PGS-2/spectrographic	0.74	99.95 %	[55]
Sc	14 REEs	PGS-2/spectrographic	0.37	99.99 %	[47]
Tm	14 REEs	PGS-2/spectrographic	0.74	99.99 %	[56]
Lu	14 REEs	PGS-2/spectrographic	0.74	99.99 %	[57]
Y	14 REEs	PGS-2/spectrographic	0.74	99.99 %	[58]
La	14 REEs	PGS-2/spectrographic	0.74	99.99 %	[59]
Ce	14 REEs	PGS-2/spectrographic	0.36	99.95 %	[60]

Yet the sensitivity of ICP-OES is not high enough for the analysis of REE with purity higher than 99.99 %; the spectral interference is serious, especially for those REE matrix with complex spectral background; matrix matching is often needed due to the matrix effect; and direct solid sample analysis is expected. It should be pointed out that the ability of analyzing high-purity REE by ICP-OES is affected by the complex spectral background of REE matrix, and the high dilution of the sample along with the low nebulization efficiency limits the determination performance of ICP-OES to a great extent.

6.4.1.1 Detection limit of REEs in REE matrix

The conventional detection limit (C_L) is obtained with the absence of other coexisting elements – no consideration of matrix effect in real-world sample. Boumans proposed real detection limit ($C_{L,t}$) which can be expressed as

$$C_{L,t} = \frac{2}{5} \times \frac{X_i(\lambda_a)}{S_a} + C_L$$

where S_a is the sensitivity of the analytical line, and $X_i(\lambda_a)$ is the net signal of interference obtained at the analytical line. Thus, $C_{L,t}$ is often higher than C_L .

Velichkov employed $C_{L,t}$ for the selection of analytical line in the determination of single RE in high-purity RE materials [61]. Table 6.26 lists a comparison of detection limits for REEs obtained under different circumstances, where A represents the detection limit with the presence of matrix ($C_{L,t}$), B represents the detection limit without the presence of matrix (C_L) and C is the detection limit obtained after the removal of matrix. As can be seen, in the presence of RE matrix, the obtained real detection limit is higher than the obtained conventional detection limit; the increase of the detection limit depends on the spectrum complexity of the RE matrix, and the detection limit is much higher when the spectrum of RE matrix is more complicated; $C_{L,t}$ is increasing with the increase of the matrix concentration; the detection limit could be improved by removing the matrix and enriching target analytes.

6.4.1.2 Analytical line and internal line

For the direct determination of trace REEs impurities in high-purity RE, the selection of analytical lines should consider the following factors: (1) sensitive analytical lines are commonly considered; (2) when the most sensitive line is interfered, other sensitive lines should be selected instead; (3) the interference type (partly or complete overlapping) and extent should be investigated by wavelength scanning; (4) instrument with high dispersive power can be used to avoid or reduce the spectral interference; (5) appropriate dilution of the sample can reduce the spectral interference caused by the matrix to some extent.

Application of a certain internal standard would avoid the problems caused by variation of ICP discharging parameters and nebulization condition, ensuring the

Table 6.26: The detection limits of REEs under different conditions [61].

Element	Analytical lines (nm)	Detection limits corresponding to dissolved solids (matrix is Pr or Sm) (%)		
		A	B	C
Sc II	424.683	4.6×10^{-4}	1.5×10^{-4}	1.8×10^{-5}
Y II	324.228	1.0×10^{-3}	–	2.4×10^{-5}
La II	333.749	4.1×10^{-3}	–	7.6×10^{-5}
Ce II	446.021	1.7×10^{-2}	2.1×10^{-3}	2.3×10^{-4}
Pr II	418.948	–	1.6×10^{-2}	4.1×10^{-4}
Nd II	430.358	–	1.3×10^{-3}	5.0×10^{-4}
Sm II	360.949	4.4×10^{-3}	–	1.8×10^{-4}
Eu II	412.970	–	1.3×10^{-3}	1.4×10^{-4}
	272.778	1.5×10^{-3}	–	1.3×10^{-4}
Gd II	301.013	3.1×10^{-3}	–	1.8×10^{-4}
	310.050	–	6.9×10^{-3}	1.8×10^{-4}
Tb II	370.286	–	1.0×10^{-2}	2.7×10^{-4}
Dy II	353.170	5.9×10^{-3}	6.5×10^{-4}	–
Ho II	339.898	–	4.0×10^{-4}	6.5×10^{-5}
Er II	337.271	–	2.6×10^{-4}	3.0×10^{-5}
Tm II	346.220	–	3.3×10^{-4}	7.0×10^{-5}
Yb II	289.138	9.5×10^{-4}	–	6.0×10^{-5}
	328.937	–	4.2×10^{-4}	2.0×10^{-5}
Lu II	261.542	1.0×10^{-4}	1.6×10^{-4}	7.4×10^{-6}

reproducibility and accuracy of the method. Table 6.27 lists the analytical lines of REEs in high-purity RE matrix.

6.4.1.3 Matrix concentration and solid detection limit

The relative solid detection limit of the method could be improved by increasing the concentration of the sample (matrix concentration), while matrix effect would deteriorate the detection limit. Thus, it is necessary to select an appropriate concentration of the sample matrix. The aqueous detection limit of target analyte can be expressed as

$$C_L = \frac{k \cdot (\text{RSD})_B \cdot C_o}{I_L/I_B}$$

where k is an integer determined by confidence, generally $k = 3$, $(\text{RSD})_B$ is the RSD of background signal, I_L/I_B is the signal-to-background ratio, and C_o is the concentration of target analyte.

Actually, the solid detection limit in the original sample is more interested in high-purity RE analysis. Dividing both sides of the formula by the matrix concentration (C_{matrix}) simultaneously, the solid detection limit can be obtained:

$$C'_L = \frac{k \cdot (\text{RSD})_B \cdot C'_o}{I_L/I_B}$$

Table 6.27: Reference analytical lines for ICP-OES detection of REE impurities in high-purity RE matrix.

Matrix	Analytical lines of RE impurities (nm)							
	Ce	La	Pr	Nd	Sm	Eu	Gd	Tb
La	338.10	–	474.02	384.90	408.67	480.67	333.75	–
Ce	–	418.66	456.05	415.47	413.38	446.02	418.66	413.38
Pr	422.54	417.94	–	410.07	440.88	422.29	414.31	422.52
Nd	406.11	406.11	–	–	430.35	406.11	415.61	399.46
Sm	359.26	373.91	446.73	336.59	–	442.43	388.5	359.26
Eu	388.97	397.19	–	309.71	272.77	–	372.49	412.97
Gd	364.62	354.93	–	376.84	376.84	335.05	–	385.24
Tb	332.44	350.91	–	350.92	332.44	387.42	367.64	–
Dy	340.78	353.17	–	–	394.46	338.50	394.46	400.04
Ho	345.60	345.60	–	450.39	381.07	345.60	–	381.07
Er	337.27	337.27	–	390.63	337.27	349.91	369.27	349.91
Tm	336.26	342.51	–	336.29	384.80	329.1	313.13	–
Yb	369.42	328.93	–	398.80	328.93	328.93	297.06	–
Ln	347.20	307.76	–	350.74	261.54	291.14	307.76	–
Y	324.22	371.02	332.78	354.90	371.02	324.22	371.02	377.43

Matrix	Analytical lines of rare earth impurities (nm)						
	Dy	Tm	Yb	Lu	Y	Y	Sc
La	379.48	423.83	423.83	423.83	408.67	408.67	333.74
Ce	404.08	424.86	429.66	418.66	413.76	413.38	422.57
Pr	390.84	440.88	418.95	417.94	417.94	422.53	422.39
Nd	401.25	438.56	415.60	406.10	401.22	396.31	410.34
Sm	359.26	428.08	446.73	425.64	356.82	428.08	403.43
Eu	381.97	420.50	393.05	397.19	443.55	390.71	393.05
Gd	342.25	335.08	354.93	354.93	335.04	342.24	342.24
Tb	350.92	400.55	400.55	356.17	387.41	350.91	350.91
Dy	–	444.97	397.85	353.17	400.04	353.17	400.04
Ho	345.60	442.05	348.48	345.60	347.42	339.89	345.60
Er	369.26	390.63	390.63	369.26	337.27	337.27	323.05
Tm	346.22	–	367.13	346.22	342.51	342.51	342.51
Yb	328.94	328.93	–	328.93	369.42	328.93	328.93
Ln	350.74	350.74	350.74	–	261.54	291.13	347.24
Y	377.43	371.02	437.49	324.22	–	–	324.22

where C'_0 is the content of target analyte in solid sample. For a specific sample, C'_0 , k and $(RSD)_B$ are constants; thus, $C'_L C'_L$ is proportional to reciprocal of I_L/I_B .

To find the appropriate matrix concentration, the following procedure can be processed.

The sample solution is diluted stepwise and a series of sample solutions with different matrix concentration are obtained. The corresponding I_B/I_L is determined and plotted to matrix concentration (C_{matrix}), resulting to a curve of relationship between

the solid detection limit and matrix concentration (Figure 6.18). As can be seen, with the increasing of the matrix concentration, the solid detection limit of target analyte is decreased; with further increasing of the matrix concentration, the solid detection limit decreases slowly and becomes constant. Based on it, an appropriate matrix concentration can be selected.

Besides, when the matrix concentration is too high, nebulizer clogging or analytes deposition on ICP torch would occur. Consequently, matrix concentration of less than 10 mg/mL is usually employed.

6.4.2 REE ores analysis by ICP-OES

Acid or alkaline digestion is usually employed to transform the ores into aqueous solution prior to ICP-OES detection. Table 6.28 lists the application of ICP-OES for the direct

Table 6.28: Application of ICP-OES for the direct determination of REEs in ores.

Sample	Target analyte	Sample preparation	Detection limit	Reference
Phosphate Mine	REEs	Sample is digested by HNO ₃ + HF + HCl, vaporized and diluted by diluted HNO ₃ for ICP-OES detection	40–300 µg/g	[62]
Geological samples	13 REEs	Sample is microwave-digested by HNO ₃ + HF at 14 atm, vaporized and diluted by 2 mol/L HNO ₃ for ICP-OES detection	0.01–1 µg/g	[63]
Sediments	La, Sc, Y, etc.	Sample is digested by HNO ₃ + HF + HClO ₄ , vaporized and diluted by diluted HCl for ICP-OES detection	µg/g level	[64]
Phosphate Mine	REEs	Sample is digested by hot H ₂ SO ₄ , filtered, and the filtrate is diluted to the REEs concentration range of 10–500 µg/mL for subsequent ICP-OES detection	1–40 ng/mL	[65]
Monazite	REEs	Sample is digested by H ₂ SO ₄ and vaporized; the residue is decomposed by HCl, and diluted with water, spiked with Cd as internal standard	ng/mL level	[66]

determination of REEs in ores. It should be pointed out that the sensitivity of ICP-OES is limited and the possible spectral interference caused by coexisting ions should be corrected.

6.4.3 Trace REE analysis by ICP-OES in alloys

ICP-OES has been widely employed in the determination of REEs and non-REEs in various types of RE alloys (e.g., aluminum alloys, copper alloys, magnetic and superconducting materials). The operation is very simple, and the sample is often decomposed by using some inorganic acids, diluted properly, and can be directly introduced into ICP for subsequent detection – no need for any chemical separation pretreatment. Main components and trace components can be determined simultaneously; for example, the content of Pr and Sm in Pr-Sm-Co alloy is determined by ICP-OES to be 12–20 %. Besides, the reproducibility of ICP-OES detection can be maintained at around 1 %. Table 6.29 lists the application of ICP-OES in the analysis of REEs in metal and alloy samples.

Table 6.29: Application of ICP-OES in the analysis of REEs in metal and alloy samples.

Sample	Analyte	Sample preparation	Detection limit	Reference
Magnetic materials	REEs	Sample is digested by $\text{HNO}_3 + \text{HF} + \text{HClO}_4$, vaporized and diluted by diluted HCl for ICP-OES detection	1–40 $\mu\text{g/g}$	[67]
RE-Co magnetic materials	Sm, Ce, Y, Mn, Hf, Co, Fe, Cu, Zr	Sample is digested by aqua regia and prepared into sample solution with matrix concentration of 5 mg/mL. About 4 mL of the sample solution is diluted to 1 L with 1.2 mol/L HCl for ICP-OES detection, with Be as the internal standard	–	[68]
Rare Earth Steel	La, Ce, Pr, Nd	Sample is digested by $\text{HNO}_3 + \text{HCl} + \text{HClO}_4$, vaporized and diluted by 0.1 mol/L HClO_4 for ICP-OES detection	0.1–1 $\mu\text{g/g}$	[69]

References

- [1] Daskalova N, Velichkov S, Krasnobaeva N, Slavova P. Spectral interferences in the determination of traces of scandium, yttrium and rare-earth elements in pure rare-earth matrices by inductively coupled plasma atomic emission-spectrometry i. cerium, neodymium and lanthanum matrices. *Spectrochim Acta Part B-A Spectrosc* 1992, 47, E1595–E620.
- [2] *Massachusetts Institute of Technology Wavelength Tables*. Cambridge, MA, The MIT Press, 1969.
- [3] Yang JF, Piao ZX, Zeng XJ, Chen XH, Zhang ZY, Guan QD. Resolution of closely spaced lines with kalman filtering in inductively coupled plasma atomic emission spectrometry. *Acta Chim Sin* 1993, 03, 283–8.
- [4] Jiang ZC, Chen H, Zhang SX. Some problems in the determination of trace rare earth impurities in complicated rare earth matrix by using a ICP spectrometer. *Chem J Chin Univ* 1990, 11, 1283–5.
- [5] Biswas SS, Sethumadhavan A, Murty PS. Determination of Y, Sm, Eu, Gd, Dy, Ho, Er in high-purity terbium oxide by ICP-AES. *Mikrochim Acta* 1991, 1, 71–7.
- [6] Li B. Determination of impurities in pure lanthanum oxide by inductively-coupled plasma emission spectrometry. *Rock Mineral Anal* 1994, 01, 20–4.
- [7] Yang JF, Zeng XJ, Huang BL. Determination of trace amount of 14 rare earth impurities in high purity yttrium oxide with ICP-AES. *Acta Chim Sin* 1990, 09, 903–8.
- [8] Boorn AW, Cresser MS, Browner RF. Evaporation characteristics of organic solvent aerosols used in analytical atomic spectrometry. *Spectrochim Acta Part B: At Spectrosc* 1980, 35, 823–32.
- [9] Chen H, Kong LY, Jiang ZC, Zeng YE. Study on the separation and preconcentration of trace amounts of rare earth impurities from high-purity sodium chloride and mechanism of ethanol enhancement effect on line intensities of rare earth elements. *Spectrosc Spectral Anal* 1988, 06, 24–8.
- [10] Boorn AW, Cresser MS, Browner RF. Evaporation Characteristics of Organic Solvent Aerosols Used in Analytical Atomic Spectrometry, *Spectrochimica Acta Part B: Atomic Spectroscopy*, 1980, 35(11–12): 823-32.
- [11] Xu JR, Kawaguchi H, Mizuike A. Effects of organic acids and solvents in inductively-coupled plasma emission spectrometry. *Anal Chim Acta* 1983, 152, 133–9.
- [12] Yang JF, Pei AL, Huang BL. Effects of ethanol and desolvation on rare earth line intensities in ICP-AES. *Chin J Anal Chem* 1988, 03, 198–202.
- [13] Chen JG, Jiang ZC, Kong LY. Enhancement effect of organic solvents on rare earth elements in ICP-AES. *J Chin Rare Earth Soc* 1991, 03, 278–80.
- [14] Chen JG, Jiang ZC, Kong LY. Determination of trace rare earth impurities in high purity La₂O₃ with TBP extraction-ICP-AES. *J Chin Rare Earth Soc* 1992, 01, 89–91.
- [15] Bentlin FRS, Pozebon D. Direct Determination of lanthanides in environmental samples using ultrasonic nebulization and ICP OES. *J Braz Chem Soc* 2010, 21, 627–34.
- [16] Lara R, Olsina RA, Marchevisky E, Gasquez JA, Martinez LD. ICP-OES Determination of rare earth elements in silicate rocks using ultrasonic nebulization and on-line ion-exchange iron separation. *At Spectrosc* 2000, 21, 172–8.
- [17] Dressler VL, Pozebon D, Matusch A, Becker JS. Micronebulization for trace analysis of lanthanides in small biological specimens by ICP-MS. *Int J Mass Spectrom* 2007, 266, 25–33.
- [18] Ružička J, Hansen EH. Flow injection analyses: Part I. A new concept of fast continuous flow analysis. *Anal Chim Acta* 1975, 78, 145–57.
- [19] Fang ZL. Flow injection analysis. *Chin J Anal Chem* 1981, 03, 369–72.
- [20] Ito T, Kawaguchi H, Mizuike A. Inductively coupled plasma emission-spectrometry of microliter samples by a flow-injection technique. *Bunseki Kagaku* 1980, 29, 332–6.

- [21] Fu LS, Ren Y. Application of flow injection analysis in rare earth determination. *Metall Anal* 1995, 02, 30–5.
- [22] Chen H, Jiang ZC, Zeng YE, Lingying Kong, Study on the FIA-ICP-AES Spectrographic method (I) determination of 14 rare earth impurities in high purity yttrium oxide. *J Chin Rare Earth Soc* 1988, 04, 65–9.
- [23] Luo JB, Zhang ZX, Qian HW. Study on the effects of three sample feeding devices on the matrix interferences in ICP-AES. *J Instrum Anal* 1989, 04, 23–7.
- [24] Shen Q, Jiang ZC, Liao ZH. The application of flow injection standard addition method to ICP-AES for the analysis of mixed rare earth samples. *Chin J Anal Lab* 1991, 02, 45–7.
- [25] Grebneva ON, Kuz'min NM, Tsysin GI, Zolotov YA. On-line-sorption preconcentration and inductively coupled plasma atomic emission spectrometry determination of rare earth elements. *Spectrochim Acta Part B: At Spectros* 1996, 51, 1417–23.
- [26] Liao ZH, Ji HN, Li LZ, Jiang ZC. Determination of trace rare earth elements in high purity zinc by inductively coupled plasma-atomic emission spectrometry with micro-column preconcentration in a flow injection system. *Chin J Anal Chem* 1995, 11, 1319–22.
- [27] Fan SH, Fang ZL. The Determination of trace amounts of lanthanum in natural waters by a flow-injection on-line preconcentration ICP system. *Spectrosc Spectral Anal* 1992, 05, 63–6.
- [28] Liang YZ, Yin NW. On-line Separation and preconcentration FIA-ICP-AES system for simultaneous determination of REEs and yttrium in geological samples. *At Spectrosc* 1995, 16, 243–7.
- [29] Huang CZ, Jiang ZC, Hu B. Mesoporous titanium dioxide as a novel solid-phase extraction material for flow injection micro-column preconcentration on-line coupled with ICP-OES determination of trace metals in environmental samples. *Talanta* 2007, 73, 274–81.
- [30] Jerez J, Isaguirre AC, Bazan C, Martinez LD, Cerutti S. Determination of scandium in acid mine drainage by ICP-OES with flow injection on-line preconcentration using oxidized multiwalled carbon nanotubes. *Talanta* 2014, 124, 89–94.
- [31] Sabarudin A, Lenghor N, Oshima M, et al. Sequential-injection on-line preconcentration using Chitosan resin functionalized with 2-amino-5-hydroxy benzoic acid for the determination of trace elements in environmental water samples by inductively coupled plasma-atomic emission spectrometry. *Talanta* 2007, 72, 1609–17.
- [32] Arrowsmith P. Laser ablation of solids for elemental analysis by inductively coupled plasma mass-spectrometry. *Anal Chem* 1987, 59, 1437–44.
- [33] Lin SL, Peng CF. Studies on the application of laser sampling-inductively coupled plasma atomic emission-spectrometry to the determination of rare-earth and refractory elements. *J Anal At Spectrom* 1990, 5, 509–14.
- [34] Nixon DE, Fassel VA, Kniseley RN. Inductively coupled plasma-optical emission analytical spectroscopy. Tantalum filament vaporization of microliter samples. *Anal Chem* 1974, 46, 210–3.
- [35] Gunn AM, Millard DL, Kirkbright GF. Optical emission spectrometry with an inductively coupled radiofrequency argon plasma source and sample introduction with a graphite rod electrothermal vaporization device. Part I. Instrumental assembly and performance characteristics. *Analyst* 1978, 103, 1066–73.
- [36] Gray AL, Date AR. Inductively coupled plasma source-mass spectrometry using continuum flow ion extraction. *Analyst* 1983, 108, 1033–50.
- [37] Jiang ZC, Cai RX, Zhang HS, *Rare Earth Elements Analytical Chemistry*, Science Press, Beijing, China, 2000.
- [38] Jiang ZC, Hu B, Qin Y, Zeng YE, Fluorination assisted electrothermal vaporization inductively coupled plasma atomic emission spectrometry: an effective method for direct determination of refractory elements in solid biological samples, *Microchem J*, 1996, 06, 326–36.

- [39] Kantor T. Interpreting some analytical characteristics of thermal dispersion methods used for sample introduction in atomic spectrometry. *Spectrochim Acta Part B: At Spectrosc* 1988, 43, 1299–320.
- [40] Jiang ZC, Qin YC, Cai XX, Zhang SX, Zeng YE. Direct determination of trace lanthanum in biological samples by fluorination assisted electrothermal vaporization inductively coupled plasma emission spectrometry, *Journal of The Chinese Rare Earth Society*, 1995, 04, 351–4.
- [41] Huang M, Jiang ZC, Zeng YE. Fluorination and volatilization of refractory elements from a graphite-furnace for sample introduction into an inductively coupled plasma by using a polytetrafluoroethylene slurry, *J Anal At Spectrom* 1991, 6, 773–9.
- [42] Dittrich K, Berndt H, Broekaert JAC, Schaldach G, Tölg G. Comparative-study of injection into a pneumatic nebulizer and tungsten coil electrothermal vaporization for the determination of rare-earth elements by inductively coupled plasma optical-emission spectrometry. *J Anal At Spectrom* 1988, 3, 1105–10.
- [43] Fan ZF, Hu B, Jiang ZC, Li SQ. Low-temperature electrothermal vaporization of thenoyltrifluoroacetone complex of Sc(III) and Y(III) for sample introduction in an inductively coupled plasma atomic emission spectrometry, and their determination in biological samples. *Anal Bioanal Chem* 2004, 378, 456–9.
- [44] Peng TY, Jiang ZC. Volatilization studies of lanthanum, yttrium and europium as their 1-phenyl-3-methyl-4-benzoylpyrazolone 5 complexes from an electrothermal vaporizer for sample introduction in inductively coupled plasma atomic emission spectrometry. *J Anal At Spectrom* 1998, 13, 75–8.
- [45] Chen SZ, Peng TY, Jiang ZC. Determination of trace europium in zirconium dioxide by electrothermal vaporization inductively coupled plasma-atomic emission spectrometry with 1-phenyl-3-methyl-4-benzoyl-pyrazone [5] as extractant and chemical modifier. *Chin J Anal Chem* 1998, 06, 762–5.
- [46] Li JY, Yang J, Dong ZR. Determination of 14 rare earth elements in high purity europium oxide by ICP-AES. *Spectrosc Spectral Anal* 1995, 71–4.
- [47] Yuan F, Qi WD, Chen XH. Determination of trace rare earth impurities in high purity metallic cerium by ICP-AES and correction of spectral interferences. *Spectrosc Spectral Anal* 1992, 02, 75–8.
- [48] Biswas SS, Kaimal R, Sethumadhavan A, Murty PS. Determination of Ce, Pr, Nd and Sm in high-purity La_2O_3 by inductively coupled plasma atomic emission-spectrometry. *Anal Lett* 1991, 24, 1885–95.
- [49] Zhang CX. Direct determination of rare earth impurities in high-purity praseodymium oxide by ICP-OES. *Spectrosc Spectral Anal* 1990, 04, 54–8.
- [50] Zhang YD, Liu GB, Xia YM. Direct determination of 14 rare earth impurity in high purity samarium oxide by ICP-AES. *Phys Test Chem Anal Part B: Chem Anal* 1994, 02, 91–2.
- [51] Huang ZR, Chen XK, Liu ZX, Wang WQ. Study on spectral interference correction method on analysing high purity Nd_2O_3 samples by ICP spectrography. *Chin J Anal Lab* 1993, 02, 61–3.
- [52] Liu WH, Gong JH, Li XJ, Xu XQ. ICP-AES Determination of rare earth impurities in europium oxide. *Chin J Anal Lab* 1995, 04, 53–5.
- [53] Zhang SX, Shen GY. Direct Determination of 14 rare earth impurities in pure gadolinium oxide by ICP-AES. *J Chin Soc Rare Earth* 1991, 02, 170–3.
- [54] Chen JW, Zhou T, Tian SJ. Determination of rare earth elements in pure terbium oxide by ICP-OES. *Spectrosc Spectral Anal* 1992, 03, 55–8.
- [55] Li RH, Guo DF, Yan XQ. X. Chen, Determination of 14 rare earth impurities in highly pure thulium oxide by model ICP-PGS2 scanning inductively coupled plasma atomic emission spectrometer. *Spectrosc Spectral Anal* 1993, 02, 61–8.
- [56] Piao ZX, Pei AL, Huang BL. Determination of 14 rare earth impurities in high purity thulium oxide by ICP-AES. *Spectrosc Spectral Anal* 1989, 03, 40–3.

- [57] Piao ZX, Pei AL, Huang BL. Determination of 14 rare earth impurities in high purity Lu_2O_3 by ICP-OES. *Chin J Anal Chem* 1988, 09, 864–5.
- [58] Yuan F, Qi WD, Ling C, et al. Determination of trace rare earth impurities in yttrium oxide of phosphor grade for colour TV sets by ICP-AES. *Spectrosc Spectral Anal* 1994, 06, 71–6.
- [59] Piao ZX, Pei AL, Huang BL. Determination of rare earth elements by inductively coupled plasma atomic emission spectrometry I. Determination of 14 rare earth impurities in high-purity lanthanum oxide. *Chin J Anal Chem* 1989, 01, 61–4.
- [60] Wang SY, Liu J, Chen XH. Determination of trace 14 rare earth elements in cerium oxide by inductively coupled plasma-atomic emission spectrometry. *Chin J Anal Chem* 1992, 11, 1273–6.
- [61] Velichkov S, Daskalova N, Slavova P. Spectral interferences in the determination of traces of scandium, yttrium and rare-earth elements in pure rare-earth matrices by inductively-coupled plasma-atomic emission-spectrometry 2. Praseodymium and samarium. *Spectrochim Acta Part B-At Spectrosc* 1993, 48, E1743–89.
- [62] Eid MA, Broekaert JAC, Tschöpel P. Application of ICP-AES to the determination of rare earth elements in phosphate samples. *Fresenius' J Anal Chem* 1992, 342, 107–12.
- [63] Grebneva ON, Bayunov PA, Kubrakova LV, Kuzmin NM. Inductively coupled plasma atomic emission determination of 13 rare-earth elements and yttrium in geological samples after microwave decomposition. *J Anal Chem* 1996, 51, 927–30.
- [64] Imai N. Multielement analysis of stream sediment by ICP-AES. *Bunseki Kagaku* 1987, 36, T41–5.
- [65] Fujino O, Araki K, Kometani Y, Sugiyama M, Matsui M. Determination of rare-earth elements in phosphate minerals by inductively coupled plasma atomic emission-spectrometry. *Bunseki Kagaku* 1985, 34, 386–91.
- [66] Iwasaki K, Fuwa K, Haraguchi H. Simultaneous Determination of 14-lanthanides and yttrium in rare-earth ores by inductively coupled plasma atomic emission spectrometry. *Anal Chim Acta* 1986, 183, 239–49.
- [67] Fries T, Lamothe PJ, Pesek JJ. Determination of rare-earth elements, yttrium and scandium in manganese nodules by inductively-coupled argon-plasma emission-spectrometry. *Anal Chim Acta* 1984, 159, 329–36.
- [68] Iwasaki K, Uchida H. Rapid determination of major and minor elements in rare earth-cobalt magnets by inductively coupled plasma atomic emission spectrometry. *Anal Sci* 1986, 2, 261–4.
- [69] Grossman AM, Ciba J, Jurczyk J, Spiewok W. Determination of lanthanum, cerium, praseodymium and neodymium in alloy-steels by inductively coupled plasma atomic-emission spectrometry. *Talanta* 1990, 37, 815–8.

Jörg Niederstraßer

7 Application of Spark Atomic Emission Spectrometry for the Determination of Rare Earth Elements in Metals and Alloys

Abstract: Within the framework of determining the chemical composition of solids using rapid analysis methods, spark atomic emission spectrometry numbers among the standard procedures of most laboratories found within the metal-producing and -processing industries as well as many other companies and institutes nowadays. For analysis purposes, samples must be both electrically conductive and sufficiently homogeneous. Prior to routine use, a spark spectrometer must first be calibrated using certified standard samples. Subsequently, only about 20–30 s are needed to perform a complete quantitative analysis, during which around 70 chemical elements can be determined across all materials. These requirements mean that of all rare earth applications only those in which they are found as alloying or trace elements within the field of metallurgy are of importance for spark emission spectrometry. In this context, the most common rare earths are lanthanum (La) and cerium (Ce), followed by praseodymium (Pr), neodymium (Nd), scandium (Sc), yttrium (Y) and samarium (Sm), while the materials are mainly aluminium, magnesium, cast iron, steel and zinc alloys. The calibration functions of several examples will be shown, discussed and validated. The detection limits lie in the $\mu\text{g/g}$ region regardless of the given matrix and are thus sufficient for most applications. Repeatability for concentrations larger than 0.1 % is less than 1 % relative, and is in the percentage range for low concentrations.

7.1 Introduction

In the past few decades, spark emission spectrometry has become a standard procedure for quickly determining the composition of metals and metal alloys and now forms an integral part of almost every laboratory within the metal-producing industry, but also increasingly the metal-processing sector. While the focus was on determining only main elements during the early years, up to 30 or more elements can now be analysed simultaneously.

The use of rare earths in many different applications has increased at an extremely brisk rate. But for which of these applications can spark emission spectrometry serve as an analysis method? After an introduction to the method, the following will shed light on this question and present a selection of analytical performance data.

7.2 Spark emission spectrometry basics

Spark emission spectrometry belongs to the group of optical atomic emission spectrometric analysis methods [1]. All of these methods have in common that free atoms or

ions must initially be excited from a base energy state (E_0) to a higher energy state (E_1) by the application of energy and the associated change of state of the outer electron shells. During a spontaneous emission of radiation, these free atoms or ions then fall back into their base state, either directly or via the detour of an excitation state, a sort of “halfway house” in energy terms. The attribute “optical” here points to the fact that the emitted radiation is ultraviolet, visible or infrared light.

Planck’s Law describes the link between energy and the spectral wavelength of the emitted radiation:

$$\Delta E_{10} = E_1 - E_0 = h \times \nu_{10} = \frac{h \times c}{\lambda_{10}} \quad (7.1)$$

ΔE_{10} : Energy difference between the excited state 1 and the base state 0; E_1 : energy of the excited state 1; E_0 : energy of the base state 0; h : Planck’s constant; ν_{10} : frequency of the emitted radiation; c : speed of light; λ_{10} : wavelength of the emitted radiation.

Every chemical element displays a collective of individual energy transitions, its line spectrum. An example of such a spectrum can be found in Figure 7.1, which presents several iron lines ranging between 270 and 273 nm.

As a result, proving the existence of one or more such lines enables qualitative analysis. But the fact that the intensity of the radiation is proportionate to the number of atoms or ions present makes it possible to perform both qualitative and quantitative analyses.

Solid samples must first be transitioned into a gaseous state and dissociated to guarantee excitation is free from interferences from any neighbouring atoms or ions. In the case of spark emission spectrometry, this energy is supplied by an electric spark, i.e. a brief electrical discharge between (at least) two electrodes. The sample itself

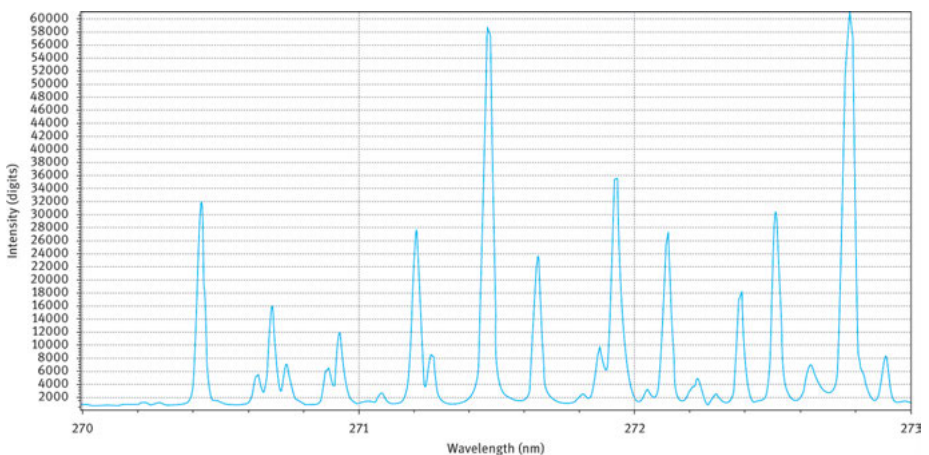


Figure 7.1: Line spectrum of iron in a pure iron sample between 270 and 273 nm.

actually constitutes one of these electrodes, namely the cathode. It therefore follows that, as a fundamental prerequisite of the method, the sample must be electrically conductive or at least powdered and mixed with an electrically conductive material such as graphite. However, generally self-conductive compact samples such as metals or metal alloys are analysed. Tungsten has established itself as a material for the so-called counter electrode, a metal that is characterised by both a high melting point and by extreme hardness, both of which are essential if the counter electrode is to remain easy to clean using mechanical means.

The spark discharge usually occurs in an argon atmosphere and not in air, for which there are diverse reasons:

- argon comes with the advantage of delivering good transparency of element lines below 190 nm,
- no oxidation processes occur and
- the heavy Ar ions cause an extreme cathode fall region, meaning the majority of the energy is transferred to the surface of the sample, which acts as the cathode, and not to the counter electrode. The temperature at the sample is consequently high, while the temperature at the counter electrode remains low.

A high-voltage ignition pulse initially causes an electrical spark to be discharged from the counter electrode to the sample, during which sample material (approx. 30 ng per spark discharge) is removed and transported into the plasma, which consists of Ar atoms, Ar ions and electrons. At temperatures $>10,000^{\circ}\text{C}$, a part of the sample material is vaporised, dissociated into atoms or ions and thermally excited to emit light (see above). The sample retains a so-called spark spot, which is characterised by a very fine metal distribution owing to fused micro-regions. Figure 7.2 shows a schematic of such a system.

However, not just the element lines of the vaporised elements are emitted within this Ar plasma, but equally a spectral background. This is mainly made up of the line spectrum of the plasma gas and continuum radiation, which results from the recombination processes between positive ions and electrons as well as electron *bremsstrahlung* (braking radiation). This, in turn, results from the change in kinetic energy that occurs given collisions between free-moving electrons and heavy plasma portions such as ions and atoms [2]. However, as the described processes are not only dependent on the electron and ion density, but also on the gas composition and temperature, the intensity of the background radiation is sample- and wavelength-specific.

Yet the analytical method used with spark emission spectrometry does not rely on observing a single spark discharge, but is actually based on a longer sparking process that is made up of several steps. To begin with, the area between the sample and the counter electrode is purged with argon to displace any excess air. What follows is the so-called pre-sparking period, in which several thousand spark discharges with a frequency of up to 1,000 Hz serve to remelt and thus to

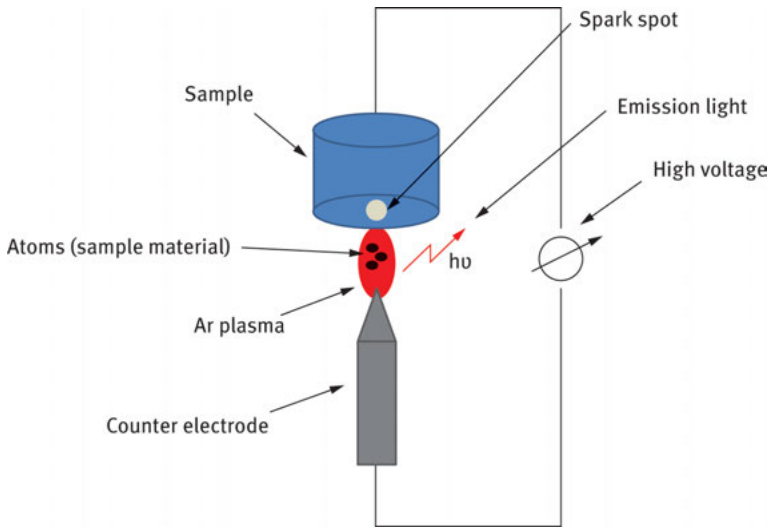


Figure 7.2: Spark emission between the sample and the counter electrode.

homogenise a portion of the sample surface. Structural influences such as inclusions can thus be eliminated or reduced. In the best possible case, this pre-sparking period ends in a so-called stationary sparking state, which is to say a point in time at which the magnitude of the emitted radiation no longer changes. This pre-sparking period is followed by the actual analysis process, during which the emitted radiation is measured and integrated over several thousand individual spark discharges, and finally converted into percentages by weight with the help of calibration functions.

7.3 Setup of a spark emission spectrometer

Modern spark emission spectrometers can generally be divided into mobile units for positive material identification purposes and stationary laboratory devices. But since mobile spectrometers have to be small, easy to handle and simple to transport, they also come with compromises in terms of spectral resolution, stability and, ultimately, their analytical capabilities. Among other things, the larger and better stabilised optical system that characterises laboratory spectrometers results in improved analysis capabilities; these devices range from small table-top units right up to automated high-end analysers.

Since they are based on the same physical principle, almost all spark spectrometers are similar in design. As an example, the following will discuss the QSG 750-II laboratory spectrometer made by the company OBLF GmbH, shown in Figure 7.3. The dimensions of the device are 100 cm (width), 90 cm (depth) and 130 cm (height).



Figure 7.3: OBLF QSG 750-II spark emission spectrometer. Source: OBLF GmbH.

The general design of a spark emission spectrometer is shown in Figure 7.4. The following then briefly describes the individual components.

7.3.1 Argon supply

The spark spectrometer is usually supplied with argon (1) of quality 4.8 (purity of 99.998 %). Should elements such as nitrogen or oxygen need to be analysed, argon supply using quality 5.0 or 6.0 is recommended, or the use of a gas purifier (3) for cleaning the argon. In this case, argon flows with a primary pressure of approx. 10 bar (2) through small pipes that are filled with various chemicals. While titanium causes chemical bonding of nitrogen and oxygen, copper oxide makes carbon monoxide and hydrocarbons oxidise into carbon dioxide and water, which are then physically bonded to a molecular sieve. Downstream of the gas purifier argon pressure is reduced to 3 bar (4).

7.3.2 Spark stand

The spark stand (5) consists of a top plate and a chamber with the counter electrode (6). The top plate is a hardened stainless steel plate with a circular opening (diameter: 12 mm), onto which the sample (7) is positioned in such a way that the opening is completely blocked off to prevent any ingress of air. The spark stand chamber is

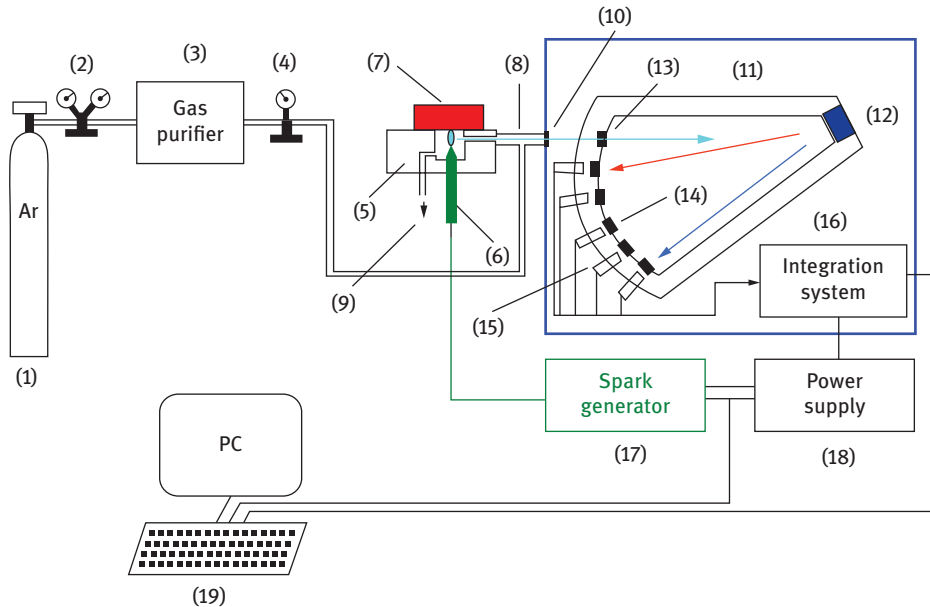


Figure 7.4: Schematic of a spark emission spectrometer [1]: (1) Ar cylinder; (2) reducing valve (output 10 bar); (3) gas purifier; (4) reducing valve (3 bar); (5) spark stand; (6) counter electrode; (7) sample; (8) light tube; (9) gas outlet; (10) entrance window and vacuum lock; (11) optical frame; (12) optical grating; (13) entrance slit; (14) exit slit; (15) photomultiplier; (16) integration system; (17) spark generator; (18) power supply; (19) control and evaluation PC.

constructed in such a way as to ensure it is well purged by the argon flow. The argon that is contaminated with burn-off (9) lands in a filter or is directly discharged into the open air.

7.3.3 Spectrometer optical system

The emission light generated in the spark stand reaches the evacuated optical system via a light pipe (8) and an entrance window (10), which is made of quartz or magnesium fluoride. The vacuumised optical system is under 0.005 mbar of pressure and contains a polychromator array with a Paschen–Runge mount assembly (11). In this regard, the concave reflection grating (12), the entrance slit (13) and the exit slits (14) are arranged in a Rowland circle. In this case, the grating and exit slits are rigid, the entrance slit can be moved in order to vary the target area of the light on the grating. Depending on the respective analytical task, the number of lines on the reflection grating can differ. The default number is at 2,400 lines per millimetre, which results in a reciprocal linear dispersion of 0.56 nm/mm. The width of the entrance slit is less than 20 μm , while the width of the exit slits varies between 25 and 50 μm . The light that

escapes through the exit slits is then detected with the help of photomultiplier tubes (15) and integrated into the data acquisition system (16). Following an analogue-to-digital conversion, these measured values are transferred to the spectrometer's PC where the measured intensities are then converted into percentages by weight. As an alternative to photomultiplier tubes other spark spectrometers use semiconductor sensors (CCD or CMOS) for light detection purposes.

7.3.4 Spark generator

As one of the core elements of any spark emission spectrometer, the spark generator (17) is responsible for generating the spark discharge. Classic discharge circuits contain a power supply, a reservoir capacitor, a coil, a resistor and the analysis spark gap. So-called medium-voltage discharges, in which the applied voltage lies within a range from 400 to 1,500 V, have established themselves for practical use. But as such a voltage is insufficient to ignite the analysis spark gap, ignition is effected externally either with the help of a so-called auxiliary spark gap or by using a high-voltage pulse. Subsequently, the reservoir capacitor can discharge via the new electrically conductive spark gap, with the discharge characteristics being dictated by the capacity of the capacitor, the inductivity of the coil and the size of the discharge resistor. The resulting supercritical attenuation ensures a unipolar discharge.

Modern spark generators, however, increasingly use transistor switches. In contrast to the classic spark generation method, these transistor switches are characterised by a current cut-out function. As long as the switch is closed, energy flows into the spark gap. Apart from the specific inductivity used, the maximum current is only dependent on the length of time the transistor switch is activated. The type of spark generation employed in this case is called a gated discharge source and is also the type used in the QSG 750-II. Should the switch be activated again during the current decay time, energy will continue to flow into the spark gap and the discharge period as well as the light emission period will be prolonged. This makes it possible to generate both short, spark-like as well as longer, arc-like discharges. The graph at Figure 7.5 shows the respective emitted light intensity curves as a function of time for various discharge types.

Given a shorter discharge time (blue function), the maximum light emission is also lower and is reached earlier than with a longer discharge time (pink function). The green function finally shows the curve produced upon the transistor switch being reactivated twice.

7.3.5 Power supply

A central power supply (18) supplies all voltages needed for the spark generator, data acquisition and all other systems.

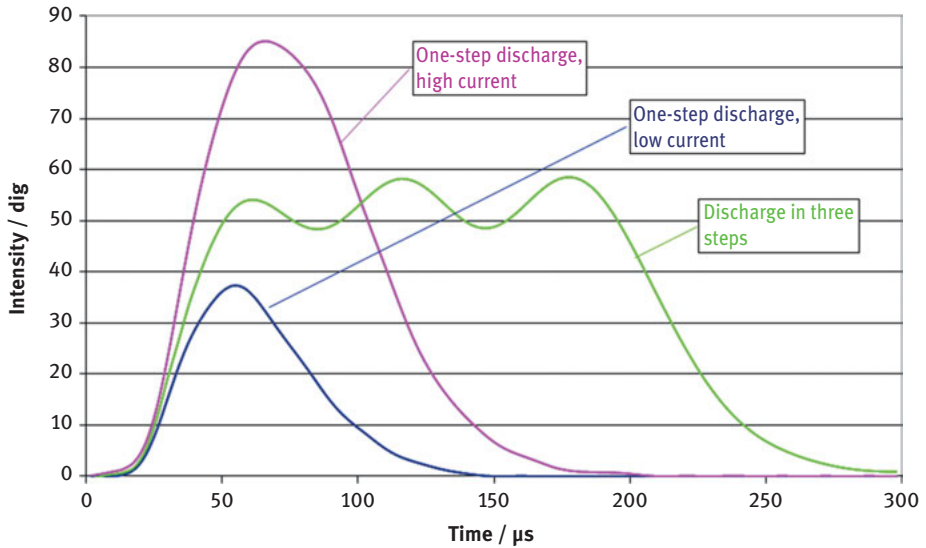


Figure 7.5: Emission curve with various discharge types.

7.3.6 Operation and evaluation PC

A conventional PC (19) serves to operate the spectrometer and to evaluate measured data.

7.4 The analysis process

A spectrometer-compliant sample must be provided prior to any actual analysis. This must be a homogeneous, electrically conductive solid sample that can be well positioned on the spark stand. One side of the sample must display a flat surface with a diameter of >12 mm. Samples of smaller diameters (between 7 and 12 mm) can be analysed using a special overlay mask. Wires with diameters of <7 mm can fundamentally also be sparked using a special wire sample holder, but in this case, analytical adjustments need to be made to guarantee correct analysis. The sample thickness should be between 0.2 and approx. 60 mm. Thinner metal sheets are difficult to analyse due to the applied heat and the danger of burning through. Higher samples can be fixed on the spark stand using extra-long retainers.

The sample surface to be used for analysis purposes must first be prepared prior to the process. This sample preparation serves to remove scale and any surface contamination. Various methods have established themselves for different metals. While turning or milling are standard methods for soft metals such as aluminium, magnesium, copper, lead or zinc, grinding with a grain size of 60 or 80 is preferred

for iron, nickel or cobalt alloys. In contrast to image analysers for which a polished and “perfect” sample surface is preferred, electrical sparks like points of attack on the sample such as the striations left by grinding or milling. This guarantees that the sparks spread out evenly over the sample surface.

Once the prepared sample is at hand, it is placed on the spark stand and the analysis can begin. The time taken for an individual measurement varies according to the type of sample between 15 and 50 s. On the one hand, this is dictated by the sample-specific pre-sparking period. While, for instance, standard steels already display a homogenised structure after a pre-sparking time of 9 s, it can take around 40 s to homogenise the many and dominant manganese sulphide precipitations found in semi-finished free-cutting steels. On the other hand, the integration process can consist of one or several cycles with various excitation energies. In contrast to the standard steel elements, exciting nitrogen atoms requires much more powerful spark discharges. However, as a result of the elevated spectral background these are counterproductive with regard to standard steel elements. Consequently, the only option for the spectrometer is to analyse the elements over various integration cycles. Finally, the measuring frequency also plays a central role. To ensure adequate statistical certainty, approx. 1,000–3,000 individual spark events are averaged or integrated. As matrices such as zinc degrade considerably more strongly than, for instance, iron, the pause between two individual spark discharges must be substantially longer. This leads to a spark succession frequency of 100–200 Hz in contrast to 800 Hz with iron.

In practice, though, an analysis never consists of taking a measurement at only one spot on the sample. As samples can display segregations or blowholes, a complete analysis is always made up of at least two so-called sparkings at different places on the sample. Using the statistical software function, the comparability of both individual results is then verified. Should a sufficient degree of certainty be given, both individual results are automatically averaged and the analysis is completed.

One of the latest developments in the field of spark emission spectrometry was introduced at the CETAS conference in Luxembourg (city) in the year 2011 and constituted the launch of a so-called double electrode spark stand, which features two electrodes instead of only one [3]. These two electrodes permit two spark processes to be conducted on the sample surface without having to reposition the sample in between sparkings. The purging process at the beginning of the analysis naturally needs to be completed only once. The pre-sparking process is conducted at double the frequency in an alternate manner. Depending on the analysis system, the actual measuring process can also be performed alternately. This makes it possible to carry out two spark processes in about the same space of time it would take to complete one using a standard system. If both spark processes are comparable, the analysis is completed. The advantage of the system is of particular benefit to users who are called upon to carry out numerous analyses per day.

7.5 Quantitative analysis

Simply proving the existence of an element within a sample, which is to say performing a qualitative analysis, is generally not sufficient for users of spark emission spectrometry. Instead, the aim is to deliver as precise a determination of the composition of a sample as possible, which requires a quantitative analysis.

7.5.1 Calibration and recalibration

Although a theoretical connection exists between the measured intensity of an element line and the concentration of the element within the plasma and the sample, respectively, a direct determination is made impossible due to a surfeit of underlying parameters. For this reason, a spark emission spectrometer must be calibrated using certified samples. In contrast to other analysis methods, the evaluation function is not the calibration function $I = f(c)$, but rather the analysis function $c = f(I)$ (I = intensity, c = percentage by weight). As the amount and composition of the sample material that enters the plasma from the sample are dependent on numerous parameters such as viscosity, vaporisation enthalpy and thermal conductivity, and as the composition of the vaporised material can in turn influence the plasma temperature and the associated excitation processes, the measured intensity must be standardised. The intensity of a reference line, usually the line of the matrix element such as iron is in a steel sample, is used as a standardisation factor. When multiplied by the so-called scaling factor S_{kt} , a typical intensity of the reference line, an absolute intensity $I_{abs,El}$ delivers the relative intensity $I_{rel,El}$:

$$I_{rel,El} = \frac{I_{abs,El}}{I_{abs,Ref}} \times S_{kt} \quad (7.2)$$

$I_{rel,El}$ = relative element intensity, $I_{abs,El}$ = absolute element intensity, $I_{abs,Ref}$ = absolute reference intensity, S_{kt} = scaling factor.

Owing to the resolution of the spectral unit and the line broadening within the plasma, spectral interferences can occur due to the overlapping of element lines, but also due to band coincidences of any non-dissociated molecules. The analysis function takes these “additive interference signals” into account by means of a linear correction.

Apart from these spectral interferences, the sample’s physical and chemical properties and the resulting vaporisation and excitation characteristics within the plasma also affect any analytes, an effect that is not fully compensated by the signal’s reference to the matrix intensity. The severity of this “matrix effect” is dependent on the concentration of the interfering element as well as of the analyte itself and is also taken into account in the analysis function.

Theoretically, there is a linear correlation between the concentration of the analytes within the sample and the measured intensity, but this is usually only given if

the concentration is low. Owing to the optically dense spark plasma, higher concentrations give rise to a self-absorption effect, i.e. non-excited atoms or ions in their base state absorb light emitted by their own kind, which in turn leads to their excitation.

The emission lines to be used in the respective application are mostly specified by the spectrometer manufacturer. The selection is based on information provided by the customer in the form of matrices, elements and concentration ranges or materials that need to be analysed. Material databases or reference literature such as the Key to Steel [4] enable spectrometer manufacturers to collate the first-named information themselves.

Unfortunately, not all elements can be measured with only one emission line each, for which the reasons are as follows:

- The self-absorption effect causes the curve of an analysis line to rise too steeply upwards of a certain concentration → the line cannot be used for high element concentrations.
- The spectral background is too large to achieve a good signal-to-background ratio → the line cannot be used for low element concentrations.
- The slope of the analysis function is too high → the line is not sensitive enough and cannot be used for low element concentrations.
- The spectral interferences are extremely high, e.g. due to matrix lines or due to main alloy components → if available, a different line should be used.

Calibrating a spark emission spectrometer involves a lot of effort since a sufficient number of certified samples are required for each analyte; this is necessary not only to describe a basic function, but also to calculate all requisite additive and matrix corrections. As a result, it is not uncommon for the calibration of a complex steel matrix to require around 300–400 samples – for which reason this “basic calibration” is performed only once in the course of a spectrometer’s lifecycle. However, as changes in the analysis sensitivity, e.g. due to soiling of the spark stand and the entrance window or fluctuations in argon quality, can lead to variations in measured intensities, it must be mathematically possible to return the system to its calibrated state with the help of recalibration samples. In the event of a commonly performed two-point recalibration, two recalibration samples are supplied for each analysis channel: a “low sample” and a “high sample”, each of which contains a low or high concentration, respectively, of the analyte. The “target intensities” of these samples are initially recorded prior to the start of the actual calibration. The recalibration samples then form part of the scope of delivery and remain with the customer. After renewed analysis at a later point in time (to ascertain “actual intensities”), target and actual intensities are used to generate correction factors with whose help every intensity of a production sample can be corrected to reflect the state of the original calibration. Depending on the number of samples, some users perform such a recalibration on a daily or a monthly basis.

7.5.2 Evaluation of calibration and analysis results

Once calibrated, the spectrometer program displays graphs of the analysis functions. An example is shown in Figure 7.6, which details a calibration of chromium in low-alloy steel.

Relative intensity is plotted on the x -axis and relative concentration on the y -axis. Relative concentration is defined by the absolute concentration of the element, divided by the matrix concentration (in this case the iron concentration), multiplied by 100 %. Each measuring point represents a certified standard sample.

The quality of the smoothing function is given by the correlation coefficient R and residual scatter SR . A0–A3 represent the coefficients of the function, which in this case is of the third degree.

In accordance with DIN 32 645 [5], the detection limit of an analysis process is calculated using the following formula:

$$\chi_{DL} = \Phi_{n,\alpha} \times \frac{s_L}{b} \quad (7.3)$$

χ_{DL} : detection limit; $\Phi_{n,\alpha}$: factor to quickly estimate the detection limit; n : number of measurements to ascertain s_L ; α : significance level; s_L : standard deviation of the intensity of a pure metal sample; b : slope of the calibration line (sensitivity).

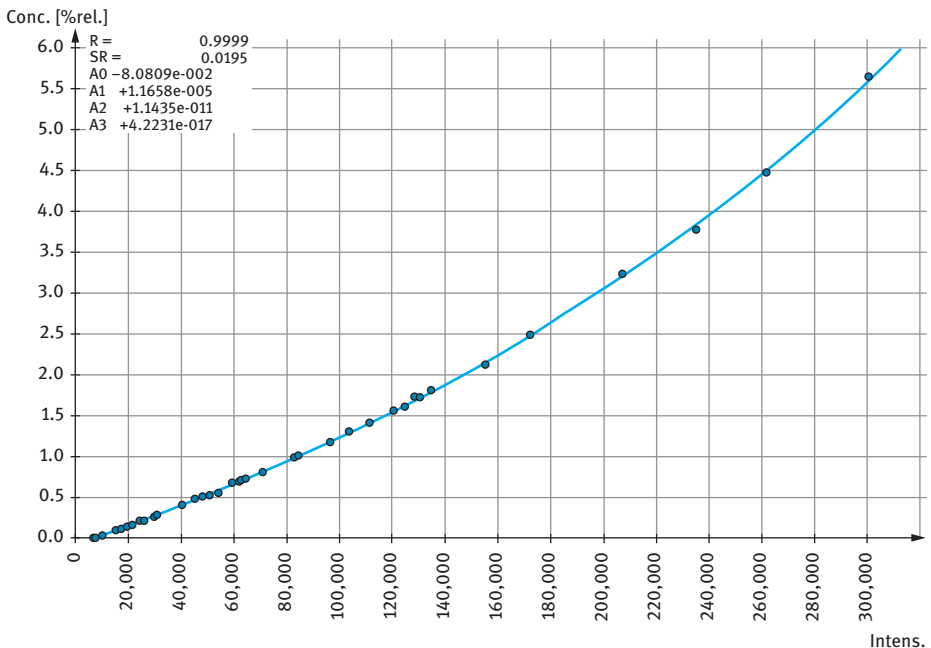


Figure 7.6: Analysis function of chromium in low-alloy steel.

The quick estimation factor $\Phi_{n;\alpha}$ is dependent on the number of measurements n that are taken and the significance level α . As a result, the detection limit must always be specified along with the data for n and α . For reasons of uniformity, a factor of three, which corresponds to ten measurements and a significance level of 0.01, is mostly used for spectrometry purposes.

Further factors used to assess the analysis process are accuracy, repeatability and reproducibility. Calibration quality is decisive for the accuracy of the analysis data. Validation measurements taken after calibration provide a good impression of the analysis results. Repeatability generally refers to the standard deviation of a multiple analysis that has been completed in a short time. Reproducibility, on the other hand, refers to long-term stability over a period of several hours, days, weeks or months. This is dependent on not just the spectrometer's stability itself, but also on parameters such as the recalibration and sample preparation.

7.6 Using spark emission spectrometry

Spark emission spectrometry provides many advantages in comparison to other analysis methods:

- short analysis times,
- numerous elements that can be analysed,
- direct analysis using a solid sample,
- relatively few requirements regarding the sample,
- fully functional in rough environments,
- simple operation, even by staff with little experience and
- the option of automation.

As a result of all these benefits, spark emission spectrometry has established itself as a standard procedure in almost all enterprises within the metal-producing industry during the last 40 years. Nowadays, no steel plant is in a position to manufacture its products without having tracked the production process with the help of spark discharges. In the same vein, almost all foundries as well as manufacturers of aluminium, copper, magnesium, nickel, cobalt, titanium, tin, lead and zinc alloys as well as, in part, precious metals are equipped with spark emission spectrometers nowadays. However, quality assurance requirements mean metal-processing companies are also often called upon to not simply put their trust in the supplied works certificates of the primary producer, but to carry out incoming quality control measures themselves. Thanks to the flexibility of the technology, further areas of application can be found among materials testers and other establishments such as universities and institutes where there such testing is carried out. In such cases, the equipment not only serves

H																		He
Li	Be											B	C	N	O	F	Ne	
Na	Mg											Al	Si	P	S	Cl	Ar	
K	Ca	Sc	Ti	V	Cr	Mn	Fe	Co	Ni	Cu	Zn	Ga	Ge	As	Se	Br	Kr	
Rb	Sr	Y	Zr	Nb	Mo	Tc	Ru	Rh	Pd	Ag	Cd	In	Sn	Sb	Te	I	Xe	
Cs	Ba	La-Lu	Hf	Ta	W	Re	Os	Ir	Pt	Au	Hg	Tl	Pb	Bi	Po	At	Rn	
Fr	Ra	Ac-Lr	Rf	Ha														
		La	Ce	Pr	Nd	Pm	Sm	Eu	Gd	Tb	Dy	Ho	Er	Tm	Yb	Lu		
		Ac	Th	Pa	U	Np	Pu	Am	Cm	Bk	Cf	Es	Fm	Md	No	Lr		

Figure 7.7: Elements suitable for analysis using spark emission spectrometry and elements analysed in practice (shown in green).

the provision of external services such as contract laboratories, but is also used for research and teaching purposes.

Many application areas of spark emission spectrometry, even though not all, are covered by operation procedures and standards, e.g. for the analysis of carbon and low-alloy steels [6, 7], austenitic steels [8], manganese steels [9], cast iron [10], aluminium and aluminium alloys [11], magnesium and magnesium alloys [12], as well as zinc and zinc alloys [13]. In many industrial sectors, inter-laboratory comparability is established with the help of round-robin tests, which are often carried out by sector institutes within, e.g. the steel or foundry industries.

The number of elements requiring analysis has risen dramatically, especially in the last few years. While the focus was only on standard steel elements like carbon, silicon, manganese, phosphorous and sulphur as well as chromium, nickel or molybdenum alloys 40 years ago, the number of elements requiring analysis can amount to 30 or more in a modern steel plant.

Figure 7.7 shows elements within the periodic table that are analysable in the various matrices and/or that are routinely analysed more or less often.

General and advanced literature on the topic of spark emission spectrometry can be found, among others, in the works by Slickers [14] and Thomsen [15].

7.7 Analysing rare earths using spark emission spectrometry

Given the right physical conditions, i.e. the existence of suitable analysis lines, there is nothing to stop rare earths from being analysed with the help of spark emission spectrometry. However, since sample homogeneity and its metallic (conductive) character are two prerequisites that must be fulfilled to permit analysis in practice, as described above, the industrial fields of application of rare earths must first be

discussed and it must be ascertained whether the requirements for spark spectrometry purposes are fulfilled.

7.7.1 Industrial use of rare earths

In the year 2011, the CIBC (Canadian Imperial Bank of Commerce) published the data shown in Figure 7.8 on the use of rare earths in industry [16].

In most applications, rare earths are found in sintered form as a magnetic material, with a crystalline structure in fluid-cracking catalysts, as complex alloys in rechargeable NiMH batteries, in oxidised form as polishing agents, in catalytic converters for automotive use and as glass additives or in other ionically bonded form, all of which are either not well suited (magnet, NiMH batteries) or entirely unsuitable for spark emission spectrometry. The only application with materials relevant for spark emission spectrometry can be found in the form of alloying elements in the field of metallurgy with the aim of producing materials with specific mechanical properties. Several applications will be briefly presented in the following.

7.7.1.1 Magnesium alloys

Mainly Ce, La, Nd and Pr, but increasingly also other rare earths, are used in the production of high-tensile materials that are required in the aviation or automotive industries [17, 18]; concentration range of up to 5 %.

7.7.1.2 Aluminium alloys

In this case, Sc increases strength and comes with structure-stabilising as well as grain-size-refining effects, especially in AlLi alloys [19], Ce and La also improve material properties, e.g. ductility [20]; concentration range <1 %.

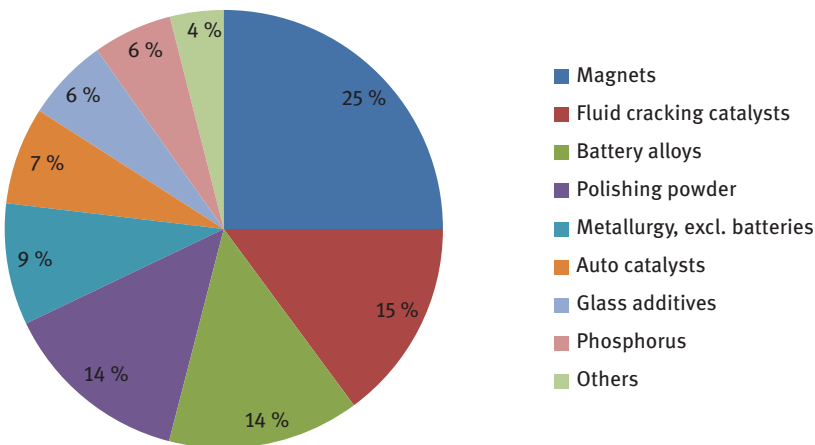


Figure 7.8: Industrial use of rare earths in 2010. Source: CIBC [16].

7.7.1.3 Cast iron and steel

Ce and La increase the number of and optimise the size distribution of graphite spheres in spheroidal graphite [21], while various other rare earths improve the material properties of steel [22]; concentration range <0.1 %.

7.7.1.4 Zinc alloys

Ca and La reduce grain boundary effects in ZnAl alloys, above all in GalfanTM, which are used as coating materials for sheet and/or plate steel. These rare earths result in improved corrosion resistance, a more homogeneous grain distribution and ultimately make the material more weldable, paintable and ductile; concentration range <0.1 % [23].

Performing general analyses of the named alloys and materials has long belonged to the main tasks to which spark emission spectrometry is put, but the inclusion of rare earths is a more recent development.

7.7.2 Spectrometric prerequisites

Once the prerequisites for an analysable sample have been met, suitable wavelengths must first be found for the respective elements. Wavelength tables such as those published by Saidel, Prokofjew and Raiski [24] and the Massachusetts Institute of Technology [25] can serve as a basis, or online databanks such as the one hosted by the American NIST Institute [26]. Table 7.1 provides an overview of the most commonly used wavelengths or wavelengths that research has shown to be the most promising, all of which fall within a range from 290 to 460 nm.

In each case, Table 7.1 also details several neighbouring wavelengths of other rare earths that constitute potential spectral interferences and should or must be taken into consideration during calibration. The severity of these spectral interferences is dependent on the analysis and interference lines, the distance between both of these, the resolution of the optical system and the width of the exit slits. It must be stated, though, that due to the fact that rare earth elements all share a certain similarity at atomic level, it is not possible to analyse any of the rare earths without there also being interferences from others. How severe these interferences are and whether they are of real-life importance can only be determined with regard to each respective application.

However, since calibration depends on more than samples containing the respective rare earth element, but must also include samples with differing concentrations of potential interference elements, the question initially poses itself as to whether there are enough commercially available reference samples that satisfy the requirements.

7.7.3 Calibration samples

In general, in-house or certified reference samples can be used for calibration purposes. In-house samples come with the advantage of being as close to the company's

Table 7.1: Potential analysis and interference lines of rare earths.

Element	Most used or possible wavelength (nm)	Interference wavelength (nm)
Sc	402.04	Sm 402.00, Nd 402.09, Dy 402.09
Y	467.48	Nd 467.46, Er 467.48
La	433.37	Pr 433.31, Pr 433.39, Sm 433.41
Ce	399.92	Nd 399.87, Pr 399.92
	413.76	Gd 413.71, Nd 413.80, Pr 413.82
Pr	422.53	Gd 422.51, Dy 422.52, Sm 422.53, Gd 422.59
Nd	406.11	Gd 406.13
	410.95	Sm 410.94, Pr 410.94, La 410.95
Sm	356.83	Lu 356.78, Nd 356.89
	443.43	Ce 443.37, Pr 443.49
Eu	459.40	Ce 459.96, Sm 495.53
Gd	364.62	Pr 364.47, Dy 364.59, Pr 364.63
	379.64	Tm 379.59
Tb	387.42	Ho 387.41, Pr 387.45
Dy	353.17	Tb 353.17
	421.17	Nd 421.13, Pr 421.19, Gd 421.20
Ho	293.68	Yb 293.72
Er	369.27	Sm 369.28, 369.28
	400.80	Sm 400.81
Tm	376.13	Gd 376.09, Nd 376.16
Yb	398.80	Gd 398.78, La 398.85
Lu	451.86	Dy 451.85

own production output in terms of composition. However, prior to being used as a calibration sample, such in-house samples need to be analysed to determine “target concentrations,” a process that is usually completed with the help of a wet-chemical or spectrometric reference procedure. Often, though, suitable sample material is not yet available prior to equipment calibration. Not just for this reason, but mainly due to quality assurance requirements (laboratory certification or accreditation), calibration must include nationally and/or internationally certified reference samples.

As an example, Table 7.2 lists the number of samples by matrix along with the highest concentration that can be made available by one of the largest and best known manufacturers and distributors of such samples.

In contrast to samples with standard elements for steel and aluminium, which are available in their hundreds and that even permit individual calibrations for special alloys, the sample range for rare earths is rather sparse. While elements with the highest industrial application density, which is to say Sc, La and Ce in aluminium, La, Ce and Nd in magnesium as well as Ce and La in cast iron, steel and zinc, are naturally the most commonly available, the variety of samples is only just sufficient to complete a basic calibration for some of these elements.

Especially in recent times, though, requests are repeatedly reaching spectrometer manufacturers for the analysis of additional rare earths, e.g. Sm and Er in aluminium,

Table 7.2: Certified reference samples for rare earths, available for purchase. Source: Brammer Standard Company, Inc. [27].

Elem.	Al		Mg		Cast iron		Steel		Zn		Ni		Co		Ti	
	No.	Max (%)	No.	Max (%)	No.	Max (%)	No.	Max (%)	No.	Max (%)	No.	Max (%)	No.	Max (%)	No.	Max (%)
Sc	12	0.54														
Y			2	0.04											5	0.01
La	6	0.03	17	0.37	7	0.02	2	0.02	12	0.06			2	0.05		
Ce	7	0.05	21	1.86	41	0.11	6	0.06	14	0.08						
Pr			2	0.07												
Nd	2	0	6	0.18												
Sm																
Eu																
Gd			2	0.05												
Tb																
Dy																
Ho																
Er																
Tm																
Yb																
Lu																

Table 7.3: Maximum concentrations of calibration samples held by OBLF.

Element	Al	Mg	Cast iron	Steel	Zn	Ni	Co	Ti
	Max (%)	Max (%)	Max (%)	Max (%)	Max (%)	Max (%)	Max (%)	Max (%)
Sc	0.3							
Y	0.01	4.8				0.8		0.008
La	0.3	1.2	0.03	0.02	0.06	0.5	0.05	
Ce	0.6	3	0.1	0.05	0.07	1.5		
Pr	0.08	0.5						
Nd	0.25	3.2						
Sm	0.02	0.1						
Eu		0.01						
Gd		0.3						
Tb		0.05						
Dy		0.35						
Ho		0.07						
Er		0.15						
Tm		0.015						
Yb		0.1						
Lu		0.01						

or Sm, Y, Er and Gd in magnesium. With the help of a few still existing, but unfortunately no longer commercially available, samples and a few that are only available on the Chinese market, OBLF can at present perform calibrations up to higher concentrations and/or for further elements. Table 7.3 details the maximum concentrations available at present.

However, overall it can be said that there is a great need for certified reference samples, a situation that no doubt not only results from the fact that samples are difficult as well as work-intensive to produce and certify, but also due to the demand for them.

Using existing and/or reference samples provided by the customer, it is possible to carry out calibrations. In the following, several examples from the aluminium, magnesium, iron and zinc matrices will be presented and analytical performance data discussed.

7.8 Analysis of aluminium alloys

7.8.1 Calibration (analysis function) and accuracy

Of the rare earth elements, Sc, Y, La, Ce, Pr, Nd and Sm can in general be calibrated in aluminium at present. As the most often analysed elements, Ce and La (Figures 7.9

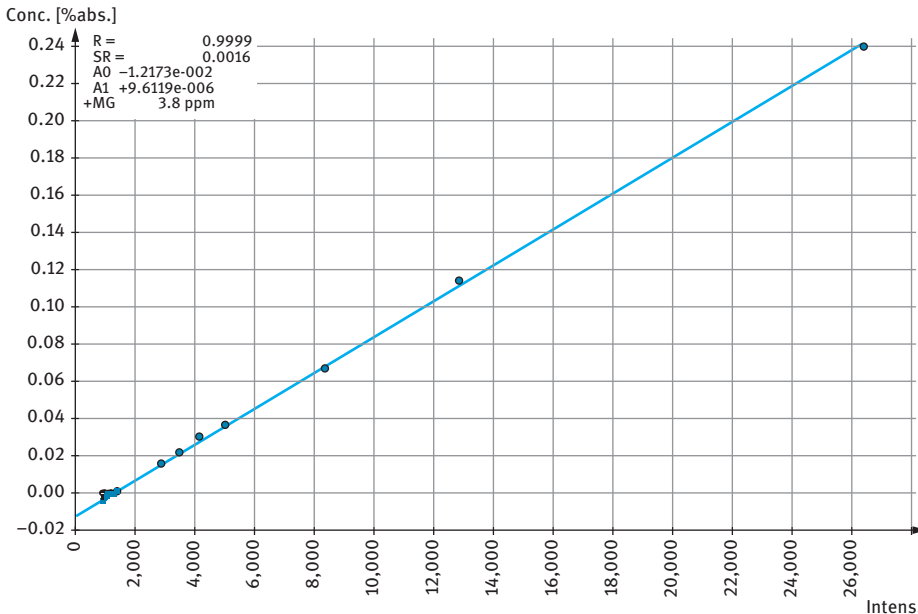


Figure 7.9: Analysis function of La in aluminium.

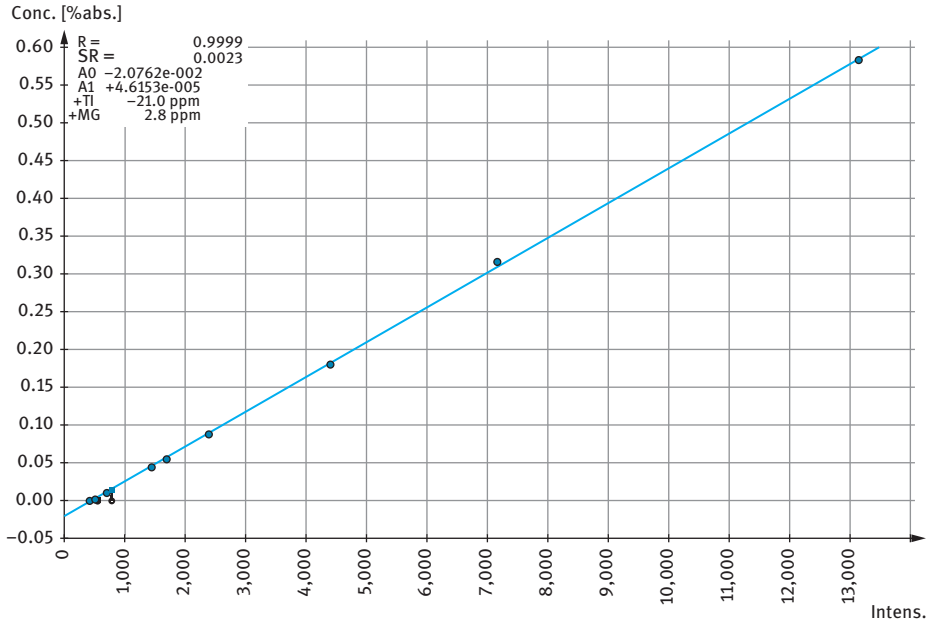


Figure 7.10: Analysis function of Ce in aluminium.

and 7.10) serve as examples for analysis functions. Wavelength 413.76 nm was used for Ce and 433.37 nm for La. Both functions display a linear curve within the concentration range of up to 0.6 % (Ce) and 0.24 % (La). For Ce, an additive Ti correction (413.73 nm) of 21 µg/g/% Ce is necessary. The lowest concentration range requires an additive Mg correction, which is not based on a line overlapping, but rather on a shift of the background signal, and thus constitutes a matrix correction.

Table 7.4 details the validation as a test of the accuracy of the calibration. The sample set was a Chinese series that already served as a basic calibration framework. As a result, the requirement of an independent validation using independent samples could not be met due to a lack of suitable samples, as was also the case for the other matrices.

Table 7.4: Validation of La and Ce in aluminium.

Sample	La in aluminium		Ce in aluminium	
	Setpoint (%)	Meas. val. (%)	Setpoint (%)	Meas. val. (%)
SE1	0.022	0.021	0.054	0.056
SE2	0.037	0.036	0.087	0.089
SE3	0.067	0.067	0.180	0.181
SE4	0.114	0.112	0.316	0.309
SE5	0.239	0.237	0.584	0.579

Meas. val. = Measured value.

Table 7.5: Detection limits in aluminium.

Element	Sc	Y	La	Ce	Pr	Nd	Sm
Detection limit ($\mu\text{g/g}$)	0.1	*	3	3	3	3	2

*Calibration is possible, but has yet to be carried out.

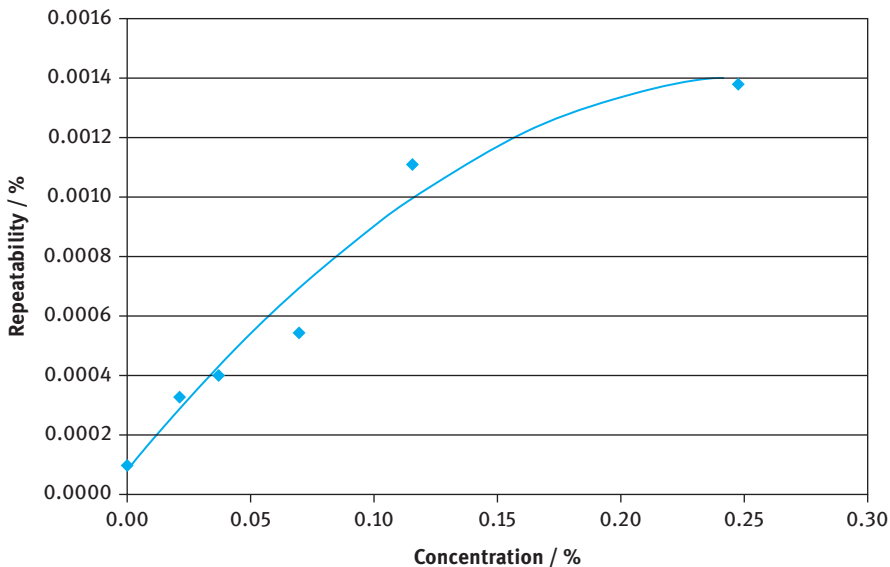
The degree of correspondence with the certified values is very good. However, if rare earth samples with a higher number and variety of concentrations were to be routinely analysed, more samples would have to be included in the calibration due to the interference situation.

7.8.2 Detection limits

A tenfold analysis of a pure aluminium sample delivered the detection limits of the individual elements. These are detailed in Table 7.5 for all elements determined in aluminium.

7.8.3 Repeatability

To determine repeatability, several samples were sparked 10 times in quick succession, followed by a calculation of the mean values and standard deviations. A comparison of the values for Ce and La is shown in Figures 7.11 and 7.12.

**Figure 7.11:** Representation of repeatability of La in aluminium.

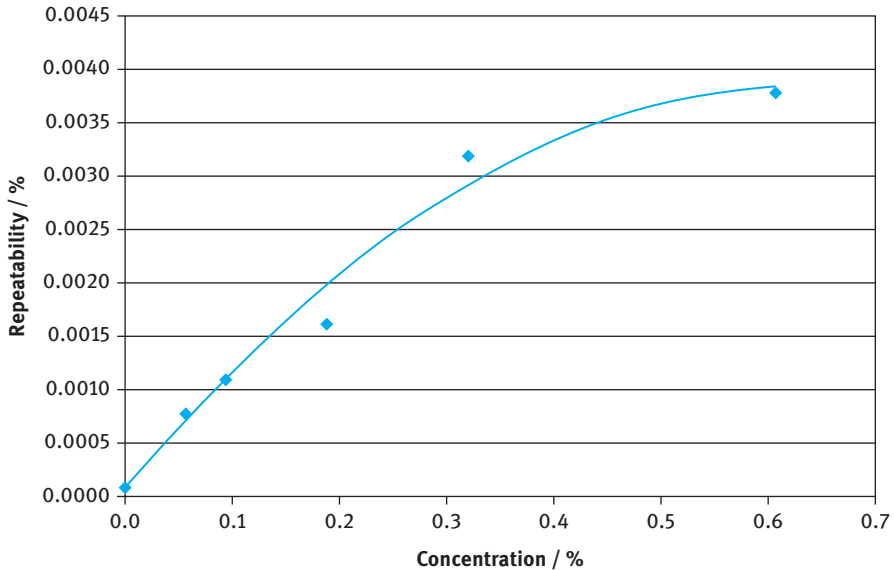


Figure 7.12: Representation of repeatability of Ce in aluminium.

Given an example concentration of 0.2 %, repeatability for La corresponds to a relative standard deviation of 0.6 %, and for Ce with a concentration of 0.5 % to a relative standard deviation of 0.7 %.

7.9 Analysis of magnesium alloys

7.9.1 Calibration (analysis function) and accuracy

The calibration samples provided by the Norwegian company Norsk Hydro were still available for purchase up until a few years ago, but unfortunately are now no longer commercially available. A few of these samples are still held by OBLF and can be used for calibration purposes. In comparison to the values cited at Brammer Standard (see Table 7.2), the OBLF calibration limits are considerably higher and permit – at least as a basic function – the calibration of almost all rare earths. As a rule, the elements ordered by customers are mainly La, Ce, Nd, Pr and less often Y and Sm. As La and Ce were discussed for aluminium, the focus will now be on the elements Nd and Pr, as examples, for magnesium. The analysis functions of up to 3 % in the case of Nd and up to 0.5 % in the case of Pr are shown in Figures 7.13 and 7.14.

In contrast to Pr, the Nd samples do not display a linear function, which can be explained by the self-absorption effect. In this case, a second-degree polynomial serves to describe the function. As the concentrations of rare earths are generally higher in comparison to aluminium, some of the spectral interferences described in Table 7.1 are

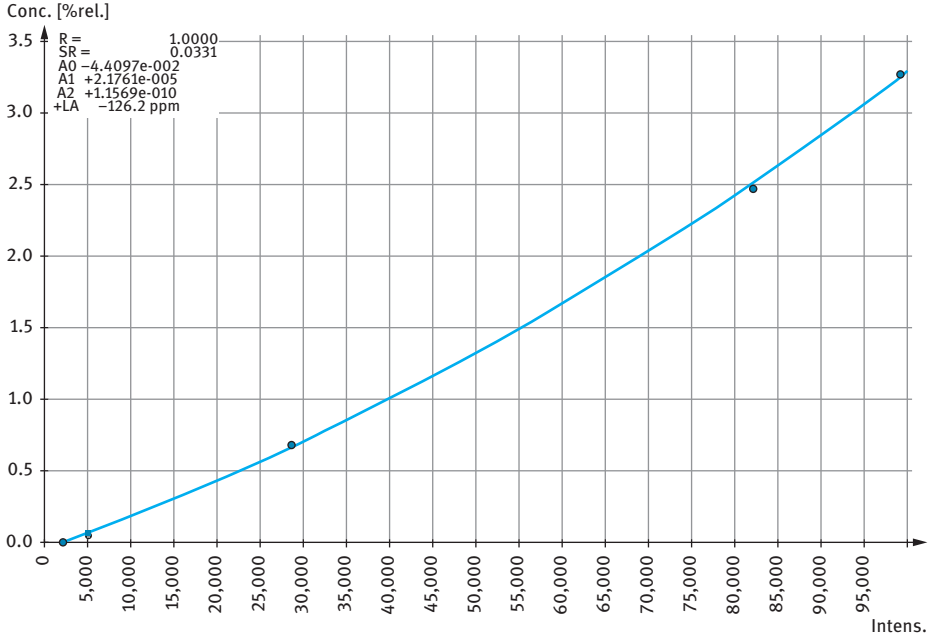


Figure 7.13: Analysis function of Nd in magnesium.

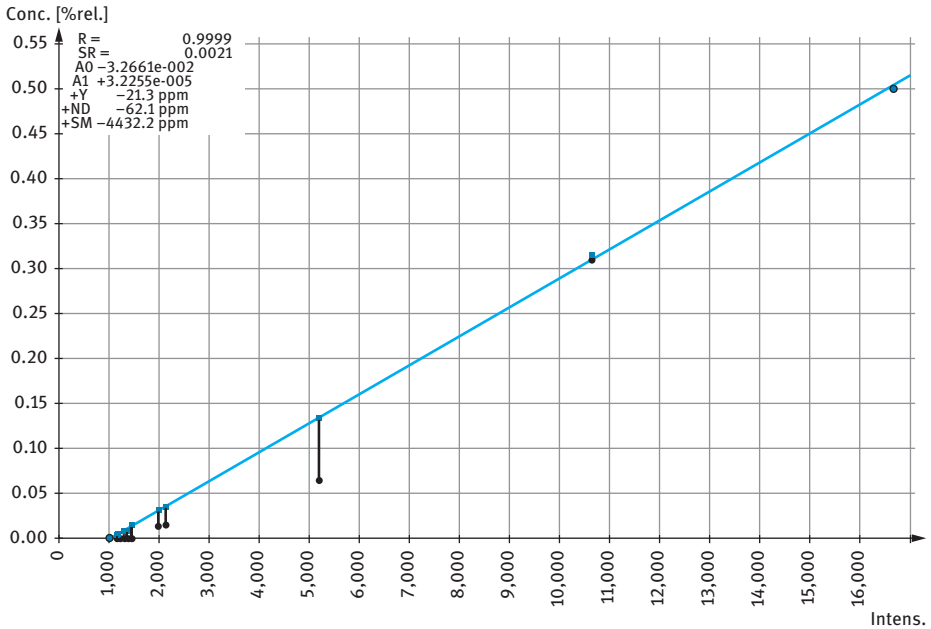


Figure 7.14: Analysis function of Pr in magnesium.

Table 7.6: Validation of Nd and Pr in magnesium.

Sample	Nd in magnesium		Pr in magnesium	
	Setpoint (%)	Meas. val. (%)	Setpoint (%)	Meas. val. (%)
MGH2B	0.044	0.041	0.013	0.013
MGF1B	0.050	0.050	0.48	0.48
AEH93	0.61	0.59	0.28	0.27
MGY1A	2.26	2.30	0.059	0.059
MGH1B	3.05	3.02	0.014	0.015

Meas. val. = Measured value.

easily visible. The interference of Y on Pr is particularly noticeable, but not mentioned in the table. Going by the measured calibration samples, the interference is, however, clear to see.

Some of these samples were subsequently sparked in concentration mode. The results are shown in Table 7.6.

The degree of correspondence is again very good in this case. However, in practice care must be exercised when dealing with materials that are alloyed with a large variety of rare earths. This would most definitely require a more extensive calibration, ideally using the precise materials required in each case.

7.9.2 Detection limits

The detection limits in Table 7.7 show that spark emission spectrometry is not a suitable method for analysing rare earths in the lowest $\mu\text{g/g}$ or even sub- $\mu\text{g/g}$ ranges. In such cases, a wet-chemical method would no doubt deliver more reliable data. The advantages of spark analysis can, by contrast, be seen in the possibility of analysing higher concentrations, coupled with the high speed of the method.

7.9.3 Repeatability

Figures 7.15 and 7.16 again show the repeatability of Nd and Pr as examples. In the case of Nd, the relative standard deviations lie within the 2 % region at 0.6 % and for

Table 7.7: Detection limits in magnesium.

Element	Y	La	Ce	Pr	Nd	Sm	Eu	Gd	Tb	Dy	Ho	Er	Tm	Yb	Lu
Detection limit ($\mu\text{g/g}$)	12	5	10	8	9	27	*	*	*	*	*	5	*	*	*

*Calibration possible, but has yet to be carried out.

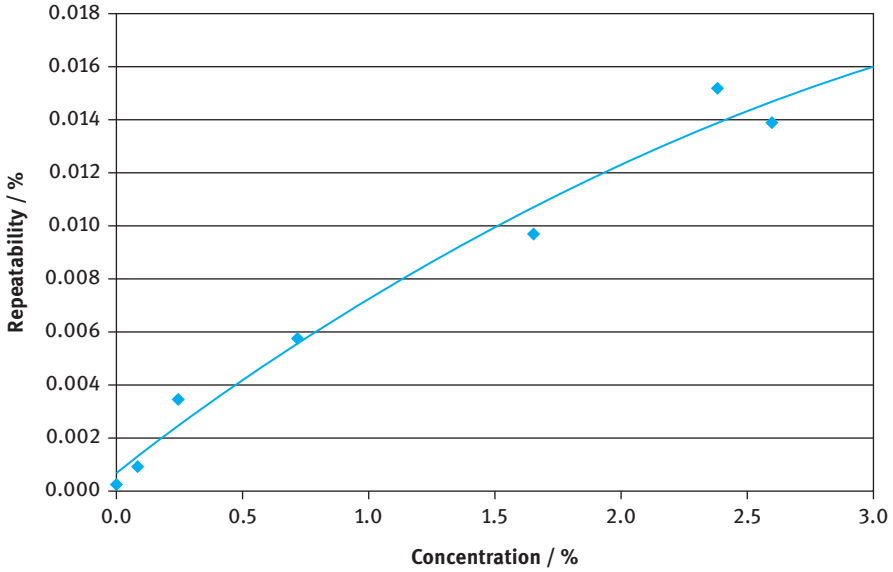


Figure 7.15: Representation of repeatability of Nd in magnesium.

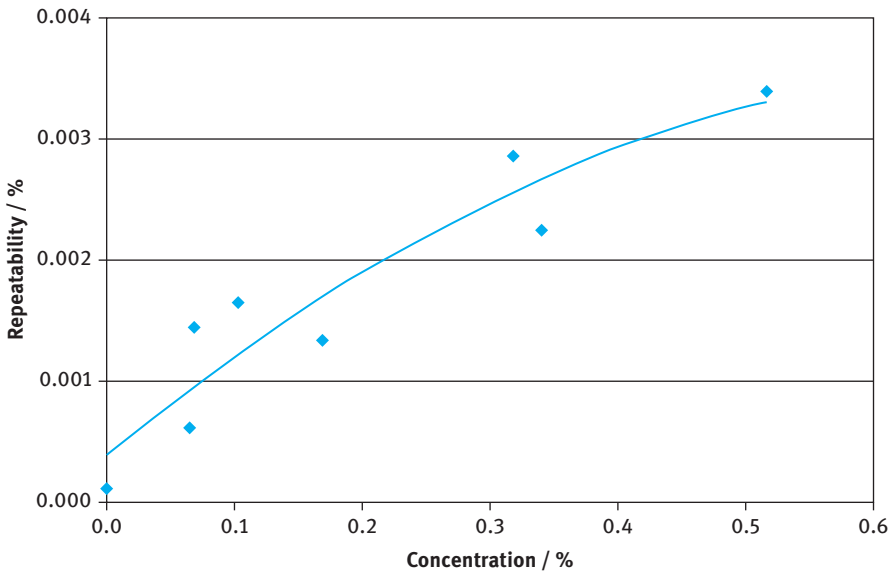


Figure 7.16: Representation of repeatability of Pr in magnesium.

Pr with a concentration of 0.5 % also at 0.6 %, and are thus within the normal spark spectrometry range.

7.10 Analysis of iron alloys

7.10.1 Calibration (analysis function) and accuracy

Although the use of rare earths in the area of steel production has yet to make great strides, the use of La and Ce in cast iron has almost become a standard application nowadays. For that reason, the focus will be on cast iron in the following. Figures 7.17 and 7.18 detail the analysis functions.

In comparison to the aluminium and magnesium matrices, the spectral interferences affecting the analysis functions are substantially more severe with a height of many $\mu\text{g/g}/\%$, especially of elements that are characteristic of cast iron, e.g. C, Mn, Cr and Ni. While these interferences can be corrected with relative ease, they also make routine analysis anything but simple. As shown in Table 7.8, the validation looks good for both elements, but when analysing unknown samples of differing composition, deviations of $\pm 0.001\text{--}0.002\%$ may well arise, even down to the lowest concentrations. In such a case, a selective calibration would again be helpful.

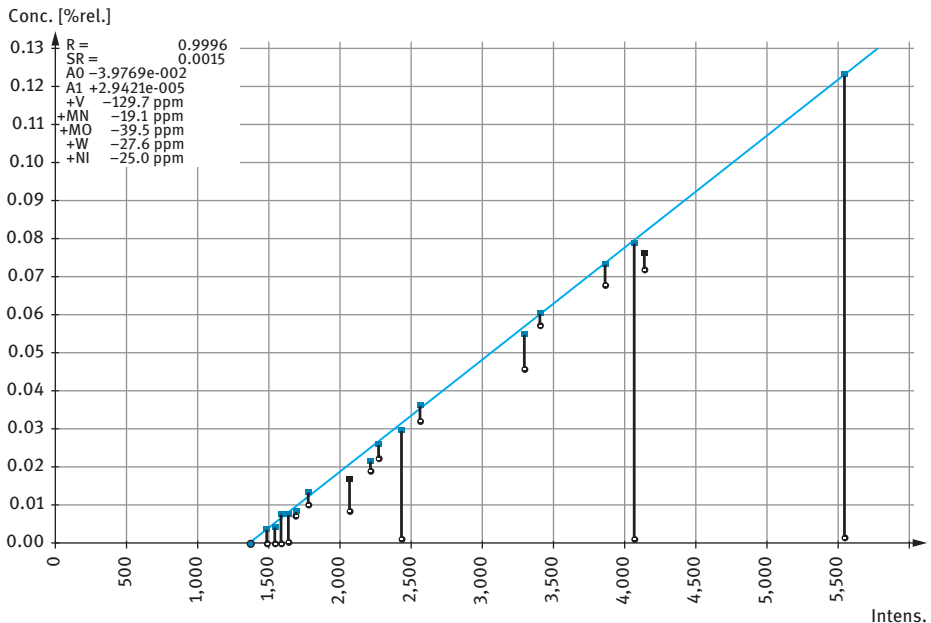


Figure 7.17: Analysis function of Ce in cast iron.

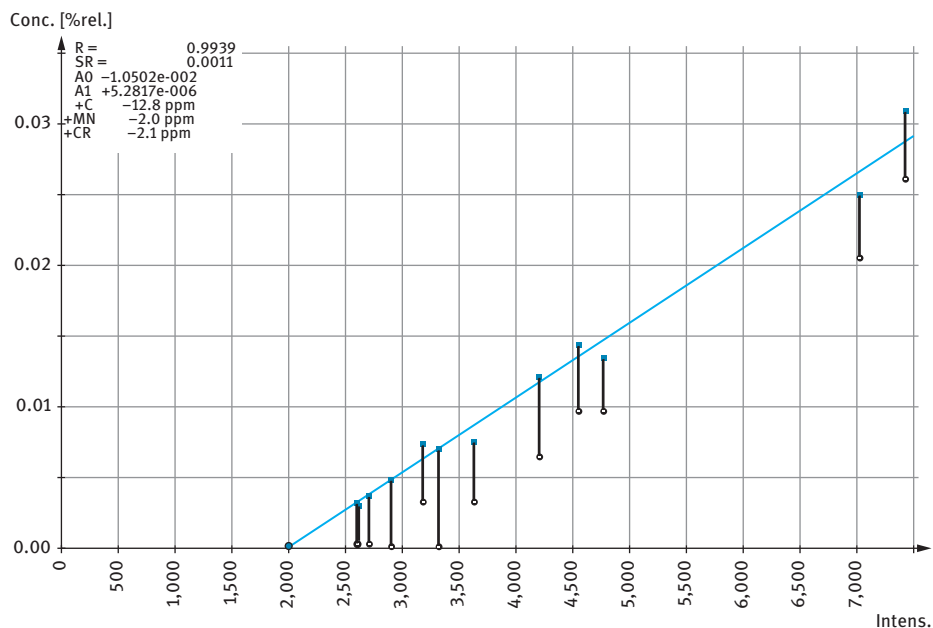


Figure 7.18: Analysis function of La in cast iron.

Table 7.8: Validation of Ce and La in cast iron.

Sample	La in cast iron		Ce in cast iron	
	Setpoint (%)	Meas. val. (%)	Setpoint (%)	Meas. val. (%)
246B	0.003	0.002	0.007	0.008
244B	0.009	0.010	0.018	0.020
249B	0.006	0.006	0.021	0.022
669/11	–	–	0.042	0.044
247B	0.019	0.020	0.053	0.053
667/11	–	–	0.062	0.062

Meas. val. = measured value.

7.10.2 Detection limits

The detection limits detailed in Table 7.9 show that analysis is possible within the $\mu\text{g/g}$ range. However, calibration should be carried out using samples that are as close to the material as possible in order to minimise the above-mentioned inter-elemental influences.

Table 7.9: Detection limits in cast iron and steel.

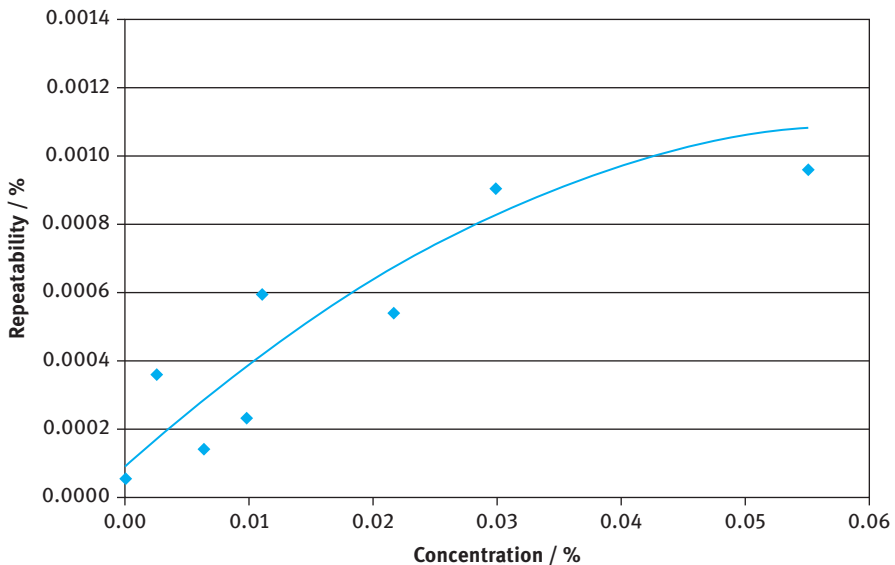
Element	La	Ce
Detection limit ($\mu\text{g/g}$)	2	5

7.10.3 Repeatability

The degrees of repeatability of La and Ce are shown for a series of samples in Figures 7.19 and 7.20. With the exception of the highest La samples, the values correlate to the concentration in a linear fashion. At 0.05 %, the relative standard deviation is at approx. 1.8–2 %.

7.10.4 Long-term stability

Long-term stability is a key criterion for assessing analytical performance. Routine use and evaluation of control samples are good options for ascertaining this long-term stability. As an example, Figure 7.21 shows the La concentration curve of a control sample analysed at a foundry over a period of approx. four weeks. In each case the mean value is shown, calculated on the basis of two spark events. Several hundred

**Figure 7.19:** Representation of repeatability of La in cast iron.

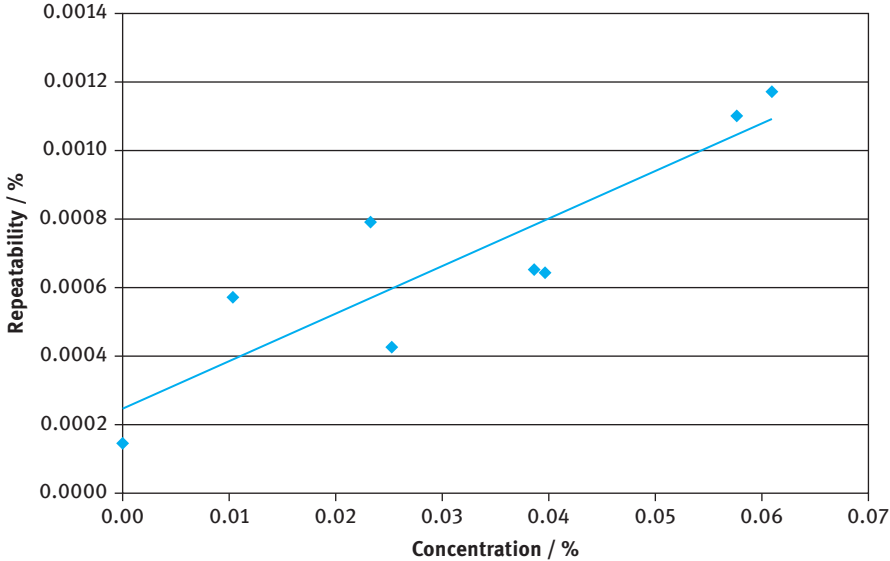


Figure 7.20: Representation of repeatability of Ce in cast iron.

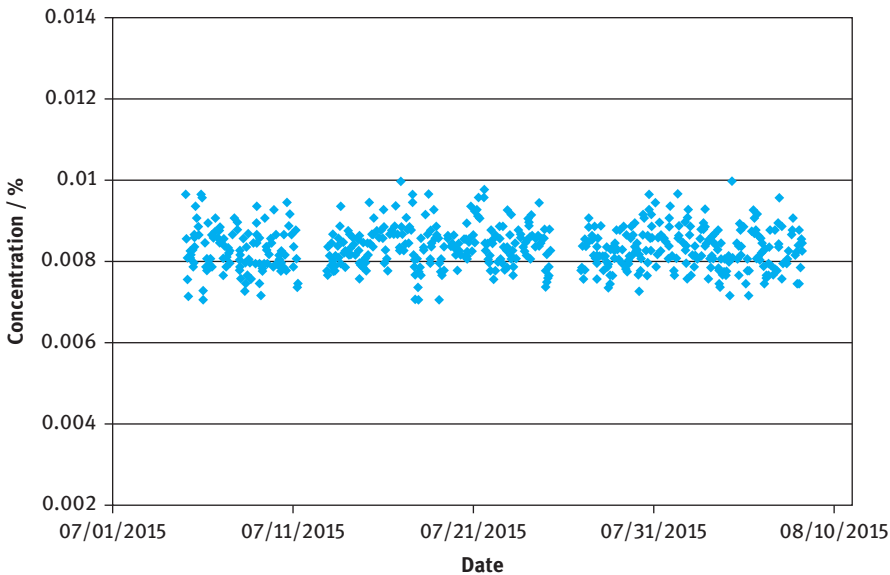


Figure 7.21: Signal record regarding the long-term stability of La in cast iron.

production samples were also analysed in between the control sample measurements on each day. Recalibration was carried out on a weekly basis.

Over the entire period, the standard deviation remained at 0.0005 %, which makes it only approx. 0.0001 % higher than the standard deviation for repeatability.

7.11 Analysis of zinc alloys

7.11.1 Calibration (analysis function) and accuracy

The only two rare earths that are used in zinc alloys are La and Ce, and predominantly in an alloy called GalfanTM, which is used as a coating for sheet steel [28]. It therefore comes as little surprise that only these elements are available as certified samples and can be calibrated. At present customer requests for analysis of these two elements are still relatively few so that only few reference samples are available at OBLF. The following calibrations (Figures 7.22 and 7.23) were therefore carried out with three (for La) and four (for Ce) reference samples.

Since no further rare earths are present, but also – with the exception of aluminium and copper – as a result of further material elements only being present in low concentrations, the functions are not affected by other elements.

7.11.2 Detection limits

The detection limits ascertained via the generated calibration function are shown in Table 7.10 and were at 1 µg/g for La and 4 µg/g for Ce. According to the ASTM standard, the sum of La and Ce must range between 0.03 % and 0.10 %, which are nowhere near the ascertained detection limits [28].

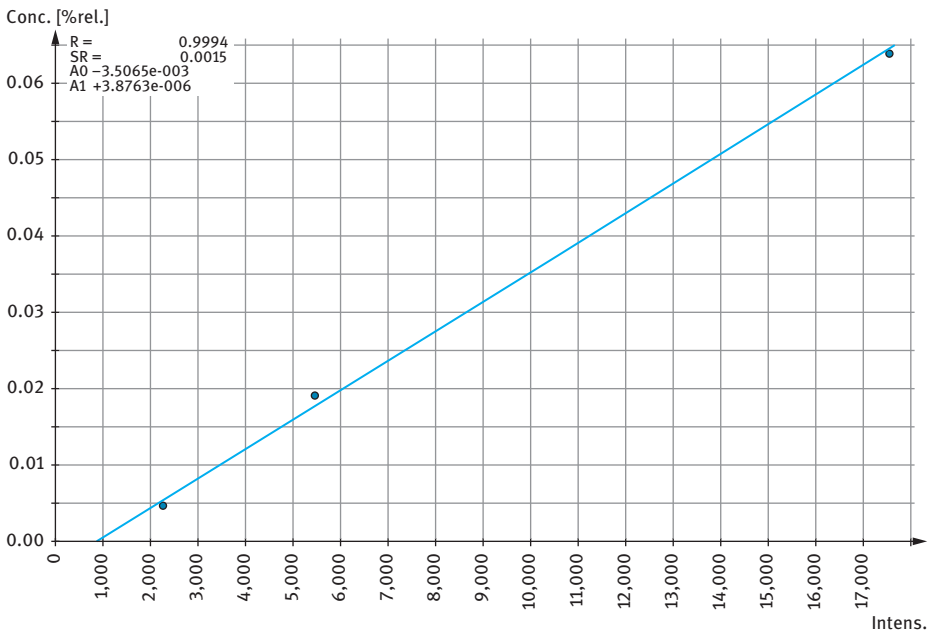


Figure 7.22: Analysis function of La in zinc.

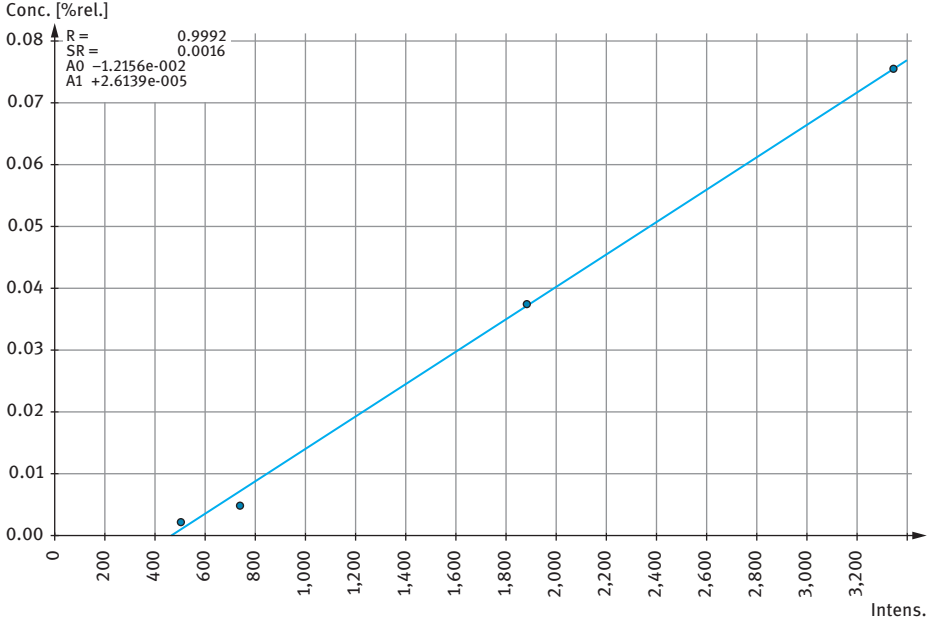


Figure 7.23: Analysis function of Ce in zinc.

Table 7.10: Detection limits in zinc.

Element	La	Ce
Detection limit ($\mu\text{g/g}$)	1	4

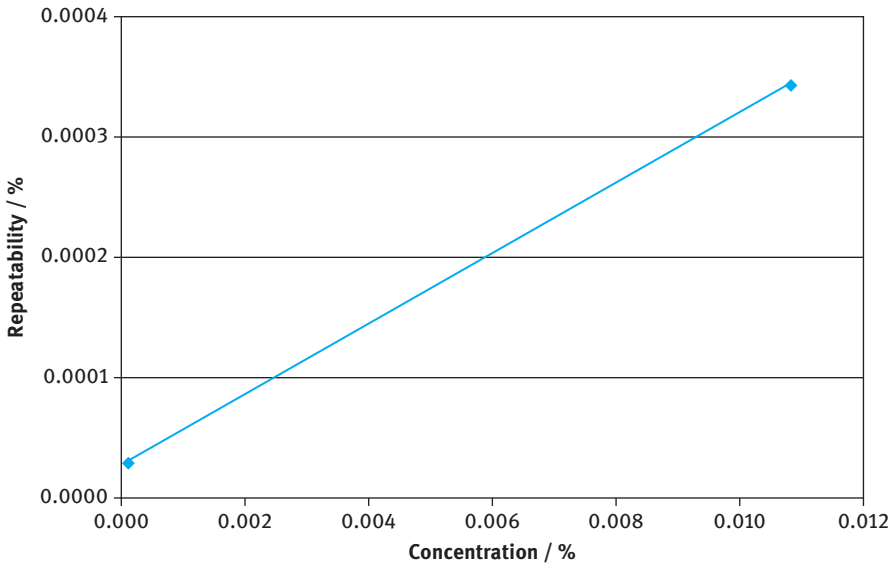


Figure 7.24: Representation of repeatability of La in zinc.

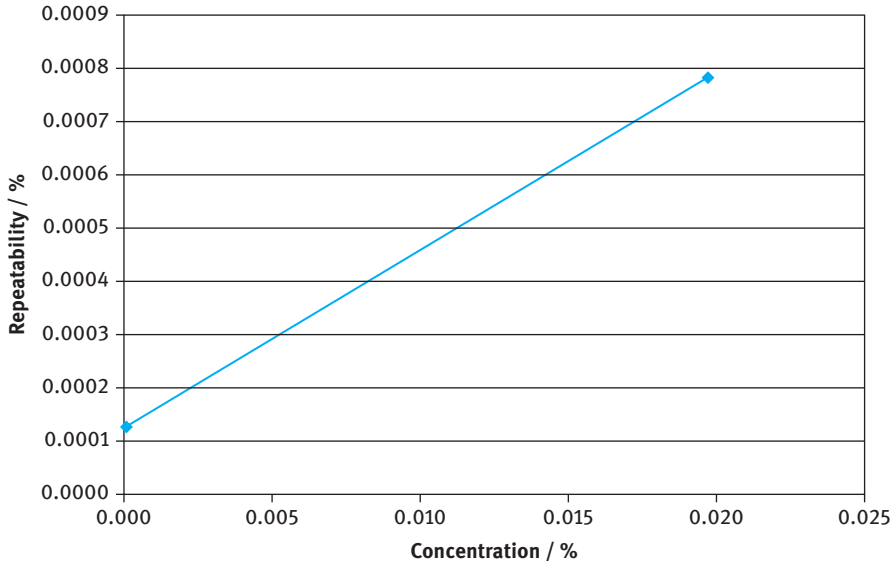


Figure 7.25: Representation of repeatability of Ce in zinc.

7.11.3 Repeatability

A tenfold analysis of two samples resulted in the repeatability values shown in Figures 7.24 and 7.25. In the upper region at 0.01 % for La and at 0.025 % for Ce, they are at 3 % relative. Based on the detection limits and repeatability the analytical prerequisites are given for routinely determining La and Ce in zinc alloys. Calibration should, however, be extended and validated with further standard samples.

7.12 Conclusion

Spark emission spectrometry is a means of analysing and determining the chemical composition of metallic (conductive) solid samples both quickly and without involving lengthy sample preparation. Applications involving rare earths need to be metals or metal alloys if they are to satisfy the requirement of metallic conductivity and homogeneous element distribution. In this context, iron (cast iron and steel), aluminium, magnesium and zinc alloys are additionally alloyed with rare earths in a range from a few tens of $\mu\text{g/g}$ to several per cent. At present, calibration samples are mainly available for the most common alloys and the most commonly used rare earths. As this spectrum is constantly growing, there is a backlog demand for calibration standards that contain more than certified concentrations of Ce and La.

Analytical performance data show that detection limits are in the $\mu\text{g/g}$ region regardless of the specific matrix. Repeatability values for concentrations larger than

0.1 % are, in part, considerably lower than 1 % relative; for concentrations less than 0.1 % these values range between 1 % and 3 % relative. Using the reproducibility of cast iron as an example shows that processability is given.

References

- [1] Niederstraßer J. Funkenspektrometrische Stickstoffbestimmung in niedriglegierten Stählen unter Berücksichtigung der Einzelfunkenspektrometrie. Doctorate thesis, Gerhard-Mercator-Universität – Gesamthochschule Duisburg, 2003.
- [2] Drost H. Plasmachemie. Berlin, Germany, Akademie-Verlag Berlin, 1978.
- [3] Niederstraßer J, Overkamp B. A new generation in spark emission spectrometry. Proceedings of the 8th international workshop on progress in analytical chemistry & materials characterisation in the steel and metals industries, Luxembourg, 2011.
- [4] Stahlschlüssel – Key to Steel, Marbach, Germany, Verlag Stahlschlüssel Wegst GmbH, 2016.
- [5] DIN 32645:2008-11: Chemical analysis – decision limit, detection limit and determination limit under repeatability conditions – Terms, methods, evaluation, 2008.
- [6] ASTM International. Standard practice for evaluation an optical emission vacuum spectrometer to analyze carbon and low-alloy steel. Designation E1009–95 (reapproved 2006), ASTM International, 2006.
- [7] ASTM International. Standard test method for the analysis of carbon and low-alloy steel by spark atomic emission spectrometry. Designation: E415–14, ASTM International, 2014.
- [8] ASTM International. Standard test method for analysis of austenitic stainless steel by spark atomic emission spectrometry. Designation: E1086–14, ASTM International, 2014.
- [9] ASTM International. Standard test for analysis of high manganese steel using atomic emission spectrometry. Designation E2209–02 (reapproved 2006), ASTM International, 2006.
- [10] ASTM International. Standard test method for analysis of cast iron by spark atomic emission spectrometry. Designation E1999–11, ASTM International, 2011.
- [11] ASTM International. Standard test method for analysis of aluminium and aluminium alloys by spark atomic emission spectrometry. Designation E1251 – 11, ASTM International, 2011.
- [12] ASTM International. Standard test method for analysis of magnesium and magnesium alloys by atomic emission spectrometry. Designation B954–15, ASTM International, 2015.
- [13] ASTM International. Standard test method for analysis of zinc and zinc alloys by spark atomic emission spectrometry. Designation E634–12, ASTM International, 2012.
- [14] Slickers K. Automatic Atomic-Emission-Spectroscopy. Gießen, Germany, Brühlsche Universitätsdruckerei Gießen, 1993.
- [15] Thomsen VB. Modern Spectrochemical Analysis of Metals: An Introduction for Users of Arc/Spark Instrumentation. Materials Park, OH, ASM International, 1996
- [16] Gibson M, Parkinson I. Once ignored on the periodic table, don't ignore them now – a rare earth element industry overview. CIBC Report, CIBC World Markets Inc., 6 March 2011.
- [17] Angelini V, Boromei I, Ceschini L, Morri A. Microstructure and mechanical properties of a rare earth rich magnesium casting alloy. Metallurgia Ita Italy 2015, 107, 37–42.
- [18] Lue Z, Zhou J, Sun ZM, Chen RS. Effect of rare earth elements on the structures and mechanical properties of magnesium alloys. Chin Sci Bull Germany 2013, 58, 816–20.
- [19] Røyset J, Ryum N. Scandium in aluminium alloys. Int Mater Rev UK 2005, 50, 19–44.
- [20] Liu GL, Si NC, Sun SC, Wu QF. Effects of grain refining and modification on mechanical properties and microstructure of Al-7.5Si-4Cu cast alloys. Trans Nonferrous Met Soc China Netherlands 2014, 24, 946–53.
- [21] Pedersen KM, Tiedje NS. Influence of rare earth on shrinkage porosity in thin walls ductile cast iron. Int J Cast Metal Res UK 2009, 22, 302–05.

- [22] Liu JH, Xie DY, Li CS, Shao L, Zhang RJ. Influence of rare earth on property of low chromium semi-steel. *J Iron Steel Res Int Netherlands* 2003, 10, 50–53.
- [23] Amadeh A, Pahlevani B, Heshmati-Manesh S. Effects of rare earth metal addition on surface morphology and corrosion resistance of hot-dipped zinc coatings. *Corros Sci* 2002, 44, 2321–31.
- [24] Saidel AN, Prokofjew WK, Raiski SM. *Spektraltabellen*. Berlin, Germany, VEB Verlag Technik Berlin, 1955.
- [25] The Massachusetts Institute of Technology. *Wavelength Tables*. Cambridge, MA, MIT Press, 1969.
- [26] NIST atomic spectra database lines form. http://physics.nist.gov/PhysRefData/ASD/lines_form.html (accessed April 2016)
- [27] Brammer standard online database <http://www.brammerstandard.com/form.cfm> (accessed November 2015).
- [28] ASTM International. Standard specification for GALFAN (zinc-5 % aluminium-mischmetal) alloy in ingot form for hot-dip coatings. Designation B750-12, ASTM International, 2012.

Rainer Schramm

8 Use of X-ray Fluorescence Analysis for the Determination of Rare Earth Elements

Abstract: X-ray fluorescence spectrometry (XRF) is a powerful tool for the analysis of solid material. That is the reason why the technique was applied for the determination of rare earth elements (REEs) since about 1970. At present, energy-dispersive XRF and wavelength-dispersive XRF are used for the analysis of pressed powder pellets or fused Li-borate beads containing REEs. The production of reliable results can only be achieved by careful optimization of the parameter, in particular the selection of spectral lines. The quantification is based on a calibration realized by using reference samples.

8.1 Introduction

The use of X-ray fluorescence spectroscopy (XRF) for the analysis of rare earth elements (REEs) is divided into the analysis of minors and traces in materials with natural origin and the analysis of industrial products containing REEs as main, minor or trace components.

The advantage of XRF is the direct analysis of solid material which could be presented directly as powder or pressed pellet. The disadvantage could be a high error and a high average lower limit of detection (LLD) of about 1–10 µg/g.

Nevertheless, XRF is very often used as a rapid method with high throughput. For some applications, the measurement error could be reduced by using fusion technology as sample preparation method. The LLD could be further reduced by using preconcentration methods.

One typical application is the analysis of REE in geological materials as overview or screening in addition to other techniques like inductively coupled plasma-optical emission spectrometry (ICP-OES) or inductively coupled plasma-mass spectrometry (ICP-MS).

Other typical applications are the analysis of REE as tracer in polymers [1], as impurity in pure chemicals, as component in glass, e.g., light-emitting diodes, as component in polishing powders, as component in magnets and generally as component in recycling processes.

For all these applications, the sample preparation procedure as well as the measurement conditions has to be adapted to the REE present in the samples.

8.2 Principle of X-ray fluorescence analysis

X-ray fluorescence radiation is an electromagnetic radiation with high energy. Energetically, it lies between γ -radiation and UV radiation.

X-ray fluorescence is generated by, among other processes, the ionization of the inner shell of an atom if radiation with high energy (0.1–100 keV) interacts with an atom. However, the probability that it will occur is small and is also dependent on the atomic number of the atom. Most of the excitation energy is translated into heat, which is the reason that XRF instruments always need to be more or less cooled.

If ionization of an inner shell does occur, i.e., an electron is removed, then the hole is filled by an electron from a higher energy shell. The energy difference is released as X-ray fluorescence radiation and is characteristic for the element. Depending on which transition takes place, it is called radiation: K, L or M.

Figure 8.1 shows the typical electron transitions for the different shells. The lower line represents the innermost shell of an atom. The arrows symbolize an electron transition that is accompanied by the formation of an X-ray fluorescence line, e.g., $K\alpha_1$. The intensity of the lines decreases in the order $K\alpha$, $K\beta$, $L\alpha$, $L\beta$.

For example, an electron e_K leaves the K-shell if the energy $h \times \nu$ of the exciting radiation is higher than the binding energy $h \times \nu_K$ of the electron e_K (Figure 8.2). The characteristic X-ray fluorescence radiation is created. However, if this fluorescence radiation leads to an ionization of the M-shell, an electron e_M will leave the atom. This effect is called Auger effect and is in competition to the fluorescence effect. The fluorescence yield expresses the number of photons created in relation to the number of holes created by ionization and increases with atomic number.

The most important equations for XRF are listed in Table 8.1.

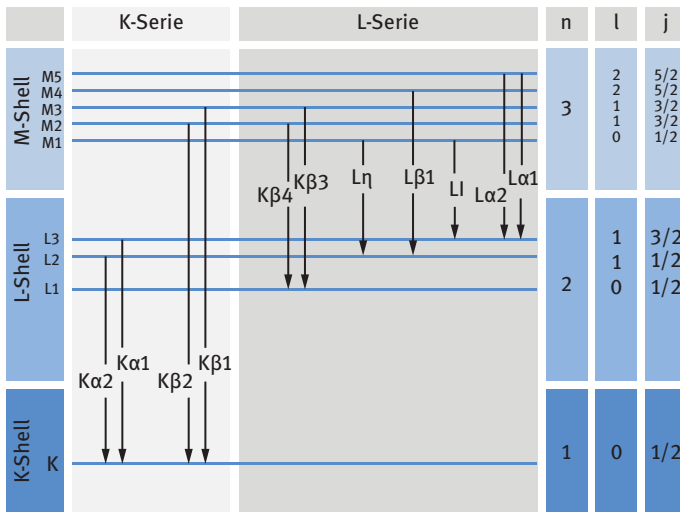


Figure 8.1: Transition of electrons in inner shells (a schematic setup of the energy levels for the single X-ray emission lines of the K- and L-series).

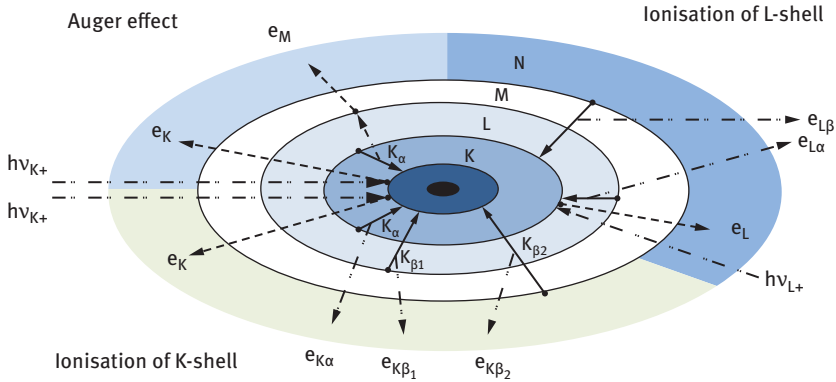


Figure 8.2: A schematic setup of the excitation of X-ray fluorescence analysis.

Table 8.1: Basic equations for X-ray fluorescence analysis.

Moseley's law

ν_K : Frequency of K transition, C_K : constant, σ_K : screening constant for K transition

$$\nu_K = C_K (Z - \sigma_K)^2$$

Fluorescence yield

I_K : Total number of characteristic K X-ray photons

n_K : Number of primary K-shell vacancies

$$\omega_K = \frac{I_K}{n_K}$$

Bragg's law

d : Interplanar distance, θ : scattering angle, n : positive integer, λ : wavelength

$$2d \cdot \sin \theta = n\lambda$$

Theoretical fluorescence intensity (K-shell)

$I_{i,K\alpha}$: Intensity of element i for $K\alpha$ line, I_{ex} : intensity of monochromatic excitation, c_i : concentration of element i , $\mu_{i,ex}$: mass absorption of the exciting radiation in element i , μ_{ex} : mass absorption of the exciting radiation in the sample, μ_i : mass absorption for the $K\alpha$ fluorescence radiation of element i in the sample, J_i : K jump ratio, ω_i : fluorescence yield, f_i : fraction of ω_i for $K\alpha$, Ψ' , Ψ'' : room angles, $\Omega/4\pi$: geometry factor

$$I_{i,K\alpha} = \left(\frac{I_{ex} \cdot c_i \cdot \mu_{i,ex}}{\mu_{ex} \cdot (1/\sin \Psi') + \mu_i \cdot (1/\sin \Psi'')} \right) \cdot (J_i \cdot \omega_i \cdot f_{i,K\alpha}) \cdot \left(\frac{1}{\sin \Psi'} \right) \cdot \left(\frac{\Omega}{4\pi} \right)$$

8.3 XRF methods

Depending on the method of detection, instrument technology is divided into energy-dispersive (EDXRF) and wavelength-dispersive (WDXRF) X-ray fluorescence analysis [2–9].

8.3.1 Energy-dispersive X-ray fluorescence analysis

With EDXRF, the sample is excited by the X-ray tube directly or through a filter (Figure 8.3). A semiconductor detector (e.g., silicon–lithium semiconductor, pin diode or

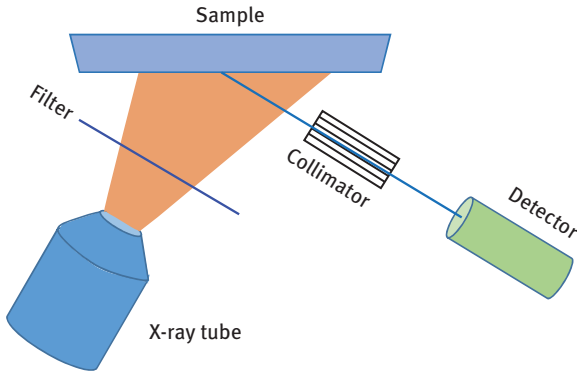


Figure 8.3: A schematic setup of an energy-dispersive X-ray fluorescence spectrometer with direct excitation.

silicon drift chamber) analyzes the X-ray fluorescence radiation that comes directly from the sample.

Here, the detector together with the associated electronics counts and sorts, according to energy, all of the photons that reach it. A pulse height spectrum that indicates the number of photons or impulses for a given energy is established. The detector typically has only a few μs for processing, so that in case of a modern silicon drift detector (SDD), processing is accordingly limited to approximately 1,000,000 pulses/s. Using a filter, a portion of the exciting radiation can be screened out to avoid overloading the detector.

XRF with polarizing excitation represents an alternative design for EDXRF (Figure 8.4). Here, the radiation coming from the tube is deflected by 90° and is then used to irradiate the sample. The detector must be perpendicular to the plane determined by the tube, target and sample. The most important effect is that by deflecting the

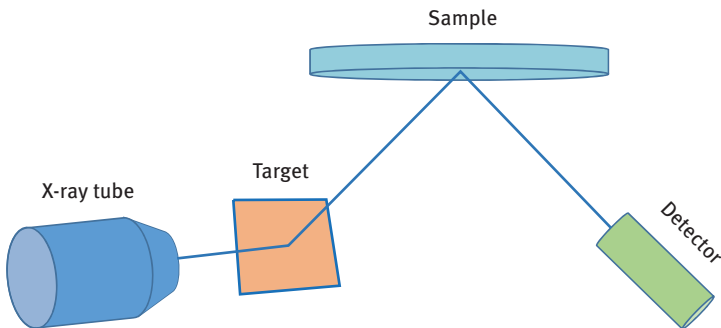


Figure 8.4: 4c vector – “Configuration of an energy-dispersive X-ray fluorescence spectrometer with polarized excitation”.

X-ray radiation by 90° , the radiation is polarized and the spectral background in the spectrum is reduced.

The analysis of REE by EDXRF suffers from big overlaps between the spectroscopic lines so that detector resolution becomes the limiting factor.

8.3.2 Wavelength-dispersive X-ray analysis

WDXRF uses, like some EDXRF, direct excitation (Figure 8.5). Here, it is also possible to work with filters to block or weaken components of the excitation radiation. The major difference is the method of detection of the X-ray fluorescence radiation for WDXRF. Using a goniometer, only one wavelength from the spectrum is fed to the detector, i.e., it measures only one line from one element. In order to conduct multiple element analyses, it is necessary to create a serial measuring program that drives to and analyzes all of the lines of interest, one after another. There are, however, so-called simultaneous spectrometers: In this case, there is a set channel for each element consisting of a fixed crystal with corresponding detector arranged around the sample. When combined with a goniometer, this forms a very fast, high-performance XRF instrument that is especially useful for process control.

Most of the XRF spectrometers nowadays are equipped with an X-ray tube with a target “Rh”. Nevertheless, for the analysis of REE, an X-ray tube with targets “Au” and “W” would be a better choice than Rh to excite the K- and L-lines of the REE [10].

The analysis of REE by WDXRF still remains a challenge even if the resolution of the goniometer is much better than for EDXRF. There are still a lot of line overlaps which cannot be totally resolved. The final performance of the XRF analysis of REE is therefore strongly depending on the availability of overlap-free analyte lines which could be used for the determination.

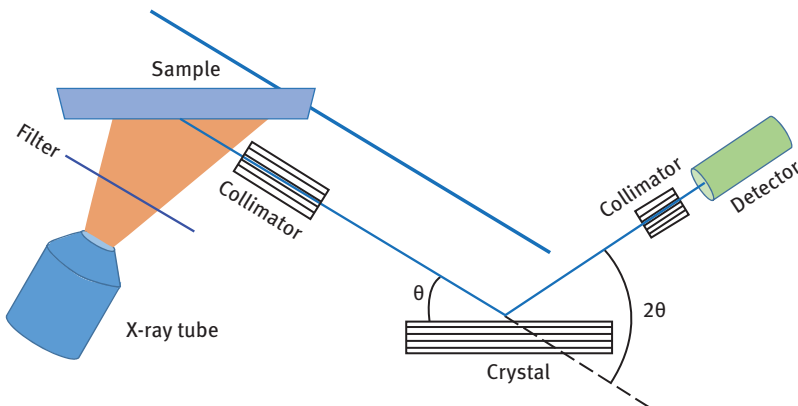


Figure 8.5: Schematic setup of a wavelength-dispersive X-ray fluorescence spectrometer.

8.3.3 Comparison of EDXRF–WDXRF

In general, it is possible to say that the two techniques are complimentary; one supplements the other. EDXRF has a time advantage, as all elements are measured simultaneously, whereas the (serial) WDXRF measures the elements one after another.

WDXRF has a resolution and sensitivity advantage which is especially useful in the range of atomic numbers up to 30 and 55–80 which also includes most of REEs.

8.3.4 Other XRF techniques

8.3.4.1 Handheld XRF instruments

Handheld XRF instruments are based on EDXRF with direct excitation. Combined with a low-power X-ray tube, they suffer from low resolution and low sensitivity for REE analysis.

8.3.4.2 Total reflection XRF

Total reflection is a special version of XRF which works only with liquid samples. Therefore, the sample needs to be digested first and then a small amount is dried on a quartz disk which then is irradiated by X-rays under total reflection conditions [11]. An example for the determination of REE in geological materials is described in Ref. [12].

8.4 Sample preparation

The performance of XRF for REE analysis is strongly dependent on sample preparation. However, the sample preparation strategy must be in agreement with the chosen measurement conditions especially the analyte lines, K- or L-series.

8.4.1 Pressed pellets techniques

Pressing a sample leads to a defined density in the pellet. This guarantees reproducible sample preparation.

The Following procedures are used to press samples:

- Direct pressing
- Pressing in aluminum trays
- Pressing in rings
- Pressing with binders
- Pressing onto a backing material

It is important for XRF that the pressed sample is mechanically stable. The sample is subject to a vacuum when placed into the analytical instrument and returned to an air environment after the measurement. High stability is required to be sure that the

sample does not break during these procedures. Only a few materials display this type of stability, which can be increased by pressing into aluminum trays. Mixing with a binder is obligatory for most materials.

Manually mixing with mortar and pestle is arduous and not very effective. This is why, I recommend using a simple mixer, whereby the high reproducibility is also ensured.

8.4.1.1 In practice: Making a pellet

The complete procedure for making a pellet, from preparation of the sample to pressing, is shown in Figure 8.6 [2].

After grinding the sample, 4 g of the sample is mixed with 1 g binder (e.g., wax [2]). Before pressing, the pressing tool can be covered with a pellet film, which prevents subsequent sticking, simplifies cleaning and prevents contamination of the pellet from the hardened steel (Cr, Fe). Aluminum cups help stabilize the pellet and enable easy labeling but have no additional usefulness. Table 8.2 presents figures based on experience for the pressure required depending on the diameter of the pressed pellet. Here, it is important to remember that the pressing procedure must be reproducible,



Grinding of the whole sample



Weigh 4g sample



Add 1g binder



2 minutes mixing



Use pelletfilm or



Aluminium cup



Pour the mix into the die



And press:



Perfect pressed pellet

Figure 8.6: Illustration of all steps to produce a pressed pellet with binder.

Table 8.2: Recommended pressure depending on the diameter of the pressed pellet.

Diameter	Pressure (t)
32 mm	15–20
40 mm	20–30
35-mm ring inside	max. 30

i.e., the same density must be obtained in each pressed pellet. Direct pressing from 0 to, e.g., 30 tons can prevent the air contained in the sample from completely escaping. This leads to cracks in the pressed pellet. Use of a lower pressure or a pressing procedure in several steps is recommended.

When there is not enough sample material, but a stable pressed pellet is still required, then the sample can be pressed onto a backing. In literature [13], this is presented for yttrium oxide: 400 mg of sample (dissolved in acid and precipitated as oxalate) is mixed with an equal amount of boric acid and then pressed on a boric acid layer as backing. However, since December 1, 2010, boric acid is classified as GHS08 health hazard which means that it should be replaced by a non-hazardous material. In Ref. [2], a cellulose-type material called BOREOX is presented as a good non-hazardous replacement.

It has to be mentioned that sample thickness should always be higher than the penetration depth of the XRF line used for calibration. Table 8.3 lists recommended minimum sample thicknesses or masses depending on K- or L-lines for REE analysis.

8.4.2 Fusion technology

In XRF, most solid samples are prepared as pressed pellets, whereby the achievable precision suffers from so-called particle size effects. They describe the phenomenon that the intensity of X-ray fluorescence is depending on particle size and shape. If the achieved precision with pressed pellets is not sufficient, the sample must be prepared using a fusion process.

Table 8.3: Minimum required sample thickness [2] or mass [10] of a pressed pellet for REE analysis depending on the analyte line and pellet diameter.

REE XRF lines	Minimum sample thickness (mm)	Minimum mass/diameter
L-lines	0.5	2 g/D30 mm
K-lines	8	20 g/D30 mm 40 g/D40 mm

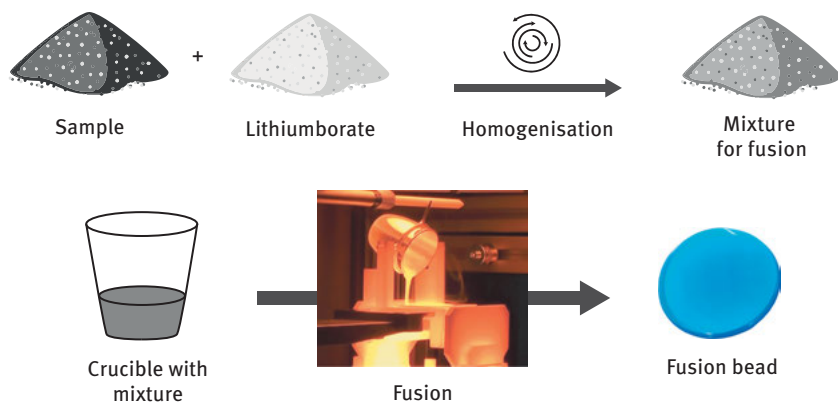


Figure 8.7: Principle of the fusion process.

The fusion provides an ideally homogeneous sample with a defined density and without particle size effects. In addition, homogeneity and a perfect surface lead to a much smaller calibration error.

Figure 8.7 shows the fundamentals of the fusion process.

The following conditions must be fulfilled for fusion of a sample:

- Finely ground oxidic sample material
- Borate as the fusion material and glass-forming agent
- Platinum–gold crucible
- Platinum–gold casting dishes
- Temperatures higher than the borate melting point

Modern automatic fusion systems are used to obtain reproducible fusions. As base for the technique, either a muffle furnace, a gas burner or an induction furnace is used. In most of the systems, the sample is mixed with the flux then placed into a platinum crucible. The crucible is set onto the melting position and then the sample is fully automatically oxidized, melted, stirred and cast. After approximately 10–15 min, the cold fusion bead can be placed into the XRF for measurement.

For ICP-OES or ICP-MS measurements, the melted sample could be cast directly into the acid instead of casting a bead.

Further sample preparation methods using fusion known from literature:

Rock samples are mixed 1:5 with lithiumtetraborate and fused at 1,000°C in a muffle furnace. Then dissolved in HF and HNO₃ followed by a separation of REE from the matrix by anion exchange and subsequent preconcentration. Finally, the REE are coprecipitated with rhodizonate and tannin. The precipitate is collected on membrane filter which is measured with XRF [14].

To fuse REE rock samples, three different dilutions between sample and flux are suggested by Nakayama and Nakamura [15]:

A ratio of 1:1 for REE, 1:2 for Th and U and 1:10 for major and minor elements. It is a challenge to perform a low-dilution fusion with a ratio 1:1 to avoid inclusions and

bubbles. Therefore, the fusion had to be repeated a second time and LiCl was added to avoid devitrification. The LLDs achieved with this method are in the range of 0.6 (Th, U) and 0.7–6.5 µg/g for REE.

The authors of Ref. [16] describe a method for raw materials with major and minor concentrations of REE: the REEs are separated from the main matrix by dissolving them with HF/HNO₃ and Na₂CO₃/Na₂O₂ and final precipitation as oxalate. Then, a fusion of the residue with lithiumtetraborate was done. Cr and Mo were used as internal standard. Results are presented for light REEs, Y and Th over a wide concentration range (La, Ce, Nd, Pr 0.02–25 %; Sm, Gd, Eu, Y and Th 0.005–1 %).

In Ref. [10], monazite samples were fused with pure lithiumtetraborate or a mixture of lithiumtetraborate and lithiummetaborate (90:10) in a ratio of 0.5 g sample and 9.5 g flux and a few drops of LiBr (25 %) as releasing agent.

8.4.3 Additional sample preparation techniques

Roelandts [17] describes the analysis of REEs in apatite. The sample is dissolved in HNO₃, then the REEs are separated by a mixed solvent anion exchange and kept by the resin which is then analyzed by XRF on top of a disk.

Another preconcentration method in combination with a thin film measurement is presented in Ref. [18]: 1-g sample was fused with 4-g Na₂O₂ and finally dissolved in acid. The REEs were separated from the main components by ion exchange. The XRF measurement was done at an ion-exchange paper.

Also in Ref. [19], the XRF measurements were performed directly on a filter. After digestion of the sample with acid, the REEs are preconcentrated by using an arsenazo III complex which was collected on a filter by chemofiltration.

8.5 Practical application of REEs determination

8.5.1 Reference materials

To perform and to verify an XRF calibration, reference materials are required. Table 8.4 lists the reference materials mentioned in the literature cited in this article. Most of

Table 8.4: Reference materials cited in REE literature.

Reference material	Producer
SRM 613	NIST, National Institute of Standards and Technology, USA
JG-1a, JR-2, JR-3, JG-1, JB-1	GSJ, Geological Survey of Japan
SARM 1 (NIM-G)	SARM, Mintek South Africa
IGS-36	BGS, British Geological Survey
BCR-1, G-2, GSP-1, BHVO-1	USGS, U.S. Geological Survey

Table 8.5: Free accessible databases for the search of reference materials containing REEs.

Database	Reference
FLUXearch	www.fluxearch.com
COMAR	www.comar.bam.de
GeoReM	georem.mpch-mainz.gwdg.de

them are already sold out. However, there are replacements and many other reference materials which could easily be explored by free accessible databases in the internet. Table 8.5 gives an overview.

8.5.2 Measuring parameters

Starting the configuration of an XRF spectrometer for the determination of REE, first the spectral line for calibration must be selected. REEs have three K-lines and about seven L-lines which could be used. However, the sensitivity of the analyte lines differs a lot. From the K-line series, the $K\alpha_1$ line and for the L-lines, the $L\alpha_1$ and $L\beta_1$ show the highest sensitivity.

K series lines could be used for La, Ce, Pr, Nd, Sm if pressed pellets are used as sample preparation. Based on the large penetration depth, particle size effects will be reduced.

Figure 8.8 shows the K series lines for La to Sm measured with WDXRF equipped with a target X-ray tube “Rh”, 60 kV excitation, lithium fluoride (LiF) 220 crystal, 0.15° fine collimator and SC as detector. The graph demonstrates how the sensitivity decreases from La to Sm.

For comparison, Figure 8.9 shows the K series lines of the elements La to Sm measured with an EDXRF equipped with a target X-ray tube “W”, 60 kV excitation combined with a Al_2O_3 polarizer target and a Silicon SDD. The resolution is better than in WDXRF and there are less line overlaps in the spectrum. Based on the fact that the concentrations for the REE shown in Figure 8.8 are 40,000 $\mu\text{g/g}$ each and the concentrations for the REE shown in Figure 8.9 are only 100 $\mu\text{g/g}$ each, it can be seen that also the sensitivity is much higher.

L-series lines must be used with fusion disks because of infinite thickness limitations. Figures 8.10–8.12 show the complete L-line spectra of La, Gd and Lu as an example measured with WDXRF, Rh target X-ray tube, 40 kV excitation, LiF 220 crystal, 0.15° fine collimator and flow counter detector (FPC). The L-lines show always the same line pattern (out of the $L\beta_4$ line).

For comparison, Figure 8.13 shows the overlap of single element L-line spectra of the REE measured with an EDXRF with W target X-ray tube, 40 kV excitation with a Mo secondary target and an SDD. However, the resolution of the detector is not sufficient to resolve the different lines.

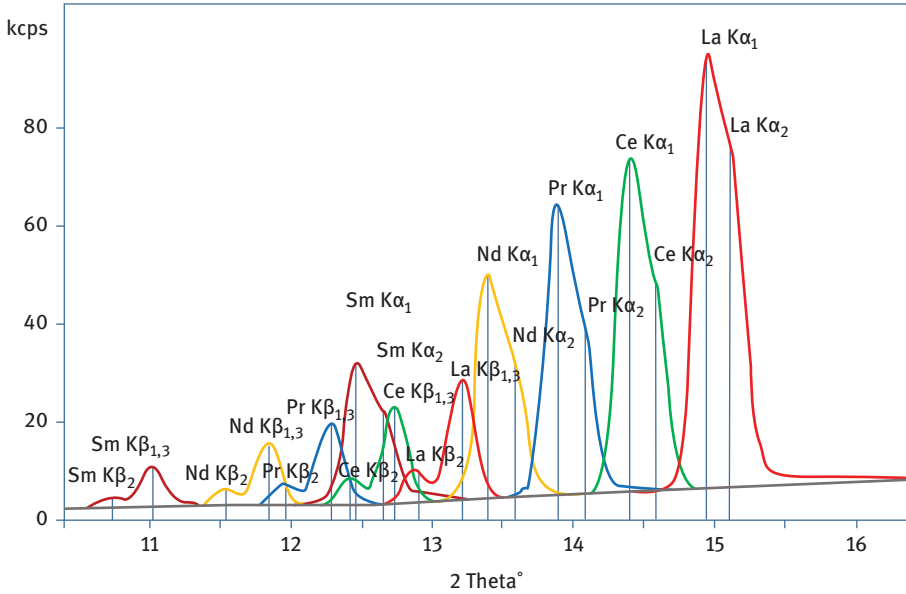


Figure 8.8: Overlapped K-line spectra of REE measured at 40,000 µg/g single element samples from FLUXANA, WDXRF, Rh tube 60 kV, LIF 220, 0.15°, SC.

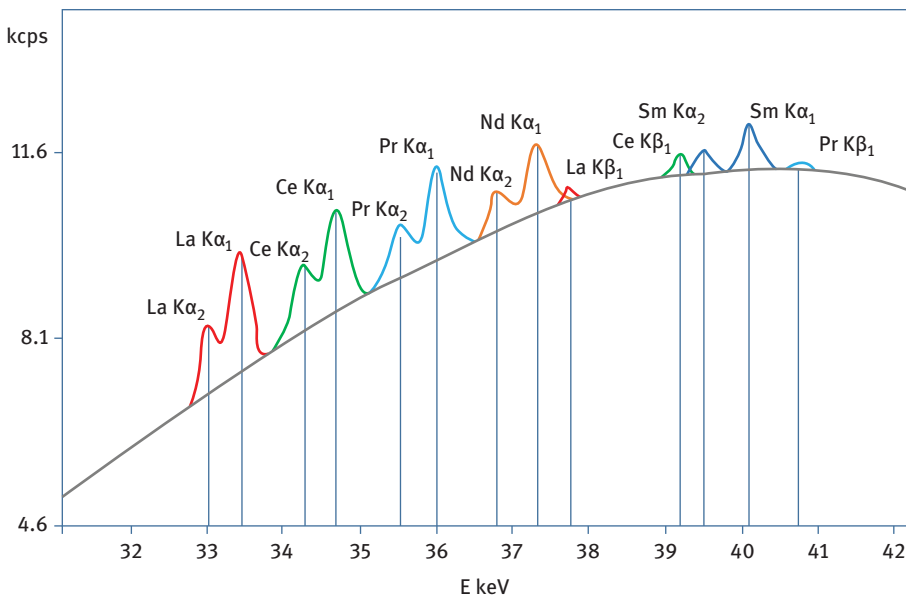


Figure 8.9: Overlapped K-line spectra of REE measured at 100 µg/g single element samples from FLUXANA, EDXRF, W tube, 60 kV, Al₂O₃ polarizer, SDD.

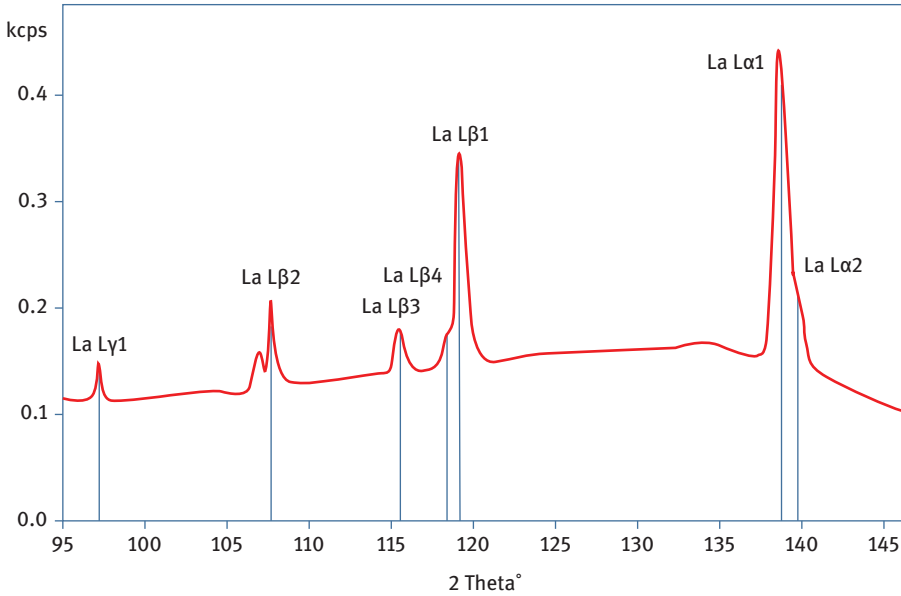


Figure 8.10: L-series lines of 100 µg/g La in cellulose measured with WDXRF, Rh-tube, 40 kV, LIF 220, 0.15°, FPC.

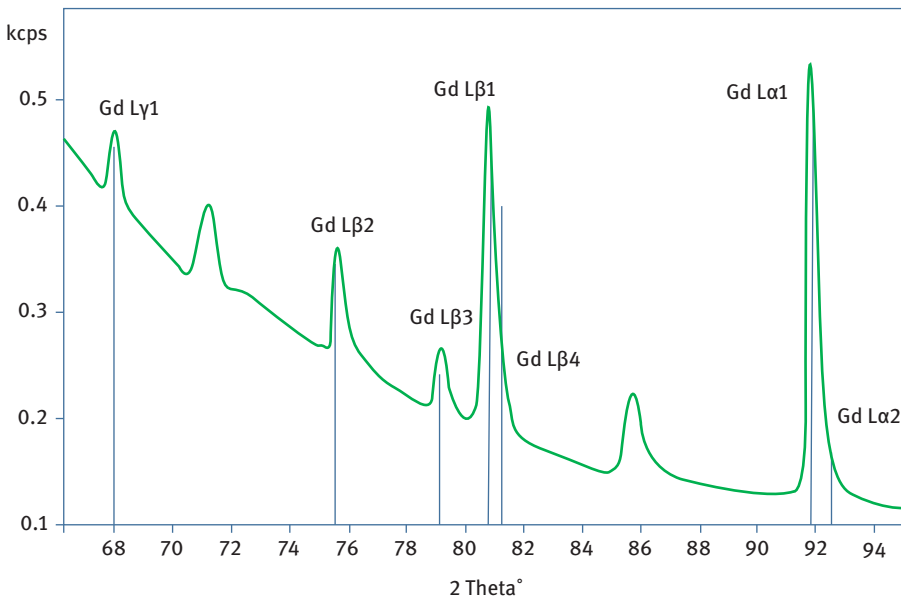


Figure 8.11: L-series lines of 100 µg/g Gd in cellulose measured with WDXRF, Rh-tube, 40 kV, LIF 220, 0.15°, FPC.

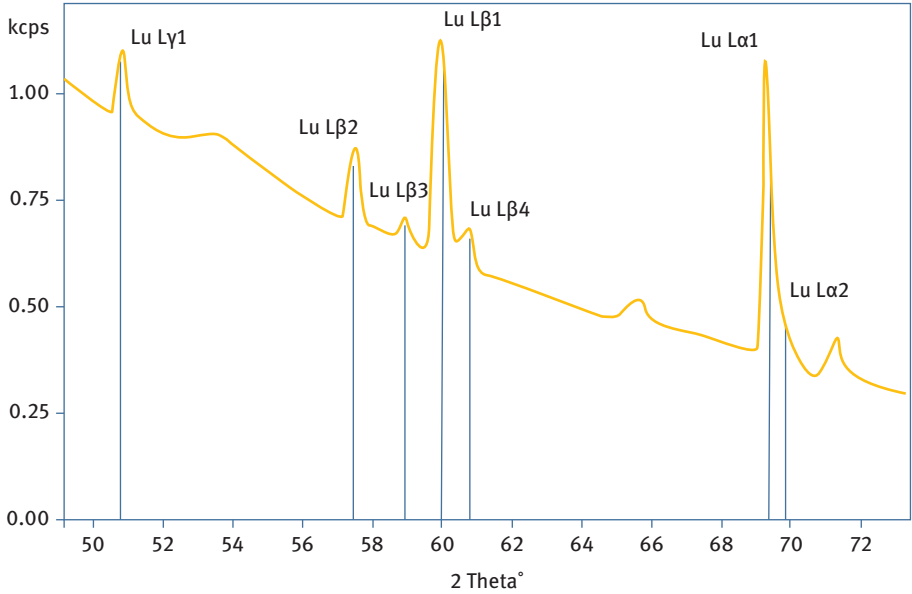


Figure 8.12: L-series lines of 100 µg/g Lu in cellulose measured with WDXRF, Rh-tube, 40 kV, LIF 220, 0.15°, FPC.

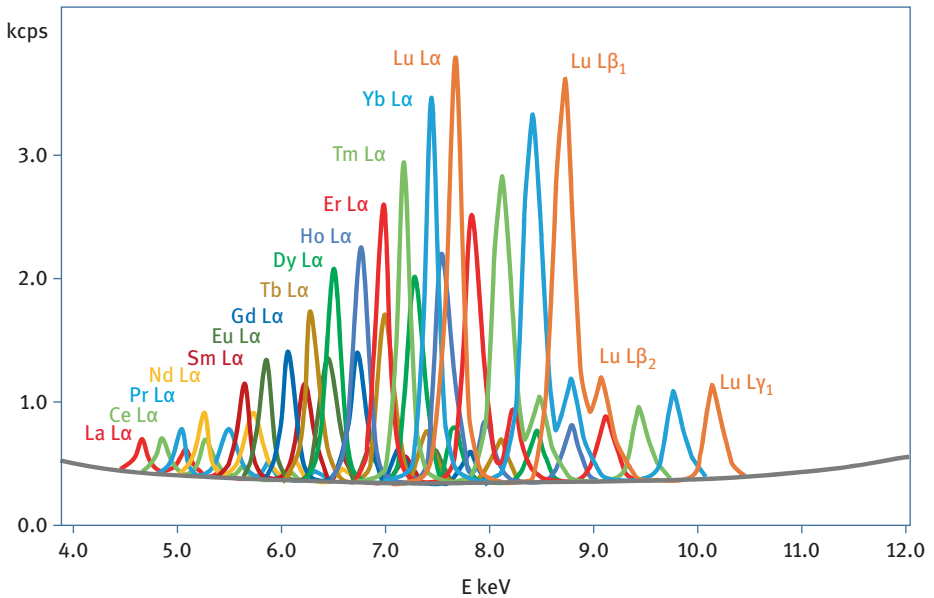


Figure 8.13: Overlapped L-line spectra of REE measured at 100 µg/g single element samples from FLUXANA, EDXRF, W tube, 40 kV, Mo secondary target, SDD.

The most difficult work in creating a measurement program for REEs is the selection of the analyte lines and the corresponding background positions. Because of the high numbers of line overlaps, a general recommendation is very difficult. Figures 8.14–8.17 show a full scan of all analyte lines in the region of the REE lines. This measurement was performed on the glass drift monitor sample FLX-S13 from FLUXANA which contains most of the elements which show lines in this spectrum. The detailed study of all line marks gives a good impression of where to select the analyte lines and the corresponding background positions for the required application.

Table 8.6 lists all X-ray fluorescence lines of REE which show relevant intensities and Figure 8.18 lists all line overlaps which have to be taken into account for REE.

8.5.3 Analyte lines

Table 8.7 gives an indication which analyte lines should be selected for the analysis of REE. The selection considers a minimum of line overlaps which have to be taken into account by spectrum scans or the measurement of single element standards. Also, background positions have to be chosen based on individual measurements on the samples which have to be investigated.

A complete measurement program for WDXRF equipped with target x-ray tube “Rh” to measure rock samples is presented in Ref. [15].

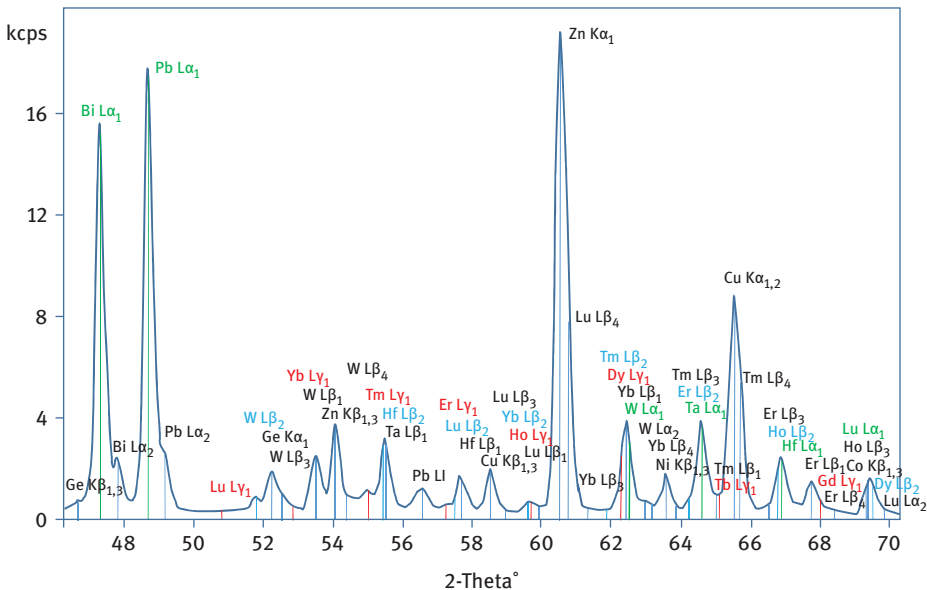


Figure 8.14: Scan 1/4 of FLUXANA drift monitor sample FLX-S13 with WDXRF, Rh tube 40 kV, LIF 220, 0.15°, FPC.

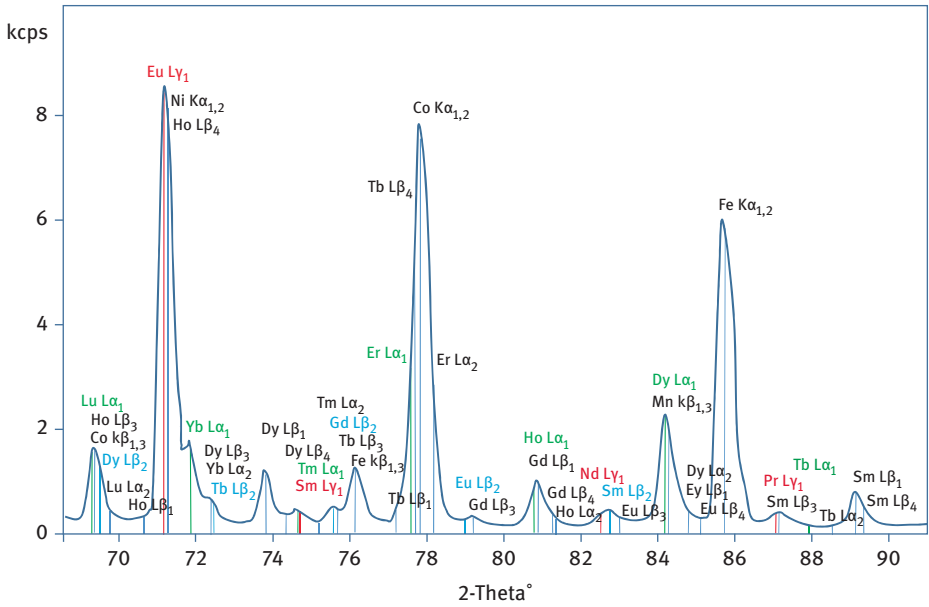


Figure 8.15: Scan 2/4 of FLUXANA drift monitor sample FLX-S13 with WDXRF, Rh tube 40 kV, LIF 220, 0.15°, FPC.

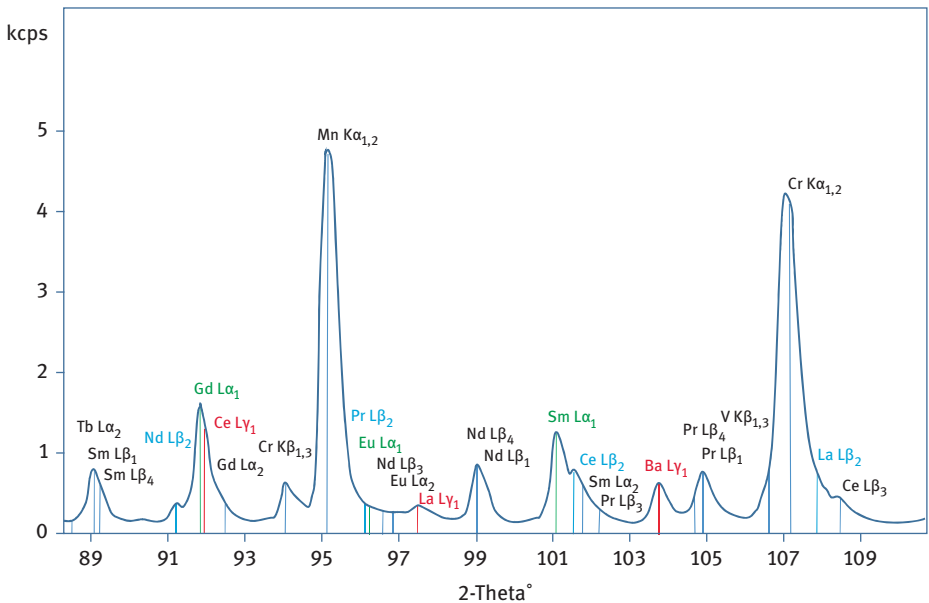


Figure 8.16: Scan 3/4 of FLUXANA drift monitor sample FLX-S13 with WDXRF, Rh tube 40 kV, LIF 220, 0.15°, FPC.

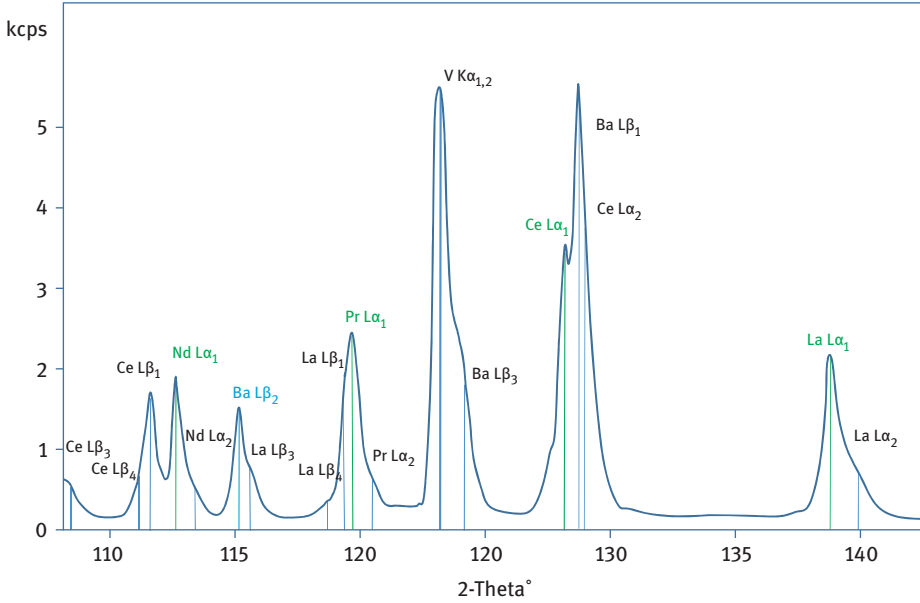


Figure 8.17: Scan 4/4 of FLUXANA drift monitor sample FLX-S13 with WDXRF, Rh tube 40 kV, LIF 220, 0.15°, FPC.

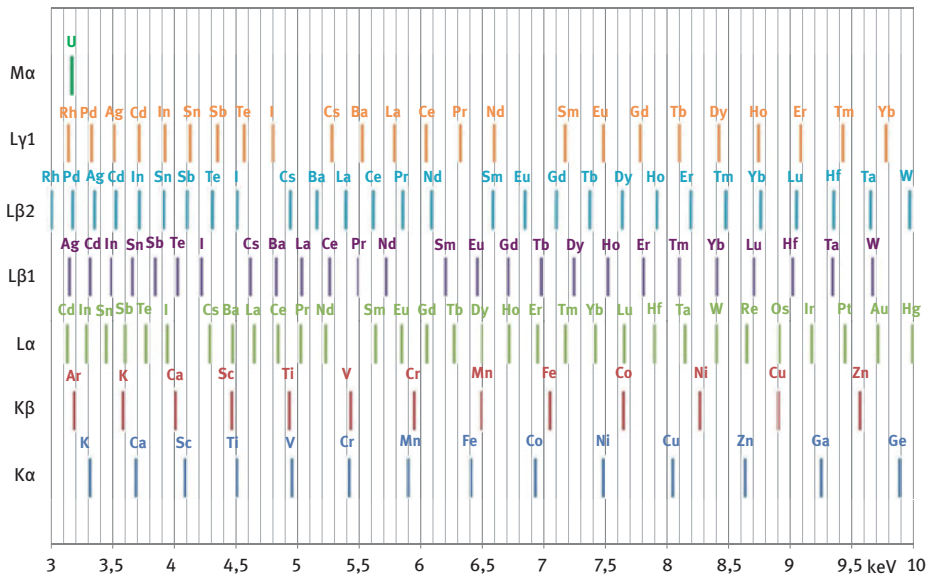


Figure 8.18: X-ray fluorescence line overlaps relevant for REE in the range of 3–10 keV [2].

Table 8.6: Fluorescence lines from REE in keV [20, 21].

Z	Element	K α_1	K α_2	K β_1	L α_1	L α_2	L β_1	L β_2	L β_3	L β_4	L γ_1	M α_1
57	La	33.4418	33.0341	37.801	4.65097	4.63423	5.0421	5.3835	5.1434	5.0618	5.7885	0.833
58	Ce	34.7197	34.2789	39.2573	4.8402	4.823	5.2622	5.6134	5.3653	5.2774	6.052	0.883
59	Pr	36.0263	35.5502	40.7482	5.0337	5.0135	5.4889	5.85	5.5918	5.4981	6.3221	0.929
60	Nd	37.361	36.8474	42.2713	5.2304	5.2077	5.7216	6.0894	5.8294	5.7216	6.6021	0.978
62	Sm	40.1181	39.5224	45.413	5.6361	5.609	6.2051	6.586	6.3180	6.1962	7.178	1.081
63	Eu	41.5422	40.9019	47.0379	5.8457	5.8166	6.4564	6.8432	6.3716	6.4378	7.4803	1.131
64	Gd	42.9962	42.3089	48.697	6.0572	6.025	6.7132	7.1028	6.8310	6.6873	7.7858	1.185
65	Tb	44.4816	43.7441	50.382	6.2728	6.238	6.978	7.3667	7.0961	6.9403	8.102	1.24
66	Dy	45.9984	45.2078	52.119	6.4952	6.4577	7.2477	7.6357	7.3702	7.2039	8.4188	1.293
67	Ho	47.5467	46.6997	53.877	6.7198	6.6795	7.5253	7.911	7.6518	7.4711	8.747	1.348
68	Er	49.1277	48.2211	55.681	6.9487	6.905	7.8109	8.189	7.9392	7.7453	9.089	1.406
69	Tm	50.7416	49.7726	57.517	7.1799	7.1331	8.101	8.468	8.2309	8.0258	9.426	1.462
70	Yb	52.3889	51.354	59.37	7.4156	7.3673	8.4018	8.7588	8.5368	8.3132	9.7801	1.521
71	Lu	54.0698	52.965	61.283	7.6555	7.6049	8.709	9.0489	8.8470	8.6065	10.1434	1.581

Table 8.7: Recommended analyte lines of REE from the author with alternatives in brackets. For comparison, also the recommendations from literature are given.

Z	Element	Author	[10]	[22]	[3]	[16]
57	La	$L\alpha_1$	$L\alpha_1$	$L\alpha_1$	$L\alpha_1, L\beta_1$	$L\alpha_1$
58	Ce	$L\beta_1 (L\alpha_1)$	$L\beta_1$	$L\alpha_1$	$L\beta_1$	$L\beta_1$
59	Pr	$L\beta_1 (L\alpha_1)$	$L\beta_1$	$L\beta_1$	$L\beta_1$	$L\beta_1$
60	Nd	$L\alpha_1$	$L\beta_1$	$L\alpha_1$	$L\alpha_1$	$L\beta_1$
62	Sm	$L\beta_1 (L\alpha_1)$	$L\beta_1$	$L\beta_1$	$L\alpha_1, L\beta_1$	$L\beta_1$
63	Eu	$L\alpha_1 (L\beta_1)$	$L\alpha_1$		$L\alpha_1$	$L\beta_1$
64	Gd	$L\alpha_1$	$L\alpha_1$	$L\alpha_1$	$L\alpha_1$	$L\beta_1$
65	Tb	$L\alpha_1$	$L\alpha_1$	$L\alpha_1$	$L\alpha_1$	
66	Dy	$L\beta_1$	$L\alpha_1$	$L\beta_1$	$L\beta_1$	
67	Ho	$L\beta_1$	$L\alpha_1$	$L\beta_1$	$L\alpha_1$	
68	Er	$L\alpha_1$	$L\alpha_1$	$L\beta_1$	$L\alpha_1$	
69	Tm	$L\alpha_1$	$L\alpha_1$		$L\alpha_1$	
70	Yb	$L\alpha_1$	$L\alpha_1$	$L\alpha_1$	$L\alpha_1$	
71	Lu	$L\alpha_1 (L\beta_1)$	$L\alpha_1$		$L\alpha_1$	

8.5.4 Lower limit of detection (LLD)

Figures 8.19 and 8.20 show LLDs of REE in different matrices and measured with WDXRF equipped with a target x-ray tube “Rh” and EDXRF equipped with a target x-ray tube, W both working with 60 kV. While EDXRF shows here a higher sensitivity for the K-lines, WDXRF shows a higher sensitivity for most of the L-lines.

8.6 Calibration

The calibration strategy is depending on the sample preparation. For pressed pellets, particle size effects and matrix effects dominate the interelement corrections. To build up a calibration, many standard materials analyzed by other analytical methods are required. Most of the instrument manufacturers offer such calibration packages already. In fused bead sample preparation, the sample is totally dissolved and doesn't show any particle size effects. Additionally, matrix effects could be reduced because of the dilution or the presence of a strong absorber element. Fusion shows the advantage of building an independent calibration traceable to the weights of pure chemicals. An example of building such a calibration is given in Ref. [15]. For such a calibration, less calibration samples are required and the need of external standard materials is small. Also, FLUXANA offers calibration sets for REE applications as fused beads.

Attention has to be paid to sample thickness if K-lines are used for analysis. There is a possible risk that the samples are not infinitely thick for the high energies of K-lines. If a target x-ray tube “Rh” is used, a possible correction for the imperfect

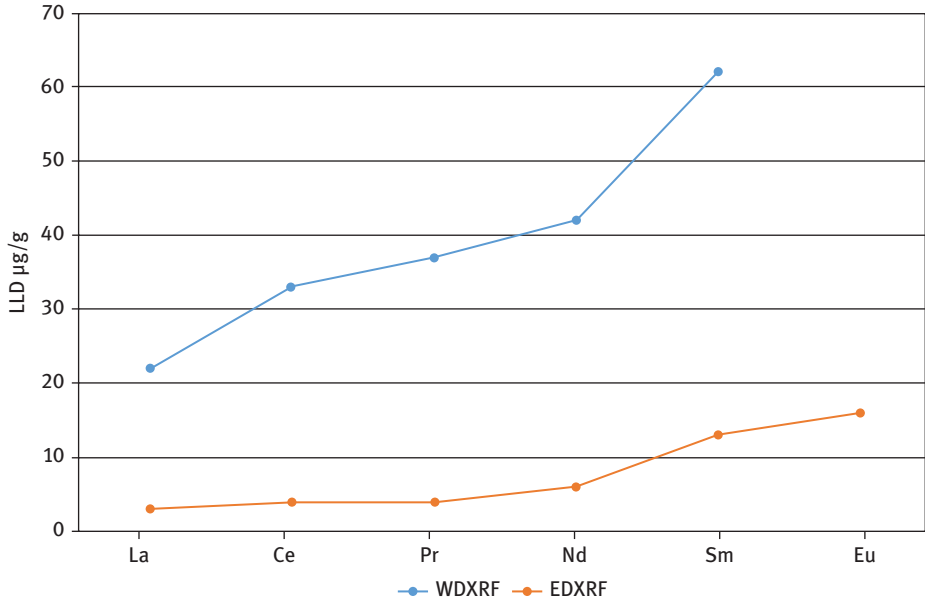


Figure 8.19: LLD of REE measured with $K\alpha_1$ -line (WDXRF: 20 s per line in lithiumtetraborate matrix, EDXRF: 600 s in cellulose matrix).

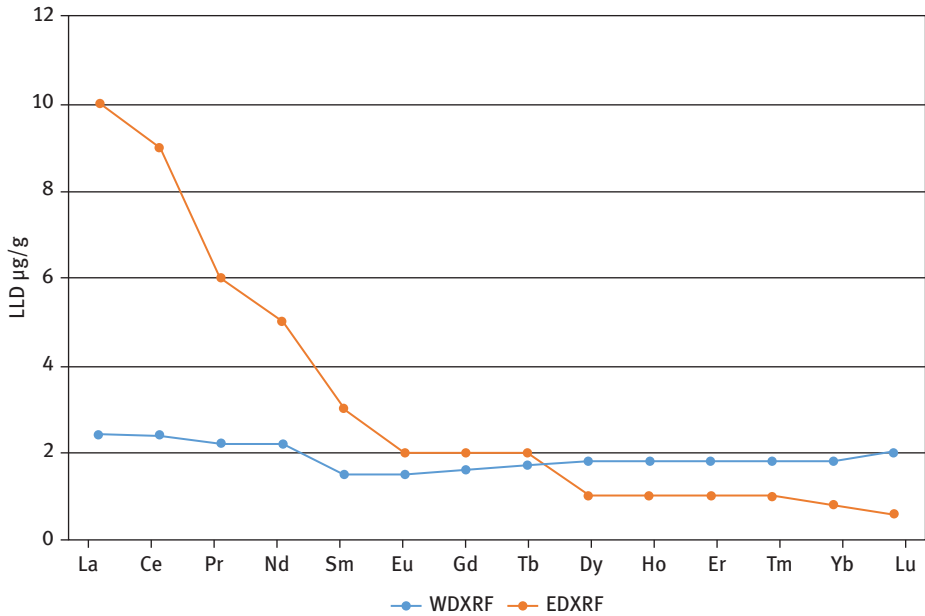


Figure 8.20: LLD of REE measured with $K\alpha_1$ -line (WDXRF: 20 s per line, EDXRF: 600 s, both in cellulose matrix).

thickness and additionally for any kind of matrix effects could be the normalization to the Rh K α Compton Peak because no absorption edges are found in between.

8.6.1 Other calibration strategies mentioned in literature

Macháček and Weiss [16] describe for the calibration of REE an empirical correction in combination with internal standard elements Cr and Mo.

Michelsen [22] gave an overview about the use of an internal standard like Sr for Y, the use of standard addition for REE in rock samples and dried solutions on filters.

8.7 Summary

The analysis of REE with X-ray fluorescence analysis remains a challenge. An XRF application of REE requires an extensive and careful development by the analyst. The significance of the final result depends on the choice of the sample preparation method, the measurement conditions, the calibration strategy and the selection of standard materials.

The choice of fusion or pressed pellets will influence the sensitivity. Sample thickness must be in agreement with line selection. The choice of the analyte line and the corresponding background has to take into account possible line overlaps. Calibration must consider matrix effects and interelement effects.

In literature, several examples are given on how to use XRF successfully for REE analysis. However, there could be always limitations based on particle size effects, line overlaps or poor sensitivity, so that other techniques like ICP-MS have to be used instead.

Finally, an intense study of the application problem has to prove that XRF could be used successfully to analyze REE in a certain sample type.

References

- [1] Bezati F, Froelich D, Massardier V, Maris E. Addition of tracers into the polypropylene in view of automatic sorting of plastic wastes using X-ray fluorescence spectrometry. *Waste Manage* 2009, 30, 591–6.
- [2] Schramm R. *X-Ray Fluorescence Analysis: Practical and Easy*. Bedburg-Hau, FLUXANA, 2012.
- [3] Willis JP, Feather C, Turner K. *Guidelines for XRF analysis*. James Willis Consultants, 2014.
- [4] Willis JP, Duncan AR. *Understanding XRF Spectrometry*. Panalytical B.V., 2008.
- [5] Hahn-Weinheimer P, Hirner A, Weber-Diefenbach K. *Röntgenfluoreszenzanalytische Methoden: Grundlagen und praktische Anwendungen in den Geo-, Material- und Umweltwissenschaften*. Braunschweig and Wiesbaden, Vieweg, 1995.
- [6] Jenkins R. *X-Ray Fluorescence Spectrometry*. 2nd edn. New York, John Wiley & Sons, Inc., 1999.
- [7] Grieken RE Van, Markowicz A. (ed.). *Handbook of X-Ray Spectrometry*. New York, Marcel Dekker, 1992.

- [8] Grieken RE Van, Markowicz A. (ed.). *Handbook of X-Ray Spectrometry*. 2nd edn. New York, Marcel Dekker, 2002.
- [9] Beckhoff B, Kanngießler B, Langhoff N, Wedell R, Wolff H (eds.). *Handbook of Practical X-Ray Fluorescence Analysis*. Berlin Heidelberg, Springer-Verlag, 2006.
- [10] McNew EB, Willis JP. An evaluation of the analysis of Monazite and REE compounds by WDXRFs: a spectroscopist's nightmare (or challenge?). *Adv X-ray Anals* 1999, 41, 829.
- [11] Klockenkämper R, von Bohlen A. *Total-Reflection X-ray Fluorescence Analysis and Related Methods*. New Jersey, Wiley, 2015.
- [12] Muia L, Grieken RV. Determination of rare earth elements in geological materials by total reflection X-ray fluorescence. *Anal Chim Acta* 1991, 251, 177.
- [13] Dixit RM, Deshpande SS. An XRF method for the determination of common rare earth impurities in high purity yttrium oxide. *Fresenius' Z Anal Chem* 1977, 288, 180–2.
- [14] Bauer-Wolf E, Wegscheider W, Posch S, Knapp G, Kolmer H, Panholzer F. Determination of traces of rare earth elements in geological samples. *Talanta* 1993, 40, 9.
- [15] Nakayama K, Nakamura T. X-ray fluorescence analysis of rare earth elements in rocks using low dilution glass beads. *Anal Sci* 2005, 21, 7, 815–22.
- [16] Macháček V, Weiss D. X-ray fluorescence determination of light rare earth elements, Y and Th, by the fusion technique, *X-Ray Spectrometry* 1998, 14, 53.
- [17] Roelandts I. Determination of light rare earth elements in apatite by X-ray fluorescence spectrometry after anion exchange extraction. *Anal Chem* 1981, 53, 4, 676–80.
- [18] Robinson P, Higgins NC, Jenner GA. Determination of rare-earth elements, yttrium and scandium in rocks by an ion exchange-X-ray fluorescence technique. *Chem Geol* 1986, 55, 121.
- [19] De Vito IE, Olsinaab RA, Masiab AN. Preconcentration and elimination of matrix effects in XRF determinations of rare earth elements by preparing a thin film through chemofiltration. *J Anal At Spectrom* 2001, 16, 275–8.
- [20] <http://www.med.harvard.edu/JPNM/physics/refs/xrayemis.html> (accessed 11 June 2012), from Bearden JA. *X-Ray Wavelengths*. *Review of Modern Physics* 1967, 1, 86–99.
- [21] Zschornack G. *Handbook of X-Ray Data*. Berlin Heidelberg, Springer, 2007.
- [22] Michelsen OB. *Analysis and Application of Rare Earth Materials*. Nato Advanced Study Institute. Kjeller, Norway, Universitetsforlaget, 1972.

Heinz-Günter Stosch

9 Neutron Activation Analysis of the Rare Earth Elements (REE) – With Emphasis on Geological Materials

Abstract: Neutron activation analysis (NAA) has been the analytical method of choice for rare earth element (REE) analysis from the early 1960s through the 1980s. At that time, irradiation facilities were widely available and fairly easily accessible. The development of high-resolution gamma-ray detectors in the mid-1960s eliminated, for many applications, the need for chemical separation of the REE from the matrix material, making NAA a reliable and effective analytical tool. While not as precise as isotope-dilution mass spectrometry, NAA was competitive by being sensitive for the analysis of about half of the rare earths (La, Ce, Nd, Sm, Eu, Tb, Yb, Lu). The development of inductively coupled plasma mass spectrometry since the 1980s, together with decommissioning of research reactors and the lack of installation of new ones in Europe and North America has led to the rapid decline of NAA.

9.1 Introduction

The principle of neutron activation analysis (NAA) was proposed by von Hevesy and Levi in 1936, following the detection of the neutron by James Chadwick in 1932 [1, 2]. The practical application of NAA, of course, had to await the development of neutron-generating devices, in particular the nuclear reactor, after World War II, which made high neutron fluxes ($10^{12} \text{ cm}^{-2} \text{ s}^{-1}$ and above) available for analytical purposes. For more than 20 years, from the mid-1960s to the late 1980s, NAA remained the most widely employed method for the analysis of the rare earth elements (REEs) as well as a number of other elements, present at the trace element level in geological and biological materials. An excellent account of the state of NAA towards the end of this period is provided by Potts [3]. A web page with much useful information is maintained by Kubešová [4].

9.2 Principles of neutron activation: activation equation, cross sections

An atomic nucleus that is hit by a neutron (n) may undergo a variety of nuclear reactions, depending upon the energy of the neutron. At low-to-intermediate kinetic energies, below about one million electron volts (MeV), (n, γ) reactions prevail, meaning that the neutron is captured by the nucleus which then emits a γ -ray. Higher kinetic energies of the neutron cause reactions such as (n, p), by which the neutron

is captured and a proton p is emitted, or (n, α) , which indicates that an α -particle (a helium nucleus) is emitted. As neutrons do not carry an electric charge, they experience no repulsion by an atomic nucleus. For this reason, neutrons with very small kinetic energies can be captured by a nucleus. In fact, neutrons, thermal are most commonly utilized in NAA. Thermal neutrons carry kinetic energies less than about 0.1 eV ($1 \text{ eV} = 1.602 \times 10^{-19} \text{ J}$). Using the relation $E = k_B \times T$, where k_B is Boltzmann's constant ($8.617 \times 10^{-5} \text{ eV K}^{-1}$), we calculate that a temperature of 300 K corresponds to an energy of just 0.026 eV.

If a target which contains atomic nuclei of kind X is exposed to a beam of neutrons (or other particles), the number N of nuclei Y , formed by a reaction, can be calculated:

$$\frac{dN_Y}{dt} = \sigma \times \Phi \times N_X \quad (9.1)$$

where dN_Y/dt is the production rate of Y , σ is the cross section, neutron (cm^2), Φ is the neutron flux ($\text{cm}^{-2} \text{ s}^{-1}$), assumed to remain constant across the target, and N_X the number of nuclei X , also assumed to remain essentially constant. The cross section σ indicates the probability of the reaction to occur. It is commonly associated with the apparent cross section of nucleus A for a neutron that approaches the nucleus. Historically, the word "barn, neutron cross section" has been coined as the unit for the cross section where 1 barn (b) = 10^{-24} cm^2 ; 1 b corresponds approximately to the cross section of a uranium nucleus. For thermal neutrons, σ decreases approximately as a function of $1/v$, where v is the speed of the neutron. The slower the neutron is, the larger is the probability that it is captured by a nucleus. Above the thermal energy range, there is the range of epithermal energies up to about 100 eV. This range is characterized by sharp increases in σ at well-defined energies that correspond to resonances, the formation of a compound nucleus in discrete excited states (Figure 9.1) [5].

Neutron capture of an atomic nucleus results in the formation of an isotope of the same element in an excited state. A prompt γ -ray is released immediately and carries away part or all of the excitation energy, depending upon the existence and stability of excitation levels. Prompt γ -ray NAA is one of the methods of neutron activation. It requires the detector to be set up close to the neutron source, for example, a reactor. It may be the method of choice if only stable isotopes of an element are produced during neutron irradiation or if only radioactive isotopes with very short half-lives are generated. Among the REEs, only Sm and Gd can be reasonably well analysed at normal concentrations in rock samples [6]; prompt γ -ray NAA will not further be considered here.

In many cases, Y is a radioactive isotope that decays with its characteristic half-life $t_{1/2}$ into a stable isotope or into another radioactive isotope of a different element. The β^- decay results in the formation of an element with a higher atomic number $Z + 1$ by emission of an electron or to an isotope of an element with a lower atomic

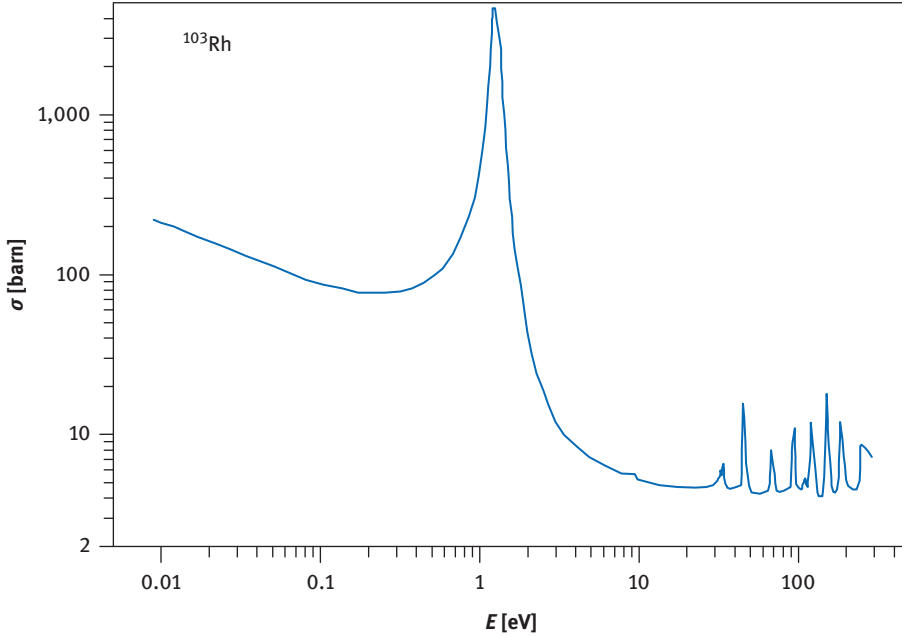
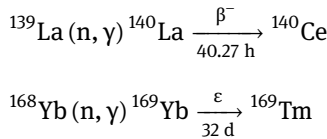


Figure 9.1: Dependence of the neutron-absorption cross section σ upon the neutron energy displaying the decrease of σ with neutron energy for thermal neutrons and neutron capture resonances at epithermal energies (redrawn from De Soete et al. [5]). ^{103}Rh displays a strong resonance at an energy of 1.26 eV (and more resonances at higher energies). This corresponds to an excited state of the compound nucleus ^{104}Rh , which forms with a high probability when natural rhodium is irradiated with neutrons with appropriate energy. This compound nucleus decays rapidly ($\approx 4 \times 10^{-15}$ s by γ -emission into ^{104m}Rh and ^{104}Rh , which both are radioactive and decay by β^- emission into stable ^{104}Pd).

number $Z - 1$ by the nucleus capturing an orbiting electron, more rarely by emission of a positron from the nucleus (β^+ decay), for example,



where ϵ denotes electron capture, h and d time in hours and days, respectively. Half-life and decay constant λ are related by

$$t_{1/2} = \frac{\ln(2)}{\lambda} \tag{9.2}$$

At least part of the decays by β^- , β^+ or electron capture results in the formation of a nucleus in an excited state. The excitation energy is immediately released by emission

of one or more γ -rays with characteristic energies. These γ -rays are registered and evaluated in NAA.

A decay scheme is used to illustrate the decay of a radioactive isotope. This is illustrated in a simplified form in Figure 9.2 for the decay of ^{140}La into stable ^{140}Ce . Almost all β^- decays go into excited levels of ^{140}Ce which decay through γ -ray emission. The four strongest decays at 328.8, 487.0, 815.8 and 1,596.6 keV are most suitable for γ -ray counting.

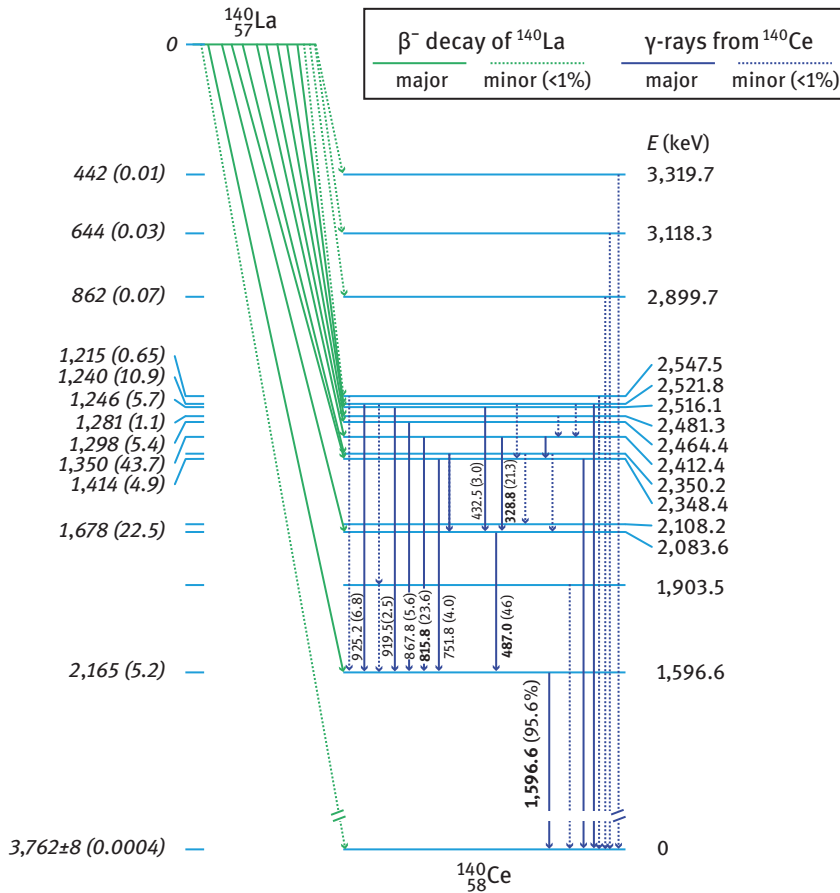


Figure 9.2: Decay of radioactive ^{140}La into stable ^{140}Ce . β^- decays to various excited states and to the ground state of ^{140}Ce are displayed by green arrows; decay of the various excited states by γ -emission is shown by dark blue arrows. Levels of excited states of ^{140}Ce are shown in light blue. The total decay energy between the ground state of ^{140}La and the ground state of ^{140}Ce amounts to 3,762 keV. More than 99% of all β^- decays end up at excited levels of ^{140}Ce which release their excitation energies through γ -emission. Values in parentheses are γ -ray abundances per 100 β^- decays. Modified after Ref. [7].

If nuclide Y, produced according to eq. (9.1), is radioactive, it will start to decay during neutron irradiation and we must subtract its rate of decay

$$-\frac{dN_Y}{dt} = \lambda \times N_Y$$

from eq. (9.1) which gives:

$$\frac{dN_Y}{dt} = (\sigma \times \Phi \times N_X) - (\lambda \times N_Y) \quad (9.3)$$

Assuming that N_X remains essentially constant during irradiation and that $N_Y = 0$ at the beginning of irradiation, the integration of this equation provides

$$N_Y = \frac{\sigma \times \Phi \times N_X}{\lambda} \times (1 - e^{-\lambda t}) \quad (9.4)$$

with t being the duration of irradiation and N_Y being the number of radioactive nuclei at the end of irradiation. As NAA counts the number of decays within a defined period of time, it is convenient to replace N_Y by the activity A_Y , where $A = \lambda \times N$. We then obtain

$$A_Y = \sigma \times \Phi \times N_X \times (1 - e^{-\lambda t}) \quad (9.5)$$

Typical irradiation times range from seconds to several days. For a given nuclide 50 % of the maximum activity is reached after irradiating the sample for one half-life, 90 % are reached after 3.3 half-lives. After the end of irradiation, the induced activity decays away as a function of decay time t_d :

$$A_Y = \sigma \times \Phi \times N_X \times (1 - e^{-\lambda t}) \times e^{-\lambda t_d} \quad (9.6)$$

After seven half-lives less than 1 % of the original activity is still present; this represents an approximate limit where a nuclide can be quantitatively measured with an acceptable precision. In a natural sample such as a piece of rock, many radioactive nuclides with different half-lives will be produced during irradiation. A nuclide with a short half-life, such as ^{165}Dy (2.35 h), has reached its saturation activity after an irradiation time of one day whereas a nuclide with a long half-life such as ^{160}Tb (72.3 d) has achieved only about 1 % at that time (Figure 9.3). Whereas the activity of ^{165}Dy must be counted within about 12 h after the end of irradiation, the activity of nuclides with long half-lives is counted much later when all short-lived activities have decayed. In practice, it is preferable to split the sample, irradiate one split for a short time (minutes) and count the induced activities of the short-lived nuclides within less than a day after the end of irradiation, and irradiate the second split for a longer time (hours to days) and let the short-lived activities decay before counting the activities of the long-lived nuclides.

Normally, NAA is used as a relative method; this eliminates the need to precisely know the value of the neutron flux Φ (and flux variations) as well as the cross

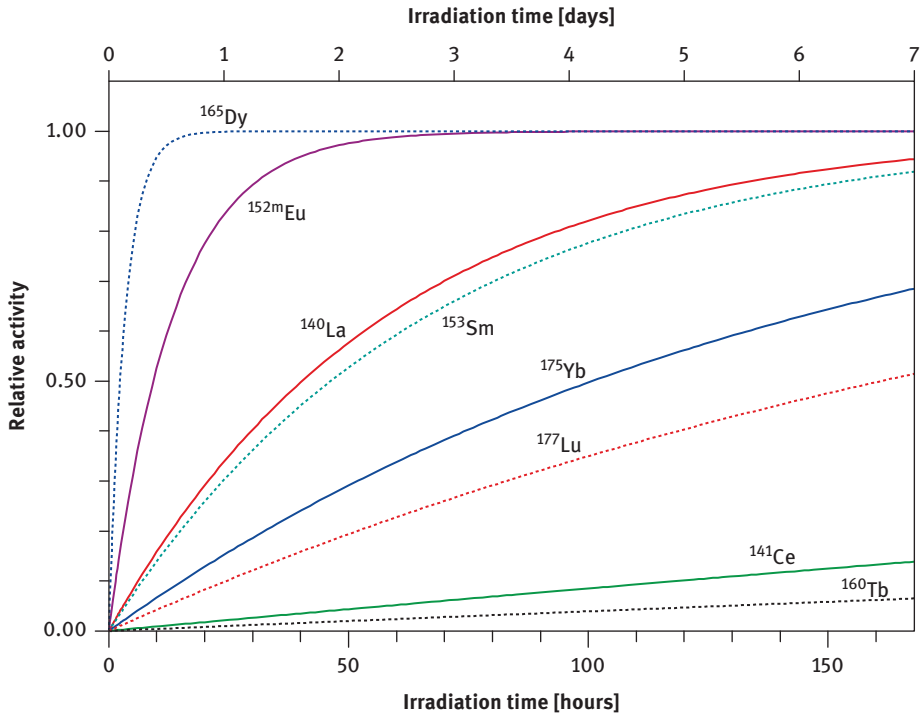


Figure 9.3: The saturation factor, $NAA (1 - e^{-\lambda t})$ as a function of irradiation time for nuclides of the REE with different half-lives.

section σ . Instead, single- or multi-element standards are irradiated together with the samples of interest (see Section 9.4.2). However, considerable efforts have also been undertaken to develop the single-comparator method where only one element or isotope, in particular ^{197}Au , is required for standardization [8–10].

9.3 Equipment

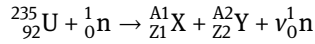
9.3.1 Neutron sources

Obviously, NAA depends upon the availability of powerful neutron sources. By far the most important source is the fission reactor. Other sources are accelerators and the bombardment of light nuclei by α - or γ -rays.

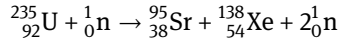
9.3.1.1 The fission reactor

Research fission reactors produce neutrons through fission of ^{235}U by using uranium fuel enriched in this isotope. ^{235}U is fissionable by thermal neutrons with a high (n, f) cross section of 586 b (f = fission). Fission of ^{235}U produces two large fragments plus,

on average, 2.5 neutrons that are required to entertain a chain reaction. Schematically, the fission reaction can be written as



with X and Y denoting the two fragments with mass A and atomic number Z and ν being the number of neutrons generated per reaction, for example,



${}^{95}\text{Sr}$ and ${}^{138}\text{Xe}$ are both radioactive and undergo several β^- decays into ${}^{95}\text{Mo}$ and ${}^{138}\text{Ba}$, respectively. Figure 9.4 shows the fission yield for ${}^{235}\text{U}$ (yields taken from Ref. [11]). It can be seen that the two large fragments centre around masses 90–100 and 133–143, respectively. In a sample to be analysed, ${}^{235}\text{U}$, of course, undergoes the same fission by thermal neutrons. This will lead to the production of light REE and may constitute a major source of error in NAA in particular of Ce and Nd if abundances of uranium exceed those of the light REE ([12] and Section 9.4.5).

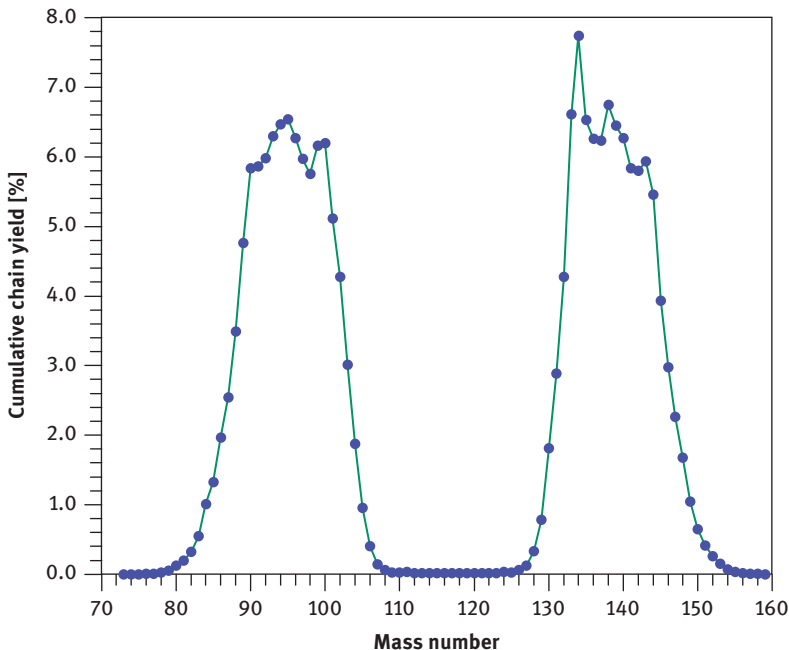


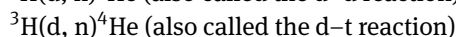
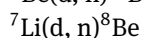
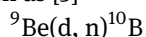
Figure 9.4: Cumulative chain yield for the fission of ${}^{235}\text{U}$ with thermal neutrons as a function of mass number. Because fission of one ${}^{235}\text{U}$ yields two heavy fragments, the sum of the yields equals 200 %.

The two to three neutrons released during fission of ^{235}U are neutrons, fast that, on average, carry away a total energy of about 5 MeV. Before they can be absorbed by another ^{235}U nucleus or be utilized for standard NAA, they must be thermalized through elastic collisions with a moderator, that is, with nuclei of light elements, in particular hydrogen, carbon and oxygen until equilibrium is achieved with the thermal motion of the moderator. Current research reactors reach thermal neutron flux densities between about 10^{12} and 10^{15} $\text{n cm}^{-2} \text{s}^{-1}$.

In 2012, there were about 382 research reactors in operation worldwide [13] with many facing decommissioning within a few years. In Germany, for example, there are currently only three research reactors left (Berlin, Mainz and Munich) whereas some 40 years ago there were about a dozen in operation. It is evident, therefore, that today NAA is of little importance in this country and many others as small new neutron generating facilities, in particular neutron generators, are still in the state of development.

9.3.1.2 Accelerators, neutron generators, isotopic neutron sources

Accelerator-generated neutrons have been employed in NAA since the 1970s. Charged particle accelerators (cyclotron, linear accelerator, Van de Graaff accelerator) can be used to bombard isotopes of light elements with deuterium, causing reactions such as [5]



(d, n) denotes that the target (isotopes of Be, Li, H) is bombarded with deuterons leading to the formation of a compound nucleus which emits a neutron and decays into isotopes of B, Be and He.

The last three reactions provide monoenergetic neutrons or nearly so. The d-d and the d-t reactions generate high neutron yields already at low bombarding energies and therefore are particularly useful to manufacture neutron generators with small footprints (in principle, tabletop machines) and thus have been in the focus of research in recent years [13, 14]. The d-d fusion reaction currently is capable of producing 10^{10} n s^{-1} using a neutron generator in which a deuterium beam, produced with a radio-frequency generated plasma and 100–140 kV of acceleration voltage is focused on a target, commonly metal hydride [15, 16]. However, the maximum thermal neutron flux at sample position was only 2×10^7 $\text{n cm}^{-2} \text{s}^{-1}$, insufficient for trace element analysis. The d-d reaction is being explored for prompt γ -ray NAA as well as for standard NAA. Deuterium (${}^2\text{H}$) has the advantage over tritium (${}^3\text{H}$) to be easily available and stable whereas the latter is radioactive (half-life 12.3 years [a]) and must be manufactured through nuclear reactions. Neutron generators employing the d-d reaction contain no radioactivity and thus are safe when switched off. The d-t reaction produces high-energy neutrons (14.7 MeV). Such fast neutrons may be employed in the

determination of light elements like carbon, nitrogen and oxygen through (n, p), (n, α) and (n, 2n) reactions; these elements are not well activated by (n, γ) reactions [17].

Isotopic neutron sources have been (and are) of little importance in NAA due to rather low neutron intensities of less than 10^7 n s^{-1} [13]. They require an α -emitting radioactive source such as ^{241}Am (half-life 432.2 a) or ^{226}Ra (1600 y) and a target, in particular Be, to induce (α , n) reactions, for example, $^9\text{Be}(\alpha, \text{n})^{12}\text{C}$. Photon activation using a radioactive source of high-energy γ -rays, in particular ^{124}Sb (half-life 60.3 d) is essentially limited to the analysis of Be through the reaction $^9\text{Be}(\gamma, \text{n})^8\text{Be}$ where the latter instantaneously disintegrates into two ^4He atoms. Upon decaying into ^{124}Te , ^{124}Sb emits a γ -ray of energy 1.69 MeV which is just barely energetic enough to induce the (γ , n) reaction on ^9Be that requires a threshold energy of 1.67 MeV. Almost all other (γ , n) reactions have threshold energies in excess of 8 MeV [5]. Photons exceeding this energy are produced as bremsstrahlung by firing a high-energy electron beam from an accelerator on a target metal. In this way, some REE can be analysed by photon activation in geological and biological materials if present at concentration levels of tens of ppm [18].

9.3.2 The counting system

A NAA counting system consists of a detector and the pulse-processing electronics. The latter comprises preamplifier, main amplifier, a multichannel analyser that includes an analogue-to-digital converter and an output device (computer) (Figure 9.5) [3]. The amplifiers are required to amplify the small signal registered in the detector and to achieve a high signal-to-noise ratio. The multichannel analyser sorts and stores the incoming signals as a function of γ -ray energy. Evaluation of the spectra (calculation of photopeak areas) is carried out by dedicated software on a computer.

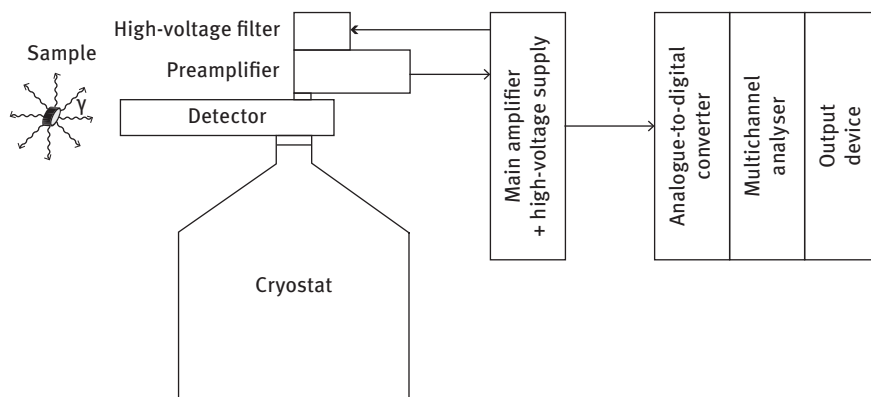


Figure 9.5: Schematic sketch of an NAA counting system (modified after [3]).

9.3.2.1 Detectors

During the early years of NAA the most suitable detector was a scintillation detector, commonly a big transparent single crystal (or polycrystalline material) of NaI doped with Tl as an activator (order of 0.1 mol%), connected to a photocathode and a photomultiplier. The energy of γ -rays entering such a crystal is absorbed and transferred to electrons which are caught by the activator. A tiny flash of light is then emitted during transition from the excited to the ground state. The light is converted to an electric signal by the photocathode and the signal is amplified by a photomultiplier. The advantage of the Tl-doped NaI detector is that the crystals are fairly easy to grow from the melt to large sizes [19]. Sizes of 3 in. (diameter) by 3 in. (height) were the standard in the 1960s. They were able to register a large fraction of the incoming γ -rays. In contrast to semiconducting diodes, they also can be operated at ambient temperatures. The main disadvantage of the Tl-doped NaI detector is its poor energy resolution. NAA of the REE in geological materials at that time required the chemical separation of each REE using time-consuming ion-exchange techniques [20]. NaI scintillation detectors are still used today when it is important to detect as large a fraction of the incoming γ -rays as possible, for example, in nuclear medicine or environmental sciences.

The high-resolution Ge semiconductors that are used today were developed in the early 1960s [21, 22]. Ge has a higher atomic number than Si that is used as detector material in X-ray fluorescence and therefore Ge is much better suited to stop the high-energy γ -rays. Moreover, to create an electron–hole pair requires only an energy of 2.95 eV at the operating temperature of about 80 K (3.72 eV in Si at the same temperature). Absorption of a 1-MeV γ -ray will then create about 3.4×10^5 electrons equivalent to a charge of 5.7×10^{-14} C [3]. Until the 1980s, the process of growing germanium left unacceptably high levels of impurity inside the crystal which acted as p-type (“positive holes” in the valence band, due, for example, to atoms with three valence electrons instead of the four in germanium, causing the formation of acceptor levels in the forbidden energy region between valence band and conduction band) or n-type semiconductors (negative charges, e.g. by atoms with five valence atoms, forming donor levels). Such impurities cause conduction of the germanium under an electrostatic field even in the absence of ionizing radiation. In order to compensate for this effect, Li, which enters interstitial sites in the Ge, was diffused into a cylinder of p-type Ge, leaving only the central part of the cylinder as a p-type semiconductor [3]. These crystals were thus called coaxial Ge(Li) detectors. As lithium diffuses fairly rapidly through germanium at room temperature, these crystals had always to be cooled to the temperature of liquid nitrogen, even if not in use. High-purity Ge became gradually available during the 1970s, initially as small crystals only, eliminating the need of Li drifting. These crystals were first used to manufacture “planar” (disc-shaped) Ge detectors with a typical volume of $\leq 10^0$ cm³ and an active area of 0.X mm² that were employed in the detection of low-energy γ -rays (≈ 60 –250 keV). The maximum volume of high-purity Ge detectors has increased about linearly from the mid-1970s (less than 100 cm³) to about 800 cm³ in 2003 [23], thus permitting the fabrication of detectors for any need.

The quality of a detector is judged by its efficiency, of a detector to detect a signal as well as its resolution. The absolute efficiency is the fraction of γ -rays emitted from a sample that cause an event in the detector. This parameter is strongly dependent upon the geometry, in particular the distance between sample and detector, as the sample will emit photons isotropically in all directions (Figure 9.5). More important is the relative efficiency which permits a comparison to be made between different detectors. Relative efficiency is the relative photopeak efficiency (total absorption of a γ -ray in the crystal by the photoelectric effect, see below) of a detector compared to that of a 3 in. \times 3 in. NaI(Tl) detector at an energy of 1,333 keV (^{60}Co) and a distance of 25 cm between source and detector [24]. Obviously, relative efficiency increases with the volume of the detector and values of more than 100 % are nowadays reached for high-purity Ge detectors. The efficiency decreases with γ -energy, above about 300 keV approximately proportional to $E^{-0.5}$. A large Ge(Li) or Ge detector possesses a maximum efficiency at about 100 keV and it decreases by about one order of magnitude at 1,333 keV. A planar Ge detector has a maximum efficiency below about 50 keV and it decreases by about one order of magnitude at 200 keV.

The resolution, of a detector is reported as full width at half maximum (FWHM), that is the width of a peak at half its maximum intensity. For coaxial Ge(Li) and big high-purity Ge detectors, resolution is usually specified for the 1,333 keV line of ^{60}Co (see Figure 9.6), either as an absolute value in keV or as a relative one ($100 \times \text{FWHM}$ divided by the energy of the γ -peak). For planar Ge detectors resolution is reported for

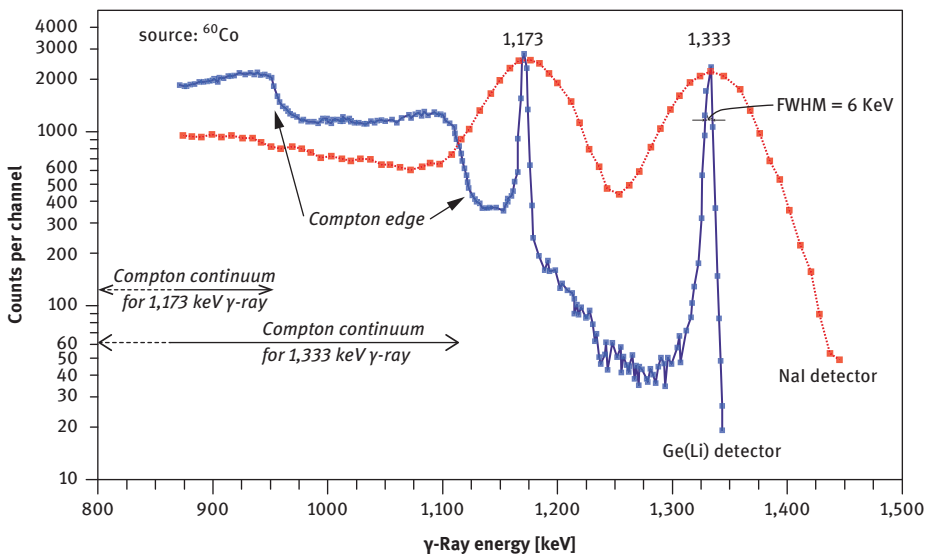


Figure 9.6: The high-energy part of a γ -ray spectrum of ^{60}Co showing the superior energy resolution of a Li-drifted Ge detector over a Tl-doped NaI scintillation detector [21]; $\text{keV} = 1,000 \text{ eV}$. The resolution of the Ge(Li) detector is shown for the 1,333 keV γ -ray (FWHM = full width at half maximum).

the 122.1 keV γ -peak of ^{57}Co or the 121.8 keV peak of ^{152}Eu . In the former case, resolution is about 2 keV absolute or 0.15 relative, 20–30 times better than the resolution of a NaI(Tl) detector, in the latter case it may be about 0.55 keV absolute or 0.45 % relative. As high-energy γ -rays are much less likely to be absorbed in a planar Ge detector than in a high-volume Ge detector, the Compton background (see next section) is much diminished which makes the planar detector the detector of choice for detecting γ -rays with energies below ≈ 150 keV.

9.3.2.2 Interaction of electromagnetic radiation with matter

The absorption, of radiation of X-rays or γ -rays by matter follows an exponential relation:

$$I = I_0 \times \exp(-\mu \times d) \quad (9.7)$$

where I_0 is the initial intensity of the photon beam, I is the remaining intensity after having travelled distance d (cm) through matter and μ (cm^{-1}) is the absorption coefficient. The latter is the sum of three terms, the photoelectric effect, the Compton effect and the pair-production effect, plotted for Ge and Si in Figure 9.7.

In the *photoelectric effect* the entire energy of the photon is transferred to an orbital electron, in about 80 % of cases to a K electron and in 20 % to an L electron [5]. The energy of the electron corresponds to the energy of the photon minus the binding energy of the electron. Instantaneously an electron from the next higher shell fills the gap, thus emitting a characteristic X-ray. The energies of the photoelectron and the X-ray are absorbed by ionization of detector atoms. There is a small probability for the X-ray to escape from the detector, thus giving rise to an “escape peak” with an energy of the original photon minus the energy of the X-ray. The photoelectric effect is most important for atoms with high atomic number and low photon energies (Figure 9.7). It is essentially these photons that are of interest in NAA.

The *Compton effect* is the result of elastic scattering between a photon and an electron, most likely an outer orbital one, of the interacting atom. Only part of the energy of the photon is transferred to the electron, thereby reducing the energy of the photon that is deflected at an angle ϑ relative to its incident direction. The energy of the scattered photon is dependent upon ϑ [5]:

$$E_\gamma = \frac{E_0}{1 + \frac{E_0}{m_0 \times c^2} \times (1 - \cos \vartheta)} \quad (9.8)$$

where E_γ is the energy of the photon after collision, E_0 is the energy of the photon prior to collision and $m_0 \times c^2$ is the rest mass of the electron ($9.109 \times 10^{-31} \text{ kg} \times 299,792,458^2 \text{ m}^2 \text{ s}^{-2} = 8.187 \times 10^{-14} \text{ J}$ or 511 keV as $1 \text{ eV} = 1.602 \times 10^{-19} \text{ J}$). E_γ attains its maximum for $\vartheta = 0$ ($E_\gamma = E_0$) and its minimum value for $\vartheta = 180^\circ$ ($E_0/[1 + 2E_0/(m_0 \times c^2)]$). For $\vartheta = 180$, the maximum energy of the Compton electron

$$E_{e-\text{max}} = E_0 - E_{\gamma-\text{min}}$$

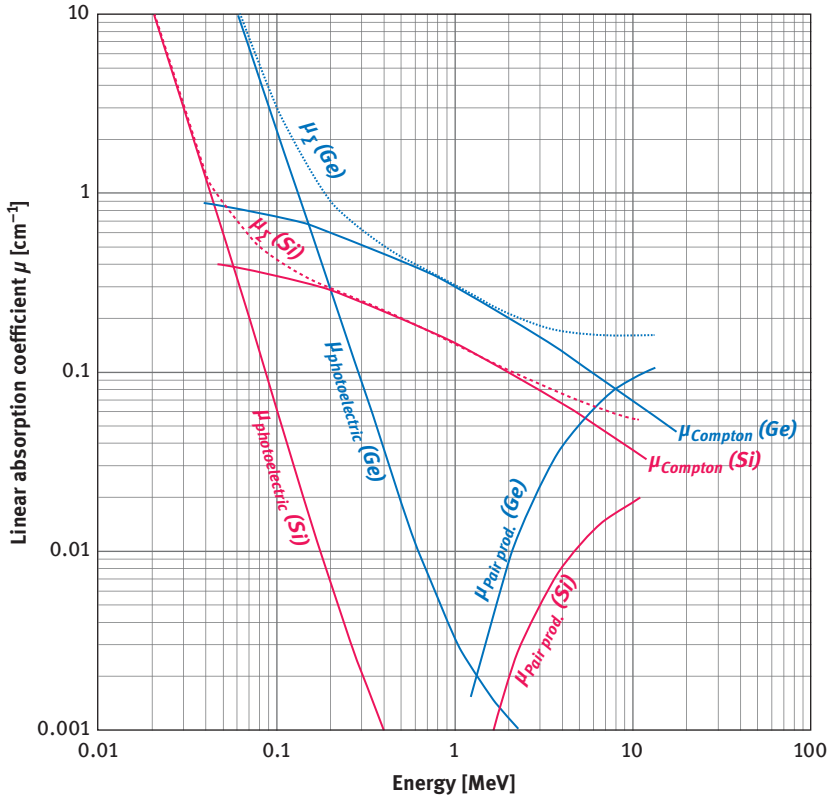


Figure 9.7: Linear absorption coefficients for germanium and silicon plotted against γ -ray energy. μ_{Σ} is the sum of the three individual terms (plotted with data extracted from Ref. [25]). μ_{Σ} is equal to μ in eq. (9.7).

will then be

$$E_{e\text{-max}} = \frac{E_0}{1 + \frac{m_0 \times c^2}{2E_0}} \quad (9.9)$$

As E_{γ} may vary continuously between its minimum and maximum values, so may the energy of the Compton electron E_e between the value calculated from eq. (9.9) and zero. The scattered photon can undergo further Compton interactions, be totally absorbed by the photoelectric effect or escape from the detector. If only the energy of the scattered electron is absorbed in the detector whereas the scattered photon escapes, it contributes to the Compton continuum, a region with an undesired high background in a γ -spectrum. For the 1,333 keV γ -ray of ^{60}Co , eq. (9.9) provides a value of 1,119 keV; this is called the Compton edge (see Figure 9.6). Similarly, the 1,173 keV line of ^{60}Co produces a Compton edge at 949 keV and a Compton continuum below that value. γ -Ray absorption due to the Compton effect dominates μ at intermediate

energies and also decreases with energy, but less steeply so than the photoelectric effect (Figure 9.7).

At very high energies of the γ -rays the *pair production effect* begins to dominate μ , for Ge in excess of about 10 MeV (Figure 9.7). Such a photon can interact with the strong electromagnetic field of an absorber nucleus to produce an electron–positron pair. The minimum energy of the photon that can give rise to pair production equals the rest masses of electron plus positron (511 keV each), that is 1,022 keV. Excess energies of the incident photon will be shared as kinetic energy by electron and positron. After the positron has lost its kinetic energy, it annihilates by reaction with another electron, generating two 511 keV γ -rays. These photons may subsequently be absorbed through the photoelectric effect or the Compton effect.

9.4 Practical considerations

9.4.1 Instrumental versus radiochemical NAA

Two types of NAA are commonly distinguished, instrumental NAA (INAA) and radiochemical NAA (RNAA). In Instrumental neutron activation analysis (INAA) γ -ray counting is carried out after neutron irradiation without further manipulation of the sample, except, maybe, of re-packaging. As NAA is a true multi-element method, for a rock like basalt INAA typically permits the analysis of about 15–20 elements (Na, Sc, Cr, Mn, Fe, Co, Sb, Cs, La, Ce, Nd, Sm, Eu, Tb, Yb, Lu, Hf, Ta, Th, U), depending upon their concentration.

In Radiochemical neutron activation analysis (RNAA), the sample is chemically treated after irradiation in order to separate the element(s) of interest from the matrix prior to counting of the photopeaks. This, of course, requires access to a laboratory where radiochemistry can be carried out. Apart from taking time, this generates additional radioactive waste, in particular in liquid form. All REE are, in principle, accessible to RNAA.

Figure 9.8 shows the naturally occurring REE nuclides together with those employed in NAA. Table 9.1 provides additional information on cross sections for neutron absorption and γ -lines that can be evaluated for analysis (analytical photopeak data from Refs [29, 30]; other data from Refs [11, 31]). In natural rocks, where the light REE (La–Nd) are present at the 10^1 or even 10^2 ppm level and the heavy REE (Ho–Lu) at the 10^0 ppm level, the elements La, Ce, Nd, Sm, Eu, Tb, Yb and Lu can normally be analysed by INAA whereas Pr and Er can only be measured after REE separation from the matrix activity. Due to the short half-life of ^{165}Dy (2.35 h), Dy can only be measured after a separate short (few minutes) irradiation and immediate transport of the activated samples from the reactor to the laboratory for γ -ray counting which must be finished within about five half-lives when the induced activity has decayed to about 3 % of the value at the end of irradiation. This short irradiation is also beneficial for the determination of ^{166}Ho the signal of which is severely enhanced by second-order activation of ^{164}Dy in irradiations of long duration (Section 9.4.5).

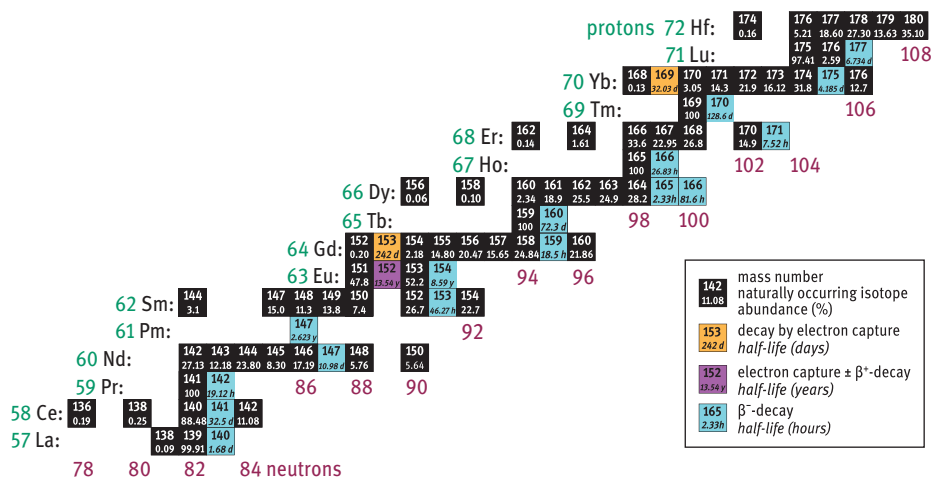


Figure 9.8: Excerpt from the chart of the nuclides [11] showing isotopes, naturally occurring isotopes, radioactive, used in NAA of the REE and Hf in black and radioactive ones employed in NAA in various colours. Small fractions (<5 %) of ^{142}Pr , ^{154}Eu and ^{170}Tm also decay by electron capture to ^{142}Ce , ^{154}Sm and ^{170}Er , respectively. Whereas La, Ce, Nd, Sm, Eu, Tb, Yb and Lu can commonly be analysed by INAA in geological samples, the analysis of Pr and Er always requires RNAA (see also Table 9.1). Among the naturally occurring REE nuclides, some are very weakly radioactive and form the basis of decay systems that are used in geochronology and isotope geochemistry: ^{147}Sm decays, with a half-life of 106×10^9 years, by α -emission into ^{143}Nd [26]. ^{176}Lu decays by β^- emission into ^{176}Hf (half-life 37.2×10^9 years [27]). ^{138}La undergoes a branched decay, by electron capture into ^{138}Ba and by β^- emission into ^{138}Ce ; only the latter is of some importance (partial decay constant $\lambda_{\beta} \approx 2.37 \times 10^{-12} \text{ a}^{-1}$ [28]).

9.4.2 Samples and standards

Samples and standards are commonly irradiated as solids but liquids and even gases can also be used if care is taken to avoid leakage during and after neutron irradiation. Sealed SiO_2 glass tubes or ampoules are particularly suited as containers for liquids and gases. Biological samples may be freeze-dried prior to irradiation. Geological samples, if necessary, can simply be dried in an oven to remove moisture. During neutron irradiation prompt γ -rays are emitted by the sample due to neutron absorption and scattering; in addition, decay of the formed radioactive isotopes releases radiation. Partial absorption of this radiation by the sample produces heat. This causes radiolytic decomposition of H_2O and biological materials during long irradiations (hours and more, depending upon the neutron flux) and a build-up of pressure in the sample containers; organic material may even carbonize [5].

Geological samples will normally be present as finely ground powders but irradiation of rock chips or single mineral grains is also acceptable, provided that they are representative of the bulk samples. It is useful to have a broad idea on the range of REE concentrations to be expected in order to adjust the quantity of sample for irradiation. Quantities between less than 1 mg and a few grams are used, with the most

Table 9.1: Information on isotopes, naturally occurring isotopes, radioactive, used in NAA reaction cross sections and analytical photopeaks for the REE, Y and some other elements that are commonly analysed by INAA.

Element	Isotope mass number	Nat. abundance (at%)	Activation cross section [b]	Product isotope	Half-life ^a	Analytical photopeaks [keV] ^b	Decay product(s)	Method	Irradiation time ^c	Comment
La	139	99.91	9	¹⁴⁰ La	40.272 h	328.75 (21.3),	¹⁴⁰ Ce	INAA, RNAA	Short, long	
						487.03 (45.7), 815.8 (23.6), 1,596.2 (96.0)				
Ce	140	88.48	0.58	¹⁴¹ Ce	32.5 d	145.45 (49.3)	¹⁴¹ Pr	INAA, RNAA	Long	
Pr	141	100	11.5	¹⁴² Pr	19.13 h	1,575.9 (3.7)	¹⁴² Nd	RNAA	Long	4 b for formation of metastable ^{142m} Pr which decays into ground state with half-life of 14.6 min; 7.5 b for formation of ¹⁴² Pr in ground state
Nd	146	17.19	1.4	¹⁴⁷ Nd	10.98 d	91.10 (28.3), 531.0 (13.5)	¹⁴⁷ Pm → ¹⁴⁷ Sm ¹⁵³ Eu	INAA, RNAA	Long	
Sm	152	26.7	206	¹⁵³ Sm	46.27 h	103.18 (28.2)		INAA, RNAA	Short, long	
Eu	151	47.8	3,150	^{152m} Eu	9.3 h	121.78 (9.0), 841.6 (13.0), 963.5 (12.0)	¹⁵² Gd (72 %), ¹⁵² Sm (28 %)	INAA, RNAA	Short	^{152m} Eu is a metastable state of ¹⁵² Eu
						121.78 (33.2), 344.27 (31.4), 778.85 (15.2), 964.0 (17.3), 1,407.92 (24.3)				
			6,000	¹⁵² Eu	13.33 a			INAA, RNAA	Long	

Element	Isotope mass number	Nat. abundance (at%)	Activation cross section [b]	Product isotope	Half-life ^a	Analytical photopeaks [keV] ^b	Decay product(s)	Method	Irradiation time ^c	Comment
Gd	152	0.20	900	¹⁵³ Gd	239.47 d	97.50 (30.0), 103.20 (22.5)	¹⁵³ Eu	RNAA, rarely INAA	Long	
Tb	159	100	23.1	¹⁶⁰ Tb	72.3 d	86.79 (20.9), 298.54 (35.0)	¹⁶⁰ Dy	INAA, RNAA	Long	
Dy	164	28.2	2,700	¹⁶⁵ Dy	2.35 h	94.60 (4.0)	¹⁶⁵ Ho	RNAA, rarely INAA	Short	1,700 b for formation of metastable ^{165m} Dy which decays into the ground state with a half-life of 1.3 min; 1,000 b for formation of ¹⁶⁵ Dy
Ho	165	0	5,500	¹⁶⁶ Dy	81.5 h	82.45 (12.0)	¹⁶⁶ Ho	RNAA	Long	2,000 b for neutron capture of ^{165m} Dy, 3,500 b for neutron capture of ¹⁶⁵ Dy in the ground state
Er	165	100	61	¹⁶⁶ Ho	26.8 h	80.60 (5.4)	¹⁶⁶ Er	RNAA, rarely INAA	Long, short	
	170	14.9	6	¹⁷¹ Er	7.52 h	111.60 (25.0), 124.03 (11.0), 295.90 (28.0), 308.30 (63.0)	¹⁷¹ Tm → ¹⁷¹ Yb	RNAA	Long, short	
Tm	169	100	105	¹⁷⁰ Tm	128.6 d	84.26 (10.0)	¹⁷⁰ Yb	RNAA, rarely INAA	Long	
Yb	168	0.13	2,400	¹⁶⁹ Yb	32 d	63.50 (45.0), 110.00 (18.0), 130.70 (11.0), 177.00 (22.0), 197.80 (40.0), 307.50(10.0)	¹⁶⁹ Tm	INAA, RNAA	Long	

Element	Isotope mass number	Nat. abundance (at%)	Activation cross section [b]	Product isotope	Half-life ^a	Analytical photopeaks [keV] ^b	Decay product(s)	Method	Irradiation time ^c	Comment
	174	31.8	100	¹⁷⁵ Yb	4.2 d	113.50 (1.9), 282.60 (3.7), 396.10 (6.0)	¹⁷⁵ Lu	INAA, RNAA	Long, short	
Lu	176	2.59	1,780	¹⁷⁷ Lu	6.71 d	112.96 (6.5), 208.34 (11.0)	¹⁷⁷ Hf	INAA, RNAA (RNAA)	Long, short	
Y	89	100	1.25	⁹⁰ Y	64.1 h	1,760.7 (0.02)	⁹⁰ Zr			No useful γ -rays; requires β^- counting
Na	23	100	0.53	²⁴ Na	14.96 h	1,368.6 (100), 2,754.1 (98.85)	²⁴ Mg	INAA	Short, long	
Sc	45	100	27	⁴⁶ Sc	83.82 d	889.3 (100), 1,120.5 (100)	⁴⁶ Ti	INAA	Long	
Cr	50	4.345	16	⁵¹ Cr	27.7 d	320.1 (9.8)	⁵¹ V	INAA	Long	
Mn	55	100	13.3	⁵⁶ Mn	2.58 h	846.6 (99.0), 1,811.2 (30.0), 2,112.6 (15.5)	⁵⁶ Fe	INAA	Short	
Fe	58	0.28	1.3	⁵⁹ Fe	44.503 d	142.54 (0.81), 192.23 (2.80), 1,099.27 (56.0), 1,291.58 (44.0)	⁵⁹ Co	INAA	Long	
Co	59	100	37.2	⁶⁰ Co	5.272 a	1,173.23 (99.88), 1,332.52 (100)	⁶⁰ Ni	INAA	Long	
Sb	123	42.64	4.06	¹²⁴ Sb	60.3 d	602.71 (98.1), 722.78 (10.8), 1,691.04 (50.0)	¹²⁴ Te	INAA	Long	

Element	Isotope mass number	Nat. abundance (at%)	Activation cross section [b]	Product isotope	Half-life ^a	Analytical photopeaks [keV] ^b	Decay product(s)	Method	Irradiation time ^c	Comment
Cs	133	100	29	¹³⁴ Cs	2.06 a	569.33 (15.8), 604.7 (98.0), 795.79 (89.0)	¹³⁴ Ba	INAA	Long	
Hf	180	35.1	13	¹⁸¹ Hf	42.39 d	133.05 (41.0), 136.25 (6.9), 345.95 (12.0), 482.16 (83.0)	¹⁸¹ Ta	INAA	Long	
Ta	181	99.988	20	¹⁸² Ta	114.43 d	100.10 (11.9), 152.44 (7.1), 222.11 (7.98), 1,121.19 (37.0), 1,188.95 (17.1), 1,221.31 (28.9), 1,230.93 (12.1)	¹⁸² W	INAA	Long	
Th	232	100	7.37	²³³ Pa	27 d	98.44 (13.5), 111.0 (4.85), 300.11 (6.6), 311.9 (38.0), 340.47 (4.43)	²³³ U	INAA	Long	²³³ Th decays with a half-life of 22.3 m to ²³³ Pa which has a half-life of 27.0 d
U	238	99.2745	2.7	²³⁹ Np	2.355 d	99.5 (11.0), 103.7 (18.0), 106.13 (21.06), 117.7 (6.3), 228.19 (9.5), 277.6 (12.1)	²³⁹ Pu	INAA	Long, short	²³⁹ U decays with a half-life of 23.5 m to ²³⁹ Np which has a half-life of 2.355 d

^ah: hours, d: days, a: years.

^bBold face: preferred γ -line for analysis if two or more lines can be used; values in parentheses: relative intensities (in %).

^cShort: minutes, long: hours to days.

typical quantities being on the order of 100 mg. Pulverized samples can be put into aluminium or SiO₂ glass containers and sealed; coarse grains or chips can be simply wrapped in Al foil. For short irradiations or irradiation in reactors with low neutron fluxes polyethylene foil or vials may also be used. In high-flux reactors, polyethylene foil becomes brittle within several minutes. In addition, in the manufacturing process compounds of antimony are employed as catalysers (e.g. [32]), that are a source of high-energy γ -rays from the decay of ¹²⁴Sb and, consequently, cause an appreciable Compton background during counting. SiO₂ tubes and Al foil are available at very high purity, eliminating the need to transfer the irradiated samples to inactive containers before γ -ray counting. Safely encapsulating powder in Al foil, however, is difficult and thus not advisable. If low-purity Al containers are used, the samples must be transferred to inactive containers prior to γ -ray counting.

Although eq. (9.6) can be solved for N_X , the number of atomic nuclei of interest, thus making NAA an absolute analytical method, this equation is not practical to employ. First, the absolute value of the activity A_Y cannot be easily derived and depends upon the counting geometry (mainly the distance between sample and detector) and the efficiency of the detector. Second and more importantly, the neutron flux Φ is not precisely known and may fluctuate. Major- and minor-element isotopes of geological and biological samples (H, C, N, O, Na, Mg, Al, Si, P, S, Ca, Ti, Fe) have small cross sections for neutron absorption (less than a few barns). Therefore, it can be safely assumed that the neutron flux remains constant across a set of samples during irradiation. The neutron flux, however, varies as a function of distance in the core region of a reactor. Whereas flux variations across samples are small in the core of a large graphite-moderated reactor ($\leq 0.5\% \text{ cm}^{-1}$), they may reach $10\% \text{ cm}^{-1}$ in the core of a small water-moderated reactor [5]. These uncertainties are eliminated by the irradiation of two or more sets of standards and, sometimes, flux monitors together with the samples. The single-comparator method, NAA not further considered here, requires precise knowledge of γ -ray intensities, isotopic abundances, and thermal neutron cross sections from which a “ k_0 -factor” can be calculated [4, 33].

The flux monitor, NAA may be a thin rod or wire of a metal such as Fe, Co or Au. Short wires (few centimetres) may be wrapped around each sample in order to precisely record the neutron dose (flux \times time) at the position of the sample. Thin metal sheets may be placed inside aluminium cans, large containers used for irradiation, in between individual samples or layers of samples [3]. Flux monitors are recommended if samples are to be irradiated in small research reactors and accelerators and/or if the highest possible analytical precision is to be achieved.

Standards can be prepared from commercially available multi-element or single-element standard solutions for inductively coupled plasma mass spectrometry (ICP-MS) analysis. They may, of course, also be prepared by dissolving metals or compounds. If oxides are used, care has to be employed with regard to the exact stoichiometry. Terbium, for example, forms a stable oxide Tb₄O₇ instead of the normal REE₂O₃ composition. If stock solutions must be diluted, this should be done

shortly before use in order to minimize loss of elements by adsorption to the walls of polyethylene or PTFE containers. Appropriate quantities of the solutions may be pipetted on small sheets of high-purity Al foil or into SiO₂ glass containers and dried. Quantities varying between a few micrograms (Sm, Eu, Lu) and about 100 µg (Gd) are considered reasonable. This is at least one order of magnitude more than present in most geological samples. When combining several elements in preparing standards, interferences of γ-lines must be avoided. For example, uranium can often be measured in geological samples through the decay of ²³⁹Np (²³⁸U(n, γ)²³⁹U $\xrightarrow[23.5 \text{ m}]{\beta^-}$ ²³⁹Np $\xrightarrow[2.35 \text{ d}]{\beta^-}$ ²³⁹Pu), which has a half-life only slightly larger than ¹⁵³Sm and has a fairly intense photopeak at 103.70 keV that cannot be resolved from the 103.18 keV photopeak of ¹⁵³Sm. Moreover, neutron absorption by ²³⁵U causes fission, producing nuclides in the mass range of the light REE with high yields (Figure 9.4). Gd and Ho are subject to interference by second-order reactions of Eu and Dy; pure standards of Eu and Dy are required to correct for these interferences.

International reference standards should also be included in a set of samples in order to estimate the accuracy of the concentration data. As REEs (and other trace element concentrations) are vastly different in different types of geological materials, it is advisable to select a standard similar in composition to the samples, for example, a standard granite for the analysis of granites or a standard ultramafic rock for the analysis of peridotites. These rocks will have REE concentrations that typically differ by more than two orders of magnitude.

For the purpose of neutron irradiation in a reactor, the samples are packed into an aluminium can which may have a diameter of 1.5–3 cm and a length of ≈10 cm. About 10–40 samples fit into such a can, each ≈100-mg sample sealed in SiO₂ glass or an aluminium container. In order to correct for neutron flux gradients, the position of each sample and standard inside the can must be known. As the induced activity A_{γ} is a linear function of the neutron flux (eq. (9.6)) and as the irradiation time is the same for all samples and all standards, two sets of element standards, one set placed at the bottom and the other at the top of the irradiation can, are sufficient to correct for neutron flux variations by linear interpolation. More sets of standards or flux monitors, of course, will improve the flux correction at the cost of additional time for γ-ray counting. In large research reactors, the variation in neutron flux between top and bottom of an aluminium can with a length of 10 cm will typically be on the order of 10 % only.

9.4.3 Counting strategies

Before irradiating the samples, the subsequent counting strategies should be considered and irradiation parameters adjusted.

If all REEs are to be measured, radiochemical separation is indispensable. In this case, each sample is split into two portions. One split should be irradiated for a short

time (on the order of 10 min) and immediately (after a delay of no more than 1 h) be transferred to the radiochemistry laboratory. This split serves for γ -ray counting of ^{165}Dy and ^{166}Ho , and possibly ^{171}Er , $^{152\text{m}}\text{Eu}$, ^{140}La and ^{153}Sm . The second split should be irradiated for at least several hours up to about 1 week, depending upon the expected REE concentrations. After a delay of 1–2 days (“cooling time”), these samples are transferred to the laboratory for performing radiochemical separation of the REE and subsequent counting. The most critical isotope to be measured is ^{171}Er ($t_{1/2} = 7.52$ h); for its detection, not much more than 1 day (\approx three half-lives) should be allowed to pass between the end of irradiation and γ -ray counting, together with isotopes having half-lives less than about 1 week (^{142}Pr , ^{166}Ho , ^{140}La , ^{153}Sm , ^{175}Yb , ^{177}Lu). Two to 4 weeks later, after the short-lived activities have decayed, the longer lived nuclides can be measured, i.e. ^{147}Nd , ^{141}Ce , (^{177}Lu), ^{169}Yb , ^{160}Tb , ^{170}Tm , ^{153}Gd , and ^{152}Eu . ^{142}Pr and ^{140}La have no low-energy γ -lines; for their detection, a large-volume Ge(Li) or Ge detector is required. All other REE nuclides listed in Table 1.1 can, in principle, be analysed using a planar Ge detector. In the energy range below ≈ 150 keV, the planar detector is the preferred one due to its lower Compton background and better resolution.

If no radiochemistry laboratory is accessible or if other elements, in addition to the REE are to be measured, then the instrumental NAA method must be employed. In this case, the short irradiation is of little benefit as ^{56}Mn , and in favourable cases ^{165}Dy , are the only nuclides that cannot be detected in geological samples after the long irradiation. The long (hours to days) irradiation requires a cooling time of about 2 days or more before the first series of γ -ray counting can be started, targeting at ^{140}La , ^{153}Sm , ^{175}Yb , ^{177}Lu , ^{24}Na , and ^{239}Np . At that time, ^{24}Na may still constitute the main activity in many geological and biological samples (Figures 9.9(a) and 9.10(a)); its high-energy γ -rays contribute highly to the Compton background. The second γ -ray counting may take place about 3–5 weeks after the end of irradiation. At this time, the short-lived nuclides have decayed to negligible values and the Compton background of geological samples is now determined by ^{59}Fe and ^{46}Sc and, maybe, ^{60}Co (Figure 9.9(b)). Among the REEs, ^{141}Ce , ^{147}Nd , ^{152}Eu , ^{160}Tb and ^{169}Yb can now be expected to be detectable as shown in Figure 9.10(b and c) for the case of a volcanic rock.

As the behaviour of the REE in nature is predictable and mainly a function of the differences in ionic radii and, in the case of Ce and Eu, of oxygen fugacity, the REE patterns of rocks and minerals can commonly be constructed from the elements accessible by INAA. Under reducing conditions, a portion of the Eu will be divalent, giving rise to Eu behaving differently from Sm or Gd, visible as a Eu “anomaly” in many rocks. The magnitude of this anomaly can only be interpolated between Sm and Tb as Gd cannot be measured precisely by INAA. Moreover, the ^{153}Gd photopeak at 97.5 keV is interfered by the 98.44 keV photopeak of ^{233}Pa (from the decay of ^{233}Th , Figure 9.10(c)). For measuring Gd by INAA, it therefore is useful to let ^{233}Pa decay for about half a year (7 half-lives of this isotope) – if time is not essential.

9.4.4 Radiochemical neutron activation analysis (RNAA) – a fast separation scheme

Radiochemical neutron activation involves the separation of the elements of interest from the matrix activity. At the time when the samples arrive at the laboratory, 1 or 2 days after the end of irradiation, geological and biological materials are highly radioactive. All chemical work, therefore, must be carried out minimizing the exposure of the operator to the radiation. This includes manipulating the samples behind

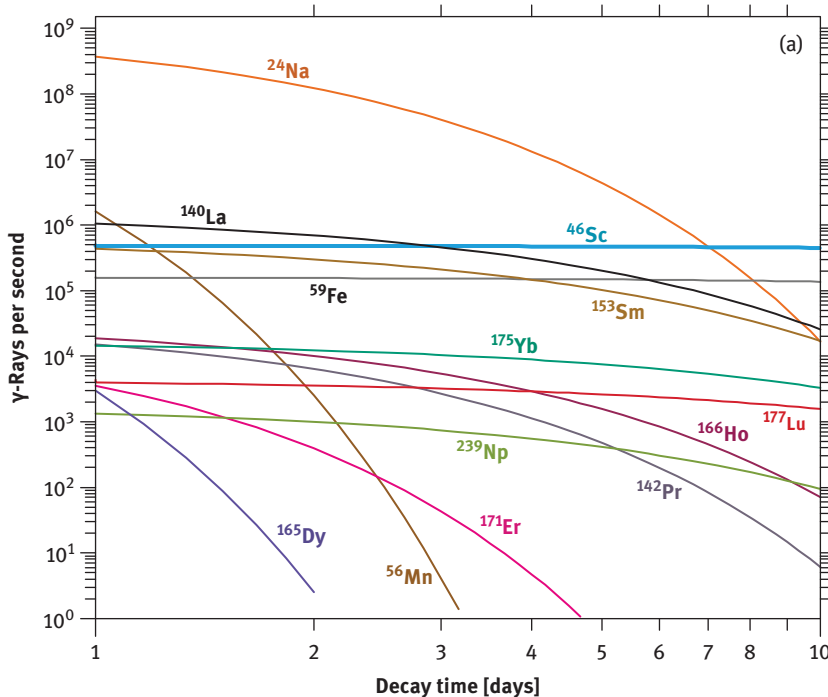


Figure 9.9: γ -Activities of a number of nuclides as a function of cooling time for the international standard rock basalt BCR-1 released by the US Geological Survey, the supply of which is long exhausted. For each nuclide, only the activity of the main γ -ray, displayed in boldface in Table 9.1, has been calculated as $A = \lambda \times N \times$ relative intensity (where more than one γ -line is highlighted, the one with the higher intensity was used, except for ^{239}Np (277.6 keV)). The energy-dependent efficiency of the detectors has not been considered. Calculations were performed for a thermal neutron flux of $5 \times 10^{13} \text{ cm}^{-2} \text{ s}^{-1}$ and an irradiation time of 24 h. Recommended concentrations in BCR-1 are Na 2.43, Sc 32.8, Mn 1410, Fe 9.41, Co 36.3, La 25.0, Ce 53.7, Pr 6.9, Nd 28.7, Sm 6.58, Eu 1.96, Gd 6.68, Tb 1.05, Dy 6.35, Ho 1.11, Er 3.61, Tm 0.59, Yb 3.39, Lu 0.512, Hf 4.90, Ta 0.79, Th 6.04, U 1.71 (all values in ppm, except Na and Fe in %) [34]. Although many of these activities are high, be aware that only a small fraction of the γ -rays are registered by the detector. In INAA, the activity is dominated by ^{24}Na during the first week after irradiation. Afterwards, ^{46}Sc , ^{59}Fe and ^{60}Co are the main contributors. All these nuclides release high-energy γ -rays during decay, thus causing a high Compton background, in particular in the large-volume Ge detector.

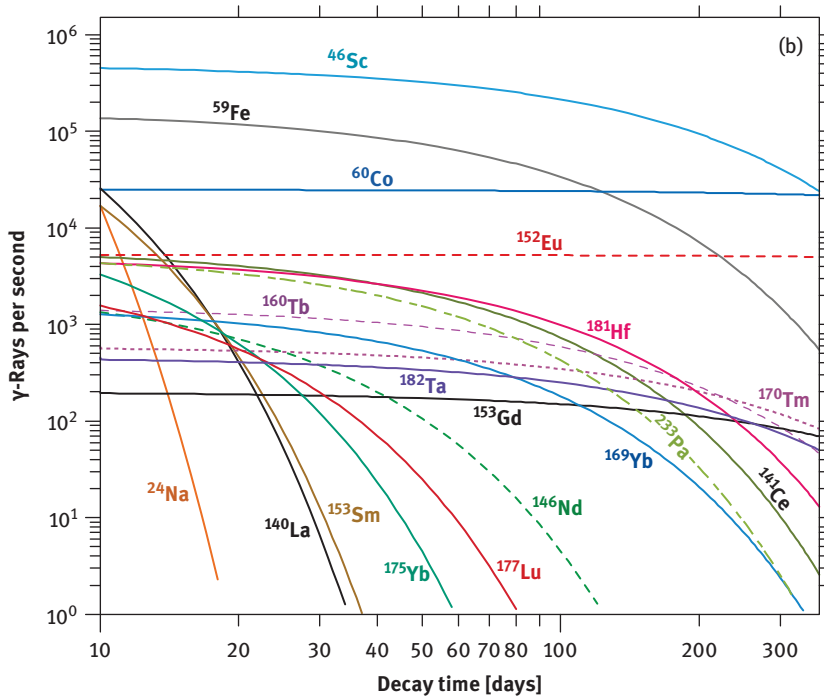


Figure 9.9: (continued)

protective shielding (usually made by bricks of lead, about 5 cm thick) and following a quick-and-dirty chemical procedure. As all chemicals that are used during digestion of the samples and separating the REE are inactive, there is little danger of introducing contamination, except through cross-contamination between samples. Prior to the development of the high-resolution Ge detectors, all REE had to be separated from one another which involved time- and labour-consuming extraction or ion-exchange techniques [35, 36]. With the advent of the coaxial Ge(Li) and planar Ge detectors, the chemical work was reduced to separate the REE as a group from the matrix. At the University of Cologne, we have applied the separation technique outlined in Figure 9.11 and described in more detail by Carl [37]. In many geological samples, ^{46}Sc accounts for the main activity between about 1 week and 1 year after the end of irradiation. It is, therefore, indispensable to remove at least the major portion of ^{46}Sc from the REE. We achieved this by precipitating Sc using phytic acid [38]. Chemical yields of the REE were typically between about 90 % and 95 % as determined from the analysis of international reference materials or by re-irradiation and γ -ray counting of samples. To our experience, two people working together can process about 20 samples in 10 h.

By employing this separation scheme and irradiating $\approx 10^{-1}$ g of sample at a flux of 8×10^{13} n cm $^{-2}$ s $^{-1}$, we were able to analyse the REE in minerals from peridotites containing ppb levels of the REE only (Figure 9.12). Even sub-ppb levels are accessible

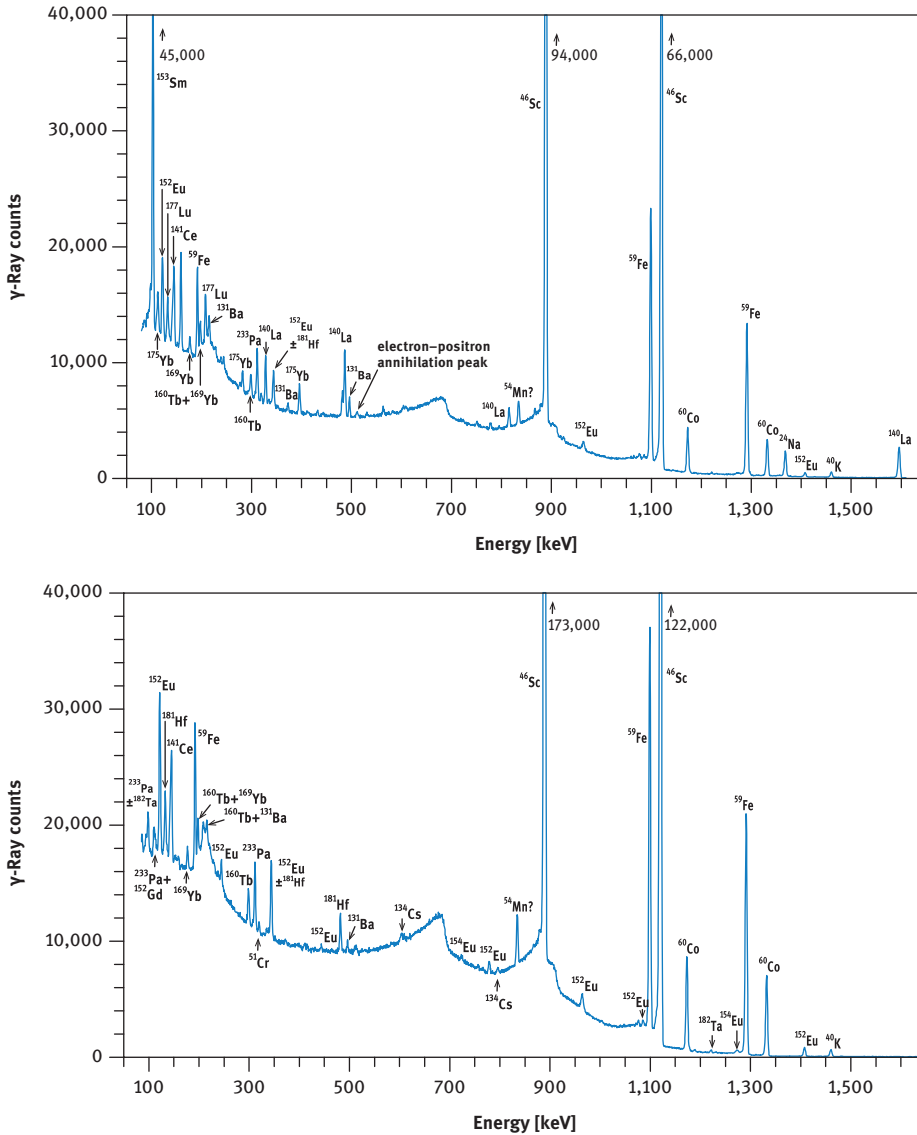


Figure 9.10: γ -Ray spectra of international reference rock basalt BCR-1. (a) Spectrum taken with a coaxial Ge(Li) detector about 8 days after end of irradiation, (b) spectrum taken with a coaxial Ge(Li) detector about 30 days after end of irradiation, (c) part of spectrum taken with a planar Ge detector about 28 days after end of irradiation. Irradiation conditions: neutron flux $5 \times 10^{13} \text{ cm}^{-2} \text{ s}^{-1}$ for 12 h at the research reactor “DIDO” of the former “Kernforschungsanlage Jülich” (now “Forschungszentrum Jülich”) in September 1993. γ -Ray counting was performed at the former “Institut für Kernchemie”, University of Cologne. The dead time of the counting system was kept below 3 % by adjusting the distance between sample and detector. Counting times were 3 h (a), 4 h (b) and 10 h (c).

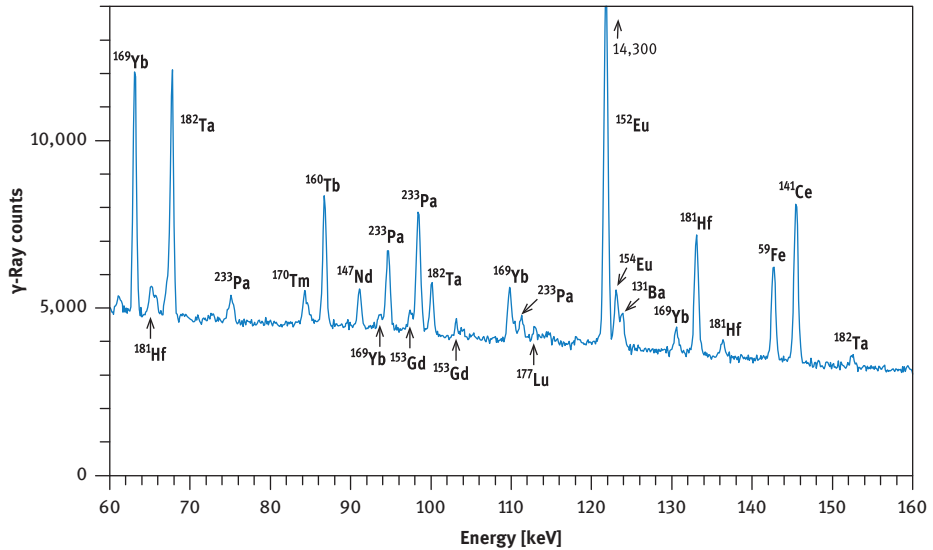


Figure 9.10: (continued)

1. transfer sample to Ni crucible & add 20 mg of inactive REE_2O_3 carrier (containing all REE) + 2 mg Sc_2O_3
- ↓
2. fuse with 5 g NaOH + 1 g Na_2O_2 for 5 minutes
- ↓
3. transfer melt quantitatively to glass beaker containing 50–100 ml H_2O and stir / shake gently
- ↓
4. transfer contents to centrifuge vial and centrifuge for ≈ 5 minutes; discard supernatant solution
- ↓
- 4a. wash precipitate with water, centrifuge and again discard supernatant solution
- ↓
5. dissolve the precipitate in ≈ 1 n HCL; dilute with H_2O to a volume of ≈ 100 ml
- ↓
6. add phytic acid ($\text{C}_6\text{H}_{18}\text{O}_{24}\text{P}_6$) or its K-salt to precipitate Sc; centrifuge & discard precipitate
- ↓
- 6a. again add Sc carrier and repeat previous step (for ultramafic rocks only)
- ↓
7. add HF to the clear solution to precipitate REE as fluorides; it helps to heat (not boil) the solution
- ↓
8. centrifuge precipitate, then transfer it with H_2O on filter paper ($\varnothing 15$ mm), dry gently and seal in polyethylene foil
- ↓
9. start γ -ray counting

Figure 9.11: Separation scheme for REE from silicate minerals and rocks (modified after [37]). Steps 4a and 6a should be included if samples with very low REE concentrations are processed.

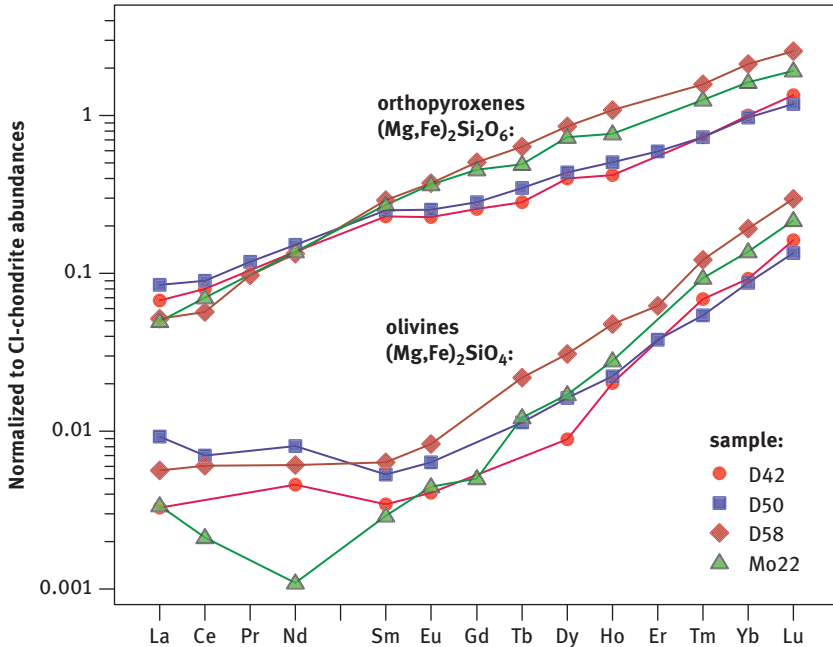


Figure 9.12: REE in olivines $(\text{Mg, Fe})_2\text{SiO}_4$ and orthopyroxenes $(\text{Mg, Fe})_2\text{Si}_2\text{O}_6$ from peridotites (redrawn from data published in Ref. [39]). Peridotites are rocks from the Earth's upper mantle brought to the surface as inclusions in basaltic volcanic rocks. REE were separated from the matrix (sample weights between 100 and 300 mg) according to the procedure outlined in Figure 9.11. CI-chondrite normalization values from Ref. [40]. The sample with the lowest REE concentration has REE abundances corresponding to detected quantities of approximately 1 ng for La, 1.5 ng for Ce, 0.7 ng for Nd and 0.5 ng for Sm. Even lower concentrations were observed in spinel $(\text{Mg, Fe})(\text{Al, Cr})_2\text{O}_4$, corresponding to detected quantities of ≈ 0.06 ng for La, 0.03 ng for Sm and 0.06 ng for Lu [39]. The patterns indicate crystal-chemical control of REE^{3+} incorporation into the lattice of olivine and orthopyroxene with the largest of the REE being most strongly excluded from incorporation. Higher than expected concentrations of the light REE in olivine are likely to be due to physical contamination, in particular fluid inclusions.

for the most sensitive elements La, Sm, Eu, Yb and Lu. In contrast, by INAA, we would have detected only Eu, Yb and Lu in orthopyroxene and none of the REE in olivine.

9.4.5 Data reduction and sources of error

Data reduction following γ -ray spectroscopy comprises calculation of the peak area and standard error. This procedure is comparable to the task encountered in energy-dispersive X-ray spectroscopy and is discussed in detail by Potts [3]. In most cases (La, Ce, Nd, Sm, Eu, Tb, Yb and Lu in INAA and all REE in RNAA), well-resolved γ -ray lines can be chosen to evaluate the net peak area by subtracting the interpolated

background from the total peak area. Deconvolution of photopeaks is rarely required. As the 1σ -error is estimated from the square root of γ -ray counts of total peak as well as background, 1σ of the net peak area N_{Peak} is calculated as $\sqrt{N_{\text{Peak}} + 2N_{\text{Background}}}$. As the background is particularly high at low energies (Figures 9.10(a–c)), its value may contribute more to the total error in this region than the photopeak, at least in INAA. If the counts at the background are of the same magnitude as the net peak area, a couple of thousand counts must be accumulated for the net peak area in order to keep the standard error below about 3 %. At high energies, the background is low and the error of a photopeak is determined by the number of counts in the peak, but due to the much lower efficiency of the detector at high energies, the number of counts is much smaller, again leading to higher 1σ -errors. The energy dependence of the efficiency is seen in Figure 9.10(a) by comparing the γ -lines of ^{140}La at 487 keV and 1,596 keV. According to Table 9.1, the 1,596 keV line should be more intense by about a factor of two compared to the 487-keV line, whereas in Figure 9.10(a) the latter line is the stronger one (by a factor of 1.85 if counts under the peak area are calculated and if the obvious interference at slightly lower energy is incorrectly included as ^{140}La).

Although NAA is poor in interferences, NAA from competing reactions leading to the formation of the same nuclide, caution must be exercised when analysing Gd and Ho. “Second-order reactions” may severely enhance the signals of ^{153}Gd and ^{166}Ho [41, 42]. Such interferences arise during long irradiations and/or high neutron fluxes, when a radioactive nuclide $^{A+1}_Z\text{X}$, formed during irradiation from a stable isotope ^A_ZX of element X, decays into a stable isotope $^{A+1}_{Z+1}\text{Y}$, the (n, γ) -reaction of which – producing $^{A+2}_{Z+1}\text{Y}$ – is used to determine the concentration of element Y. Alternatively, $^{A+1}_Z\text{X}$ may capture another neutron to form $^{A+2}_Z\text{X}$ which decays into $^{A+2}_{Z+1}\text{Y}$.

Second-order activation can be calculated from the Bateman–Rubinson equation [5, 43]:

$$N_n(t) = \Lambda_1^* \times \Lambda_2^* \times \dots \times \Lambda_{n-1}^* \times N_1^0 \times \sum_{i=1}^n C_i \times e^{(-\Lambda_i \times t)} \quad (9.10)$$

where $N_n(t)$ is the number of nuclides $^{A+2}_{Z+1}\text{Y}$ produced after irradiation time t in a reactor from the interfering reaction, N_1^0 is the initial number of (inactive) nuclides ^A_ZX . $\Lambda_i = \lambda_i + \sigma_i \times \Phi$ and $\Lambda_i^* = \lambda_i^* + \sigma_i^* \times \Phi$ where λ_i is the decay constant of nuclide i , λ_i^* is the partial decay constant (producing, e.g. ^{152}Gd from $^{152\text{m}}\text{Eu}$, whereas λ_i is the total decay constant, generating $^{152}\text{Gd} + ^{152}\text{Sm}$ from $^{152\text{m}}\text{Eu}$), σ_i is the total reaction cross section and σ_i^* the partial cross section (leading, e.g. from ^{151}Eu to $^{152\text{m}}\text{Eu}$, whereas σ_i is the value leading from ^{151}Eu to $^{152\text{m}}\text{Eu} + ^{152}\text{Eu}$); Φ is the neutron flux.

The factors C_i are defined as

$$C_i = \prod_{j=1}^i \frac{1}{\Lambda_j - \Lambda_i} \quad (j \neq i)$$

In the above example, $n = 4 \left({}^A_Z X, {}^{A+1}_Z X, {}^{A+1}_{Z+1} Y, {}^{A+2}_{Z+1} Y \right)$, C_1 is then calculated as

$$C_1 = \frac{1}{\Lambda_2 - \Lambda_1} \times \frac{1}{\Lambda_3 - \Lambda_1} \times \frac{1}{\Lambda_4 - \Lambda_1}.$$

${}^{151}\text{Eu}$ possesses a cross section of 3,150 b to form ${}^{152\text{m}}\text{Eu}$. About three quarters of this nuclide decay with a half-life of 9.3 h into stable ${}^{152}\text{Gd}$ (Table 9.1). Whereas ${}^{151}\text{Eu}$ has a natural abundance of almost 50 %, the abundance of ${}^{152}\text{Gd}$ is only 0.20 %. For a sample with a chondritic abundance ratio of Gd/Eu (≈ 3.5), irradiating a sample at a flux of $5 \times 10^{13} \text{ n cm}^{-2} \text{ s}^{-1}$ for just 1 day enhances the total amount of ${}^{153}\text{Gd}$ by more than 10 %. For an elemental Eu/Gd ratio of 1:1 the increase is about 50 % and a neutron flux of $1 \times 10^{14} \text{ n cm}^{-2} \text{ s}^{-1}$ will almost double the ${}^{153}\text{Gd}$ signal (Figure 9.13). Five days of irradiation at $5 \times 10^{13} \text{ n cm}^{-2} \text{ s}^{-1}$ will more than double the ${}^{153}\text{Gd}$ signal for a chondritic Eu/Gd ratio and increase it by a factor of 4 for a 1:1 ratio. A standard of pure Gd must

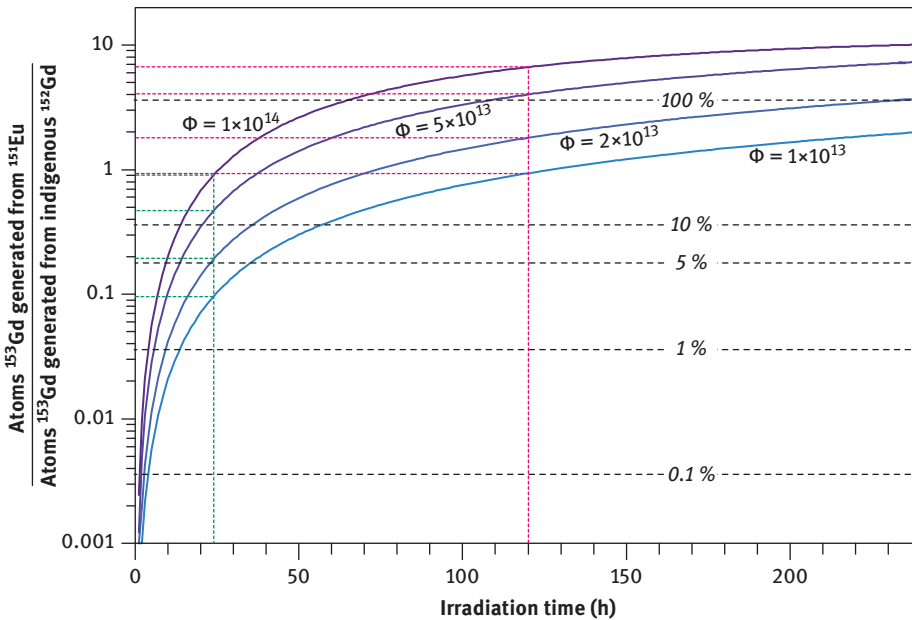


Figure 9.13: Interference from ${}^{151}\text{Eu}$ on the ${}^{153}\text{Gd}$ signal as a function of irradiation time and neutron flux as computed from eq. (9.10). ${}^{153}\text{Gd}$, activated from ${}^{152}\text{Gd}$ indigenous to the sample, was calculated from eq. (9.3). The y-axis has been scaled to a 1:1 elemental Eu/Gd ratio. Most geological samples will have lower ratios, closer to the chondritic one ($\approx 1/3.5$, chondritic ratios are indicated by black broken lines). Green and red broken lines serve to illustrate the interference for irradiation times of 1 and 5 days, respectively. Calculations have been carried out employing the Bateman–Rubinson equation [5, 43], using isotopic abundances, activation cross sections and half-lives as given in Table 9.1. For equal concentrations of Eu and Gd in a sample, for example, 1 ppm, irradiating the sample for 1 day at a neutron flux of $1 \times 10^{13} \text{ n cm}^{-2} \text{ s}^{-1}$ will increase the ${}^{153}\text{Gd}$ signal by about 10 % whereas irradiation at a flux of $1 \times 10^{14} \text{ n cm}^{-2} \text{ s}^{-1}$ will almost double the signal.

be used to correct for this interference by counting ^{152}Eu and ^{153}Gd in standard and unknowns. Reducing the irradiation time to much less than one day or the neutron flux is not a good option in this case in view of the long half-life of ^{153}Gd and, hence, its low activity (compare Figure 9.9).

^{164}Dy forms ^{165}Dy by neutron capture with a cross section of 2,700 b which decays into stable ^{165}Ho with a half-life of 2.35 h, thus increasing the concentration of Ho as a function of irradiation time and neutron flux in the reactor. ^{165}Dy may also capture another neutron ($\sigma = 3,500$) to form ^{166}Dy , which decays into ^{166}Ho with a half-life of 81.5 h, about three times longer than the half-life of ^{166}Ho . This has the consequence that the interference of Dy on the determination of the Ho content is not only dependent upon the neutron flux and duration of irradiation but also on the time when the decay of ^{166}Ho is counted. The interference can only be kept small (<3 %) if the sample is irradiated for no longer than about 1 h and γ -ray counting is carried out within about three half-lives of ^{166}Ho [42].

A second source of error arises from the presence of uranium in a sample if its concentration matches, or is even higher than, those of Ce and Nd (see also Section 9.3.1.1). In these cases fission of ^{235}U by thermal neutrons produces fragments with masses within the range of the light REE (Figure 9.4). Particularly high, for our concern, are the fission yields Y_i for masses 140 (6.268 %), 141 (5.837 %), 142 (5.796 %) and 147 (2.265 %). Initially, these nuclides have an excess number of neutrons, leading them to decay by β^- emission into stable nuclides. The decay of nuclide 142 ends at stable ^{142}Ce , thus shielding ^{142}Pr from being affected by U fission (Figure 9.8). The decay of nuclide 140 is somewhat modulated by ^{140}Ba due to its half-life of 12.75 d. As ^{140}La is analysed within a few days after the end of irradiation and $\sigma_{(n,\gamma)}$ is much higher for ^{139}La than for ^{140}Ce and ^{147}Nd , contribution from fission of ^{235}U is expected to remain small. No long-lived nuclides, however, are encountered during decay of nuclides 141 and 147 until they reach ^{141}Ce and ^{147}Nd .

The activity ratio of ^{141}Ce produced by fission of ^{235}U relative to ^{141}Ce produced by the (n, γ) reaction from ^{140}Ce can be estimated from eq. (9.5):

$$\frac{A_{235\text{U}}(n, f)}{A_{141\text{Ce}}(n, \gamma)} = \frac{\sigma_{(n,f)} \times \Phi \times N_{235\text{U}} \times Y_{i141} (1 - e^{-\lambda_{141} \times t})}{\sigma_{(n,\gamma)} \times \Phi \times N_{140\text{Ce}} \times (1 - e^{-\lambda_{141} \times t})}$$

The neutron flux Φ and the irradiation time, of course, are identical for uranium and cerium in the sample. The equation thus simplifies to

$$\frac{A_{235\text{U}}(n, f)}{A_{141\text{Ce}}(n, \gamma)} = \frac{\sigma_{(n,f)} \times N_{235\text{U}} \times Y_{i141}}{\sigma_{(n,\gamma)} \times N_{140\text{Ce}}} = \frac{\sigma_{(n,f)} \times (c_{235\text{U}}/U_{\text{at. weight}}) \times \text{Ab}_{235\text{U}} \times N_{\text{Av}} \times Y_{i141}}{\sigma_{(n,\gamma)} \times (c_{140\text{Ce}}/\text{Ce}_{\text{at. weight}}) \times \text{Ab}_{140\text{Ce}} \times N_{\text{Av}}}$$

where c stands for concentrations, Ab for isotope abundances and N_{Av} for Avogadro's number. If concentrations of U and Ce are equal, this results in

$$\frac{A_{235\text{U}}(n, f)}{A_{141\text{Ce}}(n, \gamma)} = \frac{586 \times (1/238.03) \times 0.0072 \times 0.06268}{0.58 \times (1/140.115) \times 0.8848} = 0.30$$

For the contribution to ^{147}Nd from fission of ^{235}U in the case of equal concentrations the result is

$$\frac{A_{^{235}\text{U}}(n, f)}{A_{^{141}\text{Ce}}(n, \gamma)} = \frac{586 \times (1/238.03) \times 0.0072 \times 0.02265}{1.4 \times (1/144.24) \times 0.1719} = 0.24$$

Interferences of this magnitude can be corrected reasonably well by γ -counting of ^{239}Np , ^{141}Ce and ^{147}Nd in uranium standards and samples, provided that concentrations of Ce, Nd and U are at least on the order of 10^1 ppm to allow γ -ray counting by INAA with small statistical errors. For most geological materials fission interference is much smaller. The averages concentrations of the continental crust are estimated at 1.3 ppm U, 43 ppm Ce and 20 ppm Nd [44]. The basalt standard BCR-1 contains only 1.7 ppm U compared to 53.7 ppm Ce and 28.7 ppm Nd [34]. In alkaline rocks such as syenites, however, uranium may become strongly enriched. For example, for the international standard syenite SY-2 a U concentration of 284 ppm is given, compared to 73 ppm Nd [45]. In NAA of this rock, the contribution from ^{235}U fission to the ^{147}Nd photopeak would match the contribution from ^{146}Nd . Analysing the light REE in uranium ores, Gd in compounds of Eu, and Ho in compounds of Dy by NAA without pre-irradiation chemical separation would surely be a challenge.

9.5 Conclusion

NAA is an effective and sensitive tool for REE analysis. Its role is nowadays greatly diminished by the decommissioning of nuclear research reactors in parts of the world as well as by the development of competitive techniques, namely ICP-MS. NAA is a true multi-element technique capable of routinely determining the concentrations of some 15–20 elements in geological samples. In ICP-MS, great care must be exercised to ensure dissolution of all minerals in rocks using high-purity acids, in particular zircon, which may contain a significant portion of the heavy REE. Both INAA and RNAA are little susceptible to contamination because no pre-irradiation treatment of samples is necessary. On the other hand, NAA takes a long time to complete (1 month or more) due to the necessity of letting short-lived activities decay in order to decrease the background during γ -ray counting. Potential health risks of the analyst through exposure to γ - and β^- radiation must also be considered as well as the requirements for disposing nuclear waste when selecting an analytical method for REE analysis.

Acknowledgements

I am grateful to the staff of the Institut für Kernchemie, in particular U. Herpers, Universität zu Köln/Germany, where I was able to carry out NAA from 1976 until 1993. I extend my thanks to the people in charge of the two research reactors “MERLIN” and “DIDO” of the former “Kernforschungsanlage Jülich” – which both are now decommissioned.

References

- [1] Hevesy G, Levi H. The action of neutrons on the rare earth elements. Det Kgl Danske Videnskabernes Selskab, Matematisk-fysiske Meddelelser 1936, XIV, 5, 1–34.
- [2] Hevesy G, Levi H. Action of slow neutrons on rare earth elements. Nature 1937, 137, 185.
- [3] Potts PJ. A Handbook of Silicate Rock Analysis. Glasgow, Blackie, 1992.
- [4] Neutron Activation Analysis. <http://www.naa-online.net/> (accessed: 26 November 2015).
- [5] De Soete D, Gijbels R, Hoste J. Neutron Activation Analysis. London, John Wiley & Sons, 1972.
- [6] Gladney ES, Curtis DB, Perrin DR. Determination of selected rare earth elements in 37 international geochemical reference materials by instrumental thermal neutron capture prompt gamma-ray spectrometry. Geostand News 1985, 9, 25–30.
- [7] Baer HW, Reidy JJ, Wiedenbeck ML. The decay of ^{140}La to levels in ^{140}Ce . Nucl Phys A 1968, 113, 33–56.
- [8] Simonits A, De Corte F, Hoste J. Single-comparator methods in reactor neutron activation analysis. J Radioanal Nucl Chem 1975, 24, 31–46.
- [9] Moens L, et al. k_0 -measurements and related nuclear data compilation for (n, γ) reactor neutron activation analysis. J Radioanal Nucl Chem 1984, 82, 385–452.
- [10] De Corte F. The standardization of standardless NAA. J Radioanal Nucl Chem 2001, 248, 13–20.
- [11] Pfennig G, Klewe-Nebenius H, Seelmann-Eggebert W. Karlsruher Nuklidkarte (Chart of the Nuclides). Lage, Marktdienste Haberbeck, 1995.
- [12] Ila P, Jagam P, Muecke GK. Multielement analysis of uraniferous rocks by INAA: Special reference to interferences due to uranium and fission of uranium. J Radioanal Chem 1983, 79, 215–32.
- [13] International Atomic Energy Agency. (ed) Neutron Generators for Analytical Purposes. Vienna, International Atomic Energy Agency, 2012, 162.
- [14] Reijonen J, et al. First PGAA and NAA experimental results from a compact high intensity D–D neutron generator. Nucl Instrum Methods Phys Res Sect A 2004, 522, 598–602.
- [15] Bergaoui K, et al. Development of a new deuterium–deuterium (D–D) neutron generator for prompt gamma-ray neutron activation analysis. Appl Radiat Isot 2014, 94, 319–27.
- [16] Bergaoui K, et al. Prompt gamma-ray neutron activation analysis of boron using Deuterium–Deuterium (D–D) neutron generator. J Radioanal Nucl Chem 2015, 303, 115–21.
- [17] Filby RH. Isotopic and nuclear analytical techniques in biological systems: A critical study. Part IX. Neutron activation analysis. Pure Appl Chem 1995, 67, 1929–41.
- [18] Řanda Z, Kučera J, Mizera J, Frána J. Comparison of the role of photon and neutron activation analyses for elemental characterization of geological, biological and environmental materials. J Radioanal Nucl Chem 2007, 271, 589–96.
- [19] NaI scintillation detector. http://www.horiba.com/uploads/media/RE09-18-098_03.pdf (accessed 5 August 2015).
- [20] Haskin LA, Wildeman TR, Haskin MA. An accurate procedure for the determination of the rare earths by neutron activation. J Radioanal Chem 1968, 1, 337–48.
- [21] Tavendale AJ, Ewan GT. A high resolution lithium-drift germanium gamma-ray spectrometer. Nucl Instrum Methods 1963, 25, 185–7.
- [22] Ewan GT, Tavendale AJ. Application of high resolution lithium-drift germanium gamma-ray spectrometers to high energy gamma-rays. Nucl Instrum Methods 1964, 26, 183–6.
- [23] Luke PN, Amman M, Tindall C, Lee JS. Recent developments in semiconductor gamma-ray detectors. J Radioanal Nucl Chem 2005, 264, 145–53.
- [24] Gamma ray spectrometry. <http://www.cnstn.nrrt.tn/afra-ict/NAT/gamma/html/Gamma%20Spec%20V1.pdf> (accessed 4 August 2015).
- [25] Review of the physics of semiconductor detectors. [http://www.ortec-online.com/download/Review of the Physics of Semiconductor Detectors.pdf](http://www.ortec-online.com/download/Review%20of%20the%20Physics%20of%20Semiconductor%20Detectors.pdf) (accessed 7 August 2015).

- [26] Kossert K, Jörg G, Nähle O, Lierse v. Gostomski C. High-precision measurement of the half-life of ^{147}Sm . *Appl Radiat Isot* 2009, 67, 1702–6.
- [27] Scherer EE, Münker C, Mezger K. Calibration of the lutetium–hafnium clock. *Science* 2001, 293, 683–7.
- [28] Tanimizu M. Geophysical determination of the ^{138}La β^- decay constant. *Phys Rev C: Nucl Phys* 2000, 62, 017601, 1–4.
- [29] Erdtmann G, Soyka W. The gamma-ray lines of radionuclides, ordered by atomic and mass number. Part I. $Z = 2 - 57$ (Helium–Lanthanum). *J Radioanal Nucl Chem* 1975, 26, 375–495.
- [30] Erdtmann G, Soyka W. The gamma-ray lines of radionuclides, ordered by atomic and mass number, Part II. $Z = 58 - 100$ (Cerium – Fermium). *J Radioanal Nucl Chem* 1975, 27, 137–286.
- [31] The Lund/LBNL nuclear data search. <http://nucleardata.nuclear.lu.se/toi/> (accessed 7 December 2015).
- [32] Shotykh W, Krachler M, Chen B. Contamination of Canadian and European bottled waters with antimony from PET containers. *J Environ Monit* 2006, 8, 288–92.
- [33] De Corte F, et al. Recent advances in the k_0 -standardization of neutron activation analysis: extensions, applications, prospects. *J Radioanal Nucl Chem* 1993, 169, 125–58.
- [34] Gladney ES, Burns CE, Roelandts I. 1982 compilation of elemental concentrations in eleven United States Geological Survey rock standards. *Geostand Newsl* 1983, 7, 3–226.
- [35] Schmitt RA, Mosen AW, Suffredini CS, Lasch JE, Sharp RA, Olehy DA. Abundances of the rare-earth elements, lanthanum to lutetium, in chondritic meteorites. *Nature* 1960, 186, 863–6.
- [36] Haskin LA, Frey FA. Dispersed and not-so-rare earths. *Science* 1966, 152, 299–314.
- [37] Carl C. Neutronenaktivierungsanalytische Untersuchungen über die Verteilung der Seltenen Erden und anderer Spurenelemente in kohligen Chondriten und in metamorphen Gesteinen der Ostalpen. Universität zu Köln, 1979, 181.
- [38] Beck G. Die scandiumspezifische Gruppe der Pyrophosphorsäuren. *Mikrochemie* 1951, 36–37, 790–2.
- [39] Stosch H-G. Rare earth element partitioning between minerals from anhydrous spinel peridotite xenoliths. *Geochim Cosmochim Acta* 1982, 46, 793–811.
- [40] McDonough WF, Sun S-S. Composition of the earth. *Chem Geol* 1995, 120, 223–53.
- [41] Kubota M. Interferences by neutron induced second order nuclear reaction in activation analysis of rare earths. *J Radioanal Chem* 1977, 36, 565–76.
- [42] Kramar U. The importance of second order activation in the determination of trace elements in geological samples by instrumental neutron activation analysis. *Geochim Cosmochim Acta* 1980, 44, 379–82.
- [43] Rubinson W. The equations of radioactive transformation in a neutron flux. *J Chem Phys* 1949, 17, 542–7.
- [44] Rudnick RL, Gao S. Composition of the continental crust, in: Rudnick RL (ed.) *The Crust*. Oxford, Elsevier–Pergamon, 2005, 1–64.
- [45] Gladney ES, Roelandts I. 1988 compilation of elemental concentration data for CCRMP Reference Rock Samples SY-2, SY-3 and MRG-1. *Geostand Newsl* 1990, 14, 373–458.

Sven Sindern and F. Michael Meyer

10 Automated Quantitative Rare Earth Elements Mineralogy by Scanning Electron Microscopy

Abstract: Increasing industrial demand of rare earth elements (REEs) stems from the central role they play for advanced technologies and the accelerating move away from carbon-based fuels. However, REE production is often hampered by the chemical, mineralogical as well as textural complexity of the ores with a need for better understanding of their salient properties. This is not only essential for in-depth genetic interpretations but also for a robust assessment of ore quality and economic viability. The design of energy and cost-efficient processing of REE ores depends heavily on information about REE element deportment that can be made available employing automated quantitative process mineralogy.

Quantitative mineralogy assigns numeric values to compositional and textural properties of mineral matter. Scanning electron microscopy (SEM) combined with a suitable software package for acquisition of backscatter electron and X-ray signals, phase assignment and image analysis is one of the most efficient tools for quantitative mineralogy. The four different SEM-based automated quantitative mineralogy systems, i.e. FEI QEMSCAN and MLA, Tescan TIMA and Zeiss Mineralogic Mining, which are commercially available, are briefly characterized.

Using examples of quantitative REE mineralogy, this chapter illustrates capabilities and limitations of automated SEM-based systems. Chemical variability of REE minerals and analytical uncertainty can reduce performance of phase assignment. This is shown for the REE phases parisite and synchysite. In another example from a monazite REE deposit, the quantitative mineralogical parameters surface roughness and mineral association derived from image analysis are applied for automated discrimination of apatite formed in a breakdown reaction of monazite and apatite formed by metamorphism prior to monazite breakdown.

SEM-based automated mineralogy fulfils all requirements for characterization of complex unconventional REE ores that will become increasingly important for supply of REEs in the future.

10.1 Introduction

The Rare Earth Elements (REEs) comprise the lanthanides, a group of 15 metals, as well as Sc and Y because they tend to occur in the same mineral assemblage as the lanthanides and exhibit similar chemical properties. All the rare earths except Pm are available in the geological environment. Following a common pattern within the periodic table, the lanthanides with even atomic numbers are more common in nature, and in general, REE with lower atomic numbers are more common

ionic constituents in REE minerals and occur in greater abundance than the REE with higher atomic numbers. The trends in the Earth's crustal abundance suggest a division between light and heavy REEs [1]. Although variation exists, commonly the lanthanides are subdivided according to their atomic weight into light rare earths (LREEs) comprising La through Gd, and heavy rare earths (HREEs) including Tb through Lu, and Y.

Industrial consumption of REE indicates that demand is driven by the rapid development of emerging industries. These include hybrid electric vehicles and wind power generation, which rely on the use of rare earths such as Nd for permanent magnets. Other consumer sectors include FCC catalysts, battery alloys, metallurgical products, phosphors, ceramics, catalytic converters, as well as chemical, military and satellite industries [2].

Given this global demand for green and sustainable products in energy, military and manufacturing industries, REE demand throughout the world is projected to increase. Consequently, the REEs are increasingly becoming more attractive commodity targets for the mineral industry. Almost all current mine production of REEs is derived from less than ten minerals, and in particular, bastnaesite, monazite and xenotime [3]. There is, however, a problem especially with monazite as it may contain deleterious impurities like Th, which imparts an unwanted radioactivity to the ores. The cost of handling and disposing of radioactive material is a serious impediment to the economic extraction of the more radioactive REE-rich minerals [4]. Another problem arises from the fact that the REE portfolio produced by current mining is dominated by Ce and La, accounting for 77 % of the total world supply. There is no indication of change in the near future since known ore reserves of producing mines have an even higher share of Ce plus La with close to 80 %. This leads to an imbalance between the REE mix produced by current mining and the industrial demand, as not all of the 15 REEs are of the same industrial importance. For example, REEs used for high-performance permanent magnets are Pr, Nd, Tb and Dy, while Eu, Tb, Er and Y are components of other products such as phosphors and ceramics [5]. The imbalance between industrial need for certain REEs and the mine production portfolio can be assessed by the critical REE ratio of $(La + Ce)/(Nd + Eu + Tb + Dy + Y)$. This ratio is 4.5 for the 2014 production and 5.4 for the REE reserves known in the same year. Adding up the 2014 commodity prices [6] for each REE, this ratio is 0.00545. In other words, the cumulative unit value for Nd + Eu + Tb + Dy + Y is 183.5 times higher than that for La + Ce.

This unfavourable ratio calls for a paradigm shift from conventional high LREE ores to unconventional REE ores with HREE enrichments. The distribution of individual REEs in minerals is not even and certain minerals will hold enrichments or depletions of light or heavy REEs, respectively. This renders most REE ores mineralogically and chemically complex. This, together with a wide textural variability, demands sufficient understanding of the salient characteristics of REE ores, essential for a robust assessment of the quality and economic viability of a potential REE

deposit. In that sense, it is important to identify and quantify all the REE-phases present in the ore and to evaluate the elemental department of the different REEs into the different REE-bearing phases.

Following the production chain, mineral processing requires additional information on mineral associations, grain size distributions as well as grain liberation characteristics. Nowadays, mineral processing is generally capable of sequential separation of multiple mineral phases, but when the REEs are found in two or more mineral hosts, with each behaving differently during extraction, beneficiation can become relatively inefficient and costly [7]. From that, it would appear that deposits in which the REEs are preferentially concentrated in a single mineral phase have a competitive advantage. On the other hand, mining of REEs as by-product of additional or major commodities has a significant price advantage since extraction costs are shared by the bundle of metals mined. However, polymetallic ores, by nature, contain a complex and diverse mineral assemblage, which may require special beneficiation strategies to become technically and economically viable. The design of cost-efficient processing for such ores depends heavily on information that can be made available employing automated quantitative process mineralogy [8].

10.2 Quantitative mineralogy

Quantitative mineralogy assigns numeric values to compositional and textural properties of mineral matter (e.g. rocks, ores and processing products). Compositional properties are related to the kind and quantity of mineral phases in a sample. This is known as the modal composition, which specifies the relative proportions in volume% or mass% from highly abundant rock forming minerals to less abundant accessory phases.

Textural properties comprise a multitude of information on the grains forming the sample as well as on their spatial arrangement. Grains are characterized by their size and shape. Further quantitative mineralogical parameters related to size are grain size distributions, either of the total sample or a specific mineral fraction. The spatial distribution of grains can be described by properties such as alignment, orientation or spacing [9]. Quantitative mineralogy thus attempts to convert rock properties to numbers, which often are only described in a qualitative way by geoscientists. As numeric procedures can only handle quantitative data, this represents an important contribution to the development of computer models, e.g. on beneficiation processes [10].

A variety of methods including polarization microscopy, electron microscopy, X-ray diffraction, differential thermal analysis and infrared and optical emission spectrometry has been applied in the last decades for quantitative mineralogical studies, e.g. [11–13].

Automated procedures to generate quantitative mineralogical data require unattended identification of mineral phases. Furthermore, not only to account for target

elements of mining but also in order to identify deleterious elements (e.g. U, Th), such systems should allow element detection. Any of the previously mentioned textural properties can only be quantified if information on phases and chemistry are related to images. Imaging must be performed with high spatial resolution to be suitable for fine-grained rocks. Thus, accessory phases or complex intergrowth of minerals can reliably be quantified. Finally, all data sets must be available in digital form for image analysis. Scanning electron microscopy (SEM) meets most of these requirements and is one of the most efficient tools for quantitative mineralogy.

10.3 Scanning electron microscopy

In a SEM, an electron beam is generated from a tungsten filament or a field emission gun. The electron beam is focussed and can be directed on a single spot or it can be scanned over a specimen. Among the interactions between the electrons penetrating the specimen and the sample elements, the electrons scattered back from the incident beam (backscatter electrons, BSEs) and fluorescence X-ray photons generated by excitation of atoms in the specimen are most important for quantitative mineralogy. Both yield information on sample composition (Figure 10.1).

The intensity of the BSE signal is primarily correlated to the mean atomic number of the sample [14]. This allows differentiation of minerals; in particular, minerals containing elements with higher atomic number, such as the REE, are characterized by high BSE intensity and can be distinguished from silicates or carbonates composed of lighter elements. The energy of fluorescence photons is characteristic

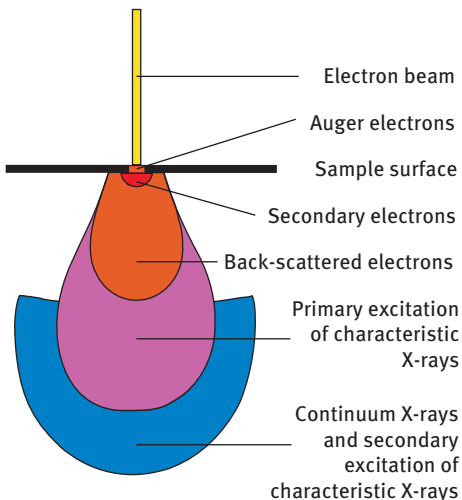


Figure 10.1: Schematic sketch showing interaction volume of electrons in sample, not to scale, according to Refs [14, 16, 17]. Pear shape is typical of materials with low mean atomic numbers such as silicate or carbonate minerals.

of the excited elements while their intensity is proportional to the concentration of these elements. As both BSE and fluorescence photons are generated by an interaction of sample atoms and electrons, they represent a larger volume of the specimen than only the area of the incident electron beam ([15], Figure 10.1). In an untitled sample, the volume of interaction depends on mean atomic number, density and beam energy [16, 17]. The latter is a function of the potential applied for acceleration of electrons emitted from the electron gun. At usual analytical conditions, i.e. acceleration voltages between 15 and 25 kV, the width of the interaction volume limits the spatial resolution of the technique in most mineral matrices to values between 2 and 5 μm .

Polished samples – either as a thin section on glass or a polished epoxy resin mount – are preferred to avoid surface effects on BSE intensity. As most mineral samples are not conductive, the samples are coated with carbon prior to analysis.

10.4 SEM-based automated quantitative mineralogy

Software packages, which make a conventional SEM applicable for automated quantitative mineralogy, are complex key components of such analytical systems. They control the entire analytical procedure of one or more samples in an unattended way. This comprises control and optimization of instrumental parameters as well as acquisition and storage of BSE and X-ray signals. Furthermore, software packages must offer a diversity of image analysis functions.

Grains with coherent properties and their boundaries must be identified in an image built up by the signals according to the scanning pattern (segmentation, e.g. [18, 19]). In a further step, the grains must be mineralogically identified, and the software should be able to separate touching grains for further image analysis (de-agglomeration). Data are transformed to digital images displaying mineral species with user-defined colours. Proportions of different minerals (i.e. modal abundance) can be calculated simply by counting pixels quantifying the area assigned to each mineral. According to the Delesse principle, this is equivalent to volume proportions. Using density information that is included in a database implemented in the software package modal abundance in volume% can be transferred to mass%.

These basic digital image data allow computation of quantitative textural parameters. Grains, either imaged in a mount of separate grains or numerically de-agglomerated from an image of a rock sample, can further be characterized in terms of size parameters (area, perimeter and diameter). Many software packages derive these values after calculation of equal area circles or ellipses for each grain. Furthermore, grains can be characterized with respect to their shape applying mathematical shape parameters. Numerous parameters converting quantitative values of grain-radius, -diameter, -area or -perimeter to grain shape are described in the literature (i.e. aspect ratio [20], circularity [21], convexity [22], eccentricity [23], projection shape factor [24],

projection sphericity [25], radial shape factor, roughness factor [24], solidity [22] and surface roughness [23]).

Image data can also be used for the quantification of textural parameters that, for example, describe orientation as well as contact relationships or mineral associations.

Orientation can be expressed as a statistics on the angles of long axes of elongated particles. Pixels along shared boundaries of two phases can be counted yielding a statistics of mineral associations if applied to all mineral grains forming contacts in a rock sample.

Finally, quantitative image analysis data can be combined to derive parameters that are directly applicable to processing of ores and to the evaluation of beneficiation processes. Mineral liberation serves as a good example. It may be either defined as the modal proportion of an ore mineral in a particle or as the proportion of an ore mineral boundary, which is associated with the mounting resin to the total boundary of a particle. The latter indicates the free surface of an ore mineral amenable to processing operations (e.g. flotation, hydrometallurgy).

According to the authors' knowledge, currently, there are four SEM-based automated quantitative mineralogy systems commercially available (in alphabetical order of companies): FEI (QEMSCAN, MLA), Tescan (TIMA) and Zeiss (Zeiss Mineralogic Mining).

10.4.1 Quantitative Evaluation of Minerals by Scanning Electron Microscopy

Early generations of the QEMSCAN (Quantitative Evaluation of Minerals by Scanning Electron Microscopy) were developed by CSIRO (Commonwealth Scientific and Industrial Research Organisation) in Australia in the middle of the 1970s as QEM*SEM automated mineragraphy [15, 26]. The actual system is based upon FEI Quanta 650 and Quanta 650F SEMs, and in addition to a standard version, it is offered as product models “express” and “well site” (www.fei.com). The instrument is equipped with a Bruker Dual X-Flash5030 energy-dispersive X-ray spectroscopy (EDS) detector. Up to 14 round epoxy-mounted samples (diameter 30 mm) or 12 standard thin sections can be placed in the sample chamber.

The workflow of a QEMSCAN analysis is displayed in Figure 10.2. The specimen is scanned on a grid basis with an electron beam step width usually varying between 0.8 and 10 μm (Figure 10.2(a) and 10.2(b)). For each step, which is represented by an image pixel in the resulting dataset, the system acquires the BSE intensity and X-ray fluorescence spectrum consisting of 1,000–5,000 counts at acceleration voltages of 15, 20 or 25 kV (Figure 10.2(c)). Information on up to 72 elements is derived from peak signals within the spectrum. Count rates at spectral peaks are transferred to information on element abundance.

Mineral identification is performed comparing pixel information with a database (Species Identification Protocol, SIP) defining a range of element compositions, BSE values and detector count rates for each phase. Mineral assignment is done at first

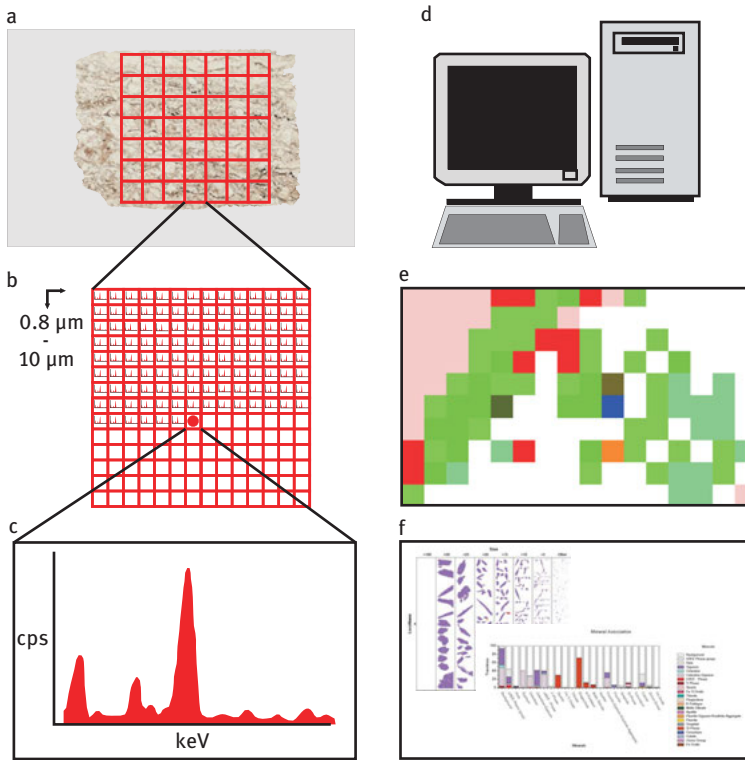


Figure 10.2: Workflow of a QEMSCAN Analysis, (a) Pattern of frames on a carbon-coated polished thin section of a rock. Frames are sequentially scanned. (b) Each frame is scanned with an electron beam step width varying between 0.8 μm (minimum value) and usually 10 μm . (c) Acquisition of BSE intensity and fluorescence spectrum with EDS X-ray detectors usually on the basis of 1,000–5,000 counts. (d) Data storage on hard disc and phase assignment to each pixel by correlation of X-ray and BSE data with a database. (e) Generation of images with colour coding for different mineral phases. (f) Image analysis, generation of quantitative mineralogical data (e.g. modal composition, particle size and size distribution, mineral association, particle shape and textural parameters).

match within a sequence of phases also defined in the SIP (Figure 10.2(d) and 10.2(e)). Image data generated in these steps constitute the basis for further quantitative mineralogical evaluation of the samples (Figure 10.2(f)).

Among the measurement modes of QEMSCAN, two are most often applied. The fieldscan/field image mode is recommended for the study of non-fragmented rocks showing their original texture. This mode generates images displaying the total scanned area, which offers data for mineral abundance and textural analysis. An example of such a fieldscan image is given in Figure 10.3, which shows a rock formed by a groundmass of plagioclase and muscovite as well as by larger irregularly shaped

quartz grains indicated by different colours. Less abundant mineral phases, such as the REE-mineral monazite (REEPO_4) as well as apatite or clinzoisite-epidote, are detected by QEMSCAN and can easily be recognized due to dark blue, dusky pink and lavender colour coding, respectively.

The time-consuming effort of high-resolution pixel-by-pixel X-ray mapping is highly appropriate for the study of materials composed of fine-grained minerals with similar BSE properties. This is illustrated in Figure 10.3. While phase assignment for muscovite, plagioclase and quartz is clear using X-ray data, these minerals, which are characterized by similar and relatively low densities, can hardly be distinguished in BSE images at a BSE scale suitable for distinction of heavier phases.

In contrast to the fieldscan mode for non-fragmented rocks, samples consisting of particulate material (crushed rocks, ore concentrates and unconsolidated sediments) mounted in a resin representing specimen surface that is not of interest are

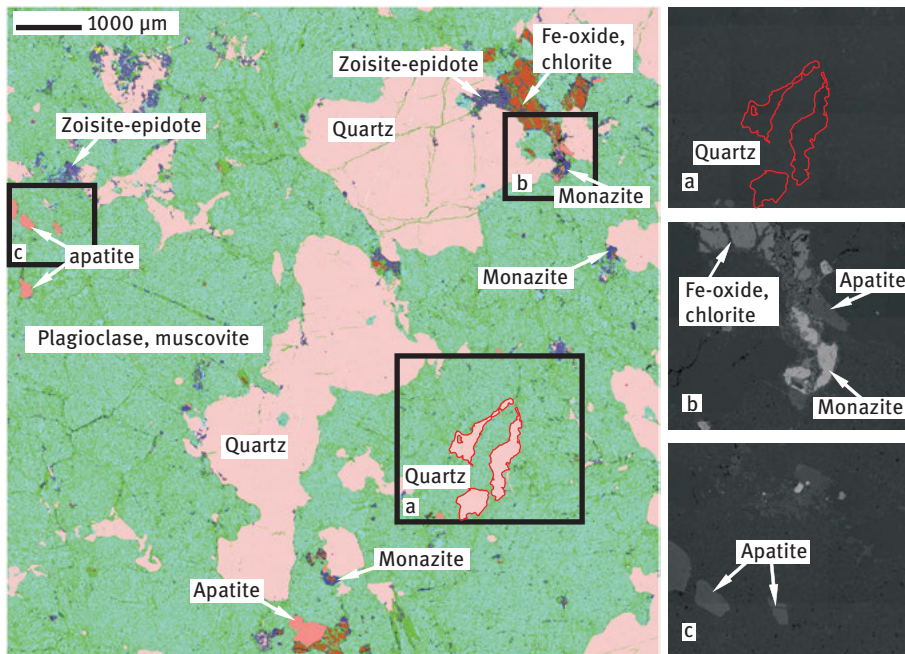


Figure 10.3: QEMSCAN fieldscan image of a monazite (REEPO_4) bearing rock. Minerals are indicated by colour coding as indicated in the image (apatite = dusky pink, chlorite = dark green, Fe-oxide = brown, monazite = dark blue, muscovite = light green, plagioclase = bluish green, quartz = pink and zoisite-epidote = lavender). The sample areas of insets a, b and c are alternatively displayed as BSE image on the right side. Monazite is characterized by a high density compared to other phases and thus shows highest BSE intensity. Contours of three quartz grains are highlighted by red lines in inset a. BSE scaling appropriate for distinction of minerals with elevated density (e.g. apatite, Fe-oxide and monazite) in insets b and c is not suitable for distinction of lighter phases like muscovite, plagioclase and quartz, which dominate in inset a.

best analysed with the “Particle Mineral Analysis” (PMA) mode. Here, sample areas not exceeding a user-defined BSE threshold value indicative of background resin are not analysed. Further, measurement modes of QEMSCAN are described in Ref. [26].

10.4.2 Mineral Liberation Analyser

Originally, the MLA was developed by the JKMRC (Julius Kruttschnitt Mineral Research Centre, University of Queensland) in the 1990s [27]. Today, the system is provided by the FEI Company and the hardware basis is identical to QEMSCAN.

Its software also allows pixel-by-pixel determination of BSE and EDS data along a grid pattern on the sample (GXMAP mode). The characteristic and probably most often used measurement mode discriminates grains first on the basis of their BSE intensity, which is calibrated to a range of atomic numbers. Finally, a single X-ray analysis is performed on each grain for phase assignment in combination with the BSE values according to best spectral match of analytical data with those of mineral standard spectra available in a mineral reference library [19]. This XBSE mode reduces analysis time due to limitation of the time-consuming step of EDS analysis. It is most appropriate for samples composed of larger grains with coherent BSE values. Further, measurement modes are described in Refs [19, 27, 28].

10.4.3 Tescan-Integrated Mineral Analyser

The hardware basis of the Tescan-integrated mineral analyser (TIMA) is either formed by a MIRA field emission or a VEGA thermal emission SEM equipped with up to four EDS detectors (www.tescan.com). BSE and spectral information obtained for each pixel is used for identification of mineral phases. So far, literature information on this recently released analytical system is not available.

10.4.4 ZEISS Mineralogic Mining

The Mineralogic Mining System was released by Zeiss in 2014. It can be run on the different SEM platforms offered by the company (e.g. Zeiss EVO, Zeiss SIGMA HD, as well as mobile systems designed for on-site mineral processing purposes, MinScan, www.zeiss.com). The software allows various modes of data acquisition [29]. Mineral classification can be performed using BSE greyscale values as well as in combination with X-ray spectra that are acquired by one or more EDS detectors for all image pixels. Furthermore, in a mode comparable to MLA, touching pixels with common BSE intensity are combined and mineral identification is performed using a single EDS analysis.

Prior to phase assignment, X-ray data are transferred to quantitative element concentrations [29, 30]. Element wt.% values are then compared to minimum and

maximum ranges indicative for phases of interest listed in a database. The use of quantitative values (i.e. data directly related to mineral stoichiometry) makes phase assignment independent of instrumental parameters affecting the EDS spectrum (e.g. acceleration voltage [29]).

To enhance the volume of information and to support phase identification, the system allows the correlation of SEM data with images obtained from external sources (e.g. polarization light and cathodoluminescence microscopy, 2D virtual slices through 3D X-ray tomographic datasets [30]).

10.5 Quantitative REE mineralogy

REE minerals are chemically highly variable and show complex formulae. Rocks in which they occur in high abundance that could serve as REE ores generally show complicated textures. Both, petrologists who want to understand the origin of such rocks and mining engineers who develop concepts for ore processing need to study chemical and textural variability of such minerals. This represents a challenge for automated quantitative mineralogy but also a field for which this technology is highly applicable, as will be illustrated by following examples.

Owing to mainly identical charges (3^+) and minor variations in ionic radii, various REEs isostructurally substitute in mineral phases. Most REE minerals are thus characterized by a range of chemical compositions rather than by one specific stoichiometry.

For example, the common REE ore minerals parisite and synchysite, which can in a simplified way be expressed as $\text{CaREE}_2(\text{CO}_3)_3(\text{F, OH})_2$ and $\text{CaREE}(\text{CO}_3)_2(\text{F, OH})$, respectively, do not only show incorporation of the different lanthanoids La, Ce, Pr, Nd or Sm but also replacement of these elements by Y and Th as well as of Ca by other elements such as Sr, Ba or Fe. A review of published data [31–34] on these minerals reveals the following compositional ranges for both minerals (in part recalculated for $\text{Ca} + \text{Sr} + \text{Ba} + \text{Fe} = 1$ per 3 CO_3):

Parisite: $\text{Ca}_{0.89-1.00}\text{Sr}_{0.00-0.04}\text{Ba}_{0.00-0.09}\text{Fe}_{0.00-0.03}\text{La}_{0.29-0.67}\text{Ce}_{0.77-1.16}\text{Pr}_{0.08-0.11}$
 $\text{Nd}_{0.18-0.37}\text{Sm}_{0.01-0.05}\text{Eu}_{0.00-0.01}\text{Gd}_{0.00-0.02}\text{Y}_{0.00-0.04}\text{Th}_{0.00-0.01}(\text{CO}_3)_3(\text{F, OH})_2$

Synchysite: $\text{Ca}_{0.89-1.00}\text{Sr}_{0.00-0.03}\text{Fe}_{0.00-0.03}\text{La}_{0.24-0.39}\text{Ce}_{0.47-0.53}\text{Pr}_{0.03-0.06}\text{Nd}_{0.08-0.19}$
 $\text{Sm}_{0.01-0.02}(\text{CO}_3)_2(\text{F, OH})$

Calculated fluorescence spectra representative of these variable compositions obtained in an SEM analysis are displayed in Figure 10.4. In accordance with the mineral stoichiometry, parisite is characterized by higher signals of REE as well as F and lower signals of Ca compared to synchysite. However, the signal ranges of La, Ce, Pr and Nd for both minerals show an overlap. Furthermore, automated quantitative mineralogical systems dominantly use spectral information from limited photon counts (e.g. 1,000–5,000) for phase assignment – independent of the software solutions offered

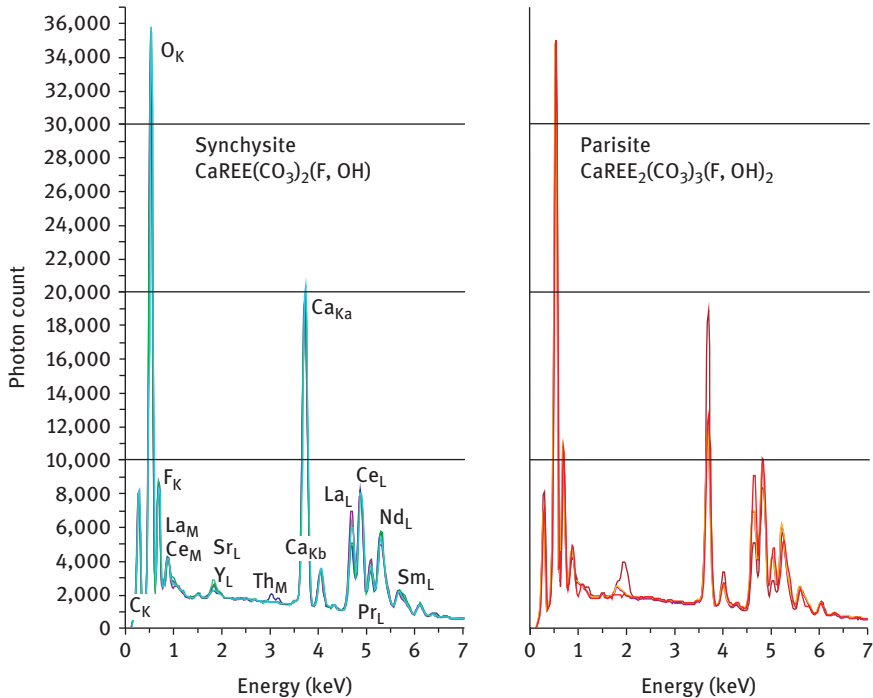


Figure 10.4: Fluorescence spectra of synchysite and parisite calculated for mineral compositions published by [31–34], calculation performed with the iDiscover[®] software by FEI-company assuming an acceleration voltage of 15 kV. The indices K and L denote spectral information belonging to the K- and L-series, respectively. Only in the case of Ca K_{α} (Ka) and K_{β} (Kb), radiation is indicated.

by different companies. Thus, counting statistics, detector noise as well as surface effects lead to uncertainty of signal intensity. In consequence, chemical variability of REE minerals as illustrated by the example in Figure 10.4 and analytical uncertainty can reduce the performance of phase assignment. In such cases, minerals that cannot be distinguished have to be combined in a group of phases.

Monazite (REEPO_4) is one of the most important ore minerals for LREE. It is an important constituent of magmatic as well as of placer deposits and belongs to the first mineral phases used for extraction of REE [1].

In addition to a quantitative evaluation of a REE ore, which implies the determination of the modal abundance of monazite or other REE minerals, it is important to understand ore-forming processes. The definition of parameters controlling monazite stability that are indicated by monazite-forming as well as by monazite-consuming mineral reactions is an important basis for such study. This is illustrated in Figure 10.5, which displays details of the QEMSCAN image in Figure 10.3 showing a monazite-bearing metamorphic rock.

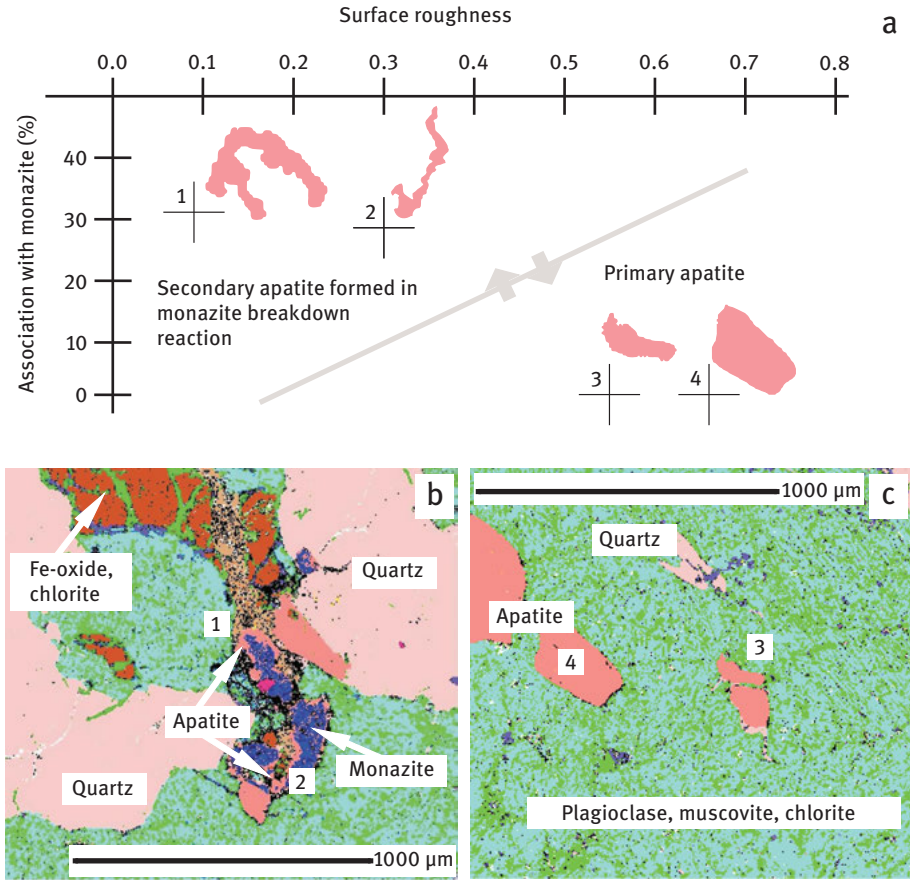
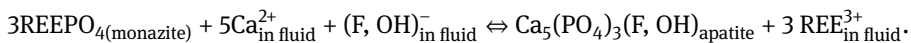


Figure 10.5: Example of image analysis applied for the distinction and quantification of primary apatite and apatite formed by breakdown of monazite. (a) Grains 1–4 are characterized by the parameters association and surface roughness. Association indicates the proportion of monazite pixels in contact with an apatite grain in % of the total amount of pixels defining the perimeter of the apatite grain. The surface roughness is defined as $(2 \times \pi \times (\text{area pixels}/\pi)^{1/2} / \text{perimeter pixels})$. Apatite formed by reaction of monazite (grains 1 and 2) is characterized by high association and low surface roughness values. (b) Position of apatite grains 1 and 2 in a reaction rim around monazite, sample area is identical to inset b in Figure 10.3(c). Examples of primary metamorphic apatite grains (3 and 4) in a matrix composed of plagioclase and muscovite with minor chlorite, sample area identical to inset c in Figure 10.3.

Monazite (REEPO_4) shown by dark blue colour coding is surrounded by a corona of apatite ($\text{Ca}_5(\text{PO}_4)_3(\text{OH}, \text{F})$) (dusky pink), which formed in a breakdown reaction indicating the limit of monazite stability. The reaction can be formulated in a simplified way as:



The abundance of apatite thus could be considered as an indicator for this breakdown reaction, which was probably triggered by a retrograde albitization of plagioclase releasing Ca^{2+} to the fluid. However, the image shows that next to fine-grained and irregularly shaped apatite from the coronas, a second type can be observed. Apatite of this type, which is texturally not associated to monazite and which forms larger rounded grains with smooth boundaries, is genetically not related to monazite. Rather, it belongs to the original metamorphic assemblage.

Both types of apatite must be distinguished in order to indicate apatite as monazite breakdown product. Shape parameters allow transferring the descriptive characterization of both types to measurable numeric data in an automated quantitative mineralogical approach that is independent of the experience or optical impression of a mineralogist performing individual microscopic grains inspection.

The surface roughness parameter compares the actual perimeter of a grain (formed by neighbouring pixels of the same kind) with the perimeter of a circle with equivalent area quantified by the amount of pixels representing the grain. Thus, the regularly shaped apatite grains with smooth boundaries, which belong to the metamorphic assemblage, are characterized by high roughness parameters close to 1, whereas the irregularly shaped apatite grains forming the coronas around unstable monazite yield low roughness parameters.

Grain association is another parameter of image analysis that can be applied for discrimination of both types, because apatite formed by monazite breakdown generally is in contact with monazite. In contrast, metamorphic apatite is almost exclusively associated to other minerals than monazite.

A combination of both parameters, roughness and association, thus provides a criterion for automated discrimination of both types of apatite, which is illustrated in Figure 10.5. In a series of samples, image analysis could be applied to quantify volumes of both reaction partners and consequently to show progress of monazite breakdown.

10.6 Concluding remarks

Although based on concepts from the 1970s automated quantitative mineralogy is a field that has shown significant progress in the last years due to hardware and software developments of the SEM manufacturers. The examples outlined in this chapter underline the capabilities of automated quantitative mineralogy for phase identification and textural analysis. Therefore, this technology fulfils all requirements for characterization of complex unconventional REE ores with HREE enrichment that will become increasingly important for supply of REEs in the future.

Acknowledgements

QEMSCAN measurements by R. Klinghardt and L. Gronen are gratefully acknowledged. We thank G. Günther for retrieval of literature.

References

- [1] Chakmouradian AR, Wall F. Rare earth elements: Minerals, mines, magnets (and more). *Elements* 2012, 8, 333–40.
- [2] Alonso E, Sherman AM, Wallington TJ, Everson MP, Field FR, Roth R, Kirchain RE. Evaluating rare earth element availability: A case with revolutionary demand from clean technologies: *Environ Sci Technol* 2012, 46, 3406–14.
- [3] Hellman PL, Duncan RK. Evaluation of rare earth element deposits: *IMM Trans B: Appl Earth Sci*, 2014, 123, 107–17.
- [4] USEPA. Rare earth elements: A review of production, processing, recycling, and associated environmental issues: Cincinnati, U.S. Environmental Protection Agency (USEPA), 2012, 135.
- [5] USDOE. Critical mineral strategies: US Department of Energy, 2010, 165.
- [6] HEFA, Rare earth metal prices: HEFA Rare Earth Inc., www.mineralprices.com. 2014. Accessed: October 15, 2015.
- [7] Jordens A, Cheng YP, Waters KE. A review of the beneficiation of rare earth element bearing minerals. *Miner Eng* 2013, 41, 97–114.
- [8] Gu Y, Schouwstra RP, Rule C. The value of automated mineralogy. *Miner Eng* 2014, 58, 100–3.
- [9] Butcher AR. Automated mineralogy & petrography for geometallurgy. 11th Freiberg short course in economic geology 2012, December 5–7, 175p.
- [10] Lund C, Lamberg P. Geometallurgy – A tool for better resource efficiency. *Eur Geol* 2014, 37, 39–43.
- [11] Lyon RJ, Tuddenham WM. Quantitative mineralogy as a guide in exploration. *Min Eng* 1959, 11, 1–5.
- [12] Davies BL, Walawender MJ. Quantitative mineralogical analysis of granitoid rocks: A comparison of X-ray and optical techniques. *Am Miner* 1982, 67, 1135–43.
- [13] Kile DE, Eberl DD. Quantitative mineralogy and particle-size distribution of bed sediments in the Boulder Creek Watershed, Colorado, in: Murphy SF, Verplanck PL, Barber LB (eds.) *Comprehensive water quality of the Boulder Creek Watershed, Colorado, during high-flow and low-flow conditions*, 2000. US Geological Survey Water-Resources Investigations Report 03–4045, 2003, 173–84.
- [14] Knight RD, Klassen RA, Hunt P. Mineralogy of fine-grained sediment by energy-dispersive spectrometry (EDS) image analysis – a methodology. *Environ Geol* 2002, 42, 32–40.
- [15] Pignolet-Brandom S, Reid KJ. Mineralogical characterization by QEM*SEM, in: Carson DJ, Vassiliou AH (eds.) *Process Mineralogy VIII*. Warrendale, PA, USA, The Minerals, Metals & Materials Society 1988, 337–46.
- [16] Potts PJ. *A Handbook of Silicate Rock Analysis*. London, Glasgow, Weinheim, New York, Tokyo, Melbourne, Madras, Blackie Academic & Professional, 622p.
- [17] Jones MP. *Methoden der Mineralogie*. Stuttgart, Ferdinand Enke Verlag, 260p.
- [18] Heilbronner R, Barret S. *Image Analysis in Earth Sciences*. Berlin, Heidelberg, Springer-Verlag, 2014.
- [19] Gu, Y. Automated scanning electron microscope based mineral liberation analysis. *J Miner Met Charact Eng*, 2003, 2, 33–41.
- [20] Schneiderhöhn P. Eine vergleichende Studie über Methoden zur quantitativen Bestimmung von Abrundung und Form an Sandkörnern. *Heidelb Beitr Mineral Petrogr* 1954, 4, 172–91.
- [21] Rodriguez J, Johansson J, Edeskär T. Particle shape determination by two-dimensional analysis in geotechnical engineering. *Proceedings of Nordic Conference on Soil Mechanics and Geotechnical engineering*, NGM 2012, 207–18.
- [22] Olson E. Particle shape factors and their use in image analysis – part 1: Theory. *J GXP Compliance* 2011, 15, 85–96.

- [23] Podczeczek F, Newton JM. The evaluation of a three-dimensional shape factor for the quantitative assessment of the sphericity and surface roughness of pellets. *Int J Pharm* 1995, 124, 253–59.
- [24] Bouwman AM, Bosma JC, Vonk P, Wesselingh, JH, Frijlink HW. Which shape factor(s) best describe granules? *Powder Technol* 2004, 146, 66–72.
- [25] Podczeczek F, Rahman SR, Newton JM. Evaluation of a standardised procedure to assess the shape of pellets using image analysis. *Int J Pharm* 1999, 192, 123–38.
- [26] Pirrie D, Rollinson GK. Unlocking the applications of automated mineral analysis. *Geol Today* 2011, 27, 235–44.
- [27] Sylvester P. Use of the Mineral Liberation Analyzer (MLA) for mineralogical studies of sediments and sedimentary rocks, in: Sylvester P (ed.) *Quantitative Mineralogy and Microanalysis of Sediments and Sedimentary Rocks*. Mineralogical Association of Canada Short Course Series 2012, 42, 1–16.
- [28] Fandrich R, Gu Y, Burrows D, Moeller K. Modern SEM-based mineral liberation analysis. *Int J Miner Process* 2007, 84, 310–20.
- [29] Graham SD, Brough C, Cropp A. An introduction to Zeiss Mineralogic Mining and the correlation of light microscopy with automated mineralogy: a case study using BMS and PGM analysis of samples from a PGE-bearing chromitite prospect. *Precious Metals '15*, 2015, Falmouth UK, 10p.
- [30] Graham SD, Cropp A. Advances in mineral characterisation techniques: emerging tools and workflows. *Proceedings of the 13th Biennial SGA Meeting 2015*, 24–27 August, Nancy France, 1403–5.
- [31] Manfredi TR, Bastos Neto AC, Pereira VP, Barbanson L, Schuck C. The parisite-(Ce) mineralization associated with the Fazenda Varela carbonatite (Correia Pinto, SC). *Pesquisas em Geociencias* 2013, 40, 295–307.
- [32] Petrella L. The nature and origin of REE mineralization in the Misery syenitic intrusion, northern Québec, Canada. Master thesis 2012, McGill University Montreal, 130p.
- [33] Ni Y, Post JE, Hughes JM. The crystal structure of parisite-(Ce), $Ce_2CaF_2(CO_3)$. *Am Miner* 2000, 85, 251–8.
- [34] Zaitsev AN, Wall F, LeBas MJ. REE-Sr-Ba minerals from the Khibina carbonatites, Kola Peninsula, Russia: their mineralogy, paragenesis and evolution. *Miner Mag* 1998, 62, 225–250.

Larissa Müller, Heike Traub and Norbert Jakubowski

11 Novel Applications of Lanthanoides as Analytical or Diagnostic Tools in the Life Sciences by ICP-MS-based Techniques

Abstract: Inductively coupled plasma mass spectrometry (ICP-MS) is a well-established analytical method for multi-elemental analysis in particular for elements at trace and ultra-trace levels. It has found acceptance in various application areas during the last decade. ICP-MS is also more and more applied for detection in the life sciences. For these applications, ICP-MS excels by a high sensitivity, which is independent of the molecular structure of the analyte, a wide linear dynamic range and by excellent multi-element capabilities. Furthermore, methods based on ICP-MS offer simple quantification concepts, for which usually (liquid) standards are applied, low matrix effects compared to other conventional bioanalytical techniques, and relative limits of detection (LODs) in the low pg g^{-1} range and absolute LODs down to the attomol range.

In this chapter, we focus on new applications where the multi-element capability of ICP-MS is used for detection of lanthanoides or rare earth elements, which are applied as elemental stains or tags of biomolecules and in particular of antibodies.

11.1 Introduction

Inductively coupled plasma mass spectrometry (ICP-MS) is a well-established analytical method for multi-elemental analysis in particular for elements at trace and ultra-trace levels. It has found acceptance in various application areas during the last decade and is also more and more applied for detection in the life sciences.

In Analysis and Speciation of Lanthanoides by ICP-MS, we have already discussed the ICP-MS technology in detail and have presented the determination and speciation of Gd-containing contrast agents to study the fate from clinical application to the distribution in the environment and its interaction with the biosphere as a typical application. In this chapter, we focus on new applications using the multi-element capability of ICP-MS where lanthanoides are applied as elemental stains for detecting or tagging of biomolecules and in particular of antibodies. The concept of metal tagging has already been used for detection of biomolecules by ICP-MS (for more details, see Bettmer et al. [1]), and it is already quite popular for detection and quantification of metalloproteins (for more details, see a perspective article by Swart and Jakubowski [2]). However, most of the biomolecules being of analytical interest do not contain elements detectable by ICP-MS, so that artificial tagging known as bio-conjugation by metals, in particular by lanthanoides, are more and more applied. This new concept

of bio-conjugation is already successfully used to extend the capabilities of ICP-MS in the life sciences for toxicological, biochemical and medical applications.

Many methods and technologies discussed in this chapter are quite analogous to the application of fluorescence spectroscopy using lanthanoides as fluorophores, but this is discussed in Analysis and Speciation of Lanthanoides by ICP-MS.

11.2 Bio-conjugation of biomolecules

Trend setting in this new application area for lanthanoides is the technology of bio-conjugation of biomolecules (mainly of peptides, proteins, DNA, RNA and antibodies) using metal tags. These metallic tags, in particular from the group of the rare earth elements (REEs), are chemically bound to the molecule of interest using a reactive group to which a chelating compound is connected, which chelates the metal of interest. The best choice of metals for this purpose are the lanthanoides due to the following advantages:

1. The lanthanoides all show a very similar chemistry, thus a method once elaborated for one element can easily be transferred to other elements of this group.
2. The concentration of the lanthanoid elements in biological or medical samples is rather low, so that blank correction is not needed.
3. All lanthanoides can easily be ionized with an efficiency near 100 % due to a low first ionization potential; thus, the sensitivity in ICP-MS is high and the limits of detection (LODs) are quite low.
4. Lanthanoides are nearly not hampered by spectral interferences; many isotopes can be obtained enriched with purities better than 95 %. The only interference which should be mentioned here is the isobaric interference for elements with multiple naturally occurring isotopes used without enrichment and to certain extends interferences based on oxide formation.

11.2.1 Fundamentals

In principle, the chemistry applied for bio-conjugation (tagging) in ICP-MS is very similar to the chemistry used for the development of contrast agents in magnetic resonance imaging (MRI). For ICP-MS application mainly bifunctional ligands were investigated as tagging reagents. They consist of two parts, a metal chelating compound and a reactive group which connects the chelate – if possible covalently – to the biomolecule of interest and in particular to antibodies. Concerning the chelates, macrocyclic compounds based on 1,4,7,10-tetraazacyclododecane-1,4,7,10-tetraacetic acid (DOTA) or linear chelates such as diethylenetriaminepentaacetic acid are promising candidates and can easily be loaded by different metals preferentially by lanthanoides or their isotopes. The 15 lanthanoid elements provide at least 37 isotopes that are non-redundantly unique masses allowing the design of highly multiplexed/multi-parametric cell assays, because the mass resolution achieved in ICP-MS even in low mass resolution is always sufficient to separate isotopes at mass m from adjacent

masses ($m \pm 1$). Some of the isotopes are interfered by isobaric interferences as mentioned before, but this limitation has been solved by application of enriched and stable isotopes. Additionally, the chelating compounds applied offer improved water solubility and they have a high-stability constant in order to be resistant against metal exchange which otherwise could compromise their application. For more details, see the reviews related to metal tagging and in which the chemistry of tagging is described in more detail [3, 4].

Concerning the reagents used as reactive group, isothiocyanatobenzyl residues (SCN) and *N*-Hydroxysuccinimid ester (NHS) are often applied, because they bind preferentially to amino-groups of amino acids. Alternatively, maleimidoethylacetamide residues are used for conjugation to sulfhydryl (SH) residues after selective reduction of the proteins or antibody's cysteine-based disulfide bridges. In both cases, the reaction step with the biomolecule is always critical, because it will significantly change the physical and chemical properties of the antibody and in case of immunoassays it might also affect the antibody's binding efficiency and specificity.

Additionally, glycoproteins and in particular antibodies, which are always glycosylated in nature, can be derivatized at their sugar residues after oxidation to form aldehydes, which then can react with lanthanoide-containing chelating tags carrying the reactive group, a hydrazide or primary amine [5]. In a similar way, the 5'- and 3'-end ribose sugars of RNA can be oxidized to aldehydes, using the same reactive groups mentioned before [6]. A different way for detection of DNA is based on application of base-complementary oligonucleotide groups synthesized with reactive amine or SH groups for which the same conjugation chemistry can be used as for antibodies.

11.2.2 Bio-conjugation of antibodies

Historically, chelating compounds were first employed in combination with radioactive tracers. McDevitt et al. presented a method for binding ^{225}Ac to a SCN-DOTA and attached the complex to an immunoglobulin G (IgG) antibody [7]. The use of a NHS linker attached to DOTA was described by Lewis et al. who performed bio-conjugation with the radioactive isotopes ^{111}In and ^{90}Y [8]. Due to the fact that such assays can be analyzed only in laboratories specialized in radiochemistry and additionally to overcome health hazards caused by the radioactive materials, soon fluorescent lanthanoides (Eu, Sm, Tb, Dy) replaced the radioactive central ions (see for instance, AutoDELFIATM). The DELFIATM approach offered a (fourfold) multi-parametric assay and was already applied in 2002 in one of the first multi-parametric assays using ICP-MS detection [9]. However, one of the first immunoassays with ICP-MS detection was discussed in literature for the quantification of the thyroid-stimulating hormone thyroxinein (TSH) by Zhang et al. [10]. The authors used a Eu-tagged antibody for detection of the hormone. The Eu signal measured after digestion was directly proportional to the serum TSH concentration. The assay was linear and the limit of detection was sufficient to cover the whole diagnostic relevant range. The precision was better

than 10 % and the TSH results obtained by ICP-MS were in good agreement with the result obtained by a radioimmunoassay which was used for validation.

Metal coding was first discussed by Whetstone et al. [11] and a year later Krause et al. [12] applied for a patent for a DOTA-based reagent with a cysteine reactive maleimide group, and a biotin modification for purification and enrichment of tagged peptides via biotin–avidin affinity chromatography, named and patented as metal-coded affinity tag (MeCAT).

Concerning the development of immunoassays most applications at the beginning of this method have used tags containing only one detectable element, but the sensitivity of an ICP-MS can be significantly increased if each single tag consists of more than one metal atom. As a consequence, polymer tags were developed by Lou et al. [13] for single cell assays analyzed by the CyTOFTM technology (see Analysis and Speciation of Lanthanoides by ICP-MS). Application of the polymer tag provides a gain in sensitivity of the ICP-MS detection of up to a factor of 100 in comparison to single atomic tags. As mentioned before, a maleimide group at one end of the polymer chain was used for coupling the polymer to the free SH groups generated by partial reduction of the disulfide bridges of proteins and antibodies.

11.3 Applications

The different applications where bio-conjugation (tagging) of biomolecules was used for ICP-MS detection can be divided into two main categories:

- (A) Identification and quantification strategies in MS for DNA, proteins and peptides.
- (B) Immunoassays and metallo-stains.

They all have in common that lanthanoides are used as metal for ICP-MS detection.

11.3.1 Development of identification and quantification strategies for DNA, peptides and proteins in mass spectrometry

As said before, lanthanoid elements are often applied as tags for multiplexed and targeted analysis of peptides, proteins, DNA and RNA using MS for detection (for more details, see a review from de Bang and Husted [14]).

Besides the specific detection of biomolecules, after tagging the quantification of peptides and proteins is gaining more importance. The first study where a ligand based on DOTA was loaded with lanthanoides for MS-based applications was presented by Whetstone et al. already in 2004 for the differential tagging of peptides [11]. The authors showed that this approach was applicable in combination with reversed phase chromatography separation of peptides and subsequent MS/MS experiments. In a study by Ahrends et al. [15] reaction parameters for MeCAT were optimized, and the new method was used to analyze proteins of the *Sus scrofa* eye lens as a model system to demonstrate the applicability [16]. LC-ICP-MS was used for separation and

quantification of metal-tagged polypeptides from a protein digest. The quantitative information from ICP-MS was then used for calibration of organic MS (electrospray ionization (ESI)-MS). The low matrix effects of biological samples in ICP-MS, and the use of simple, non-species specific metal-containing standards opened up a new possibility for absolute quantification of proteins and peptides to be used as homemade calibration standards in organic MS. The limit of detection for Ho³⁺-tagged bovine serum albumin was calculated for the ICP-MS detection as low as ~100 attomol only. Furthermore, an investigation of variations in an *Escherichia coli* (*E. coli*) proteome due to different growth temperatures was conducted with this tagging technique. An implementation of MeCAT to absolute peptide and standard protein quantification was published recently [17]. For absolute quantification, selected peptides were tagged with MeCAT-Eu and quantified by isotope dilution ICP-MS using liquid tracers. A peptide mix at different concentrations was separated by reversed-phase (RP) chromatography before ICP-MS detection and thus, a calibration was performed in one run. For quantitative protein identification, a lysozyme and a bovine serum albumin tryptic digest were tagged with MeCAT-Eu. The resulting peptides were analyzed by LC-ICP-MS and LC-(RP)-ESI-ion trap Fourier transform ion cyclotron resonance MS.

A ICP-MS-based method is discussed by El-Khatib et al. for relative and absolute quantification of sulfenic acid (SA) in peptides and proteins, which is an important biomarker for protein oxidation often involved in intracellular redox-mediated events by reactive oxygen species altering structure and function of proteins in many diseases [18]. A new metal-containing reagent (Ln-DOTA-Dimedone) was synthesized and shown to react specifically with SA. The high sensitivity, structure-independent signal and multiplexing capabilities of ICP-MS were demonstrated together with the specificity of Ln-DOTA-Dimedone and Ln-MeCAT for detection of SAs and thiol residue in a simultaneous detection approach.

In a proof of concept experiment, three thiolated complementary DNA probes (derivatized with Eu, Tb and Ho, respectively) have been applied by López-Fernández et al. for detection of three oligonucleotides by ICP-MS using size exclusion for separation [19]. The LODs achieved range between 5 and 11 fmol absolute.

Brueckner et al. describe a hybridization assay based on biotin-streptavidin affinity combining this with lanthanoide-tagged reporter oligonucleotide probes and biotinylated capture oligonucleotide probes. For the improvement of the sensitivity and sequence specificity of the assays, it was combined with target amplification by the ligase chain reaction. The proof of principle experiment demonstrated that the target amplification step resulted in a 6,000-fold increase of sensitivity, and finally an LOD of only 2.6 amol was achieved with a double-stranded DNA target [20].

11.3.2 Analytical and diagnostic applications of lanthanoids

Immunoassays are based on the specific binding of antibodies with their corresponding antigens and thus can be used for identification of proteins (antigens) or their quantification. For this purpose, it is common to tag the antibody by

a compound which can be easily detected by photometry, fluorescence or atomic detection, in particular, ICP-MS as it will be discussed in this section in more detail.

Usually, antibodies of the IgG-type are employed for this purpose. The first description of an antibody carrying a tag for subsequent detection was published by Coons in 1941 [21], who introduced the coupling of fluorescein by an isothiocyanate derivate. The first clinical immunoassay, making use of the specificity of antigen–antibody reactions, was developed for the determination of insulin in human blood by Yalow and Berson in 1960 [22].

11.3.2.1 Applications of lanthanoides in mass cytometry

The state-of-the-art for characterizing proteins of many biological cells individually is flow cytometry. A cell sample is treated with a fluorescence probe (e.g. fluorescent-tagged antibodies) and the cell suspension is formed to a liquid stream which allows the cells aligned in the center of a capillary to pass a light beam for fluorescence sensing or sorting. But the optical technique is limited by fluorescence dye quenching and auto-fluorescence of the sample and the containers. Additionally, the number of colors is limited due to broad and overlapping emission and absorption bands and sophisticated strategies have to be elaborated for massively multi-parametric assays. However, this technology is a benchmark very often applied in many clinical environments.

To overcome these limitations, a novel technique for real time analysis of massively multi-parametric assays of single cells at high-throughput was developed by Scott Tanner and colleagues using ICP-MS [23]. For this purpose, antibodies are modified with metal tags as described in Section 11.2.2 instead of fluorophores conventionally employed in polychromatic flow cytometry.

The mass cytometer (a schematics is shown already in Analysis and Speciation of Lanthanoides by ICP-MS), which was introduced to the market as CyTOF™ by DVS Sciences Inc. (now Fluidigm), is a novel adaptation of ICP-MS, better to say of ICP-TOF-MS (time of flight: TOF) for cell counting [24]. A TOF-MS is a very fast scanning mass analyzer which allows to measure transient signals with μs time resolution. The sample introduction of a cell suspension into the CyTOF™ is based on a micro-concentric pneumatic nebulizer which is connected to a heated spray chamber, to which a make-up argon gas flow is supplied via a mass flow controller. In the spray chamber, the gas flow containing droplets with imbedded cells is dried (all water droplets without cells are vaporized). The technology employs the total consumption sample introduction system limiting sample aspiration rate to $\sim 45 \mu\text{L}/\text{min}$. All water vapors reach the plasma source. The dried cells are injected into the plasma ion source where they are undergoing rapid thermolysis, atomization and ionization. The ions are passing through the atmosphere-vacuum interface, ion beam forming optics, low mass cutoff filter, time-of-flight mass analyzer, and finally, are registered by the detector and data acquisition system as a transient event: ion intensity versus time.

The stochastic sample introduction leads to possible overlap of the ion signals limiting the maximum rate of cell introduction to $\sim 1,000/\text{s}$. A longer or shorter than

expected ion signal indicates coincidence of cells in one integration window or presence of cell fragments. Spectra are recorded at 13 μs intervals. Between cell events, the spectra are largely blank. When an ion cloud arrives at the detector, a series of some 20 spectra reflect the Gaussian-like transient signal of a single cell event which lasts up to 400 μs and contains all of the metal ions associated within the cell, including those metal or lanthanoid isotopes that were intentionally attached as tags or stains (of antibodies, intercalators to stain the DNA and metallic viability indicator stains). Lanthanoid containing μm -sized polymer particles are used as quality control standards and for instrumental optimization.

An example is provided in Figure 11.1 showing a screen capture during the analysis of a human peripheral blood mononuclear cell (PBMc) sample stained with 27 metal-tagged antibodies using enriched lanthanoid isotopes. The display indicates a peak each time an ion signal is recorded and shows the masses along the X-axis and the sequential spectra of each antibody along the vertical axis. It is clear that the raw data clusters in two dimensions are aligned indicating a complex and unique ion structure of every cell event. The different antibodies (cluster of differentiation [CD]2–CD117 and human leukocyte antigen – antigen D-related [HLA-DR]) are binding to receptors on the surface of a cell and are thus able to differentiate different cell populations. Iridium-containing DNA intercalators are used as trigger for a cell event and dead cells are identified by a metal-containing stain based on a treatment with a cisplatinum or rhodium intercalator. These dead cell events are separated from

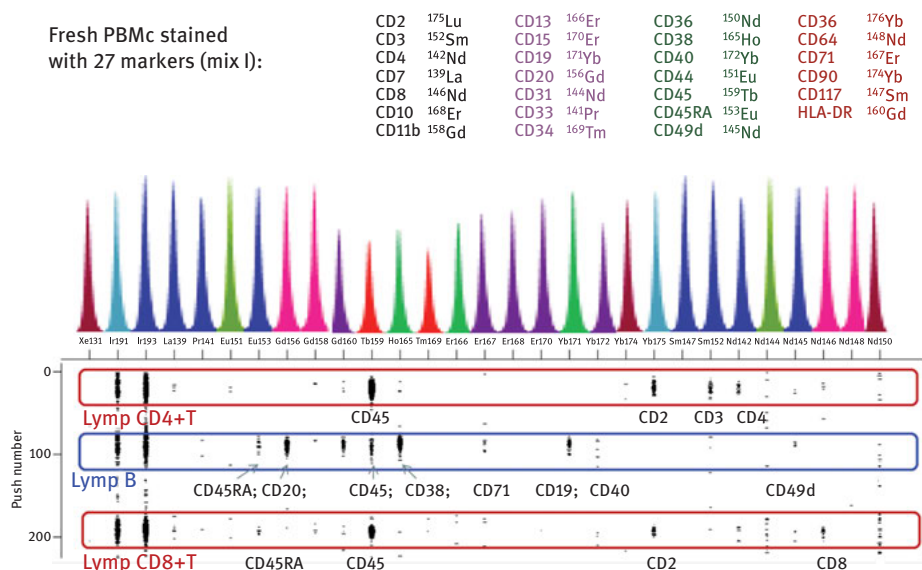


Figure 11.1: A screen capture of raw digitized data for slurry nebulization of a human PBMc sample stained with 27 metal-tagged antibodies and with Ir-containing DNA-intercalator. The concomitance of the metal tag and intercalator signals identify a single-cell event. (By permission of ABC.)

the total number of all cells measured. Again all antibodies and stains are measured simultaneously and time resolved in each single cell event.

Analytically, such a concept can be used for instance to identify the differentiation type of diseased blood cells in childhood leukemia, where the success of a chemotherapy strongly depends on the subtypes of the disease, or in stem-cell research where differentiation can now be followed (for more details, see a recent review [25]).

For more details about data handling of massively multi-parametric single cell assays analyzed by CyTOF™ technology, please see a recent review [26] and for more information on CyTOF™ developments the reviews of Björnson et al. [27] and Bendall et al. [28] are recommended for further reading.

The applications of mass cytometry will have an important impact on fundamental, clinical and pharmaceutical research, and in principle, it is an important new analytical tool on the way to a personalized diagnosis.

11.3.2.2 Applications of lanthanoides in bio- and immuno-imaging

In recent years, significant progress has been made in the development and application of imaging mass spectrometric techniques such as matrix-assisted laser desorption/ionization MS and secondary ion mass spectrometry for the determination of the distribution of organic compounds and elements in biological tissue samples [29]. The main drawback of the mentioned methods however is the quantification step because the analytical signal is strongly dependent on the matrix and its local environment. Exactly here, laser ablation inductively coupled plasma mass spectrometry (LA-ICP-MS) has significant advantages, because a simple calibration strategy is often allowed by use of homemade matrix matched standards.

Concerning the analytical capabilities, LA-ICP-MS combines a few very important features. It provides spatially resolved information on element distribution (qualitative and quantitative) in thin sections of biological samples for instance of brain tissue to study neurodegenerative diseases or tumor growth [30]. By rastering with a laser across the sample, a two-dimensional image can be reconstructed that shows the relative intensities of the respective elements. In the past, this technique was most often applied for qualitative imaging of biological samples (bio-imaging) only, due to a lack of internal standards and quantification concepts.

11.3.2.2.1 Internal standard and calibration concepts for LA-ICP-MS

Presently, LA-ICP-MS detection is mainly used as a qualitative imaging method while the development of suitable calibration concepts and internal standards for quantification and improvement of the reproducibility and accuracy are still under investigation [31].

In liquid analysis, the internal standard is used for drift correction and calibration and thus it is required that the standard should have physical and chemical properties similar to the analyte element during the pneumatic nebulization process, the transport, ionization and transmission into the ICP-MS. In LA, it should correct

additionally for differences in the ablation process by laser instabilities or changes of sample properties to compensate variations or drift effects during the LA process.

For internal standardization elements such as ^{13}C in nitrocellulose (NC) membranes [32], the iodination of intact proteins [33] or gold deposition on sample surfaces of tissues [34] are used for signal normalization only but cannot yet be used for the development of quantification schemes. Concerning development of calibration strategies for LA-ICP-MS different techniques are described in literature. Often solid materials such as metals or glasses or alternatively matrix matched in-house standards are used in order to account for matrix effects as well as variations in ablated and transported mass, and instrumental drift [35]. Various normalization approaches and quantification strategies are aiming these critical properties described in detail in the reviews from Konz et al. [34] and Hare et al. [31].

Feldmann et al. [36] used an ink-jet pattern to optimize the wash out of a LA cell for detection of hetero-elements in proteins blotted onto membrane by LA-ICP-MS while Bellis et al. used commercial inks with ordinary copper content as a reference for biological samples in LA-ICP-MS [37].

In 2014, Hoesl et al. [38] investigated a new approach using inks of a commercial inkjet printer, which are spiked with different elements (In, Th, Er and Pr), printed onto the top of a sample for internal standardization and calibration in LA-ICP-MS. For this purpose, two different types of inks were spiked with characteristic metal contents. The first set of ink contains indium as an internal standard whereas the second ink contains multiple lanthanoid metals for a calibration of proteins and antibodies tagged by a metal. Simultaneous detection of all elements by LA-ICP-MS was tested in a model investigation using proteins separated by sodium dodecyl sulfate polyacrylamide gel electrophoresis (SDS-PAGE) and electro-blotted onto an NC membrane.

The printed internal standard (In) achieved adequate RSD values of 5 % for homogeneity of the printed areas and 2 % for the reproducibility. Additionally, the calibration approach revealed excellent relative process standard deviations of 1 % and detection limits as low as 1–4 fmol only. While each of the approaches for standardization and calibration can be used independently, their combination is even more powerful. Standard proteins have been tagged before PAGE separation and could be quantified on the electroblot membrane by use of the metal doped ink. Thus, the comparison of the original amount of protein loaded onto the gel and the fraction of protein detected on the membrane allowed to calculate the losses during the gel separation and the electrotransfer (of less than 1 %). Additionally, the evaluation of the newly developed inkjet-mediated standardization and calibration was utilized for indirect protein quantification using metal-tagged antibodies in a Western blot immunoassays of three model proteins. In future, these studies can be used to develop work flows for quantitative proteomics.

Recently, the printing strategy for internal standardization by use of lanthanoides was adapted for LA-ICP-MS analysis of tissue sections by Hoesl et al. [39] and Moraleja

et al. [40]. The latter researcher extended this approach for standardization (Ir) and for isotope dilution (Pt isotopes for Pt-containing drugs) by using isotopic spike solutions to improve the accuracy in the quantification step.

The authors of this chapter are very much convinced that standardization will open a new door in clinical applications and drug research. Additionally, real quantification is a completely new dimension on the way of quantitative proteomics and microscopy. Similar to fluorescence spectroscopy, lanthanoides will play a very central role for the development of stains and tags for biomarkers in mass cytometry and quantitative mass microscopy.

11.3.2.2.2 Application for protein tagging

The potential of LA-ICP-MS to detect, quantify and map biomolecules was first described by Neilsen et al. [41] in electrophoresis gels. In the beginning of this new technology, metal tagging was mainly applied for indirect detection of specific proteins via the metal tag. In principle, the tagging chemistry cannot be applied only for tagging of a single protein but for a whole set of biomolecules and even for a whole proteome. Such a tagging procedure would allow developing analytical strategies comparable to differential expression studies which are well-known for gel electrophoresis (difference gel electrophoresis): Such a technology allows the study of different proteomes from different experiments after stimulation of the protein expression by an external stimulus, for instance, oxidative stress and each experiment is coded by a (fluorescence) color [42]. Although this technology looks very promising, only a few applications have been presented in literature so far for ICP-MS applications, although it was applied already first for metallodrugs to study metal-protein adduct formation [43]. He et al. studied the proteome differential expression in *E. coli*, in response to heat stress using bio-conjugation of two proteomes: a control and a heat stress proteome [44]. Both whole proteomes have been tagged by two different lanthanoides (Tm, Lu). LA-ICP-MS was used for detection to locate Heat Shock Proteome expressed differentially by the heat shock in a two-dimensional gel electrophoresis by a comparison of the signal intensities of the different lanthanoides representing the two sample states. Whereas LA-ICP-MS was used for screening of the differential expression of proteins in protein spots on the gel, these spots were then analyzed by organic MS (ESI-MS) to identify the proteins that showed the differential expression. Due to the excellent sensitivity of LA-ICP-MS, new potential heat shock proteins with very low abundance were found. As said before, differential expression studies have been performed already in biochemistry using fluorescence colors, however, MS now can extend the number of “colors” significantly.

A multiplexed quantification of plant thylakoid proteins on Western blots using lanthanoid-tagged antibodies and LA-ICP-MS was discussed by de Bang et al. [45]. The method allowed reproducible and multiplexed quantification of five thylakoid proteins extracted from chloroplasts of the plant species “*Arabidopsis thaliana*” and

was capable of measuring the L subunit in a photosystem I protein of an *Arabidopsis* mutant containing only less than 5 % of this particular protein, relative to the wild-type.

The multiplex detection of cytochromes P450 (CYP) by different lanthanoide-tagged antibodies in electrophoretically separated and electroblotted liver microsomal protein samples of rats treated with xenobiotic or cancerogenic compounds has been investigated by Waentig et al. [46]. CYP P450 is a family of iron-containing enzymes strongly involved in the metabolism of xenobiotic compounds such as toxicants and drugs. Quantitative analysis of CYP patterns of cells and tissues is an important aspect in toxicological and pharmacological research. Detection limits in the medium fmol range were achieved. Competition of antibody binding could be neglected as the quantitative data obtained by single immunoassays were comparable to the multiplex assay. This offers the use of high-throughput microarray instead of sample separation by electrophoresis and blotting procedures, which are time consuming and vulnerable to sample losses.

Microarrays allow the arrangement of hundreds of protein spots just on a single microscopic slide by use of conventional spotter technology. After spotting, the array is incubated with metal tagged antibodies directed against biomarkers indicative for a specific disease or for expression of relevant proteins. Such microarray platform exists already but with antibodies tagged by fluorescence tags. Again, as it was the case for mass cytometry, the same advantages are valid here. Consequently, a new multi-parametric protein microarray embracing the multi-analyte capabilities of LA-ICP-MS was developed for CYP P450 detection in a proof of principle experiment by Waentig et al. [47].

By use of LA-ICP-MS for detection of the multi-parametric protein microarray, it was possible to simultaneously determine the expression of 8 cytochromes (color coded by the lanthanoide intensity in Figure 11.2) in 14 different rat experiments (coded by the position on the microarray). Each array spot has a diameter of 400 μm , so that about 224 spots (single samples) on a single microscopic slide can be analyzed (see also Figure 11.2). The methodology presented here shows excellent detection

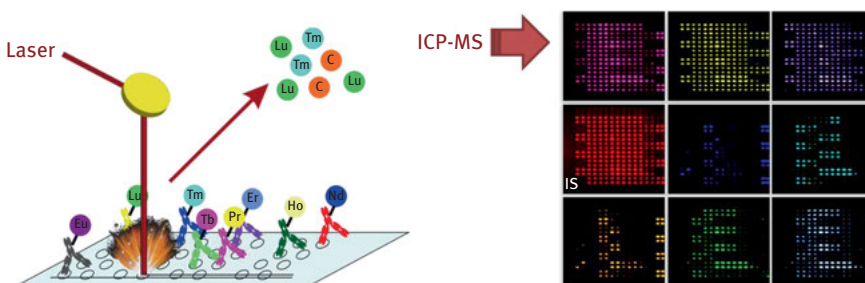


Figure 11.2: Workflow of the protein microarray.

limits in the lower attomol range and a very good linearity which is a prerequisite for development of further quantification strategies. Again, such an assay looks promising for a personalized diagnosis because hundreds of patient samples can be tested for many biomarkers in one run.

11.3.2.2.3 Application for single-cell analysis

Protein spots in a Western blot assay or microarray are rather large structures at mm sizes. However, protein staining also works at cellular levels, which will be demonstrated in the next example. For such an application, the laser diameter needs to be reduced to the low μm scale, thus by a factor of roughly 1,000. Reducing the laser spot size is inherently related to a reduction in sensitivity, due to the fact that the volume/area and thus the number of atoms in this ablated volume (area) is tremendously reduced. Thus, a compromise between sensitivity and spot size is usually driven by the application and this was the reason why imaging with single-cell resolution has not been investigated frequently for essential elements in cells. However, single-cell resolution was demonstrated already in a few publications where either elemental staining or uptakes of metallic nanoparticles by cells are presented (for more details, see review [25]). Concerning the latter application, it should be mentioned that depending on the size, metallic nanoparticles can be taken up by cells by endocytosis and are enriched in the cells. Thus, the metal atoms become locally enriched in the cell, so that sensitivity is not a limiting factor anymore. LA-ICP-MS therefore has already been applied for these types of application [48]. In this work, the sample (a biological cell) has been ablated in a line scan using a differential scanning mode, which is discussed in more detail elsewhere [25]. This scanning mode allows a local resolution for very thin samples (thin cuts of tissues and cells) which are smaller than the laser spot size and mainly limited only by the dispersion of the LA system. Such a methodology will become even more important, because in many technical processes lanthanoides are already applied in the form of nanoparticles, e.g. as cerium(IV) oxide. An example for the detection of lanthanoid-containing nanoparticles is presented in the next chapter.

Gd-containing contrast agents are often used for MRI in clinical diagnosis and in an experiment presented by Managh et al., human CD4⁺ T cells were incubated with commercially available Gd-based MRI contrast agents (Omniscan and Dotarem, see Analysis and Speciation of Lanthanoides by ICP-MS) [49]. In the chelated form, these substances are not toxic and are taken up easily by living cells. Up to 10⁸ Gd atoms/single cell were detected under optimal conditions. In this example, the cell diameter (about 10 μm) was much smaller than the applied laser spot diameter (25 μm), so that in each laser shot, just a single cell was completely ablated. The LA-ICP-MS measurements of single cells showed that the contrast agent could still be detected in the cell for up to 10 days after labeling.

Reifschneider et al. applied thulium as a metallo-stain to investigate the transport of single cells in a mouse model [50]. The stained cells, in particular macrophages and

tumor cells, have been injected intravenously and have been detected by LA-ICP-MS in tissues from different organs (liver, lung and spleen).

Recently, Mueller et al. used a maleimide-DOTA loaded with thulium as a central ion for the elemental staining of a whole single cell [51]. As mentioned in Section 11.2.1, the reactive maleimide group binds covalently to free SH groups such as cysteine and thus this stain is representing the distribution of proteins in a cell. A short incubation time of a few minutes was sufficient for application of LA-ICP-MS imaging of a whole cell proteome with a local resolution in the μm range (see Figure 11.3). Improvements of the local resolution to the sub-micrometer range look feasible if improved LA systems, which are described already in literature, will become commercially available [52].

11.3.2.2.4 Application for tissue analysis

A first investigation where nanoparticles doped with REE are tested for clinical diagnosis should be discussed here. For the development of very small iron oxide nanoparticles (VSOP) for MRI, Prussian blue iron staining was already often applied for iron detection in tissues by microscopy. However, this staining approach is unspecific when tissues contain substantial endogenous iron in particular in a particulate form. Scharlach et al. tested whether microscopy by LA-ICP-MS is sensitive enough to analyze accumulation of VSOP doped with Europium (Eu) in tissue sections and found that this technique is very sensitive and specific for this application [53]. An example is shown in Figure 11.4.

The Eu signals clearly demonstrate that the nanoparticle can penetrate deeply into the tissue in those areas where atherosclerotic plaques have been identified, giving a hint that the barrier of the blood vessel is damaged already in this area possibly by inflammation, because no particles are detected in the intact regions.

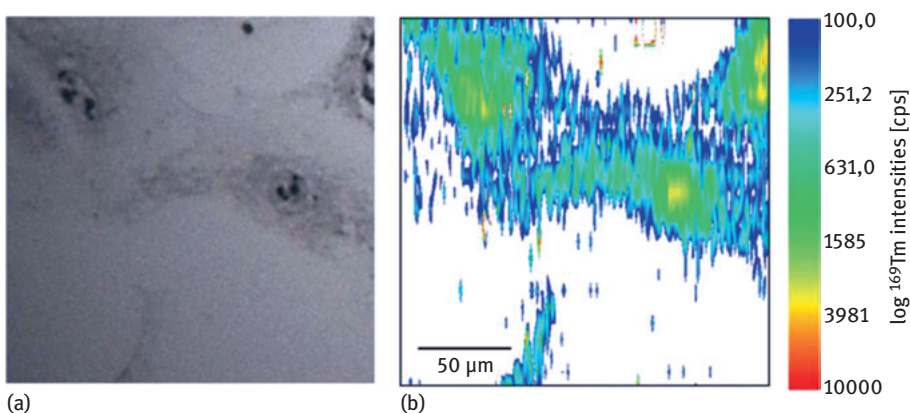


Figure 11.3: A: Microscopic picture of fixed and thulium-stained 3T3 fibroblast cells with Maleimide-DOTA-Tm. B: LA-ICP-MS intensity profile of thulium distribution. Pixel $6.0 \times 0.3 \mu\text{m}^2$.

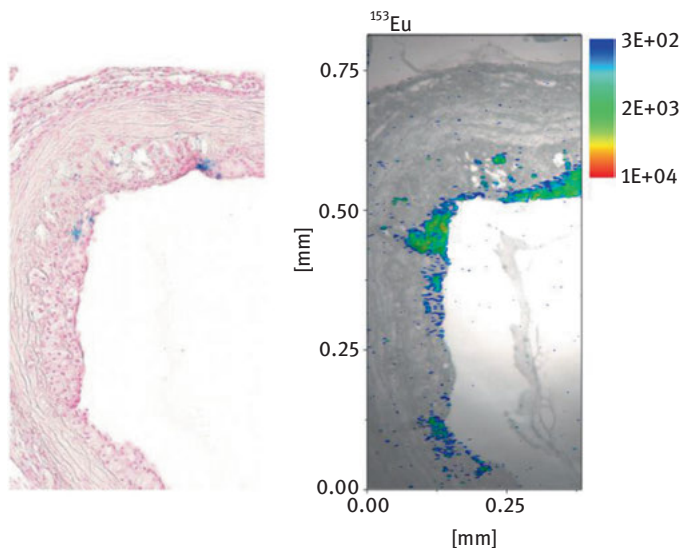


Figure 11.4: Correlation of Eu–VSOP distribution with Prussian blue stained tissue sections (left). Bright field image of an aortic root section and a LA-ICP-MS image of an adjacent slice (right) superimposed on an unstained bright field image. Pixel: $8.0 \times 0.4 \mu\text{m}^2$.

With respect to CyTOF™ technology, it was discussed already that tagging of antibodies is a powerful tool for cell cytometry, where the cells are measured as a suspension in solution. Of course, the same chemistry can also be applied for imaging of cells and tissues placed onto microscopic slides as it is done already in immunohistochemistry (IHC). The principle for this application is often applied already routinely in pathology. In conventional IHC, a primary antibody which is directed against a biomarker (e.g. a protein which is expressed during cancer) is applied and binds directly to surface proteins or receptors on a cell surface of a thin cut of a tissue or a biopsy sample. In IHC, a secondary antibody is applied which carries the analytical information which becomes visible by a color change or a fluorescence signal. The analytical information is read out by use of a microscope and visual inspection. Thus, the color and the morphology of the tissue are the relevant parameters for the diagnosis and have an important impact for instance on the choice of an adequate therapy. Due to the fact that color changes are very sensible and have only a very small linear dynamic range, the protocols used in the clinical environment are very strict and have to be developed for each new biomarker. If LA-ICP-MS imaging is applied for IHC, only the primary antibody is needed and is coded not by color but by a lanthanoid metal, which then can be detected using a LA system for imaging of the lanthanoid distribution on the surface of the tissue. Again, as before, many different antibodies can be applied simultaneously, so that many biomarkers can be evaluated in the same sample (multiplexing)

but under compromise conditions. The reason for this much higher flexibility is based on the extension of the linear dynamic range by many orders of magnitude so that even compromised conditions lead to outstanding signal to noise ratios and therefore offers the new capability of multiplex analysis even in IHC applications. Such a strategy can increase sample throughput and would lower the analysis costs. Finally, the integration of the lanthanoid ion intensities over tissue areas by application of imaging software delivers a number, and if an internal standardization and calibration is applied, these numbers can become quantitative and thus comparable. This would be an outstanding advantage compared to the present technology.

The direct detection of biomarkers in tissue sections was investigated by Hutchinson et al. who applied Eu- and Ni-tagged secondary antibodies for LA-ICP-MS imaging of beta-amyloid deposits in mouse brain tissue to study Alzheimer's plaques which were highlighted by the Eu signals [54].

The first multiplexed immunohistochemical approach was presented by Giesen et al. who used three tumor markers tagged with lanthanoids for detection in a single cancerous tissue section [55]. In this case, primary antibodies against the human epidermal growth factor receptor 2 (Her 2), mucin 1 (MUC 1 – a membrane-associated protein), and cytokeratin 7 (CK7 – a type II cytokeratin, which is specifically expressed in glandular epithelia) were tagged with holmium, terbium and thulium via the reagent SCN-DOTA, respectively.

A breast cancer tissue section of 5 μm thickness was incubated with the lanthanoid labeled antibody pool simultaneously. As said before, in this case, no secondary antibody was needed. The expression levels of the tumor markers could be directly compared with the same section which is of great benefit for standardization of the results in IHC. Moreover, the LA-ICP-MS analysis indicated different expression levels for Her 2, Muc 1 and CK7, which was not obvious from the conventionally stained IHC sections. This method had been improved over the last years so that the state-of-the-art is presented in a very recent paper of Giesen et al. [56]. Here a formalin-fixed, paraffin-embedded (FFPE) Her 2-enriched breast cancer tissue section incubated with a polymer (including Ho) tagged antibody against Her 2 was investigated. The resulting image had a pixel size of $1 \times 1 \mu\text{m}$ and allows a precise analysis of the cell membrane-bound anti-Her 2. More recently, Giesen and coworkers used the same LA cell in combination with a simultaneous detecting CyTOFTM (see also Analysis and Speciation of Lanthanoids by ICP-MS) for spatial resolved multiplexing immunomaging of 32 proteins and their modifications in FFPE breast cancer tissue samples and human mammary epithelial cells [56]. The results were validated with conventional immunofluorescence microscopy and no significant changes in specificity and performance of the antibodies used for fluorescence and the CyTOFTM measurements could be observed. Furthermore, it could be shown that even high numbers of metal-tagged antibodies didn't interfere with each other during the immune reaction. The study reached subcellular resolution for the first time in a multiplex immunomaging approach using the previously mentioned polymer-tagged antibodies and LA-ICP-TOF-MS.

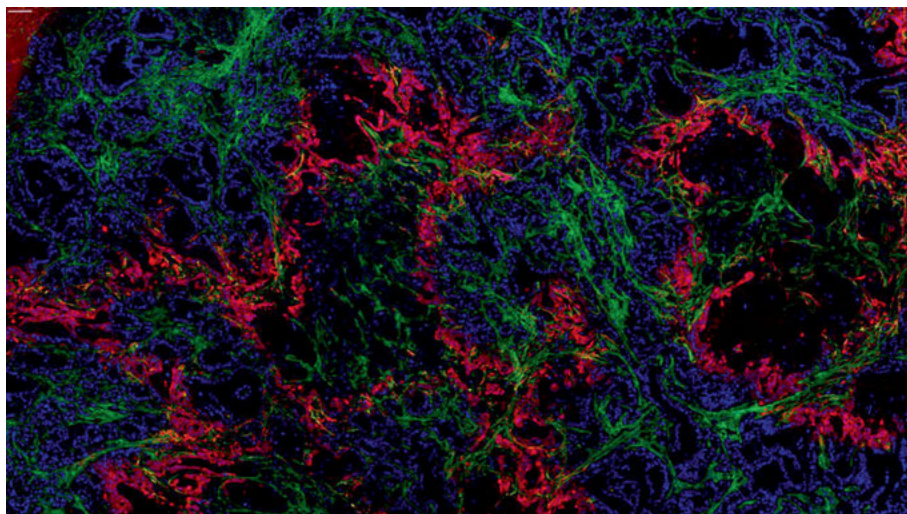


Figure 11.5: A color coded LA-ICP-MS measurement of a pancreatic xenograft tissue sample. Anti-pimonidazole: red; anti-collagen I: green; anti-histone H3: blue. Ablation area: $3,840 \times 2,160 \mu\text{m}$. Scale bar: $100 \mu\text{m}$, shown in the top left corner (with courtesy of Vladimir Baranov, Fluidigm Corp.).

For illustration of the state of the art, a color-coded LA-ICP-MS measurement of pancreatic xenograft tissue sample (patient pancreatic tumor implanted into an immunodeficient mouse) is shown in Figure 11.5. Three biomarkers which play a role in the development of pancreatic cancer are shown as an example with micrometer laser spot size resolution. The antibody directed against pimonidazole, a hypoxia tracer administered to the mouse prior to tissue harvest, is tagged with Ho and is used as a marker of tumor cells in regions of low oxygen (hypoxia) (shown in red color). The antibody directed against collagen I is tagged with Tm (shown in green color) and stains the mouse stroma, whereas the antibody directed against the histone H3 conjugated to ^{176}Yb tag (shown in blue color) shows all cell nuclei. Results are presented here only for 3 out of 18 biomarkers measured simultaneously.

To summarize, this new technology of metal-tagged antibodies allows multiplex analysis of clinical biomarkers relevant for normal and disease processes at cellular levels in tissues; however, many problems have still to be solved to implement LA-ICP-MS as an imaging method which is emerging from “bench to bedside” (for more details, see a recent review [57]).

11.4 Outlook

In the last decade, different ICP-MS-based methods for the detection and quantification of all kinds of biomolecules (peptides, proteins, DNA, RNA and antibodies) using lanthanoides as metal tags or stains have successfully been developed. But, as

a conclusion, the authors want to summarize that the immunoassays and metal-staining techniques presented here in combination with mass cytometry and with bioimaging using LA-ICP-MS are up to now only used for basic discovery and healthcare applications. However, they have the potential in future to be applied as a very new and promising approach toward personalized diagnosis and therapies. Moreover, with the new technologies developed for LA-ICP-MS, a quantitative elemental microscope becomes feasible.

To summarize, the immunoassays presented here have already opened a new door for quite different novel applications of most lanthanide elements in clinical diagnostics where up to now only Gd-containing contrast agents are well established.

References

- [1] Bettmer J, Jakubowski N, Prange A. Elemental tagging in mass spectrometric bioanalysis. *Anal Bioanal Chem* 2006, 386, 7–11.
- [2] Swart C, Jakubowski N. Update of the status of metrology for metalloproteins. Sent for publication to *J Anal At Spectrom* 2016, 31, 1756–65.
- [3] Giesen C, Wäntig L, Jakubowski N, Panne U. History of (LA) ICP MS based immunoassays *spectrochim. Acta Part B* 2012, 76, 27–39.
- [4] Schwarz G, Müller L, Beck S, Linscheid MW. DOTA based metal labels for protein quantification: A review. *J Anal At Spectrom* 2014, 29, 221–33.
- [5] Hermanson GT. *Bio-conjugation Techniques*. Oxford, Elsevier Ltd, 2nd revised edn (REV), 2008.
- [6] Mayer G. The chemical biology of aptamers. *Angew Chem Int Ed* 2009, 48, 2672–89.
- [7] McDevitt MR, Ma DS, Simon J, Frank RK, Scheinberg DA. Design and synthesis of Ac-225 radioimmunopharmaceuticals. *Appl Radiat Isotopes* 2002, 57, 841–7.
- [8] Lewis MR, Raubitschek A, Shively JE, Facile A. Water-soluble method for modification of proteins with DOTA – use of elevated-temperature and optimized Ph to achieve high specific activity and high chelate stability in radiolabeled immunoconjugates. *Bioconjugate Chem* 1994, 5, 565–76.
- [9] Baranov V, Quinn Z, Bandura DR, Tanner SD. A sensitive and quantitative element-tagged immunoassay with ICPMS detection. *Anal Chem* 2002, 74, 1629–36.
- [10] Zhang C, Wu F, Zhang X. ICP-MS-based competitive immunoassay for the determination of total thyroxin in human serum. *J Anal At Spectrom* 2002, 17, 1304–7.
- [11] Whetstone PA, Butlin NG, Corneillie TM, Meares CF. Element-coded affinity tags for peptides and proteins. *Bioconjugate Chem* 2004, 15, 3–6.
- [12] Krause M, Scheler C, Böttger U, Weisshoff H, Linscheid MW. Verfahren und Reagenz zur spezifischen Identifizierung und Quantifizierung von einem oder mehreren Proteinen in einer Probe. German Patent. Patent Number 10227599 B4 (2005).
- [13] Lou XD, Zhang GH, Herrera I, Kinach O, Ornatsky O, Baranov V, Nitz M, Winnik MA. Polymer-based elemental tags for sensitive bioassays. *Angew Chem Int Ed* 2007, 46, 6111–4.
- [14] de Bang TC, Husted S. Lanthanide elements as labels for multiplexed and targeted analysis of proteins, DNA and RNA using inductively-coupled plasma mass spectrometry. *Trends in Anal Chem* 2015, 72, 45–52.
- [15] Ahrends R, Pieper S, Kühn A, Weisshoff H, Hamester M, Lindemann T, Scheler C, Lehmann K, Taubner K, Linscheid MW. A metal-coded affinity tag approach to quantitative proteomics. *Mol Cell Proteomics* 2007, 6, 1907–16.
- [16] Ahrends R, Pieper S, Neumann B, Scheler C, Linscheid MW. Metal-coded affinity tag labeling: A demonstration of analytical robustness and suitability for biological applications. *Anal Chem* 2009, 81, 2176–84.

- [17] Esteban-Fernández D, Scheler C, Linscheid MW. Absolute protein quantification by LC-ICP-MS using MeCAT peptide labeling. *Anal Bioanal Chem* 2011, 401, 657–66.
- [18] El-Khatib A, Esteban-Fernández D, Linscheid MW. Inductively coupled plasma mass spectrometry-based method for the specific quantification of sulfenic acid in peptides and proteins. *Anal Chem* 2014, 86, 1943–8.
- [19] López-Fernández L, Blanco-González E, Bettmer J. Determination of specific DNA sequences and their hybridisation processes by elemental labelling followed by SEC-ICP-MS. *Analyst* 2014, 139, 3423–8.
- [20] Brückner K, Schwarz K, Beck S, Linscheid MW. DNA Quantification via ICP-MS using lanthanide-labelled probes and ligation-mediated amplification. *Anal Chem* 2014, 86, 585–91.
- [21] Coons AH, Creech H J, Jones R N. Immunological properties of an antibody containing a fluorescent group. *P Soc Exp Biol Med* 1941, 47, 200–2.
- [22] Yalow RS, Berson SA. Immunoassay of endogenous plasma insulin in man. *J Clin Invest* 1960, 39, 1157–75.
- [23] Tanner SD, Bandura DR, Ornatsky O, Baranov V, Nitz M, Winnik MA. Flow cytometer with mass spectrometer detection for massively multiplexed single-cell biomarker assay. *Pure Appl Chem* 2008, 80, 2627–41.
- [24] Bandura D, Baranov V, Ornatsky O, Antonov A, Kinach R, Lou XD, Pavlov S, Vorobiev S, Dick JE, Tanner SD. Mass cytometry: technique for real time single cell multitarget immunoassay based on inductively coupled plasma time-of-flight mass spectrometry. *Anal Chem* 2009, 81, 6813–22.
- [25] Mueller L, Traub H, Jakubowski N, Drescher D, Kneipp J, Baranov V. Trends in single cell analysis by ICP-MS. *Anal Bioanal Chem* 2014, 406, 6963–77.
- [26] Zivanovic N, Jacobs A, Bodenmiller B. A Practical Guide to Multiplexed Mass Cytometry. Chapter in the book: High-dimensional single cell analysis, Springer Series Fienberg, Harris G. et al. (eds.) *Curr Top Microbiol Immunol* 2014, 377, 95–109. ISBN 978-3-642-54827-7.
- [27] Bjornson ZB, Nolan GP, Fantl WJ. Single-cell mass cytometry for analysis of immune system functional states. *Current Opin Immunol* 2013, 25, 484–94.
- [28] Bendall SC, Nolan GP, Roederer M, Chattopadhyay P. A deep profiler's guide to cytometry. *Trends Immunol* 2012, 33, 323–32.
- [29] Adam F, Barbante C. Chemical Imaging Analysis. Series Comprehensive Analytical Chemistry ed. by Barcelo, D. Series 69, Amsterdam, Wilson & Wilson, Elsevier, 2015. ISBN 978-0-44463439-9.
- [30] Limbeck A, Galler P, Bonta M, Bauer G, Nischkauer W, Vanhaecke F. Recent advances in quantitative LA-ICP-MS analysis: Challenges and solutions in the life sciences and environmental chemistry. *Anal Bioanal Chem* 2015, 407, 6593–617.
- [31] Hare D, Austin C, Doble P. Quantification strategies for elemental imaging of biological samples using laser ablation-inductively coupled plasma-mass spectrometry. *Analyst* 2012, 137, 1527–37.
- [32] Fan TW, Pruszkowski E, Shuttleworth SJ. Speciation of selenoproteins in Se-contaminated wildlife by gel electrophoresis and laser ablation-ICP-MS. *J Anal At Spectrom* 2002, 17, 1621–3.
- [33] Jakubowski N, Messerschmidt J, Garijo Anorbe M, Waentig L, Hayen H, Roos PH. Labelling of proteins by use of iodination and detection by ICP-MS. *J Anal At Spectrom* 2008, 23, 1487–96.
- [34] Konz I, Fernandez B, Fernandez ML, Pereiro R, Sanz-Medel A. Laser ablation ICP-MS for quantitative biomedical applications. *Anal Bioanal Chem* 2012, 403, 2113–25.
- [35] Macedone JH, Gammon DJ, Farnsworth PB. Factors affecting analyte transport through the sampling orifice of an inductively coupled plasma mass spectrometer. *Spectrochim Acta Part B-Atomic Spectrosc* 2001, 56, 1687–95.
- [36] Feldmann I, Koehler CU, Roos PH, Jakubowski N. Optimisation of a laser ablation cell for detection of hetero-elements in proteins blotted onto membranes by use of inductively coupled plasma mass spectrometry. *J Anal At Spectrom* 2006, 21, 1006–15.

- [37] Bellis DJ, Santamaria-Fernandez R. Ink jet patterns as model samples for the development of LA-ICP-SFMS methodology for mapping of elemental distribution with reference to biological samples. *J Anal At Spectrom* 2010, 25, 957–63.
- [38] Hoesl S, Neumann B, Techritz S, Linscheid MW, Theuring F, Scheler C, Jakubowski N, Mueller L. Development of a calibration and standardization procedure for LA-ICP-MS using a conventional ink-jet printer for quantification of proteins in electro- and Western-blot assays. *J Anal At Spectrom* 2014, 29, 1282–91.
- [39] Hoesl S, Neumann B, Techritz S, Sauter G, Simon R, Schlüter H, Linscheid MW, Theuring F, Jakubowski N, Mueller L. Internal standardization of LA-ICP-MS immuno imaging via printing of universal metal spiked inks onto tissue sections. *J Anal At Spectrom* 2016, 31, 801–8.
- [40] Moraleja I, Esteban-Fernández D, Lázaro A, Humanes B, Neumann B, Tejedor A, Luz Mena M, Jakubowski N, Gómez-Gómez MM. Printing metal-spiked inks for LA-ICP-MS bioimaging internal standardization: Comparison of the different nephrotoxic behavior of cisplatin, carboplatin, and oxaliplatin. *Anal Bioanal Chem* 2016, 408, 2309–18.
- [41] Neilsen JL, Abildtrup A, Christensen J, Watson P, Cox A, McLeod CW. Laser ablation inductively coupled plasma-mass spectrometry in combination with gel electrophoresis: A new strategy for speciation of metal binding serum proteins. *Spectrochim Acta Part B-Atom Spectrosc* 1998, 53, 339–45.
- [42] Unlü M, Morgan ME, Minden JS. Difference gel electrophoresis: A single gel method for detecting changes in protein extracts. *Electrophoresis* 1997, 18, 2071–7.
- [43] Moreno-Gordaliza E, Esteban-Fernández D, Giesen C, Lehmann K, Lázaro A, Tejedor A, Scheler C, Cañas B, Jakubowski N, Linscheid M, Gomez M. LA-ICP-MS and nHPLC-ESI-LTQ-FT-MS/MS for the analysis of cisplatin–protein complexes separated by two dimensional gel electrophoresis in biological samples. *J Anal At Spectrom* 2012, 27, 1474–83.
- [44] He Y, Esteban-Fernández D, Neumann B, Bergmann U, Bierkandt F, Linscheid MW. Application of MeCAT-Click labelling for protein abundance characterization of *E. coli* after heat shock experiments. *J Proteomics* 2016, 136, 68–76.
- [45] de Bang CT, Shah, P, Cho, SK, Yang SW, Husted S. Multiplexed quantification of plant thylakoid proteins on western blots using lanthanide-labeled antibodies and laser ablation inductively coupled plasma mass spectrometry (LA-ICP-MS). *Anal Chem* 2013, 85, 5047–54.
- [46] Waentig L, Jakubowski N, Roos PH. Multi-parametric analysis of cytochrome P450 expression in rat liver microsomes by LA-ICP-MS. *J Anal At Spectrom* 2011, 26, 310–19.
- [47] Waentig L, Jakubowski N, Techritz S, Roos PH. Multi-parametric microarray for protein profiling: Simultaneous analysis of 8 different cytochromes via differentially element tagged antibodies and laser ablation ICP-MS. *Analyst* 2013, 138, 6309–15.
- [48] Drescher D, Giesen C, Jakubowski N, Traub H, Panne U, Kneipp J. Quantitative imaging of gold and silver nanoparticles in single eukaryotic cells by LA-ICP-MS. *Anal Chem* 2012, 84, 9684–8.
- [49] Managh AJ, Edwards SL, Bushell A, Wood K J, Geissler EK, Hutchinson JA, Hutchinson RW, Reid HJ, Sharp BL. Single cell tracking of gadolinium labeled CD4+ T cells by laser ablation inductively coupled plasma mass spectrometry. *Anal Chem* 2013, 85, 10627–34.
- [50] Reifschneider O, Wentker KS, Strobel K, Schmidt R, Masthoff M, Sperling M, Faber C, Karst U. Elemental Bioimaging of thulium in mouse tissues by laser ablation-ICPMS as a complementary method to heteronuclear proton magnetic resonance imaging for cell tracking experiments. *Anal Chem* 2015, 87, 4225–30.
- [51] Mueller L, Herrmann A. Bilder einzelner Zellen aus dem Elementmikroskop. *Nachr Chem* 2015, 63, 1196–9.
- [52] Wang HA, Grolimund D, Giesen C, Borca CN, Shaw-Stewart JR, Bodenmiller B, Guenther D. Fast chemical imaging at high spatial resolution by laser ablation inductively coupled plasma mass spectrometry. *Anal Chem* 2013, 85, 10107–16.

- [53] Scharlach C, Mueller L, Wagner S, Kobayashi Y, Kratz H, Ebert M, Jakubowski N, Schellenberger E. LA-ICP-MS allows quantitative microscopy of europium-doped iron oxide nanoparticles and is a possible alternative to ambiguous Prussian blue iron staining. *J Biomed Nanotech* 2016, 12, 1001–10.
- [54] Hutchinson RW, Cox AG, McLeod CW, Marshall PS, Harper A, Dawson EL, Howlett DR. Imaging and spatial distribution of beta-amyloid peptide and metal ions in Alzheimer's plaques by laser ablation-inductively coupled plasma-mass spectrometry. *Anal Bioanal Chem* 2005, 346, 225–33.
- [55] Giesen C, Mairinger T, Khoury L, Wöntig L, Jakubowski N, Panne U. Multiplexed immunohistochemical detection of tumor markers in breast cancer tissue using laser ablation inductively coupled plasma mass spectrometry. *Anal Chem* 2011, 83, 8177–83.
- [56] Giesen C, Wang HA, Schapiro D, Zivanovic N, Jacobs A, Hattendorf B, Schöffler PJ, Grolimund D, Buhmann JM, Brandt S, Varga Z, Wild PJ, Guenther D, Bodenmiller B. Highly multiplexed imaging of tumor tissues with subcellular resolution by mass cytometry. *Nature Methods* 2014, 11, 417–22.
- [57] Bodenmiller B. Multiplexed epitope-based tissue imaging for discovery and healthcare applications. *Cell Syst* 2016, 2, 225–38.

Jürgen Meinhardt, Martin Kilo, Ferdinand Somorowsky
and Werner Hopp

12 Lanthanoides in Glass and Glass Ceramics

Abstract: Many types of glass contain lanthanoides; among them, special glass for optical applications is the one with the highest content of lanthanoides. The precise determination of the lanthanoides' concentration is performed by inductively coupled plasma-optical emission spectrometry (ICP-OES). However, up to now, there are no established standard processes guaranteeing a uniform approach to the lanthanoid analysis. The knowledge of the lanthanoides' concentrations is necessary on the microscale in some cases, especially if a suitable separation and recycling procedure is to be applied. Here, the analysis is performed by energy-dispersive X-ray (EDX) or wavelength-dispersive X-ray (WDX) analytics in the scanning electron microscope.

12.1 Introduction

Glass is one of the oldest materials used by mankind. The first glass was produced in ancient Egypt about 4,000 years B.C. Nowadays, it exists in plenty of types and it can be either a mass product with millions of tons of annual production, but also a specialty product with only a few kg of annual production. Currently, about 100 million tons of glass is produced worldwide. There are different types of glass [1]:

1. Container glass (44 % total market amount by weight);
2. flat glass (29 % total market amount by weight);
3. glass fibers (12 % total market amount by weight); and
4. specialty and technical glass and glass ceramics (15 % total market amount by weight).

The first two glass types, covering almost 75 % of the global market volume (in tons, not in money) are only covered by soda-lime glass and besides of coloring elements, the main components of such glass are Na_2O , K_2O , CaO , MgO , Al_2O_3 , and SiO_2 , leading to silicate glass. Glass fibers also usually consist of silicate glass, with the main component SiO_2 . For specialty glass, other elements, like boron oxide, lead oxide, germanium oxide, phosphorous oxide, and others can be the network-forming main component. Regarding special applications, even non-oxidic glass like fluoride glass (for specific optical glass fibers) or chalcogenide glass (for infrared optics) is needed and can be doped with lanthanoides for these applications.

Glass fibers and in particular specialty and technical glass can contain a much larger number of elements than container glass and flat glass. When the composition of the glass is developed, one of the unique material properties of glass is used. Glass as an amorphous component can dissolve almost all elements in considerable amounts. Therefore, glass chemists have developed glass compositions, containing almost all

elements of the periodic system of elements. Modern glass compositions can consist of more than 15 intentionally added cations, each playing a unique role in the final glass or glass ceramics.

Nevertheless, being in a metastable state, glass has always a tendency to crystallize. While this is an unwanted effect for typical container and flat glass or glass fibers, the crystallization of glass is willingly triggered in the case of glass ceramics in order to get new materials with new and specific properties.

Due to the very broad and large application of specialty glass, lanthanoides can be added to the glass for many different reasons, the most relevant being:

1. Coloring agents, amounts <2–3 wt% [2]
2. Mechanical properties, amount <10–15 wt% [3]
3. Tuning optical properties, amount <60 wt% [4]
4. Crystallization agent, amount <3 wt% [5]
5. High Abbe number glass, amount <50 wt%
6. Laser glass, amount <5 wt%

For the production of specialty glass, chemicals of high purity are needed in contrast to container glass and flat glass. Therefore, a good recycling strategy of lanthanoides from specialty glass would be very helpful. At present, a successful recycling is hindered by many different glass systems, corroborated with the fact that almost all lanthanoides containing specialty glass is not a component of glassware but in a system where it has to be extracted. One example for this might be the current cell phone camera: The optical system consists of lenses or prisms made by special glass, containing a large amount of pure lanthanoides like lanthanum oxide or neodymium oxide (up to 20 %). However, the amount of the glass per cell phone is very small, and, depending on the manufacturer, different glass types are used. Another example might be dental glass ceramics. Here, various lanthanoides like samarium, ytterbium, or terbium are added in order to get a natural fluorescence. These lanthanoides are very rare and expensive, but a recycling even of production waste is currently not possible, since the different materials contain different types and amounts of lanthanoides.

Regarding all aspects, a precise knowledge of the chemical composition is mandatory in order to establish lanthanoid recycling strategies.

12.2 Literature survey of rare earth chemical analysis in glass

12.2.1 Laser-ablation inductively coupled plasma mass spectrometry (LA-ICP-MS)

Glass samples containing rare earth oxides, especially trace concentrations, mostly were analyzed using LA-ICP-MS. Historical samples [6–14] and historical silicate ceramics [15] were analyzed also applying this method.

12.2.2 Laser-ablation inductively coupled plasma atomic emission spectrometry (LA-ICP-AES)

This method was applied for the analysis of [8]:

- nuclear waste glass ceramics [16, 17],
- reference glass [18–24], and
- various glass materials [25, 26].

12.2.3 ICP-MS analysis of solutions

The analysis of solutions containing rare earth elements by ICP-MS was published in several papers [17, 20, 21, 27–29].

The dissolution of the sample was performed by hydrofluoric acid digestion, microwave digestion, or melting with lithium metaborate and subsequent dissolution of the melt.

ICP-AES (Inductively Coupled Plasma-Atomic Emission Spectroscopy) after hydrofluoric acid digestion is reported in [30].

12.2.4 X-ray fluorescence analysis (XRF)

XRF for the analysis of low amounts of rare earth oxides suffers from a poor sensitivity. So, high-energy X-rays from a synchrotron were used to quantify rare earth oxides in glass [14, 31–33], even for forensic purpose [34, 35]. “Normal” XRF was used to examine historical silicate ceramics [36–38].

12.3 Analytical methods for the determination of main components of glass (except lanthanoides)

Details of ICP and X-ray fluorescence (XRF) are presented in chapters 5–6 and 8 of this book, respectively. Comparing methods, it is to be mentioned that it is easier to prepare a multielement standard solution for ICP than to produce or acquire a solid standard for XRF or ICP analysis. On the other hand, direct measurements of solids need less time than a procedure with decomposition of the solid. The reproducibility of XRF is better than of ICP. The detection limits are lower for ICP, especially ICP-MS.

There are some specific features of glass analysis:

In the case of XRF, glass can either be measured directly or, because of its relative low melting point, converted to a fused bead by remelting without fluxing agent. The benefit is a higher sensitivity that means lower detection limits compared to sample preparation by diluting with a fluxing agent.

Some glass contains B_2O_3 or Li_2O or both of them. If a complete analysis of the glass sample (a sum of 100 %) is required, these components have to be determined. For physical reasons, it is impossible to measure Li_2O by XRF. B_2O_3 can be determined in glass samples prepared without fluxing agent. Because of an information depth of

the boron radiation below 1 μm , it is necessary to have planar polished surfaces [39]. Otherwise, the B_2O_3 determination is performed as the Li_2O determination, e.g., by ICP-OES in solution after decomposition (see next chapter).

For the analysis with ICP, glass can be decomposed by hydrofluoric acid digestion which leads to an acid solution free of Si (in most cases, the main component of the glass) and B. Therefore, a higher sample weight can be used which lowers the detection limits.

SiO_2 is determined gravimetrically after melting the sample with sodium carbonate, dissolving the melt in HCl and precipitation of the SiO_2 . The precipitated SiO_2 is filtered, ignited, and then weighed [40, 42].

B_2O_3 is determined by ICP-OES after melting the sample with sodium carbonate, dissolving the melt in HCl and filtering from precipitated material [41, 42].

Fluorine in glass can be determined by XRF or by wet chemistry [42, 43]. One digestion method is the pyrohydrolysis in a tube furnace at 1,050°C with superheated water vapor in presence of a catalyst. The fugitive fluorine components are distilled into water. The second method is sintering the glass powder with a mixture of sodium carbonate and zinc oxide at 1,000°C. After cooling, the melt is extracted. In both cases, the fluoride ion can be measured electrometrically (fluoride-sensitive electrode), by ion chromatography or photometrically (alizarin–ethylenediaminetetraacetic acid complex).

12.4 Preparation of sample solutions for glass analysis by ICP-OES

12.4.1 Hydrofluoric acid digestion

The most common procedure for dissolution of glass samples in order to analyze the components except SiO_2 and B_2O_3 is the hydrofluoric acid digestion. The advantage of this method is the removal of the matrix components SiO_2 (and B_2O_3 if present) and of the harmful hydrofluoric acid by evaporation. Several variations exist:

12.4.1.1 Hydrofluoric acid–sulfuric acid digestion (procedure B)

The powdered glass sample is weighed into a platinum dish and soaked with deionized water [44]. Then hydrofluoric acid and sulfuric acid are added carefully. The mixture is heated slowly on a heating plate until the sulfuric acid begins to fume. After cooling, the mixture is heated with additional hydrofluoric acid until all liquid is evaporated. After heating in a muffle furnace and cooling, the dry residue is dissolved in hydrochloric acid.

12.4.1.2 Hydrofluoric acid–perchloric acid digestion (procedure C)

The powdered glass sample is weighed into a platinum dish and soaked with deionized water [44]. Then hydrofluoric acid and perchloric acid are added. After stirring

and waiting for 30–60 min, the mixture is heated on a heating plate until all liquid is evaporated. After cooling, the evaporation is repeated with hydrofluoric acid and perchloric acid. After cooling, again the dry residue is dissolved in hydrochloric acid.

12.4.1.3 Modified hydrofluoric acid–perchloric acid digestion

In several laboratories, a modified procedure is used: The powdered glass sample is weighed into a graphite crucible. Then a mixture of HNO_3 , HF, and HClO_4 is added. By heating it to 110°C and then to 140°C , all acids are evaporated. After cooling, the dry residue is dissolved in hydrochloric acid.

This procedure can be performed in a closed system where the harmful hydrofluoric acid is neutralized after evaporation by a sodium hydroxide solution.

12.4.2 Melt digestion

Some components which resist the hydrofluoric acid digestion can be dissolved by melt digestion. The disadvantage of the method is a high concentration of matrix elements (e.g., Na, Si) in the measuring solution which limits the range for the application in an ICP-OES spectrometer. The solution has to be diluted, and the use of an ultrasonic nebulizer is rather impossible. Several variations exist:

12.4.2.1 Sodium carbonate melt digestion (procedure A)

The powdered glass sample is weighed into a platinum dish, mixed with sodium carbonate, and then heated to $1,000^\circ\text{C}$. After cooling, the melt is dissolved with water and nitric acid [44].

12.4.2.2 Sodium carbonate/potassium carbonate melt digestion (procedure 10.4)

The powdered glass sample is weighed into a platinum crucible, mixed with sodium carbonate, potassium carbonate, and sodium peroxide and then heated to $1,000^\circ\text{C}$ [45]. After cooling, the melt is dissolved with water and nitric acid.

12.5 ICP-OES analysis of rare earth elements

ICP-OES measurements can be performed according to DIN 51086-2 [45]. Specific wavelengths for some rare earth elements are given (Table 12.1). DIN 51086-2 is being extended for the missing rare earth elements (Table 12.2).

12.6 Analysis of special optical glass

Two samples of optical glass were analyzed in ISC by hydrofluoric acid–perchloric acid digestion described in Chapter 4.1.3. SiO_2 and B_2O_3 were determined according to DIN [40, 41]. The results are given in Table 12.3.

Table 12.1: Frequently used emission lines for the analysis of rare earth elements in glass by ICP-OES, lower limits of the range of application for 1 g sample weight in 100 ml solution and important disturbing elements according to DIN 51086-2 [45].

Element	Emission line [nm]	Lower limit of the range of application [mg/kg]	Important disturbing elements
Ce	413.380	30	Fe, V
	418.660	30	
Er	337.271	5	V
	349.910	10	
Eu	381.967	1	Fe
	412.970	2	
La	333.749	5	Fe, Ti
	408.672	5	
Nd	401.225	30	Cr, Ti V
	430.358	40	
Pr	390.844	20	Fe, U, Ni
	414.311		
Yb	328.937	1	Y
	369.419		

Table 12.2: Frequently used emission lines for the analysis of rare earth elements in glass by ICP-OES, lower limits of the range of application for 1 g sample weight in 100 ml solution and important disturbing elements according to extension of DIN 51086-2 (in processing).

Element	Emission line [nm]	Lower limit of the range of application [mg/kg]	Important disturbing elements
Dy	353.171	0.5	Ce, Mn, Th
	387.211	1	Ho, Sm
	394.468	0.5	Ce, Eu, Er
Gd	342.246	0.5	Ce Th, W, Eu
	376.840	1	
Ho	345.600	2	Ce, Dy, Nd Tm, Hf
	348.484	3	
	381.074	2	
Lu	219.556	0.5	W, Ta Ni
	261.541	0.5	
	547.668	1	
Sm	359.259	3	Nd, Gd, Th, W Pr, Cr, Zr, Nb, Ta, Ce, Co Ce, Gd
	388.528	3	
	446.734	5	
Tb	332.440	5	Cr, Nb, Th Ho Nb, Cr, Fe, Er, Dy
	350.914	3	
	367.636	2	
Tm	313.125	0.5	Tb Zr, Th, Ti Ce, Y, U, Er
	336.261	5	
	384.802	1	

Note: No spectral interferences emerge from the main components of glass (Si, Na, K, Mg, Ca, Al, B). The spectra of minor elements as Fe, Ti, Cr show interferences with some rare earth lines; however, many interference emerge between the rare earth and many other elements.

Table 12.3: Analytical results for two optical glass samples, concentrations are given in mass%.

Element oxide	Sample 1 (%)	Sample 2 (%)
SiO ₂	4.98	10.21
B ₂ O ₃	30.3	12.9
BaO	0.49	0.48
CaO	–	15.2
ZnO	2.94	–
ZrO ₂	7.85	7.44
La₂O₃	44.9	24.8
Y ₂ O ₃	7.94	–
TiO ₂	–	8.93
Nb ₂ O ₅	0.48	19.8
Sum	99.9	99.8

It can be seen that the sum of determined components for both samples is near to 100 %. Due to the fact that the measurement precision for ICP-OES is higher compared to ICP-MS, definitely no important component was overlooked.

Li₂O cannot be determined by XRF. The measurement of B₂O₃ is difficult or impossible in case of borate-fused beads. The XRF quantification to 100 % can hardly be performed without information from other methods, e.g., ICP-OES.

12.7 Analysis of glass by topochemical analysis

A precise analysis of element contents in glass and glass ceramics is obtained by methods described above. Sometimes, it might be useful to determine the element contents locally too, i.e., on a scale of micrometers or nanometers. This is not necessary for glass of a high-grade purity and homogeneity, but e.g., for glass ceramics. Glass ceramics are formed by tempering glass that contains nucleating agents, such as titanium or zirconium oxide. Crystals are formed during a defined heat treatment because of these nucleating agents. At the end of the production process, a microstructure, consisting of crystals and glass is formed (Figure 12.1). During development of glass ceramics, local analyses of the elemental concentrations are mandatory to understand what happens during heat treatment. In case of recycling of glass ceramics, the total concentration of the single elements rather plays the predominant role. To measure them exactly, it is necessary to chemically dissolve first the glassy as well as the crystalline phases and then analyze them by ICP. The knowledge of the chemical composition of the various glassy and especially crystalline phases may be useful here to develop appropriate chemical dissolution and precipitation routines. For these two reasons, i.e., for the development of glass ceramics on one hand and for the development of chemical dissolution and separation processes on the other, a closer look at a sample is needed by using the so-called topochemical analysis EDX. Topochemical

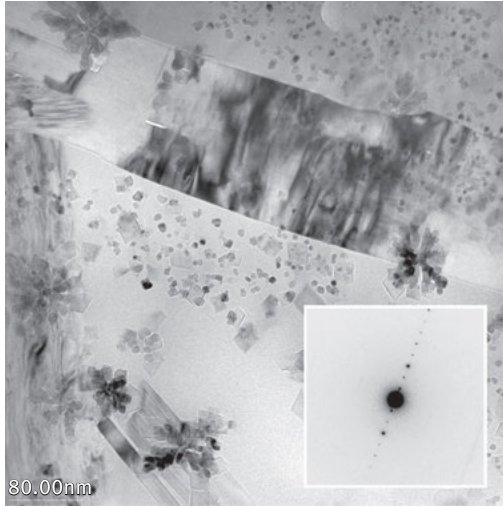


Figure 12.1: Transmission electron micrograph of a glass ceramic. Image Fraunhofer ISC.

analysis EDX is usually performed in two ways: First, an EDX device is mounted on a scanning electron microscope (SEM) or a transmission electron microscope (TEM). Second, it can be combined with a WDX device, which is either a stand-alone device or it is mounted on a SEM. The functionality of these two methods is described in other chapters of this book. This chapter describes the procedure of the analysis and should be considered in more detail.

In both methods, a focused electron beam impinges on the sample surface and penetrates into the sample. By inelastic interaction processes between the primary electrons (the electrons of the electron beam) and the electrons of the atoms of the sample, heat energy arises (amongst others) that leads to a local heating of the sample. The degree of heating depends on the kinetic energy of the primary electrons, the current intensity (beam current), i.e., how many primary electrons per unit time are incident on the sample surface, as well as the cross section of the electron beam, i.e., the size of the incident on the sample. In extreme cases, temperatures of 1,000°C may arise during the analysis by EDS in TEM. Figure 12.2 shows the resulting temperature during the analysis by EDS in TEM, depending on the current strength and thermal conductivity. It may happen that samples melt or vaporize locally when no appropriate care in the analysis is taken.

During analyses in a SEM by EDS or WDS, the resulting temperatures are lower, but can still be significant (Figure 12.3).

The local stoichiometry changes by melting or even vaporizing, but this is trivial. It is also soon obvious that increased atomic mobility – that means increased diffusivity – arises due to the increased temperature. But another effect happens, namely the formation of a space charge inside the sample. It arises because here a part of the primary electrons is quasi landfilled. Spray and Rae described this effect in 1995 [47]. The following (Figure 12.4) is obtained from this article.

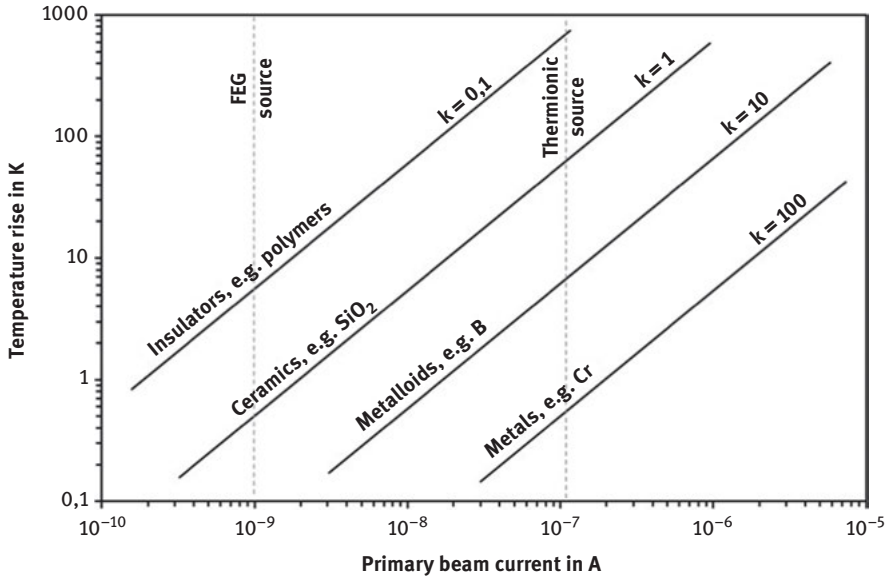


Figure 12.2: Possible local sample temperatures during the analysis in TEM by EDS, depending on the beam current and the thermal conductivity k [51].

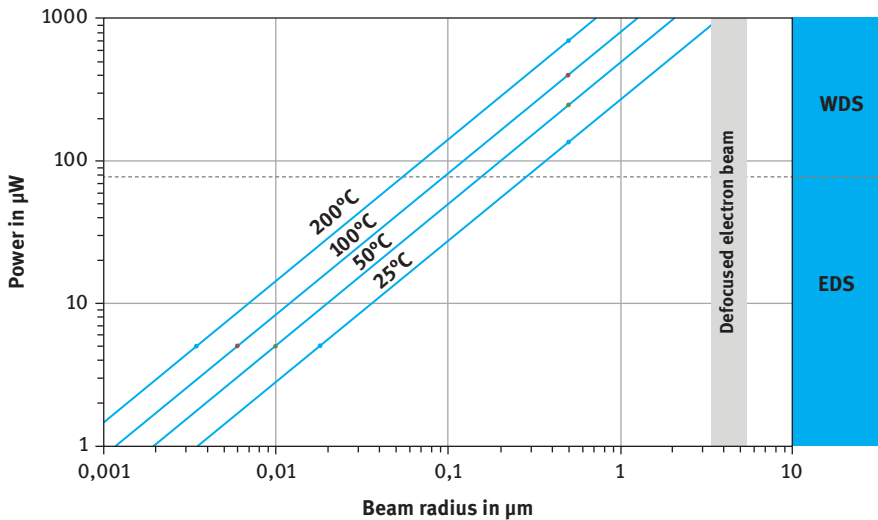


Figure 12.3: Local sample temperature depending on the diameter of the electron beam and the electron beam power [47].

Due to the increased diffusivity by temperature rise and the driving force created by the space charge region, the very mobile ions such as Na^+ , but also Li^+ , diffuse deeper into the sample and the stoichiometry in the analysis area changes.

Lanthanoides are not directly affected by this effect due to their usually relatively low diffusion rate. But as the concentration of other elements changes in the

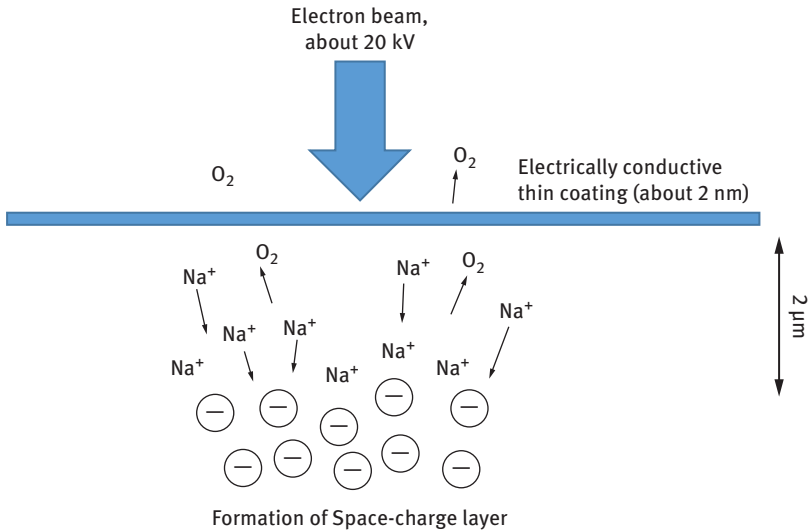


Figure 12.4: Formation of a space charge zone during the EDS or WDS analysis [47].

environment of lanthanoides, a false concentration of lanthanoides is measured. This effect should be also taken into consideration.

There is another important parameter to be considered during local analysis: the pressure. In the electron microscope is a very low pressure of about 10⁻⁵ mbar. If the vapor pressure of some elements is very high, then a change in the stoichiometry is carried out by evaporation also.

To prevent these two effects, a consistent cooling of the samples is recommended during the analysis in order to avoid an increase in temperature and therefore an increased diffusivity.

A final aspect concerns the different hydrolytic resistance of glass. This has to be considered in the preparation that should be water-free; it should be carried out with petroleum for example. If water is used and the glass is very sensitive to an aqueous attack, then the alkali and alkaline earth metal ions are especially leached. With the standard soda-lime glass for windows, changes of 10 % in the sodium concentration may arise.

In summary, the following recommendations for a good local chemical analysis with EDS and WDS can be made:

- Use cooling stages (liquid nitrogen) to avoid high sample temperature.
- Avoid water during grinding and polishing.
- If possible, avoid high beam current and focusing of the beam.
- Observe the time dependent peak development during the measurement.
- Don't forget that the surface of glass can be strongly different from the bulk.

In the articles [46–51] the thermal effects are described based on studies.

References

- [1] Bange K, Durán A, Parker JM. Making Glass Better – ICG Roadmaps of Glass R&D with a 25 Year Horizon, 2nd edn. Madrid, International Commission of Glass, 2014.
- [2] Scholze H. Glas – Natur, Struktur und Eigenschaften, Springer Verlag, Berlin Heidelberg, 1977.
- [3] Varshneya AK. Fundamentals of Inorganic Glass. New York, Academic Press, Inc, Harcourt Brace & Co., 1994.
- [4] Lange J. Rohstoffe der Glasindustrie, Weinheim, Wiley-VCH, 1993.
- [5] Vogel W. Glaschemie. Springer Verlag, 1992.
- [6] Di Bella M, Quartieri S, Sabatino G, Santalucia F, Triscari M. The glass mosaics tesserae of Villa del Casale, Piazza Armerina, Italy: A multi-technique archaeometric study. *Archaeolog Anthropolog Sci* 2014, 6, 4, 345–62.
- [7] Robertshaw, P, Wood, M, Haour, A, Karklins, K, Neff, H. Chemical analysis, chronology, and context of a European glass bead assemblage from Garumele, Niger. *J Archaeolog Sci* 2014, 41, 591–604.
- [8] Siqin B, Li Q, Gan F. Analysis of ancient Chinese potash glass by laser ablation inductively coupled plasma-atomic emission spectrometry/mass spectrometry. *Fenxi Huaxue* 2013, 41, 9, 1328–33.
- [9] Smit Z, Milavec T, Fajfar H, Rehren Th, Lankton JW, Gratuze B. Analysis of glass from the post-Roman settlement Tonovcov grad, Slovenia, by PIXE-PIGE and LA-ICP-MS. *Nucl Instrum Meth Phys Res, Sect B: Beam Interact Mater At* 2013, 311, 53–59.
- [10] Wedepohl KH, Simon K, Kronz A. Data on 61 chemical elements for the characterization of three major glass compositions in Late Antiquity and the Middle Ages. *Archaeometry* 2011, 53, 1, 81–102.
- [11] De Francesco AM, Scarpelli R, Barca D, Ciarallo A, Buffone L. Preliminary chemical characterization of Roman glass from Pompeii. *Periodico di Mineralogia* 2010, 79, 3, 11–19.
- [12] Robertshaw P, Benco N, Wood M, Dussubieux L, Melchiorre E, Ettahiri A. Chemical analysis of glass beads from medieval Al-Basra (Morocco). *Archaeometry* 2010, 52, 3, 355–79.
- [13] Smit Z, Janssens K, Bulska E, Wagner B, Kos M, Lazar I. Trace element fingerprinting of Facon-de-Venise glass. *Nucl Instrum Meth Phys Res, Sect B: Beam Interact Mater At* 2005, 239, 1–2, 94–99.
- [14] De Raedt I, Janssens K, Veeckman J, Vincze L, Vekemans B, Jeffries TE. Trace analysis for distinguishing between Venetian and facon-de-Venise glass vessels of the 16th and 17th century. *J Anal Atom Spectrom* 2001, 16, 9, 1012–17.
- [15] Scarpelli R, De Francesco AM, Gaeta M, Cottica D, Toniolo L. The provenance of the Pompeii cooking wares: Insights from LA-ICP-MS trace element analyses. *Microchem J* 2015, 119, 93–101.
- [16] Wang X, Motto-Ros V, Panczer G, et al. Mapping of rare earth elements in nuclear waste glass-ceramic using micro laser-induced breakdown spectroscopy. *Spectrochim Acta, Part B: At Spectrosc* 2013, 87, 139–46.
- [17] Tabersky D, Luechinger NA, Rossier M, et al. Development and characterization of custom-engineered and compacted nanoparticles as calibration materials for quantification using LA-ICP-MS. *J Anal At Spectrom* 2014, 29, 6, 955–62.
- [18] Tu XL, Zhang H, Deng WF, et al. Application of Resolution in-situ laser ablation ICP-MS in trace element analyses. *Diqiu Huaxue* 2011, 40, 1, 83–98.
- [19] Strnad L, Mihaljevic M, Sebek O. Laser ablation and solution ICP-MS determination of rare earth elements in USGS BIR-1G, BHVO-2G and BCR-2G glass reference materials. *Geostand Geoanal Res* 2005, 29, 3, 303–14.

- [20] Hu Z, Gao S, Liu Y, Chen H, Hu S. Accurate determination of rare earth elements in USGS, NIST SRM, and MPI-DING glasses by excimer LA-ICP-MS at high spatial resolution. *Spectrosc Lett* 2008, 41, 5, 228–36.
- [21] Jochum KP, Stoll B, Herwig K, et al. MPI-DING reference glasses for in situ microanalysis: new reference values for element concentrations and isotope ratios. *Geochem, Geophys, Geosyst* 2006, 7, 2.
- [22] Eggins SM, Shelley JM. Compositional heterogeneity in NIST SRM 610-617 glasses. *Geostand Newsl* 2002, 26, 3, 269–86.
- [23] Horn I, Hinton RW, Jackson SE, Longerich HP. Ultra-trace element analysis of NIST SRM 616 and 614 using laser ablation microprobe-inductively coupled plasma-mass spectrometry (LAM-ICP-MS): a comparison with secondary ion mass spectrometry (SIMS). *Geostand Newsl* 1997, 21, 2, 191–203.
- [24] Norman MD, Pearson NJ, Sharma A, Griffin WL. Quantitative analysis of trace elements in geological materials by laser ablation ICPMS: Instrumental operating conditions and calibration values of NIST glasses. *Geostand Newsl* 1996, 20, 2, 247–61.
- [25] Payne JL, Pearson NJ, Grant KJ, Halverson GP. Reassessment of relative oxide formation rates and molecular interferences on in situ lutetium-hafnium analysis with laser ablation MC-ICP-MSO. *J Anal At Spectrom* 2013, 28, 7, 1068–79.
- [26] Stix J, Gauthier G, Ludden JN. A critical look at quantitative laser-ablation ICP-MS analysis of natural and synthetic glasses. *Can Mineral* 1995, 33, 2, 435–44.
- [27] Zhang J, Xie F, Liang Y. The impact of the mechanical properties with rare earth elements on the black shale glass-ceramic. *International Conference on Materials for Renewable Energy and Environment*, Chengdu, China 2013, 2, 569–72.
- [28] Mirti P, Pace M, Ponzzi MM, Aceto M. ICP-MS analysis of glass fragments of Parthian and Sasanian epoch from Seleucia and Veh Ardasir (central Iraq). *Archaeometry* 2008, 50, 3, 429–50.
- [29] Smit Z, Janssens K, Bulska E, Wagner B, Kos M, Lazar I. Trace element fingerprinting of Facon-de-Venise glass. *Nucl Instrum Methods Phys Res Sect B: Beam Interact Mater At* 2005, 239, 1–2, 94–99.
- [30] Mizusuna Hirobumi, Nakayama Mokichi. Determination of rare earth elements in glass by ICP-AES (inductively coupled plasma-Atomic emission spectroscopy). *Jpn Kokai Tokkyo Koho* 1993, JP05079983A19930330.
- [31] Abe Y, Kikugawa T, Nakai I. Development of nondestructive heavy elemental analytical method of ancient glass artefacts using high-energy (116 keV) synchrotron radiation X-ray fluorescence spectrometry. *X-sen Bunseki no Shinpo* 2014, 45, 251–68.
- [32] Chen JR, Chao EC, Back JM, et al. Rare earth element concentrations in geological and synthetic samples using synchrotron x-ray fluorescence analysis. *Nucl Instrum Methods Phys Res Sect B: Beam Interact Mater At* 1993, B75, 1–4, 576–81.
- [33] Nakai I, Terada Y, Itou M, Sakurai Y. Use of highly energetic (116 keV) synchrotron radiation for X-ray fluorescence analysis of trace rare-earth and heavy elements. *J Synchrotron Radiat* 2001, 8, 4, 1078–81.
- [34] Nakanishi T, Nishiwaki Y, Miyamoto N, Shimoda O, Watanabe S, Muratsu S, Takatsu M, Terada Y, Suzuki Y, Kasamatsu M, Suzuki S. Lower limits of detection of synchrotron radiation high-energy X-ray fluorescence spectrometry and its possibility for the forensic application for discrimination of glass fragments. *Forensic Sci Int* 2008, 175, 2–3, 227–34.
- [35] Nishiwaki Y, Nakanishi T, Terada Y, Ninomiya T, Nakai I. Nondestructive discrimination of small glass fragments for forensic examination using high energy synchrotron radiation X-ray fluorescence spectrometry. *X-Ray Spectrom* 2006, 35, 3, 195–99.

- [36] Baklouti S, Maritan L, Laridhi Ouazaa N, Mazzoli C, Larabi Kassaa S, Joron JL Fouzai B, Casas Duocastella L, Labayed-Lahdari M. African terra sigillata from Henchir Es-Srira archaeological site, central Tunisia: Archaeological provenance and raw materials based on chemical analysis. *Appl Clay Sci* 2015, 105–106, 27–40.
- [37] Facetti-Masulli JF, Kump P, Gonzalez VR, Diaz Z. Geochemical studies of Guarani ethnic groups pottery with XRF. *J Radioanal Nucl Chem* 2010, 286, 2, 489–94.
- [38] Beckhoff B, Kolbe M, Hahn O, Karydas AG, Zarkadas C, Sokaras D, Mantler M. Reference-free x-ray fluorescence analysis of an ancient Chinese ceramic. *X-Ray Spectrom* 2008, 37, 4, 462–65.
- [39] Bach H, Krause D. *Analysis of the Composition and Structure of Glass and Glass Ceramics*. Berlin, Heidelberg, Springer Verlag, 2013, 83.
- [40] Deutsche Norm DIN 52340-2. Prüfung von Glas; Chemische Analyse von ungefärbten Kalk-Natron-Gläsern, Teil 2: Bestimmung von SiO₂, 1974.
- [41] International Standard ISO 21078-1. Determination of boron (III) oxide in refractory products – Part 1: Determination of total boron (III) oxide in oxidic materials for ceramics, glass and glazes, 2008.
- [42] American Standard ASTM C169–92. Standard test methods for chemical analysis of soda-lime and borosilicate glass, 2011.
- [43] Deutsche Norm DIN 51084. Prüfung von oxidischen Roh- und Werkstoffen für Keramik, Glas und Glasuren – Bestimmung des Gehaltes an Fluorid (Testing of oxidic raw and basic materials for ceramic, glass and glazes – Determination of fluoride content) – in German, 2008.
- [44] Deutsche Norm DIN 52340-3. Prüfung von Glas; Chemische Analyse von ungefärbten Kalk-Natron-Gläsern, Teil 3: Aufschlußverfahren, 1990.
- [45] Deutsche Norm DIN 51086-2. Prüfung von oxidischen Roh- und Werkstoffen für Keramik, Glas und Glasuren – Teil 2: Bestimmung von Ag, As, B, Ba, Be, Bi, Ca, Cd, Ce, Co, Cr, Cu, Er, Eu, Fe, La, Mg, Mn, Mo, Nd, Ni, P, Pb, Pr, S, Sb, Se, Sn, Sr, Ti, V, W, Y, Yb, Zn, Zr durch optische Emissionsspektrometrie mit induktiv gekoppeltem Plasma (ICP OES) (Testing of oxidic raw materials and materials for ceramics, glass and glazes – Part 2: Determination of Ag, As, B, Ba, Be, Bi, Ca, Cd, Ce, Co, Cr, Cu, Er, Eu, Fe, La, Mg, Mn, Mo, Nd, Ni, P, Pb, Pr, S, Sb, Se, Sn, Sr, Ti, V, W, Y, Yb, Zn, Zr by optical emission spectrometry with inductively coupled plasma (ICP OES)) – in German, 2004.
- [46] Borom MP, Hanneman RE. Local compositional changes in alkali silicate glasses during electron microprobe analysis. *J Appl Phys* 1967, 38, 2406.
- [47] Spray JG, Rae DA. Quantitative electron microprobe analysis of alkali silicate glasses: A review and userguide. *Can Mineral* 1995, 33, 323–32.
- [48] Varshneya AK, Cooper AR, Cable M. Changes in composition during electron micro-probe analysis of K₂O–SrO–SiO₂ Glass. *J Appl Phys* 1966, 37, 2199.
- [49] Nielsen CH, Sigurdsson H. Quantitative methods for electron microprobe analysis of sodium in natural and synthetic glasses. *Am Mineral* 1981, 66, 547–52.
- [50] Vassamillet LF, Caldwell VE. Electron probe microanalysis of alkali metals in glasses. *J Appl Phys* 1969, 40, 1637.
- [51] Williams DB, Carter CB. *Transmission Electron Microscopy: Basics I*. New York, Springer Science & Business Media Inc., 1996.

Sven Sindern

13 Analysis of Rare Earth Elements in Rock and Mineral Samples by ICP-MS and LA-ICP-MS

Abstract: The group of the rare earth elements (REEs) serves as valuable indicator of numerous geological processes such as magma formation or fluid–rock interaction. The decay systems of the radioactive REE isotopes ^{138}La , ^{147}Sm and ^{176}Lu are used for geochronometric dating of a range of events, starting from first steps of planetary formation to younger steps of geodynamic development. Thus, the abundance of all REEs occurring in a large range of concentrations as well as precise isotope ratios must be analysed in different geomaterials.

The inductively coupled plasma (ICP) ion source and various types of mass spectrometers (MS) represent the basis to fulfil the analytical requirements of geoscientific studies. Today, ICP-quadrupole MS and ICP-sector field MS (SFMS) with a single detector or multiple ion collection (MC-ICP-MS) are standard instruments for REE analyses in the geosciences. Due to the need for in situ analysis, laser ablation (LA)-ICP-MS has become an important trace element microprobe technique, which is widely applied for determination of REE concentrations and isotope compositions in geoscientific laboratories.

The quality of concentration analysis or isotope ratio determination of REEs by ICP-MS and LA-ICP-MS is affected by many parameters. Most significant are interferences caused by polyatomic oxide and hydroxide ion species formed in the plasma as well as fractionation effects leading to non-stoichiometric behaviour during element determination or to biased isotope ratio measurements. Laser-induced fractionation and isobaric interferences have to be considered as additional effects for LA-ICP-MS. As analyte elements and matrix are unseparated, mineral standards matching the matrix of samples are a prerequisite for accurate and precise REE concentration and isotope ratio determination. Application of fs lasers instead of the more common ns lasers in LA-ICP-MS systems turns out to be a significant step to reduce laser-induced fractionation and to overcome effects of sample matrices.

13.1 Introduction

The rare earth elements (REEs, i.e. lanthanides) are a ubiquitously distributed group of elements in nature and present in many earth materials, but at low concentration. In a range of element abundance in the earth's crust ([1], noble gases not considered), they rank between positions 24 (Ce, 60 $\mu\text{g/g}$) and 61 (Tm, 0.3 $\mu\text{g/g}$). Their concentrations are similar to those of common metals such as Zn (65 $\mu\text{g/g}$), Ni (56 $\mu\text{g/g}$), Cu (25 $\mu\text{g/g}$) and Pb (14.8 $\mu\text{g/g}$), but significantly higher than the concentrations of precious metals such as Ag (0.07 $\mu\text{g/g}$), Au (0.0025 $\mu\text{g/g}$) and Pt (0.0004 $\mu\text{g/g}$) [1]. Only within a rare but complex group of minerals, the REEs reach major element levels.

The geochemical behaviour of REEs is controlled by their ionic radii, charge and complexation behaviour [2]. Owing to their electron structure and progressive filling of the 4f orbitals, REEs are characterized by the principal oxidation number of +3 and a steadily decreasing ionic radius with increasing atomic number (lanthanide contraction). Accordingly, within the group of REEs slightly different geochemical properties can be observed, leading to gradually varying smooth distribution patterns (e.g. [3, 4]) that are characteristic of different rock types (Figure 13.1). Exceptions to this behaviour can be observed for Ce and Eu, which may adopt the oxidation numbers +4 and +2, respectively, depending on the geochemical system. Furthermore, smoothly varying REE patterns can show significant perturbations as a consequence of fractionation caused by contrasting complexation behaviour of different REEs. This is a function of the

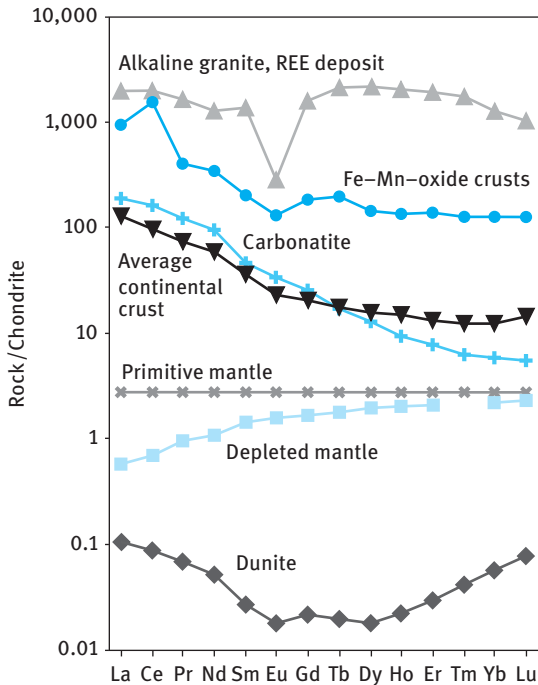


Figure 13.1: Chondrite-normalized REE patterns for major domains of the silicate earth and different rock types are indicative of geological formation processes (chondrite values in ref. [5]). Diverging patterns of the average continental crust [1] and depleted mantle [6] relative to primitive mantle [5] reflect REE fractionation during formation of magmatic melts. Dunites (values of DTS-1 in ref. [7]) are residual rocks of the earth's mantle formed after extraction of magmatic melts. Carbonatites [2] and alkaline granites [8] represent magmatic melts ascending in the crust. They can enrich REE and form deposits of these elements. Fe-Mn-oxide crusts are precipitates of the seawater [2] and reveal REE fractionation due to differences in marine particle reactivity. In particular, they show fractionation of Ce due to precipitation of CeO_2 .

electron configuration of different REEs as well as of the type of the complexing ligand and thus of the geochemical environment in which a mineral or rock was formed [2].

The group of REEs thus serves as highly valuable indicator of numerous geological processes like magma formation and differentiation [9] as well as interaction of hydrothermal fluids and rocks including the formation of ore deposits [2]. REEs can also reflect redox conditions in magmatic, hydrothermal or sedimentary systems (e.g. [10, 11]), and more and more they show the anthropogenic emission of REEs used in medical or technical applications to natural environments [12–14] (Figure 13.1).

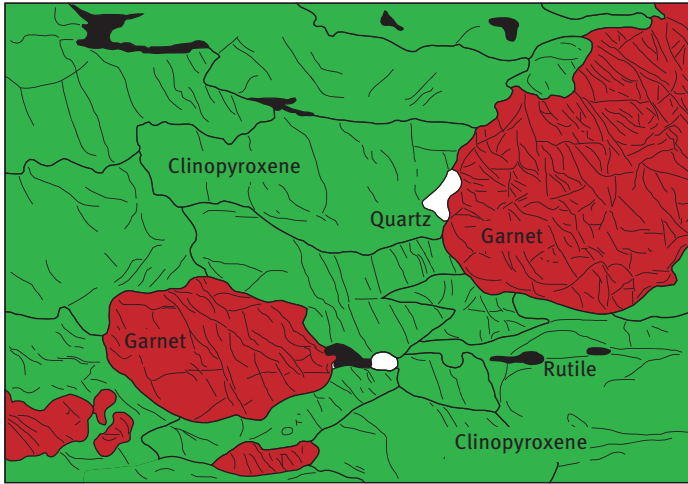
Three of the REEs (i.e. La, Sm and Lu) have natural radioactive isotopes with half-lives in the order of magnitude of the earth's age. Thus, considerable decay of the radioactive parent isotopes (^{138}La , ^{147}Sm and ^{176}Lu) and increase of the radiogenic daughter isotopes (^{138}Ce , ^{138}Ba , ^{143}Nd and ^{176}Hf) occur within the timescale of the earth's history and can be used for geochronometric dating, starting from first steps of planetary formation taking place after onset of solar system condensation to crust formation or younger geodynamic events [15–24]. Figure 13.2 illustrates the concept of the Sm–Nd isochron dating of a metamorphic rock. Application of the ^{138}La – ^{138}Ce / ^{138}Ba -, ^{147}Sm – ^{143}Nd - and ^{176}Lu – ^{176}Hf -decay systems requires determination of isotope ratios, particularly in minerals that strongly fractionate the parent over the daughter isotope [25, 26]. To use the latter decay system, Hf isotopes must be analysed, which is addressed in this chapter too, although this element does not belong to REEs. For the application of the short-lived ^{146}Sm – ^{142}Nd decay system for the study of early differentiation of the earth, see refs [27, 28].

Furthermore, stable isotopes may also show isotopic fractionation serving as indicator of a natural process. Slight anomalies of the $^{153}\text{Eu}/^{151}\text{Eu}$ ratio in meteorite samples are interpreted to reflect early stages of planetary history, such as magnetic separation processes in the early ionized fraction of the solar nebula [29].

In nature, REE concentration patterns as well as isotope compositions can vary on a mineral grain scale. Complexly zoned minerals, such as zircon, monazite or garnet, can therefore serve as monitor for major geodynamic processes, for example crust formation or growth and collapse of mountain chains [31, 32], if they are studied in detail.

These brief explanations show that a large range of analytical capabilities is required for the study of REEs in geosciences. Usually all members of the group of REEs must be addressed for the determination of element concentrations in order to reveal the characteristic distribution patterns. Thus, the concentration range from several wt.% down to the sub- $\mu\text{g/g}$ or sub- ng/L level has to be covered in different earth materials like minerals, bulk rock or soil samples as well as natural water. Furthermore, precise determination of isotope ratios is a prerequisite for application of the ^{138}La – ^{138}Ce / ^{138}Ba -, the ^{147}Sm – ^{143}Nd - and ^{176}Lu – ^{176}Hf -decay systems or for the investigation of fractionation of heavy stable isotopes (e.g. $^{153}\text{Eu}/^{151}\text{Eu}$). Both, element and isotope analyses are performed on bulk samples after chemical processing and also in situ using probe techniques, which allow analytical work with high spatial resolution.

(a)



(b)

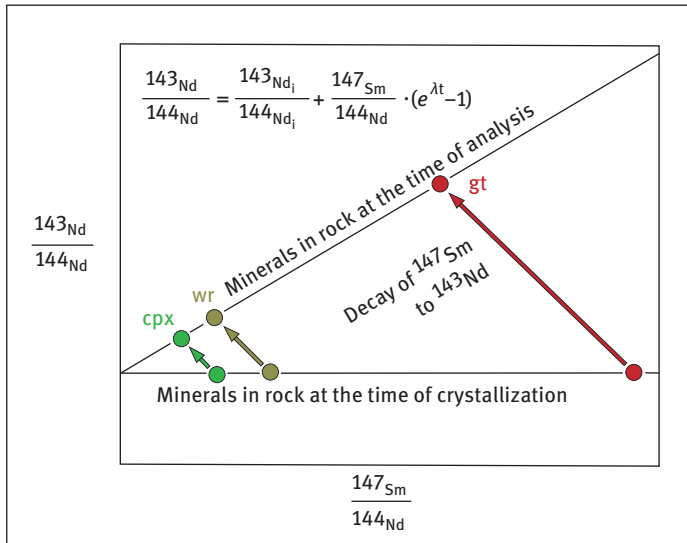


Figure 13.2: Samarium–neodymium isochron dating of rock formation. (a) Eclogite – a metamorphic rock formed during subduction of oceanic crust – composed of the minerals clinopyroxene (green), garnet (red) with minor amounts of quartz (white) and rutile (black). Sketch is drawn according to ref. [30]. (b) Isochron diagram showing the principles of dating using the ^{147}Sm – ^{143}Nd system according to the decay equation displayed in the upper part of the diagram. The index “i” indicates the initial ratio of $^{143}\text{Nd}/^{144}\text{Nd}$ present at the time of crystallization of the rock, and λ denotes the decay constant of ^{147}Sm ($\lambda = 6.54 \times 10^{-12}$ /year, e.g. [19]). Rock-forming minerals, garnet (gt) and clinopyroxene (cpx), accessories (not considered) and accordingly also a whole rock sample (wr) initially are at isotopic equilibrium during formation of the eclogite (i.e. at metamorphic crystallization) and plot on a horizontal line. Due to radioactive decay of ^{147}Sm to ^{143}Nd , the isotopic signatures of mineral fractions and whole rock shift in an undisturbed system to a position on a line with positive slope – the isochron. Its slope ($e^{\lambda t} - 1$) indicates the time elapsed since rock formation and can be calculated after determination of $^{147}\text{Sm}/^{144}\text{Nd}$ and $^{143}\text{Nd}/^{144}\text{Nd}$ ratios [19, 25].

The inductively coupled plasma (ICP) ion source and various types of mass spectrometers (MS) represent the basis to fulfil the analytical requirements in the geosciences. This will be addressed in the following sections of this chapter. The important role of ICP-MS and laser ablation (LA) as efficient techniques for sample introduction and in situ analysis of solid matter to fulfil the analytical requirements in the geosciences are highlighted.

13.2 Technical development

Starting in the 1980s, ICP-quadrupole MS (ICP-QMS) has become the standard instrument for REE analyses in the geosciences. Within a few years, ICP-QMS-based analytical procedures replaced instrumental neutron activation analysis or procedures applying isotope dilution thermal ionization mass spectrometry (TIMS), which represented the standard methods since the 1960s. Most important arguments in favour of ICP-QMS were lower prime and operating cost, relatively low duration of analysis and large sample throughput as well as the option to cover all REEs in one step [33–38].

The combination of the ICP ion source with magnetic sector field (SF) mass filters represented a major step in the field of isotope geochemistry and cosmochemistry [39, 40]. Owing to the flat top peak signals and the ability of the plasma source to ionize most elements, ICP-SFMS systems allow precise isotope ratio measurements also for poorly ionizing elements such as Zr, Hf or W. In particular, geochronometry applying the Lu–Hf system was limited due to insufficient sensitivity of conventionally used TIMS for Hf [15]. The application of multiple ion collection (MC) in MC-ICP-SFMS instruments and simultaneous mass detection was a further step to enhance the precision of isotope ratio measurements [41, 42].

In contrast to QMS, double-focusing ICP-SFMS systems, commercially available today either with multiple or single ion collection, can be operated with significantly higher resolution at still reasonable sensitivity [43, 44]. Despite prices approximately >5 times higher than those of quadrupole instruments, (MC)-ICP-SFMS have become common equipment in most isotope geochemistry laboratories worldwide.

Due to the particular need for in situ trace element and isotope ratio determination with high spatial resolution, LA-ICP-MS has become an important technique in geosciences. After first steps in the late 1980s [36, 45–47], the potential of a technique for REE analysis avoiding the step of sample dissolution was intensively explored [48–50]. As an alternative to ICP-QMS and ICP-SFMS, time-of-flight MS (ICP-TOFMS) were used for LA-ICP-MS. However, due to limited ion counting rate and low sensitivity of such MSs, LA-ICP-TOFMS systems so far are not as effective as those applying QMS or SF-MS analysers [51]. In comparison to secondary ionization mass spectrometry, which has comparable analytical capabilities and which can also be considered an alternative method, LA-ICP-MS requires larger spot sizes but is significantly cheaper and faster, and does not require vacuum [52]. LA-ICP-MS thus turned out to be one of the

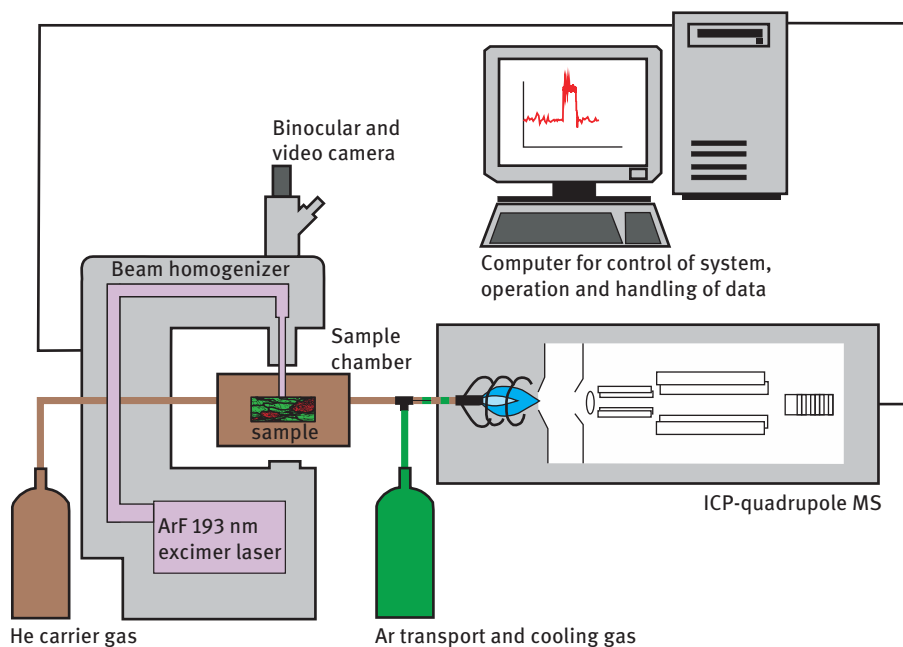


Figure 13.3: Schematic diagram of a common LA-ICP-MS system based on an ns-ArF excimer laser and an ICP-QMS.

“most affordable and most widely applicable trace element microprobe” techniques in geoscientific laboratories [53].

For LA-ICP-MS analysis, a pulsed high-energy laser beam is focused on the surface of a solid sample, which is placed in an air-tight sample chamber flushed with a carrier gas (Figure 13.3). Irradiation causes the release of aerosol particles from the sample surface, which are transported to the ICP ion source in which they are vaporized and finally ionized (e.g. [53, 54] and references therein). Helium allows better uptake of aerosol particles than Ar and usually serves as carrier gas [55, 56]. Small flows of other gases (e.g. N_2 and H_2) may be added to the carrier gas to suppress oxide formation and to enhance sensitivity [57, 58].

After intensive technical development in the last 20 years, different lasers providing pulsed laser light are used in LA-ICP-MS systems. Lasers differ with respect to the pulse length, which can be in the range of 3–20 ns (ns lasers) or in the sub-picosecond range (often 60–150 fs, generalized as fs lasers [58–60]). Furthermore, lasers differ with respect to the type. In commercial instruments, ns laserlight is either produced in solid-state Nd:YAG or ArF excimer lasers. The latter laser type, which is more expensive but delivers higher photon energy, has a fundamental wavelength of 193 nm, whereas in a Nd:YAG laser such light is produced from the fundamental wavelength of 1,064 nm using an optical parameter oscillator ([51] and references therein). Solid-state Nd:YAG ns lasers emitting light with 266 or 213 nm, which have been most

common in earlier commercial systems, become less attractive for application in geoscientific laboratories.

Femtosecond LA systems, which are based on solid-state lasers (Ti:sapphire), are significantly more complex than ns instruments and have become commercially available only in the last years [61].

13.3 Physical and chemical effects on concentration and isotope ratio determination

The quality of concentration or isotope ratio determination by ICP-MS and LA-ICP-MS is affected by many factors. In addition to general aspects related to any analytical activity (e.g. memory effects and contamination) or general technical conditions (e.g. signal drift, dead time of ion detector and plasma stability), there are further factors, which are specifically associated with physical and chemical processes in the ICP source leading to interference and fractionation (e.g. [62]).

The occurrence of polyatomic ion species due to oxide and hydroxide formation of REEs and Ba as well as of BaCl in the plasma is a well-known phenomenon causing serious interference mainly on Eu, Gd, Tb, Yb and Lu [34, 35]. Oxide production is influenced by the availability of oxygen, which is significantly higher in solution-ICP-MS than at “dry plasma” conditions in LA-ICP-MS [36, 63]. Different to sample introduction by solution LA-ICP-MS allows routine analytical procedures during which oxide contributions to most REE isotopes chosen for analysis can be neglected [64].

In addition to interferences, fractionating effects have to be considered. Plasma temperature is important for the degree of ionization and ion energies, which have an effect on mass-dependent vaporization, diffusion or ion trajectories in the plasma ([65] and references therein). In addition, space charge effects causing mutual repulsion of positively charged ions lead to enhanced deflection of the lighter masses in the ion beam [66, 67]. In combination, these physical processes, which occur in the plasma, between sampler and skimmer cones as well as immediately behind the skimmer cone, are the reason for mass-dependent fractionation [65, 68]. Any instrumental parameter affecting these physical processes in plasma and interface region, in turn, has an influence on fractionation that is reflected by non-stoichiometric behaviour during element determination or by biased isotope ratio measurement. Such instrumental parameters are nebulizer gas flow, extraction lens voltage, torch position, rf power and cone design [65, 67]. Furthermore, as the total ion current also affects physical conditions in the plasma sample, related parameters like concentration or sample matrix influence mass-dependent fractionation, too.

Other instrumental factors, such as focusing and shape of the ion beam, collision or scatter of ions in the flight tube or in the ion collection system, inefficient suppression of secondary electrons or nonlinear response of resistors, lead to

mass-independent fractionation effects [41]. These are most obvious if the beam is split into various parts in MC-ICP-MS.

All of these factors leading to elemental and isotopic fractionation are independent of the method of sample introduction (solution or LA). Such instrumental mass bias must be distinguished from laser-induced fractionation processes, which are specifically associated with sample uptake by LA (Figure 13.4). Elemental and isotopic fractionation may occur immediately in or around the ablation pit during laser sampling due to non-congruent evaporation and redistribution of elements on the basis of different volatilities between subsolidus phases (vapour and melt) forming in the ablation pit or condensing around it [59, 63 and references therein, 69, 70].

Differential transport properties of ablation products (i.e. melt droplets, vapour phase condensates, solid fragments and agglomerates) were invoked to cause fractionation during passage through the transfer tubing [71 in 63]. Most studies on laser-induced fractionation point to the crucial role of melt formation at the ablation site (Figure 13.4).

While incomplete vaporization and ionization of larger particles in the plasma are shown to lead to preferential transmission of more volatile elements and lighter isotopes, enhanced loading of the plasma with aerosol particles causes element-dependent suppression of signal intensity [63, 65, 72, 73]. Although the latter effects occur in the plasma they are controlled by the properties of laser-derived aerosols and thus belong to laser-induced fractionation.

Other studies explore the role of the position of a sample in a large-volume open design ablation cell on variation of Sm–Nd inter-element and Nd isotope fractionation [74]. Two-volume ablation cells help to establish constant conditions of fractionation [59].

The physical processes of aerosol formation and interaction occurring during ablation are controlled by absorption of the laser energy by the solid sample. Thus, in addition to the sample matrix, instrumental parameters that influence absorption also have an effect on laser-induced fractionation. Numerous studies conducted in this field have shown that laser wavelength and power density as well as laser pulse length are most important (see [63] for further parameters). Different to ns pulses, thermal diffusion, which is the reason for melt production in an ablation pit, does not occur during ablation with fs pulses [58, 63]. Taking the crucial role of melts for laser-induced fractionation into consideration fs-LA-ICP-MS can be regarded as a major step to reduce laser-induced fractionation and to overcome effects of sample matrices on fractionation [58, 76, 77].

For ns LA-ICP-MS, the application of deep UV wavelengths (in particular 193 nm) turned out to be absorbed best by transparent matrices [53, 72, 78]. This allows efficient ablation of silicates (e.g. zircon and feldspar) or oxides (e.g. quartz) that constitute a dominant part among mineral and rock samples.

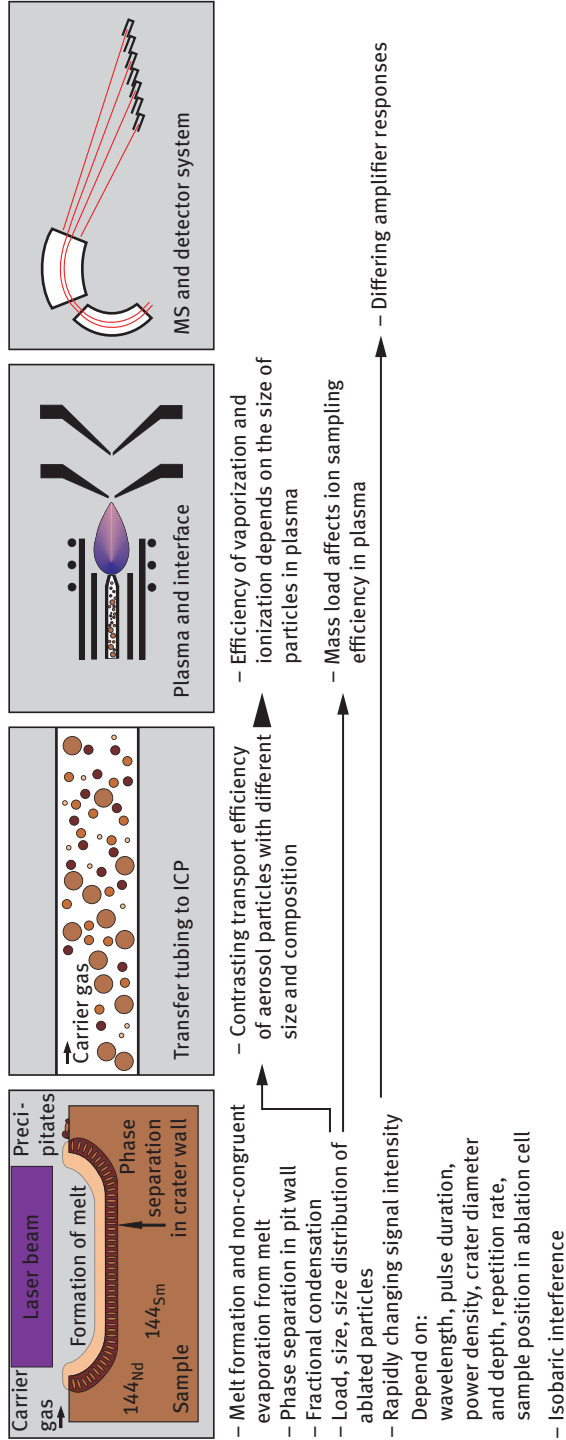


Figure 13.4: Schematic overview of processes causing laser-induced fractionation and interference in (ns-)LA-ICP-MS system on the way of an analyte element from the ablation pit in a solid sample with unseparated matrix via transfer tubing and ICP interface to the detector system [59, 63, 69, 70, 72, 74, 75].

13.4 Determination of REE concentrations

13.4.1 Sample preparation

The standard procedure of operation requires sample supply to the ICP ion source as liquid aerosol droplets via a nebulizer and a spray chamber. Therefore, dissolution is the first sample preparation step of earth materials after homogenization and separation of a representative aliquot.

As a characteristic feature of the REE department in earth materials, their abundance is often controlled by accessory minerals such as allanite, apatite, monazite, xenotime or zircon [79]. Some of these accessories are of low solubility, which has to be considered for the choice of dissolution procedures. Acid dissolution is usually performed with mixtures of either HNO_3 or HClO_4 and HF necessary to attack silicates and quartz that are dominant in many rocks. Evaporation to dryness leads to disappearance of Si. Residues are taken up with either HCl or HNO_3 . Pressure containers are preferred because they allow digestion of accessory minerals of low solubility. Procedures employing microwave digestion systems are also successfully applied for analysis of REEs in silicate rocks [80].

Furthermore, effective digestion of solid earth materials can be achieved by fusion dissolution with lithium borate. Glasses formed in this step can further easily be digested in HCl or HNO_3 [43].

Bulk rock REE analyses are also performed on homogenized solid samples applying LA as sampling tool. For this purpose, pressed powder pellets have been applied [48, 81]. Limited precision due to heterogeneity on the scale of a single laser spot is compensated by averaging results from a raster of laser spots [36]. Better homogenization of rock samples is achieved in samples, which are fused either directly or using a flux. Application of the relatively expensive method of direct fusion for REE analysis in rock samples is less common [82, 83] but sometimes rock glasses suitable for LA-ICP-MS are provided by natural volcanic processes [84]. Flux-based methods, using mixtures of Li-borates added to the sample at ratios ranging between 7:1 and 5:1, are applied most often [36, 43, 49, 85, 86].

13.4.2 Quantification

Quantification of REE concentrations by solution-ICP-MS is mainly based on external calibration using dilutions of stock solutions [33, 34]. The methods of standard additions and isotope dilution are alternative ways of calibration, which are less vulnerable to complex matrices in earth materials and thus offer better accuracy and precision of REE analysis [87]. However, both methods require labour-intensive and time-consuming steps of sample handling, which also leads to higher costs of analyses. Therefore, they are usually not applied as routine methods in geoscientific laboratories.

Drift of signal intensity is corrected by internal standards for which elements that are naturally not contained in the sample are added at defined concentrations. For analysis of REEs in earth materials, Ru or Rh and Re are appropriate as their masses bracket the range of masses of REEs [88].

While one or more isotopes free of isobaric interferences exist for each REE, the interferences caused by polyatomic oxide and hydroxide species can be significant for the group of REEs and can require correction applying experimentally derived factors accounting for yields of formation of interfering ions in the plasma [34, 42] unless high mass resolution is available using double-focusing ICP-SFMS. Increasing the resolution ($m/\Delta m$) to values in the range of 8,000–10,000 REE-oxide ions can be separated from REE-atom ions, which, however, leads to a significant decrease in sensitivity [43, 89]. Several authors explore the effects of high resolution, collision cell technology and doubly charged ions to minimize interferences [37, 90, 91].

Detection limits and precision are not entirely dependent on instrumental parameters as they are also affected by factors such as laboratory blank and numerous processes during the entire analytical procedure starting from the sample preparation and ending with data reduction and concentration calculation. Using solution-ICP-MS for determination of REE concentrations, even with quadrupole mass filters, detection limits ranging around 1 ng/g (in solid samples) and run-to-run (external) precision <5 % for REE concentrations $\geq 0.1 \mu\text{g/g}$ can be reached. Accuracy of REE determinations based on repeated dissolution and analysis of certified rock standards varies between 5 % and 10 % [34, 88].

Quantification of REE concentration in homogenized rock or mineral samples by LA-ICP-MS is mainly performed after external calibration using solid reference materials. As reference materials, either synthetic glasses or rock glasses produced by melting of natural rocks or minerals as well as synthetic crystalline material or natural minerals are applied for REE analysis [92, 93]. Synthetic polyethylene-based REE standards have been tested but are not common today [94]. The glasses 610 and 612 synthesized by the National Institute of Standards and Technology (NIST) are certainly most widely applied for LA-ICP-MS mineral and rock analysis; see GeoReM database in refs [95, 96]. Mineral standards, for which REE concentrations are known, are zircon 91500 [97], zircon Plesovice [98] or titanite TIT-200 [99]. An alternative technique based on simultaneous ablation of a Li-borate blank disc and nebulization of a standard solution was tested by Pickhardt et al. [100].

It has to be considered for external LA-ICP-MS calibration that the absolute mass of material ablated per time unit (ablation yield) varies between different materials [53, 63, 70], which leads to systematic errors if standard materials are different to samples. Therefore, at least one element with independently determined concentrations in standard and sample serving as internal reference standard is required for quantification of concentrations using the equation:

$$\frac{C_a^u}{C_r^u} = \frac{C_a^{st}}{C_r^{st}} \cdot \frac{I_a^u \cdot I_r^{st}}{I_r^u \cdot I_a^{st}} \cdot \frac{S_a^u \cdot S_r^{st}}{S_r^u \cdot S_a^{st}}$$

[53, 101]. Here, C and I denote concentrations and signal intensities, respectively, in an unknown sample (upper index u) and a standard (upper index st). The lower index a indicates the analyte element, whereas r marks the internal reference element. Usually external calibration standards and samples are analysed in a bracketing sequence, which also helps to correct for drift effects.

As physical processes responsible for laser-induced fractionation are controlled by material-dependent absorption of laser energy in the solid (see 13.3), signal intensities obtained in a standard are not representative for an individual sample unless both matrices are identical. Such differences in sensitivity can be corrected with element-specific factors (S) accounting for contrast of sensitivity between internal reference element and the analyte element [63]. Owing to their overall similarity, sensitivities within the group of the REE as well as those of Y and Sc are almost identical. Furthermore, sensitivities of REEs are not significantly different from those of the alkaline earth elements Mg, Ca, Sr and Ba [70]. Therefore Ca, which is abundant in many rock types and minerals as well as in the NIST 600 series standards, can be recommended as suitable internal standard element for REE analysis. In such case, errors caused by insufficiently constrained sensitivity correction factors are minimized. When using a LA-ICP-MS system affected by mass- and element-dependent fractionation (particularly for ns LA-ICP-MS) these errors can only be neglected if matrix-matched standards are applied.

This has an effect on accuracy of LA-ICP-MS, which is known to be <10 % when analysing silicate minerals without matrix matching but may be reduced to <5 % if matrix matched standards are used [33, 63]. External precision has improved since the early days of REE analysis by LA-ICP-MS (e.g. [94]) and now is similar to precision of solution-ICP-MS. Jochum et al. [102] report precision of 0.8–3.5 % (RSD) for REE analysis by 193 nm ns LA-ICP-SFMS in the concentration range of 38 and 51 $\mu\text{g/g}$ in natural glass standards after repeated analysis. The potential to improve precision as well as to overcome matrix dependency using fs LA-ICP-MS is shown in Refs [103, 104]. Detection limits for LA-ICP-MS significantly depend on the size of the laser pit and on the isotope used for detection next to the sensitivity of the instrument. For a beam diameter of 100 μm sensitive LA-ICP-SFMS systems can reach detection limits for REEs as low as 0.001 $\mu\text{g/g}$ [86, 102].

In addition to concentration analysis, LA can also be used as a tool for chemical imaging if operated in a raster mode. Cook et al. [105] create REE distribution maps of mineral grains based on LA-ICP-MS signal intensities with a spatial resolution of 7–12 μm .

13.5 Determination of isotope ratios by multi-collector (MC)-ICP-MS

The application of ^{138}La , ^{147}Sm , ^{146}Sm or ^{176}Lu decay for geo- or cosmochronological studies or the use of isotope ratios as geochemical tracers requires the precise

determination of isotope ratios (Figure 13.2). These include ratios of the radiogenic daughter isotopes and a non-radiogenic stable reference isotope of the same element in the denominator (i.e. $^{138}\text{Ce}/^{142}\text{Ce}$, $^{143}\text{Nd}/^{144}\text{Nd}$, $^{142}\text{Nd}/^{144}\text{Nd}$, $^{176}\text{Hf}/^{177}\text{Hf}$) as well as ratios of the radioactive parent isotope and the reference (i.e. $^{138}\text{La}/^{142}\text{Ce}$, $^{147}\text{Sm}/^{144}\text{Nd}$, $^{146}\text{Sm}/^{144}\text{Nd}$, $^{176}\text{Lu}/^{177}\text{Hf}$).

For this analytical task, MC-ICP-MS offers best ionization of REEs and Hf in the ICP source as well as most precise isotope ratio determination due to MC, which allows simultaneous mass detection. This enhances precision because effects due to fluctuations in signal intensity cancel out [41, 42]. Isotope ratio determination is either performed in static mode with stable magnetic field or in dynamic mode, in which the field is changed to detect individual masses in different collectors. While the static mode allows faster analysis, the latter helps to circumvent errors caused by different efficiencies within the array of ion collectors [41].

The following parts, therefore, focus on MC-ICP-MS. For isotope ratio determination by MC-ICP-MS, sample uptake is done by solution as well as by LA.

13.5.1 Solution-MC-ICP-MS

For solution-MC-ICP-MS, powdered bulk rock samples or mineral grains must be dissolved. Due to blank restrictions and in order to keep the sample matrix simple, only acid dissolution, mainly with mixtures of HF and HClO_4 or HNO_3 , is performed using Teflon® vessels (with steel jacket if necessary) in clean air laboratory environment.

While ratios of two isotopes of the same element can be determined in one step, isotope ratios involving two elements (e.g. $^{147}\text{Sm}/^{144}\text{Nd}$ and $^{176}\text{Lu}/^{177}\text{Hf}$) are determined in two separate steps of concentration analysis using isotope dilution [25]. Therefore, mixed spike solutions usually enriched with the isotopes ^{149}Sm – ^{150}Nd , ^{176}Lu – ^{178}Hf and ^{176}Lu – ^{180}Hf are added to the sample solution.

In order to keep the matrix of the elements as simple as possible, which helps to optimize signal stability and to minimize mass discriminating effects (see 13.3) and in order to avoid isobaric interferences of atomic ions (e.g. ^{144}Sm and ^{144}Nd) as well as of molecular species forming with elements of lower masses and Ar, O, N or C, element fractions are isolated from the spiked sample solutions [41]. Several methods of extracting REE and Hf from the bulk rock or mineral matrix and subsequent purification of Nd, Sm and Lu employing different chromatographic materials (e.g. Biorad® AG50WX8 cationic resin, Eichrom® TRU resin, resins conditioned with α -hydroxyisobutyric acid/ α -HIBA, Teflon®-based resins conditioned with di(2-ethylhexyl)orthophosphoric acid/HDEHP) but also liquid–liquid extraction have been developed [106–118].

Despite chemical isolation, trace impurities can occur in the fractions of analyte elements, which impose the problem of isobaric interferences (e.g. ^{176}Yb – ^{176}Lu and ^{144}Sm – ^{144}Nd). Correction of interference-related signal intensities can be performed

using interference-free masses, such as ^{173}Yb , ^{175}Lu , ^{146}Nd or ^{145}Nd and ^{149}Sm , as monitors for the presence of the interfering masses [113].

Correction of mass bias due to fractionation effects in the ICP ion source or detection system can be performed by bracketing of the sample analysis with two standard analyses. This requires identical fractionation properties of sample and standard solutions [41]. For independent calculation of bias caused by mass-dependent factors, different mathematical approaches are known among which an exponential law is applied most [41, 42]. For the latter, a stable reference isotope ratio unaffected by interferences is required for normalization. While $^{146}\text{Nd}/^{144}\text{Nd}$, $^{147}\text{Sm}/^{153}\text{Sm}$ and $^{179}\text{Hf}/^{177}\text{Hf}$ ratios can be used for correction of unknown isotope ratios of Nd, Sm and Hf, respectively, Lu only has the two isotopes ^{176}Lu and ^{175}Lu . Mass bias of the $^{176}\text{Lu}/^{175}\text{Lu}$ ratio can be evaluated using an interference-free isotope ratio of another REE after doping of the solution (e.g. $^{167}\text{Er}/^{166}\text{Er}$ [119]) or using Yb occurring in the Lu fraction due to incomplete chromatographic separation. To avoid the incorrect assumption of identical fractionation properties of Lu and Yb, the difference in mass discrimination is externally evaluated by repeated systematic analysis of mixed Yb and Lu standard solutions – a method also allowing assessment of isobaric interference by ^{176}Yb on ^{176}Lu [15, 41]. Alternatively, normalization to the $^{187}\text{Re}/^{185}\text{Re}$ ratio of an admixed standard solution is used for correction [120].

Any mass-independent fractionation must be corrected using factors derived from the analysis of standard solutions with known isotopic composition. Thus, often a final normalization to a standard solution run during analytical sessions is applied to yield accurate and reproducible isotope ratio measurements [41, 119].

For normalization or general evaluation of accuracy and correction procedures for determination of the radiogenic isotope ratios, standard solutions prepared with pure metals or oxides such as La Jolla, Ames-Nd or JNdi-1 for Nd, JMC 475 for Hf or JMC 304, Ames-Ce for Ce are common [95, 121–123].

Precision of isotope ratio determination by MC-ICP-MS depends on instrumental properties and correction procedures as well as on concentration of the analyte element or analysis time. For common analytical conditions applied for rock and mineral analysis, external precision (2σ) obtained from repeated analysis of standard solutions is often reported to be ≤ 20 ppm for $^{176}\text{Hf}/^{177}\text{Hf}$ or $^{143}\text{Nd}/^{144}\text{Nd}$ [68, 119, 124]. For the latter element, precision of MC-ICP-MS is comparable to values determined by TIMS [125].

13.5.2 LA-MC-ICP-MS

Determination of Sm–Nd isotopes with LA-MC-ICP-MS has increasingly been applied to minerals that enrich the light REE in the last years. Minerals such as monazite, apatite, titanite or allanite in which Nd can reach concentrations of several wt.% are highly suitable for this technique because precise isotope ratio analysis can be performed

also in small laser spots [126]. Isotopes of the Lu–Hf system are mainly analysed in zircon. Such measurements in combination with other in situ trace element and isotope (U–Pb, O) data obtained from the same single crystal make zircon one of the most important tracers of the earth's crustal evolution [57, 127].

LA-MC-ICP-MS thus combines the advantage of in situ analysis at high spatial resolution with the convenience of a method that does not require time-consuming dissolution and chromatographic sample preparation. However, leaving analyte elements and matrix unseparated leads to analytical tasks that require further consideration.

Isobaric interferences are more crucial for in situ analysis than for solution-ICP-MS. The signal of ^{144}Nd can be affected by a contribution of ^{144}Sm as high as 4 % in monazite because this mineral, like other light REE-rich minerals, contains significant amounts of Sm next to Nd [75]. Likewise, the REE isotopes ^{176}Lu and ^{176}Yb interfere to higher degrees with ^{176}Hf in in situ mineral analyses than in elemental fractions after chemical separation. Correction of an interfering isotope (e.g. ^{144}Sm) can be performed using its ratio with an interference-free isotope (e.g. ^{149}Sm) and additional correction of mass bias on the ratio. However, stable non-radiogenic ratios used for normalization in mass bias correction procedures may also be affected by interfering matrix elements (e.g. ^{142}Ce on ^{142}Nd) that can have high concentrations in unseparated solid mineral matter. Different procedures for such correction are given in refs [74, 75, 126].

In general, due to laser-induced fractionation (see 13.3), which occurs in addition to fractionation caused in plasma and interface, mass bias is a more pronounced effect of in situ LA-MC-ICP-MS isotope ratio determination. Furthermore, inter-element fractionation affecting analyses of parent–reference ratios (e.g. $^{147}\text{Sm}/^{144}\text{Nd}$, $^{176}\text{Lu}/^{177}\text{Hf}$) cannot always adequately be corrected using stable isotope ratios of only one element.

In many laboratories, both insufficiently corrected mass bias of daughter–reference ratios and fractionation of parent–reference ratios are corrected using mineral standards often analysed in a standard-sample bracketing mode [74]. Thus, well-characterized and homogeneous mineral standards matching the matrix of REE-enriched minerals including zircon are a prerequisite for accurate and precise isotope ratio measurement in particular for ns LA-MS-ICP-MS, which is still more often applied than fs LA-MS-ICP-MS. Instead of mineral standards, such as zircon 91500 [97, 128, 129], synthetic glass standards have also successfully been applied [74, 75].

Precision of LA-MC-ICP-MS isotope ratio determination depends on signal intensity, and thus on the concentration of the analyte element as well as on the pit diameter. Furthermore, integration time and correction procedures also control precision [65, 129]. McFarlane and McCulloch [126] report internal precision of the $^{143}\text{Nd}/^{144}\text{Nd}$ ratio as good as in TIMS instruments (<10 ppm, 2σ) for monazite with Nd at 9 wt. % and a crater diameter of 50 μm . External precision reaches best values between 60 and 95 ppm (2σ) for analytical conditions applicable to natural minerals (e.g. zircon and $^{176}\text{Hf}/^{177}\text{Hf}$ [57, 129]).

13.6 Concluding remarks

In the last 30 years, ICP-MS has been a rapidly developing technique. The robust and versatile ICP source allows efficient ionization and can be combined with different systems of sample input as well as with different MSs (quadrupole, magnetic SF and time of flight) at various detector configurations (single collector and multi-collector). Recent advance, for example in the field of fs LA-ICP-MS and MC-ICP-MS, shows that the technical and methodological evolution is still ongoing – certainly also driven by the analytical needs of the geosciences.

The introduction of ICP-MS as a standard instrument in geochemical laboratories significantly enhanced the availability of REE analyses of rocks and minerals, and due to the excellent ionization capability of the source ICP-MS also marked a major step in isotope geochemistry and cosmochemistry. Taking the role of REEs as indicator elements for geological processes and as geochronometers based on the decay of La, Sm and Lu isotopes into consideration, the advent of ICP-MS can be considered an important step in geosciences.

Acknowledgements

The author thanks Mrs. G. Günther and M.-A. Voß for assistance with bibliographical data.

References

- [1] Wedepohl KH. The composition of the continental crust. *Geochim Cosmochim Acta* 1995, 59, 1217–32.
- [2] Bau M. Controls on the fractionation of isovalent trace elements in magmatic and aqueous systems: Evidence from Y/Ho, Zr/Hf, and lanthanide tetrad effect. *Contrib Mineral Petrol* 1996, 123, 323–33.
- [3] Krauskopf KB, Bird DK. *Introduction to Geochemistry*. New York, McGraw-Hill, Inc., 1995.
- [4] Faure G. *Principles and Applications of Inorganic Geochemistry*. New York, Macmillan Publishing Company, 1991.
- [5] McDonough WF, Sun SS. The composition of the Earth. *Chem Geol* 1995, 120, 223–53.
- [6] Workman RK, Hart SR. Major and trace element composition of the depleted MORB mantle (DMM). *Earth Planet Sci Lett* 2005, 231, 53–72.
- [7] Jain JC, Field MP, Neal CR, Ely JC, Sherrell RM. Determination of the REE in geological reference materials DTS-1 (dunite) and PCC-1 (peridotite) by ultrasonic and microconcentric desolvating nebulisation ICP-MS. *Geostand Newsl* 2000, 24, 65–72.
- [8] Kempe U, Möckel R, Graupner T, Kynicky J, Dombon E. The genesis of Zr-Nb-REE mineralization at Khalzan Buregte (Western Mongolia) reconsidered. *Ore Geol Rev* 2015, 64, 602–25.
- [9] Wilson M. *Igneous Petrogenesis, A Global Tectonic Approach*. London, Chapman & Hall, 1989.
- [10] Alexander B, Bau M, Andersson P, Dulski P. Continentally-derived solutes in shallow Archean seawater: Rare earth element and Nd isotope evidence in iron formation from the 2.9 Ga Pongola Supergroup, South Africa. *Geochim Cosmochim Acta* 2008, 72, 378–94.

- [11] Bau M, Koschinsky A. Oxidative scavenging of cerium on hydrous Fe oxide: Evidence from the distribution of rare earth elements and yttrium between Fe oxides and Mn oxides in hydrogenetic ferromanganese crusts. *Geochem J* 2009, 43, 37–47.
- [12] Möller P, Knappe A, Dulski P. Seasonal variations of rare earths and yttrium distribution in the lowland Havel River, Germany, by agricultural fertilization and effluents of sewage treatment plants. *Appl Geochem* 2014, 41, 62–72.
- [13] Klaver G, Verheul M, Bakker I, Petelet-Giraud E, Négrel P. Anthropogenic rare earth elements in rivers: Gadolinium and lanthanum. Partitioning between the dissolved and particulate phases in the Rhine River and spatial propagation through the Rhine-Meuse Delta (the Netherlands). *Appl Geochem* 2014, 47, 186–97.
- [14] Kulaksiz S, Bau M. Anthropogenic dissolved and colloid/nanoparticle-bound samarium, lanthanum and gadolinium in the Rhine River and the impeding destruction of the natural rare earth element distribution in rivers. *Earth Planet Sci Lett* 2013, 362, 43–50.
- [15] Blichert-Toft J, Boyet M, Télouk P, Albarède F. ^{147}Sm - ^{143}Nd and ^{176}Lu - ^{176}Hf in eucrites and the differentiation of the HED parent body. *Earth Planet Sci Lett* 2002, 204, 167–81.
- [16] Blichert-Toft J, Albarède F. The Lu-Hf isotope geochemistry of chondrites and the evolution of the mantle-crust system. *Earth Planet Sci Lett* 1997, 148, 243–58.
- [17] Dickin AP. *Radiogenic Isotope Geology*, 2nd edition. Cambridge, New York, Melbourne, Madrid, Cape Town, Singapore, Sao Paulo, Cambridge University Press, 2005.
- [18] Doucelance R, Bellot N, Boyet M, Hammouda T, Bosq C. What coupled cerium and neodymium isotopes tell us about the deep source of oceanic carbonatites. *Earth Planet Sci Lett* 2014, 407, 175–86.
- [19] Faure G. *Principles of Isotope Geology*. New York, Chichester, Brisbane, Toronto, Singapore, John Wiley & Sons, 1986.
- [20] Gao Y, Ling W, Qiu X, Chen Z, Bai X. La-Ce isotopic system: Application status and advances. *Earth Science. J China Univ Geosci* 2011, 36, 33–42, in Chinese, English abstract.
- [21] Harrison TM, Blichert-Toft J, Müller W, Albarède F, Holden P, Mojzsis SJ. Heterogeneous Hadean Hafnium: Evidence of continental crust at 4.4 to 4.5 Ga. *Science* 2005, 310, 1947–50.
- [22] Marshall CP, Fairbridge RW. *Encyclopedia of Geochemistry*. Dordrecht, Boston, London, Kluwer Academic Publishers, 1999.
- [23] Patchett PJ. Importance of the Lu-Hf isotopic system in studies of planetary chronology and chemical evolution. *Geochim Cosmochim Acta* 1983, 47, 81–91.
- [24] Tanaka T, Shimizu H, Kawata Y, Masuda A. Combined La-Ce and Sm-Nd isotope systematics in petrogenetic studies. *Nature* 1987, 327, 113–17.
- [25] Baxter EF, Scherer EE. Garnet geochronology: Timekeeper of tectonometamorphic processes. *Elements* 2013, 9, 433–8.
- [26] Smit MA, Scherer EE, Mezger K. Lu-Hf and Sm-Nd garnet geochronology: Chronometric closure and implications for dating petrological processes. *Earth Planet Sci Lett* 2013, 381, 222–33.
- [27] Caro G, Bourdon B, Birck JL, Moorbath S. High-precision $^{142}\text{Nd}/^{144}\text{Nd}$ measurements in terrestrial rocks: Constraints on the early differentiation of the earth's mantle. *Geochim Cosmochim Acta* 2006, 70, 164–91.
- [28] Harper CL, Jacobsen SB. Evidence from coupled ^{147}Sm - ^{143}Nd and ^{146}Sm - ^{142}Nd systematics for very early (4.5-Gyr) differentiation of the earth's mantle. *Nature* 1992, 360, 728–32.
- [29] Moynier F, Bouvier A, Blichert-Toft J, Telouk P, Gasperini D, Albarède F. Europium isotopic variations in Allende CAIs and the nature of mass-dependent fractionation in the solar nebula. *Geochim Cosmochim Acta* 2006, 70, 4287–94.
- [30] Matthes S. *Mineralogie*. Berlin, Heidelberg, New York, Tokyo, Springer-Verlag, 1983.
- [31] Harley SL, Kelly NM, Möller A. Zircon behaviour and the thermal histories of mountain chains. *Elements* 2007, 3, 25–30.

- [32] Scherer EE, Whitehouse MJ, Münker C. Zircon as a monitor of crustal growth. *Elements* 2007, 3, 19–24.
- [33] Becker JS, Dietze HJ. Inorganic mass spectrometric methods for trace, ultratrace, isotope, and surface analysis. *Int J Mass Spectrom* 2000, 197, 1–35.
- [34] Dulski P. Interferences of oxide, hydroxide and chloride analyte species in the determination of rare earth elements in geological samples by inductively coupled plasma-mass spectrometry. *Fresenius' J Anal Chem* 1994, 350, 194–203.
- [35] Jenner GA, Longerich HP, Jackson SE, Fryer BJ. ICP-MS – a powerful tool for high-precision trace-element analysis in earth sciences: Evidence from analysis of selected U.S.G.S. reference samples. *Chem Geol* 1990, 83, 133–48.
- [36] Perkins WT, Pearce NJG, Jeffries TE. Laser ablation inductively coupled mass spectrometry: A new technique for the determination of trace and ultra-trace elements in silicates. *Geochim Cosmochim Acta* 1993, 57, 475–82.
- [37] Taylor HE, Huff RA, Montaser A. Novel applications of ICPMS, in: Montaser A (ed.) *Inductively Coupled Plasma Mass Spectrometry*. New York, Chichester, Weinheim, Brisbane, Singapore, Toronto, Wiley-VCH, 1998, 681–807.
- [38] Jarvis KE. Inductively coupled plasma mass spectrometry: A new technique for the rapid or ultra-trace level determination of the rare-earth elements in geological materials. *Chem Geol* 1988, 68, 31–39.
- [39] Gäbler HE. Applications of magnetic sector ICP-MS in geochemistry. *J Geochem Explor* 2002, 75, 1–15.
- [40] Walder AJ, Platzner I, Freedman PA. Isotope ratio measurement of lead, neodymium and neodymium-samarium mixtures, hafnium and hafnium-lutetium mixtures with a double focusing multiple collector inductively coupled plasma mass spectrometer. *J Anal At Spectrom* 1993, 8, 19–23.
- [41] Albarède F, Telouk P, Blichert-Toft J, Boyet M, Agranier A, Nelson B. Precise and accurate isotopic measurements using multiple-collector ICP-MS. *Geochim Cosmochim Acta* 2004, 68, 2725–44.
- [42] Olesik JW. Inductively coupled plasma mass spectrometers, in: Elias SA (ed.) *Treatise on Geochemistry*, 2nd edition, Volume 15. *Analytical Geochemistry/Inorganic INSTR. Analysis*, Amsterdam, Boston, Heidelberg, Elsevier, 2014, 309–36.
- [43] Becker JS. *Inorganic Mass Spectrometry – Principles and Applications*. Chichester, John Wiley & Sons, 2007.
- [44] Turner PJ, Mills DJ, Schröder E, Lapitajs G, Jung G, Iacone LA, Haydar DA, Montaser A. Instrumentation for low- and high-resolution ICPMS, in: Montaser A (ed.) *Inductively Coupled Plasma Mass Spectrometry*. New York, Chichester, Weinheim, Brisbane, Singapore, Toronto, Wiley-VCH, 1998, 421–501.
- [45] Gray AL. Solid sample introduction by laser ablation for inductively coupled plasma source mass spectrometry. *Analyst* 1985, 110, 551–6.
- [46] Jackson SE, Longerich HP, Dunning GR, Fryer BJ. The application of laser-ablation microprobe-inductively coupled plasma-mass spectrometry (LAM-ICP-MS) to in situ trace-element determinations in minerals. *Can Miner* 1992, 30, 1049–64.
- [47] Sylvester PJ. Laser-ablation-ICPMS in the earth sciences – preface, in: Sylvester P (ed.) *Laser-Ablation-ICPMS in the Earth Sciences – Principles and Applications*. Mineralogical Association of Canada Short Course Series 2001, 29, iii–iv.
- [48] Jarvis KE, Williams JG. Laser ablation inductively coupled plasma mass spectrometry (LA-ICP-MS): A rapid technique for the direct, quantitative determination of major, trace and rare-earth elements in geological samples. *Chem Geol* 1993, 106, 251–62.
- [49] Brätz H, Klemd R. *Analyses of Rare Earth Elements in Geological Samples by Laser Ablation-Inductively Coupled Plasma Mass Spectrometry (LA-ICP-MS)*. Agilent Technologies Inc. Publication Number 5988-6305EN, 2002, 1–6.

- [50] Gaspar M, Knaack C, Meinert LD, Moretti R. REE in skarn systems: A LA-ICP-MS study of garnets from the Crown Jewel gold deposit. *Geochim Cosmochim Acta* 2008, 72, 185–205.
- [51] Longerich HP. Laser ablation-inductively coupled plasma-mass spectrometry (LA-ICP-MS); an introduction, in: Sylvester P (ed.) *Laser Ablation-ICP-MS in the Earth Sciences – Current Practices and Outstanding Issues*. Mineralogical Association of Canada Short Course Series 2008, 40, 1–18.
- [52] Longerich H, Diegor W. Introduction to mass spectrometry, in: Sylvester P (ed.) *Laser-Ablation-ICPMS in the Earth Sciences – Principles and Applications*. Mineralogical Association of Canada Short Course Series 2001, 29, 1–19.
- [53] Heinrich CA, Pettke T, Halter WE, et al. Quantitative multi-element analysis of minerals, fluid and melt inclusions by laser-ablation inductively-coupled-plasma mass-spectrometry. *Geochim Cosmochim Acta* 2003, 67, 3473–97.
- [54] Hattendorf B, Latkoczy C, Günther D. Laser ablation ICP-MS. *Anal Chem* 2003, August 1, 341A–347A.
- [55] Horn I, Guillong M, Günther D. Wavelength dependant ablation rates for metals and silicate glasses using homogenized laser beam profiles – implications for LA-ICP-MS. *Appl Surf Sci* 2001, 182, 91–102.
- [56] Günther D. Quantitative fluid inclusion analysis using a 193 nm excimer laser-ablation system coupled to ICP-MS, in: Sylvester P (ed.) *Laser-Ablation-ICPMS in the Earth Sciences – Principles and Applications*. Mineralogical Association of Canada Short Course Series 2001, 29, 47–61.
- [57] Hawkesworth CJ, Kemp AIS. Using hafnium and oxygen isotopes in zircons to unravel the record of crustal evolution. *Chem Geol* 2006, 226, 144–62.
- [58] Shaheen ME, Gagnon JE, Fryer BJ. Femtosecond (fs) lasers coupled with modern ICP-MS instruments provide new and improved potential for in situ elemental and isotopic analyses in the geosciences. *Chem Geol* 2012, 330–31, 260–73.
- [59] d'Abzac FX, Czaja AD, Beard BL, Schauer JJ, Johnson CM. Iron distribution in size-resolved aerosols generated by UV-femtosecond laser ablation: Influence of cell geometry and implications for in situ isotopic determination by LA-ICP-MS. *Geostand Geoanal Res* 2014, 38, 293–309.
- [60] Seydoux-Guillaume AM, Freydier R, Poitrasson F, d'Abzac FX, Wirth R, Datas L. Dominance of mechanical over thermally induced damage during femtosecond laser ablation of monazite. *Euro J Mineral* 2010, 22, 235–44.
- [61] Freydier R, Candaudap F, Poitrasson F, Arbouet A, Chatel B, Dupré B. Evaluation of infrared femtosecond laser ablation for the analysis of geomaterials by ICP-MS. *J Anal At Spectrom* 2008, 23, 702–10.
- [62] Pickhardt C, Dietze HJ, Becker JS. Laser ablation inductively coupled plasma mass spectrometry for direct isotope ratio measurements on solid samples. *Int J Mass Spectrom* 2005, 242, 273–80.
- [63] Sylvester P. Matrix effects in LA-ICP-MS, in: Sylvester P (ed.) *Laser ablation-ICP-MS in the earth sciences – current practices and outstanding issues*. Mineralogical Association of Canada Short Course Series 2008, 40, 67–78.
- [64] Kent AJR, Ungerer CA. Production of barium and light rare earth oxides during LA-ICP-MS microanalysis. *J Anal At Spectrom* 2005, 20, 1256–62.
- [65] Pearson NJ, Griffin WL, O'Reilly SY. Mass fractionation correction in laser ablation multiple-collector ICP-MS: Implications for overlap corrections and precise and accurate in situ isotope ratio measurement, in: Sylvester P (ed.) *Laser Ablation-ICP-MS in the Earth Sciences – Current Practices and Outstanding Issues*. Mineralogical Association of Canada Short Course Series 2008, 40, 93–116.

- [66] Douglas DJ, Tanner SD. Fundamental considerations in ICP-MS, in: Montaser A (ed.) *Inductively Coupled Plasma Mass Spectrometry*. New York, Chichester, Weinheim, Brisbane, Singapore, Toronto, Wiley-VCH, 1998, 615–79.
- [67] Heumann KG, Gallus SM, Rädlinger G, Vogl J. Precision and accuracy in isotope ratio measurements by plasma source mass spectrometry. *J Anal At Spectrom* 1998, 13, 1001–8.
- [68] Vance D, Thirlwall M. An assessment of mass discrimination in MC-ICPMS using Nd isotopes. *Chem Geol* 2002, 185, 227–40.
- [69] d'Abzac FX, Beard BL, Czaja AD, Konishi H, Schauer JJ, Johnson CM. Iron isotope composition of particles produced by UV-femtosecond laser ablation of natural oxides, sulfides, and carbonates. *Anal Chem* 2013, 85, 11885–92.
- [70] Jackson S. Calibration strategies for elemental analysis by LA-ICP-MS, in: Sylvester P (ed.) *Laser Ablation-ICP-MS in the Earth Sciences – Current Practices and Outstanding Issues*. Mineralogical Association of Canada Short Course Series 2008, 40, 169–88.
- [71] Koch J, Feldmann I, Jakubowski N, Niemax K. Elemental composition of laser ablation aerosol particles deposited in the transport tube to an ICP. *Spectrochim Acta B At Spectrosc* 2002, 57, 975–85.
- [72] Guillong M, Horn I, Günther D. A comparison of 266 nm, 213 nm and 193 nm produced from a single solid state Nd:YAG laser for laser ablation ICP-MS. *J Anal At Spectrom* 2003, 18, 1224–30.
- [73] Krosiakova I, Günther D. Elemental fractionation in laser ablation-inductively coupled plasma-mass spectrometry: Evidence for mass load induced matrix effects in the ICP during ablation of a silicate glass. *J Anal At Spectrom* 2007, 22, 51–62.
- [74] Fisher CM, McFarlane CRM, Hanchar JM, Schmitz MD, Sylvester PJ, Lam R, Longerich HP. Sm-Nd isotope systematics by laser ablation-multicollector-inductively coupled plasma mass spectrometry: Methods and potential natural and synthetic reference materials. *Chem Geol* 2011, 284, 1–20.
- [75] Iizuka T, Eggins SM, McCulloch MT, Kinsley LPJ, Mortimer GE. Precise and accurate determination of $^{147}\text{Sm}/^{144}\text{Nd}$ and $^{143}\text{Nd}/^{144}\text{Nd}$ in monazite using laser ablation-MC-ICPMS. *Chem Geol* 2011, 282, 45–57.
- [76] Steinhöfel G, Horn I, von Blanckenburg F. Matrix-independent Fe isotope ratio determination in silicates using UV femtosecond laser ablation. *Chem Geol* 2009, 268, 67–73.
- [77] Horn I, von Blanckenburg F, Schoenberg R, Steinhöfel G, Markl G. In situ iron isotope ratio determination using UV-femtosecond laser ablation with application to hydrothermal ore formation processes. *Geochim Cosmochim Acta* 2006, 70, 3677–88.
- [78] Guillong M, Günther D. Effect of particle size distribution on ICP-induced elemental fractionation in laser ablation-inductively coupled plasma-mass spectrometry. *J Anal At Spectrom* 2002, 17, 831–7.
- [79] Bea F, Montero P. Behavior of accessory phases and redistribution of Zr, REE, Y, Th, and U during metamorphism and partial melting of metapelites in the lower crust: An example from the Kinzingite formation of Ivrea-Verbano, NW Italy. *Geochim Cosmochim Acta* 1999, 63, 1133–53.
- [80] Balaram V, Rao TG. Rapid determination of REEs and other trace elements in geological samples by microwave acid digestion and ICP-MS. *At Spectrosc* 2003, 24, 206–12.
- [81] Morrison CA, Lambert DD, Morrison RJS, Ahlers WW, Nicholls IA. Laser ablation-inductively coupled plasma-mass spectrometry: An investigation of elemental responses and matrix effects in the analysis of geostandards materials. *Chem Geol* 1995, 119, 13–29.
- [82] Fedorowich JS, Richards JP, Jain JC, Kerrich R, Fan J. A rapid method for REE and trace-element analysis using laser sampling ICP-MS on direct fusion whole-rock glasses. *Chem Geol* 1993, 106, 229–49.

- [83] Becker JS, Pickhardt C, Dietze HJ. Laser ablation inductively coupled plasma mass spectrometry for determination of trace elements in geological glasses. *Mikrochim Acta* 2000, 135, 71–80.
- [84] Jenner FE, O'Neill HSC. Major and trace analysis of basaltic glasses by laser-ablation ICP-MS. *Geochem Geophys Geosyst* 2012, 13, doi:10.1029/2011GC003890.
- [85] Becker JS, Dietze HJ. Determination of trace elements in geological samples by laser ablation inductively coupled plasma mass spectrometry. *Fresenius J Anal Chem* 1999, 365, 429–34.
- [86] Ødegård M, Dundas SH, Flem B, Grimstvedt A. Application of a double-focusing magnetic sector inductively coupled plasma mass spectrometer with laser ablation for the bulk analysis of rare earth elements in rocks fused with $\text{Li}_2\text{B}_4\text{O}_7$. *Fresenius J Anal Chem* 1998, 362, 477–82.
- [87] Cheatham MM, Sangrey WF, White WM. Sources of error in external calibration ICP-MS analysis of geological samples and an improved non-linear drift correction procedure. *Spectrochim Acta* 1993, 48B, E487–E506.
- [88] Dulski P. Reference materials for geochemical studies: New analytical data by ICP-MS and critical discussion of reference values. *Geostand Newsl* 2001, 25, 87–125.
- [89] Jakubowski N, Moens L, Vanhaecke F. Sector field mass spectrometers in ICP-MS. *Spectrochim Acta Part B* 1998, 1739–63.
- [90] Du Z, Houk RS. Attenuation of metal oxide ions in inductively coupled plasma mass spectrometry with hydrogen in a hexapole collision cell. *J Anal At Spectrom* 2000, 15, 383–8.
- [91] Mason PRD, Kraan WJ. Attenuation of spectral interferences during laser ablation inductively coupled plasma mass spectrometry (LA-ICP-MS) using an rf only collision and reaction cell. *J Anal At Spectrom* 2002, 17, 858–67.
- [92] Jochum KP, Stoll B, Herwig K et al. MPI-DING reference glasses for in situ microanalysis: New reference values for element concentrations and isotope ratios. *Geochem Geophys Geosyst* 2006, 7, 1–44, doi:10.1029/2005GC001060.
- [93] Jochum KP,ENZWEILER J. Reference materials in geochemical and environmental research, in: ELIAS SA (ed.) *Treatise on Geochemistry*, 2nd edition. Volume 15, Analytical Geochemistry/Inorganic INSTR. Analysis, Amsterdam, Boston, Heidelberg, Elsevier, 2014, 43–70.
- [94] Cousin H, Magyar B. Precision and accuracy of laser ablation-ICP-MS analysis of rare earth elements with external calibration. *Mikrochim Acta* 1994, 113, 313–23.
- [95] Jochum KP, Nohl U, Herwig K, Lammel E, Stoll B, Hofmann AW. GeoReM: A new geochemical database for reference materials and isotopic standards. *Geostand Geoanal Res* 2005, 29, 333–8.
- [96] Jochum KP, Stoll B. Reference materials for elemental and isotopic analyses by LA-(MC)-ICP-MS: Success and outstanding needs, in: SYLVESTER P (ed.) *Laser Ablation-ICP-MS in the Earth Sciences – Current Practices and Outstanding Issues*. Mineralogical Association of Canada Short Course Series, 2008, 40, 147–68.
- [97] Wiedenbeck M, Hanchar JM, Peck WH, et al. Further characterization of the 91500 zircon crystal. *Geostand Geoanal Res* 2004, 28, 9–39.
- [98] Sláma J, Košler J, Condon DJ, et al. Plešovice zircon – a new natural reference material for U-Pb and Hf isotopic microanalysis. *Chem Geol* 2008, 249, 1–35.
- [99] Ødegård M, Skår Ø, Schiellerup H, Pearson NJ. Preparation of a synthetic titanite glass calibration material for in situ microanalysis by direct fusion in graphite electrodes: A preliminary characterization by EPMA and LA-ICP-MS. *Geostand Geoanal Res* 2005, 29, 197–209.
- [100] Pickhardt C, Becker JS, Dietze HJ. A new strategy of solution calibration in laser ablation inductively coupled plasma mass spectrometry for multielement trace analysis of geological samples. *Fresenius J Anal Chem* 2000, 368, 173–81.

- [101] Longerich HP, Jackson SE, Günther D. Laser ablation inductively coupled plasma mass spectrometric transient signal data acquisition and analyte concentration calculation. *J Anal At Spectrom* 1996, 11, 899–904.
- [102] Jochum KP, Stoll B, Herwig K, Willbold M. Validation of LA-ICP-MS trace element analysis of geological glasses using a new solid-state 193 nm Nd:YAG laser and matrix-matched calibration. *J Anal At Spectrom* 2007, 22, 112–21.
- [103] Gonzales J, Dundas SH, Liu CY, Mao X, Russo RE. UV-femtosecond and nanosecond laser ablation-ICP-MS: Internal and external repeatability. *J Anal At Spectrom* 2006, 21, 778–84.
- [104] Jochum KP, Stoll B, Weis U, Jacob DE, Mertz-Kraus R, Andreae MO. Non-matrix-matched calibration for the multi-element analysis of geological and environmental samples using 200 nm femtosecond LA-ICP-MS: A comparison with nanosecond lasers. *Geostand Geoanal Res* 2014, 38, 265–92.
- [105] Cook NJ, Ciobanu CL, O'Reilly D, Wilson R, Das K, Wade B. Mineral chemistry of Rare Earth Element (REE) mineralization, Browns Ranges, Western Australia. *Lithos* 2013, 172–73, 192–213.
- [106] Blichert-Toft J, Chauvel C, Albarède F. Separation of Hf and Lu for high-precision isotope analysis of rock samples by magnetic sector-multiple collector ICP-MS. *Contrib Mineral Petrol* 1997, 127, 248–60.
- [107] Cassidy RM, Chauvel C. Modern liquid chromatographic techniques for the separation of Nd and Sr for isotopic analysis. *Chem Geol* 1989, 74, 189–200.
- [108] Dosso L, Murthy VR. A Nd isotopic study of the Kerguelen Islands: Inferences on enriched oceanic mantle sources. *Earth Planet Sci Lett* 1980, 48, 268–76.
- [109] Eugster O, Tera F, Burnett DS, Wasserburg GJ. The isotopic composition of gadolinium and neutron capture effect in some meteorites. *J Geophys Res* 1970, 75, 2753–68.
- [110] Hooker PJ, O'Nions RK, Pankhurst RJ. Determination of rare-earth elements in USGS standard rocks by mixed-solvent ion exchange and mass-spectrometric isotope dilution. *Chem Geol* 1975, 16, 189–96.
- [111] Makishima A, Nakamura E. New preconcentration technique of Zr, Nb, Mo, Hf, Ta and W employing coprecipitation with Ti compounds: Its application to Lu-Hf system and sequential Pb-Sr-Nd-Sm separation. *Geochem J* 2008, 42, 199–206.
- [112] Morisset CE, Scoates JS, Weis D, Rahier A. Methodology and application of hafnium isotopes in ilmenite and rutile by MC-ICP-MS. *Geostand Geoanal Res* 2014, 38, 159–76.
- [113] Münker C, Weyer S, Scherer E, Mezger K. Separation of high field strength elements (Nb, Ta, Zr, Hf) and Lu from rock samples for MC-ICPMS measurements. *Geochem Geophys Geosyst* 2001, 2, 10.1029/2001GC000183.
- [114] Pin C, Santos Zalduegui JF. Sequential separation of light-rare-earth elements, thorium and uranium by miniaturization extraction chromatography: Application to isotopic analyses of silicate rocks. *Anal Chim Acta* 1997, 339, 79–89.
- [115] Rehkämper M, Gärtner M, Galer SJG, Goldstein SL. Separation of Ce from other rare-earth elements with application to Sm-Nd and La-Ce chronometry. *Chem Geol* 1996, 129, 201–8.
- [116] Richard P, Shimizu N, Allegre CJ. $^{143}\text{Nd}/^{146}\text{Nd}$, a natural tracer: An application to oceanic basalts. *Earth Planet Sci Lett* 1976, 31, 269–78.
- [117] Scherer EE, Cameron KL, Johnson CM, Beard BL, Barovich KM, Collerson KD. Lu-Hf geochronology applied to dating Cenozoic events affecting lower crustal xenoliths from Kilbourne Hole, New Mexico. *Chem Geol* 1997, 142, 63–78.
- [118] Ulrich M, Bureau S, Chauvel C, Picard C. Accurate measurement of rare earth elements by ICP-MS after ion-exchange separation; application to ultra-depleted samples. *Geostand Geoanal Res* 2012, 36, 7–20.
- [119] Lapen TJ, Mahlen NJ, Johnson CM, Beard BL. High precision Lu and Hf isotope analyses of both spiked and unspiked samples: A new approach. *Geochem Geophys Geosyst* 2004, 5, doi:10.1029/2003GC000582.

- [120] Scherer EE, Münker C, Mezger K. Calibration of the lutetium-hafnium clock. *Science* 2001, 293, 683–7.
- [121] Andreasen R, Lapen TJ. The absolute neodymium isotopic composition of standard materials – implications for accurate and precise ¹⁴²neodymium measurements and chronology. 44th Lunar and Planetary Science Conference, 2013, 2918.
- [122] Patchett PJ, Tatsumoto M. A routine high-precision method for Lu-Hf isotope geochemistry and chronology. *Contrib Mineral Petrol* 1980, 75, 263–7.
- [123] Tanaka T, Masuda A. The La-Ce geochronometer: A new dating method. *Nature* 1982, 300, 515–18.
- [124] Choi MS, Cheong CS, Kim J, Shin HS. Hafnium isotope analysis of mixed standard solutions by multi-collector inductively coupled plasma mass spectrometry: An evaluation of isobaric interference corrections. *J Anal Sci Technol* 2013, 4, 1, www.jast-journal.com/content/4/1/1
- [125] Harvey J, Baxter EF. An improved method for TIMS high precision neodymium isotope analysis of very small aliquots (1–10 ng). *Chem Geol* 2009, 258, 251–7.
- [126] McFarlane C, McCulloch M. Sm-Nd and Sr isotope systematics in LREE-rich accessory minerals using LA-MC-ICP-MS, in: Sylvester P (ed.) *Laser Ablation-ICP-MS in the Earth Sciences – Current Practices and Outstanding Issues*. Mineralogical Association of Canada Short Course Series 2008, 40, 117–33.
- [127] Kinny PD, Maas R. Lu-Hf and Sm-Nd isotope systems in zircon, in: Hanchar JM, Hoskin PWO (eds.) *Zircon*. *Rev Mineral Geochem* 2003, 53, 327–41.
- [128] Goolaerts A, Mattielli N, de Jong J, Weis D, Scoates JS. Hf and Lu isotopic reference values for the zircon standard 91500 by MC-ICP-MS. *Chem Geol* 2004, 206, 1–9.
- [129] Woodhead JD, Hergt JM, Shelley M, Eggins S, Kemp R. Zircon Hf-isotope analysis with an excimer laser, depth profiling, ablation of complex geometries, and concomitant age estimations. *Chem Geol* 2004, 209, 121–35.

Tom Lorenz and Martin Bertau

14 Recycling of Rare Earth Elements

Abstract: Any development of an effective process for rare earth (RE) recycling has become more and more challenging, especially in recent years. Since 2011, when commodity prices of REs had met their all-time maximum, prices have dropped rapidly by more than 90 %. An economic process able to offset these fluctuations has to take unconventional methods into account beside well-known strategies like acid/basic leaching or solvent extraction. The solid-state chlorination provides such an unconventional method for mobilizing RE elements from waste streams. Instead of hydrochloric acid this kind of chlorination decomposes NH_4Cl thermally to release up to 400 °C hot HCl gas. After cooling the resulting solid metal chlorides may be easily dissolved in pH-adjusted water. Without producing strongly acidic wastes and with NH_4Cl as cheap source for hydrogen chloride, solid-state chlorination provides various advantages in terms of costs and disposal. In the course of the SepSELSA project this method was examined, adjusted and optimized for RE recycling from fluorescent lamp scraps as well as $\text{Fe}_{14}\text{Nd}_2\text{B}$ magnets. Thereby many surprising influences and trends required various analytic methods to examine the reasons and special mechanisms behind them.

14.1 Recycling of rare earth elements

The development of efficient and economic strategies for RE recycling depends on different factors, for example, commodity prices, location and size of deposits, costs for disposal as well as hazard potential. Due to great worldwide deposits of RE containing ores and low commodity prices, only a few recycling processes are currently able to work on an industrial scale. However, the majority focuses only on production wastes or end-of-life (EoL) products with especially high RE contents [1–4]. Recycling of $\text{Fe}_{14}\text{Nd}_2\text{B}$ and SmCo magnets from production waste has been state of the art for a couple of decades. Currently 10–30 % of the starting alloys still accumulate as different wastes during manufacturing, such as slurry, powder or chips [2]. Most of these chiefly pyrometallurgical processes remove the plastic sockets, then grind the waste and blend the resulting powder with new starting alloys [4–6]. This strategy avoids an expensive and costly reduction of RE elements.

Regarding EoL products fluorescent lamp scraps and NiMH batteries currently serve as sources for efficient RE recycling. Although spent magnets often contain more than 30 wt.% of REM as well as there are many scientific articles dealing with this topic, yet none of the proposed strategies or processes has met the requirements for an upscale to industrial production [2, 3, 7–11]. The reasons are versatile: (i) Removing the small magnets from their sockets and housings in, for example, hard drives

or electric motors often proves to be very complicated [7–9, 12]. (ii) Besides prices for RE oxides decreased in part by more than 98 % since 2011. For instance, CeO₂ dropped from 100 US\$/kg [13] to 1.59 US\$/kg [14] within the last 5 years. (iii) Since EoL products contain REs mostly in oxidized state, either because of their application (fluorescent powders, polishing agents, ceramics, glass) or due to corrosion (magnets, alloys, batteries), pyrometallurgical treatment must not be used for recycling. The same applies for impurities, accompanying elements (e.g. Ni, Co, Zn) and housings coming along with EoL waste. Disadvantageously, the expensive RE reduction using fused salt electrolysis cannot be avoided in a hydrometallurgical process.

Nevertheless, Umicore and Solvay Rare Earths have already developed a wet chemical EoL recycling for fluorescent lamps (2008) and NiMH batteries (2011) on an industrial scale [7, 15]. By now Osram has patented a process for RE recovery from fluorescent lamp scraps, too [16]. In case of permanent magnets the MORE project (2011–14), a joint project of Siemens, Mercedes, Umicore and several German scientific institutes and universities, examined three different strategies to recycle magnets from spent electric motors. Whereas both mechanical strategies, namely the reuse of undamaged magnets as well as blending the grinded magnets with starting alloys, missed the requirements for new permanent magnets, the third hydrometallurgical route yielded the REs as sellable oxides [7–9]. But neither the MORE project nor one of the wet chemical processes developed in scientific literature has succeeded in reducing the gap between laboratory bench and industrial process so far [2, 3, 7–11]. Against this background, unconventional recycling processes get more and more attractive. One approach, the so-called solid-state chlorination, shows numerous amazing effects for RE recycling and combines high yields with an extremely low demand for chemicals combined with minor costs for disposal. Within the SepSELSA project this method was adjusted and optimized for RE recovery from fluorescent lamp scraps [17–19]. Unexpected trends and side reactions required many different methods of analysis. In this context the optimization based on statistical designs, as they are used for development of analytic techniques, proved most helpful.

14.2 Recycling from fluorescent lamp scraps

Approximately 250–300 t of Hg-contaminated fluorescent lamp scraps with average RE contents of about 10 wt.% are deposited downhole in Germany every year [16]. Prior to a wet chemical recovery such as Solvay Rare Earth runs in La Rochelle, all the quicksilver has to be removed by distillation at >357 °C. Additionally to EoL lamp scraps there are Hg-free production wastes with RE contents up to 22 wt.%. In 2009, when the regulation EG 245 came into force, higher standards for light quality were applied so that the older and RE-free halophosphate fluorescent materials couldn't achieve

anymore [20]. As a result the amount of three-band fluorescent materials and the RE content are going to rise prospectively. In this regard EoL fluorescent lamp scraps and production waste were examined by the SepSELSA¹ project in the course of process development.

14.2.1 Starting material

Both EoL scraps and production wastes always contain a mixture of different fluorescent materials whose composition varies in a wide range, due to joint repository and disposal. Alongside three-band materials and the older halophosphate these wastes embody residues of glass and metallic sockets, too. In general, the particular fluorescent materials are composed of a host lattice and one or more doped activator elements. RE elements serve mainly as activators, except for yttrium which forms a host lattice, too ($\text{Y}_2\text{O}_3:\text{Eu}^{3+}$). Overall fluorescent lamp scraps may consist of up to 19 different elements. Table 14.1 summarizes the most common components of EoL wastes.

During the SepSELSA project the first batch of waste came directly from lamp production, whereas the second batch consisted of EoL lamp scraps (Table 14.2). To determine the composition of both batches X-ray fluorescent spectroscopy (XFS) was used after removing the quicksilver by heating up to 500 °C in a stream of nitrogen gas and maintaining this temperature for 4 h. Yet an exact quantification of particular fluorescent materials remained impossible, because some elements are part of more than one fluorescent material at the same time. Therefore, SEM-EDX spectroscopy

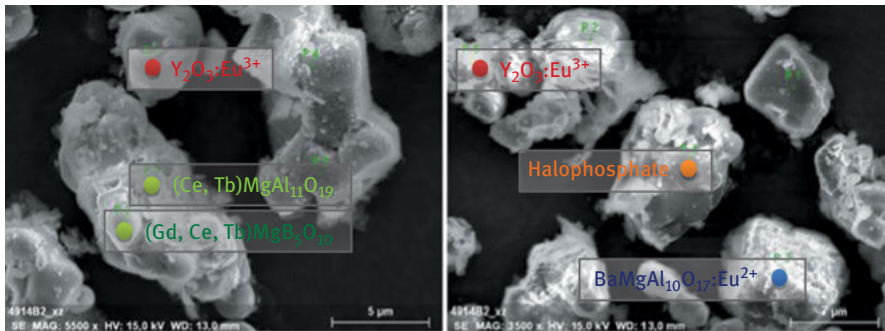
Table 14.1: Components of EoL fluorescent lamp scraps [19].

Component		Colour of emission	Source
$\text{Y}_2\text{O}_3:\text{Eu}^{3+}$	(YOE)	Red	Three-band Fluorescent materials
$\text{La}(\text{PO}_4):\text{Ce}^{3+}, \text{Tb}^{3+}$	(LAP)	Green	
$(\text{Ce}^{3+}, \text{Tb}^{3+})\text{MgAl}_{11}\text{O}_{19}$	(CAT)	Green	
$(\text{Gd}^{3+}, \text{Ce}^{3+}, \text{Tb}^{3+})\text{MgB}_5\text{O}_{10}$	(CBT)	Green	
$\text{BaMgAl}_{10}\text{O}_{17}:\text{Eu}^{2+}$	(BAM)	Blue	
$(\text{Ca}, \text{Sr}, \text{Ba})_5(\text{PO}_4)_3\text{Cl}:\text{Eu}^{2+}$	(ScAp)	Blue	
$\text{Ca}_5(\text{PO}_4)_3(\text{F}, \text{Cl}):\text{Sb}^{3+}, \text{Mn}^{2+}$		Continuous	Halophosphate fluorescent material
Hg			Medium for UV emission
SiO_2			Glass residue
Metallic pieces			Socket

¹ The authors wish to thank the Federal Ministry of Education and Research for financial support of the project (grant number 033R113B).

Table 14.2: Composition of fluorescent lamp scraps examined in the SepSELSA project.

Elements	Production waste (wt.%)	EoL waste (wt.%)
Ca	6.7	17.6
Al	12.2	4.2
P	4.5	9.3
Si	3.8	8.7
Ba	9.3	9.1
Sr	5.9	0.5
Mg	1.2	0.6
Y	15.7	5.4
Eu	1.3	0.3
Gd	0.6	0.2
Tb	1.0	0.3
La	1.3	0.8
Ce	1.8	0.7
Σ RE	21.7	7.7

**Figure 14.1:** Secondary electron images (SEI) of the used EoL fluorescent lamp scraps provided by SEM.

was used to correlate each particle by its composition with the respective fluorescent material (Figure 14.1).

By developing an efficient recycling process all efforts were concentrated on yttrium and europium representing the main part of the six RE elements with a share of 70–80 %. Yttrium solely occurs in the red-light-emitting fluorescent material together with Eu^{3+} as activator. Regarding all elements the Y concentration amounted to 5.4 wt.% for the EoL batch and 15.7 wt.% for the production waste.

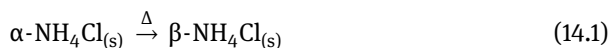
Each analysis via XFS was conducted with a wavelength-dispersive XFS (XEPOS from Spectro, Germany) and without using external standards. About 2 g of the dry and powdered sample (<100 μm) was mixed with 1 g cellulose in a ZrO_2 -based ceramic crucible and afterwards homogenized in a vibrating cup mill for 2 min. The resulting fine powder was introduced to a press (10^4 N) preparing tablets of 35 mm in diameter. The internal calibration was used for quantification, where the sample matrix was taken into account depending on the measured composition. The quantification was conducted sequentially for each particular element based on its respective characteristic X-radiation by using either a scintillation counter ($\lambda < 0.2$ nm) or a flow counter ($\lambda > 0.2$ nm). Measurement periods were altered between 12 and 24 s depending on the element. Afterwards all element contents were calculated by comparing the counts per second with the intern calibration. In summary this method suits well for survey measurement of unknown samples but is insufficient for analysing trace elements. For more accurate determination an external calibration with different standards is indispensable. If the sample dissolves completely in mineral acids other methods, for instance ICP-AES or flame-AAS, are more preferable.

In contrast to yttrium Eu^{2+} serves furthermore as activator in blue fluorescent materials such as $\text{BaMgAl}_{10}\text{O}_{17}:\text{Eu}^{2+}$ (BAM) and $(\text{Ca}, \text{Sr}, \text{Ba})_5(\text{PO}_4)_3\text{Cl}:\text{Eu}^{2+}$ (ScAp). The remaining REs lanthanum, cerium, gadolinium and terbium are components of blue and green emitting materials, but with quite low concentrations of about 0.3–1.8 wt.%. Altogether the production waste contains almost three times as much RE elements (21.7 wt.%) as the EoL lamp scraps. As expected, the content of outdated halophosphate is two to three times higher in EoL waste, as it's proved by the respective concentrations of calcium and phosphor. The same is applied for silicon coming from glass breakage produced during cutting the metal sockets.

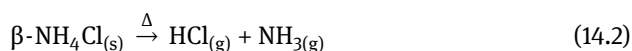
14.2.2 Solid-state chlorination

In contrast to acid leaching gaseous $\text{HCl}_{(\text{g})}$ reacts with the fluorescent lamp scraps during solid-state chlorination. Initially both batches are mixed with NH_4Cl and heated above 250 °C. At 184 °C NH_4Cl changes modification, and thermal decomposition sets in at $T > 220$ °C releasing gaseous $\text{NH}_{3(\text{g})}$ and $\text{HCl}_{(\text{g})}$.

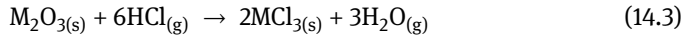
Change of modification at $T = 184.3$ °C



Thermal decomposition at $T \geq 220$ °C



Reaction with $\text{HCl}_{(g)}$ at $250 < T < 400 \text{ }^\circ\text{C}$



The last reaction yields water-soluble and nonvolatile metal chlorides. Volatile chlorides (FeCl_3 at $120 \text{ }^\circ\text{C}$) and metal chlorides with low melting temperatures (ZnCl_2 at $318 \text{ }^\circ\text{C}$) were not present in the fluorescent lamp scraps. They interfere with the gas-phase chlorination by forming liquid films on the particle surfaces, thus shielding them from further chlorination. In addition, the thermal decomposition is reversible, which allows recovering unreacted NH_4Cl in a subsequent step by allowing the gaseous phase to cool down. Yet compared to conventional acid leaching, the scrap constituent exhibits different behaviour towards gaseous HCl . Whereas $\text{Y}_2\text{O}_3:\text{Eu}^{3+}$ reacts very fast to YCl_3 and EuCl_3 , all of the phosphate, aluminate and borate fluorescent materials remain almost unaltered. By leaching the chlorinated solid with 100 g of distilled water all formed metal chlorides dissolve. For conducting this solid-state chlorination several suitable reactor types are at hand. Initially, in exploratory experiments an array of three sublimation reactors served to determine relevant influence

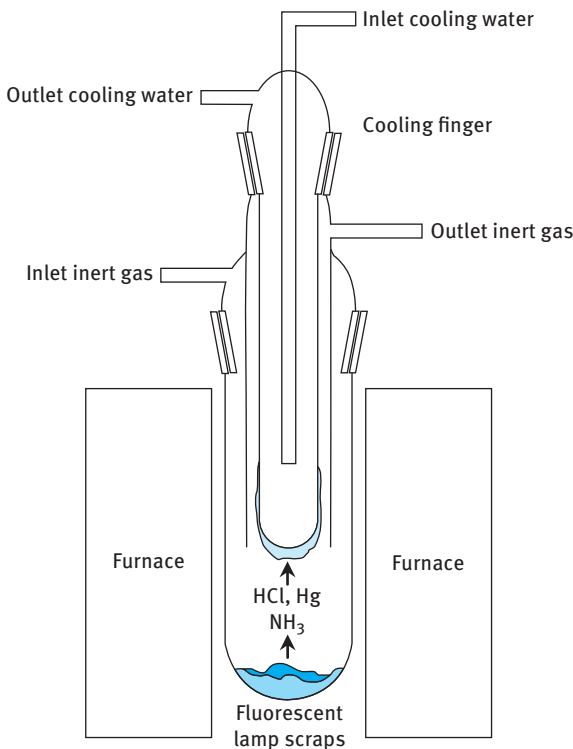


Figure 14.2: Sublimation reactor used for all attempts of orientation as well as the sequential pre-optimization.

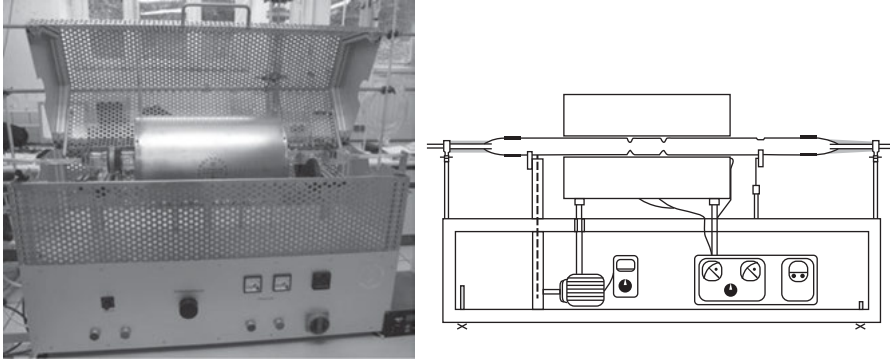


Figure 14.3: Rotary kiln used for simultaneous optimization.

factors and their respective ranges for the upcoming simultaneous optimization. As depicted in Figure 14.2, the mixture of NH_4Cl and fluorescent lamp scraps is placed on the bottom of a quartz tube reactor. A nitrogen atmosphere is required in order to prevent water-insoluble metal oxides from forming. By directing the gas flow next to a cooling finger unreacted NH_4Cl separates from the gaseous phase by depositing on the surface.

For optimizing the reaction on the basis of statistical designs the reactor type was changed to a rotary kiln operating in batch mode. Here, the mixture of NH_4Cl and fluorescent scraps was placed between two tapers in the horizontal quartz tube (Figure 14.3). Compared to conventional fixed or fluidized bed reactors as well as sublimation reactors the rotary kiln is able to operate in continuous mode, from which a significantly better performance compared with batch-type reactors is expected.

In fact, first, orienting experiments showed great differences between solid-state chlorination and classic leaching with aqueous hydrochloric acid (Figure 14.4). For comparison, in experiments with EoL lamp scraps as well as with production waste, chlorination was conducted at $T = 300^\circ\text{C}$ for 2 h with an NH_4Cl /fluorescent lamp scrap ratio (AFR) = 2.0 g/g, followed by leaching with distilled water. Acid leaching served as reference and was conducted in 3 M hydrochloric acid at 60°C for 3 h. In the leachate the concentration of the solid amounted to 15 wt.%.

The analysis of all water-based samples was conducted via atomic emission spectroscopy using an inductive coupled plasma (iCAP 6500 duo von Thermo Scientific, USA). The samples were diluted to element concentrations between 1 and 25 mg/L. For fluorescent lamp scraps two dilutions (1:10 and 1:100) were applied, due to very different concentrations of yttrium and the other RE elements. Although all samples were analysed in a low dilution of 1:10, the concentration of lanthanum, cerium, gadolinium and terbium hardly exceeded the detection limit (~ 0.1 mg/L) proving a high selectivity for yttrium and europium. For magnet analyses, a dilution of 1:200 was sufficient. Further pretreatment of the samples was not required. Before transferring each sample

Table 14.3: Measured wavelengths λ for particular RE elements.

Fluorescent lamp scraps		Fe ₁₄ Nd ₂ B magnets	
Y	371.029 nm	Fe	238.204 and 239.562 nm
Eu	381.967 nm	Nd	401.225 and 406.109 nm
Gd	342.247 nm	Dy	394.468 nm
Tb	350.917 nm		
La	379.478 nm		
Ce	456.236 nm		

to the plasma torch, a Mira Mist nebulizer connected to a cyclone spray chamber was used to produce an aerosol from the sample. For quantification, an average was calculated from intensities of three consecutive measurements (Table 14.3).

Contrary to natural RE ores wastes only contain a reduced number of RE elements. Thus, there are only few relevant disturbances that have to be taken into account, like for terbium and dysprosium at $\lambda = 353.170$ nm.

Considering the overall yield for RE elements, there is one advantage of the wet acid leaching over solid-state chlorination: metal chlorides are dissolved from particle surfaces, thus continuously regenerating a particle surface and thus preventing surface passivation. Moreover, HCl_(aq) leaching also mobilizes gadolinium, terbium, lanthanum and cerium, resulting in a slightly higher RE yield of about 5–7 percentage points. However, in view of the low concentrations of these four RE elements the differences remain small. And, these slightly higher overall yields were bought at the price of a considerably lower discrimination power between the major and minor constituents.

Consequently, mobilizing all elements results in an obvious disadvantage when it comes to RE separation. Owing to their highly similar chemical properties REs are difficult to separate, and it often requires more than 100 stages of solvent extraction. Solid-state chlorination overcomes separation problem through its higher selectivity towards the RE phosphors, allowing for selectively separating the major constituents Y and Eu. As depicted in Figure 14.4 Y–Eu selectivity towards the remaining four RE elements reached 99.6 % (production) and 99.7 % (EoL), respectively. Accordingly, the wet acid approach furnished Y–Eu selectivities, not exceeding 97.2 % for EoL products and 91.2 % for fluorescent lamp scraps from production waste.

The main difference between both methods concerns the gaseous phase leaving the reactor while chlorinating with NH₄Cl. The hot aerosol consists of NH_{3(g)}, H₂O_(g), HCl_(g) and entrained solid particles. Cooling the gaseous phase below 220 °C leads to a quantitative recombination of HCl_(g) and NH_{3(g)} to NH₄Cl, because of the reversible decomposition reaction. Both NH₄Cl and entrained particles can easily be separated from the gas flow by bag filters and recirculated afterwards. Referring to

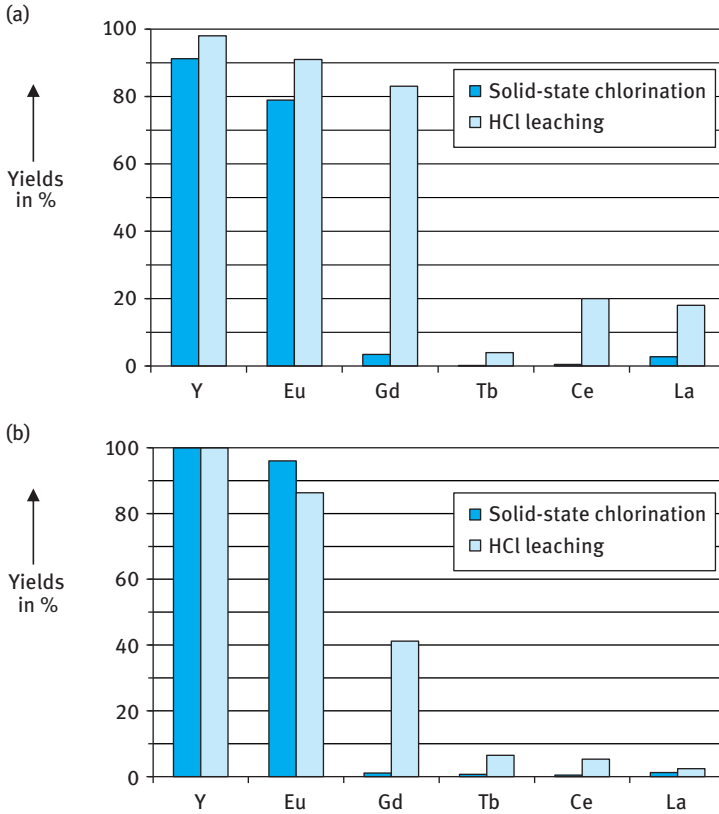


Figure 14.4: Comparison of leaching with hydrochloric acid and solid-state chlorination (SepSELSA project) for production waste (a) and EoL fluorescent lamp scraps (b) [19].

sublimation reactors this happens on the cooling fingers. In contrast, recovering excess acid from wet acid leaching processes, for example, via diffusion dialysis, is more difficult and always incomplete. After separation of NH_4Cl the remaining gaseous phase consists of $\text{H}_2\text{O}_{(\text{g})}$ and $\text{NH}_3_{(\text{g})}$. When transferred to a scrubber, NH_3 even yields a sellable by-product, if the resulting ammonia solution meets the requirements for purity.

14.2.3 Optimization of the solid-state chlorination

14.2.3.1 Choice of optimization method

There are two fundamental approaches for optimization: (a) sequential and (b) simultaneous.

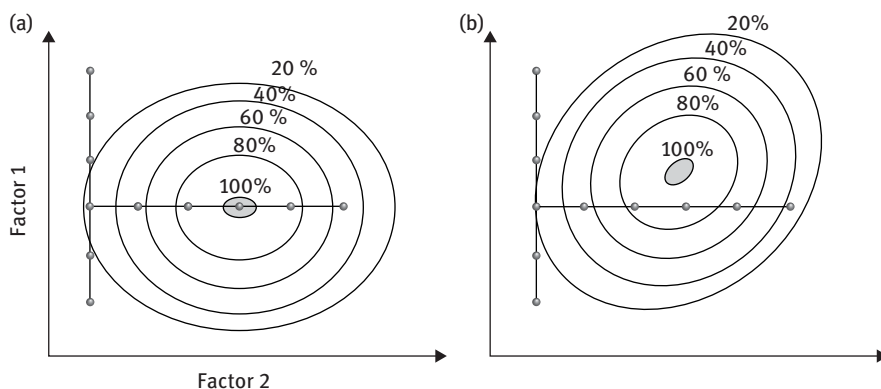


Figure 14.5: Response surfaces for sequential optimization without (a) and with correlation (b) between both factors (modified according to Ref. [21]).

Most commonly the optimum is determined by varying one influence factor after another while keeping all remaining reaction conditions constant. This one-factor-at-the-time strategy requires less experiments to obtain an optimum, but massive problems occur, when two or more factors correlate with each other (Figure 14.5). Moreover, this error may go unnoticed.

Without any correlation the optimum at 100 % is achieved accurately (Figure 14.5(A)). But if one factor cannot be varied independently without changing the second factor as well, the depicted one-factor-at-the-time strategy yields only an ostensible optimum instead (Figure 14.5(B)) [21]. Especially in complex reaction systems avoiding all correlations is often impossible. So a change of optimization methods is absolutely necessary. In this regard, the sequential simplex method using a geometric algorithm suits to determine the global optimum, but with a previously unknown count of experiments. However, the simplex method relies on prompt analyses, because every next experiment within this algorithm requires an evaluation of the previous one. If there is no prompt analysis at hand, statistical designs provide an alternative. These designs alter all factors at the same time on the basis of a symmetric plan. The evaluation takes place after conducting all experiments [21, 22]. By generating a model equation from the results covering all influences, it becomes possible to estimate the target value (e.g. the yield) at every point of the examined area. For solid-state chlorination a three-stage Box–Behnken plan was applied for optimization involving a polynomial of the second degree as model equation:

$$y = b_0 + \sum_{i=1}^k b_i x_i + \sum_{1 \leq i < j} b_{ij} x_i x_j + \sum_{i=1}^k b_{ii} x_i^2 \quad (14.4)$$

with	y	–	target (Y–Eu yield in the permeate)
	x_i	–	factors (temperature, time, AFR)
	k	–	number of factors (here: 3)
	b_0	–	ordinate intercept (here: 0)
	b_i, b_{ij}, b_{ii}	–	regression parameters covering linear and squared influences as well as correlations between different factors

Determining all regression parameters is a mathematical problem of multiple linear regressions. Already the number of three factors renders the required calculations rather laborious. They are therefore commonly conducted by evaluation software such as Statgraphics (Statpoint Technologies, Inc.). By knowing the model equation the optimum can be calculated within the examined area. Despite the chosen optimization method three preconditions must be fulfilled: (i) the experiments have to be repeatable with a preferably low distribution of measurement values, (ii) all factors must have an influence on the target value and (iii) have to be varied in an appropriate range, where the influence exceeds the experimental error. Therefore, attempts of orientation are necessarily conducted during a sequential pre-optimization of the solid-state chlorination.

14.2.3.2 Attempts of orientation

The overall yield of yttrium and europium calculated from their concentrations in the permeate was chosen as target value (simplified: Y–Eu yield). The percentage of each element dissolved in the permeate and analysed by ICP-AES refers directly to the metal chlorides produced by solid-state chlorination, because all original components of the fluorescent lamp scraps are insoluble in water. At first AFR and temperature were varied between 1.0 and 4.0 g/g and 250–400 °C, respectively.

The experiments with altered temperatures were conducted at an AFR of 3.0 g/g and with a constant reaction time of 3 h. Starting at 250 °C Y–Eu yield increased constantly achieving maximum at 300 °C but drops at higher temperatures (Figure 14.6). This trend is dominated by yttrium as the major component amongst REs, whereas the yields of the residual RE elements either remain unchanged (B) or even slightly increase with temperature (A).

The reason for this relates to the very different composition of each fluorescent material. While $\text{HCl}_{(g)}$ reacts preferably with oxidic $\text{Y}_2\text{O}_3\text{:Eu}^{3+}$ at any temperature the more acid-resistant lanthanum, cerium, gadolinium and terbium containing aluminate/borate/phosphate fluorescent materials only react at higher temperatures to a limited extent. Similar behaviour was observed for the comparative leaching with hydrochloric acid (Figure 14.4). Of these four elements gadolinium produced the highest yield with 9.3 % at 400 °C. Furthermore, temperatures beyond 300 °C lead to an accelerated decomposition of NH_4Cl resulting in a fast-expanding gaseous phase that transports unreacted $\text{HCl}_{(g)}$ out of the reaction zone. As a result, Y yield decreased at higher temperatures. In contrast to yttrium, Eu yields ranged about 71 % at >300 °C

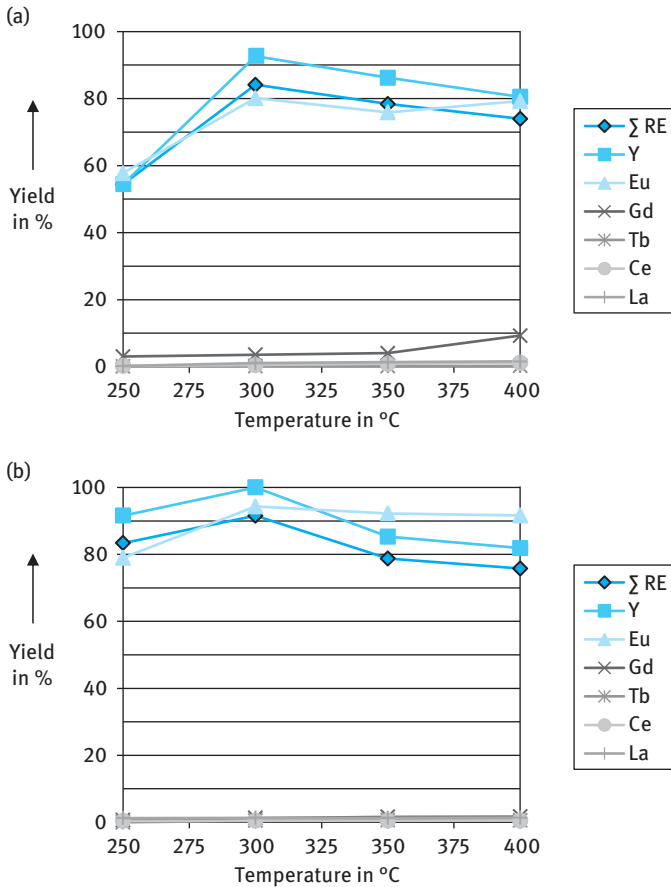


Figure 14.6: Temperature dependency of solid-state chlorination for production waste (a) and EoL fluorescent lamp scraps (b) at a constant AFR of 3.0.

(Figure 14.6), because europium is a component of both the more acid-labile $Y_2O_3:Eu^{3+}$ as well as the more acid-resistant fluorescent materials $(Ca, Sr, Ba)_5(PO_4)_3Cl:Eu^{2+}$ and $BaMgAl_{10}O_{17}:Eu^{2+}$. Therefore, temperatures from 275 °C to 325 °C are preferred for simultaneous optimization, wherein highest Y–Eu yields are expected.

As second influence on solid-state chlorination the AFR was examined at 350 °C by varying the ratio between 1.0 and 4.0 g/g. Both batches of fluorescent lamp scraps showed the same trend. Initially Y yield rose till AFR reached 2.0 g/g and decreased afterwards as the NH_4Cl amount accumulates further (Figure 14.7). This trend turns against all expectations whereby Y yields should rise while more $HCl_{(g)}$ is available for chlorination. Eu yields always stay above 70 %, but there is no real trend to observe again. Concerning lanthanum till terbium, yields follow expectations and increase slightly at higher AFR to a maximum of 4.1 % for gadolinium at 4.0 g/g (Figure 14.7(A)).

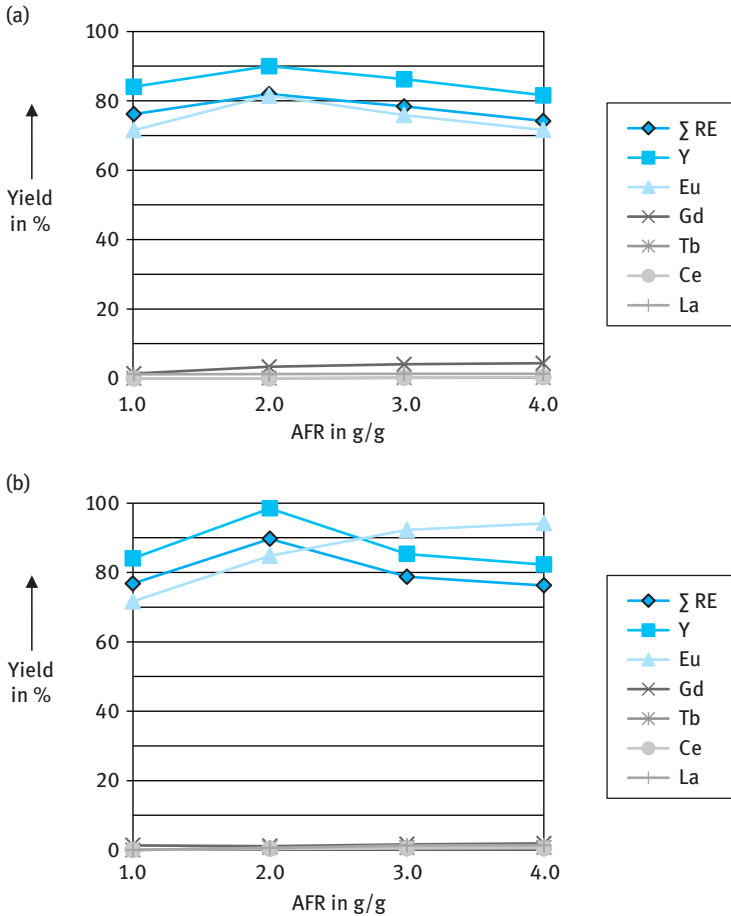


Figure 14.7: Dependency of RE yields as function of AFR for production waste (a) and EoL fluorescent lamp scraps (b) at 350 °C.

Due to this unusual trend of both fluorescent lamp scraps a side reaction was predicted, influencing Y yields at high NH_4Cl amounts in a negative way. A count of 19 different elements was made proving a real challenge. For clarification, solid filtration residues of the aqueous leachate were analysed via XFS to identify elements behaving contrary to yttrium (Figure 14.8). Because filtration residues contain the elements remaining unchlorinated, Y amount of substance shows a reverse trend and increases with rising AFR (Figure 14.8). Only two of the examined elements follow a distinct trend contrary to yttrium: calcium and barium. The first refers to outdated halophosphate, while barium is a component of the blue emitting $\text{BaMgAl}_{10}\text{O}_{17}:\text{Eu}^{2+}$. As XFS was measured without standards by using an internal calibration the results had to be verified by other means.

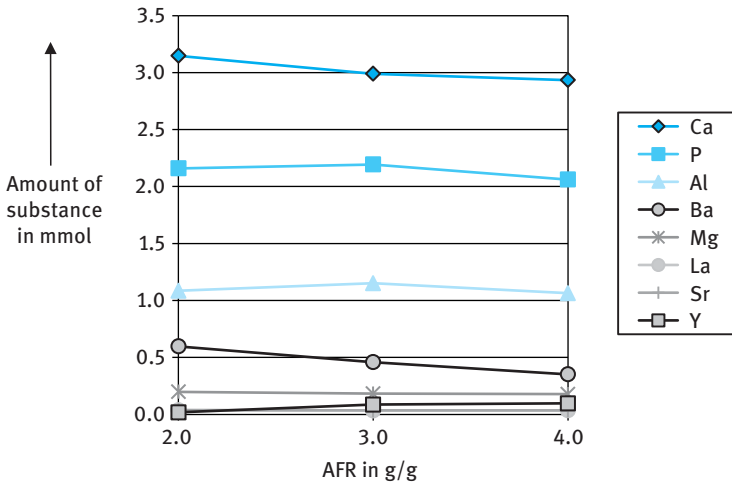


Figure 14.8: Amount of substance of selected elements in the retentate at different AFR (EoL fluorescent lamp scraps chlorinated at 350 °C).

Therefore, solid-state chlorination was conducted with model substances to avoid potential side effects of other elements. At first, equal masses of Y_2O_3 and $Ca_3(PO_4)_2$ were mixed with NH_4Cl in different ratios and chlorinated at 350 °C (Figure 14.9). While Ca yield increases constantly till 43 % Y yield meets an optimum at 78 % (NH_4Cl/Y_2O_3 ratio 2.0 g/g) and thereafter drops stepwise to 43 % at 10 g/g. Actually Ca^{2+} doesn't drop Y yields by itself, but along with Ca^{2+} mobilized phosphate ions precipitate dissolved Y^{3+} as YPO_4 . Since solubility of YPO_4 (4.2×10^{-13} mol/L at 25 °C [23]) is much lower than for $Ca_3(PO_4)_2$ (1.1×10^{-7} mol/L at 25 °C [24]) precipitation of Y^{3+} increases with rising amounts of calcium entering the solution.

Repeating these experiments with $BaMgAl_{10}O_{17} \cdot Eu^{2+}$ instead of $Ca_3(PO_4)_2$ showed no interaction with yttrium. At 4.0 g/g Y yield achieved approximately 100 %, whereas barium remains almost unreacted with yields <0.5 % (Figure 14.9). Barium had no influence on Y yields.

Concerning simultaneous optimization the global optimum is estimated for an AFR from 1.0 to 3.0 g/g, because at 2.0 g/g both fluorescent lamp scraps achieved their highest Y yields.

But before commencing further optimization, experimental procedure has to prove repeatability. The less distribution caused by experimental error the more accurate information can be gathered about influences of factors and their correlations. Insufficient repeatability of experiments heavily reduces the information value of statistical designs. Thus, at least one experiment of each design is a three-fold determination. During pre-optimization solid-state chlorination was conducted at the estimated pre-optimum of 300 °C and 2.0 g/g twice. For example, for production waste the gap between the Y–Eu yields was quite low while both experiments achieved

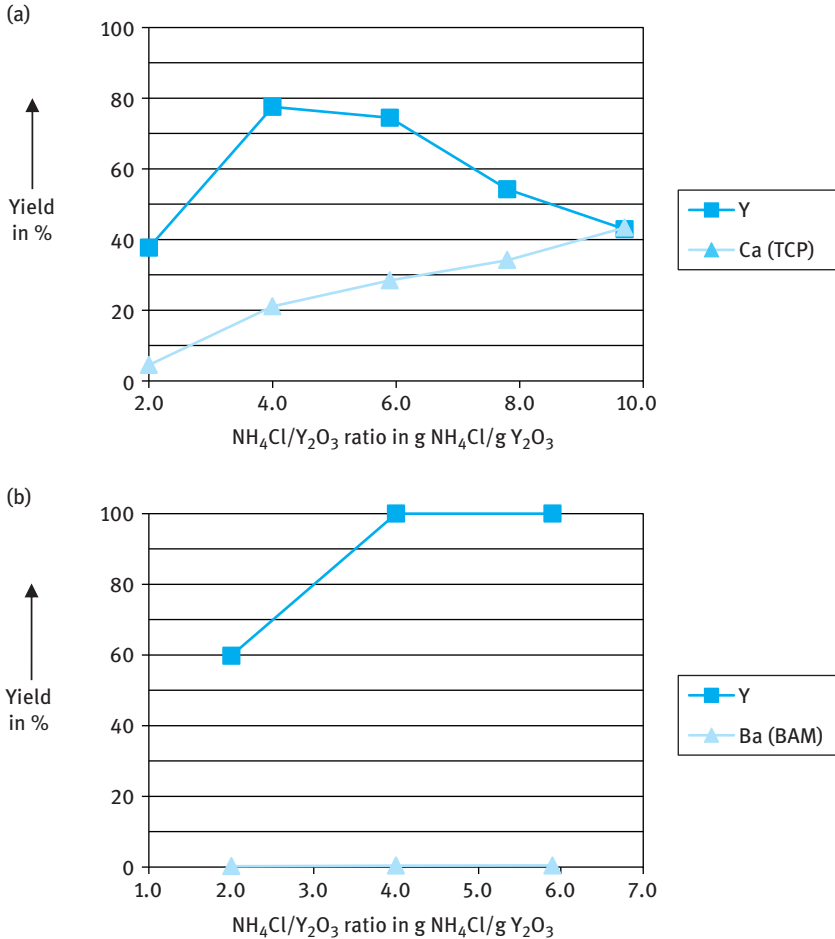


Figure 14.9: Solid-state chlorination of (a) $\text{Y}_2\text{O}_3/\text{Ca}_3(\text{PO}_4)_2$ and (b) $\text{Y}_2\text{O}_3/\text{BaMgAl}_{10}\text{O}_{17}:\text{Eu}^{2+}$ at 350°C and different $\text{NH}_4\text{Cl}/\text{Y}_2\text{O}_3$ ratios.

the highest average yields by then (90.3 % and 89.9 %). The particular yields of RE elements are depicted in Figure 14.4. Conclusively by proving repeatability and determining the proper range for the AFR all preconditions for optimization are fulfilled.

14.2.3.3 Simultaneous optimization

On the basis of the former sequential pre-optimization the target value (Y-Eu yield) and the ranges of all factors were defined. Suitable statistical designs for three factors (AFR, temperature and time) are central composite design, complete factorial design or the Box–Behnken plan. If the supposed optimum isn't located at the borders of

3³-Box–Behnken design**Target value:**

Y–Eu yield in the permeate

Factors:

Temperature

Reaction time

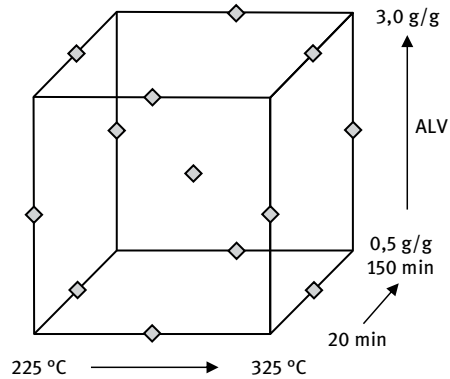
NH₄Cl/fluorescence lamp scraps ratio (AFR)

Figure 14.10: Statistical design used for optimizing the solid-state chlorination of fluorescent lamp scraps (production waste) showing all experiments (◆).

the examined area Box–Behnken plan needs the fewest count of experiments to reliably determine the optimum. Since that's the case simultaneous optimization was conducted for production waste via 3³-Box–Behnken plan (Figure 14.10).

Such a plan of three factors and three stages to even examine non-linear dependencies needs 15 experiments with a three-fold determination of the centre. Time, as third factor, was altered from 20 to 150 min, taking into account that the rotary kiln heats up with ~10 K/min. Lower times for chlorination would distort the results, since chlorination already starts during heating phase as soon as temperature rises above 220 °C.

Finishing all experiments, evaluation commences by looking at the resulting Pareto diagram (Figure 14.11). The diagram depicts all sized influences and compares them with the experimental error (black line). Where the bars cross the black line, there is a significant influence on Y–Eu yield.

Remarkably, time shows no direct influence. Only the cross effect BC, where time and temperature correlate, has a small significant impact on Y–Eu yield within the examined range of 20–150 min. This indicates a very fast chlorination being almost finished at 20 min, especially when compared to conventional leaching with hydrochloric acid taking 3 h for accomplishment. Finally, the model equation (14.5) is formed by removing nonsignificant effects from polynomial (4) and calculating the regression parameters:

$$y = -912,92 - 23,80 \cdot A + 1,07 \cdot B + 6,56 \cdot C - 8,60 \cdot A^2 + 0,23 \cdot AC - 3,9 \cdot 10^{-3} \cdot -11,4 \cdot 10^{-3} \cdot C^2 \quad (14.5)$$

where y is the target value (Y–Eu yield); A is the mass of NH₄Cl in g (per g fluorescent lamp scraps); B is the time for chlorination in min; and C is the temperature in °C.

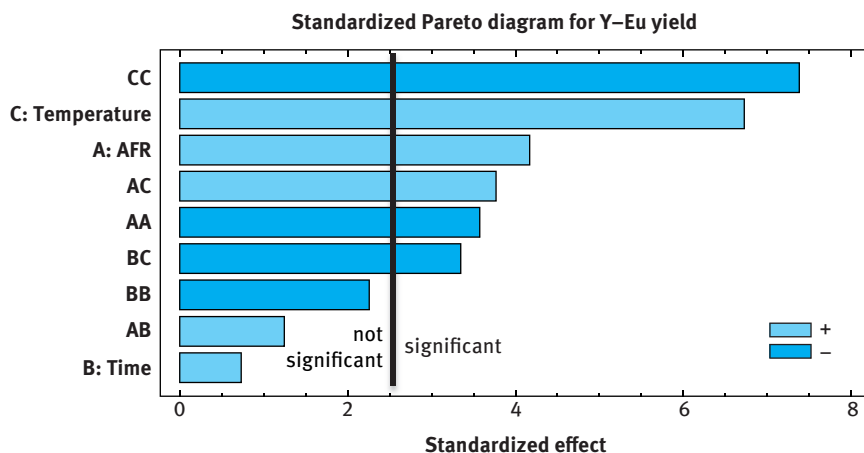


Figure 14.11: Pareto diagram with all linear (A, B, C), square (AA, BB, CC) and cross (AB, AC, BC) effects.

The estimated optimum at $86.9\% \pm 3.3\%$ was predicted for $312\text{ }^{\circ}\text{C}$, 20 min and an AFR of 2.76 g/g . Henceforth, a double-fold determination proved the optimum (90.2% and 87.0%). Alongside the missing influence of time additional positive and negative effects occurred. First of all, the five-times-larger reactor volume of the rotary kiln turned out to be disadvantageous compared to sublimation reactors. Due to spacious distribution of the gaseous phase greater amounts of $\text{HCl}_{(\text{g})}$ and $\text{NH}_{3(\text{g})}$ recombined and deposited outside the heating zone and lowered Y–Eu yields by 5–10 percentage points. This disadvantage remains valid as long as the rotary kiln runs in batch processing, where actual chlorination only takes place within a small part of the heating zone (Fig. 14.3). However, applying a rotary kiln offers new options for temperature control. A closer look at temperature dependencies reveals that local and global optima always require temperatures below the actual decomposition temperature of NH_4Cl ($338\text{ }^{\circ}\text{C}$).

Even the proved global optimum at $312\text{ }^{\circ}\text{C}$ reveals a difference of $26\text{ }^{\circ}\text{C}$. Under this reaction condition NH_4Cl only decomposes partially and forms a dynamic equilibrium between gaseous phase and solid NH_4Cl . At least two contrary effects must influence Y–Eu yield to describe this trend. Higher temperature levels generally are in favour of Y–Eu yield; however, they prove disadvantageous as soon as the respective optimum has been exceeded (dark surface in Figure 14.12). The reason for this trend must be related to the thermodynamics of decomposition. According to eq. (14.1) every mole of NH_4Cl produces 2 moles of gas. So 54 g of NH_4Cl decomposes to 102 L of gaseous products at $350\text{ }^{\circ}\text{C}$. The faster the gaseous phase expands, the more unreacted $\text{HCl}_{(\text{g})}$ is driven out of the reaction zone. On the contrary, improving Y–Eu yields requires a reduction of the gas phase volume. However, reducing temperature only poorly serves to decrease the molar volume. Truly, cooling from $350\text{ }^{\circ}\text{C}$ to $25\text{ }^{\circ}\text{C}$ halves

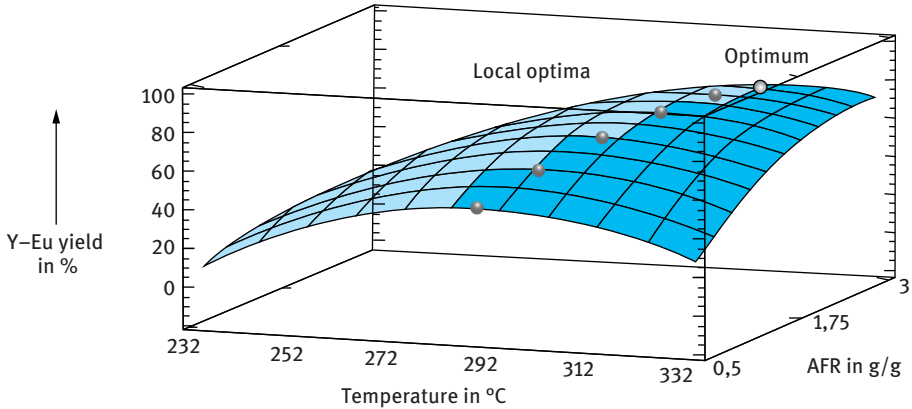


Figure 14.12: Y-Eu yield depending on temperature and AFR at a constant reaction time of 20 min.

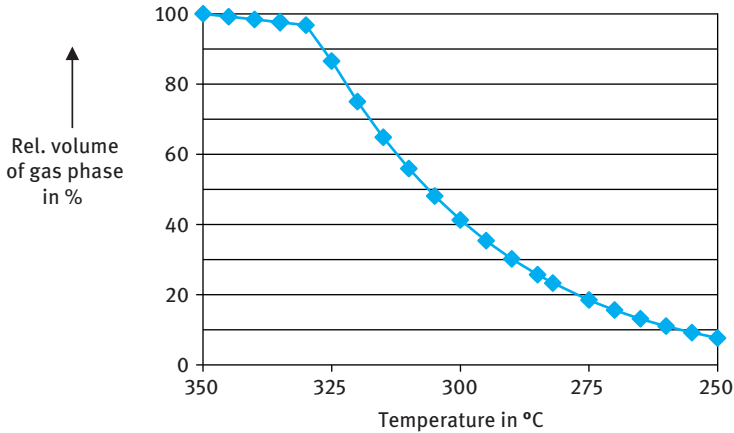


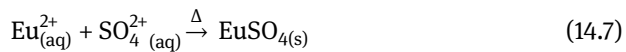
Figure 14.13: Comparative reduction of NH_3/HCl gaseous phase with decreasing temperature starting at 350 °C (=100 %).

the molar volume from ~51 L/mol to 24.4 L/mol. For NH_4Cl this trend overlaps with the decomposition equilibrium, reducing the gas volume massively, when temperature drops below 338 °C (Figure 14.13). This way it becomes feasible to almost halve the gas volume by simply reducing temperature from 350 °C to 312 °C (optimum) instead. Without the decomposition equilibrium this reduction would hardly achieve 6% between 312 °C and 350 °C. Thus, endothermic decomposition on the one hand and expansion of gas volume on the other are the two contrary trends greatly affecting temperature dependence, which shift the optimum to quite low temperatures. Although lower temperatures generally demand an extended reaction time (cross effect BC), Y-Eu yield only showed a slight time dependence between 20 and 150 min. Due to the

batch operation shorter reaction times <20 min cannot be examined with this rotary kiln. Therefore, continuous operation is required to reduce influences on Y–Eu yield by preheating.

14.2.4 Recycling process

Subsequent steps following solid-state chlorination and aqueous leaching are almost identical to wet chemical processes, yet with two exceptions. There is no strongly acidic leachate, further processing of which would require considerable amounts of NaOH. The reason is that pH values of the obtained leachate only vary between 3 and 5. In view of the expenses for the cost-intensive NaOH, it is evident that the revenues of the overall process will be rather small, if ever. The second fact concerns purity of the liquid concentrates, as solid-state chlorination separates Y/Eu from La/Ce/Gd/Tb with selectivities >99.7 %. This simplifies the laborious RE separation to separating yttrium from europium by cementation. Further purification was achieved by adding small amounts of H₂SO₄ (till pH = 3) to precipitate Ca²⁺ as CaSO₄. Potentially excess sulphate ions were subsequently removed by adding Ba²⁺. The remaining solution was funnelled through a fix bed filled with Zn granules to reduce Eu³⁺ to Eu²⁺.



Thereafter, Eu²⁺ was easily precipitated as EuSO₄ analogous to alkaline earth metals. Up to 95 % of Eu²⁺ were separated per pass. Yet EuSO₄ is no sellable product and requires further treatment, for example, treatment with NaOH_(aq) and drying to yield Eu₂O₃. When Eu³⁺ had been removed, dissolved Y³⁺ was precipitated conventionally as oxalate. Accordingly, the process yields two different concentrates for yttrium and europium while lanthanum, cerium, gadolinium and terbium remain within the solid residue. Of course, recovery of lanthanum and cerium by leaching with concentrated acids like HNO₃ is possible but uneconomic due to low commodity prices for rare earth metals. Nevertheless, current experiments provide another option simplifying RE separation. It makes use of the high magnetic susceptibilities of gadolinium and terbium. In fact, applying magnetic fields at different temperatures not only allows for easily separating Gd³⁺ and Tb³⁺ from La³⁺ and Ce³⁺. The method also efficiently separates Gd³⁺ from Tb³⁺ – in aqueous solution [25]. Since prices for La₂O₃ and CeO₂ are still very low producing respective concentrates of lanthanum and cerium is not economic at present. Figure 14.14 depicts how yttrium and europium may be recovered economically. Solid residues containing residual REs are stockpiled until economic recycling is feasible.

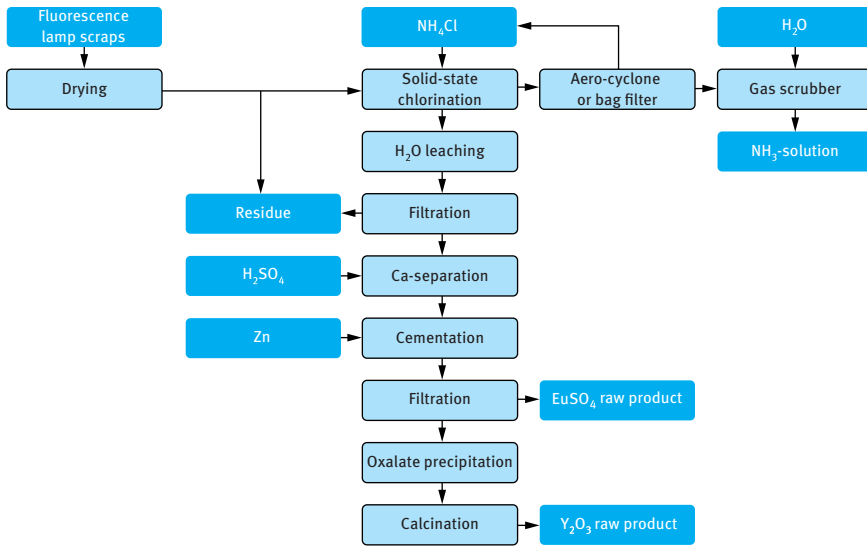


Figure 14.14: Scheme of the recycling process for fluorescent lamp scraps.

Treatment of the gaseous phase provides another feature affecting overall process economy: unreacted NH_4Cl is recovered by cooling, and $\text{NH}_3(\text{g})$ is removed by scrubbing with water. If NH_4Cl separation is complete, an ammonia solution is obtained, the chloride concentration of which is <250 mg/L. This way the process yields a market-established by-product, which to some extent contributes to compensate for production costs [26]. Compared to conventional leaching, recycling excess acid from the digestion medium is always incomplete and requires additional separation steps.

Concerning the number of process steps, both strategies developed within the SepSELSA project require fewer process steps to get the same raw concentrates compared with what has been published by Solvay and Osram. Solid-state chlorination even reduces the process effort to a half (Figure 14.15).

14.2.5 Summary

Solid-state chlorination provides a promising alternative for mobilizing RE elements from fluorescent lamp scraps. NH_4Cl as source for $\text{HCl}(\text{g})$ offers many economic advantages compared to all applied wet chemical processes. Although NH_4Cl (~110 €/t) roughly costs as much as 35 % hydrochloric acid (~135 €/t), as a solid it contains almost twice as much the molar amount HCl per weight unit (68 wt.%) [29]. Due to high selectivities, less HCl is consumed, and unreacted $\text{HCl}(\text{g})$ can be easily recovered from the gas stream leaving the reactor. Without consideration of potential revenues from selling the NH_3 solution as by-product, costs for chemicals are thus reduced by at least 50 %. Because there is no strongly acidic digestion medium, costs for downstream

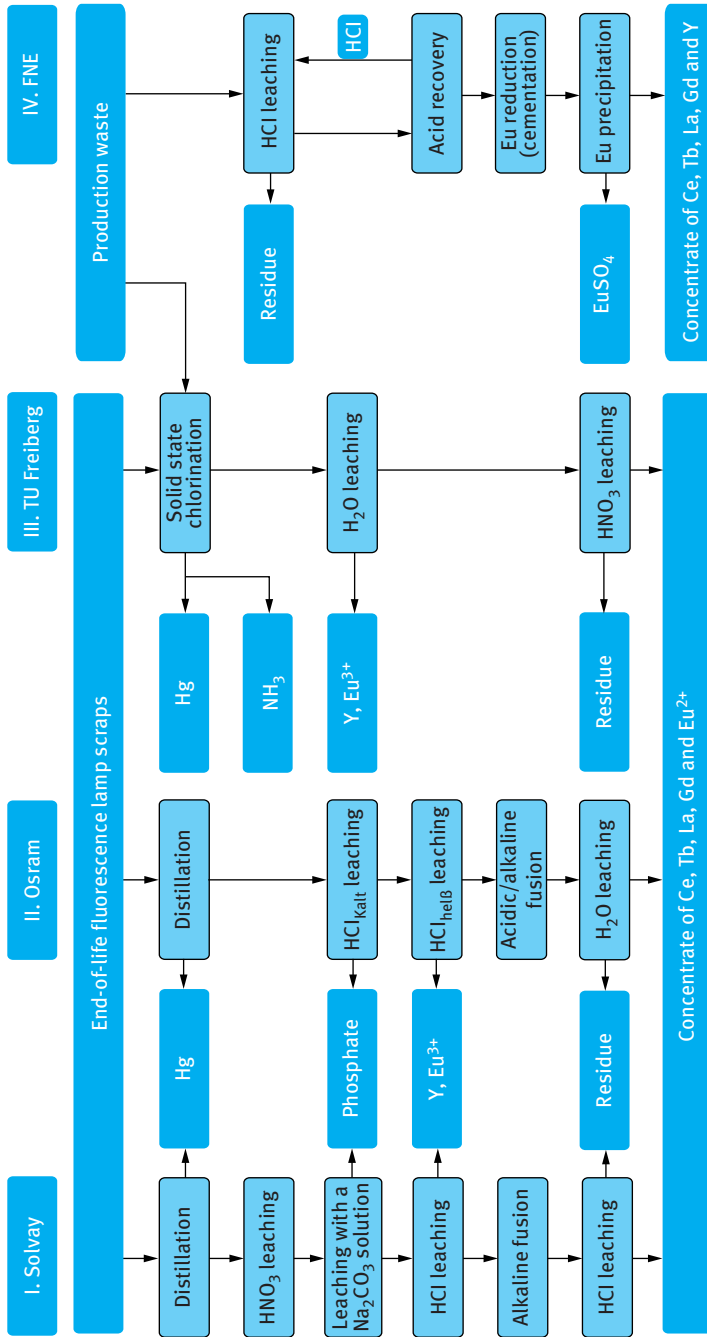


Figure 14.15: Comparison of solid-state chlorination with industrial-applied recycling processes for fluorescent lamp scraps [16, 18, 19, 27, 28].

processing and waste disposal are lower, too. Depending on heavy metal content, disposing of a strongly acidic solution may cost up to 400 €/t. Waste water with low acidity, such as it results from solid-state chlorination cuts those costs to approx. a third [30]. Furthermore, chlorination profits from high selectivity yielding two pre-separated concentrates. Although cementation of Eu^{3+} is feasible in wet chemical processes, too, pH value has to be adjusted prior to Eu winning, thus incurring additional costs for NaOH. One has to realize that increasing pH from 0.7 to 3.0 equals neutralizing 99.5 % of the acid. Furthermore, hydrometallurgical treatment yields an yttrium-rich RE oxide of lower economic value than the pre-separated Y_2O_3 provided by solid-state chlorination.

Yet a general statement on process economy cannot be made without taking into account the commodity prices, location, desired production output, personnel requirement, etc. Within the framework of the SepSELSA project a feasibility study was conducted for Freiberg (Saxony, Germany), where there is a globally acting lamp producer in the near vicinity [30]. Whereas wet chemical treatment of fluorescent lamp scraps went uneconomic between 2014 and 2016 solid-state chlorination remained at least economic for higher concentrated production wastes, although commodity prices have dropped by another 80 % within the 2 years.² At present, the main obstacle for scaling up solid-state chlorination is rotary kiln design, which implies with several different heating zones. Its development and construction are matter of current research activities at Freiberg University of Mining and Technology. Nevertheless, ~25 tons of production waste have successfully been recycled with the SepSELSA process between 2014 and 2016.

14.3 RE metal recycling from $\text{Fe}_{14}\text{Nd}_2\text{B}$ magnets

Permanent magnets containing RE metals belong to the strongest magnetic alloys currently available with magnetic energy densities up to 450 kJ/m^3 [31, 32]. Because of versatile applications in, for example, hard drives, electric motors, wind power stations or MRI scanners the demand for neodymium, dysprosium, praseodymium, samarium and terbium substantially increased within last years. For instance, demand almost doubled from 2006 to 2012 reaching 42.000 t/a. This trend continues as it can be derived from the demand of 53.000 t/a, which has been prognosticated for 2017 [33–35]. Among RE alloys $\text{Fe}_{14}\text{Nd}_2\text{B}$ magnets are the strongest ones and the most commonly used magnetic material. Consequently, a variety of processes have been developed for the treatment of production wastes, most of them pyrometallurgical

² In 2014 the Institute of Chemical Technology at Freiberg University of Mining and Technology and FNE Entsorgungsdienste Freiberg GmbH were awarded the Technology Transfer Prize by the Saxon Ministry of Science and the Arts for the development and application of the SepSELSA process for RE recycling.

ones [2–6, 12]. In the case of EoL magnets, it is corrosion, adhesives, plastics and accompanying elements, such as nickel, cobalt and zinc, which prevent the application of these well-established pyrometallurgical routes. As a consequence, hydrometallurgical treatment is almost exclusively preferred for EoL recycling [2, 3, 7–11]. Therefore, solid-state chlorination was regarded as a powerful alternative strategy for magnets, too.

14.3.1 Starting material

Prior to chemical or mechanical treatment magnet recycling starts with the systematic collection of EoL magnets and their separation from electronic scrap. Particularly the latter still represents a major challenge. It was in 2011 when the first automated process removing magnets from spent hard drives was applied by Hitachi on an industrial scale [12]. Although Fe₁₄Nd₂B magnets contain approximately as much RE (30–35 wt.%) as fluorescent lamp scraps they differ widely in structure. At first magnets are alloys containing RE metals. Because of sintering the starting materials during production, these alloys are not completely homogenous. Consequently, from grinding no distinct particles with homogeneous composition are obtained.

All SEI for magnets as well as fluorescent lamp scraps were recorded by a scanning electron microscopy (SEM) from JEOL (model JSM 7001 F) coupled with an energy-dispersive X-ray spectroscopy (EDX) from Bruker (Quantax Esprit 1.9.3). The powder samples were applied directly to a messing tab of 10 mm in diameter. A small adhesive coal bed fixed the powder on the surface. Afterwards all samples were vapourized with carbon to conduct the electrons. For taking pictures in high resolution and to avoid overexposure, the voltage was kept at 3.0 kV at a short working distance of 7.1 mm. Thus, all SEI at magnifications of 400–500 were sufficient to provide a decent overview of surface and particle structure. In contrast, EDX analysis was conducted at 15.0 kV at 13 mm (distance to the detector). The magnification of the images was ~10 times higher (3,500–5,500) to show particles in more detail. In principle the detection limit depends on the matrix, but since the average detection limit is approximately 0.1 wt.%, all elements of the samples were quantified easily (Fig. 14.1) so that particles of fluorescent lamp scraps could be assigned to certain fluorescent materials [26].

The EoL magnets examined by solid-state chlorination were derived from a rotor of a wind power plant. These 5 × 3 × 2 cm³-sized magnets were initially heated up to 350 °C for demagnetization before they were ground to particle size ≤100 μm. The grinding was conducted in two stages: magnets introduced to a horizontal impact crusher yielded small pieces applicable for the grinding in a vibrating cup mill providing a pyrophoric powder. For this reason grinding always has to be conducted under

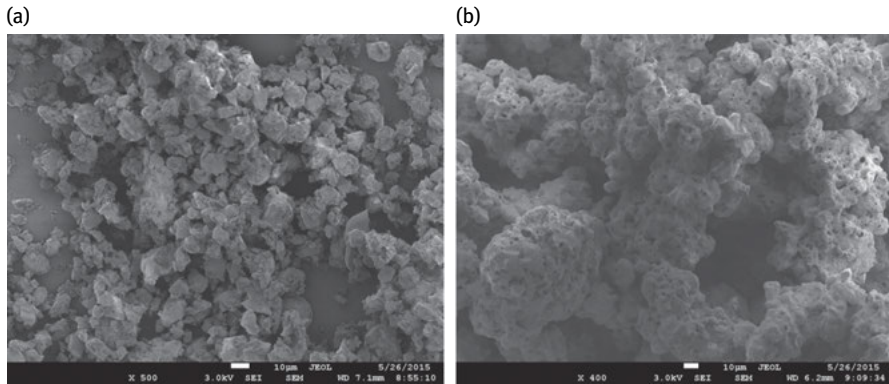


Figure 14.16: SEM-EDX analyses of magnet powders (a) before and (b) after solid-state chlorination.

Table 14.4: Composition of spent $\text{Fe}_{14}\text{Nd}_2\text{B}$ magnets.

Component	Concentration (wt.%)
Fe	65.6
Nd	29.3
Dy	4.8
B	0.3
Tb	<D.L.
Pr	<D.L.
Ni	<0.01
Other	<0.01

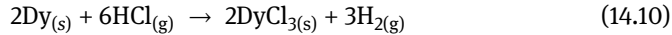
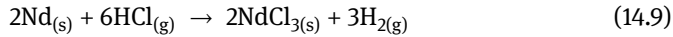
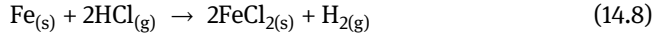
D.L., detection limit.

exclusion of oxygen. In SEM pictures the magnet powder appears as sharp-edged particles (Figure 14.16(A)).

Because of the ignoble character of $\text{Fe}_{14}\text{Nd}_2\text{B}$ alloys they may easily be dissolved in 37 % hydrochloric acid and analysed via ICP-AES afterwards. The results (Table 14.4) show a quite simple composition. The iron amounts to 65.6 wt.%, and the share of RE elements only consists of neodymium and dysprosium with an overall concentration of 34.1 wt.%. Praseodymium, which serves as cheaper substitute for neodymium, and terbium, which enhances temperature stability analogously to dysprosium, were not found in the samples examined.

14.3.2 Preliminary tests

Applying solid-state chlorination for magnet recycling also has to meet requirements first, namely the forming of water soluble as well as nonvolatile metal chlorides. Therefore, iron is the main concern, as FeCl_3 already sublimates at $T \geq 120^\circ\text{C}$:



Starting from metal alloys the redox potential of HCl_(g) is not high enough to oxidize iron to the third oxidation state (Fe³⁺). Instead nonvolatile FeCl₂ is formed. Corroded EoL magnets already containing Fe³⁺ yield small amounts of FeCl₃ that sublime during chlorination and are removed together with unreacted NH₄Cl from the gas phase. As long as these amounts remain small they will not interfere with the solid-state chlorination. In contrast to fluorescent lamp scraps all components but boron react with HCl_(g) to their respective metal chlorides. Iron as the most noble metal and main component defines the reaction conditions. Due to effective clogging of iron and RE particles in the sinter mass, iron needs to be chlorinated almost completely to achieve high yields for both RE elements. Metal chlorides form voluminous passivation layers on the particle surfaces, shielding them from further chlorination (Figure 14.16(B)). Owing to the absence of water, the metal chloride layer cannot be removed by solvation, like this would occur in the aqueous phase. It is for this reason, why solid-state chlorination suffers from lower yields. Again, the solution is provided by a rotary kiln, where the magnet powder is subjected to mechanical stress. Alternatively, unreacted magnet powder can be reused in a cycle, or the magnets are ground to even smaller particle sizes. Another important difference affects the leaching step following chlorination. This time the RE metal precipitation is highly pH sensitive, since Fe³⁺ competes for OH⁻ ions, thus causing undesired co-precipitation of mixed hydroxides. Consequently, the pH value needs to be finely adjusted in order to avoid precipitation of iron hydroxide species. Without considering the latter, leaching with distilled water leads to a partial precipitation within 3 h, thus lowering RE yields by >10 percentage points and complicating filtration due to formation of small particles with <2 μm in size (Figure 14.17(A)).

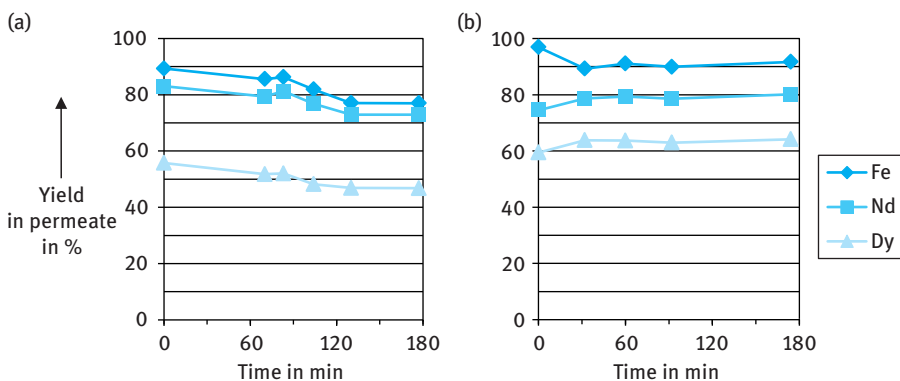
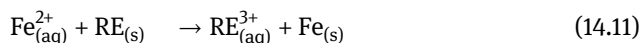


Figure 14.17: H₂O leaching following solid-state chlorination (a) without and (b) with adjusting pH value to 4 by adding hydrochloric acid.

Adjusting the pH value with $\text{HCl}_{(\text{aq})}$ prior to dissolving the metal chlorides increases all yields instantly and reduces the extent of precipitation. The equilibrium is reached after 1 h, while pH value rises slowly to approximately 6 (Figure 14.17(B)). Fe yield decreases within the first 30 min, whereas yields of neodymium and dysprosium show a contrary trend. The reason is a redox reaction between dissolved Fe^{2+} and undissolved RE metals on the particle surfaces. Analogous to eq. (14.11) this cementation may enhance RE yield up to 7 percentage points:



From this reaction one can understand why solid-state chlorination does not necessarily have to be complete in order to retrieve the entire RE content of the magnet. Of course this occurs at the expense of Fe yield. In order to avoid any undesired precipitation, pH value has to be kept constant during leaching. Since diluted $\text{HCl}_{(\text{aq})}$ provides no significant buffering capacity at pH 3–4, acetic acid (1 M) and sodium acetate were used as buffer (pH = 3) for leaching the metal chlorides. In principle, adding diluted $\text{HCl}_{(\text{aq})}$ is sufficient to prevent any precipitation, though, but this way requires higher amounts of $\text{HCl}_{(\text{aq})}$, which in addition have to be added continuously, in order to keep the pH value at 3.

14.3.3 Optimization of the solid-state chlorination

Except for the leaching step simultaneous optimization was conducted in analogy to the fluorescent lamp scraps by using a 3^3 -Box-Behnken design. The target value was represented by the yield of all REs in the pregnant solution. All factors and temperature range (225–325 °C) were kept constant (Figure 14.10). Chlorination time was varied between 60 and 240 min. Since 1 g of magnet powder served as starting material the amount of NH_4Cl varied from 1.0 to 3.0 g.

After finishing all 15 experiments, the Pareto diagram was used to surprisingly show only temperature to have a significant influence on RE yield (Figure 14.18). Although 99 wt.% of the magnets react with $\text{HCl}_{(\text{g})}$, solid-state chlorination appeared to be finished after 60 min so that all effects involving time remain insignificant (C, CC, AC, BC). Yet all influences related to NH_4Cl (A, AA, AB, AC) need a different explanation.

For chlorinating iron, neodymium and dysprosium stoichiometrically as depicted in eqs (14.8–14.10) 1.0 g of magnet powder requires approximately 1.4 g NH_4Cl . Thus, four experiments were conducted with only 70 % of the stoichiometric NH_4Cl amount. However, the RE yields range between 76 % and 84 %. So at least four experiments gave yields which appear unrealistic, although all centre points showed excellent reproducibility (RE yield at the centre: 83.5 % \pm 1.1 %). The predicted optimum of 84.2 % at 289 °C, 161 min and 1.83 g NH_4Cl could be confirmed as well by two-fold determination (83.8 % and 85.3 %). It should be noted that time and NH_4Cl

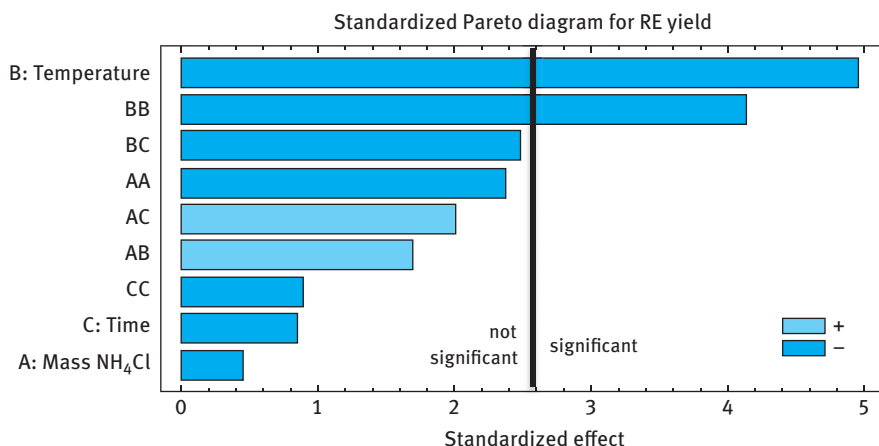


Figure 14.18: Pareto diagram with all examined effects influencing solid-state chlorination of Fe₁₄Nd₂B magnets.

amount can be chosen freely within the estimated area without affecting RE yield significantly (cf. Figure 14.18). On the basis of a correct choice of factors and ranges the missing influence of NH₄Cl must refer to at least one of two causes: (i) either leaching with the acetate buffer dissolves parts of the magnet powder at pH = 3 and distorts RE yields that way, or (ii) there is a great difference in how the several elements react with HCl_(g). In fact, the latter factor appears to apply for iron and RE metals being not associated with each other and therefore reacting separately. Both options were examined subsequently.

In case RE yields actually profit from adapting the pH value by buffering, the acetate buffer solution must be able to partially dissolve the magnet powder without solid-state chlorination. In order to check this hypothesis non-chlorinated magnet powder was subjected to leaching with acetate buffer as well as diluted HCl_(aq). Both leaching media were investigated at different pH values (Figure 14.19). Whereas diluted HCl_(aq) did not dissolve the magnets between pH 3 and 5, a substantial fraction was dissolved in 1 M acetic acid buffer: at pH = 3 almost 20 % of iron and dysprosium as well as 24 % of the neodymium were dissolved, respectively (Figure 14.19(A)). On the other hand diluted HCl_(aq) mobilized less than 0.5 % of the elements at the same pH value. As soon as pH drops below 3, HCl_(aq) contributes significantly to RE yield, too. Although pH value is the same, the concentrations of the acids may explain this different behaviour. While 37 % HCl_(aq) has to be diluted 1:10.000 (1.2 mM HCl) in order to increase pH value to 3, the 1 M buffer solution provides an 800-times-higher concentration of acetic acid. Due to the low concentration of hydrogen chloride, this solution is not suited for dissolving appreciable amounts of iron, neodymium and dysprosium.

From these findings there emerged two options for process control with the aim to avoid Fe hydroxides from precipitating: (a) either diluted HCl_(aq) is used for pH

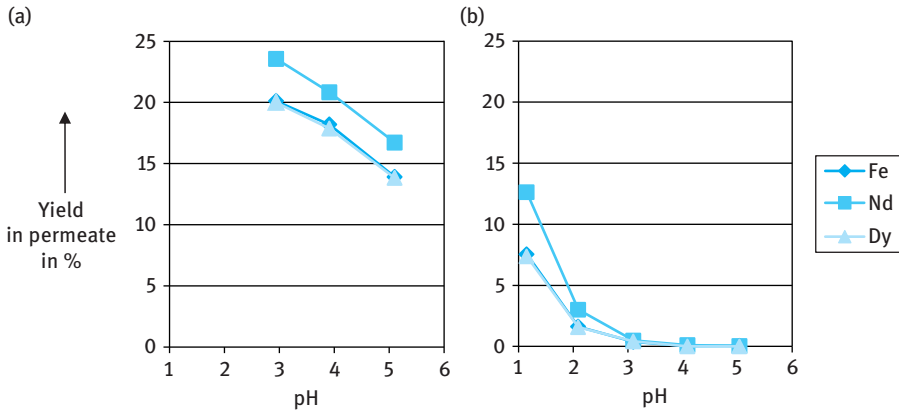


Figure 14.19: Contribution of the leaching step to RE yield by using (a) a buffer with 1 M acetic acid or (b) diluted hydrochloric acid for pH adjustment.

adjustment, which results in lower costs for chemicals or (b) acetate buffer contributes to RE yield and reduces henceforth the demand of NH_4Cl . It should be noted, though, that using acetic acid to completely dissolve the magnets is far too expensive, since the price of acetic acid is three times higher than hydrochloric acid ($\sim 450 \text{ €/t}$) [29].

For process control reducing the gas volume was most essential. Therefore, acetate buffer was chosen for further optimization. A lower NH_4Cl demand means less volume of the gas phase and consequently more magnet powder can be chlorinated within a certain time frame.

However, although the process becomes more efficient by dividing RE solubilization into two steps, namely solid-state chlorination as initial step and acid-buffered cementation as completing step, process optimization suffers from the increased amounts of parameters. The one-factor-at-the-time strategy is not applicable here, because buffer capacity and NH_4Cl amount cannot be varied independently. Further, in addition to the three factors of the Box–Behnken design buffer capacity has to be taken into account. But the range needs to be adjusted first, as previous experiments were conducted with an excess of 3.0 g acetic acid per gram magnet powder. Preferentially the range for optimization overlaps with the area of greatest changes in leaching behaviour. In order to determine this range, acetic acid concentration of the buffer was reduced stepwise from 1 M to zero. As depicted in Figure 14.20, a range between 0.025 and 0.25 mol/L was chosen for further optimization.

However, the influence of the buffer solution on RE yields does not exclude a partial selectivity during chlorination as additional reason for the missing influence of NH_4Cl . To verify a potential selectivity, buffer concentration was reduced from 1 to 0.15 M. Hereinafter two experiments were conducted under same reaction conditions at 325 °C , where only the NH_4Cl amount was altered. The first experiment was done with 0.5 g NH_4Cl equalling 35 % of the stoichiometric amount. In contrast, an excess of 1.75 g NH_4Cl (125 %) was used for the second experiment (Figure 14.21). Although

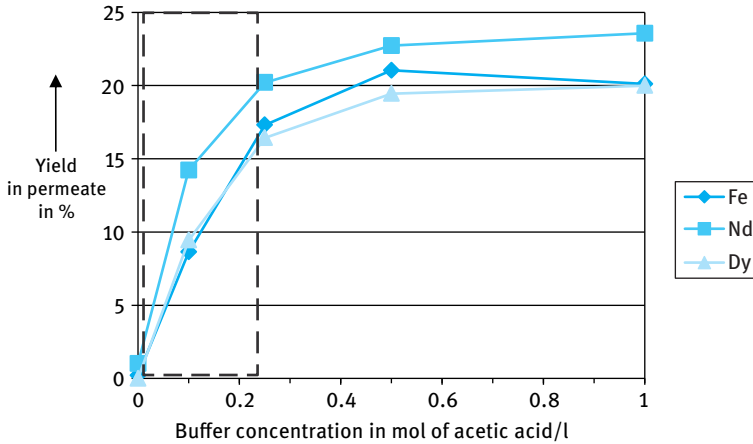


Figure 14.20: Leaching of unchlorinated magnet powder with different buffer concentrations at pH = 3 (- - adjusted range for optimization).

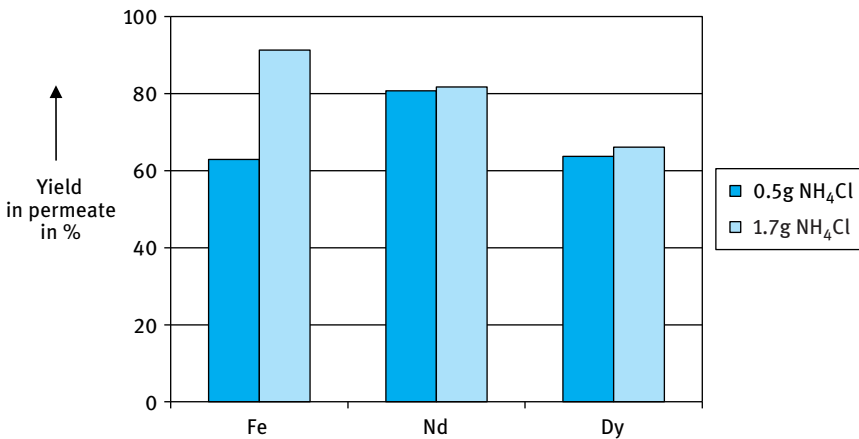


Figure 14.21: Comparison of two chlorination experiments at 325 °C (85 min) conducted with different amounts of NH₄Cl to prove partial selectivity.

leaching with a buffer enhances RE yields again, it becomes obvious that Fe yield changes exclusively and drops by 30 percentage points between both experiments. The yields of neodymium and dysprosium remain at the same levels. Seemingly NH₄Cl only affects Fe yields.

These results imply a partial selectivity. Consequently, neodymium and dysprosium are chlorinated first and form a RE-rich layer on the particle surface by their respective metal chlorides. The less ignoble iron reacts much slower with HCl_(aq) so that reduced NH₄Cl amounts affect Fe yield by far stronger than RE yields. It has to be

noted, though, that analysing liquid permeates only represents an indirect proof. For conclusive verification the chlorinated magnet powder has to be examined instead.

The mineral liberation analyser (MLA from FEI, USA) combines SEM and EDX with automated measurement systems for quantitative examination of rocks, minerals and synthetic materials. Sample preparation was decisive to prove the supposed partial selectivity. 3 g of the powder samples were mixed with the same volume of graphite to separate agglomerated particles from each other. The resulting graphite/sample mixture was casted with epoxy resin to a cylinder of 25–30 mm in diameter and hardened for 12 h. Subsequent grinding with SiC and polishing with a diamond suspension uncovered a smooth surface showing different cross sections of the particles. Coating this surface with carbon to conduct electrons represents the last step of preparation.

By electrons backscattered on a gold standard the SEM was calibrated on greyscales to enable the distinction between particles and background (e.g. epoxy resins, cracks). On this basis the measuring range of EDX is determined as well. Typical are the measurements of tens to hundreds of thousands of particles leading to millions of spectra per sample. All these spectra are compared with a reference list, formerly created for the material. This list also contains the element concentrations calculated from the spectra. Since magnets do not consist of classical minerals, no pre-recorded spectra were available and comparative spectra were collected at different locations of the sample and added to the reference list instead (Table 14.5). However, a pinpoint measurement is limited to an accuracy of 0.1–2 μm , due to the pear-shaped excitation. Therefore, mainly mixed spectra are obtained during measurement of small-sized particles or locations where compositions change strongly. Thus, assigning each measuring point to one of the references from the list is not conducted strictly, but with a previously defined tolerance. For the magnet powders, this tolerance was set to 70%. Since every element concentration of the reference list is coloured differently, it becomes possible to assign the respective colour to each measuring point for graphic illustration of the entire examined surface (Figure 14.22).

With this in mind, both experiments (Figure 14.21) were reproduced without leaching. The chlorinated powders were examined with an MLA and compared with the starting material. Since particles were cut and polished during sample preparation, it became possible to analyse the cross section to determine the composition depending on particle radius. Spectra of similar composition were combined to coloured material phases, representing the heterogeneity of particles as well as the collection of mixed spectra on spots with changing composition (Table 14.5).

As is well known, during magnet manufacturing different alloys are sintered at 1,550 °C so that magnet powders could not establish a strict homogeneous composition (Figure 14.22(A)). In accordance with Table 14.4 these magnets contain 65.6 wt.% iron. The major blue domains show the same relation, as they occupy ~90 % of the surface, whereas the residual 10 % of green-coloured domains predominantly consist of neodymium and dysprosium.

Substoichiometric amounts of NH_4Cl during solid-state chlorination turned the picture upside down (Figure 14.22(B)). Agglomerates were formed consisting of several small grains. For instance the depicted particle consists of at least 16 blue-coloured

Table 14.5: Composition key used for the analysis of magnets by MLA.

Colour	Fe content (wt.%)	Nd content (wt.%)	Dy content (wt.%)	Note
	0	>60	>23	Nd represents the main component
	13	60	0	
	3	45	23	
	21	44	9	
	29	38	6	
	42	30	10	Fe represents the main component
	51	21	10	
	74	26	0	
	77	9	0	
	79	11	0	
	94	6	0	
	–	–	–	Quartz
	–	–	–	Unknown
	–	–	–	Low counts

grains in which iron content increased compared to the original powder. Now green RE-rich layers occupy the space between all grains and on the particle surface. Some green spots even show Fe contents <1 wt.%. In fact, this proves directly the assumed partial selectivity.

Since iron has a shielding effect it has to be chlorinated almost completely to achieve high RE yields as well. Therefore, over-stoichiometric amounts of NH₄Cl are necessary to disintegrate the formed agglomerates (Figure 14.22(C)). However, the resulting mechanically instable layer of metal chlorides crumbled during sample preparation. The consequences are vast cracks in the epoxy resin and uneven surfaces of pink colour, which are inaccessible for analysis. Only few grains remained, forming the retentate of the filtration and being introduced to solid-state chlorination another time.

In summary, cases (B) and (C) offer two options for process control. On the one hand, substoichiometric amounts of NH₄Cl already furnish high RE yields ≥76 %. Unreacted residues considerably enrich iron. This option should be chosen, if economic reasons require a reduction of NH₄Cl amounts and waiving the recirculation of unreacted residues. This procedure allows for introducing larger amounts of magnet powder to the rotary kiln, thus enhancing reaction performance. On the other hand, excess amounts of NH₄Cl are necessary to enable a quantitative magnet recycling. For these purposes, Fe contents of the retentates need to be equal to or less than the starting material in order to quantitatively chlorinate all metals within a few cycles, typically 2–3 cycles.

Apart from buffer leaching influencing RE yields, the range of NH₄Cl amounts also has to be expanded to cover both scenarios. However, further optimization with

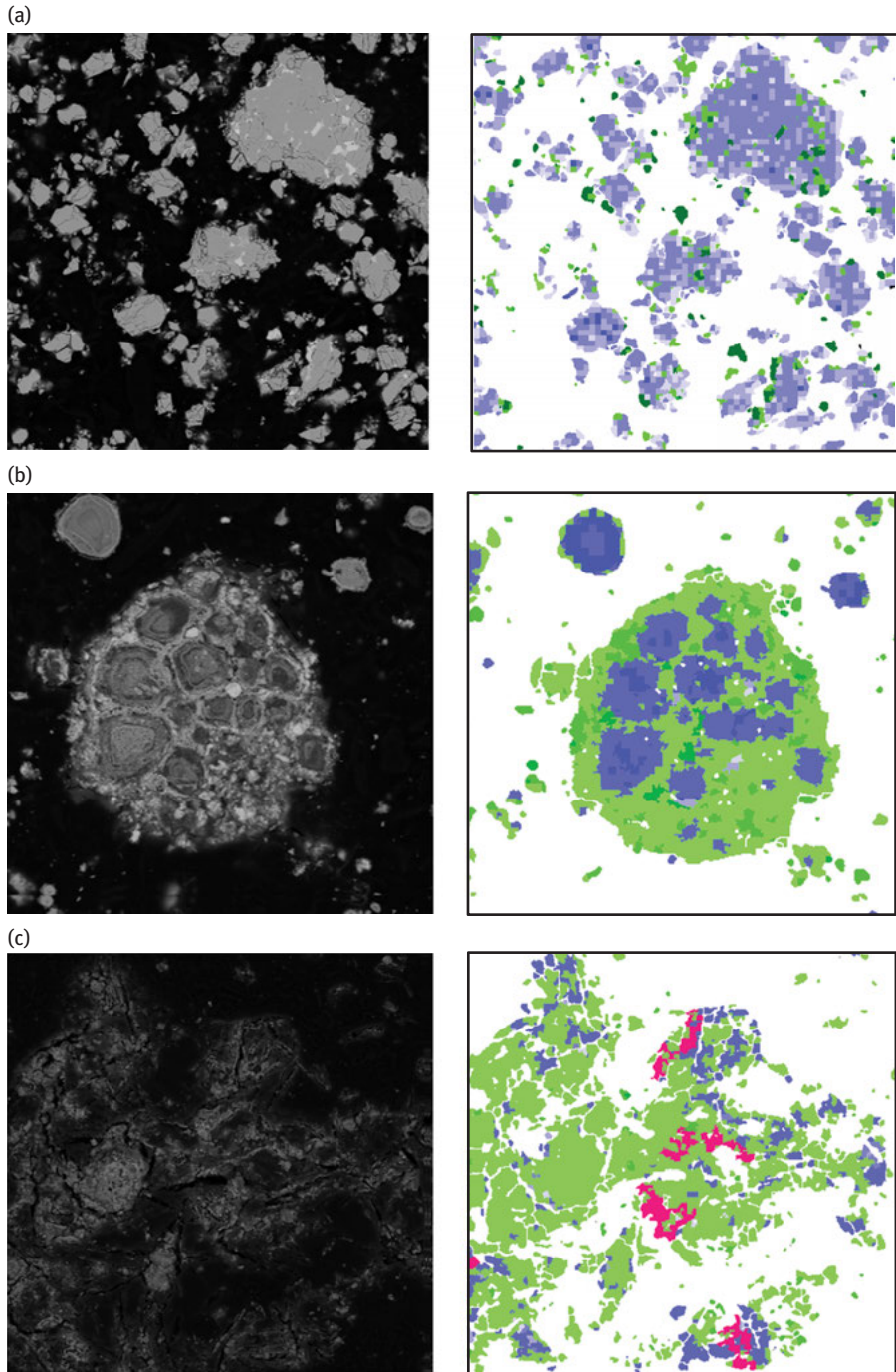


Figure 14.22: MLA examined samples of (a) untreated as well as (b) under- and (C) over-stoichiometric chlorinated magnet powders.

adjusted ranges and factors is currently continued in the MagnetoRec project³, which also comprises the development of the first rotary kiln exclusively designed for solid-state chlorination (kilogram scale). MagnetoRec has started in August 2016.

14.3.4 Recycling process

Except for some few differences the desired process resembles the one developed for fluorescent lamp scraps (Figure 14.23). At first EoL magnets need to be demagnetized and ground to particle sizes <100 μm prior to chlorination to their metal chlorides. In the course of aqueous work-up, acetate buffer (pH = 3) prevents hydroxides from precipitating and enhances RE yields by additionally leaching the magnets through cementation. Due to comparatively high pH values, any further adjustment of pH values is redundant [36–38]. The same applies for the recovery of excess acids. For precipitation oxalic acid or hydrofluoric acid can be added to the permeate after filtration with the aim of retrieving RE oxalates or fluorides. Whereas calcining the RE oxalates leads to sellable RE oxides, RE fluorides may serve as starting material for the reduction to RE metals. Nevertheless, both options for precipitation achieve quantitative yields at pH ≥ 1.

In general, designing an entire process is not necessarily the aim of developing recycling strategies. Instead extending an industrial process by one or at most a few

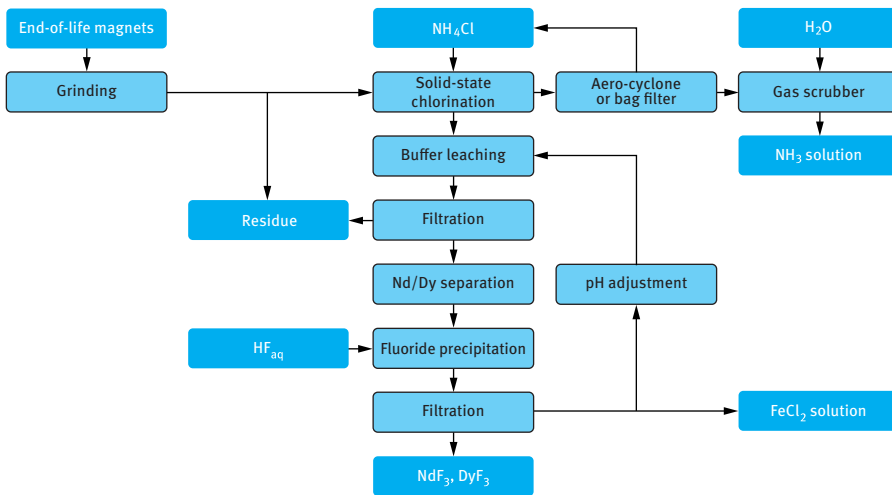


Figure 14.23: Scheme of the process developed for recycling Fe₁₄Nd₂B magnets.

³ The authors wish to thank the Federal Ministry of Education and Research for financial support of the project (grant number 033RK039B).

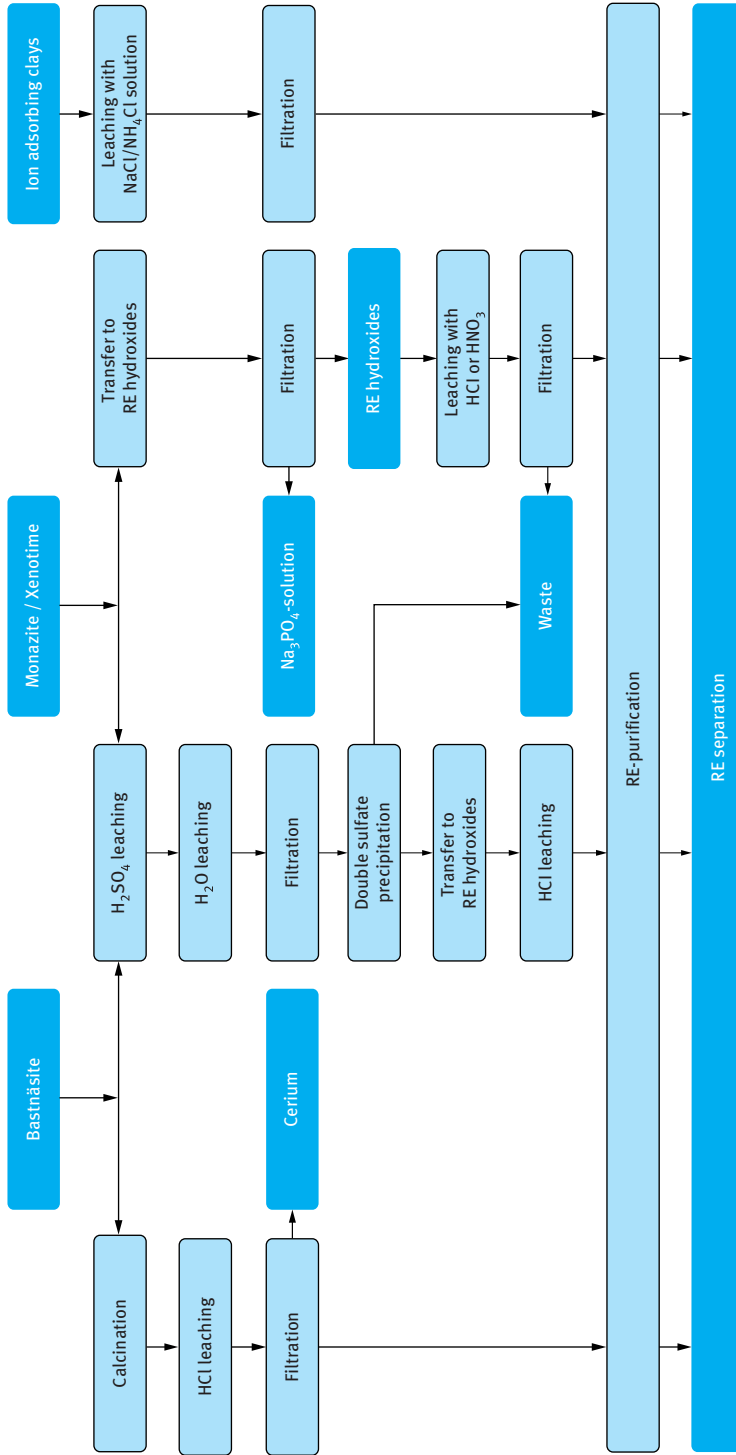


Figure 14.24: Applied industrial processes for primary RE production from different minerals [32, 36–38].

steps facilitates upscaling. Since at present there is no industrial recycling technology available, EoL recycling has to be implemented in primary RE production from their minerals and ores (Figure 14.24). This situation may be changed by transferring the solid-state chlorination on an industrial scale. It has to be noted, however, that mixed RE qualities, Nd/Dy, are obtained.

Hitherto, all processes finally furnish a mostly acidic RE concentrate, which is used for further purification and RE separation (Figure 14.24). At this point permeates coming from solid-state chlorination could be fed into primary production. Applying solid-state chlorination for primary production is conceivable, but only for carbonatic bastnäsite (Ce,La,Nd,Y)[(F,OH)CO₃]. Chlorinating monazite (La,Ce,Nd)[PO₄], xenotime (Y,Yb)[PO₄] or clays leads nowhere, since solid-state chlorination is not suited to mobilize REs from phosphates, borates or aluminates. Even industrial processes need two steps to dissolve RE elements from both phosphatic minerals. Initially either concentrated H₂SO₄ or NaOH_(aq) transfers all RE phosphates to sulphates and hydroxides, respectively. After phosphate ions were removed all RE salts are dissolved by adding acids or simply by diluting with water. For ion adsorbing clays treatment with a solution of NaCl and NH₄Cl already suffices to desorb RE ions.

14.3.5 Summary

As was shown, the solid-state chlorination of EoL magnets is saving costs for both chemicals and disposal. The chlorination protocol using NH₄Cl provides all the benefits already discussed for fluorescent lamp scraps (cf. 14.2.5). The partial selectivity of the chlorination step allows for designing processes very flexibly. In case of low commodity prices for rare earth metals, NH₄Cl demand can be reduced by more than 71 %, while concomitantly reactor performance is doubled without reducing RE yields upon magnets passing the reactor the first time (Figure 14.21). This can be achieved by using an acetate buffer which partially leaches the magnet powder and additionally enhances RE yields by a supporting cementation reaction. So there are three different effects, which allow for mobilizing RE, namely chlorination with HCl_(g), cementation of Fe²⁺ ions and leaching with small amounts of acetic acid. In this regard great expectations are placed on the MagnetoRec project, in which simultaneous optimization will finally combine solid-state chlorination and buffer leaching to recycle EoL magnets in the most efficient way.

References

- [1] Jewell S, Kimball SM. U.S. Geological Survey 2016: Mineral Commodity Summaries. Reston, US Govt. Printing Office, 2016.
- [2] Asada A, inventor; Santoku Metal Industry Co. Ltd., assignee. Method for recovering reusable rare earth compounds. US5728355 A.

- [3] Greenberg B, inventor; Pure-Etch Co., assignee. Neodymium recovery process. WO1994026665 A1.
- [4] Hirota K, Minowa T, inventor; Shin-Etsu Chemical Co. Ltd., assignee. Remelting of rare earth magnet scrap and/or sludge, magnet-forming alloy, and sintered rare earth magnet. US6960240 B2. 2002 July 10.
- [5] Hirose Y, Go T, Renda M, Kawamura N, Otaki A, inventor; Showa Denko K. K., assignee. Method and device for melting rare earth magnet scrap and primary molten alloy of rare earth magnet. WO2000039514 A1.
- [6] Onishi H, Terada T, Yamagata Y, Yamashita F, inventor; Matsushita Electric Industrial Co. Ltd., assignee. Verfahren zur Herstellung eines wiederverwendeten Pulvers für die Benutzung in einem Verbundmagnet und Verfahren zur Wiederverwendung eines Verbundmagneten. EP1096517 B1.
- [7] Bast U, Blank R, Buchert M, Elwert T, Finsterwalder F, Hörnig G, et al. Recycling von Komponenten und strategischen Metallen aus elektrischen Fährantrieben (MORE): Abschlussvorhaben zum Verbundvorhaben. Siemens AG; Daimler AG; Umicore AG&Co. KG; Vacuumschmelze GmbH&Co. KG; Universität Erlangen-Nürnberg; TU Clausthal; Öko-Institut e.V., Fraunhofer ISI, 2015.
- [8] Elwert T. Entwicklung eines hydrometallurgischen Recyclingverfahrens für NdFeB-Magnete [Dissertation]. Clausthal, TU Clausthal, 2015.
- [9] Elwert T, Goldmann D, Schmidt F, Stollmaier R. Hydrometallurgical recycling of sintered NdFeB magnets. *World Metall – Erzmetall* 2013, 66, 209–19.
- [10] Itakura T, Sasai R, Itoh H. Resource recovery from Nd–Fe–B sintered magnet by hydrothermal treatment. *J Alloys Compd* 2006, 408–412, 1382–5. doi: 10.1016/j.jallcom.2005.04.088
- [11] Lyman JW, Palmer GR. Recycling of Neodymium Iron Boron Magnet Scrap. Washington, Bureau of Mines, 1993.
- [12] Hitachi Develops Recycling Technologies for Rare Earth Metals. Tokyo, 2010.
- [13] Letcher TM, Scott JL (eds.). *Materials for a Sustainable Future*. Cambridge, Royal Society of Chemistry, 2012, 791.
- [14] Bundesanstalt für Geowissenschaften und Rohstoffe. BGR Preismonitor 03/2016. Available from: http://www.bgr.bund.de/EN/Themen/Min_rohstoffe/Produkte/Preisliste/cpl_16_03.pdf;jsessionid=FDDE38484083D1A6936FF63ED1B14F66.1_cid331?__blob=publicationFile&v=3.
- [15] Tytgat J. Umicore Battery Recycling: Recycling of NiMH and Li-ion batteries. Joint EC/Green Cars Initiative PPP Expert Workshop 2011. Brüssel, 2011.
- [16] Huckenbeck T, Otto R, Haucke E, inventor; Osram AG, assignee. Verfahren zur Rückgewinnung Seltener Erden aus Leuchtstofflampen sowie zugehörige Leuchtstoffe und Lichtquellen. WO2012143240 A2.
- [17] Lorenz T, Fröhlich P, Bertau M, inventor; FME Freiburger Metallrecycling und Entwicklungsdienstleistungen GmbH, assignee. Verfahren zur Rückgewinnung Seltener Erden aus Seltene Erden-haltigen Zusammensetzungen. DE102014206223 (A1). April 30 2014.
- [18] Lorenz T, Fröhlich P, Bertau M, inventor; FME Freiburger Metallrecycling und Entwicklungsdienstleistungen GmbH, assignee. Verfahren zur Rückgewinnung Seltener Erden aus Seltene Erden-haltigen Leuchtstoffen. DE 102014224015. 2014 Nov 25.
- [19] Lorenz T, Golon K, Fröhlich P, Bertau M. Rückgewinnung Seltener Erden aus quecksilberbelasteten Leuchtstoffen mittels Feststoffchlorierung. *Chemie Ingenieur Technik* 2015, 87, 1373–82. doi: 10.1002/cite.201400181
- [20] Verordnung (EG) Nr. 245/2009: EG 245/2009; 2009.
- [21] Otto M. *Chemometrie: Statistik und Computereinsatz in der Analytik*. Weinheim, VCH, 1997, 355.
- [22] Retzlaff G, Rust G, Waibel J. *Statistische Versuchsplanung: Planung naturwissenschaftlicher Experimente und ihre Auswertung mit statistischen Methoden*. Weinheim, Verl. Chemie, 1975, 211.

- [23] Liu X, Byrne RH. Rare earth and yttrium phosphate solubilities in aqueous solution. *Geochim Cosmochim Acta* 1997, 61, 1625–33. doi: 10.1016/S0016-7037(97)00037-9
- [24] Lide DR. *CRC Handbook of Chemistry and Physics: A Ready-Reference Book of Chemical and Physical Data*, 79th edn. Boca Raton, FL and London, CRC Press, 1998.
- [25] Seifert M, Fröhlich P, Bertau M, inventor; assignee. Vorrichtung und Verfahren zur Abtrennung und Konzentration von Bestandteilen mit magnetischem Verhalten aus einer ionenhaltigen Lösung. 102014211289.
- [26] Neufassung der Trinkwasserverordnung. Part I. Bonn, 2016, 12.
- [27] Braconnier J-J, Rollat A, inventor; Rhodia Operations, assignee. Method for recovering rare-earth elements from a solid mixture containing a halophosphate and a compound of one or more rare-earth elements. US8501124 B2.
- [28] Braconnier J-J, Rollat A, inventor; Rhodia Operations, assignee. Method of recovering rare earths from a solid mixture containing a halophosphate and a rare earth compound and solid mixtures suitable for this method. US9102998 B2.
- [29] Average commodity prizes from Alibaba, converted to Euro per t [cited June 22 2016]. Available from: www.alibaba.com
- [30] Seifert M. Economic Data for Rare Earth Recycling from Fluorescent Lamp Scraps by FNE Entsorgungsdienste Freiberg GmbH. Personal communication.
- [31] Gutfleisch O, Willard MA, Bruck E, Chen CH, Sankar SG, Liu JP. Magnetic materials and devices for the 21st century: stronger, lighter, and more energy efficient. *Adv Mater* 2011, 23, 821–42. doi: 10.1002/adma.201002180. PubMed PMID: 21294168.
- [32] Kausch P, Bertau M, Gutzmer J, Matschullat J (eds.). *Strategische Rohstoffe – Risikovorsorge*. Berlin, Heidelberg, Springer Berlin Heidelberg, 2014.
- [33] statista. Verwendung von Seltenen Erden nach Einsatzbereichen in den Jahren 2006 und 2012 [cited May 3 2016]. Available from: <http://de.statista.com/statistik/daten/studie/246406/umfrage/verwendung-von-seltenen-erden-nach-einsatzbereichen/>
- [34] Elsner H, Sievers H, Szurlies M, Wilken H. Das Mineralische Rohstoffpotential der Arktis [cited May 3 2016]. Available from: http://www.deutsche-rohstoffagentur.de/DE/Gemeinsames/Produkte/Downloads/Commodity_Top_News/Rohstoffwirtschaft/41_mineralisches-rohstoffpotenzial-arktis.pdf?__blob=publicationFile&v=4
- [35] Wilken H. Verfügbarkeit von Seltenen Erden. 21. Rostock, Dechema Kolloquium Rostock, 2016.
- [36] Dittmeyer R, Keim W, Krevsa G, Oberholz A (eds.). *Winnacker-Küchler Chemische Technik: Prozesse und Produkte. Band 6: Metalle*. 5th edn. Weinheim, Wiley-VCH, 2006.
- [37] *Ullmann's Encyclopedia of Industrial Chemistry*. Weinheim, Germany, Wiley-VCH Verlag GmbH & Co. KGaA, 2000.
- [38] Kirk RE, Othmer DF, Kroschwitz JI, Howe-Grant M. *Encyclopedia of Chemical Technology*, 4th edn. New York and Chichester, Wiley, 1998, xxviii, 912.

Index

- absorption coefficients 265
- abundance 1
- acetate buffer 35, 383, 384, 389, 391
- acid effect 158
- acid leaching 362
- acidic extraction system for REEs 30
- acidic phosphorus 19
- acidic phosphorus extractants 20
- activator 361
- activator elements 359
- activity 257
- alkaline earth metals 375
- alkyl phosphoric acid 19
- aluminium alloys 211
- amine-based extractants 20
- analysis function of Ce in aluminium 216
- analysis function of Ce in cast iron 222
- analysis function of Ce in zinc 227
- analysis function of chromium in low-alloy steel 208
- analysis function of La in aluminium 215
- analysis function of La in cast iron 223
- analysis function of La in zinc 226
- analysis function of Nd in magnesium 219
- analysis function of Pr in magnesium 219
- analysis of lanthanoides 134, 142
- analytical performance of ETV-ICP-OES, PN-ICP-OES and GFAAS 174
- apatite 297
- application of coprecipitation-ICP-OES/MS for trace REEs analysis 17
- the application of the correction factor method in high-purity yttrium oxide analysis 157
- application of ICP-OES in the analysis of REEs in metal and alloy samples 192
- application of ICP-OES in the determination of REEs impurities in high-purity REE 187
- application of ICP-OES for the direct determination of REEs in ores 191
- ashing curve of La [40]: (1) 0.2 mg/L La, 6 % PTFE; (2) biological sample, 6 % PTFE 182
- association 297, 298
- atomic emission spectroscopy using an inductive coupled plasma 363
- auger effect 232
- backscatter electrons, BSEs 289
- bastnäsite 391
- Bateman–Rubinson equation 280
- BEC and detection limits of REEs in ICP-OES 146
- β decay 254
- β^+ decay 255
- BG (k) for the fluorinating reaction of La, Y and Yb with the presence of PTFE 180
- biocompatible adsorbent particles 61
- bioimaging 317
- borate as the fusion material 239
- Box–Behnken design 382, 384
- Box–Behnken plan 366, 371, 372
- brief electrical discharge 198
- BSE 290
- buffer 384, 387, 389
- buffer leaching 391
- buffer solution 384
- calibrated 386
- calibrating a spark emission spectrometer 207
- capillary electrophoresis (CE) 74, 110, 111
- capillary microextraction (CME) 62
- carbonaceous materials 51
- the carrier (also called trapping agent) 15
- cast iron and steel 212
- ce and La in cast iron, steel and zinc 213
- central composite design 371
- centrifugal partition chromatography 99
- ceramics 358
- certified reference samples for rare earths 214
- the characteristics of FIA coupled with atomic spectroscopy 167
- characteristic X-radiation 361
- chart of the nuclides 267
- chelate extractants 23
- chelating agent 83
- chelating agent-loaded resin 77
- chelating agent for REEs extraction 24
- chelating resin 78
- chemical immobilization 57
- the chemical modifiers can be spiked into ETV system in gaseous or solid form 177
- chlorination 362, 372, 373, 378, 381, 384, 389, 391
- chromatography 74
- cinnamic acid 15

- commodity prices 357, 375, 378, 391
- commonly used spectral lines (nm) for REEs
 - analysis 151
- a comparison of analytical performance of REEs
 - in Y2O3 matrix 169
- complete factorial design 371
- complexing agent 81, 82
- compton continuum 263
- compton edge 263
- compton effect 264
- concentration of REEs in sea water 14
- continuous-flow microextraction 36
- corrosion 358
- critical REE ratio 287
- cross sections 386
- crusher 379
- CSIRO 291
- the curve of Sm concentration vs. signal intensity
 - in flow injection reverse standard addition method 170
- cyclone spray chamber 364

- decay constant 255
- decay scheme 256
- decomposition temperature 373, 374
- Delesse principle 290
- the deposition loss of analytes with and without
 - the presence of PTF 179
- derivative spectrometry 152
- design of the electrothermal vaporization (ETV)
 - device 175
- detection limit and precision for La and Y in
 - different solvents 165
- detection limit of REEs in REE matrix 188
- the detection limit of REEs with/without
 - desolvation 161
- detection limits of REEs 185
- the detection limits of REEs under different
 - conditions 189
- the detection limits for refractory elements by
 - LA-ICP-OES 173
- determination of total REEs 15
- Di(2-ethylhexyl)phosphate 16
- diffusion 329
- diffusion dialysis 365
- dimethyl oxalate 15
- diphenyl glycolic acid 15
- direct excitation 235
- dispersing solvent 40

- distribution coefficient 16
- drop-in-drop system 33
- dynamic adsorption capacity 59

- E_1 : energy of the excited state 1, 198
- the effect of desolvation temperature on the
 - spectral line intensity of REEs 161
- the effect of ethanol concentration on the signal
 - intensity of REEs in ICP-OES 164
- the effect of ethanol on the detection limit of
 - REEs 160
- the effect of ethanol on nebulization and
 - atomization efficiency 161
- the effect of HCl and matrix concentration on the
 - signal intensity of REEs [22] 168
- the effect of matrix concentration on the spectral
 - background intensity [5] 154
- the effect of PTFE slurry concentration on the
 - signal intensity of La 181
- the effect of RE matrix (Y, Yb) on the signal
 - intensity of La 184
- effect of salting-out agents on the extraction
 - efficiency of Eu³⁺ 28
- the effect of vaporization temperature on the
 - signal intensity of La 183
- the effect of Y matrix on spectral 163
- the effect of Y2O3 matrix concentration on target
 - REE signals 155
- electric motors 358, 378
- electron capture 255
- electron volts 253
- electrophoresis 108, 109
- electrothermal vaporization 173
- elements 380
- end-of-life (EoL) products 357
- energy-dispersive X-ray spectroscopy (EDX) 379,
 - 386
- enhanced sensitivity by ethanol 160
- enhanced sensitivity caused by organic solvents
 - in REEs analysis 160
- environmental monitoring 33
- EoL magnets 379, 381, 389, 391
- EoL products 358, 364
- EoL waste 358, 359, 360, 361
- epoxy resin 386, 387
- escape peak 264
- ETV-ICP-OES for REE analysis 177
- exchange resin with thin shell 76
- experimental error 367, 370, 372

- external calibration 361
- extractants for REEs 18
- extractants for REEs 19
- extracted RE complexes are neutral salts 29
- extraction ability of TBP 18
- extraction chromatography 97, 98
- extraction efficiency of REE ions 26
- extraction equilibrium 44
- extraction film 47
- extraction temperature 47
- extraction time 50

- Fe₁₄Nd₂B magnets 357, 364, 379, 380, 383, 389
- fertilizers in agriculture (especially in China) 14
- FETV technique for sample introduction 178
- FIA coupled with ICP-OES for direct determination of trace REEs 168
- field image mode, *see* fieldscan mode
- fieldscan/field image mode 292
- fieldscan mode 293
- fission reactors 258
- fission yield 259, 282
- flame-AAS 361
- flotation technique 16
- flow counter 361
- fluidized bed reactors 363
- fluorescence 289, 290
- fluorescence lines from REE in keV 248
- fluorescence yield 232
- fluorescentlamp scraps 365
- fluorescent lamp scraps (production waste) 357, 358, 359, 360, 361, 363, 364, 367, 368, 369, 370, 372, 376, 377, 379, 381, 382, 389, 391
- fluorescent material 359, 360, 362, 367, 379
- fluorescent materials 361
- fluorination-assisted (F)ETV-ICP-OES for REEs analysis 177
- food safety 33
- fullerene-like structures 51
- fusion technology 231
- fusion technology 238

- galfantm 226
- gas chromatography 107
- gaseous HCl 362
- gaseous hydrogen chloride (HCl(g)) 367, 368, 373
- gaseous phase 362, 363, 364, 365, 367, 373, 374, 376
- gas phase 381, 384

- gated discharge source 203
- Gd-based MRI contrast agent 58
- Ge semiconductors 262
- glass 358
- glass ceramics 321
- global optimum 366, 373
- gold standard 386
- group separation of REEs 16

- half life 255
- halophosphate fluorescent materials 358, 359
- handheld XRF instruments 236
- Harkins rule 2
- HCl(g) 373, 376, 381, 383
- HCl leaching 365
- heavy REEs (HREEs) 1
- hexafluorophosphate anions 42
- high-purity REE analysis by ICP-OES 187
- high-voltage ignition pulse 199
- hollow fiber liquid phase microextraction 37
- horizontal impact crusher 379
- hydrofluoric acid digestion 324
- hydrometallurgical process 358
- hydrometallurgical treatment 378, 379
- hydrophobic core 47

- IC 87, 88, 90
- ICP-AES 361, 367, 380
- ICP analysis 323
- ICP-MS 124, 125, 126, 128, 129, 130, 131, 133, 134, 135, 135, 136, 137, 138, 139, 140, 301, 302, 303, 304, 305, 306, 308, 309, 310, 311, 312, 313, 314, 315, 316, 317
- IEC 84, 87
- individual energy transitions 198
- industrial production 357
- industrial use of rare earths in 2010 211
- the influence of REE matrix on the detection limit of trace REEs 156
- influencing factors 110
- intensities 364
- internal calibration 361, 369
- internal standard compensation 156
- in-tube SPME 62
- ion chromatography 57
- ion chromatography 86
- ion-exchange chromatography 75
- ion exchange resins 78
- ionic liquids 42
- ion-imprinted polymers 60

- isocratic and gradient elution 57
- isoelectric point (IEP) 56
- Isotopic neutron sources 261
- ito et al. [20] introduced FIA into ICP-OES 167

- JKMRC 294

- kalman filtering method 152
- kinetics 47
- K series lines for La to Sm 241

- LA-ICP-OES is featured with low absolute
 - detection limit (ng to pg level) 172
- lanthanides 286, 287
- lanthanoids 295
- laser ablation (LA)-ICP-MS 308
- leaching 357, 376, 381, 384, 385, 389
- liberation 291
- Li-borate beads 231
- life sciences 301, 302
- light REEs (LREEs) 1
- light source of atomic emission spectrometry,
 - ICP 146
- line intensity of REEs under pre-desolvation 163
- line spectrum 198
- line spectrum of iron 198
- liquid chromatography 75
- liquid–liquid extraction (LLE) 15
- liquid phase microextraction (LPME) 15
- lithiumtetraborate 239
- L-line spectra of La, Gd and Lu 241
- local optimum 373
- low-dilution fusion 239
- low-temperature ETV-ICP-OES 186
- L-series lines of 100, g/g Gd in cellulose 243
- L-series lines of 100, g/g La in cellulose 243
- lumen of the hollow fiber 38

- magnesium alloys 211
- magnetic nanoparticles 58
- magnetic solid phase extraction (MSPE) 56
- magnetic susceptibilities 375
- MagnetoRec project 389
- magnet powder 380, 382, 384, 385, 386, 388
- magnifications 23, 379
- making a pellet 237
- mandelic acid 15
- mass cytometry 306, 308, 310, 311, 317
- mass-exchange characteristics 56

- matrix effect 206
- matrix effect of alkali and alkaline earth
 - metals 183
- matrix matching 156
- matrix simplification 51
- measurement program for WDXRF 245
- medium exchange 51
- medium-voltage discharges 203
- melting and boiling points (°C) for REEs and
 - corresponding compounds 178
- mesoporous nanoparticles 58
- metallic carbide-coated tube 174
- methylene phosphoric acid 15
- micelles 47
- microporous crystalline materials 60
- mineral liberation analyser (MLA) 386, 387, 388
- mobile phase 79, 80
- mobile spectrometers 200
- modal abundance 290
- model equation 366, 367, 372
- molar volume 373, 374
- molecular-imprinted polymers 60
- molecular/ion imprinted polymers 51
- monazite 296, 391
- monazite samples 240
- MORE project 358
- the most widespread and efficient type of
 - chemical reaction is halogenating reaction, especially fluorination and chlorination reaction 177
- multichannel analyser 261
- multiple linear regressions 367

- nanometer-sized powder materials 58
- nanometer-sized TiO₂ 59
- nanoparticles 58
- nano-sized inorganic oxides 58
- nanostructured materials 51
- neodymium oxide 322
- neutral phosphorus extractants for REEs
 - extraction 18
- Neutron activation analysis (NAA) 253
- NiMH batteries 357, 358
- nitrogen-containing extractants 20
- nitrogen-containing extractants for REEs 22
- non-equilibrium state 47
- nonionic surfactants, amphoteric ionic
 - surfactant 48
- nuclear reactions 253

- olivines 279
- one-factor at-the-time strategy 366, 384
- online FI separation/preconcentration ICP-OES
 - for trace REEs analysis 171
- online separation/preconcentration system
 - combined with ICP 171
- optimization 33, 370, 384, 387
- optimum 367, 372, 373, 374, 382
- organic acceptor solution 38
- organic fluorinating reagent benefits the
 - improvement of the vaporization 172
- organic resin 76
- organic solvent in ICP 159
- organic solvent and pre-desolvation 161
- orthopyroxenes 279
- ostensible optimum 366
- overlap of single element L-line spectra 241
- overlapped L-line spectra of REE 244
- overlaps 235

- pair production effect 266
- paper chromatography(PC) 102, 103
- parasite 295, 296
- Pareto diagram 372, 373, 382, 383
- partial least-squares method (PLS) 152
- Particle Mineral Analysis (PMA) 294
- particle size effects 238
- particle surface 364
- Paschen–Runge mount 202
- peridotites 279
- permanent magnets 358, 378
- permanent nanoscale pore structure 60
- pH adjustment 384
- pH value 375, 378, 381, 382, 383, 389
- pharmaceutical analysis 33
- photoelectric effect 264
- photon activation 261
- plasma torch 146, 364
- platinum–gold crucible 239
- pneumatic nebulization and ultrasonic
 - nebulization 166
- polarizing excitation 234
- polishing agents, ceramics, glass 358
- polychromator array 202
- potential analysis and interference lines of rare
 - earths 213
- precipitation 381, 382, 389
- precipitation/coprecipitation 14
- preparation 387

- pre-sparking period 199, 200, 205
- pressed pellets techniques 236
- primary production 391
- process control 383
- process economy 378
- production waste 357, 359, 360, 363, 364, 368,
 - 369, 370, 378, 378
- prompt γ -ray NAA 254
- pulse height spectrum 234
- pyrolytic graphite-coated tube 174
- pyrometallurgical processes 357, 378

- QEMSCAN 291, 292, 293, 294
- quantification of trace/ultra-trace REEs 14
- quantitative mineralogy 288

- rapid phase separation 50
- Rare Earth Elements (REEs) 74, 81, 82, 83, 84,
 - 86, 88, 90, 92, 93, 94, 95, 97, 98, 99, 102,
 - 103, 104, 106, 107, 108, 111, 115, 386
- RE alloys Fe₁₄Nd₂B magnets 378
- RE applications 2
- RE containing ores 357
- RE elements 364, 376, 381
- RE fluorides 389
- RE matrix concentration 155
- RE metals 378, 379, 382, 383, 389
- RE ores 364
- RE oxalates 389
- RE oxide 378, 389
- RE production 390
- RE reduction 358
- RE separation 364, 375, 391
- reaction zone 373
- reciprocal linear dispersion 202
- recycling processes 377
- recycling 357, 358, 379, 380, 387, 391
- REEs in biological samples 14
- REEs in groundwater 42
- REEs in seawater 57
- reference analytical lines for ICP-OES detection
 - of REE impurities in high-purity REmatrix 190
- reference list 386
- regression parameters 367, 372
- the relative deposition loss of target analytes
 - with and without the presence of PTFE 180
- repeatability 370, 371
- repeatable 367
- representation of repeatability of Ce in
 - aluminium 218

- representation of repeatability of Ce in cast iron 225
- representation of repeatability of Ce in zinc 228
- representation of repeatability of La in aluminium 217
- representation of repeatability of La in cast iron 224
- representation of repeatability of La in zinc 227
- representation of repeatability of Nd in magnesium 221
- representation of repeatability of Pr in magnesium 221
- response surfaces 366
- restricted accessed magnetic nanoparticles 61
- reusability 57
- Reverse-phase ion pair chromatography (RPIPC) 90
- rotary kiln 363, 372, 373, 375, 378, 381, 387, 389
- RP-HPLC 94
- RPIPC 92, 93, 95

- salting-out agents 28
- samarium 322
- sample preparation 386, 387
- sample pretreatment technique 50
- sampling efficiency 155
- Sc, La and Ce in aluminium, La, Ce and Nd in magnesium 213
- scanning electron microscope (SEM) 328, 379
- scintillation counter 361
- scintillation detector 262
- Secondary electron images (SEI) 360
- second-order reactions 280
- sections 386
- segmentation 290
- SEI 379
- selected spectral lines of the lanthanides and respective detection limits (mg/L) by ICPOES as a function of the nebulizer and plasma view 167
- self-absorption effect 207
- self-modeling curve resolution method (SMCRM) 152
- SEM 360, 386
- SEM-EDX analyses 380
- SEM-EDX spectroscopy 359
- sensitive lines and detection limits of REEs in ICP-OES 149
- sensitivity-enhancing effect of ethanol 161
- sensitivity-enhancing factor of organic solvent on La and Y 165
- the separation factors 26
- SepSELSA project 357, 358, 359, 360, 376, 378
- sequential optimization 365, 366
- shape parameters 290
- shielding effect 387
- signal inhibition caused by matrix effect 155
- signal profiles of Yb in the absence and presence of PTFE 179
- signal record regarding the long-term stability of La in cast iron 225
- silica gel-based ion exchanger 77
- silicon–lithium semiconductor, pin diode or silicon drift chamber 233–234
- simplex method 366
- simultaneous 365
- simultaneous back extraction 36
- simultaneous optimization 363, 372, 382
- single-drop microextraction 34
- single spark discharge 199
- sintered 386
- SIP 292
- size exclusion property 61
- size parameters 290
- size-dependent properties 58
- Sm and Er in aluminium 213
- Sm, Y, Er and Gd in magnesium 215
- SmCo magnets 357
- solid phase extraction (SPE) 15
- solid phase microextraction 15
- solid-state chlorination 357, 358, 361, 362, 363, 364, 365, 366, 368, 370, 371, 372, 375, 376, 377, 378, 379, 380, 381, 382, 383, 384, 387, 389, 391
- solid-state chlorination (SepSELSA project) 365
- solvent extraction 357, 364
- some oxygen-containing extractants for REEs 21
- sorption capacity 57
- spark discharge 199
- spark spot 199
- spark stand 201
- spark succession frequency 205
- sparkling process 199
- specialty glass 321
- speciation of Gd-containing MRI contrast agents 135, 136, 140
- Species Identification Protocol, SIP 291

- spectra 386
- spectral interferences among REEs 147
- spectrometric prerequisites 212
- spinel 279
- spontaneous emission of radiation 198
- standard addition method in FIA 169
- statgraphics 367
- stationary laboratory devices 200
- stationary sparking state 200
- statistical design 358, 363, 366, 370, 371, 372
- sublimation reactors 362, 363, 365, 373
- supercritical fluid chromatography 115
- surface functionalization 51
- surface roughness 297, 298
- survey measurement 361
- symmetric plan 366
- synchysite 295, 296
- synergistic extraction system 32

- target value 366, 367, 372
- technical glass 321
- terbium 322
- ternary component solvent system 40
- thermal decomposition 361, 362
- thermodynamics 47
- thin layer chromatography (TLC) 102, 104, 106
- three-band fluorescent materials 359
- three-phase (liquid–liquid–liquid) microextraction 36
- three-phase HF-LPME 38
- tolerance capacity of ICP for organic solvents 160

- topochemical analysis 327, 328
- total reflection XRF 236
- trace amounts of REEs in water samples 37
- tracer in polymers 231
- transmission electron microscope (TEM) 328
- tributyl phosphate 16
- two-phase HF-LPME 38
- two-phase micro-extraction mode 35
- two-phase solvent extraction 16

- use of chemical modifiers 176

- validation of Ce and La in cast iron 223
- vapor pressure 330
- vaporization mechanism of REEs
 - fluorination 178
- vibrating cupmill 379

- wavelength-dispersive XFS 361
- WDS 328
- wet chemical processes 375, 376, 378
- working distance 379

- xenotime 391
- X-ray fluorescence 323
- X-ray fluorescence line overlaps relevant for REE 247
- X-ray fluorescent spectroscopy (XFS) 359, 361, 369

- ytterbium 322

- zinc alloys 212

